Deepali Jain
Justin A. Bishop
Editors

Atlas of Sinonasal Tract Pathology

Springer

Atlas of Sinonasal Tract Pathology

Deepali Jain • Justin A. Bishop
Editors

Atlas of Sinonasal Tract Pathology

Springer

Editors
Deepali Jain
Department of Pathology
All India Institute of Medical Sciences
New Delhi, India

Justin A. Bishop
Department of Pathology
UT Southwestern Medical Center
Dallas, TX, USA

ISBN 978-981-19-7314-7 ISBN 978-981-19-7315-4 (eBook)
https://doi.org/10.1007/978-981-19-7315-4

This Springer imprint is published by the registered company Springer Nature Singapore Pte Ltd.
The registered company address is: 152 Beach Road, #21-01/04 Gateway East, Singapore 189721, Singapore

Preface

In the world of head and neck pathology, the sinonasal tract has long been an orphan of sorts. Malignancies in this region are rare, while the most frequent specimens (i.e., sinus contents) were often regarded as having little or no educational value. Because of this low status, discovery in sinonasal tract pathology historically lagged behind other head and neck sites, with classification schemes devised decades earlier persisting with little change.

Sinonasal tract pathology now, however, can no longer be overlooked. The past decade has produced a dizzying list of newly described entities and concepts in sinonasal pathology, largely the result of molecular discoveries from insightful pathologist investigators. As a result of this upheaval, one cannot be expected to learn all that needs to be known from a small section of a larger surgical pathology or head and neck pathology book. Indeed, a dedicated text focused entirely on sinonasal tract pathology is clearly needed.

It is with this background in mind, we have devised this project. In this atlas, an international group of experts in the field comprehensively detail every aspect of sinonasal tract pathology, from normal anatomy and histology and radiology to the histopathology of every conceivable tumor or tumor-like lesion in this anatomic region. The authors emphasize high-quality images over text, a crucial approach in the highly visual field of anatomic pathology. It is our sincere hope that the reader finds this book valuable in their head and neck pathology practice.

New Delhi, India — Deepali Jain
Dallas, TX, USA — Justin A. Bishop

Acknowledgments

"I am thankful to the almighty God and my family including my husband Vijay and loving son Vivaan."

—Deepali Jain

"I thank my surgical pathology mentors and my loving, supportive family."

—Justin A. Bishop

We would like to sincerely thank all coauthors for contributing their time and expertise for the completion of this book. We also thank everyone on the publishing team of Springer for their untiring efforts and assistance with this book.

Contents

About the Editors

Deepali Jain, MD, FIAC, FRCPath has done post-graduation in pathology (MD) from Post Graduate Institute of Medical Education and Research (PGIMER) Chandigarh, India and also obtained the degree of Diplomate of National Board. She was awarded research fellowship from Johns Hopkins Medical Institutions, Baltimore, MD, USA for the year 2008–09. She is Professor at All India Institute of Medical Sciences (AIIMS), New Delhi, India.

Dr Jain has more than 300 peer-reviewed national and international publications and has delivered numerous lectures in various national and international meetings. She is editorial board member of WHO 2021 Classification of Thoracic Tumors (5th edition) and first edition of International System for Reporting Lung Cytopathology by International Academy of Cytology (IAC) and International Agency for Research on Cancer (IARC) WHO. She is chapter author of WHO 2022 classification of Head and Neck Tumors and Endocrine and Neuroendocrine Tumors. In addition, she has edited and published a book *Atlas of Thymic Pathology* with Springer in 2020. She is a member of many prestigious national professional bodies including the National Academy of Medical Sciences and National Academy of Sciences of India. She is a member of pathology committee of International Association for Study of Lung Cancer (IASLC). She is section editor—*Molecular Cytopathology, Archives of Pathology and Laboratory Medicine*. Dr Jain is a recipient of numerous distinguished national and international scientific awards including IASLC Mary J Matthews Pathology/Translational research award.

Justin A. Bishop is Professor and Jane B and Edwin P Jenevein, MD Chair in pathology and Director of Anatomic Pathology at UT Southwestern Medical Center, USA. Dr Bishop completed his pathology residency at The Johns Hopkins Hospital in Baltimore. Dr Bishop is an expert in the surgical pathology diagnosis of head and neck, endocrine, and thoracic diseases. He has published more than 200 journal articles and lectured extensively both nationally and internationally. Most recently, Dr Bishop was an editor for the most recent WHO Classification of Head and Neck Tumors and the lead author of the AFIP Fascicle of Salivary Gland Tumors. He is editor-in-chief of *Seminars in Diagnostic Pathology*, associate editor for *Modern Pathology* and *JAMA Otolaryngology-Head and Neck Surgery*, and a member of several additional editorial boards.

Anatomy and Histology of Sinonasal Tract

1

Aanchal Kakkar, Kavneet Kaur, and Deepali Jain

1.1 Introduction

Knowledge of the anatomy and histology is critical in understanding the pathology of diseases that affect the sinonasal tract. They are paramount not only for diagnosing non-neoplastic and neoplastic diseases with a predilection for this location, but also for identifying the extent of tumor in resection specimens, which is required for staging of the disease.

1.2 Anatomy

The sinonasal tract includes the nose and paranasal sinuses. The nose is comprised of the external nose and the nasal cavities. There are three paired paranasal sinuses viz. maxillary, ethmoid, and frontal sinuses, and one unpaired sinus viz. sphenoid sinus. The latter is, however, separated into two parts by a septum, which may or may not be in the midline.

The external nose is pyramidal in shape, fashioned from a framework of bone and cartilage, and forms the anterior region of the nasal cavities, which open externally by apertures called nares. Posteriorly, a pair of larger apertures called choanae open into the nasopharynx. The anterior most dilated portion that forms the nostrils is known as the nasal vestibule. It contains coarse hair called vibrissae that filter inhaled particles.

The skeletal framework of the nose includes the following bones: nasal, lacrimal, maxillary and palatine bones, and the inferior turbinates, and the frontal, ethmoid, sphenoid and vomer bones which are unpaired.

The nasal cavities are wedge-shaped spaces which form the uppermost part of the respiratory tract. The midline nasal septum separates the two nasal cavities and forms their medial wall. The floor is formed by the hard palate, which separates them from the oral cavity below, and the roof is formed by the frontal, ethmoid, and sphenoid bones (from anterior to posterior) which separates them from the cranial cavity above. The lateral walls are formed by the three turbinates or conchae which are curved shelves of bone that project into the nasal cavities and divide each cavity into four air channels: the sphenoethmoidal recess between the roof and the superior turbinate, and the superior nasal meatus between the superior and middle turbinates, the middle meatus between the middle and inferior turbinates, and the inferior meatus between the inferior turbinate and the floor of the nasal cavity (Fig.1.1). The orbit and maxillary sinus are situated lateral to the upper and lower portions of the nasal cavities, respectively. The paranasal sinuses open into the roof and the lateral walls of the nasal cavity, and the nasolacrimal duct which drains the lacrimal sac opens on the lateral walls [1, 2].

The ethmoid bone forms the major portion of the nasal cavity and contributes to a part of the roof, and to the lateral and medial walls. The cribriform plate of ethmoid forms the roof of the nasal cavity, and the fibers of the olfactory nerve course through its sieve-like structure. The crista galli projects superiorly from the cribriform plate, and anchors the falx cerebri within the cranial cavity. The perpendicular plate of ethmoid projects downwards from the cribriform plate to form the upper two-thirds of the nasal septum. The ethmoidal labyrinths located on either side are formed by the orbital plate and the medial sheet, and contain the ethmoidal air cells, forming the upper lateral walls of the nasal cavity. The superior and middle turbinates arise from the medial sheet and project into the nasal cavity [3].

The paranasal sinuses are named in accordance with the bone in which they are located, viz. frontal, maxillary, sphenoidal sinuses and ethmoidal air cells (Fig. 1.2). The frontal sinuses are the superior-most sinuses situated in the frontal bones. They are triangular, with the base oriented vertically above the bridge of the nose and the apex towards the lateral aspect, above the orbit. They open onto the lateral wall of the middle meatus in the semilunar hiatus through the frontonasal duct, which travels through the ethmoidal labyrinths (Fig. 1.3).

The ethmoidal air cells located within the bilateral ethmoidal labyrinths are divided into individual air chambers: the

A. Kakkar (✉) · K. Kaur · D. Jain
Department of Pathology, All India Institute of Medical Sciences, New Delhi, India
e-mail: draanchalkakkar@aiims.edu; deepalijain76@aiims.edu

D. Jain, J. A. Bishop (eds.), *Atlas of Sinonasal Tract Pathology*, https://doi.org/10.1007/978-981-19-7315-4_1

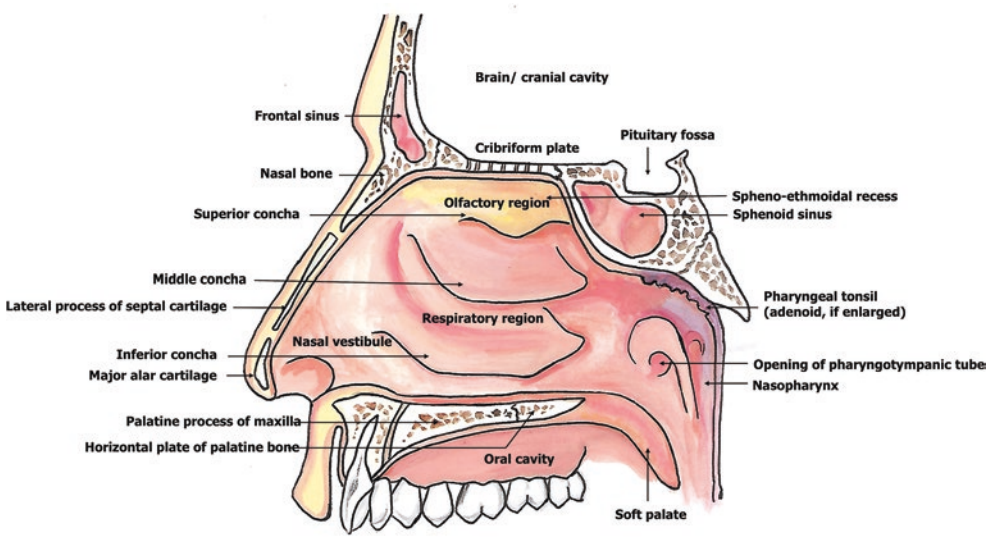

Fig. 1.1 Structures in the lateral wall of nasal cavity

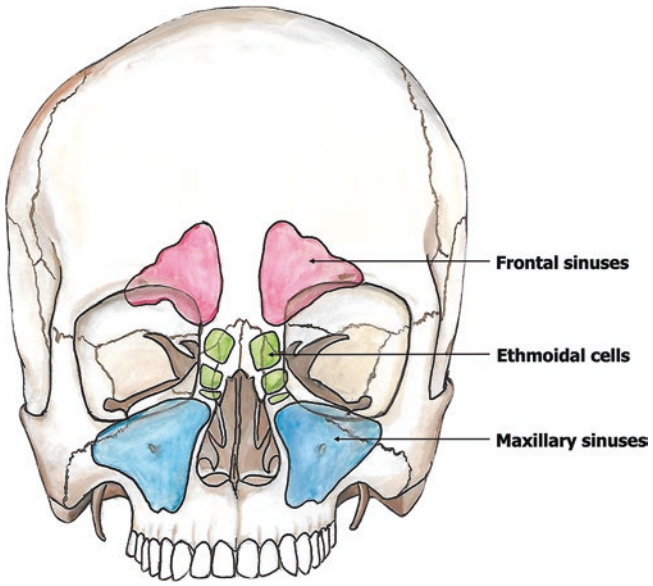

Fig. 1.2 Location of the frontal, ethmoid, and maxillary sinuses

anterior, middle, and posterior ethmoidal cells which open into the nasal cavity at the ethmoidal infundibulum, ethmoidal bulla, and into the superior nasal meatus, respectively (Fig. 1.3).

The maxillary sinuses found in the bodies of the maxillae are the largest of the paranasal sinuses. They are pyramidal in shape, with their base or the medial wall along the lateral wall of the nasal cavity and their apex pointing laterally (Fig. 1.2). The posterior walls, the superolateral walls, and the anterolateral walls are related to the infratemporal fossa posteriorly, the orbit above, and the facial muscles and the roots of the upper molars and premolars anteriorly, respectively (Fig. 1.3). The maxillary sinuses open into the nasal cavities in the middle nasal meatus in the center of the semilunar hiatus (Fig. 1.3).

The sphenoid sinus lies within the body of the sphenoid bone. It is related superiorly to the pituitary fossa of the cranial cavity and the optic chiasm, inferiorly to the nasal cavities, and laterally to the cavernous sinuses. They open into the sphenoethmoidal recess in the roof of the nasal cavity (Fig. 1.3).

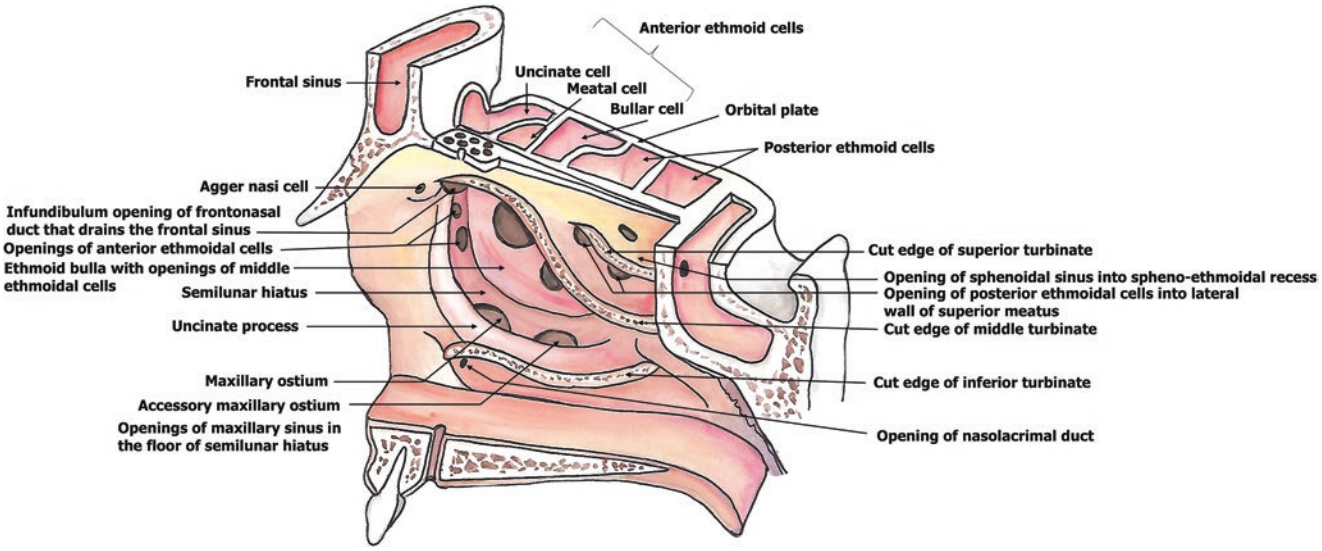

Fig. 1.3 Openings of the paranasal sinuses into the nasal cavity

1.3 Histology

The nasal vestibule is lined by keratinized stratified squamous epithelium that is continuous with the skin of the external nose, and displays skin appendages including hair follicles, sebaceous glands, and sweat glands. It extends 1 to 2 cm posteriorly from the nares to the mucocutaneous junction, i.e., limen nasi, from where the nasal cavity mucosa, also known as Schneiderian mucosa, continues posteriorly. The nasal cavity is lined by pseudostratified ciliated columnar or "respiratory" epithelium, which displays five different cell types, viz. ciliated columnar cells, basal cells, goblet cells, brush/small granule cells, and neuroendocrine cells (Fig. 1.4) [2]. First three types of cells are in majority. The apical portions of the ciliated columnar cells have cilia as well as microvilli, which are responsible for mucociliary clearance in the nasal cavity. Goblet cells are broad at the luminal aspect and have a narrow attachment to the basement membrane, and contain mucin which they secrete onto the mucosal surface through a small opening. Their luminal surface has microvilli to facilitate movement of mucin. Function of brush cells is not clear though these are proposed to have a sensory role. Non-ciliated columnar cells are more in number at the mucocutaneous junction. Some parts of the turbinates that are exposed to high air flow may show foci of squamous metaplastic epithelium.

The lamina propria consists of loose connective tissue that contains blood vessels, nerves, and seromucinous glands arranged in lobules that form superficial and deep layers (Fig. 1.5). The seromucinous glands contain serous and mucinous acini in a ratio of around 8:1. Chronic inflammatory cells viz. lymphocytes and plasma cells are seen scattered in the lamina propria.

The submucosal blood vessels in the middle and inferior turbinates (Fig. 1.6a) are thick walled and have dilated lumina. They display a prominent layer of smooth muscle in their walls, giving the turbinate tissue an erectile appearance (Fig. 1.6b). These specialized blood vessels play a role in regulating temperature and secretion in the nasal cavity. The turbinates also have a core of lamellar bone which has a scroll-like appearance on cross section (Fig. 1.6c, d), and intraosseous blood vessels coursing through the bony lamellae. Melanocytes derived from the neural crest are present in the epithelium, seromucinous glands, and the lamina propria.

The midline nasal septum is made up of hyaline/elastic cartilage anteriorly, and lamellar bone posteriorly. The mucosa that overlies the cartilage and bone is almost adherent to the perichondrium and periosteum, forming a single membrane that is referred to as mucoperiosteum. The lamina propria of the septum is rich in fibrocollagenous tissue.

The roof of the nasal cavity, including part of the superior turbinate, the cribriform plate of the ethmoid and the superior part of the nasal septum, is lined by the olfactory mucosa (Fig. 1.7). This specialized neuroepithelium is comprised of bipolar olfactory neural receptors, sustentacular or supporting cells, and basal cells. The spindle shaped olfactory receptor cells are neurons with axons at the basal aspect and apical olfactory ciliated chemoreceptors. Their axonal processes get myelinated in the lamina propria and pass through the perforations in the cribriform plate of ethmoid to reach the olfactory bulb. Sustentacular cells are supporting cells. Basal cells have stem cell potential and renew the olfactory receptor cells and sustentacular cells. Serous acini known as Bowman glands are present in the lamina propria of the olfactory mucosa, which open onto the surface via small ducts.

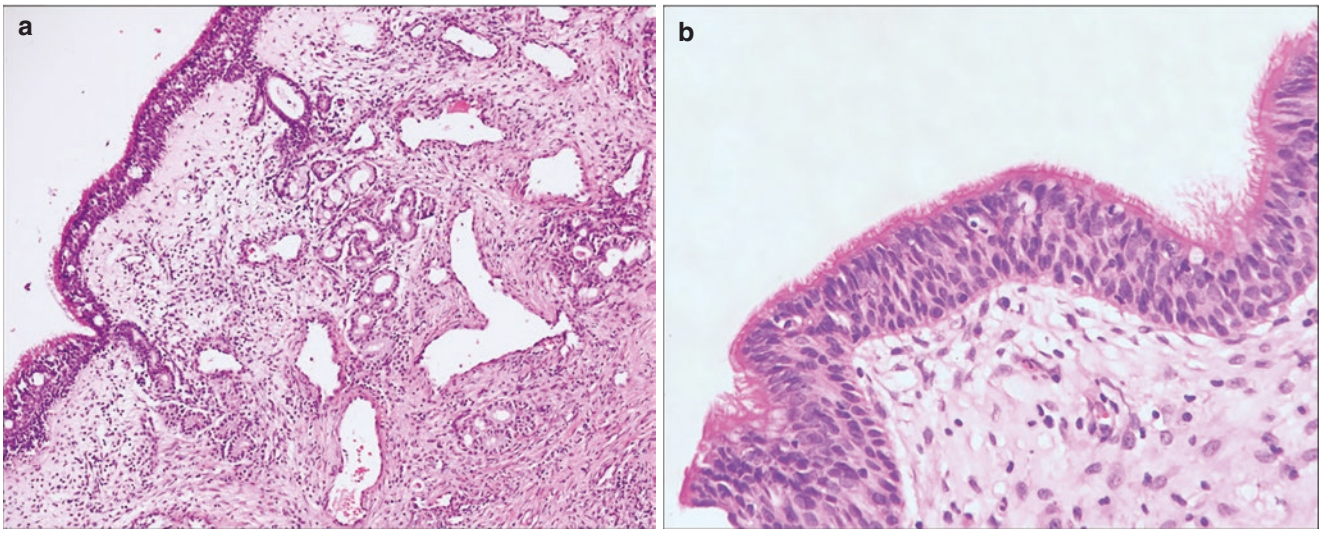

Fig. 1.4 Histology of the nasal mucosa (**a**) lined by pseudostratified ciliated columnar epithelium (**b**)

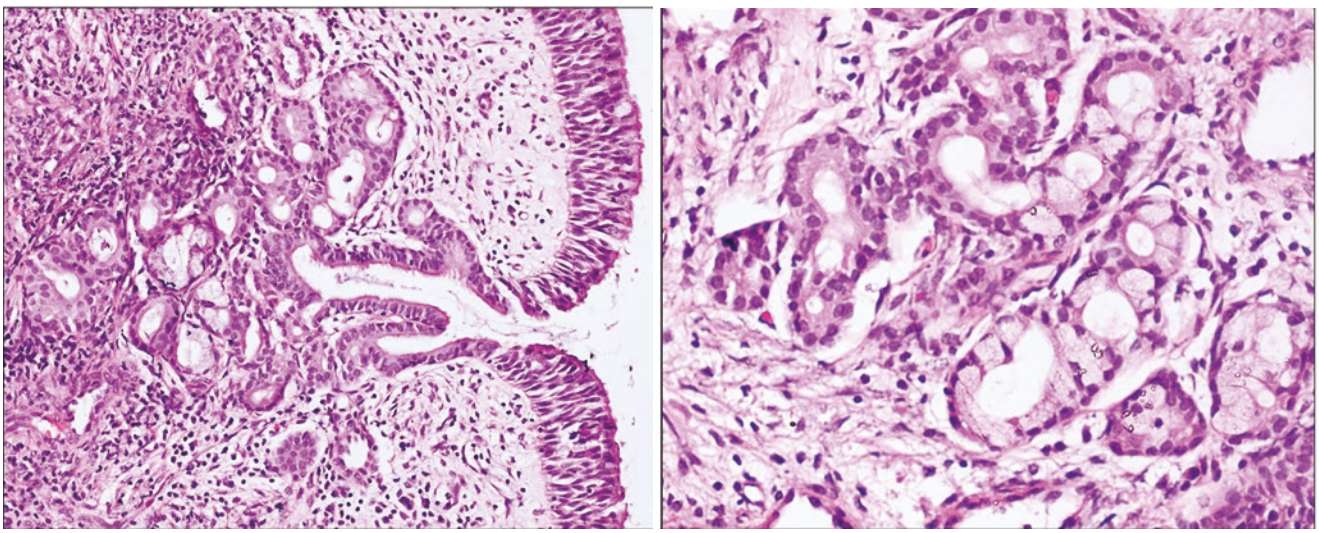

Fig. 1.5 Seromucinous glands in the lamina propria of the nasal mucosa

Like the respiratory mucosa of the nasal cavity, the paranasal sinuses are lined by pseudostratified ciliated columnar epithelium. However, the submucosa is narrower, with a relative paucity of seromucinous glands, both in size and in number, and lack of erectile appearing blood vessels (Fig. 1.8). It also has less dense fibrocollagenous tissue, permitting fluid and inflammatory cells to accumulate. A thin fibrous layer is seen adjacent to the periosteum of the bones forming the paranasal sinuses.

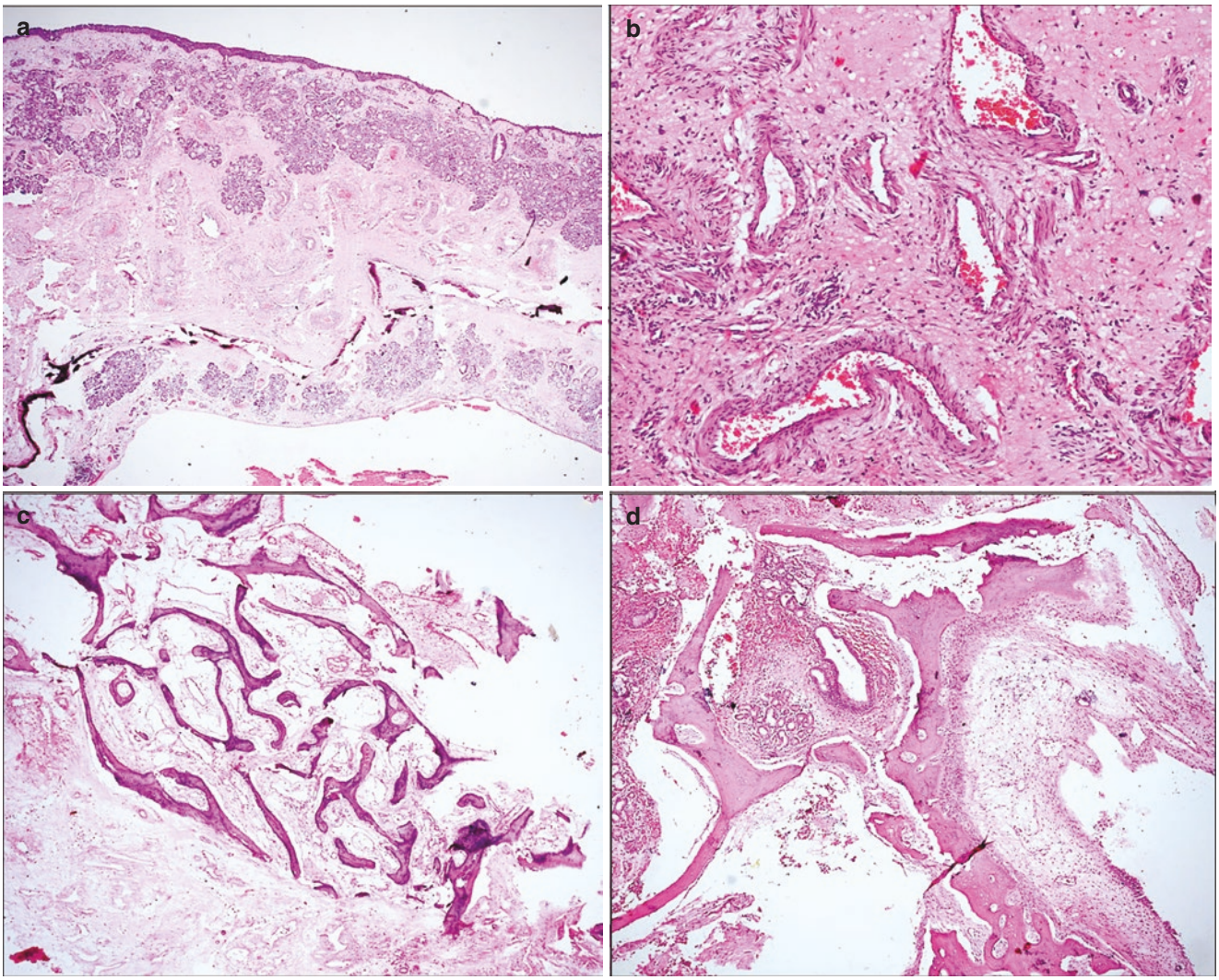

Fig. 1.6 Nasal turbinate (**a**) with thick walled erectile blood vessels (**b**) and scroll-like bone (**c**, **d**)

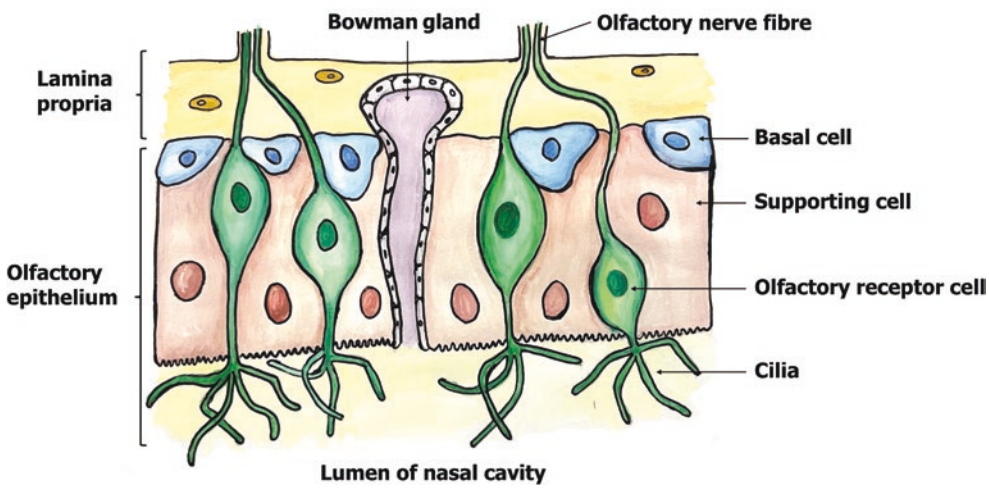

Fig. 1.7 Diagrammatic representation of histology of the olfactory mucosa

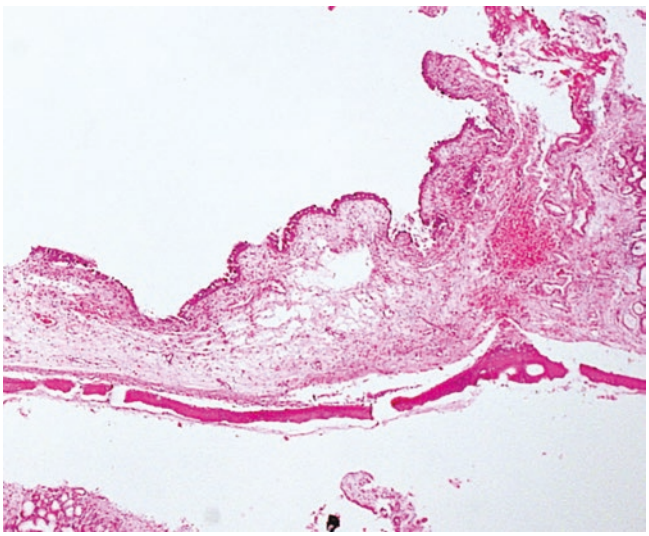

Fig. 1.8 Mucosa of paranasal sinuses

1.4 Conclusion

Knowledge of the anatomy and histology of the sinonasal tracts makes it easier to diagnose and report specimens obtained from this region, as the differential diagnosis varies with the specific location of the lesion. This knowledge also reflects in reports of resection specimens, and assists in documentation of extent of disease, staging and in clinicopathological correlation. Thus, proficiency in this subject is an essential tool in the repertoire of a head and neck pathologist.

References

1. von Arx T, Lozanoff S, Bornstein MM. Extraoral anatomy in CBCT – a literature review. Part 1: Nasoethmoidal region. Swiss. Dent J. 2019;129(10):804–15.
2. Lane AP. Nasal anatomy and physiology. Facial Plast Surg Clin North Am. 2004;12(4):387–v.
3. Ogle OE, Weinstock RJ, Friedman E. Surgical anatomy of the nasal cavity and paranasal sinuses. Oral Maxillofac Surg Clin North Am. 2012;24(2):155–vii.

Radiology of Sinonasal Tract Lesions/ Tumours

2

Ashu Seith Bhalla, Smita Manchanda, and Ankita Dhiman Nair

2.1 Introduction

Sinonasal (SN) disorders include both inflammatory/infective processes and tumours. This chapter is organized under the following headings: sinusitis, fungal diseases, tumours and miscellaneous entities.

2.2 Sinusitis

Sinusitis is essentially a clinical diagnosis with imaging being performed in specific clinical situations [1]. Plain radiographs (Modified Water's view) may be used initially (Fig. 2.1), especially in acute sinusitis. However, CT is the investigation of choice, with MRI being employed as problem-solving modality. In most cases of chronic sinusitis and recurrent sinusitis, non-contrast CT (NCCT) of the paranasal sinuses suffices. However, in cases of complicated acute sinusitis, contrast imaging is essential including the brain and orbits [1, 2].

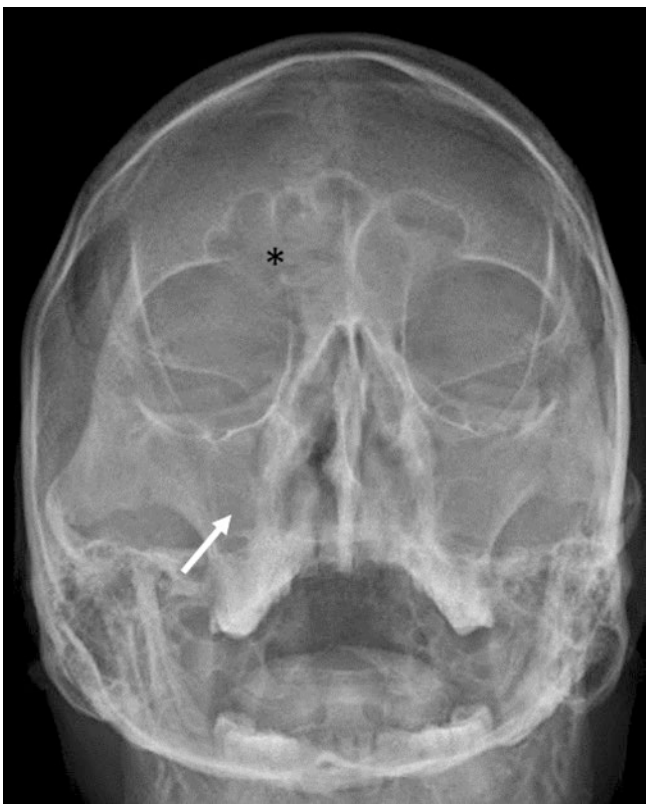

Fig. 2.1 Sinusitis. X-ray PNS Water's view shows complete opacification of bilateral maxillary sinuses (arrow), frontal (asterisk) and bilateral ethmoidal sinuses suggestive of sinusitis

A. S. Bhalla (✉) · S. Manchanda · A. D. Nair
Department of Radiodiagnosis and Interventional Radiology, All India Institute of Medical Sciences, New Delhi, India
e-mail: ashubhalla1@aiims.edu

D. Jain, J. A. Bishop (eds.), *Atlas of Sinonasal Tract Pathology*, https://doi.org/10.1007/978-981-19-7315-4_2

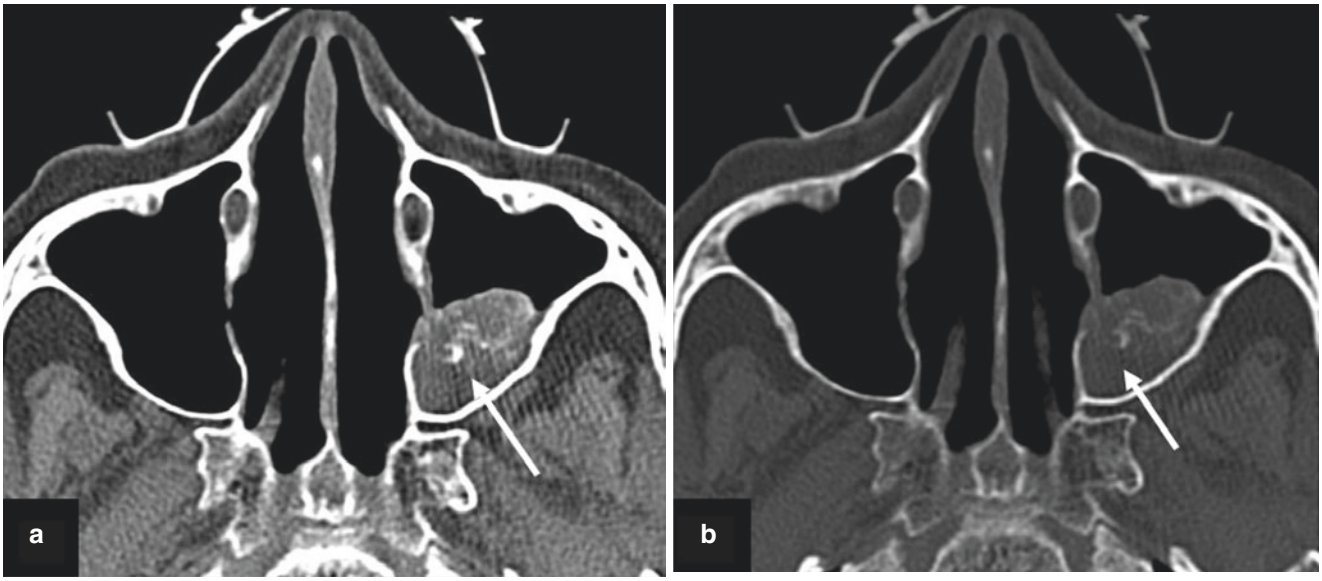

Fig. 2.2 (**a**, **b**) Maxillary Antrolith. Hypodense inspissated secretions in left maxillary antrum with calcified areas within suggestive of antrolith (arrow)

2.2.1 Chronic Sinusitis

Chronic sinusitis is characterized by opacification of the sinuses, mucosal thickening, bony sclerosis and intrasinus calcification (antrolith formation) (Fig. 2.2). The density of the secretions is variable with increased density on NCCT of the chronic inspissated secretions. As the protein concentration increases, the signal intensity on T1 and T2 weighted MRI also varies, with increased protein content becoming more hypointense on T1 and T2 weighted images [3]. Inflamed mucosal lining enhances on contrast administration, whereas fibrotic and scarred mucosa does not enhance (Fig. 2.3).

Complications of sinusitis include intraorbital complications like cellulitis, subperiosteal abscess and superior ophthalmic vein thrombosis. The intracranial complications include cavernous sinus thrombosis, meningitis, cerebritis and intracranial abscesses. These are best imaged on contrast enhanced MRI with abscesses showing peripheral rim enhancement and diffusion restriction [2, 3].

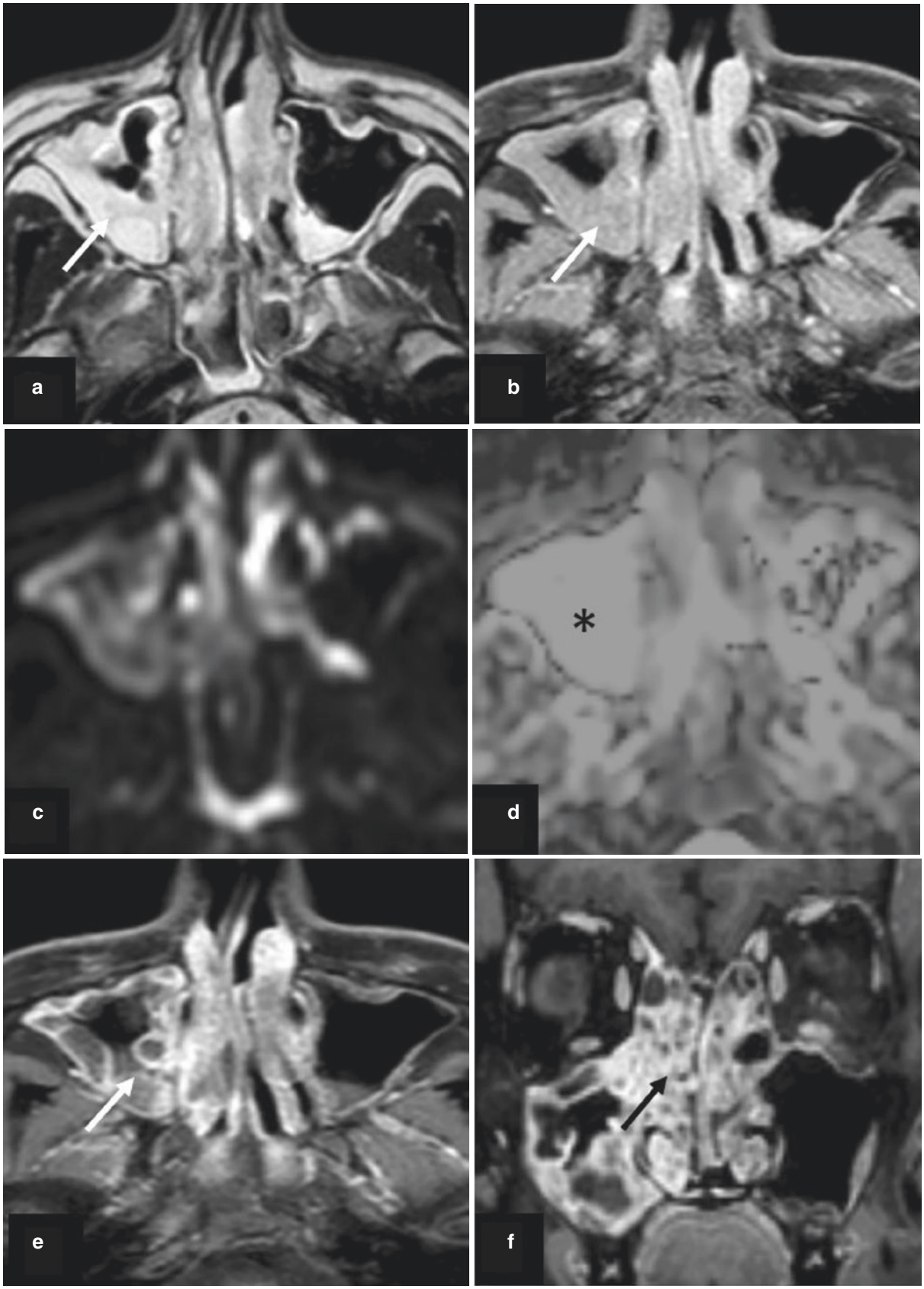

Fig. 2.3 (**a**–**f**) Chronic rhinosinusitis. (**a**, **b**) Axial T2 W and T1 W image showing diffuse polypoidal mucosal thickening in bilateral maxillary sinuses (arrows); (**c**, **d**) Facilitated diffusion in the mucosal thickening—bright on apparent diffusion coefficient (asterisk); (**e**, **f**) Diffuse mucosal enhancement seen on post-contrast images with enhancing mucosal thickening in bilateral nasal cavities also (arrows)

2.2.2 Sequelae of Chronic Sinusitis

These include retention cyst, polyps and mucocoele.

Retention cysts are well-defined, low-density, lesions along the sinus wall with convex margins on NCCT, commonly seen in the maxillary sinuses. These show rim enhancement on contrast scans.

Polyps are expansile, inflammatory sinus masses and can cause pressure erosion of the sinus walls when very large. An antrochoanal polyp is a solitary, unilateral, lesion in the maxillary antrum and nasal cavity in young adults [4]. It fills the maxillary antrum, widens the osteomeatal complex and prolapses into the nasal cavity (Fig. 2.4). Through the posterior choanae, it extends behind into the nasopharynx. It is of soft tissue density on NCCT. On MRI, it is T1 intermediate to hypointense, T2 hyperintense with hypointense linear areas and shows intense enhancement with non-enhancing linear areas (fibrotic part/desiccated secretions).

Mucoceles are the commonest expansile sinus lesions with the most common location being the frontal sinus. On NCCT, the sinus is expanded and has homogenous, hypodense/isodense (to brain parenchyma) contents. In the presence of inspissated secretions, contents can appear hyperdense on CT and isointense on T1WI and hyperintense on T2WI (Fig. 2.5). There is expansion with remodelling of the sinus walls and scalloping of the adjoining borders with thinning and deossification [4, 5]. Extensive lysis may be seen with intracranial and intraorbital extension.

It is essential to look for a cause of the mucocoele on a contrast study at the site of the obstructed drainage pathway of the sinus. These include inflammatory mucosal thickening, tumour, post-traumatic and post-operative causes [3].

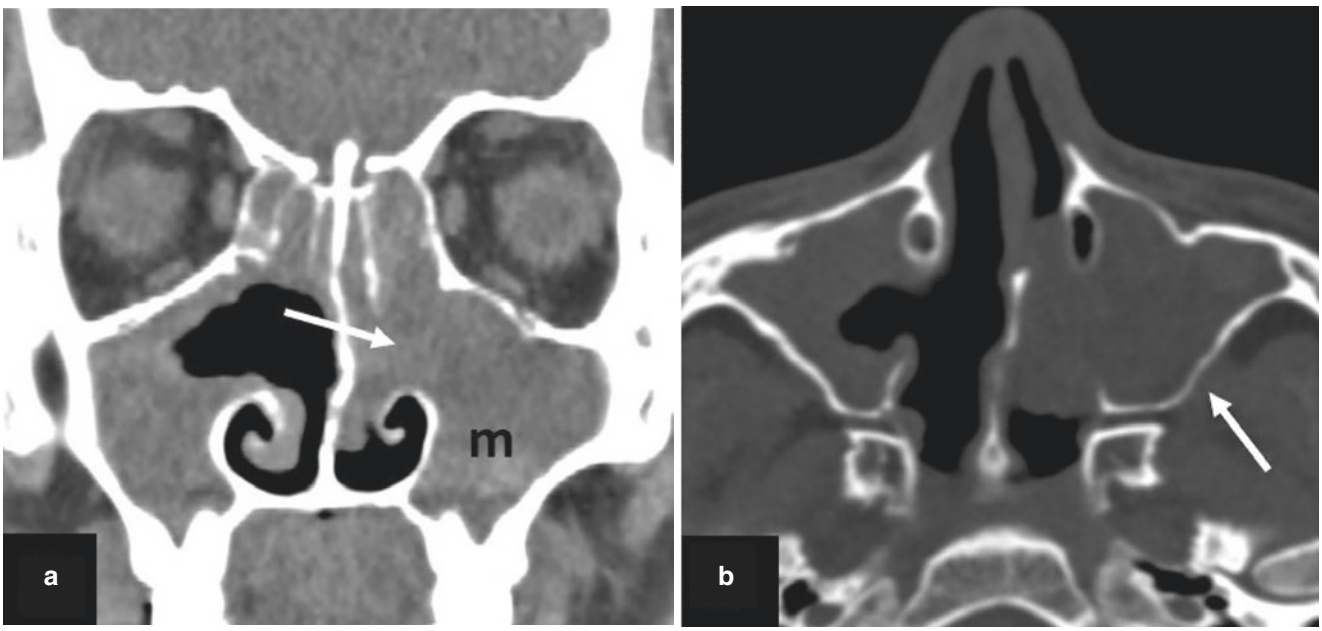

Fig. 2.4 (**a**, **b**) Antrochoanal polyp. (**a**) Complete opacification of left maxillary sinus with soft tissue (m) medially widening the left osteomeatal complex and extending into left nasal cavity (arrow); (**b**) Mild thinning of overlying walls of maxillary sinus (arrow). No erosions

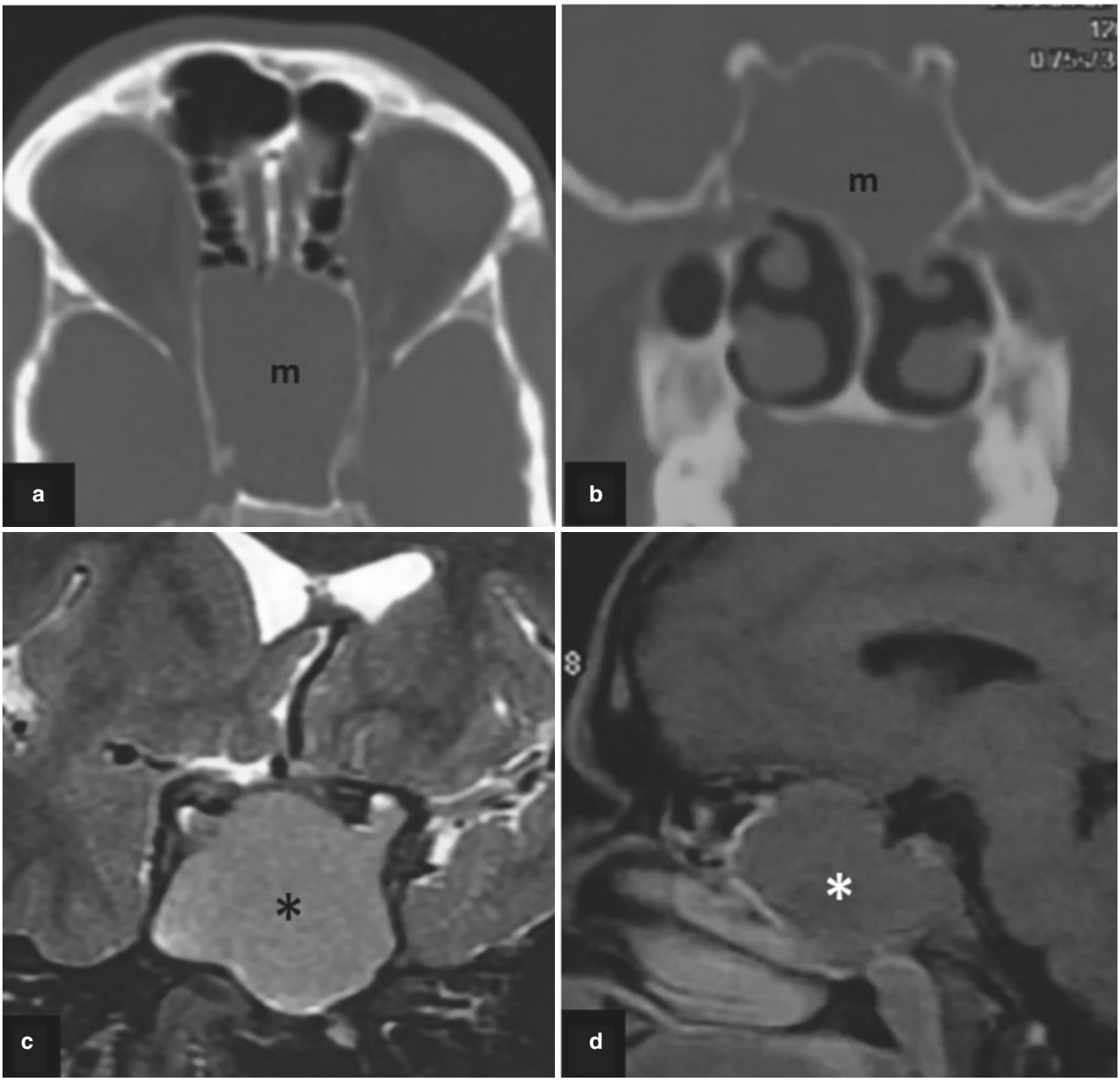

Fig. 2.5 (**a**–**d**) Mucocele. (**a**, **b**) Isolated opacification and expansion of sphenoid sinus (m); (**c**, **d**) T2 hyperintense,T1 isointense expansile sphenoid sinus mucocele (asterisk)

2.3 Fungal Disease

Fungal sinusitis has varied clinical and radiological manifestations. These are more commonly encountered now with an increase in the chemotherapy, immune suppression drugs and diabetes mellitus with the most frequent pathogen being the Aspergillus species.

It is broadly classified into non-invasive (allergic fungal sinusitis and mycetoma) and invasive (acute and chronic) forms [6].

2.3.1 Non-invasive Forms

2.3.1.1 Allergic Fungal Sinusitis (AFS)

AFS is an allergic response (IgE-mediated hypersensitivity reaction) to fungal elements. Usually there is bilateral, asymmetric involvement of multiple sinuses [6, 7].

On NCCT, it is characterized by expansion of sinuses with central hyperdense contents. A peripheral hypodensity is seen in the sinus wall and represents the inflamed mucosa. There may be erosion of lamina papyracea and intraorbital

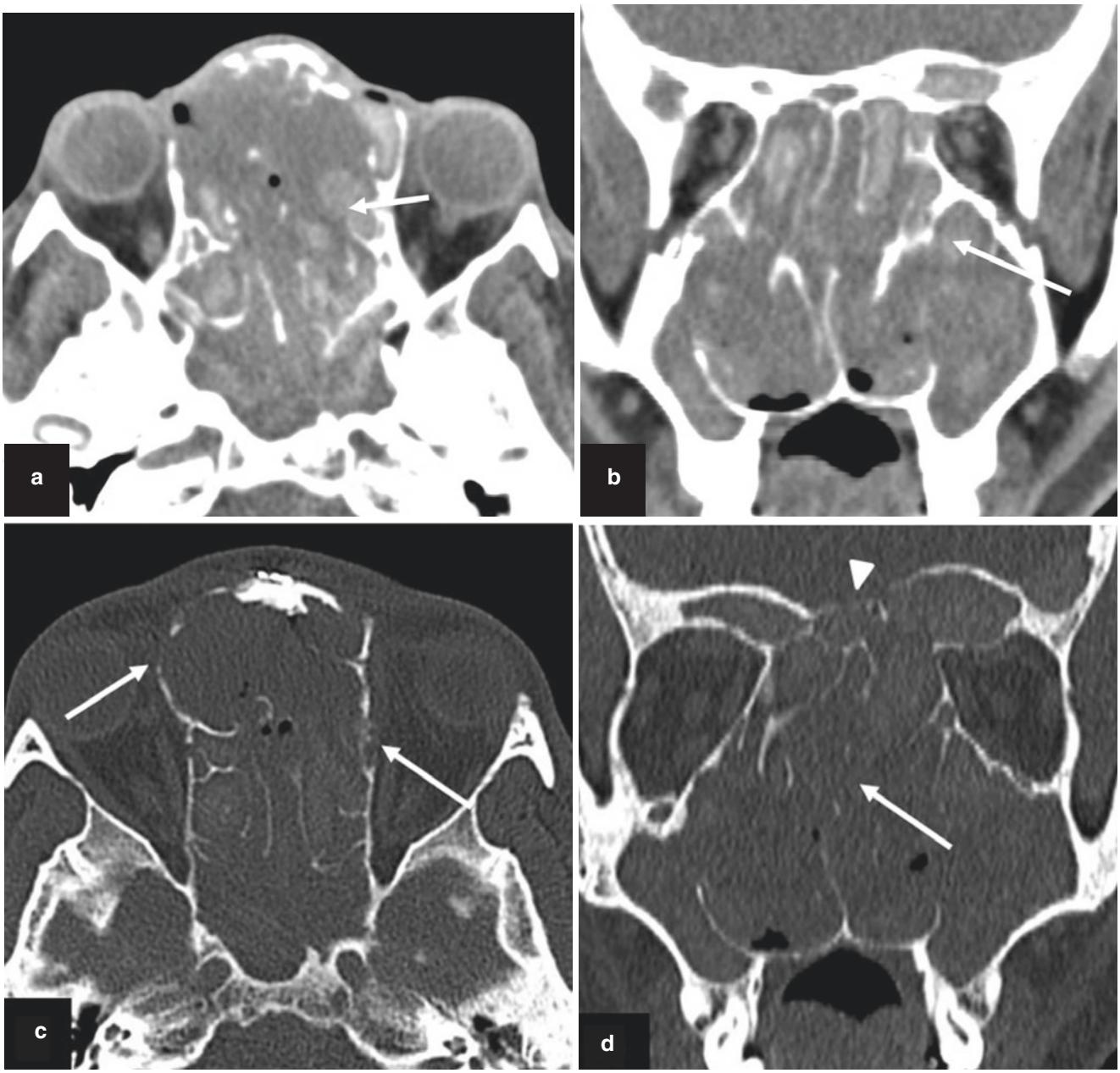

Fig. 2.6 (**a**–**d**) Allergic fungal sinusitis. (**a**, **b**) Soft tissue with hyperdense contents causing expansion of bilateral ethmoid, maxillary, frontal and sphenoid sinuses, nasal cavity (arrows); (**c**, **d**) Erosions of bilateral lamina papyracea (arrows in **c**), nasal septum, turbinates (arrow in **d**), fovea ethmoidalis (arrowhead in **d**)

extension (Fig. 2.6). Erosion of skull base leads to intracranial extension.

MRI may underestimate the disease as the low signal intensity on T2 weighted images can mimic normal aerated sinuses. Post-contrast images can delineate the enhancing mucosal lining and extrasinus soft tissue.

2.3.1.2 Fungal Ball (Mycetoma)

A mycetoma is a mass like lesion which is a dense accumulation of fungal hyphae within a sinus. It is mainly caused by *Aspergillus fumigatus* and is usually seen in the maxillary sinus in immunocompetent persons, mostly females.

On NCCT, a mycetoma appears as soft tissue opacification of the sinus with central hyperdensity and peripheral, inflamed hypodense mucosa. The bones show reactive sclerosis and periostitis.

On MRI T1 weighted images, the lesion is heterogenous, predominantly low signal intensity and with no post-contrast enhancement. Low signal intensity on the T2 weighted images is characteristic and is mainly due to the calcium, magnesium and manganese salts [8].

2.3.2 Invasive Forms

2.3.2.1 Acute Invasive Fungal Sinusitis

Also known as rhino-sino-orbito-cerebral mycosis, it is a disease of acute onset (course of disease 4 weeks or less) and rapid progression seen mostly in immunocompromised patients. There is characteristic invasion of the vessels and surrounding soft tissues, hence the bony walls may be seen as intact. Infectious spread can occur via direct extension or vascular invasion to the adjacent soft tissue, orbits and central nervous system [9].

CT findings (Fig. 2.7) are non-specific and include mucosal thickening/opacification of affected sinuses with adjacent soft tissue thickening. Bony dehiscence, inflammatory changes of the orbit, thickening of the extraocular muscles, and disease spread to retroantral fat, pterygopalatine fossa, orbital apex, inferior orbital fissure, infratemporal fossa and cavernous sinuses may be seen. These are seen as enhancing soft tissue or abscess formation in the CECT scans [7, 8].

On MRI the opacified sinuses may appear hypointense on both T1 and T2 weighted images and disease extent may be underestimated. The "Black Turbinate Sign" implies tissue necrosis, and it is the absence of enhancement in those areas which normally enhance such as nasal mucosa and the turbinates [9]. The intraorbital and intracranial extension is well seen on post gadolinium scans. The status of internal carotid

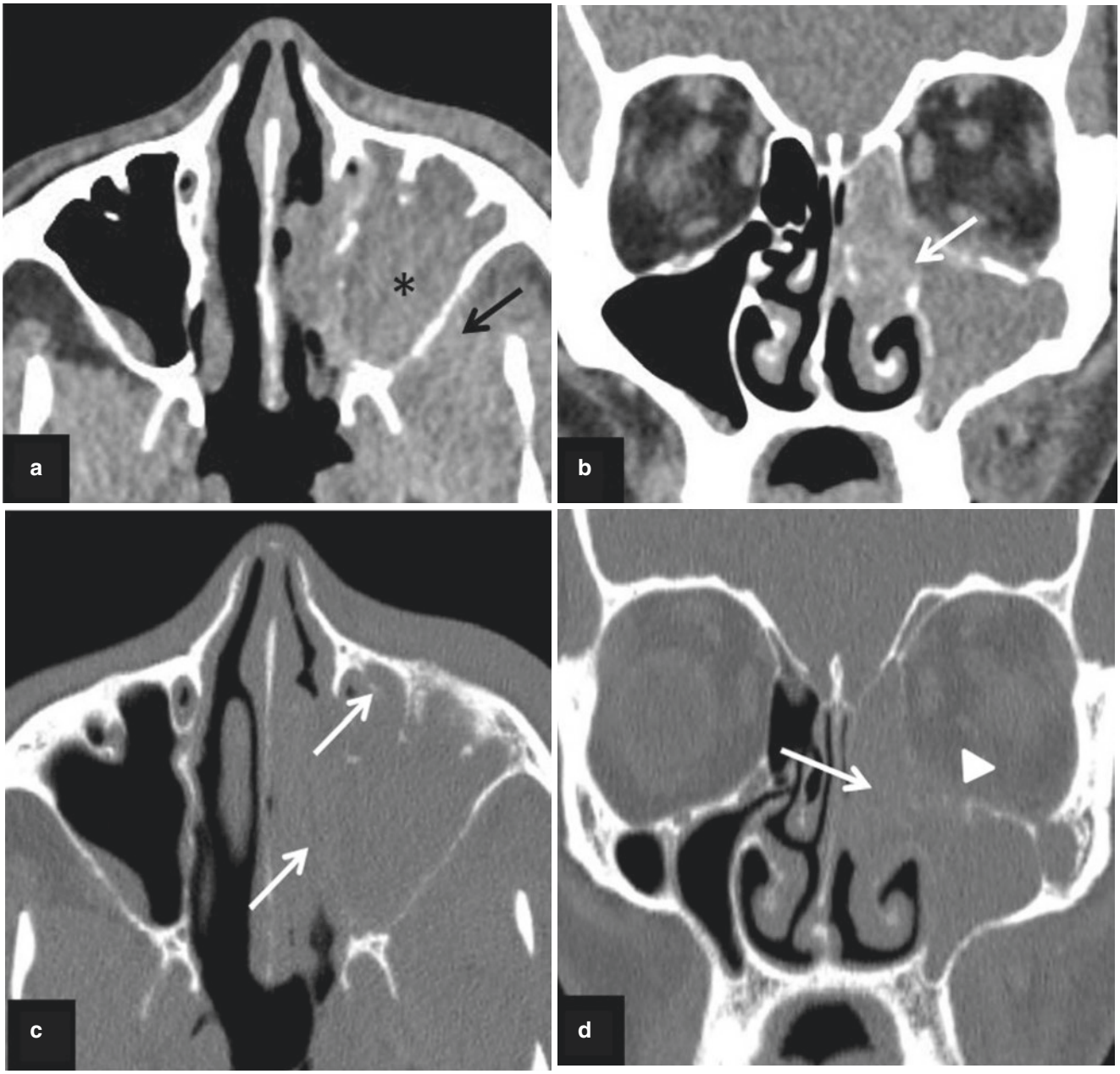

Fig. 2.7 (**a**–**d**) Acute invasive fungal sinusitis. (**a**, **b**) Soft tissue in left maxillary sinus (asterisk) extending into left nasal cavity through widened osteomeatal complex (arrow in **b**). Left retroantral fat pad is obliterated suggestive of extrasinus spread (black arrow); (**c**, **d**) Bone erosions and permeative lysis of left maxillary sinus walls (arrows in **c**), floor of left orbit (arrowhead) left nasal turbinates (arrow in **d**)

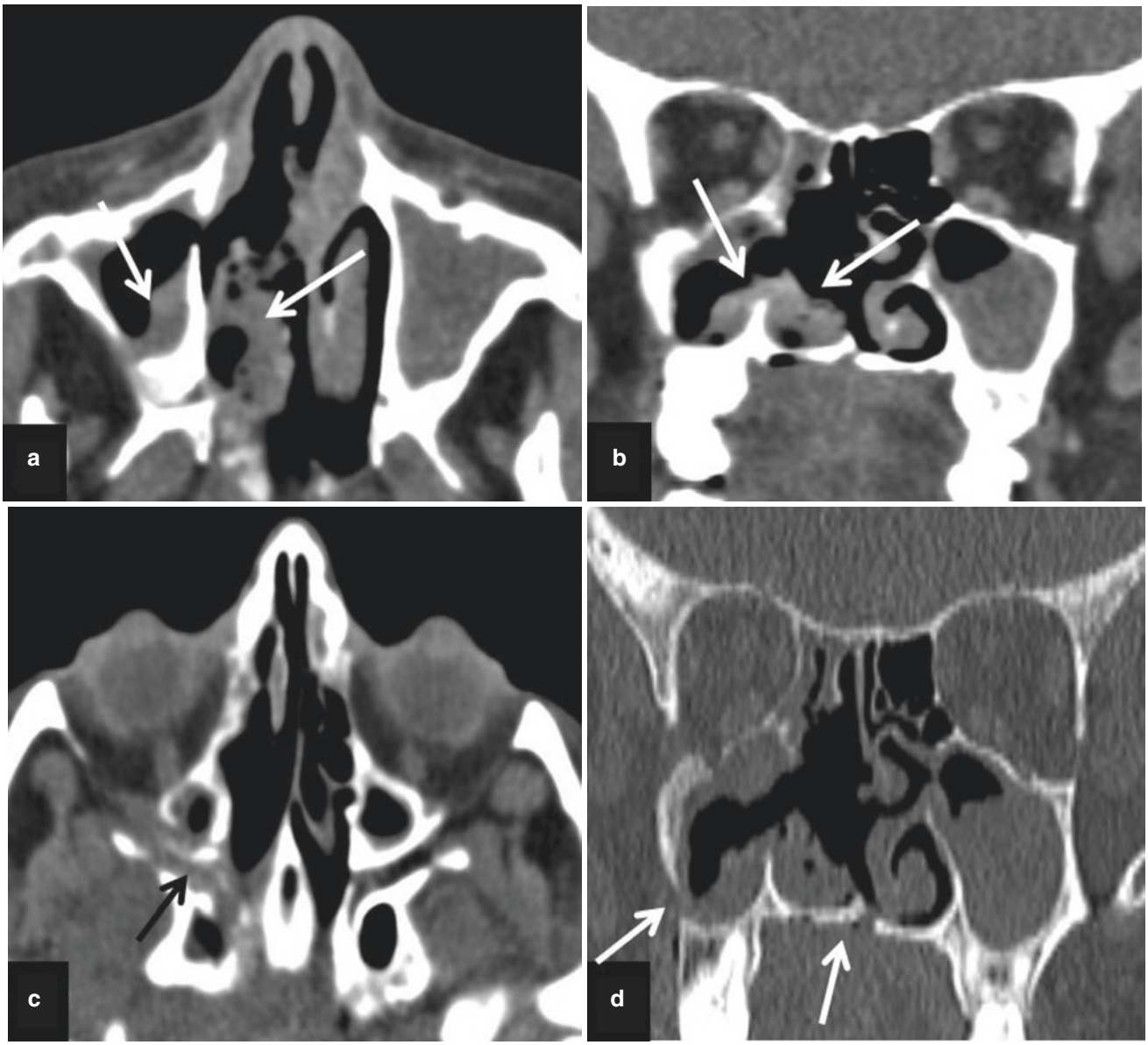

Fig. 2.8 (**a**–**d**) Chronic invasive fungal sinusitis. (**a**, **b**) Soft tissue in right maxillary sinus, right nasal cavity (arrows); (**c**) Extrasinus spread to right pterygopalatine fossa (arrow); (**d**) Erosions of hard palate and right maxillary sinus walls (arrows). Note made of post-operative changes in form of absent right middle and inferior turbinates, nasal septum

artery should be carefully evaluated for any thrombosis or mycotic pseudoaneurysm formation.

2.3.2.2 Chronic Invasive Fungal Sinusitis

Chronic invasive fungal sinusitis shows a prolonged indolent course of over more than 4 weeks and it is found in immunocompetent or slightly immunocompromised patients. It is of two types: granulomatous and non-granulomatous [8].

NCCT (Fig. 2.8) of chronic granulomatous form depicts soft tissue involving single or two sinuses with localized bone erosion. Extrasinus extent of the disease is more than the intrasinus component. The extrasinus soft tissue can be extensive involving orbits, pterygopalatine fossa and the infratemporal fossa. Bone erosions are seen at the site of extrasinus extension. *On MRI,* typical low signal intensity is seen on the T2 weighted images [9].

The imaging findings of chronic non-granulomatous form are similar to the acute invasive forms with extrasinus extension. Coarse and dense calcification is seen in the chronic form [9].

2.4 Sinonasal Tumours

Amongst the head and neck tumours, sinonasal tumours are relatively rare with malignant lesions being more common than benign ones. Imaging can help to distinguish benign from malignant lesions, narrow down the imaging differentials and delineate the extent of tumour and relationship to vital structures [10]. This recent classification divides the tumours into

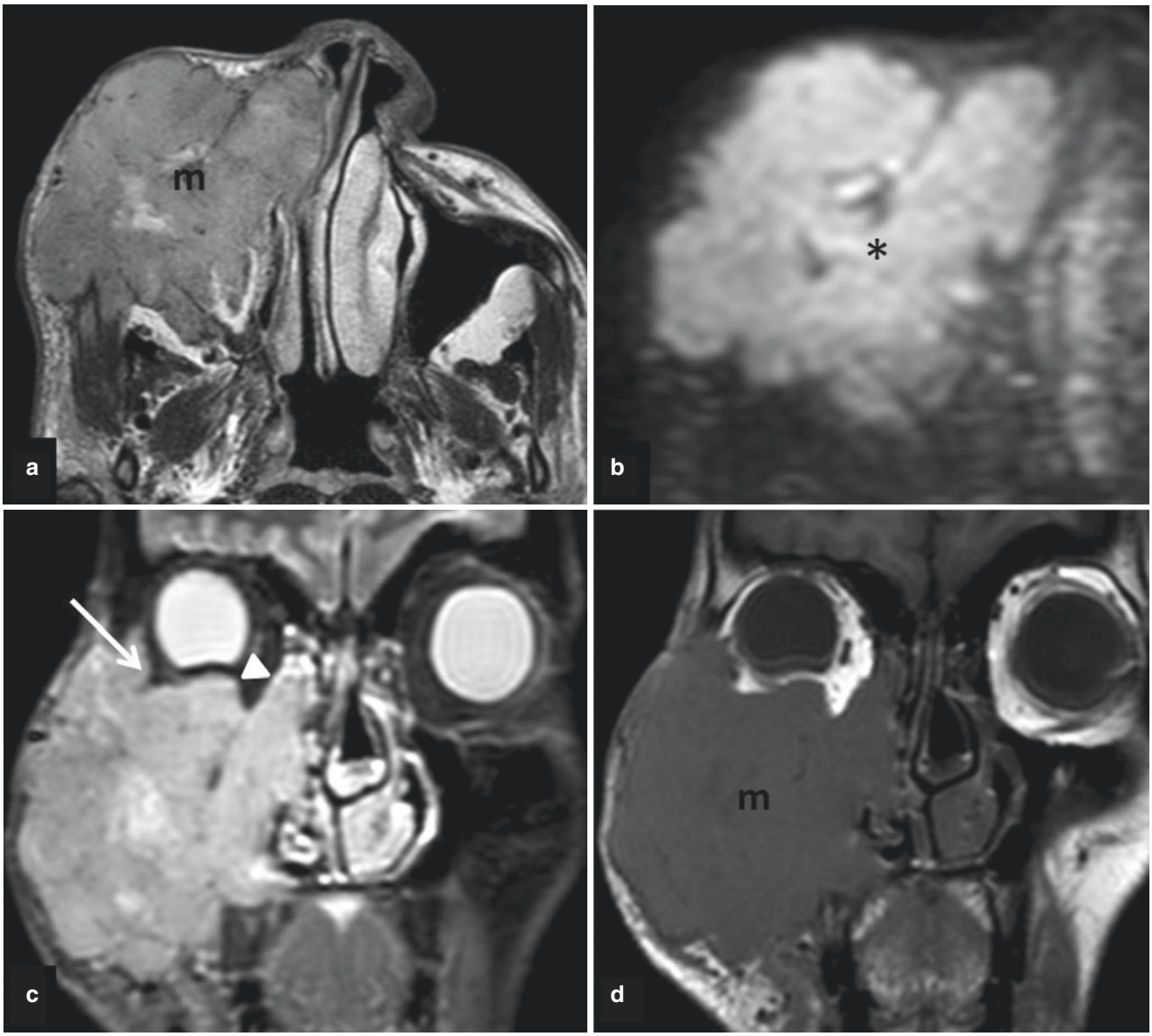

Fig. 2.9 (**a**–**d**) Maxillary sinus squamous cell carcinoma. (**a**) Large destructive T2 hypointense mass (m) in right maxillary sinus; (**b**) Restricted diffusion in the mass (asterisk); (**c**) Intraorbital extension (arrow) and extension into right nasal cavity (arrowhead); (**d**) Mass (m) is isointense on T1

broad categories of epithelial tumours, tumours of bone and cartilage, soft tissue tumours, germ cell tumours, neuroectodermal tumours, hematolymphoid tumours and secondary tumours [11, 12]. In the first four groups, these are further subdivided into benign and malignant. The neuroectodermal tumours, hematolymphoid tumours and secondary tumours include only malignant lesions [13]. The imaging characteristics of few of the common entities are described here.

2.4.1 Squamous Cell Carcinoma

It is the commonest sinonasal tumour and usually seen in the elderly males. Maxillary sinus is most commonly involved followed by the nasal cavity, ethmoid sinuses, sphenoid sinus and frontal sinus. It typically is seen as a large, heterogenous, soft tissue mass with permeative bone destruction. The disease is usually locally advanced at presentation; however, nodal disease is relatively less common [14, 15].

On CECT, it is seen as a large heterogeneously enhancing lesion with permeative bone destruction and extensive soft tissue component.

On MRI (Fig. 2.9), it is isointense on T1WI, intermediate signal intensity (SI) on T2WI and with heterogenous post-contrast enhancement and diffusion restriction. Diffusion weighted imaging (DWI) and contrast help in differentiation of tumour from inspissated secretions. It is essential to document intracranial extension, intraorbital extension and perineural spread on imaging.

2.4.2 Adenocarcinoma

Adenocarcinomas are usually seen in the fifth to sixth decades of life. The occupation related variant occurs more in males and is associated with leather dust and wood inhalation. Ethmoidal region and nasal vault are more commonly affected as the route is inhalation. The sporadic form is more common in females and commonly involves the maxillary sinus. Imaging features are non-specific [15].

Adenocarcinomas are also seen as large, heterogenous soft tissue masses with or without bony destruction on *CECT*. On *MRI*, the lesion is isointense on T1WI and intermediate signal on T2WI. The mucous producing lesions show mixed solid and fluid signals. There is evidence of heterogenous post-contrast enhancement and diffusion restriction [16, 17].

2.4.3 Adenoid Cystic Carcinoma

Adenoid cystic carcinomas are the most common salivary glands tumour in the sinonasal region. Though slow-growing lesions, there is a high propensity for local recurrence. Lesion of the palate with secondary involvement of the sinonasal space is common. Primary lesions are seen in the maxillary sinus and nasal cavity [18].

On CT, a low-grade lesion is usually polypoidal, soft tissue density with bone remodelling (rather than bone destruction). However, the high-grade lesions are aggressive with bone destruction (Fig. 2.10).

MRI reveals a lesion with high signal (low grade) or intermediate SI (high grade) on T2WI. Contrast administration helps to delineate the perineural and subperiosteal spread.

Perineural involvement is usually contiguous along the nerve and is seen as obliteration of perineural fat, thickening or irregularity of the involved nerve, abnormal enhancement compared to contralateral normal nerve and widening of neural foramina. This is commonly seen in the Meckel's cave and cavernous sinuses [16, 17]. Distant metastasis to lungs, bone, brain and lymph nodes may be seen at the time of presentation in high-grade tumours [18].

2.4.4 Sinonasal Neuroendocrine Carcinoma and Sinonasal Undifferentiated Carcinoma

These lesions are more undifferentiated, aggressive and commonly seen in the fifth and sixth decades of life.

Commonly seen in the upper nasal cavity and ethmoids, these usually present as large soft tissue masses with erosion of bones, invasion of orbits and skull base *on CT*. The lesions are mostly heterogeneously enhancing with no calcification [19].

MRI reveals an isointense mass on T1WI, isointense to hyperintense on T2WI with heterogenous post-contrast enhancement (Fig. 2.11). Lymphadenopathy and distant metastases may be seen at presentation.

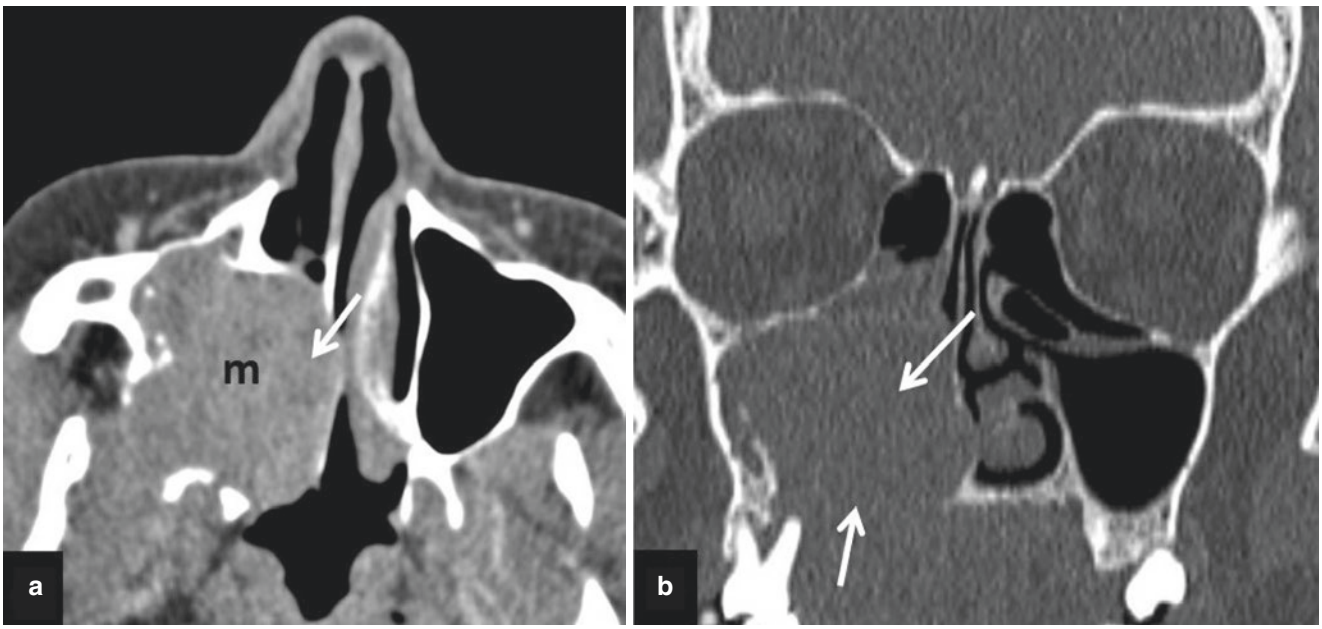

Fig. 2.10 (**a**, **b**) Adenoid cystic carcinoma right maxillary sinus. (**a**) Soft tissue mass (m) in right maxillary sinus extending medially into right nasal cavity (arrow); (**b**) Erosion of palatine process of maxilla and medial wall of right maxillary sinus (arrows)

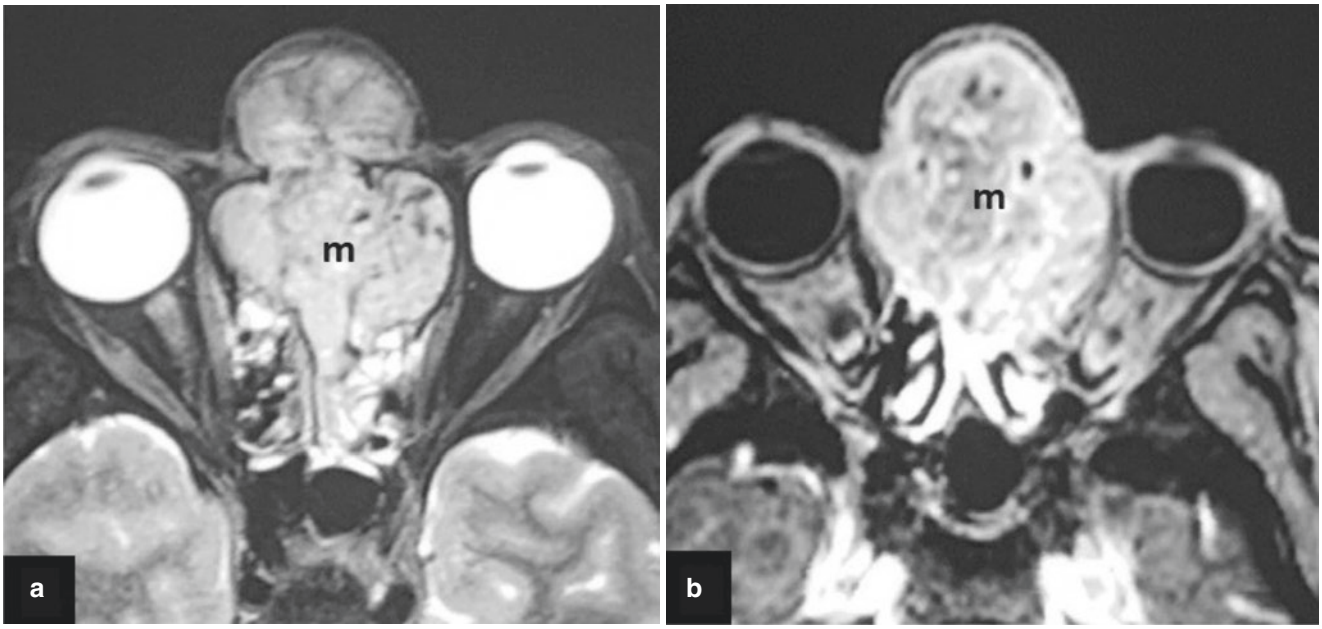

Fig. 2.11 (**a**, **b**) Sinonasal undifferentiated carcinoma. (**a**) T2 hyperintense lobulated soft tissue mass (m) in ethmoid sinus and superior nasal cavity; (**b**) Heterogenous post-contrast enhancement in the mass (m)

2.4.5 Olfactory Neuroblastoma

An uncommon malignant tumour of the sinonasal cavity which arises from the olfactory epithelium in the superior olfactory recess. The lesions have a bimodal peak in the second and sixth decade of life.

On CECT, the lesion is seen as a large mass in the upper part of nasal cavity involving the roof of ethmoidal sinuses, adjoining cribriform plate and the superior turbinates. There is bone erosion and lesion can have intraorbital and intracranial extension. Scattered, speckled calcifications may be seen. Post-contrast administration, there is moderate to intense contrast enhancement.

MRI reveals a large soft tissue mass with intermediate signal on T1WI, hyperintense on T2WI and intense post-contrast enhancement. There are characteristic cysts at brain and tumour interface (Fig. 2.12). Dural involvement needs careful assessment and reporting as larger dural defects need free flap harvesting, whereas smaller defects can be covered with a pericranial sheath. Lymph node metastasis (levels II, I, III and retropharyngeal nodes) is associated with a poorer prognosis and is now included in the staging systems [15, 20].

2.4.6 Lymphomas

The sinonasal tract is an unusual site for lymphomas with the natural killer (NK) cell, B-cell and T-cell type varieties seen. NK cell type is seen in the nasal cavity and has association with Epstein–Barr virus infection while the B-cell type has a predilection for the maxillary sinus. The *role of imaging* in SN lymphomas is to identify the primary site of disease, site for biopsy and to map the lesion in its entirety in cases of patients undergoing radiotherapy [15, 21].

The NK cell type is seen as a sheet of soft tissue in the nasal cavity with bone destruction and erosion without any sclerosis. The lesion is characteristically iso- to hypointense on T1WI and hypo- to isointense on T2WI (Fig. 2.13). Lymphadenopathy is not common; however, the lesion is associated with a poor prognosis.

B-cell type is seen commonly in maxillary sinus and causes bone remodelling (instead of bone destruction). On MRI, the lesion has an intermediate signal on T2WI (instead of the T2 hypointensity as seen with NK cell type) and shows moderate post-contrast enhancement. Burkitt's lymphoma is a type of B-cell lymphoma which has a predilection for the facial skeleton.

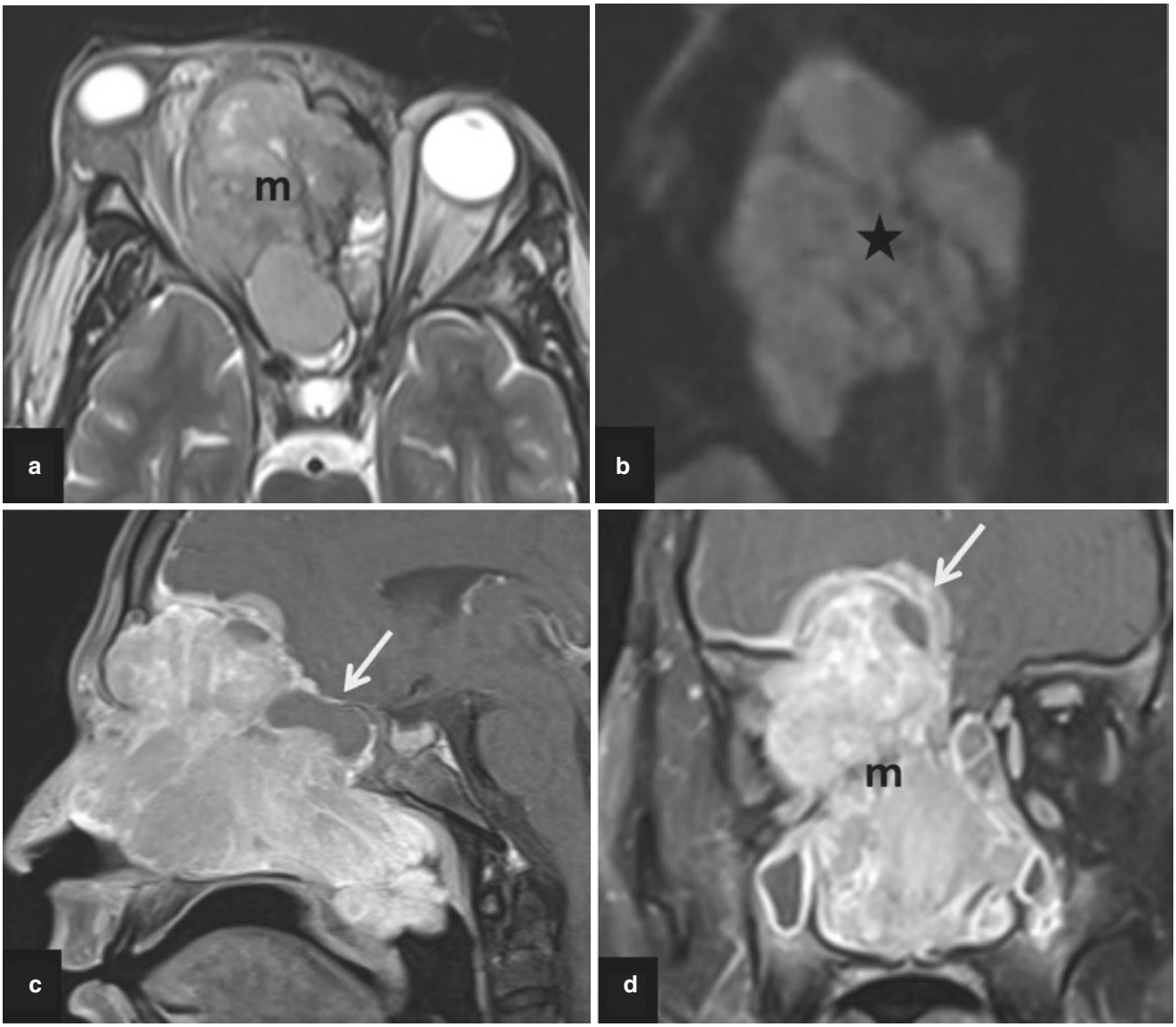

Fig. 2.12 (**a**–**d**) Olfactory neuroblastoma. (**a**) Large mass (m) with epicentre in superior nasal cavity. Hypointense signal on T2WI; (**b**) Restricted diffusion in the mass (asterisk); (**c**) Cysts in the tumour CSF interface (arrow); (**d**) Intense contrast enhancement in the mass (m). Intracranial extension of the mass also seen (arrow)

2.4.7 Rhabdomyosarcomas

Rhabdomyosarcoma is the most common sinonasal malignancy in the paediatric age group. At presentation the lesion is locally advanced with multiple sinonasal compartments involved. It is an aggressive lesion with early nodal disease and distant metastases.

CT reveals a large, heterogenous soft tissue mass lesion with bone destruction (Fig. 2.14). There may be extension into the orbits, infratemporal fossa and neck spaces.

On MRI, the mass is isointense to hyperintense on T1WI and heterogeneously hyperintense on T2WI and shows heterogenous post-contrast enhancement [14, 22].

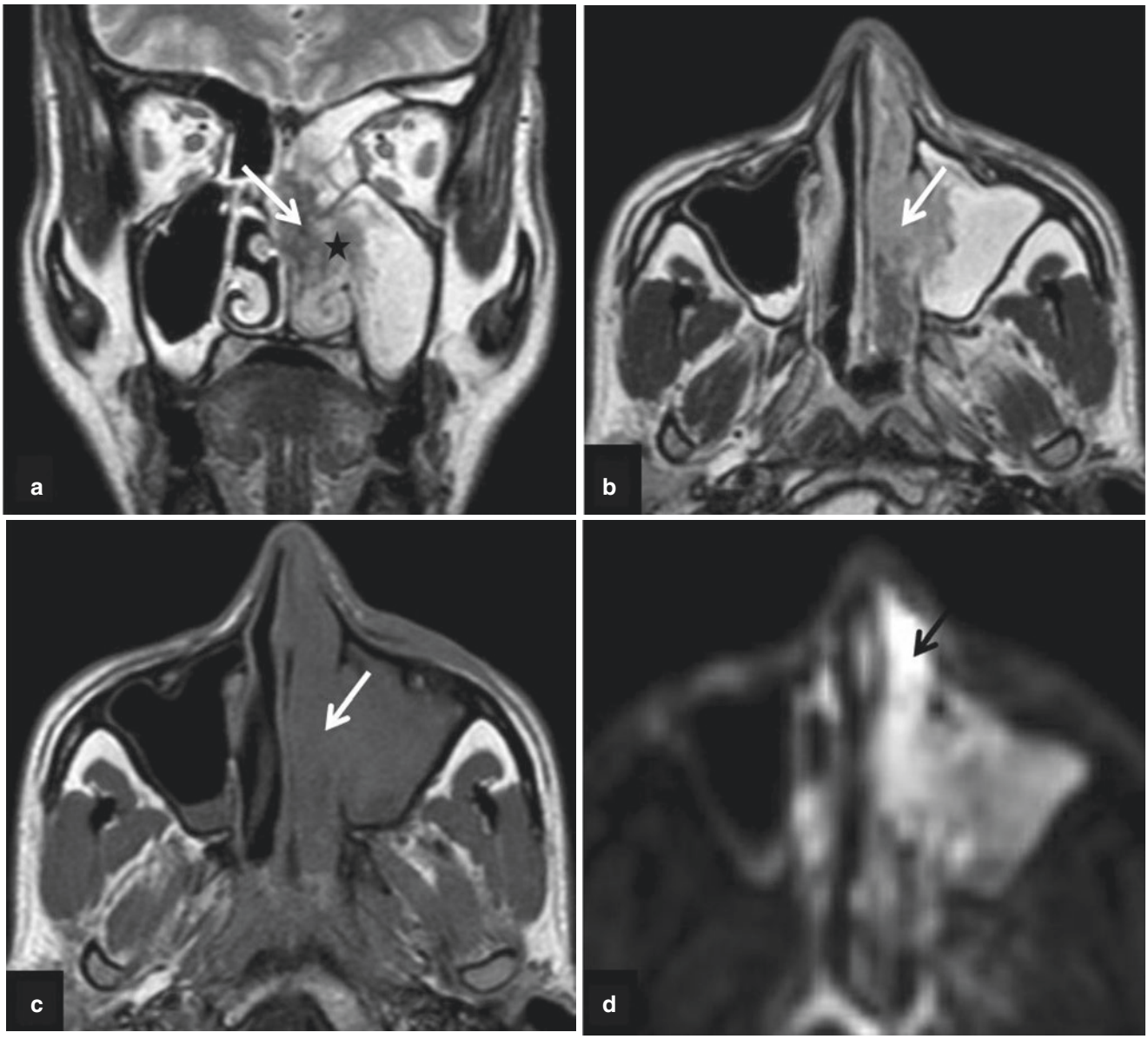

Fig. 2.13 (**a**–**d**) Natural killer T-cell lymphoma. T2 hypointense soft tissue mass in left nasal cavity with destruction of nasal turbinates (arrows in **a** and **b**). Obstruction of left osteomeatal complex (asterisk in **a**) causing opacification of left maxillary antrum. Mass is isointense on T1 (arrow in **c**) and shows restricted diffusion (arrow in **d**)

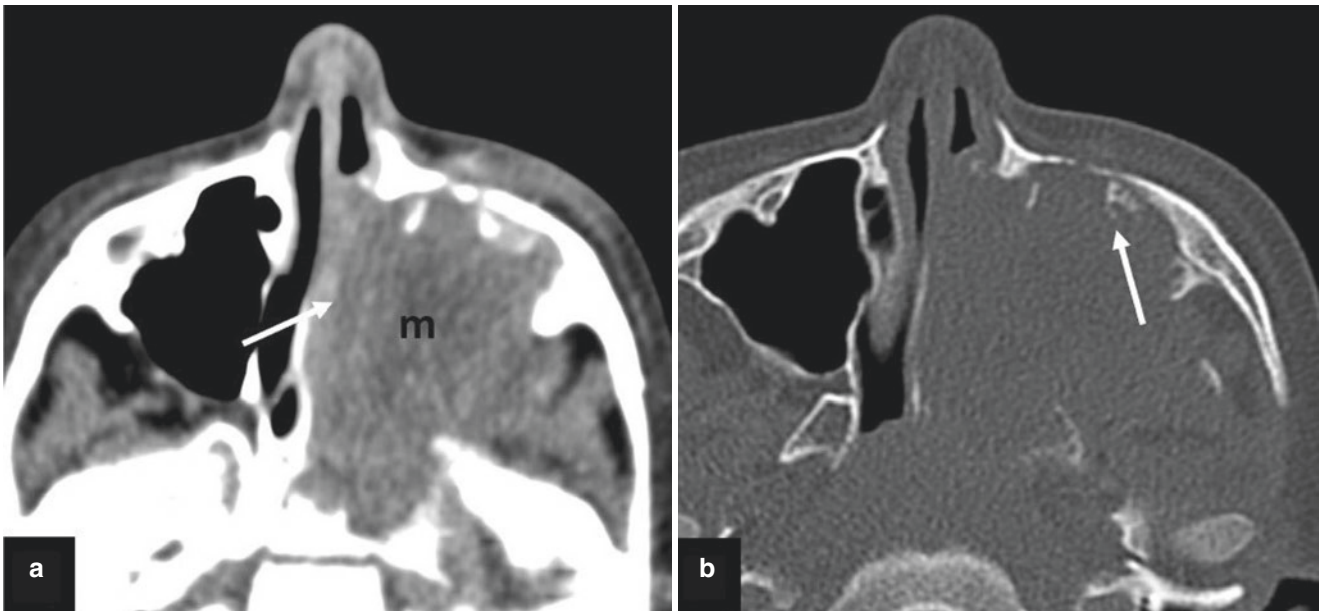

Fig. 2.14 (**a**, **b**) Rhabdomyosarcoma left maxillary sinus. (**a**) Large expansile soft tissue mass (m) in left maxillary sinus with extension into left nasal cavity (arrow); (**b**) Surrounding aggressive type of bone destruction of maxillary sinus walls (arrow)

2.5 Miscellaneous Entities

2.5.1 Sinonasal Tract Angiofibroma (STA)

CECT (Fig. 2.15) reveals an intensely enhancing mass lesion centred at the sphenopalatine foramen, posterior choana and nasopharynx. There is characteristic lateral extension into the pterygomaxillary fissure. STA causes bone expansion and remodelling with evidence of antral bowing or the Holman–Miller sign (mass effect on the posterior wall of the maxillary sinus). However, it can also show aggressive behaviour with bone erosion and destruction. The tumour demonstrates characteristic pattern of spread; anteriorly into the nasal cavity, posteriorly into the pterygoid canal and greater wing of sphenoid and posteromedially into the nasopharynx. Laterally it extends into the pterygopalatine fossa, pterygomaxillary fissure and from there into the infratemporal fossa and buccal space. Through its extension into the inferior orbital fissure, the lesion can spread into the orbits and cavernous sinuses via the superior orbital fissure.

On MRI (Fig. 2.16), STA is a heterogenous lesion with predominantly T2 hyperintense signal intensity. Multiple flow voids are often seen within the lesion and there is intense post-contrast enhancement [23–25].

2.5.2 Fibro-osseous Lesions

These are frequently encountered sinonasal lesions in practice. Tumours of osseous origin involving sinonasal (SN) cavity can arise from the bony structures within the SN cavity or from adjacent structures like anterior/central skull base, and the maxillary alveolus. Seen in young patients, the common lesions are ossifying fibroma and fibrous dysplasia.

2.5.2.1 Fibrous Dysplasia (FD)

Fibrous dysplasia involves multiple bones wherein the medulla is replaced by immature fibrous tissue and eventually osseous tissue [26]. Can have a monostotic and a polyostotic form. Craniofacial bones are frequently involved and may be part of the polyostotic form. The typical facial appearance is referred to as "Leontiasis Ossea".

On CT, there is expansion of bones with ill-defined margins with the adjoining bone. The matrix can have a lucent density, "cotton wool" appearance and may finally evolve

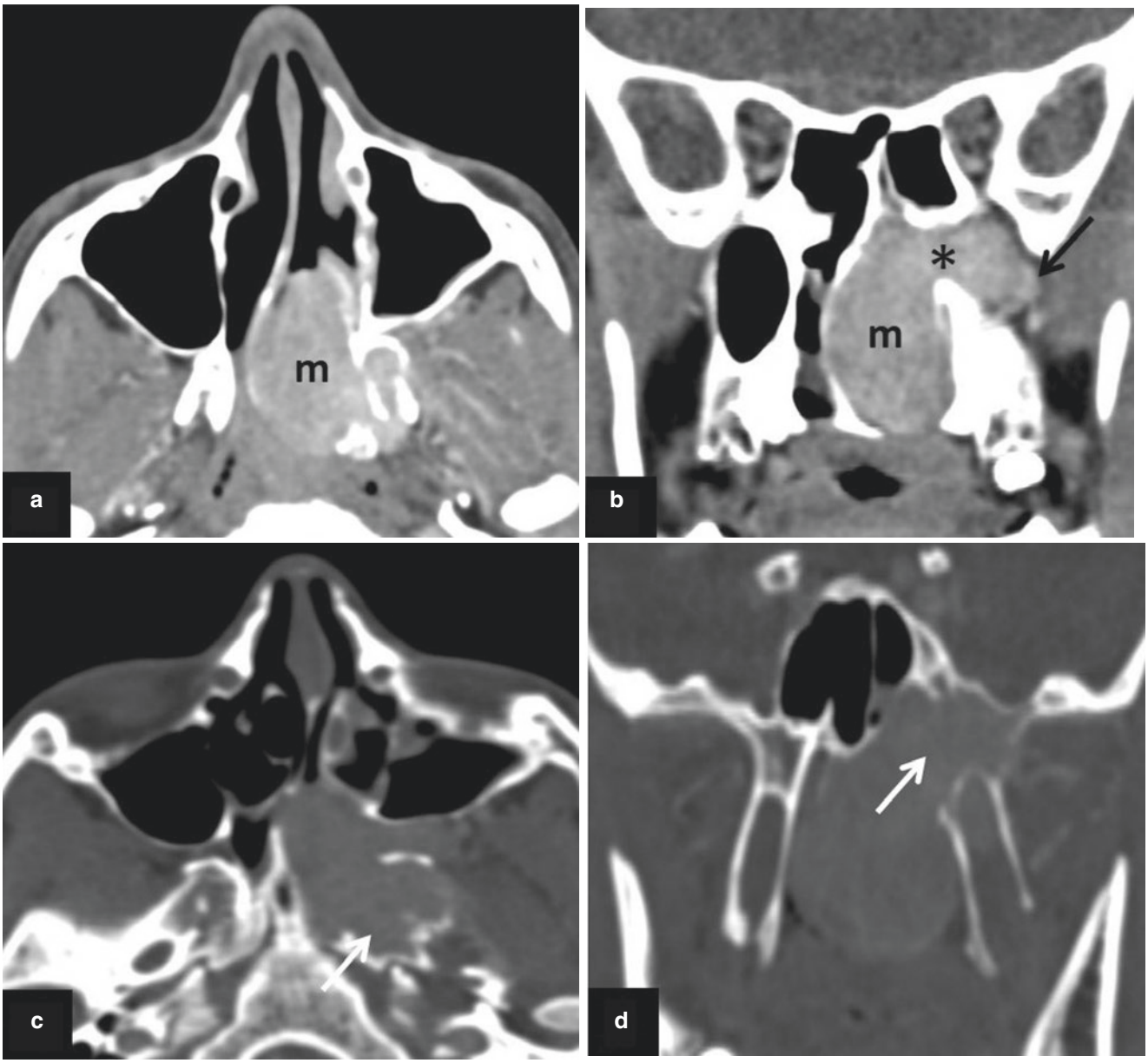

Fig. 2.15 (**a**–**d**) Sinonasal tract angiofibroma CT. (**a**) Enhancing mass extending into nasopharynx (m); (**b**) Mass in left sphenopalatine foramen, pterygopalatine fossa. Widening of pterygomaxillary fissure laterally (arrow). Mass entering nasal cavity through widened sphenopalatine foramen (asterisk); (**c**, **d**) Mass causing erosion of left pterygoid process (arrow)

into the typical "ground glass" density (Fig. 2.17). It is essential to evaluate all the skull base foramina and drainage pathways on CT.

MRI reveals intermediate signal on T1WI, intermediate or low signal intensity on T2WI with significant contrast enhancement in the fibrous tissues.

2.5.2.2 Ossifying Fibroma (OF)

It is divided into two major subtypes: conventional OF and juvenile OF. The juvenile type is seen in younger patients, has a more aggressive behaviour and is larger at presentation. It typically shows less mineralization and more bone erosion [23, 26].

CT reveals a well-defined mixed density lesion with soft tissue component. There may be matrix mineralization and calcification seen along the periphery. The density of the lesion varies with the extent of soft tissue and mineralized matrix. OF is typically a well-defined expansile lesion with occasional bone erosion (Fig. 2.18).

On *MRI*, there is heterogenous enhancement of the soft tissue component of the lesion, whereas the mineralized matrix/rim is seen as signal voids.

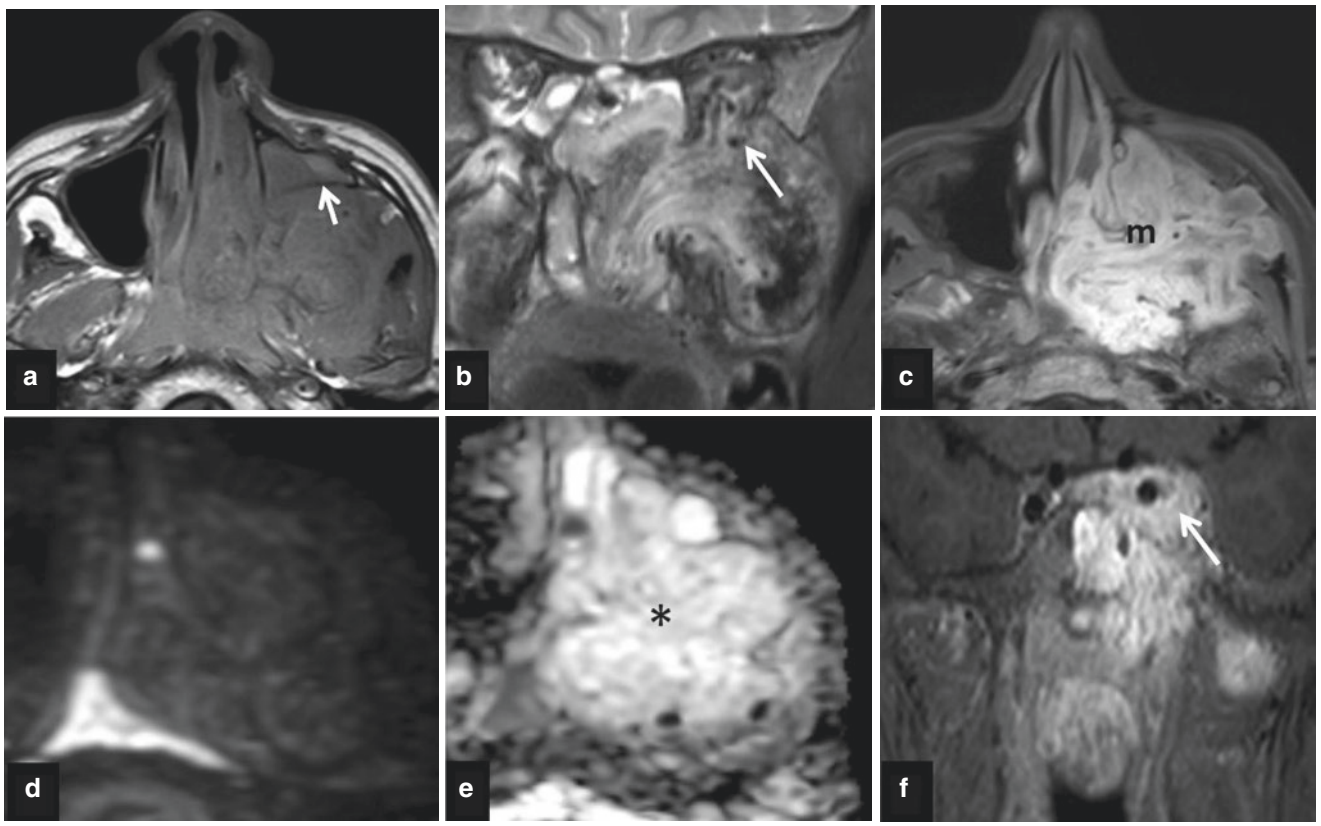

Fig. 2.16 (**a**–**f**) Sinonasal tract angiofibroma (Stage III) MRI. (**a**) Bowing of posterior antral wall (arrow); (**b**) Intermediate signal intensity with flow voids on T2 WI (arrow). (**c**) Intense post-contrast enhancement in the mass (m); (**d**, **e**) Facilitated diffusion—bright on apparent diffusion coefficient map (asterisk); (**f**) Invasion of left cavernous sinus with encasement of cavernous segment of left internal carotid artery (arrow)

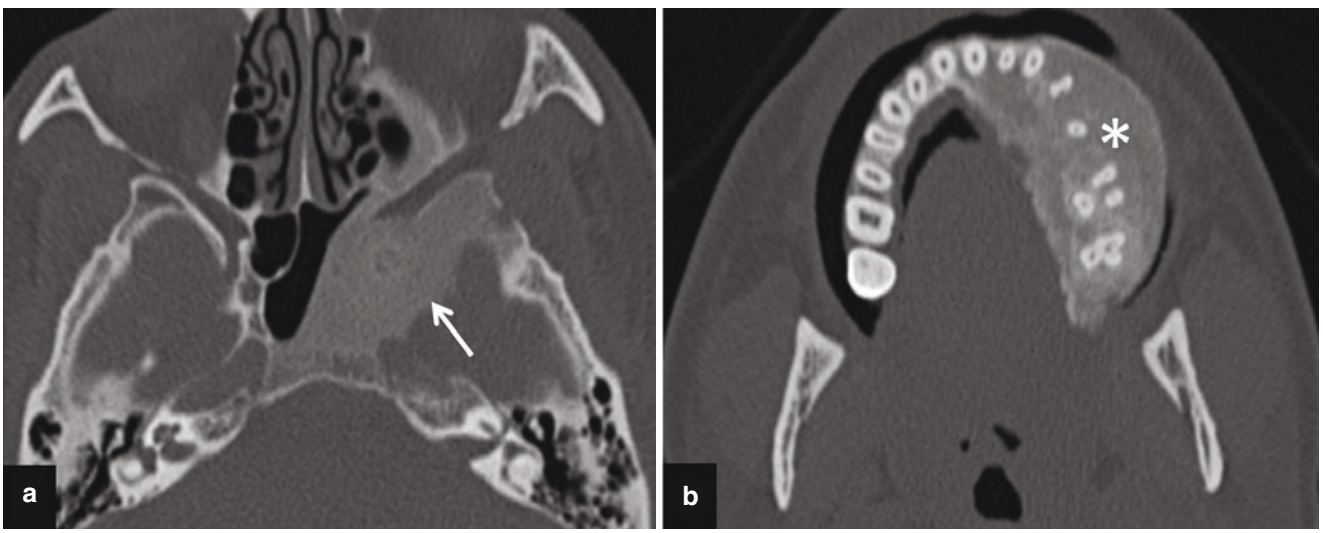

Fig. 2.17 (**a**, **b**) Fibrous dysplasia. Expansile lesion with ill-defined margins and ground glass matrix seen involving the left sphenoid bone (arrow) and left maxilla including alveolus (*) suggestive of polyostotic fibrous dysplasia

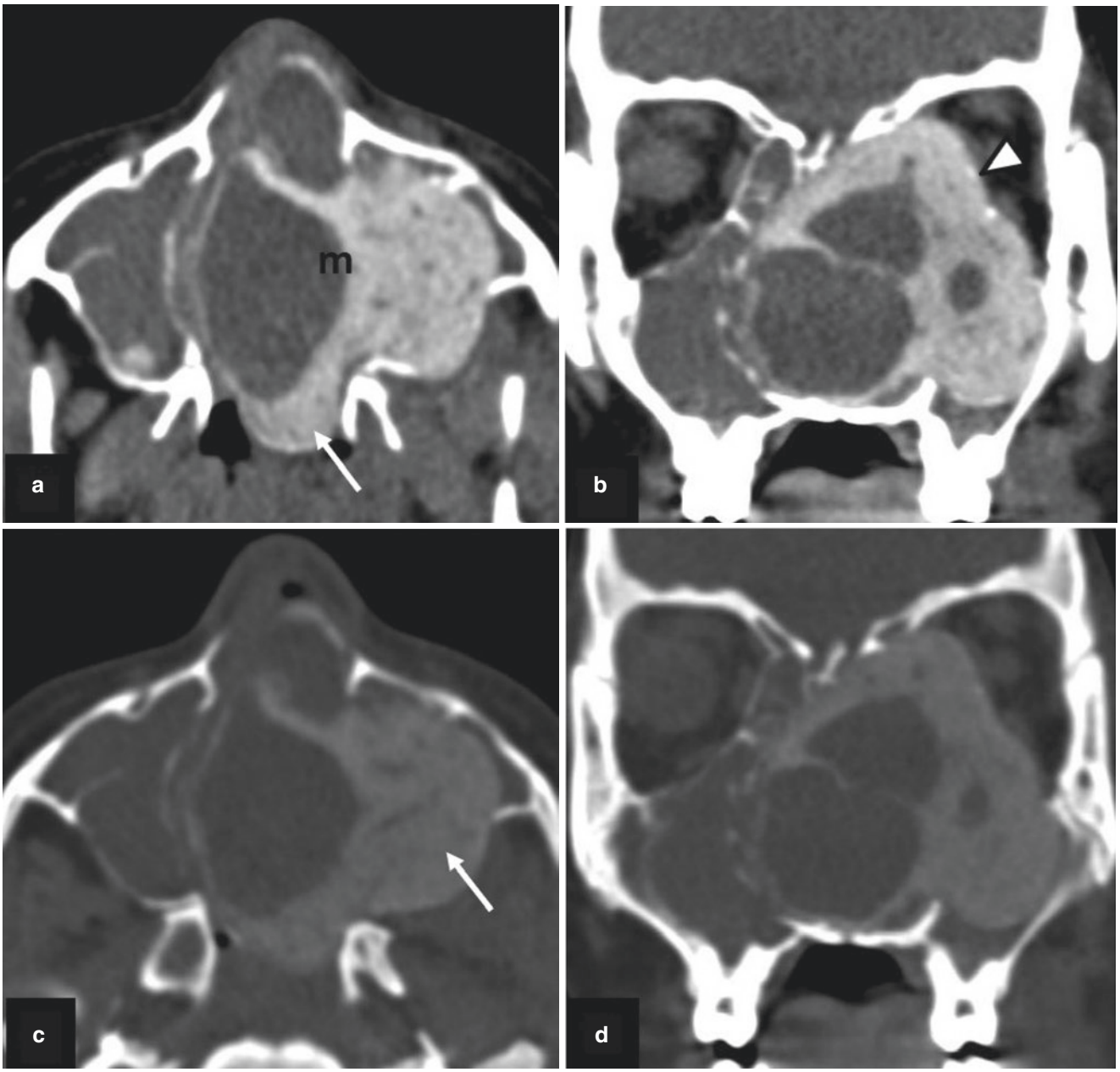

Fig. 2.18 (**a**–**d**) Ossifying fibroma. (**a**, **b**) Large well-defined mixed density expansile mass (m) in left nasal cavity and maxillary sinus, extending into left orbit (arrowhead) and nasopharynx (arrow);(**c**, **d**) Bone density areas seen on bone window images (arrow)

2.6 Conclusion

Imaging is a valuable tool for the diagnosis, management planning and follow-up of both sinusitis and neoplasia of the sinonasal cavity.

References

1. Mafee MF, Tran BH, Chapa AR. Imaging of rhinosinusitis and its complications: plain film, CT, and MRI. Clin Rev Allergy Immun. 2006;30:165–85.
2. Joshi VM, Sansi R. Imaging in sinonasal inflammatory disease. Neuroimaging Clin N Am. 2015;25:549–68.
3. Bhalla AS, Manchanda S. Imaging in Rhinosinusitis (Inflammatory Diseases). In Eds. Bhalla AS, Jana M. Sinonasal Imaging. 2018, Jaypee Brothers Medical Publishers (P) Ltd., 1st Ed, pp. 57–76.
4. Broderick DF. The opacified paranasal sinus: approach and differential. Appl Radiol. 2015;44:9–17.
5. Whyte A, Chapeikin G. Opaque maxillary antrum: a pictorial review. Australas Radiol. 2005;49:203–13.
6. Chakrabarti A, Denning DW, Ferguson BJ, et al. Fungal rhinosinusitis: a categorization and definitional schema addressing current controversies. Laryngoscope. 2009;119(9):1809–18.
7. Raz E, et al. Fungal Sinusitis Neuroimag Clin N Am. 2015;25:569–76.

8. Bhalla AS, Manchanda S. Imaging in Fungal Sinusitis. In Eds. Bhalla AS, Jana M. Sinonasal Imaging. 2018, Jaypee Brothers Medical Publishers (P) Ltd., 1st Ed, pp. 99–112.
9. Aibandi M, McCoy VA, Bazan C III. Imaging features of invasive and noninvasive fungal sinusitis: a review. Radiographics. 2007;27(5):1283–96.
10. Oren N, Vaysberg A, Ginat DT. Updated WHO nomenclature of head and neck lesions and associated imaging findings. Insights Imaging. 2019;10(1):72.
11. Thompson LDR, Franchi A. New tumor entities in the 4th edition of the World Health Organization classification of head and neck tumors: nasal cavity, paranasal sinuses and skull base. Virchows Arch. 2018 Mar;472(3):315–30.
12. Stelow EB, Bishop JA. Update from the 4th edition of the World Health Organization classification of head and neck Tumours: tumors of the nasal cavity, paranasal sinuses and Skull Base. Head Neck Pathol. 2017 Mar;11(1):3–15.
13. Davide Farina RM. Neoplasms of the sinonasal cavities. In: Hermans R, editor. Head and neck cancer imaging. 2nd ed. Berlin: Springer-Verlag; 2012. p. 207–36.
14. Sen S, Chandra A, Mukhopadhyay S, et al. Imaging approach to sinonasal neoplasms. Neuroimaging Clin N Am. 2015;25(4):577–93.
15. Sen S, Chandra A, Mukhopadhyay S, Ghosh P. Sinonasal tumors computed tomography and MR imaging features. Neuroimaging Clin N Am. 2015;25:595–618.
16. Raghavan P, Phillips CD. Magnetic resonance imaging of sinonasal malignancies. Top Magn Reson Imaging. 2007;18(4):259–67.
17. Madani G, Beale TJ, Lund VJ. Imaging of sinonasal tumors. Semin Ultrasound CT MR. 2009;30(1):25–38.
18. Kawaguchi M, Kato H, Tomita H, Mizuta K, Aoki M, Hara A, Matsuo M. Imaging characteristics of malignant Sinonasal tumors. J Clin Med. 2017;6(12):116.
19. Phillips CD, Futterer SF, Lipper MH, et al. Sinonasal undifferentiated carcinoma: CT and MR imaging of an uncommon neoplasm of the nasal cavity. Radiology. 1997;202(2):477–80.
20. Dublin AB, Bobinski M. Imaging characteristics of olfactory neuroblastoma (Esthesioneuroblastoma). J Neurol Surg B Skull Base. 2016;77(1):1–5. https://doi.org/10.1055/s-0035-1564053.
21. King AD, Lei KI, Ahuja AT, et al. MR imaging of nasal T-cell/natural killer cell lymphoma. AJR Am J Roentgenol. 2000;174(1):209–11.
22. Mondal PK, Pal I, Misra S, Biswas S, Bera SP. Rhabdomyosarcoma of nose, nasopharynx and paranasal sinuses. Indian J Otolaryngol Head Neck Surg. 2009 Dec;61(4):317–9.
23. Manchanda S, Bhalla AS. Benign Tumors of the Nose and Paranasal Sinuses: Imaging. In Eds. Bhalla AS, Jana M. Sinonasal Imaging. 2018, Jaypee Brothers Medical Publishers (P) Ltd., 1st Ed, pp. 160–181.
24. Alimli AG, et al. Juvenile nasopharyngeal Angiofibroma: magnetic resonance imaging findings. Journal of the Belgian Society of Radiology. 2016;100:1–8.
25. Das A, et al. Can diffusion weighted imaging aid in differentiating benign from malignant Sinonasal masses?: a useful adjunct. Pol J Radiol. 2017;82:345–55.
26. Eller R, Sillers M. Common fibro-osseous lesions of the paranasal sinuses. Otolaryngol Clin N Am. 2006;39(3):585–600.

Endonasal and Open Approaches to Sinonasal Tumours

3

Smriti Panda, Kapil Sikka, and Alok Thakar

3.1 Introduction

Surgery forms a corner stone in the multidisciplinary management of sinonasal tumours [1, 2]. This chapter highlights the various open and endoscopic techniques available for the management of these tumours. Expanded endonasal endoscopic procedures can provide access to a wide range of tumours arising in the sinonasal tract and extending to the pterygopalatine fossa, infratemporal fossa and the anterior cranial fossa. These approaches avoid facial incision, disassembly of the facial skeletal framework, brain retraction and provide a direct access to the tumour. This translates into reduced complication rates, shorter duration of hospital-stay and better quality of life. In carefully selected cases, oncological outcomes at par with open approaches can be obtained in case of sinonasal malignancies. Contemporary indications for open approaches are: skin involvement, involvement of the nasal bones, extensive involvement of the orbital fat, extraocular muscles, skin of the eyelid and lacrimal apparatus. Surgical Surgical approach is broadly classified into:

1. Conventional open approach
   - Requires facial incision and disassembly of facial skeletal framework.
   - Transpalatal or transoral approaches cater to strictly midline tumours.
   - Transfacial approaches can be utilised in the presence of lateral tumour spread into pterygopalatine fossa or the infratemporal fossa.
2. Endoscopic endonasal approach

   With appropriate surgical expertise and in carefully selected cases [3, 4], endoscopic endonasal approach offers a minimally invasive alternative to conventional open approaches.
3. Combined approach

Open approaches can be combined with endoscopic approaches and vice versa in case of tumours involving multiple anatomical compartments.

This chapter will focus on the case selection criteria and indications underlying open and endoscopic approaches for pathologies originating from paranasal sinuses and the anterior skull base.

3.2 Open Approaches to Paranasal Sinus and Anterior Skull Base

Non-endoscopic conventional approach to paranasal sinus tumours can be divided into soft tissue and skeletal approaches (Fig. 3.1). Soft tissue approach typically precedes the bony approach. Various options exist for soft tissue approaches for a particular bone approach according to surgical expertise and tumour extent.

S. Panda · K. Sikka (✉) · A. Thakar
Department of Otolaryngology and Head and Neck Surgery, All India Institute of Medical Sciences, New Delhi, India
e-mail: drksikka.orlhns@aiims.edu

D. Jain, J. A. Bishop (eds.), *Atlas of Sinonasal Tract Pathology*, https://doi.org/10.1007/978-981-19-7315-4_3

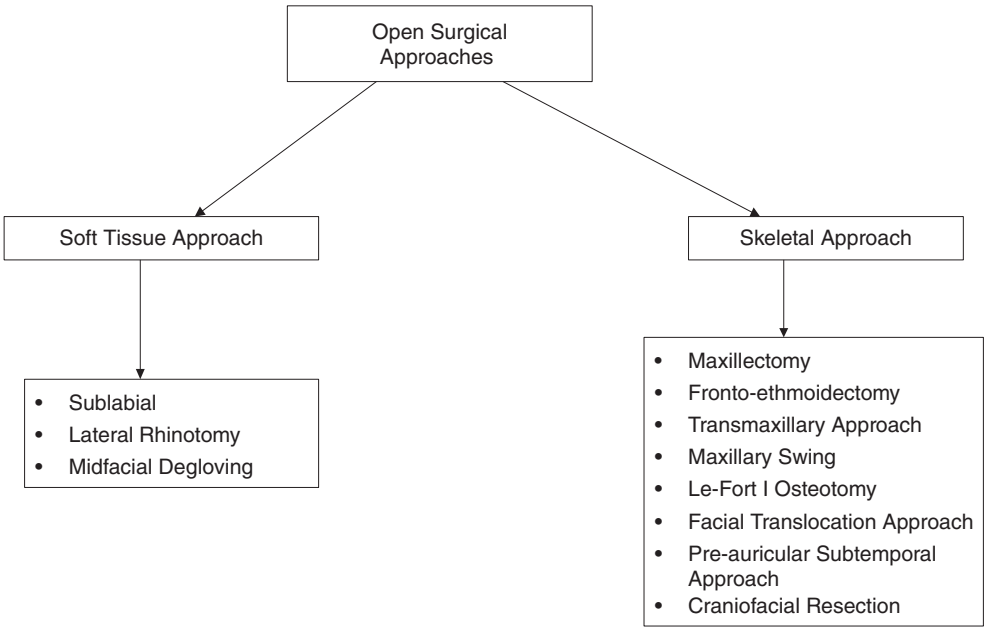

Fig. 3.1 Classification of open approaches to paranasal sinus

3.2.1 Soft Tissue Approaches

3.2.1.1 Sublabial Approach

This soft tissue approach completely avoids facial incision by concealing the incision in the sublabial area. It frequently precedes the following bony resections:

- Medial maxillectomy
- Infrastructural maxillectomy
- Transmaxillary approach to the infratemporal fossa
- Total maxillectomy: Following the sacrifice of the infra-orbital nerve. This would require the flap to be elevated till the inferior orbital margin.

Contraindications:

- Skin involvement
- Orbital invasion
- Tumour extension across the midline

3.2.1.2 Lateral Rhinotomy:

This approach has been classically described for inverted papilloma.

Bony resections which can be performed:

- Medial maxillectomy
- Infrastructural maxillectomy
- Transmaxillary approach to the infratemporal fossa
- Fronto-ethmoidectomy

Tumours arising from the following anatomical sites can be accessed by lateral rhinotomy:

- Lateral nasal wall
- Maxillary sinus
- Ethmoid sinus
- Medial and inferior aspect of the orbit
- Lacrimal fossa
- Sphenoid sinus
- Nasopharynx
- Frontal sinus
- Clivus
- Sella
- Anterior cranial fossa

Contraindication

- Palatal involvement
- Lateral extension of the tumour beyond the infraorbital foramen
- Extensive involvement of the infratemporal fossa
- Tumour extension across the midline

3.2.2 Skeletal Approaches to Paranasal Sinus Pathologies

3.2.2.1 Maxillectomy

Classification for maxillectomy depicted in Table 3.1 has been extrapolated from classification for partial maxillectomy [5]. The indications for various categories of maxillectomy have been detailed in the subsequent text.

Total Maxillectomy (Fig. 3.2)

Indications:

Table 3.1 Classification of maxillectomy (Adapted from Roy et al. [5])

Type of partial maxillectomy	Osteotomy	Indications
Infrastructural Maxillectomy	• Horizontal: Floor of nasal cavity • Palate—midline	Tumours confined to upper alveolus or upper gingivobuccal sulcus without extension to maxillary sinus or posterior extension
Subtotal Maxillectomy	Superior osteotomy: Just inferior to orbital rim Rest: Similar to total maxillectomy	Tumours of hard palate or upper gingivobuccal complex with involvement of the maxillary sinus confined to the inferior half
Medial Maxillectomy	Superior: From pyriform aperture parallel but inferior to frontoethmoidal suture line Inferior: Floor of nasal cavity Lateral: Vertically over anterior wall of maxilla medial to infraorbital foramen Posterior: Between palatine process of maxilla and pterygoid plates	Tumours arising from lateral nasal wall
Suprastructural maxillectomy	Inferior cut—floor of nasal cavity preserving the palate. Remaining osteotomies are similar to maxillectomy	Tumour involving roof of maxillary sinus with or without ethmoid sinus or orbital involvement

Malignant tumours of either epithelial or mesenchymal origin involving the maxillary sinus mucosa and all the walls of the maxilla.

Contraindications:

- Cavernous sinus involvement
- Tumour encasing internal carotid artery
- Infiltration of the sphenoid sinus, frontal sinus, and the nasopharynx
- Orbital apex involvement
- Infiltration of the brain parenchyma
- Unresectable neck metastasis
- Distant metastasis (exception: adenoid cystic carcinoma with oligometastatic disease)

Radical Maxillectomy

In case of tumour involvement of the orbital fat, extraocular muscle, eyelid and the lacrimal apparatus, orbital exenteration accompanies total maxillectomy.

Rehabilitation Following Maxillectomy

- Prosthetic rehabilitation (Fig. 3.3)
- Reconstruction with flaps

1. Pedicled flaps (temporoparietal fascial flap, temporalis muscle flap)
2. Microvascular reconstruction: Radial forearm free flap or anterolateral thigh flap

Partial Maxillectomy: Details related to the osteotomy and the indications for various partial maxillectomy have been enumerated in Table 1 [5]. Anything less than a total maxillectomy is defined as a partial maxillectomy (Fig. 3.4).

3.2.2.2 Fronto-ethmoidectomy

This procedure can be undertaken endoscopically as well as by the transfacial route.

3.2.2.3 Transmaxillary Approach

This approach provides access to the retromaxillary regions: pterygopalatine fossa and the infratemporal fossa. Transmaxillary approach can also be undertaken endoscopically. The most common tumour for which this approach is described is sinonasal tract angiofibroma. The soft tissue approach preceding the osteotomy can either be sublabial, lateral rhinotomy or midfacial degloving.

Contraindication: Tumours with lateral extension with extensive involvement of the infratemporal fossa are best managed by either maxillary swing, nasomaxillary swing or pre-auricular subtemporal approach.

3.2.2.4 Maxillary Swing

This technique was pioneered by Wei and colleagues for surgical management of recurrent nasopharyngeal carcinoma [6]. Presently this approach is found to be very suitable for sinonasal tract angiofibromas with infratemporal fossa extension (Fig. 3.5).

Fig. 3.2 Total maxillectomy. (**a**) Modified Weber Fergusson incision. (**b**) Cheek flap elevated superficial to tumour which is seen invading through anterior wall of maxilla (arrow). (**c**) Mucoperiosteal incision over midline of hard palate (arrow). (**d**) Completed osteotomy over hard palate and zygoma (arrow)

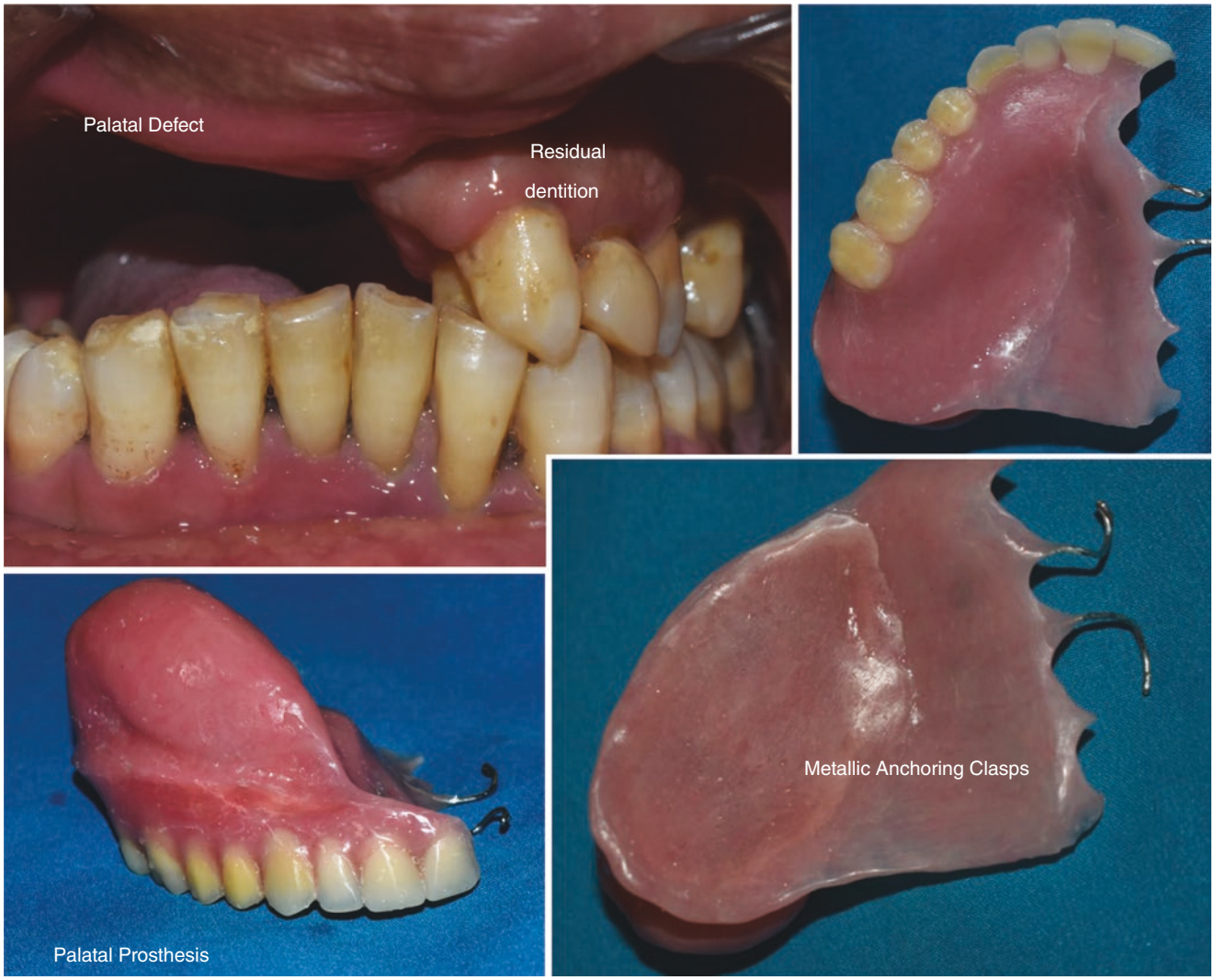

Fig. 3.3 Right sided hemipalatal defect rehabilitated with palatal obturator

Osteotomy: Prior to performing the following osteotomies, the sites are pre-plated to allow accurate approximation of the bone once the maxillary osteoplastic flap is repositioned back. The following osteotomies are performed:

- Frontal process of maxilla to the nasal bone
- Zygomatic process of maxilla
- Alveolar process in the midline
- Between the maxillary tuberosity and base of the pterygoid plates

The osteoplastic flap consists of the anterior wall of maxilla with overlying soft tissues and the floor of the orbit.

To expose the tumour located in the infratemporal fossa, posterior wall of maxilla is excised.

3.2.2.5 Cranio-facial Resection (Fig. 3.6).

Cranio-facial resection (CFR) is a single stage surgical management strategy for sinonasal tumours with extension to the anterior cranial fossa. It typically consists of a cranial part and an extracranial part. The extracranial part of the surgery can be undertaken by any of the procedures described previously.

Fig. 3.4 Sublabial infrastructural maxillectomy in a case of sinonasal mucormycosis. (**a**) Sublabial incision made and cheek flap elevated in subperiosteal plane. (**b**) Flap elevate till infraorbital foramen (single arrow) superiorly and the pyriform aperture medially (double arrow). (**c**) Palatal mucoperisoteal incision. (**d**) Final excised specimen comprised of the upper alveolus, hemipalate and inferior aspect of the maxillary sinus

3.2.2.6 Transbasal Approach (Fig. 3.7).

This approach is an alternative to CFR. Elevation of nasofrontal bone flap as shown in Fig. 3.7 allows access to the anterior skull base without resorting to unnecessary brain retraction.

3.2.2.7 Preauricular Subtemporal Approach (Fig. 3.8).

This approach offers a lateral trajectory to the infratemporal fossa. Sinonasal tumours like angiofibroma extending to infratemporal fossa with extension lateral to parasellar

Fig. 3.5 Suprastructural maxillary swing for sinonasal tract angiofibroma. (**a**) Maxillary osteoplastic flap reposited with osteotomy site plated. (**b**) Exposure of infratemporal fossa obtained after "swinging" anterior wall of maxilla (arrow). (**c**) Excised specimen of angiofibroma: Nasal part (asterisk), infratemporal fossa part (thin arrow), middle fossa part (thick arrow)

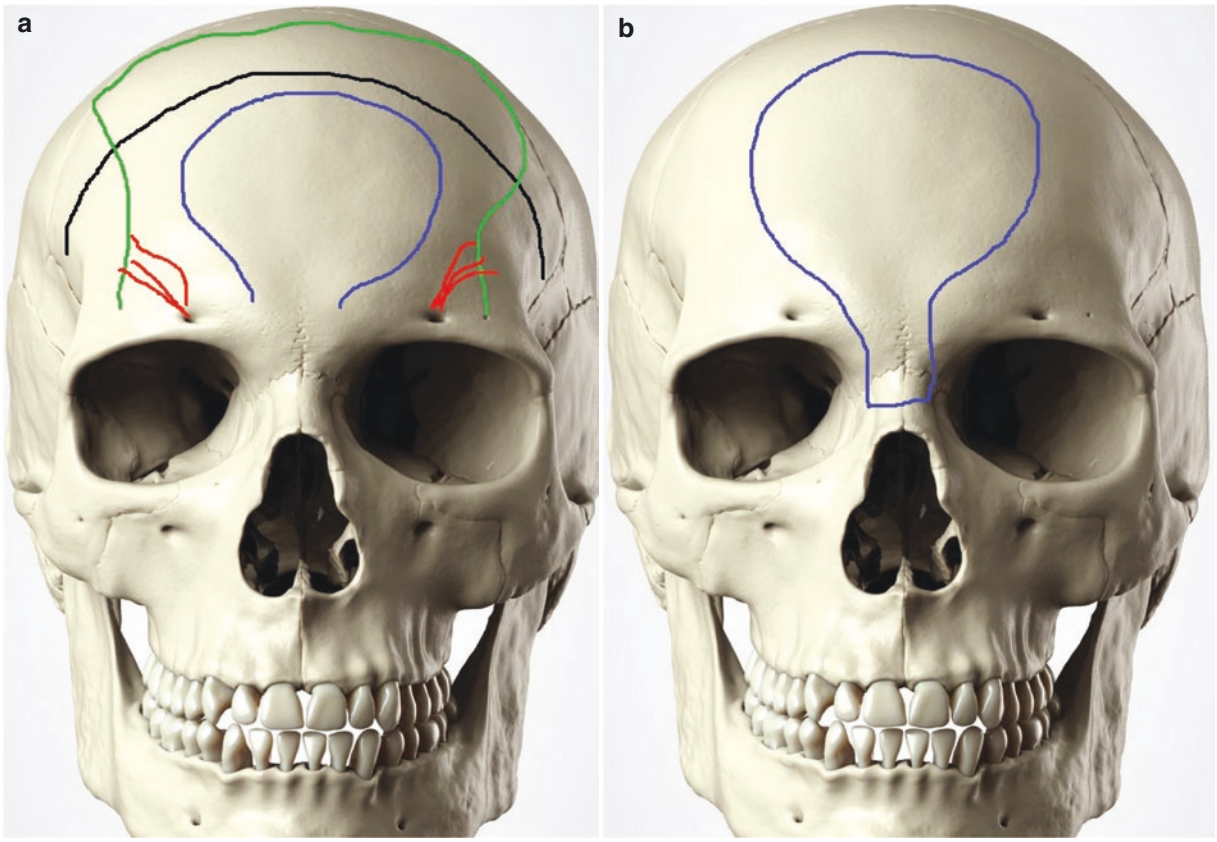

Fig. 3.6 Craniofacial resection. (**a**) Conventional bifrontal craniotomy. Black- bicoronal skin incision, green- pericranial flap pedicled on bilateral supraorbital and supratrochlear arteries (red), Frontal craniotomy (blue). (**b**) Subcranial or transbasal approach. Soft tissue approach is similar to conventional craniofacial resection. Instead of bifrontal craniotomy, Nasofrontal bone flap is elevated as shown (blue outline)

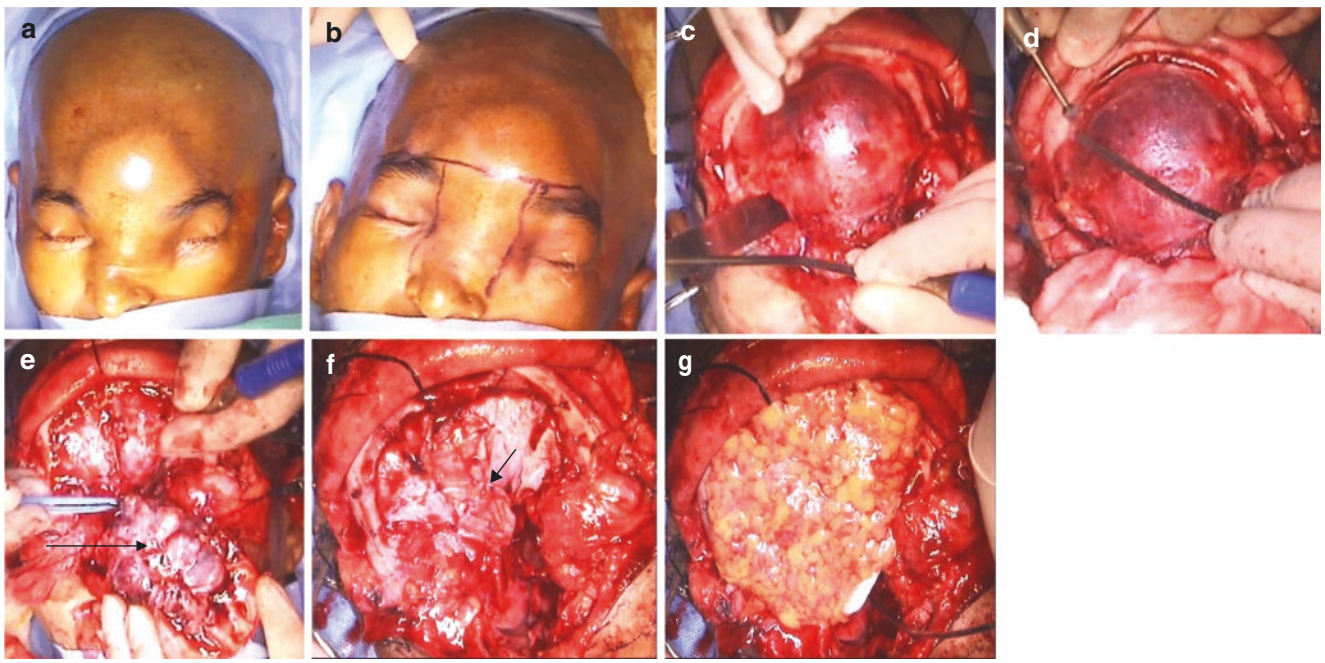

Fig. 3.7 Transbasal or subcranial approach in a sinonasal undifferentiated carcinoma. (**a**) Tumour causing erosion of outer table of the frontal bone with prominent bulge over the frontal region. (**b**) Proposed incision to accommodate bilateral frontoethmoidectomy with the craniotomy. (**c**) Flap elevated superficial to the involved tissues in subcutaneous plane over the tumour and in the subgaleal plane over the rest of the skull. (**d**) Craniotomy to elevate the nasofrontal segment. (**e**) Nasofrontal segment with the tumour reflected anteriorly (arrow). (**f**) Dural defect patched with fascia obtained from rectus abdominis (arrow). (**g**) Repair supported by abdominal fat

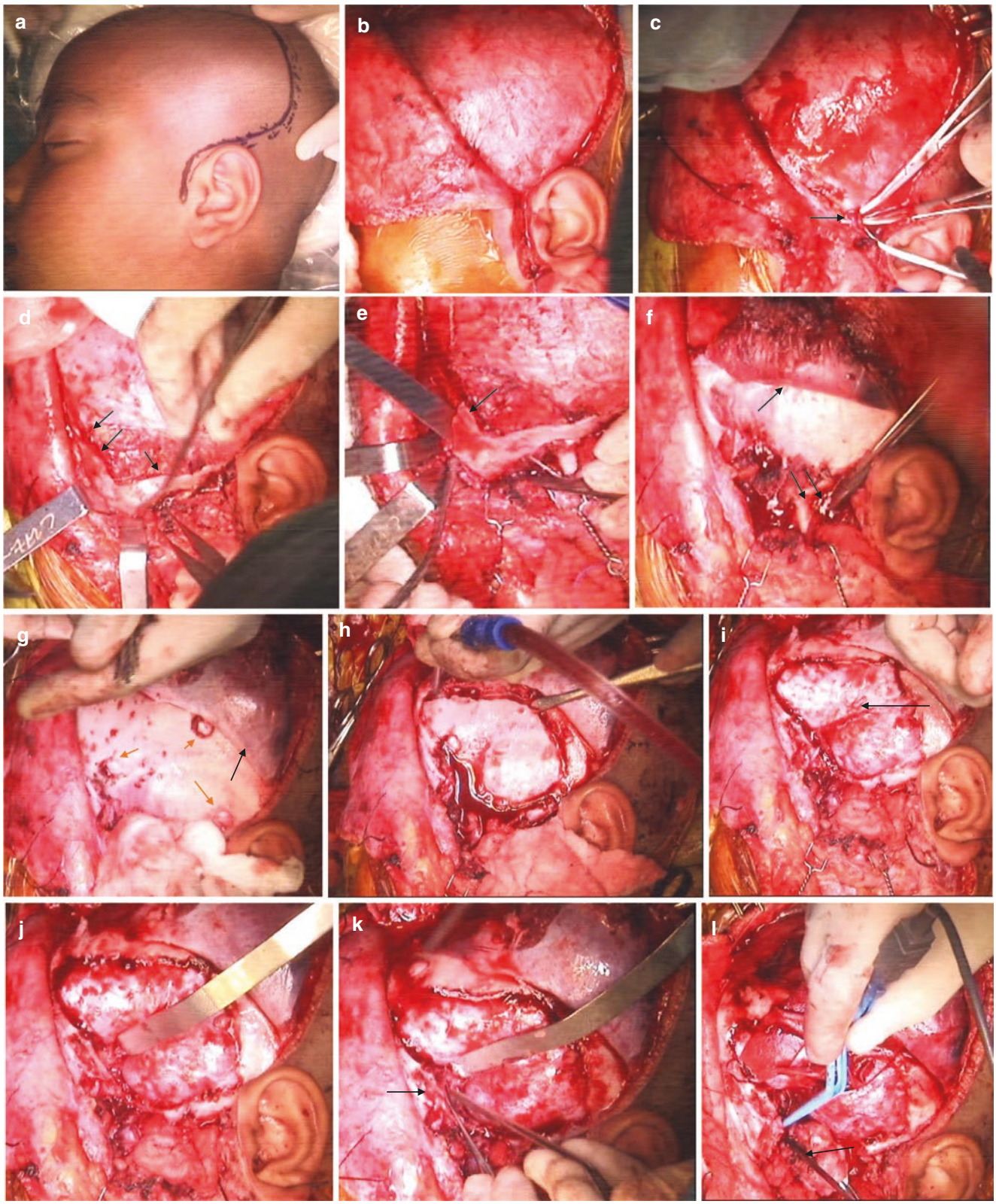

Fig. 3.8 Pre-auricular subtemporal approach in a recurrent sinonasal tract angiofibroma. (**a**) C-shaped incision over the temporal region with a vertical limb over the pre-auricular region. (**b**) Flap elevated superficial to the deep temporal fascia. (**c**) Superficial temporal artery being ligated (arrow). (**d**) Flap elevated further to expose the lateral orbital wall (double arrows) and entire length of the zygoma (single arrow). (**e**) First osteotomy at the level of the lateral orbital wall (arrow). (**f**) Exposure after complete excision of the zygoma. Condyle of the mandible is sacrificed (double arrow). Subperiosteal flap shown by single arrow. (**g**) Temporalis muscle elevated superiorly along with underlying pericranium to be used for closure at the end of the procedure (black arrow). Burr hole marked for craniotomy (orange arrow). (**h**) FTOZ (fronto-temporal-orbito-zygomatic) craniotomy being performed by connecting the burr holes. (**i**) Temporal lobe exposed after removal of the bone flap (arrow). (**j**) Temporal lobe being retracted with malleable retractor to expose the floor of the middle fossa. (**k**) Floor of middle fossa being drilled (arrow). (**l**) Tumour exposed in infratemporal fossa (arrow)

internal carotid artery require extensive lateral approaches like the pre-auricular subtemporal approach.

3.3 Endoscopic Endonasal Approach

Endoscopic endonasal approaches to the sinonasal and anterior skull base tumours provide a less morbid alternative to open approaches by providing direct access to the tumour, minimal soft tissue dissection and avoiding brain retraction. There has been considerable criticism towards the application of a purely endoscopic approach for sinonasal malignancies. This is due to tumour transection *in-situ* and the theoretical risk of tumour seeding. Literature is however replete with evidence comparing endoscopic and open approaches and have shown results comparable in terms of oncological outcomes. There still remains the following absolute contraindication to a purely endoscopic approach [3]:

- Infiltration of nasal bones
- Extension to superior and lateral recess of the frontal sinus
- Involvement of the lacrimal system and orbital contents
- Dural infiltration
- Brain parenchyma involvement

Endoscopic endonasal approaches are divided along a sagittal and coronal plane [7]. Of these endoscopic routes for sinonasal pathologies include the following:

Sagittal Plane Approaches (Anterior to Posterior) Along with their Indications:

- Transfrontal: Inflammatory lesions of the frontal sinus, repair of CSF leak
- Transplanum
- Transcribriform (Fig. 3.9): Olfactory groove meningioma and olfactory neuroblastoma

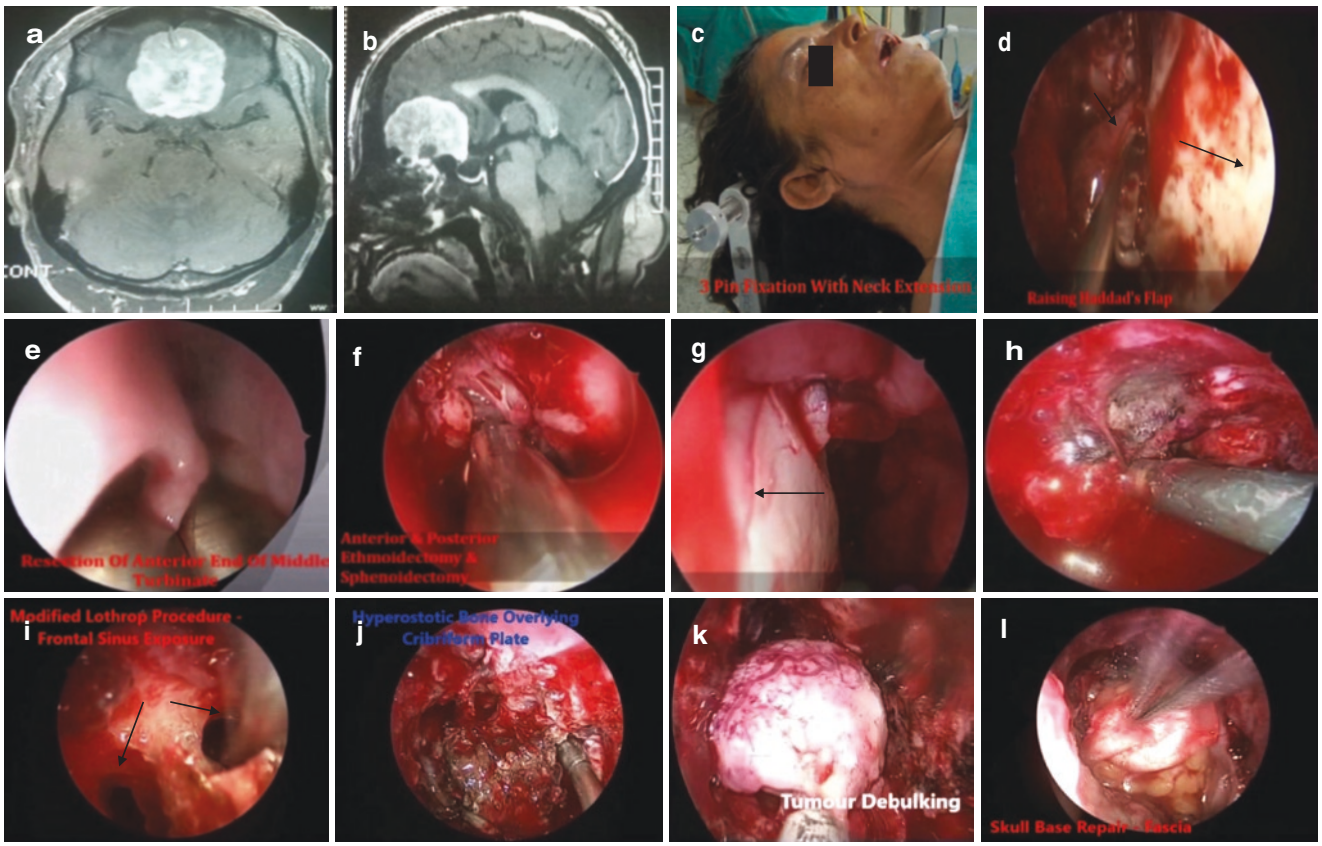

Fig. 3.9 Endoscopic Endonasal Approach in olfactory groove meningioma. (**a**, **b**) Contrast enhanced computed tomography depicting tumour arising from the olfactory groove with extradural extension to the anterior cranial fossa. (**c**) Patient positioned with slight neck extension and the head supported by 3-pin fixation. (**d**) Hadad flap being elevated on the right side. Septum—long arrow, mucoperiosteum over the septum reflected posteriorly (short arrow). (**e**) Anterior end of middle turbinate being resected. (**f**) Complete ethmoidectomy and sphenoidectomy. (**g**) Bony and cartilaginous septum (arrow) sacrificed retaining dorsal and ventral strip. This facilitates two-hand approach. (**h**) Anterior ethmoidal artery being coagulated. (**i**) Frontal sinus ostia (arrows) being exposed during endoscopic modified Lothrop procedure. (**j**) Hyperostotic bone over cribriform plate exposed and coagulated. (**k**) Tumour being debulked by use of CUSA (Cavitron Ultrsonic Suction Aspirator). (**l**) Skull base defect being reconstructed by multilayer fashion

- Transsphenoidal: Pathologies arising from the pituitary
- Transclival: Skull base chordoma
- Transodontoid: Pathologies of the craniovertebral junction

Coronal Plane Approaches: The coronal plane module includes approaches medial to lateral. Detailed description of the same is beyond the scope of this chapter. The endoscopic approach which provides access to sinonasal pathologies extending to the pterygopalatine fossa is the **transpterygoid** approach. Classical example includes transpterygoid endoscopic excision of sinonasal tract angiofibroma.

3.4 Conclusion

Conventional open approaches involve facial incision and disassembly of facial skeleton and are currently reserved for tumours infiltrating skin, palate, intraconal orbital fat, lacrimal sac, extraocular muscles, extensive involvement of infratemporal fossa. Though endoscopic endonasal approaches are ideally suited for tumours located medial to the mid-pupillary line, posteriorly based tumours and tumours displacing neurovascular structures postero-laterally, the limits of this approach can be expanded to include more extensive tumours in experienced hands and with advanced endoscopic technology.

References

1. Dulguerov P, Allal AS. Nasal and paranasal sinus carcinoma: how can we continue to make progress? Curr Opin Otolaryngol Head Neck Surg. 2006;14(2):67–72.
2. Dulguerov P, Jacobsen MS, Allal AS, et al. Nasal and paranasal sinus carcinoma:are we making progress? A series of 220 patients and a systematic review. Cancer. 2001;92(12):3012–29.
3. Snyderman CH, Pant H, Carrau RL, et al. What are the limits of endoscopic sinus surgery?: the expanded endonasal approach to the skull base. Keio J Med. 2009;58(3):152–60.
4. Castelnuovo P, Battaglia P, Turri-Zanoni M, et al. Endoscopic endonasal surgery for malignancies of the anterior cranial base. World Neurosurg. 2014;82(Suppl 6):S22–31.
5. Roy BC, Bahadur S, Thakar A. Partial maxillectomy for malignant neoplasms of Para nasal sinuses and hard palate. Indian J Cancer. 2002;39(3):83–90.
6. Wei WI, Chan JY, Ng RW, Ho WK. Surgical salvage of persistent or recurrent nasopharyngeal carcinoma with maxillary swing approach - critical appraisal after 2 decades. Head Neck. 2011 Jul;33(7):969–75.
7. Wagenmann M, Schipper J. The transnasal approach to the skull base. From sinus surgery to skull base surgery. GMS Curr Top Otorhinolaryngol Head Neck Surg. 2011;10:Doc08.

Cytology of Sinonasal Tract Lesions/Tumors

4

Felicia D. Allard and Edward B. Stelow

4.1 Introduction

Neoplastic and nonneoplastic lesions that arise in the sinonasal tract are uncommon and diverse in terms of both etiology and morphology. While surgical biopsy or resection has historically been the diagnostic mainstay, cytologic sampling of primary lesions or metastases has proven to be an effective means of establishing the diagnosis and staging these lesions. The accuracy of cytology for the detection of malignancy in sinonasal lesions is reported to range from 87.5 to 95% [1–3]. Additionally, cytologic sampling and analysis have the benefits of being minimally invasive, cost effective, widely available, and portable; other advantages include rapid processing times and less equipment required for staining and processing of the sample. Cytologic collection methods for the sinonasal tract include exfoliation, fine needle aspiration biopsy (FNAB), touch imprint of core or excisional biopsies, and nasal or sinus contents aspiration.

In some cases, cytologic sampling will show only normal components of the sinonasal tract. Additionally, we expect normal components to be present in the background of preparations in most cases, allowing pathologists to appreciate the contrasting morphology when lesional sampling is present. Therefore, it is important to recognize expected components when assessing cytologic samples from the sinonasal region. The anterior portion of the nose, the vestibule, is lined by keratinizing, stratified squamous epithelium which then transitions to non-keratinizing, stratified squamous epithelium and ciliated columnar epithelium with admixed mucinous and intermediate cells in the posterior nasal regions and sinuses. Occasional melanocytes may be present, and seromucinous glands underlie the epithelium. Additional details regarding the composition of specialized regions such as the cribriform plate can be found in Chap. 1.

Currently, sinonasal malignancies are most often sampled by cytologic means only after they have metastasized to regional lymph nodes. It is of paramount importance, then, that cytopathologists who review head and neck specimens be familiar with the range of malignancies that occur within the sinonasal tract and understand the lymph node drainage for the tract which includes the intra- and periparotid lymph nodes as well as the retropharyngeal lymph nodes and cervical chain.

4.2 Reactive and Infectious Lesions

The sinonasal tract is exposed to a number of infectious entities and environmental allergens and toxins. In large reports of sinonasal mass lesions, nonneoplastic entities outnumber neoplastic masses by more than 2:1 [4–6]. The cytologic appearance of many of these conditions can be non-specific with a differential diagnosis including infection, reactive changes, hamartomatous and neoplastic lesions (Table 4.1). Therefore, it is important to consider a broad differential and employ ancillary studies when indicated. The early identification of an infectious process can prevent delays in treatment and help guide appropriate management for these patients.

4.2.1 Infectious Lesions

Many infectious entities involving the sinonasal tract, such as viral infections that lead to acute sinusitis, are treated clinically and rarely sampled. Other fungal, bacterial and rare protozoal infections may present as mass-forming lesions or may contribute to the development of chronic sinusitis, which may present as a mass lesion, leading to biopsy or resection [7].

F. D. Allard (✉)
University of Arkansas for Medical Sciences,
Little Rock, AR, USA
e-mail: FDAllard@UAMS.edu

E. B. Stelow
University of Virginia Medical Center, Charlottesville, VA, USA
e-mail: es7yj@virginia.edu

D. Jain, J. Bishop (eds.), *Atlas of Sinonasal Tract Pathology*, https://doi.org/10.1007/978-981-19-7315-4_4

Table 4.1 Differential diagnoses of reactive and infectious lesions of sinonasal tract

Entity	Diagnostic clues
Infectious disease	
Tuberculosis	Caseating granulomas; AFB stain may reveal mycobacteria
Leprosy	Modified Ziehl–Neelsen stain often demonstrates numerous intracellular bacilli
Rhinoscleroma	Steiner stain highlights gram-negative rods within macrophages (Mikulicz cells)
Histoplasmosis	GMS stain highlights yeast forms within macrophages
Mucocutaneous leishmaniasis	Amastigotes with perinuclear kinetoplast within macrophages
Vasculitides	
Granulomatosis with polyangiitis	Positive cANCA serology; often kidney and/or lung disease as well
Allergic granulomatosis and angiitis	History of asthma and hypereosinophilia with pulmonary and cutaneous manifestations
Other	
Sarcoidosis	Hypercalcinuria and elevated serum ACE levels, pulmonary symptoms and lymphadenopathy
Intranasal cocaine use	History of intranasal drug use with necrosis of the nasal mucosa and cartilage
Myospherulosis	History of nasal packing following prior surgery/medical intervention
Peritumoral effect	Mass lesion present clinically; histochemical stains and cultures negative for microorganisms
Lymphoma	Atypical lymphoid cells present morphologically or detected on flow cytometry

4.2.1.1 Allergic Fungal Sinusitis

Allergic fungal sinusitis (AFS) is a subtype of chronic rhinosinusitis (CRS) that is characterized by the accumulation of thick, tenacious mucus containing marked eosinophilic inflammation, often called allergic-type mucus, and nasal polyposis [8, 9]. Smear slides made from intranasal swabbing or sinus aspirates in these cases can demonstrate eosinophil-rich mucin, Charcot–Leyden crystals, and scattered fungal hyphae (Fig. 4.1) [10, 11]. Giemsa or silver stains can be used to highlight fungal hyphae which are most often *Bipolaris, Curvularia, Aspergillus, Exserohilum,* and *Drechslera* species [12]. While the presence of allergic mucus is not specific to AFS and may be present in other allergic conditions, the confirmation of allergic-type mucus as well as the presence of fungal hyphae can support a clinical diagnosis of AFS when taken in the context of supporting clinical and radiologic data [13].

4.2.1.2 Sinus Mycetoma (Fungus Ball)

Mycetoma of the sinuses is most frequently caused by the ubiquitous fungus *Aspergillus fumigatus* and most commonly involves the maxillary sinuses. The material collected from fine needle aspiration biopsies will appear grossly purulent or cheesy. Smear slides or cell block preparation will demonstrate the presence of fungal hyphae, multinucleated giant cells and mixed inflammation with an absence of allergic-type mucus [14, 15]. Fungal hyphae should be readily apparent; however, silver stains can be used to highlight the hyphae which will appear thin with 45-degree angle branching (Fig. 4.2).

4.2.1.3 Invasive Fungal Sinusitis

Invasive fungal infections often present as locally destructive mass lesions in immunocompromised individuals whose clinical differential often includes infectious and malignant etiologies. The fungi most often implicated include species of *Aspergillus, Fusarium,* and the Mucorales [16, 17]. Aspirate smears from these lesions are often cellular and contain multinucleated giant cells and fungal hyphae in a background of blood and mixed, variably granulomatous inflammation [18–20]. Silver and periodic acid Schiff stains may be used to highlight fungal forms if they are not readily apparent. Of note, although eosinophils may be seen in the inflammatory milieu associated with invasive fugal sinusitis, the allergic-type mucus seen in AFS is not present.

4.2.1.4 Nasal Tuberculosis

Sinonasal tuberculosis (TB) is uncommon and generally seen secondary to pulmonary tuberculosis, although rare cases of primary sinonasal TB have been reported [21–23]. Diagnosis of nasal TB via cytologic sampling of nasal lesions is rarely reported in the literature; however, FNAB sampling of associated head and neck lymphadenopathy is reported to be highly effective in establishing a diagnosis [3, 24, 25]. Similar to the findings seen on FNAB from pulmonary TB cases, cytomorphology will reveal a mixture of granulomatous inflammation, necrosis, and epithelioid histocytes. Staining with acid-fast stains such as Ziehl–Neelsen may confirm the presence of acid-fast bacilli (Figs. 4.3 and 4.4).

4.2.1.5 Nasal Leprosy

Many regions of the world where *Mycobacterium leprae* infection is endemic have limited access to the histopathologic processing techniques required for diagnosis via biopsy. Therefore, studies have been conducted to determine the effectiveness of FNAB as a method to procure material for cytomorphologic analysis, special stains, and potential molecular studies for the diagnosis of leprosy and have shown good results [26–30]. Aspirates from *M. leprae* lesions tend to be cellular and comprised of foamy macrophages and epithelioid granulomas without necrosis. Neutrophilic or lymphocytic inflammation may be present in the background. Staining with a modified Ziehl–Neelsen stain often demonstrates numerous bacilli within the macrophages.

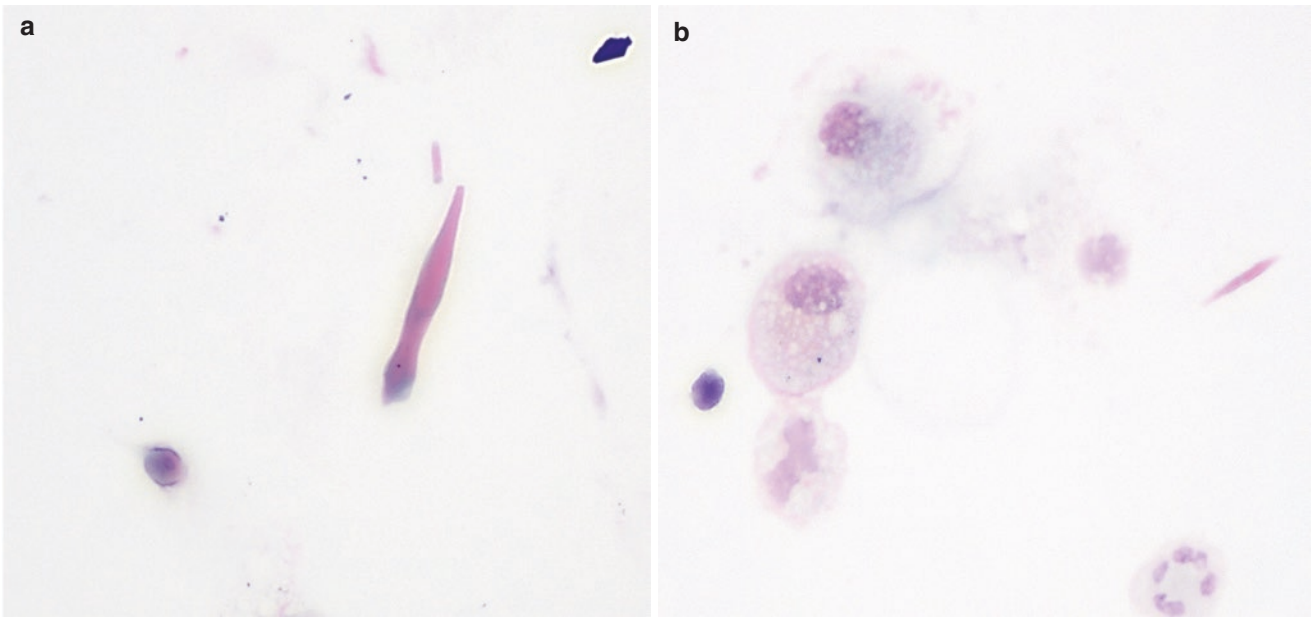

Fig. 4.1 A ThinPrep preparation of a sinus aspirate demonstrates Charcot–Leyden crystals in a background of mixed inflammation (**a**, **b**, 600x, Papanicolaou stain)

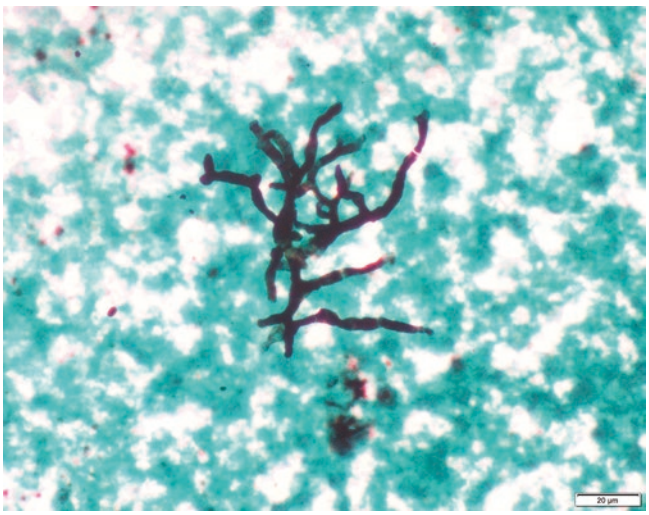

Fig. 4.2 Gomori methenamine silver stain shows acute angle branching fungal hyphae with regular constrictions/septations present in a necrotic background (600x) (contributed by Deepali Jain)

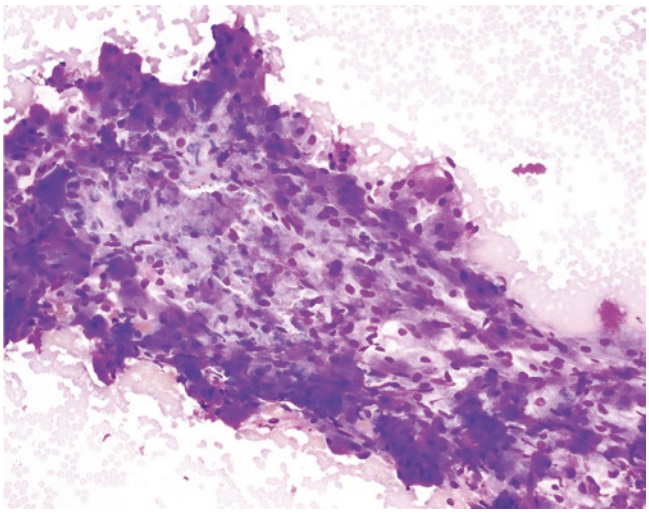

Fig. 4.3 Aspirate smears from regional lymph nodes involved by tuberculosis demonstrate granulomatous inflammation comprised of epithelioid histiocytes (200x, Romanowsky stain). A background of necrosis may be present

4.2.1.6 Rhinoscleroma

Rhinoscleroma is a chronic granulomatous disease that may involve the nasal cavity, nasopharynx, oral cavity, larynx, trachea, or bronchi and is rarely seen outside of regions in which it is endemic. It is caused by infection with the Gram-negative, encapsulated bacillus *Klebsiella rhinoscleromatis*, and is endemic to certain regions of Africa, Southeast Asia, Mexico, Central and South America, and Central and Eastern Europe [31–33]. The nasal cavity is the most frequently affected location in the body, involved in 95–100% of reported cases. Cytologic sampling of rhinoscleroma has only rarely been described in the literature. The reported cytomorphologic features mirror the histomorphologic features and include the presence of foamy macrophages in a background of lymphoplasmacytic inflammation [34].

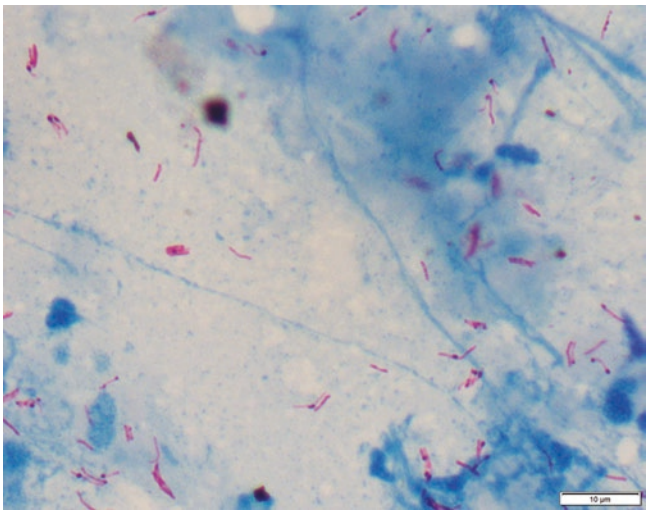

Fig. 4.4 A Ziehl–Neelsen histochemical stain demonstrates acid-fast bacilli (600x) (contributed by Deepali Jain)

Performance of a Gram, Steiner, or Warthin–Starry stain will highlight gram-negative rods within the macrophages, thus demonstrating the presence of *Klebsiella rhinoscleromatis* within the pathognomonic Mikulicz cells [35] (Fig. 4.5).

4.2.1.7 Histoplasmosis

Histoplasmosis is a systemic mycosis caused by the dimorphic fungus *Histoplasma capsulatum* that may rarely involve the mucous membranes, including the sinuses and nose, generally in immunocompromised hosts [36, 37]. Rare cases of sinus contents aspirates being used for the diagnosis of histoplasmosis have been reported [37, 38]. The cytomorphologic features described in these reports as well as in studies including FNAB of regional lymphadenopathy include the presence of foamy histiocytes, epithelioid granulomas, and multinucleated giant cells in a background of acute inflammation with variable necrosis [39]. Periodic Acid-Schiff (PAS), Gomori methenamine silver (GMS), and Giemsa stains will highlight the fungal forms present within histiocytes (Fig. 4.6).

4.2.1.8 Mucocutaneous Leishmaniasis

Another rare infectious entity that may affect the nose is the mucocutaneous form of leishmaniasis [40, 41]. Rare reports in the literature have described the use of FNAB as well as cutaneous scrape preparations in the diagnosis of cutaneous leishmaniasis presenting as nasal mass lesions [42, 43]. Smears show dense lymphohistiocytic inflammation with small oval organisms consistent with *Leishmania* amastigotes present within histiocytes (Fig. 4.7). The identification of leishmanial amastigotes with the diagnostic bar-like kinetoplast adjacent to the nucleus on Giemsa stained smears prepared from the nasal lesion is key to diagnosing this infectious lesion [44].

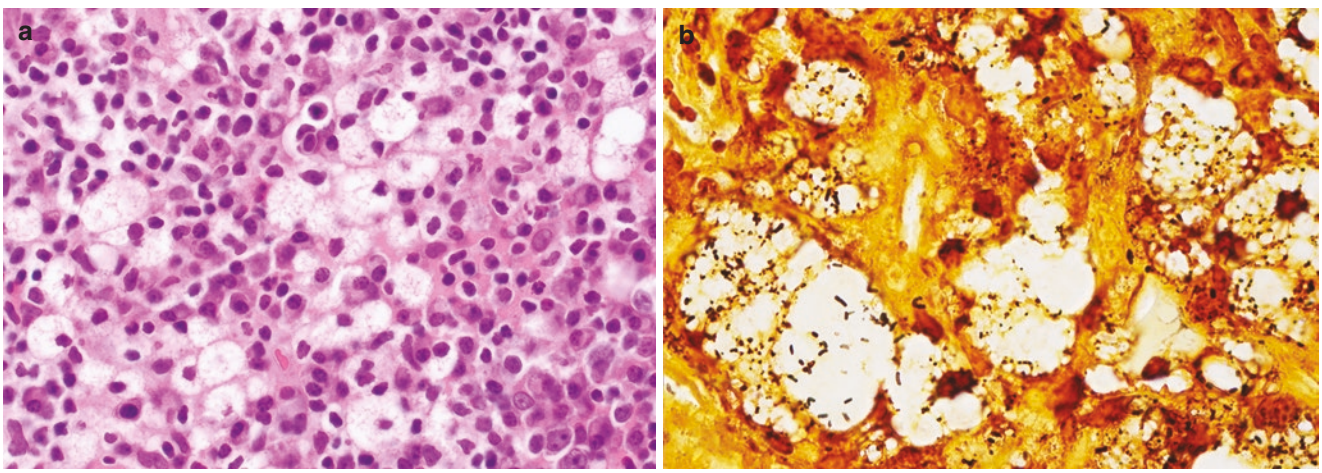

Fig. 4.5 Cell block preparations will demonstrate numerous large, foamy macrophages in a background of plasma-cell dominant chronic inflammation with occasional Russell bodies (**a**, 400x, H&E). A Steiner stain highlights numerous bacilli within the cytoplasm of the Mikulicz cells (**b**, 600x)

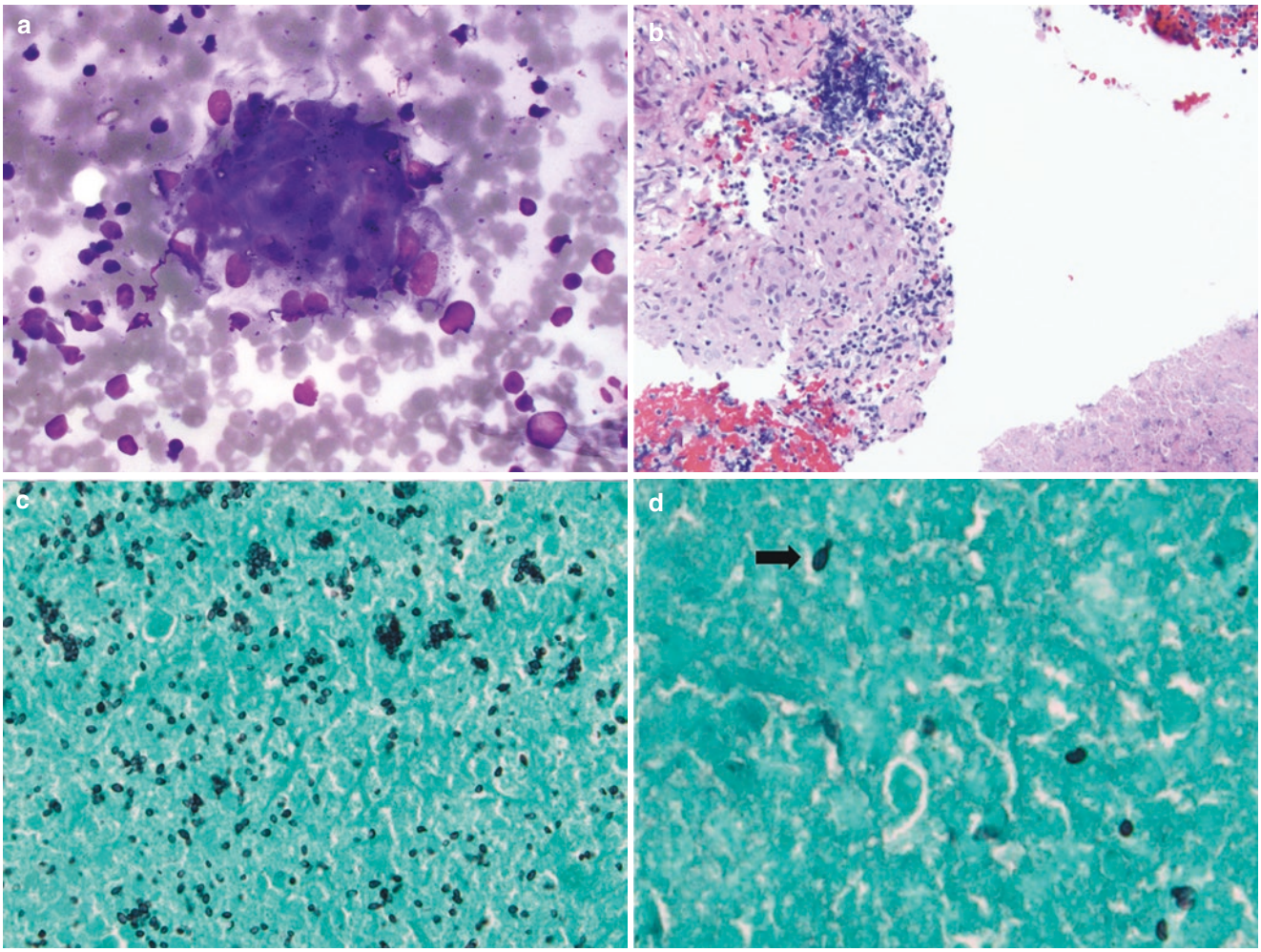

Fig. 4.6 Aspirate smear (**a**, 400x, Romanowsky stain) and cell block preparations from a lymph node involved by histoplasmosis demonstrate epithelioid granulomata with a background of necrosis seen in the cell block preparation (**b**, 200x, H&E). A silver stain highlights the intracellular yeast forms present within the macrophages (**c**, 600x, GMS), with narrow-based budding forms identified (**d**, arrow, 600x, GMS)

4.2.2 Reactive Lesions

Many chronic inflammatory processes that affect the sinonasal tract, as well as other regions of the upper respiratory tract, have significant morphologic overlap with the infectious processes described above. They can also present as mass lesions, raising clinical concern for malignancy and leading to cytologic sampling. Sarcoidosis, granulomatosis with polyangiitis (formerly Wegener's granulomatosis), and extranodal Rosai–Dorfman disease (RDD) are chronic inflammatory processes that can also involve the upper airways and may be difficult to differentiate histologically without the use of immunohistochemical and histochemical stains. These lesions will be negative for microorganisms, via histochemical stains or culture, and have other cytomorphologic and immunohistochemical features that can be helpful in their diagnosis.

4.2.2.1 Sarcoidosis

Sarcoidosis is a systemic disease that has been reported to involve the upper airways in 0.7–6% of affected patients in various studies [45, 46]. FNAB of cervical lymphadenopathy associated with cases of sinonasal sarcoidosis yield the same classic cytologic findings of noncaseating epithelioid granulomas present in a background of giant cells and lymphocytes as seen in cases of pulmonary sarcoidosis [47–49] (Fig. 4.8).

4.2.2.2 Granulomatosis with Polyangiitis

Granulomatosis with polyangiitis (GPA) frequently involves the upper airways [50, 51]. While the histopathologic features of GPA involving the sinonasal tract are well established in the literature, cytologic sampling in this location is not well described. Presumably, if GPA of the sinonasal tract was to be sampled, it would appear cytomorphologically similar to GPA of the lung and other anatomic loca-

tions where FNAB and exfoliated specimens demonstrate epithelioid granulomas, giant cells, and reactive epithelial cells in a background of blood and dirty necrosis [52] (Fig. 4.9). While these findings are non-specific, correlation with serologic studies for c-ANCA may be helpful clinically.

4.2.2.3 Sinus Histiocytosis with Massive Lymphadenopathy (Rosai–Dorfman Disease)

Sinus histiocytosis with massive lymphadenopathy (Rosai–Dorfman disease) (RDD) classically presents with massive cervical lymphadenopathy; however, extranodal involvement, including involvement of the sinonasal tract, can be present [53, 54]. Cytologic sampling of nasal RDD yields highly cellular aspirates containing numerous histocytes exhibiting the distinctive finding of emperipolesis in a background of lymphocytes and plasma cells [55, 56] (Fig. 4.10). If immunohistochemical stains are performed, they will demonstrate that the macrophages are immunoreactive for both S100 and CD68.

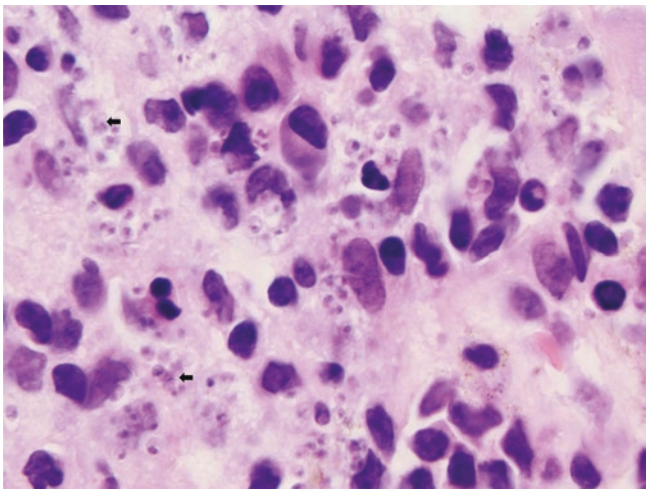

Fig. 4.7 Sampling of a skin lesion from a patient with cutaneous leishmaniasis demonstrates lymphohistiocytic inflammation with numerous leishmanial amastigotes present within the histiocytes. The diagnostic bar-like kinetoplast is visible within some amastigotes (arrows, 1000x, H&E)

4.3 Other Nonneoplastic Lesions

4.3.1 Cystic Lesions

A number of nonneoplastic cysts occur in the sinonasal tract. In one large study of all sinonasal FNAB seen in one institution over the course of 20 years, nonneoplastic cysts comprised 15.2% of total cases [3].

4.3.1.1 Mucocele

Mucoceles may occur in any of the paranasal sinuses, but most commonly occur in the frontal sinuses. They are benign cystic lesions that form secondary to obstruction of the sinus outlet. While reports of these lesions being sampled via FNAB exist in the literature, these reports do not contain a description of the cytomorphologic features [3, 57]. However, the features are likely similar to those of mucoceles of other head and neck regions, such as the oral cavity and tongue, where aspirate smears are sparely cellular, showing scattered epithelial cells and macrophages in a background of abundant mucus [58, 59].

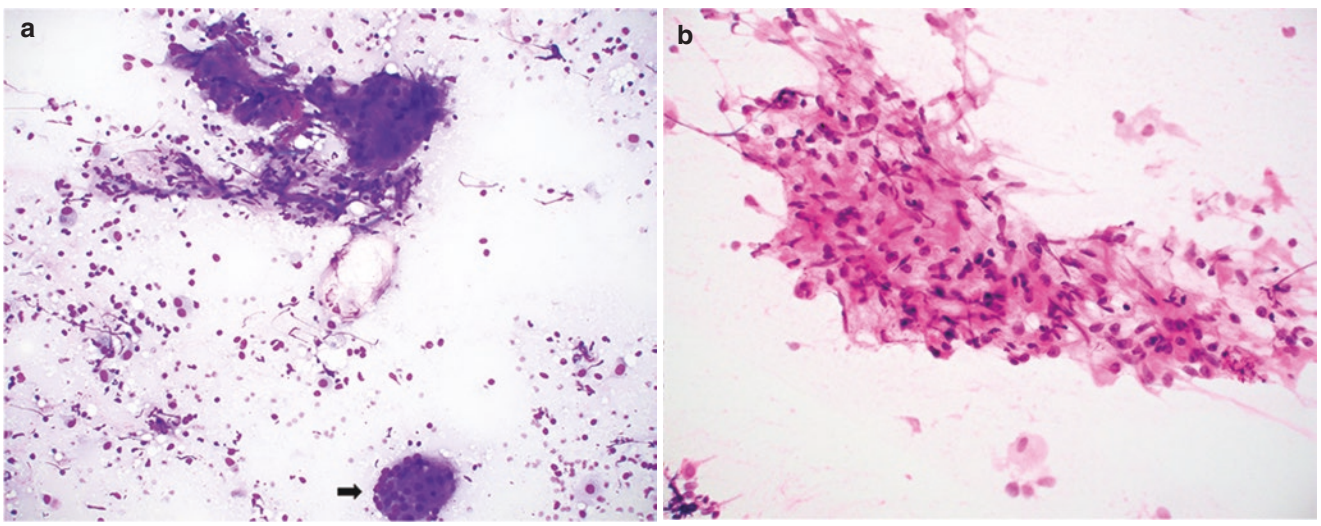

Fig. 4.8 Aspirate smears of sarcoidosis may demonstrate non-necrotizing granulomata (**a**, 200x, Romanowsky stain & **b**, 400x, Papanicolaou stain) present in a background of multinucleated giant cells (**b**, arrow)

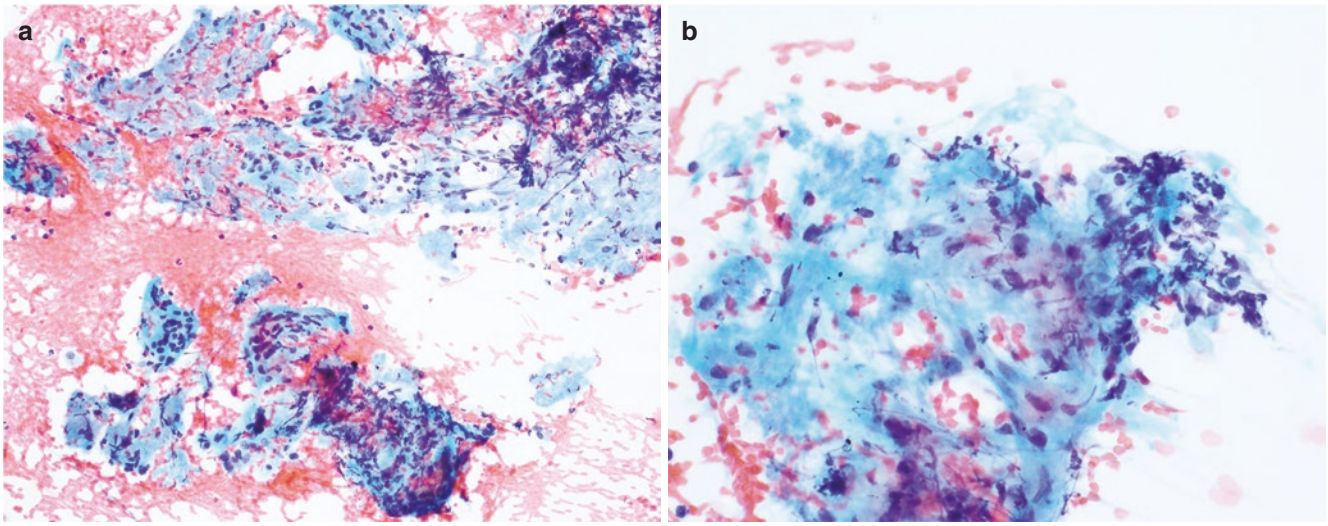

Fig. 4.9 In this example of granulomatosis with polyangiitis, aspirate smears demonstrate poorly formed granulomata and multinucleate giant cells (**a**, 200x, Papanicolaou stain) present in a background of blood and proteinaceous debris (**b**, 400x, Papanicolaou stain)

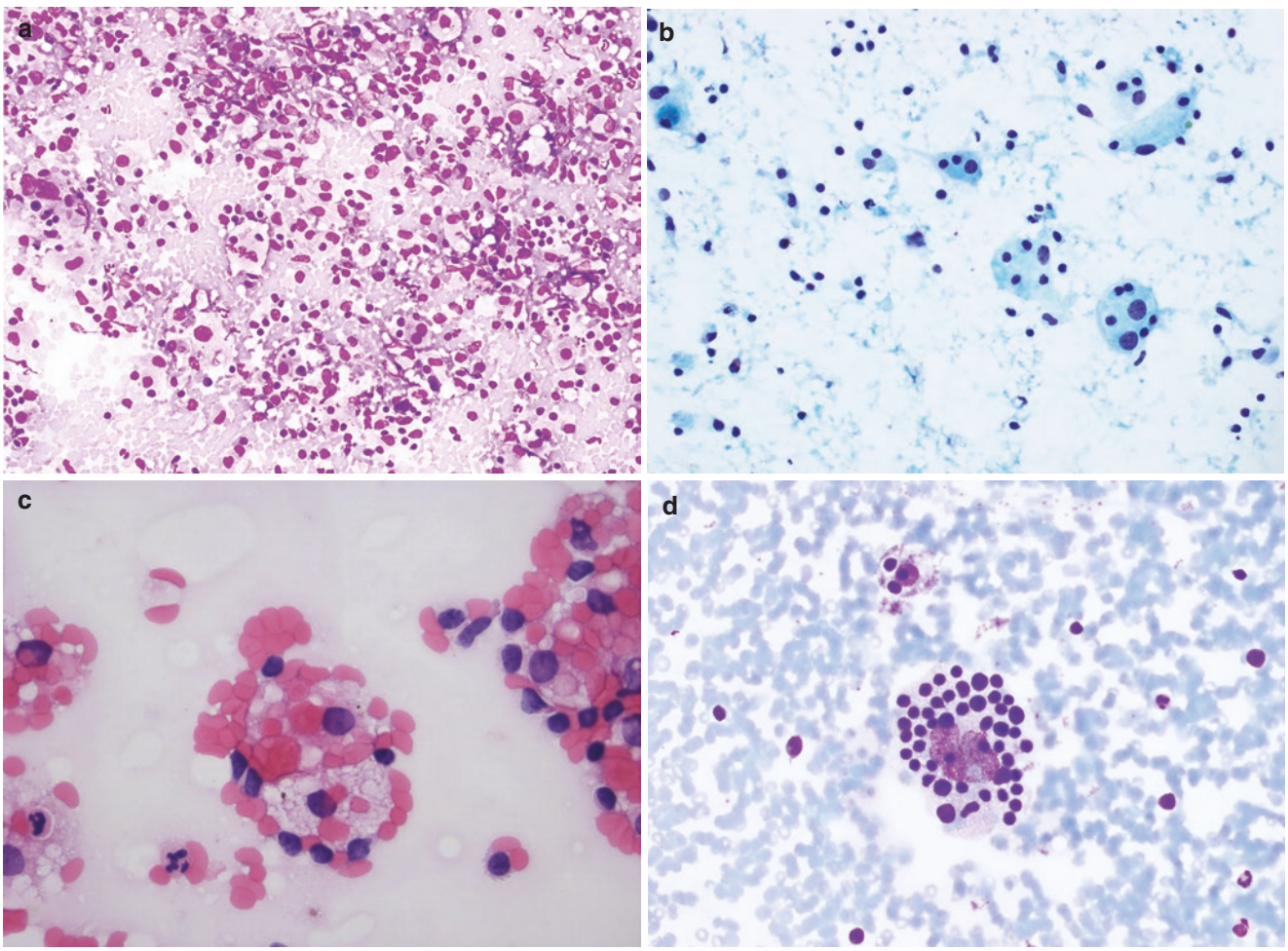

Fig. 4.10 Sinus histiocytosis with massive lymphadenopathy (Rosai–Dorfman disease) will yield cellular smears (**a**, 200x, Romanowsky stain) comprised of large histiocytes accompanied by plasma cells and lymphocytes (**b**, 400x, Papanicolaou stain). Histiocytes demonstrate emperipolesis (**c**, 600x, H&E) and may have large nuclei and some atypia (**d**, 600x, Romanowsky stain)

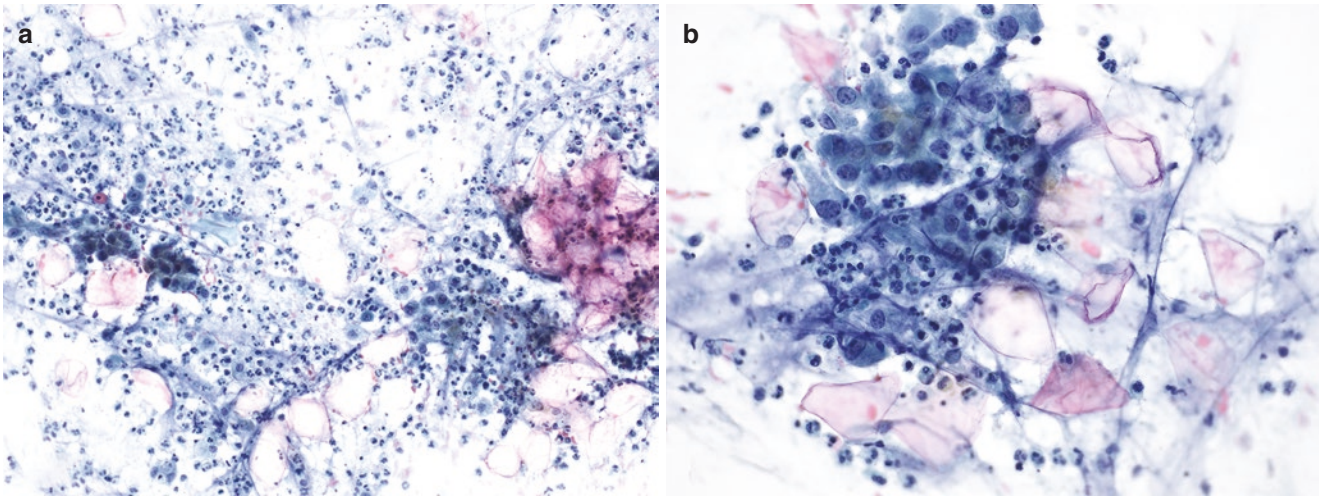

Fig. 4.11 This FNA sample of a dermoid cyst is cellular with numerous anucleate and nucleate squamous cells in a background of acute inflammation (**a**, **b**, 200x & 400x, Papanicolaou stain)

4.3.1.2 Dermoid Cyst

Dermoid cysts of the nasal tract arise from the sequestration of ectoderm during the ossification of the frontonasal plate during embryologic development [60]. These lesions are most often identified at birth and are most commonly located on the dorsum of the nose. Aspirates of dermoid cysts appear morphologically similar to aspirates of epidermal inclusion cysts. Smears are cellular with numerous anucleate and nucleate squamous cells with keratinaceous debris in the background (Fig. 4.11) [61, 62]. Histologic sections of resected lesions will demonstrate adnexal structures such as sebaceous glands, eccrine ducts, and hair follicles within the wall of the cyst that may not be apparent on FNAB.

4.4 Epithelial Neoplasms

Many neoplasms of the sinonasal tract exhibit squamous differentiation, which cytologic preparations are particularly well suited to identify. However, precise classification of many lesions remains problematic without the architecture provided by histologic evaluation of biopsy or excision specimens. Nevertheless, it is generally possible to distinguish benign and low-grade lesions from high-grade lesions. Additionally, with the recent identification of several diagnostic markers for specific lesions that involve the sinonasal tract, the ability of FNAB to collect material for immunohistochemical stains and molecular studies presents the potential to widely expand the role of cytology in the clinical management of these lesions.

4.4.1 Benign and Low-Grade Epithelial Lesions

Benign and Low-Grade Squamous Lesions

The finding of bland or mildly atypical squamous cells on cytologic preparations is not specific to any single entity or class of disease. Squamous cells with a mature, bland appearance or with mild hyperchromasia, slight nuclear enlargement, and variable background inflammation can be seen in squamous papillomas, well-differentiated squamous cell carcinomas, pseudoepitheliomatous hyperplasia, sialometaplasia, and various reactive and infectious lesions. Therefore, while these entities can be sampled and assessed cytologically, it is virtually impossible for the cytopathologist to render a specific diagnosis in this setting (Table 4.2).

4.4.2 Malignant Epithelial Tumors

4.4.2.1 Squamous Cell Carcinoma

The majority of the malignant sinonasal tract tumors are squamous cell carcinoma (SCC) and its variants. SCC of the sinonasal tract are classified as keratinizing (conventional) and non-keratinizing types, with keratinizing SCC occurring more frequently. SCC arising in the nasal cavity are generally keratinizing and well-differentiated, while those arising in the sinuses are non-keratinizing and moderately to poorly differentiated [63]. Certain SCC subtypes that occur in the sinonasal tract such as spindle cell (sarcomatoid) SCC, lymphoepithelial carcinoma, papillary SCC, and basaloid SCC pose diagnostic

challenges, especially on small biopsy and cytologic sampling, as significant morphologic overlap can be seen across these variants and other benign and malignant entities.

Keratinizing Squamous Cell Carcinoma

Keratinizing (conventional) SCC is readily recognized on cytologic preparations. Aspirate smears are generally cellular and demonstrate two-dimensional clusters of malignant squamous cells with both intracellular and extracellular keratinization. The degree of nuclear atypia and increase in nuclear-to-cytoplasmic ratio can vary, but cytologic atypia will be present. Coarse chromatin, nuclear membrane irregularities, and mitotic figures are generally seen (Fig. 4.12). Mixed inflammation and necrosis can be present.

Table 4.2 Bland-appearing squamous lesions

Reactive squamous mucosa
Pseudoepitheliomatous hyperplasia
Inflammatory polyp
Sinonasal papillomas
Well-differentiated squamous cell carcinoma variants:
Papillary squamous cell carcinoma
Verrucous squamous cell carcinoma

Non-keratinizing Squamous Cell Carcinoma

Non-keratinizing SCC (NKSCC) are less common than their keratinizing counterparts and pose a diagnostic challenge to cytopathologists as they can demonstrate morphologic overlap with other "basaloid" malignancies of the sinonasal tract (Table 4.3). NKSCC yields cellular aspirates comprised of clusters of basaloid cells showing high nuclear-to-cytoplasmic ratios, hyperchromasia, nuclear membrane irregularities, and increased mitotic activity (Fig. 4.13). Prominent nucleoli may be present and necrosis can be seen in the background. As 30–50% of sinonasal tract NKSCC harbor transcriptionally active high-risk human papilloma virus (HPV), immunohistochemical staining for p16, in addition to markers of squamous differentiation such as p40, p63, and CK5/6 may be of diagnostic utility [64–67].

Spindle Cell Carcinoma

Spindle cell carcinoma of the upper aerodigestive tract is a rare, poorly differentiated variant of SCC characterized by the spindled and/or pleomorphic morphology of the malignant cells. In most reported cases, both epithelioid and spindle cells are present in aspirates, with the spindle cells appearing as insolated cells with indistinct cytoplasmic borders, hyperchromatic, ovoid nuclei with variably prominent

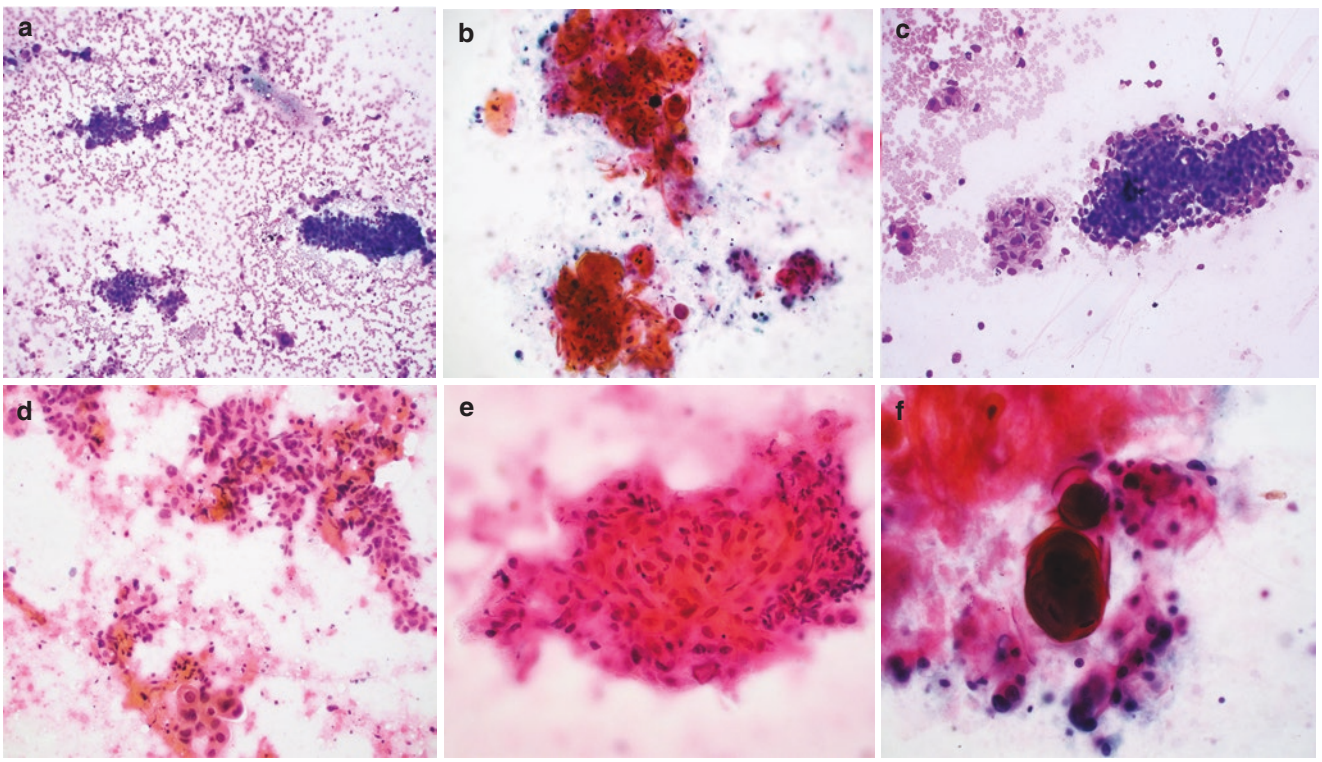

Fig. 4.12 Aspirate smears of keratinizing squamous cell carcinomas are generally cellular (**a**, 100x, Romanowsky stain & **b**, 200x, Papanicolaou stain). Smears demonstrate epithelioid cells present in two-dimensional sheets (**c**, 200x, Romanowsky stain) with a Papanicolaou stain highlighting intracellular (**d**, 200x & **e**, 400x) and extracellular (**f**, 600x) keratinization. Cytologic atypia including nuclear enlargement and hyperchromasia is present

Table 4.3 Basaloid malignancies of the sinonasal tract

Entity	Diagnostic clues
Non-keratinizing squamous cell carcinoma	Immunoreactive for p40, p63 and may be p16/HPV positive
SMARCB1 (INI-1)-deficient sinonasal carcinoma	Loss of nuclear immunoreactivity for SMARCB1 (INI-1), HPV negative, variable p40 and neuroendocrine marker expression
NUT carcinoma	Nuclear immunoreactivity for NUT immunostain, HPV negative, p40 positive, neuroendocrine markers usually negative
Sinonasal undifferentiated carcinoma	Keratin positive; p63/p40 and neuroendocrine markers are usually negative
Neuroendocrine carcinoma	Neuroendocrine markers, TTF-1, and p16 positive with dot-like keratin staining
Cellular pleomorphic adenoma	Metachromatic stroma variably present, variable myoepithelial marker expression: SMA, S100, calponin, p63
Adenoid cystic carcinoma	Metachromatic hyaline globules variably present; CD117, pankeratin, and myoepithelial marker immunoreactivity

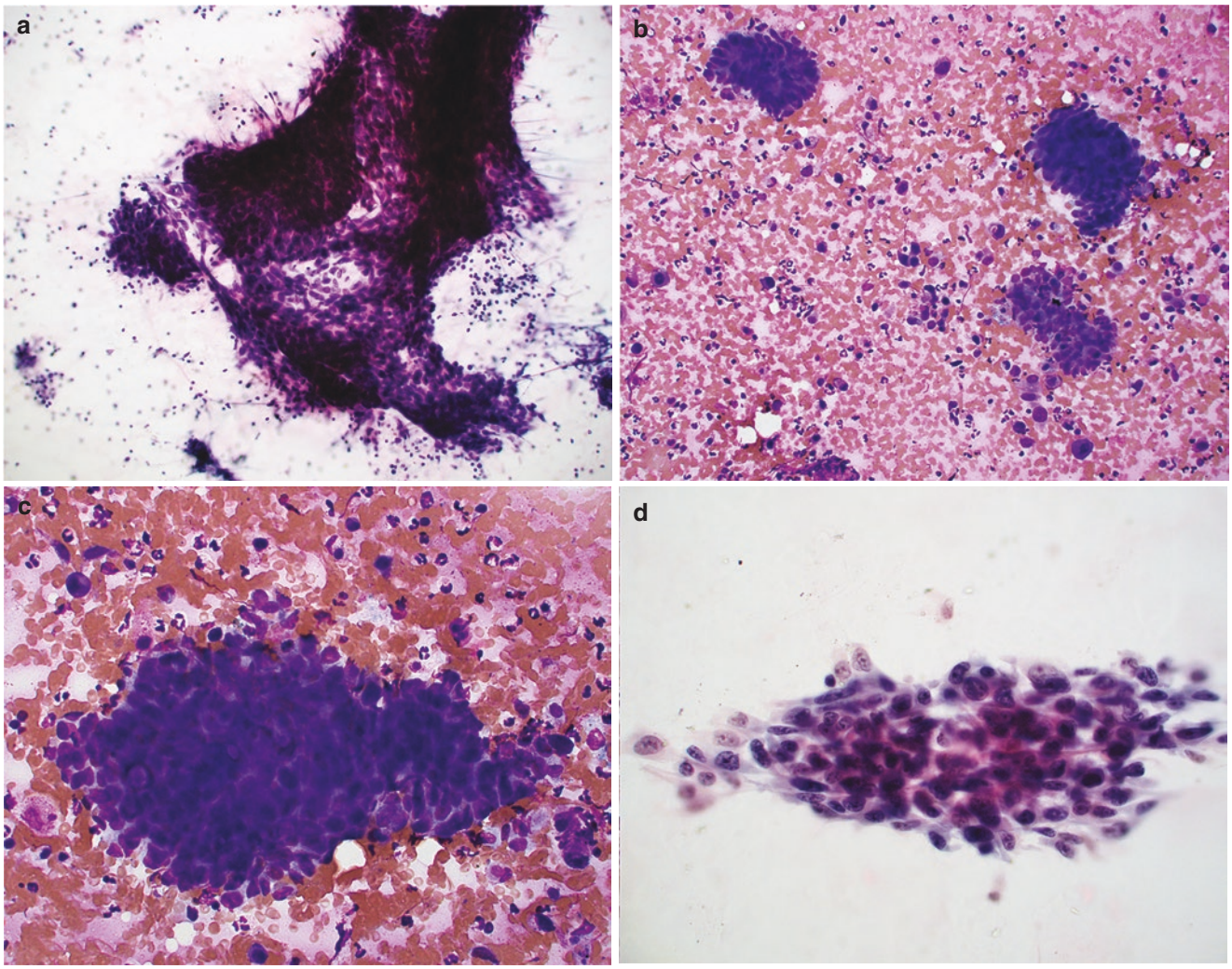

Fig. 4.13 Aspirate smears of non-keratinizing squamous cell carcinomas are generally cellular (**a**, 200x, Papanicolaou stain & **b**, 200x, Romanowsky stain). Smears demonstrate clusters of basaloid cells with high nuclear-to-cytoplasmic ratios, nuclear hyperchromasia and varying degrees of anisonucleosis and nuclear membrane irregularities (**c**, 400x, Romanowsky stain & **d**, 400x, Papanicolaou stain)

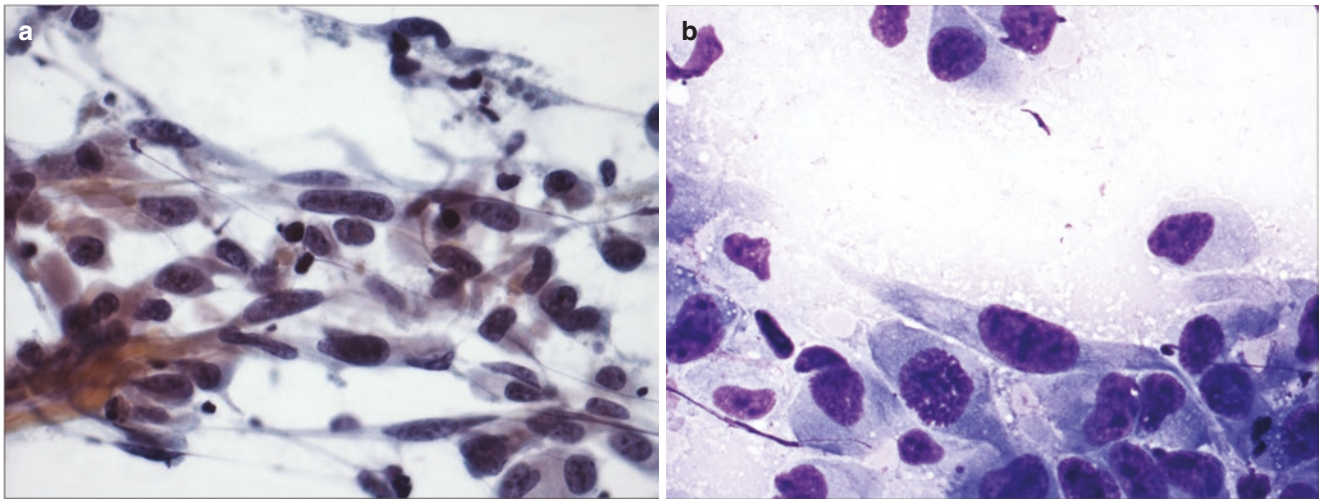

Fig. 4.14 Smear preparations of spindle cell carcinomas are often low-to-moderately cellular and comprised of moderately pleomorphic spindle cells (**a**, 400x, Papanicolaou stain) with mitotic figures generally evident (**b**, 600x, Romanowsky stain)

nucleoli, pleomorphism, and multinucleation [68–71] (Fig. 4.14). The epithelial cells show features of conventional SCC. The diagnosis and differential considered will largely depend on the components and ratio of components sampled. When the conventional SCC component is sampled, a diagnosis of SCC is readily made. If the sample is predominantly comprised of spindled cells, lesions including malignant melanoma, synovial sarcoma, and other high-grade mesenchymal neoplasms could be considered. Immunohistochemical stains may also be helpful in the diagnosis of this SCC variant, as the majority of these lesions will show immunoreactivity for cytokeratins and p63 [72].

Lymphoepithelial Carcinoma

Lymphoepithelial carcinoma is a variant of SCC morphologically similar to undifferentiated nasopharyngeal carcinoma that is highly associated with Epstein–Barr virus (EBV). This variant is rarely reported and most known cases have been in patients from Asia. FNAB yields highly cellular smears demonstrating cohesive clusters of epithelial cells in a background of mature-appearing lymphocytes. The epithelial cells are large with indistinct cytoplasmic borders, high nuclear-to-cytoplasmic ratios, and vesicular chromatin with prominent nucleoli [73–76] (Fig. 4.15).

4.4.2.2 Non-SCC Basaloid/Round Cell Epithelial Tumors

SMARCB1 (INI-1)-Deficient Sinonasal Carcinoma

SMARCB1 (INI-1)-deficient sinonasal carcinoma (IDSNC) is a malignancy defined by the inactivation of the *SMARCB1* (*INI-1*) tumor suppressor gene. The majority of FNAB of primary and metastatic lesions described in the literature produce cellular specimens with features of a non-keratinizing SCC. Aspirate smears frequently demonstrate cohesive clusters and sheets of basaloid, oval to polygonal cells with scant cytoplasm and indistinct cell borders present in a background of necrotic debris. However, some cases demonstrate oncocytic or plasmacytoid morphology, resembling myoepithelial or rhabdoid malignancies [77–80] (Fig. 4.16). The nuclei are generally small and uniform with fine chromatin, small nucleoli and mild nuclear membrane irregularities. Moderate anisonucleosis can occasionally be seen; however, overt nuclear pleomorphism has not been reported.

Cytologic features of SMARCA4-deficient SN carcinomas are included in Chap. 8.

NUT Carcinoma

NUT carcinoma is a rare high-grade malignancy that often demonstrates squamous differentiation and is defined by the presence of a fusion oncogene involving the *nuclear protein in testis (NUT) family member 1 gene* (*NUTM1*). Cytologic preparations from aspirations of primary and metastatic sites and effusions demonstrate primitive-appearing cells present singly and in sheets. These cells have high nuclear-to-cytoplasmic ratios with scant amphophilic cytoplasm. The nuclei are round to oval with vesicular chromatin and a single prominent nucleolus. Mitotic figures, apoptotic cells, and necrosis are commonly present [68, 81–83] (Fig. 4.17). A subset of cases show focal, abrupt squamous differentiation with keratinization histologically; however, the presence of keratinization is only rarely described in cytologic samples [84].

Sinonasal Undifferentiated Carcinoma

Sinonasal undifferentiated carcinoma (SNUC) lacks squamous and glandular features and is not distinguished by association with any reproducible molecular aberration or

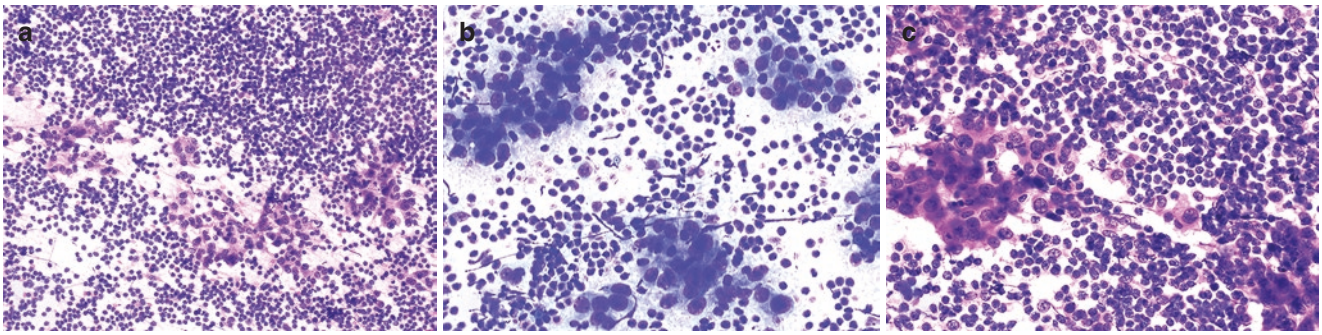

Fig. 4.15 Smear slides show a highly cellular aspirate (**a**, 200x, Romanowsky stain) with clusters of larger epithelioid cells in a background of abundant lymphocytes (**b**, 400x, Romanowsky stain). The large epithelioid cells have indistinct cell boarders and prominent nucleoli (**c**, 400x, Papanicolaou stain)

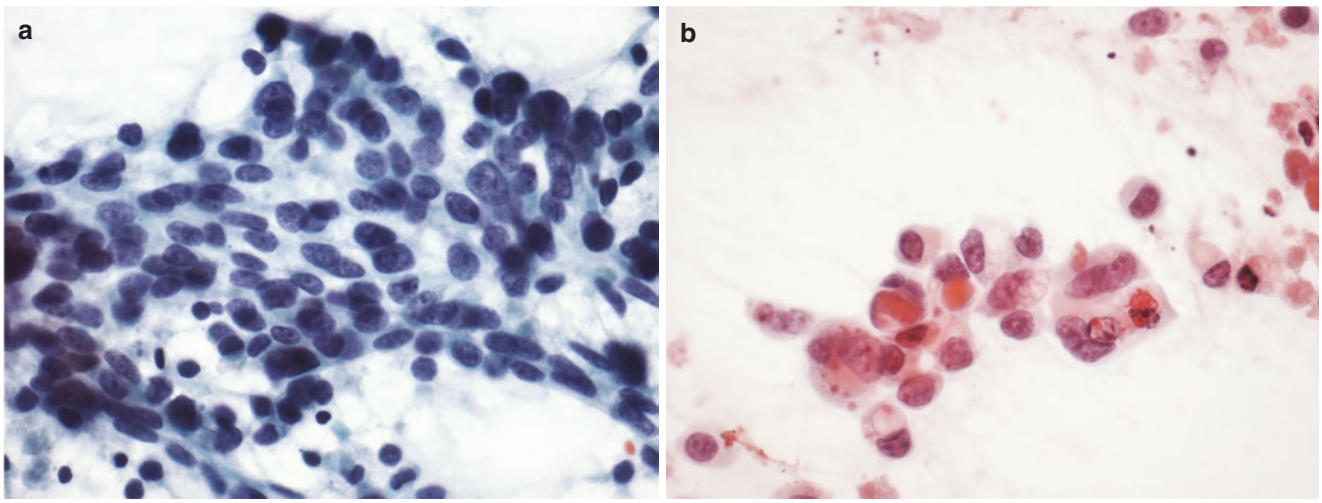

Fig. 4.16 Aspirate smears of SMARCB1-deficient sinonasal carcinoma may demonstrate a spectrum of cytomorphologies from cohesive sheets of basaloid cells (**a**, 600x, Romanowsky stain) to small clusters of cells displaying a more rhabdoid appearance with moderate anisonucleosis, vacuolated cytoplasm, nuclear membrane irregularities, and apoptotic figs. (**b**, 600x, Papanicolaou stain)

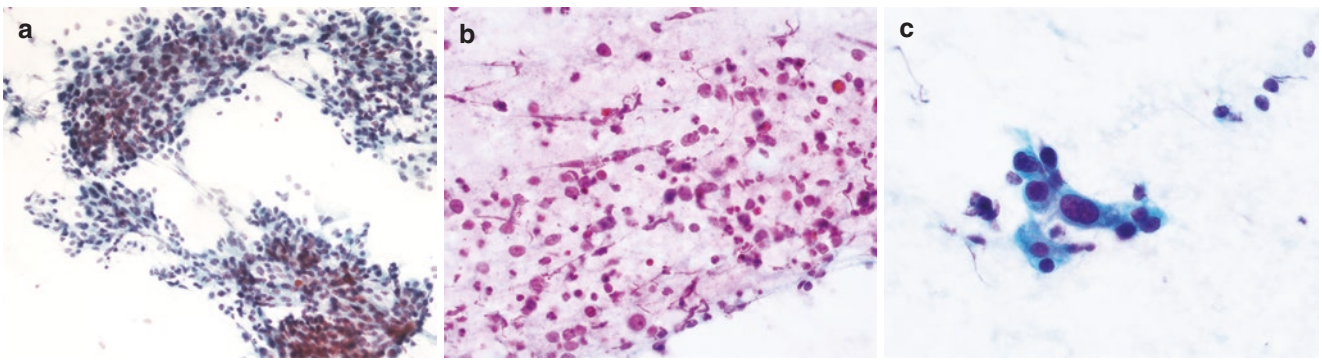

Fig. 4.17 Aspirate smears of NUT carcinomas may demonstrate two-dimensional sheets (**a**, 200x, Papanicolaou stain) or a more dispersed single cell pattern (**b**, 400x, Romanowsky stain) of malignant cells with elevated nuclear to cytoplasmic ratios, amphophilic cytoplasm, and coarse chromatin (**c**, 600x, Papanicolaou stain)

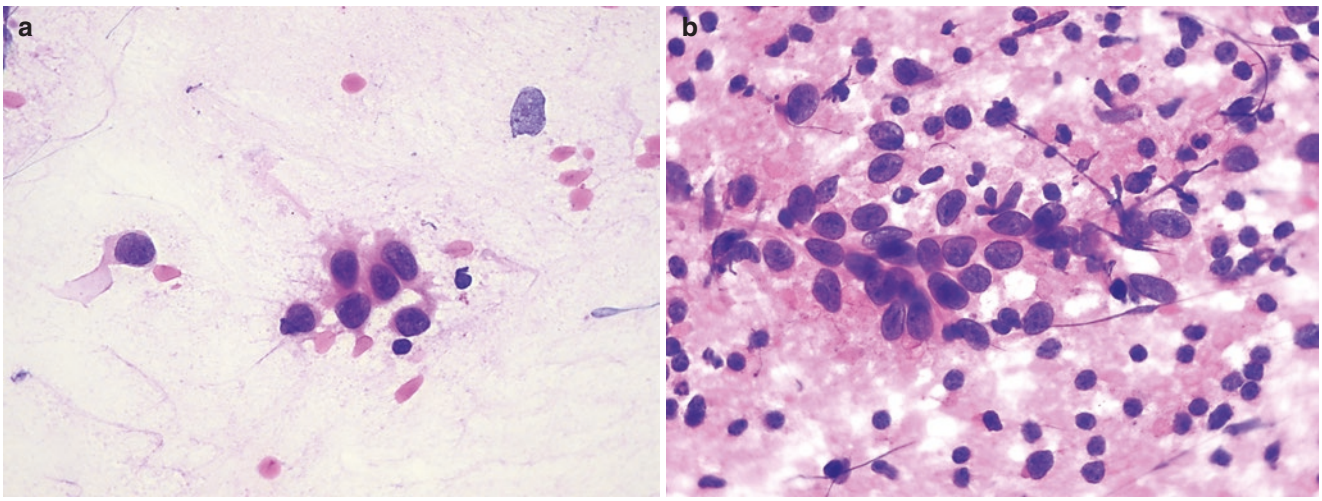

Fig. 4.18 Papanicolaou stained aspirate smears demonstrate epithelioid cells with scant, delicate cytoplasm and fine chromatin present singly and in small clusters (**a**, 600x). Stripped nuclei are present in the background inflammatory cells (**b**, 600x). Mitotic figures and a background of keratin may also be present

etiology such as EBV or HPV. Aspirates of metastatic lesions produce hypercellular smears showing malignant cells present singly and in small loose clusters. The cytoplasm is generally scant and nuclei show irregular contours with finely granular chromatin and indistinct nucleoli. Mitotic figures are readily identified. The background is significant for numerous stripped nuclei, abundant karyorrhectic debris, and mixed inflammatory cells [85] (Fig. 4.18).

4.4.2.3 Adenocarcinomas

Adenocarcinomas in the sinonasal tract can be divided into salivary type and non-salivary type, with non-salivary type being further divided into intestinal type and non-intestinal type. Distinction between the various adenocarcinoma categories that can occur in the sinonasal tract is not always possible via cytologic sampling. However, it is generally possible to separate the high-grade entities, namely: sinonasal intestinal-type adenocarcinoma and adenoid cystic carcinoma, from lower grade tumors.

Intestinal-Type Sinonasal Adenocarcinoma

Intestinal-type sinonasal adenocarcinoma (ITAC) is one of the more common adenocarcinomas to arise in the sinonasal tract and closely resembles colorectal adenocarcinomas morphologically. Rare reports of FNAB sampling of primary and metastatic lesions describe three-dimensional clusters of malignant cells in a background of mucus and inflammatory cells [2, 75, 86] (Fig. 4.19). Just as ITAC are morphologically similar to their colorectal counterparts, they are also immunophenotypically similar, with ITAC being immunoreactive for antibodies against CK20, CDX2, villin, MUC2, and SATB2 [87].

Non-Intestinal Type Adenocarcinoma

Non-intestinal type sinonasal adenocarcinoma (non-ITAC) is a heterogenous category for all adenocarcinomas that arise in the sinonasal tract that do not show features of a salivary gland tumor or intestinal morphology. Various morphologies including papillary growth patterns, oncocytic and clear-cell appearances have been reported on biopsy and resection specimens; however, cytomorphologic data on this group of entities is very limited.

4.4.2.4 Neuroendocrine Carcinomas

Small cell and large cell neuroendocrine carcinomas rarely occur in the sinonasal tract, although they occur more commonly than their well-differentiated counterparts [75]. Morphologically, they appear identical to neuroendocrine carcinomas of other sites. Small cell carcinoma appears as medium-sized cells with scant, delicate cytoplasm and the hallmark features of nuclear molding, frequent single cell necrosis, nuclear streaking, and a high mitotic rate (Fig. 4.20).

Large cell neuroendocrine carcinoma aspirates demonstrate clusters of medium to large cells with scant to moderate cytoplasm, and a nucleus with a prominent single nucleolus. Stripped nuclei, nuclear streaking, and necrosis are also common (Fig. 4.21).

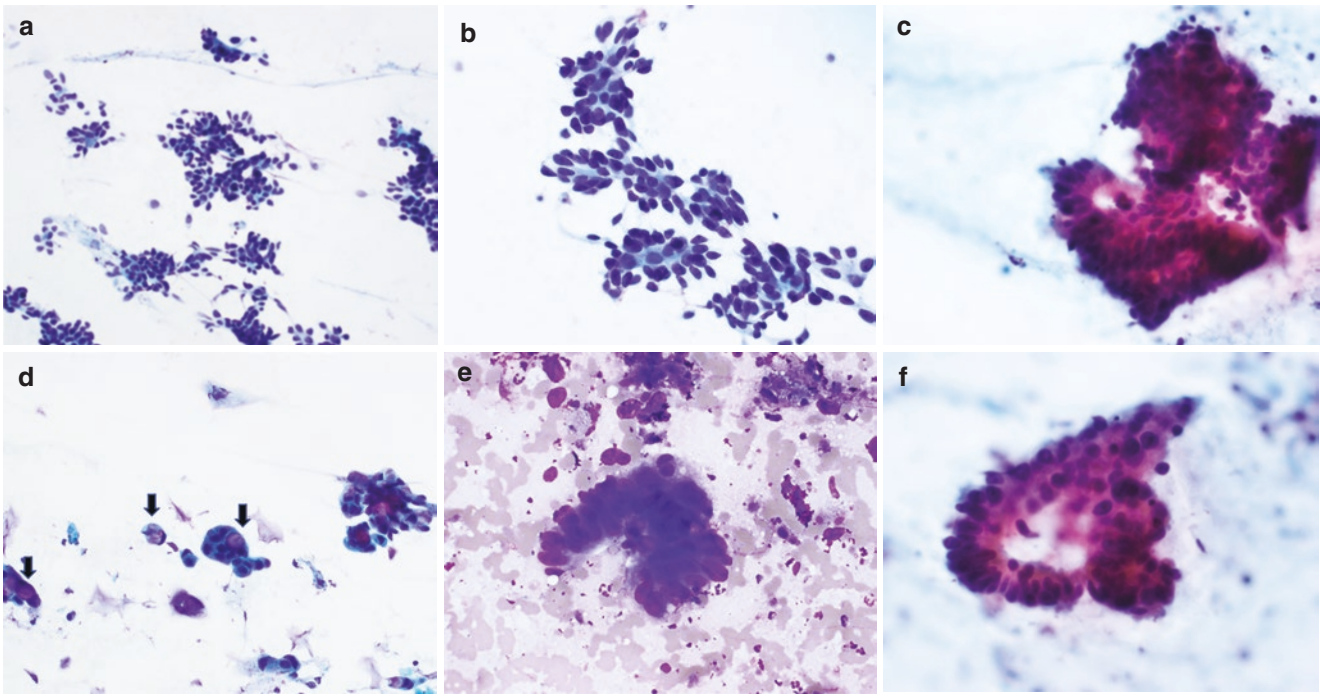

Fig. 4.19 Fine needle aspiration biopsies of intestinal-type sinonasal adenocarcinomas produce three-dimensional clusters of malignant cells (**a**, 200x, Papanicolaou stain; **b**, 400x, Papanicolaou stain & **c,** 400x, Papanicolaou stain). Mucin may be present in the form of intracytoplasmic vacuoles (arrows) or in the background (**d**, 400x, Papanicolaou stain). Some lesions may also demonstrate columnar cells with the traditional nuclear hyperchromasia and pseudostratification associated with enteric-type adenocarcinoma (**e**, 600x, Romanowsky stain; **f**, 600x, Papanicolaou stain)

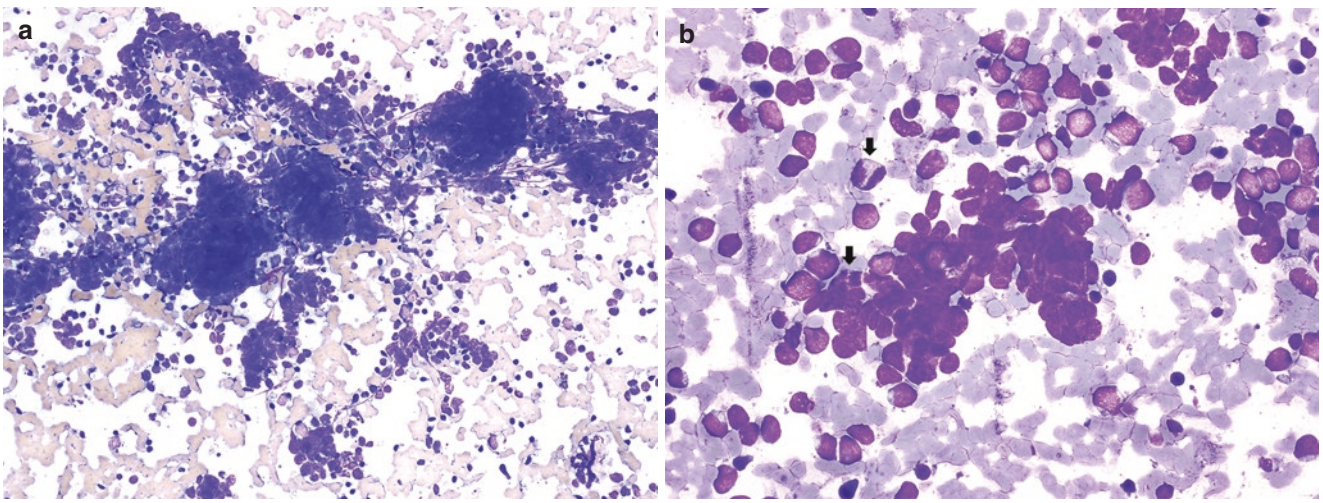

Fig. 4.20 Aspirate smears of small cell carcinomas are frequently cellular and composed of epithelioid cells with very high nuclear-to-cytoplasmic ratios present singly and in fusiform clusters (**a**, 200x, Romanowsky stain). The cytoplasm and nucleus of the malignant cells is fragile and numerous stripped and crushed nuclei are present. Nuclear molding is prominent and mitotic figures are readily identified (arrows). Intact tumor cells show scant cytoplasm and fine chromatin (**b**, 400x, Romanowsky stain)

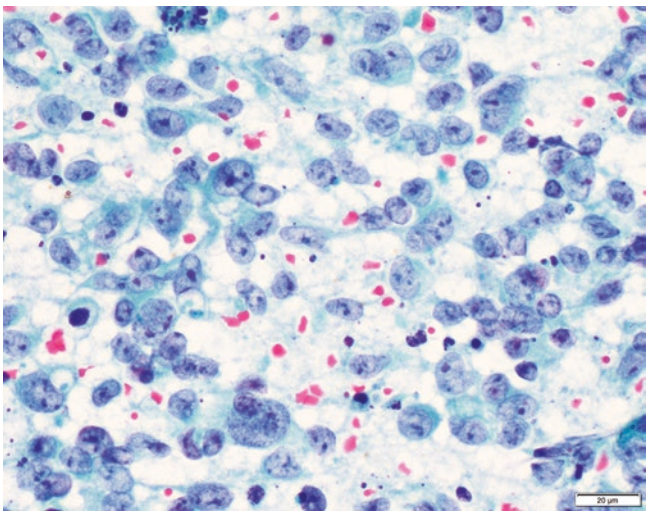

Fig. 4.21 A case of SMARCA4-deficient SN carcinoma which on morphology was large cell neuroendocrine carcinoma phenotype. Metastatic cervical lymph node FNA aspirate reveals similar morphology with large cells, moderate cytoplasm, vesicular chromatin, and prominent nucleoli. BRG1 was lost on immunohistochemistry (not shown) (400x, Papanicolaou stain) (contributed by Deepali Jain)

4.5 Salivary Gland-Type Tumors (for Details, See Chap. 9)

4.5.1 Adenoid Cystic Carcinoma

FNAB of sinonasal ACC produces smears displaying morphologic findings identical to those of ACC occurring in the salivary glands and other organs. Smears are generally cellular and contain clusters of small, uniform, basaloid cells with hyperchromatic nuclei and scant cytoplasm. These basaloid cells are seen surrounding globules and finger-like projections of uniform extracellular hyaline material with sharp borders are often present [2, 88] (Fig. 4.22). This hyaline material will stain magenta with Romanowsky stains.

4.5.2 Pleomorphic Adenoma

Pleomorphic adenomas (PA) arising in the sinonasal tract will also appear morphologically similar to their salivary counterparts, but are noted to have a more dominant epithe-

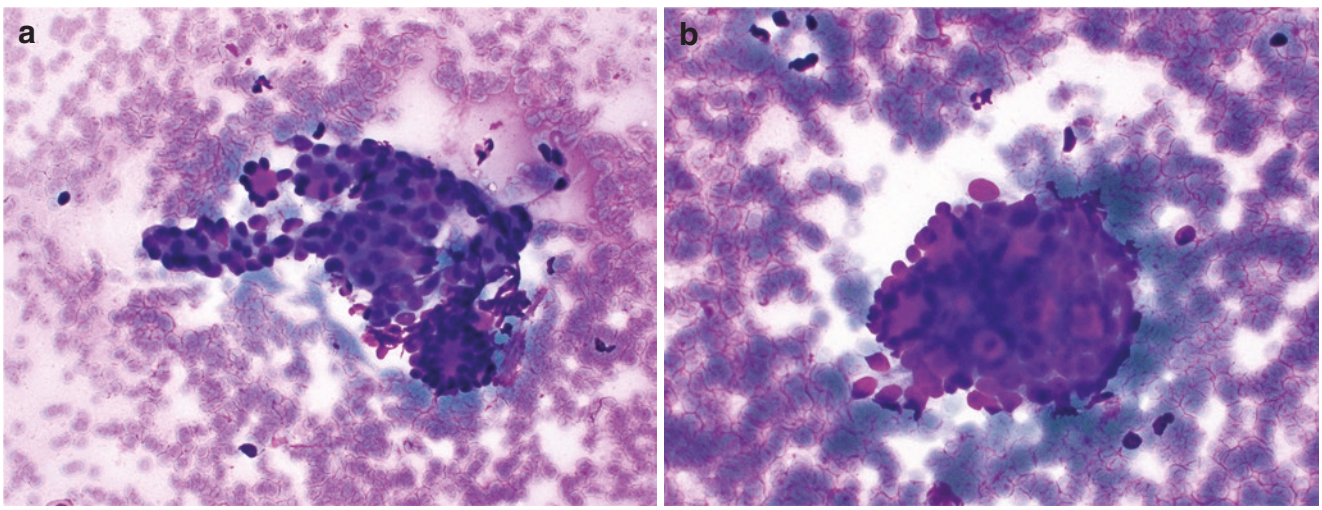

Fig. 4.22 Romanowsky stained aspirate smears demonstrate monomorphic basaloid cells surrounding spheres of dense, acellular metachromatic material (**a**, **b**, 400x)

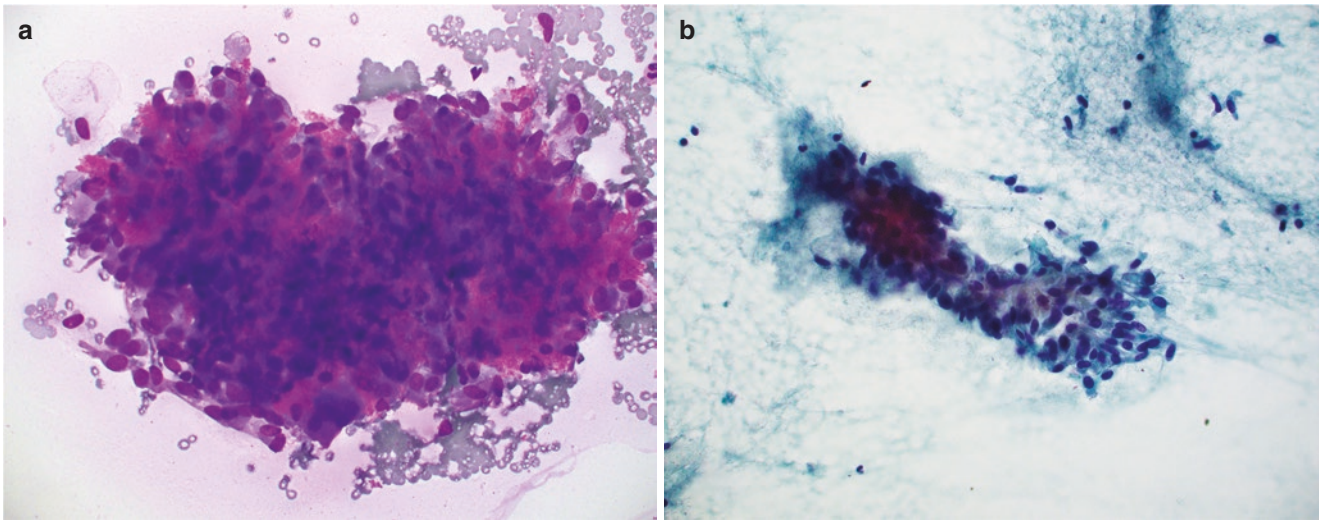

Fig. 4.23 Romanowsky (**a**, 400x) and Papanicolaou (**b**, 400x) stained smears demonstrate fragments of fibrillary, metachromatic stroma containing bland, monotonous myoepithelial cells

lial component when compared to PA occurring in the major salivary glands [75]. Smears show poorly cohesive clusters and sheets of fibrillary, chondromyxoid stroma containing admixed myoepithelial cells. The myoepithelial cells are cytologically bland and may appear round to spindled. The characteristic fibrillary stroma will appear magenta in color on Romanowsky stains [3, 86] (Fig. 4.23).

4.6 Mesenchymal Neoplasms

Mesenchymal tumors of most differentiations including vascular, fibroblastic, myofibroblastic, myogenous, cartilaginous, osseous, and neural can arise in the sinonasal tract. Certain mesenchymal entities, such as glomangiopericytoma/glomus tumor and angiofibroma, have a predilection for the sinonasal tract. Just as how significant morphologic overlap across these entities can pose significant diagnostic challenges on FNAB assessment of soft tissue masses elsewhere in the body, this same morphologic overlap exists in the sinonasal tract. More unique to the sinonasal tract, however, is that spindle cell morphology can also be seen in melanomas, carcinomas, and salivary-type neoplasms. Furthermore, the rarity of mesenchymal neoplasms of the sinonasal tract results in most cytopathologists having a lack of experience with the scope of morphology that can be encountered with these lesions. This lack of individual provider experience is currently compounded by a paucity of reports regarding the findings on FNAB sampling of these lesions. However, the clinical differential when first encountering a sinonasal mass often includes non-mesenchymal entities including epithelial and hematologic neoplasms as well as benign/reactive lesions, thus FNAB can play a key role in triaging these lesions for the correct medical management.

Despite the limitations mentioned above as well as those inherent to FNAB sampling, including sampling error and technically limited specimens, of the few case series reported in the literature regarding FNAB of sinonasal masses, cytopathologists have been able to correctly classify lesions as mesenchymal and separate low-grade lesions from malignant lesions [2, 3] (Tables 4.4 & 4.5, Fig. 4.24).

Given the ongoing discoveries of ancillary tests and a growing list of mesenchymal lesions with entity-defining cytomorphologic, immunophenotypic, and/or cytogenetic features, the utility of FNAB in diagnosing primary sinonasal mesenchymal lesions will likely continue to expand. Furthermore, given the minimally invasive nature of FNAB, cytologic sampling is well suited to confirm recurrence or metastases from known primary tumors.

In-depth cytomorphologic discussion of all possible mesenchymal neoplasms that could be encountered in the sinonasal tract is beyond the scope of this chapter. Further morphologic discussion of these entities can be found in Chapters 10 and 11.

Table 4.4 Bland-appearing spindle cell lesions

Entity	Positive immunostains
Schwannoma	S100, SOX10
Desmoid-type fibromatosis	Vimentin, beta-catenin (nuclear), SMA
Glomus tumor/ Glomangiopericytoma	Vimentin, beta-catenin (nuclear), SMA, cyclin D1, factor XIIIa
Solitary fibrous tumor	STAT6 (nuclear), CD34
Low-grade myofibroblastic sarcoma	Vimentin, SMA, desmin
Fibrosarcoma	Vimentin, limited SMA
Biphenotypic sinonasal sarcoma	S100, SMA with variable CD34, desmin, myoD1, EMA, and keratins

Table 4.5 Atypical-appearing spindle cell lesions

Entity	Positive immunostains
Undifferentiated pleomorphic sarcoma	Limited SMA staining (diagnosis of exclusion)
Spindle cell carcinoma	Keratins, variable expression of EMA and p63
Melanoma	S100, SOX10, HMB45, Melan-A/ MART1

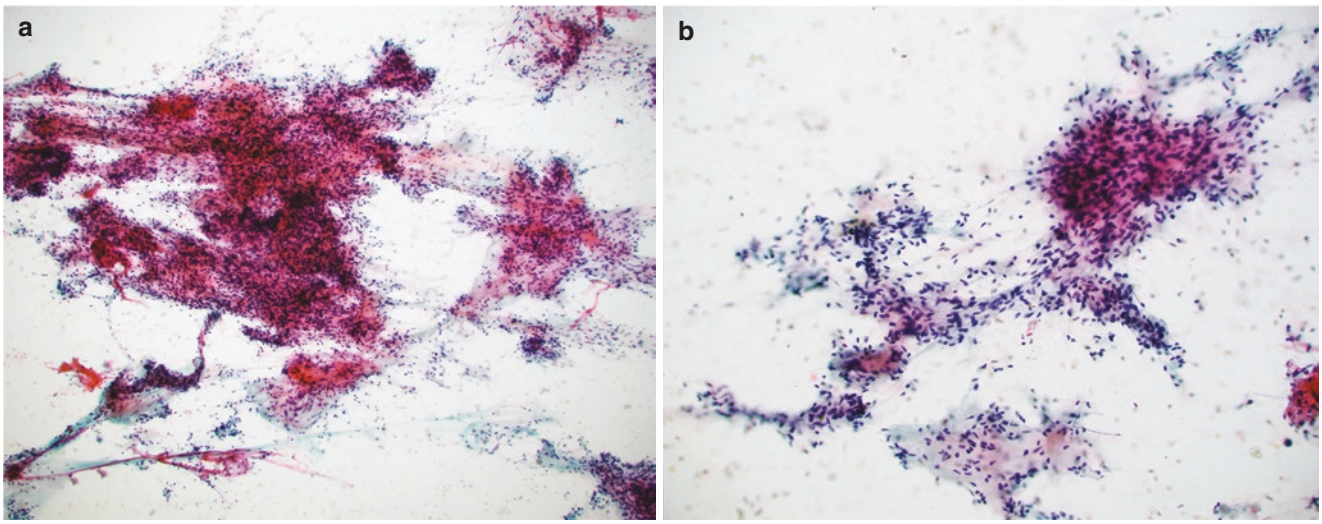

Fig. 4.24 Papanicolaou stained aspirate smears of a schwannoma demonstrate large, cohesive groups of spindle cells with irregular borders (**a**, 100x). The spindle cells demonstrate abundant cytoplasm and indistinct cells borders. The nuclei are ovoid, may be wavy, and show minimal atypia (**b**, 200x)

4.7 Neuroectodermal and Melanocytic Neoplasms

4.7.1 Ewing Sarcoma

FNAB of a primary sinonasal Ewing sarcoma would likely appear morphologically identical to other primary sites where aspirate smears show densely dispersed, small, monomorphic round cells with fine nuclear chromatin, round nuclei and scant, and vacuolated cytoplasm (Fig. 4.25). Scattered clusters and rosette-like formations can be seen. Occasional mitoses and focal nuclear molding can be present. The background of the smear is generally clean [89–92].

4.7.2 Olfactory Neuroblastoma

Olfactory neuroblastoma is a malignancy with neuroblastic differentiation that arises in the superior nasal cavity near the cribriform plate and also has a small round blue cell tumor phenotype (Table 4.6). The tumor cells are small and uniform with scant cytoplasm surrounding round, regular nuclei with fine chromatin; nucleoli are inconspicuous. Occasional Homer Wright rosettes are seen and fibrillary material can be present in the background [85, 86] (Fig. 4.26). Mitotic figures are rare in lower Hyams grade tumors, and more frequent in higher grade tumors (Fig. 4.27).

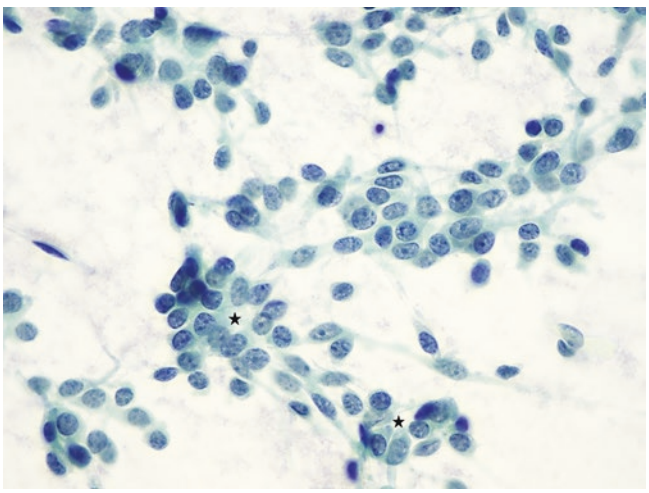

Fig. 4.25 A Papanicolaou stained smear shows small, loosely cohesive clusters of monotonous epithelioid cells with focal nuclear molding and pseudorosette formation (stars) (60x)

Table 4.6 Small round blue cell tumors of the sinonasal tract

Entity	Diagnostic clues
Ewing sarcoma/primitive neuroectodermal tumor	CD99, NSE positive; keratins, p63/p40 and neuroendocrine markers are usually negative
Olfactory neuroblastoma	Neuroendocrine markers are positive; keratins and p63/p40 are usually negative
Melanoma	S100, SOX10 positive; keratins, p63/p40 and neuroendocrine markers will be negative; HMB45, melan-A and MIFT variable
NUT carcinoma	NUT, keratins, p63/p40 positive; neuroendocrine markers are usually negative
Sinonasal undifferentiated carcinoma	Pankeratin positive; p63/p40 and neuroendocrine markers are usually negative
Alveolar rhabdomyosarcoma	Vimentin, myogenin and myoD1 positive, variable neuroendocrine marker staining, negative for keratins

4.7.3 Mucosal Melanoma

Just as in other anatomic sites, malignant melanoma arising in the sinonasal tract can show varying histomorphology from epithelioid, spindled, plasmacytoid to desmoplastic [87]. Rare reports of FNAB from sinonasal primaries report single, plasmacytoid cells with abundant cytoplasm [2, 3] (Fig. 4.28). Some cases report abundant intracytoplasmic melanin pigment. When pigment is absent, immunohistochemistry can be helpful [93].

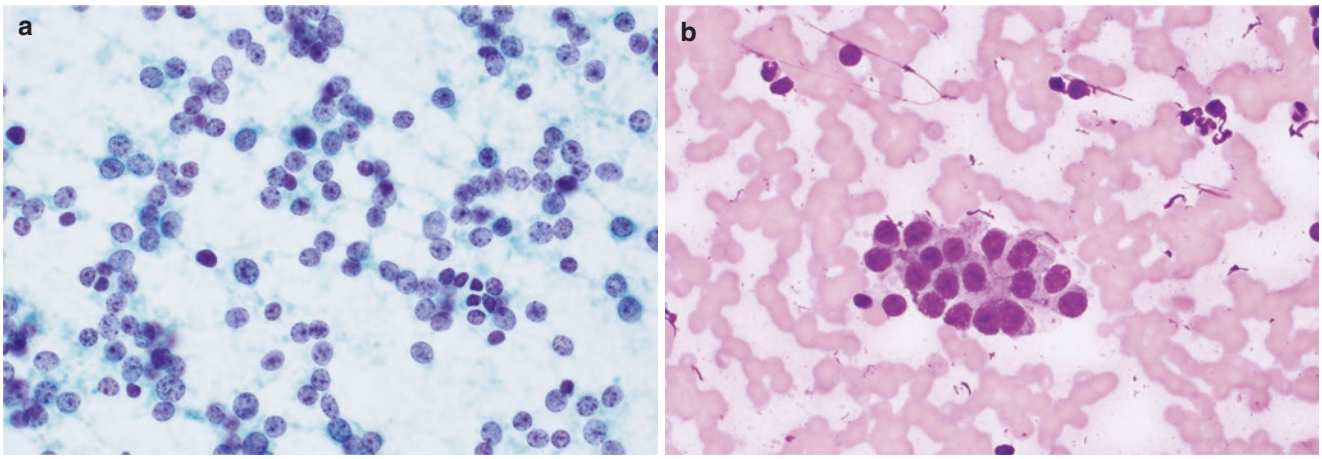

Fig. 4.26 Fine needle aspirate sampling of a low-grade (Hyams grade 1–2) olfactory neuroblastoma demonstrates small, round, monomorphic cells with scant eosinophilic cytoplasm and finely granular chromatin (**a**, Papanicolaou stain, 400x & **b**, Romanowsky stain, 600x)

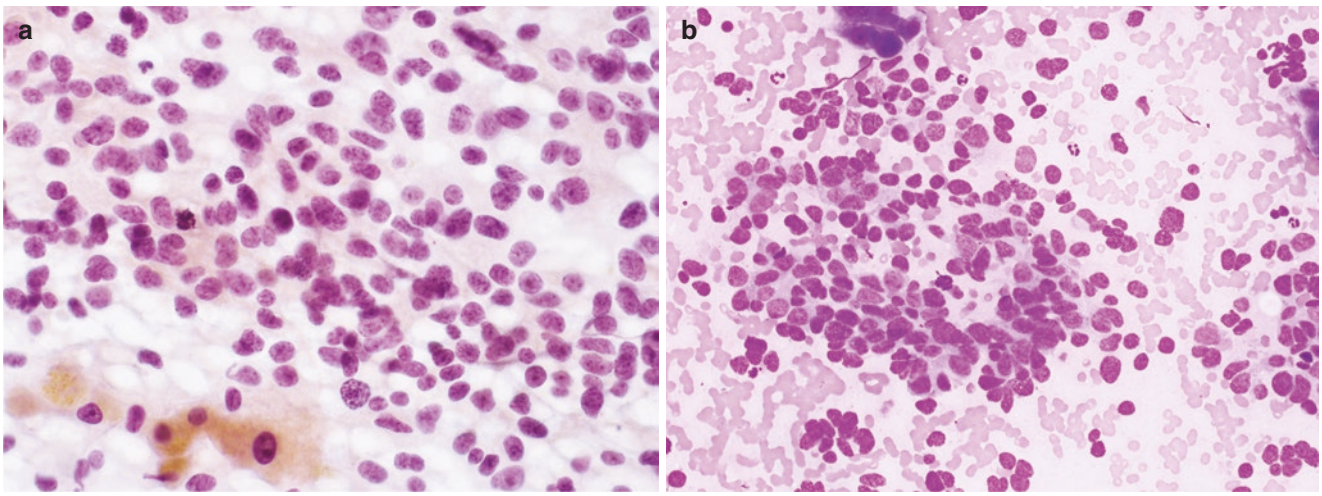

Fig. 4.27 Fine needle aspirate sampling of a higher grade (Hyams grade 3–4) olfactory neuroblastoma shows epithelioid cells with cytologic atypia including nuclear pleomorphism and scattered mitotic figs. (**a**, Papanicolaou stain, 600x & **b**, Romanowski stain, 400x)

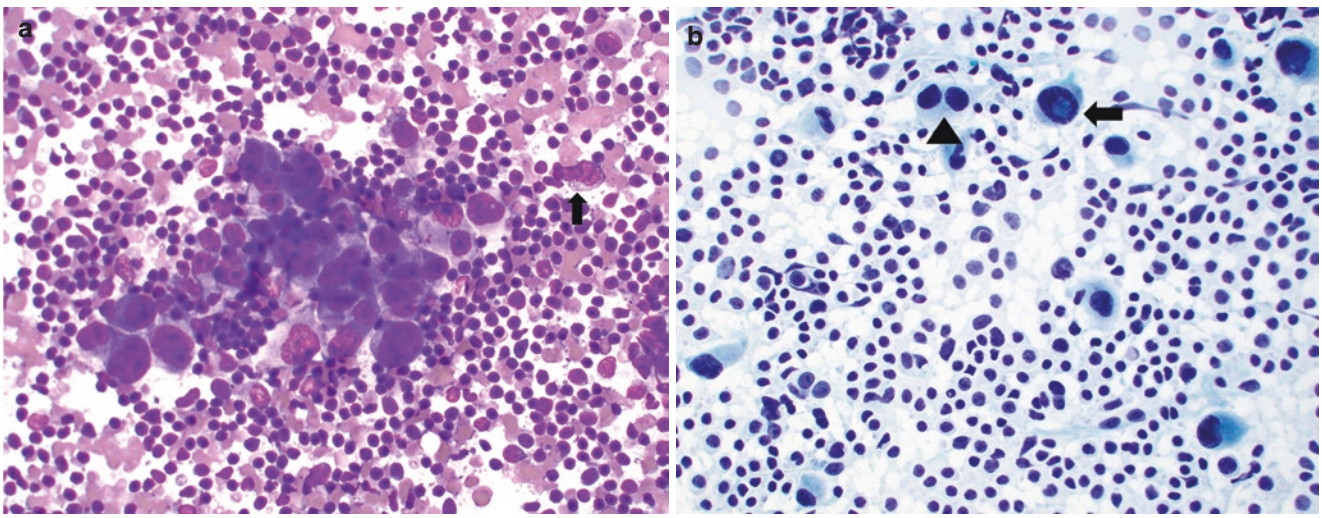

Fig. 4.28 Fine needle aspirate sampling of melanoma generally produces cellular smears comprised of large cells present singly or in loose aggregates. Malignant cells may appear plasmacytoid with abundant cytoplasm, prominent nucleoli, and fine cytoplasmic vacuoles (**a**, 400x, Romanowsky stain, arrow). Nuclear inclusions (**b**, 400x, Papanicolaou stain, arrow) and binucleated cells with spacing between mirror-image nuclei (**b**, arrowhead) are clues to the diagnosis in amelanotic cases

4.8 Other Sinonasal Neoplasms

4.8.1 Sinonasal Ameloblastoma

Ameloblastomas are rare, benign, but locally aggressive tumors of odontogenic epithelium. FNAB of maxillary sinus lesions show sheets of basaloid cells surrounded by palisading groups of columnar epithelial cells admixed with myxoid stromal fragments [94, 95].

4.8.2 Chordoma

Chordomas that arise at the base of the skull may involve the nasal cavity or sinuses. These chordomas will appear identical to those arising elsewhere in the axial skeleton. Smears will show physaliphorous cells with multiple cytoplasmic vacuoles within myxoid stroma [3]. An immunostain for brachyury can be performed to confirm the morphologic impression.

4.9 Hematolymphoid Tumors

Hematolymphoid malignancies are relatively common in the sinonasal tract (see Chap. 12 for detailed discussion). The cytologic appearance of these tumors depend on its subtype. Diffuse large B-cell lymphoma (DLBCL) is the most common lymphoid malignancy seen in this region, followed by extranodal NK/T-cell lymphoma, nasal-type (ENKTL), a malignancy unique to this location. Regardless of the subtype, diagnosis of a hematologic process can generally be established via FNAB sampling provided there is appropriate on-site triage for the procurement of adequate material for morphologic, molecular, and flow cytometric analysis.

4.9.1 Diffuse Large B-Cell Lymphoma

The utility of FNAB in the diagnosis of DLBCL involving the sinuses is established in the literature [3, 86, 96]. Aspirate smears from sinonasal tract DLBCLs will appear morphologically similar to DLBCLs arising in other sites. Morphologically, large lymphoid cells resembling immunoblasts or centroblasts will be present. These cells will display scant-to-moderate amounts of basophilic-to-amphophilic cytoplasm and have irregular nuclear contours with vesicular chromatin and prominent nucleoli (Fig. 4.29). Small, mature, nonneoplastic lymphocytes are generally present in the background and lymphoglandular bodies may also be seen. Characterization of these large cell lymphomas by flow cytometry may be difficult, so collection of material for a cell block that can be used for immunohistochemistry and molecular studies is advised.

4.9.2 Extranodal NK/T-Cell Lymphoma, Nasal-Type

This aggressive lymphoma is characterized not only by its location, but also by its association with Epstein–Barr virus (EBV) and marked prevalence amongst East Asian, indigenous Mexican, and Central and South American populations. Numerous reports of the use of both FNAB (smear and liquid-based preparations) and nasal brushing cytology for the diagnosis of this lesion make it the best cytomorphologi-

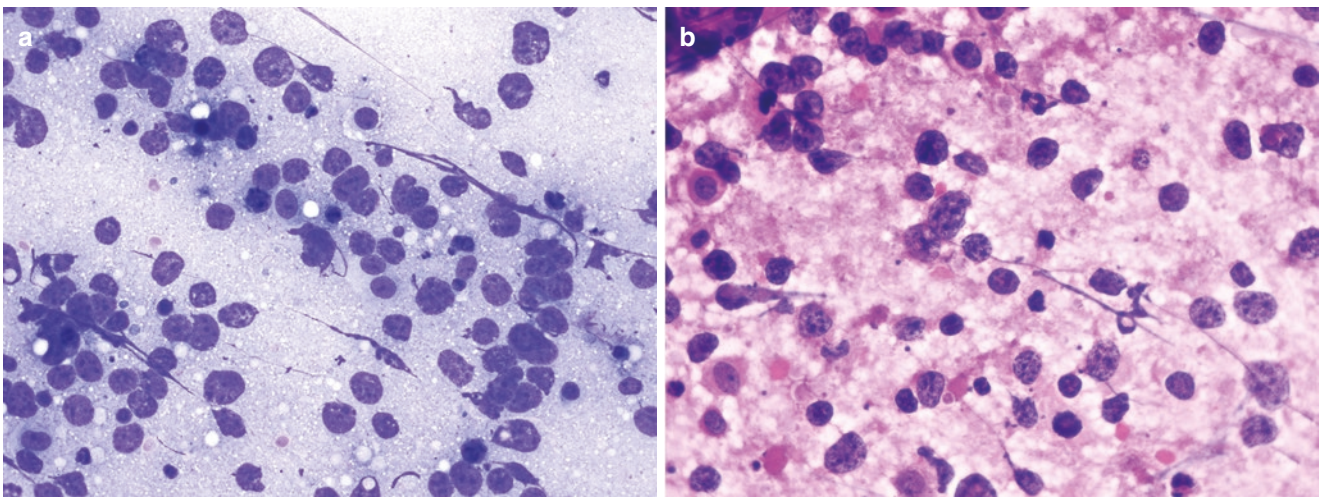

Fig. 4.29 Aspirate of diffuse large B-cell lymphomas can be variably cellular and demonstrate large, atypical cells with coarse chromatin and prominent nucleoli in a background of small, mature T-cells and lymphoglandular bodies (**a**, 400x, Romanowsky stain). Intact tumor cells show a scant to moderate amount of cytoplasm (**b**, 600x, Papanicolaou stain)

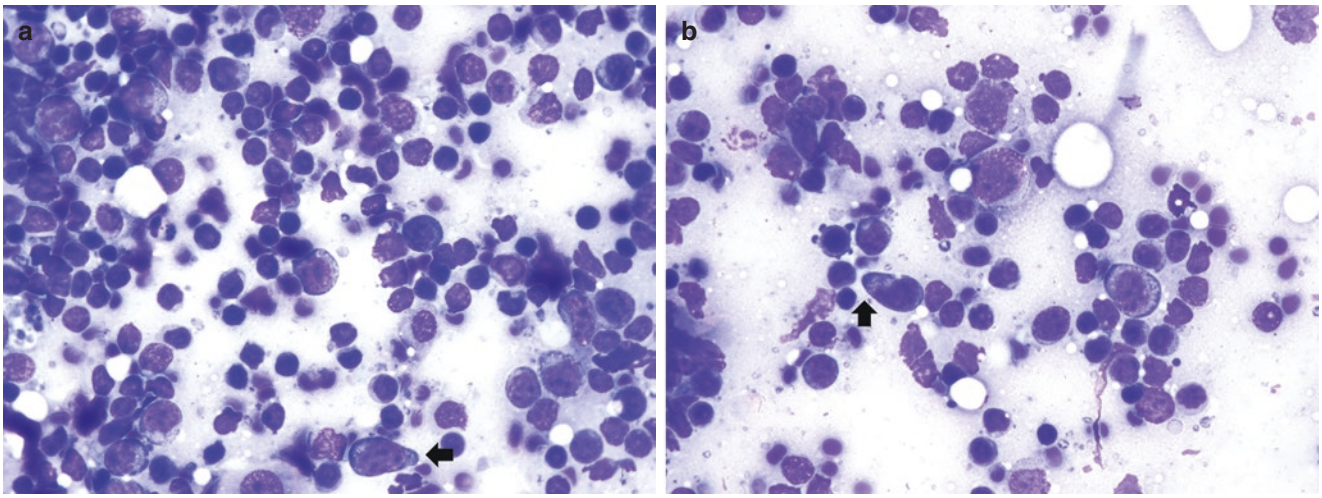

Fig. 4.30 Smear slides demonstrate a mixture of medium and large neoplastic lymphocytes with nuclear membrane irregularities, coarse chromatin, and a scant to moderate amount of cytoplasm. Scattered cells demonstrate a cytoplasmic "tongue-like" protrusion is present (arrows) (**a**, **b**, 600x, Romanowsky stain)

cally characterized hematolymphoid malignancy of the sinonasal tract. Smears demonstrate a dispersed, hypercellular sample comprised of medium-to-large lymphoid cells with scant-to-moderate amounts of pale blue, delicate cytoplasm with tongue-like cytoplasmic protrusions (Fig. 4.30). The nuclei show membrane irregularities with coarse chromatin. Clusters of neoplastic cells may be seen lining capillaries; azurophilic granules may also be present [97–100]. In contrast to the histologic findings, background necrosis is rarely reported in cytologic samples. Collection of cell block material for EBER in situ hybridization studies and additional immunostains is recommended.

4.10 Conclusion

Mass lesions that arise in the sinonasal tract are uncommon and diverse. While cytology has historically not played a large role in the primary diagnosis of these lesions in Western nations, cytologic sampling has proven to be an effective modality that can assist in the classification and management of sinonasal lesions. Published literature has shown that cytopathology is highly accurate for the detection of malignancy, as well as the distinction between high- and low-grade lesions when neoplasia is present. Given the increasing availability of ancillary tests for the diagnosis of infectious and neoplastic etiologies, and a growing list of neoplasms with entity-defining cytomorphologic, immunophenotypic, and/or cytogenetic features, the opportunity for the application of cytology in diagnosing primary sinonasal lesions will likely grow.

References

1. Tatomirovic Z, Skuletic V, Bokun R, et al. Fine needle aspiration cytology in the diagnosis of head and neck masses: accuracy and diagnostic problems. J BUON. 2009;14(4):653–9.
2. Helsel JC, Bardales RH, Mukunyadzi P. Fine-needle aspiration biopsy cytology of malignant neoplasms of the sinonasal tract. Cancer. 2003;99(2):105–12. https://doi.org/10.1002/cncr.10956.
3. Gupta N, Kaur J, Srinivasan R, et al. Fine needle aspiration cytology in lesions of the nose, nasal cavity and paranasal sinuses. Acta Cytol. 2011;55(2):135–41. https://doi.org/10.1159/000320907.
4. Garg D, Mathur K. Clinico-pathological study of space occupying lesions of nasal cavity, paranasal sinuses and nasopharynx. J Clin Diagn Res. 2014;8(11):FC04–7. https://doi.org/10.7860/JCDR/2014/10662.5150.
5. Zafar U, Khan N, Afroz N, Hasan SA. Clinicopathological study of non-neoplastic lesions of nasal cavity and paranasal sinuses. Indian J Pathol Microbiol. 2008;51(1):26–9. https://doi.org/10.4103/0377-4929.40386.
6. Satarkar RN, Srikanth S. Tumors and tumor-like conditions of the nasal cavity, paranasal sinuses, and nasopharynx: A study of 206 cases. Indian J Cancer 2016 Oct-Dec 2016;53(4):478–482. doi:https://doi.org/10.4103/ijc.IJC_551_16.
7. Lam K, Schleimer R, Kern RC. The etiology and pathogenesis of chronic rhinosinusitis: a review of current hypotheses. Curr Allergy Asthma Rep. 2015;15(7):41. https://doi.org/10.1007/s11882-015-0540-2.
8. Bush RK, Portnoy JM, Saxon A, Terr AI, Wood RA. The medical effects of mold exposure. J Allergy Clin Immunol Feb 2006;117(2):326–333. doi:https://doi.org/10.1016/j.jaci.2005.12.001.
9. Luong A, Marple BF. Allergic fungal rhinosinusitis. Curr Allergy Asthma Rep. 2004;4(6):465–70. https://doi.org/10.1007/s11882-004-0013-5.
10. Schnadig VJ, Rassekh CH, Gourley WK. Allergic fungal sinusitis. A report of two cases with diagnosis by intraoperative aspiration cytology. Acta Cytol. 1999;43(2):268–72. https://doi.org/10.1159/000330991.

11. Rane SR, Kadgi NV, Agrawal SA, Kavatkar AN. Nasal discharge cytology an important diagnostic method for allergic fungal sinusitis: report of three cases. J Clin Diagn Res. 2014;8(3):121–2. https://doi.org/10.7860/JCDR/2014/6671.4130.
12. Manning SC, Schaefer SD, Close LG, Vuitch F. Culture-positive allergic fungal sinusitis. Arch Otolaryngol Head Neck Surg. 1991;117(2):174–8. https://doi.org/10.1001/archotol.1991.01870140062007.
13. Gelardi M, Luigi Marseglia G, Licari A, et al. Nasal cytology in children: recent advances. Ital J Pediatr. 2012;38:51. https://doi.org/10.1186/1824-7288-38-51.
14. Oneson RH, Feldman PS, Newman SA. Aspiration cytology and immunohistochemistry of an orbital aspergilloma. Diagn Cytopathol. 1988;4(1):59–61. https://doi.org/10.1002/dc.2840040114.
15. Kumar Behera S, Patro M, Mishra D, Bal A, Behera B, Sahoo S. Fine needle aspiration in aspergilloma of frontal sinus: a case report. Acta Cytol. 2008;52(4):500–4. https://doi.org/10.1159/000325562.
16. deShazo RD, Chapin K, Swain RE. Fungal sinusitis. N Engl J Med. 1997;337(4):254–9. https://doi.org/10.1056/NEJM199707243370407.
17. Montone KT. Pathology of fungal rhinosinusitis: A review. Head Neck Pathol Mar 2016;10(1):40–46. doi:https://doi.org/10.1007/s12105-016-0690-0.
18. Sharma D, Mahajan N, Rao S, Khurana N, Jain S. Invasive maxillary aspergillosis masquerading as malignancy in two cases: utility of cytology as a rapid diagnostic tool. J Cytol. 2012;29(3):194–6. https://doi.org/10.4103/0970-9371.101171.
19. Singh N, Siddaraju N, Kumar S, Muniraj F, Bakshi S, Gopalakrishnan S. Fine-needle aspiration biopsy as an initial diagnostic modality in a clinically unsuspected case of invasive maxillary fungal sinusitis: A case report. Diagn Cytopathol Apr 2010;38(4):290–293. doi:https://doi.org/10.1002/dc.21216.
20. Singhal N, Raghubanshi G, Handa U, Punia RP, Singhal S. Fine needle aspiration cytology: a useful technique for diagnosis of invasive fungal rhinosinusitis. Head Neck Pathol Sep 2013;7(3):236–240. doi:https://doi.org/10.1007/s12105-013-0434-3.
21. Dey S, Misra S, Dutta M. Primary Sinonasal tuberculosis: A diagnostic challenge. Turk Arch Otorhinolaryngol Jun 2018;56(2):117–121. doi:https://doi.org/10.5152/tao.2018.3191.
22. Kim KY, Bae JH, Park JS, Lee SS. Primary sinonasal tuberculosis confined to the unilateral maxillary sinus. Int J Clin Exp Pathol. 2014;7(2):815–8.
23. Nawaz G, Khan MR. Primary sinonasal tuberculosis in north-West Pakistan. J Coll Physicians Surg Pak. 2004;14(4):221–4. doi:04.2004/JCPSP.221224
24. Prasad KC, Sreedharan S, Chakravarthy Y, Prasad SC. Tuberculosis in the head and neck: experience in India. J Laryngol Otol. 2007;121(10):979–85. https://doi.org/10.1017/S0022215107006913.
25. Mahana S, Tomar R, Agrawal R, Saksena R, Manchanda V, Gupta R. Tuberculous lymphadenitis: comparison of cytomorphology, Ziehl-Neelsen staining, and rapid mycobacterial culture at a pediatric superspecialty hospital. Cytojournal. 2016;13:17. https://doi.org/10.4103/1742-6413.187070.
26. Nigam PK, Kumar P, Pathak N, Mittal S. Fine needle aspiration cytology in reactional and non-reactional leprosy. Indian J Dermatol Venereol Leprol. 2007;73(4):247–9. https://doi.org/10.4103/0378-6323.33635.
27. De A, Hasanoor Reja AH, Aggarwal I, et al. Use of fine needle aspirate from peripheral nerves of pure-neural leprosy for cytology and polymerase chain reaction to confirm the diagnosis: A follow-up study of 4 years. Indian J Dermatol 2017 Nov-Dec 2017;62(6):635–643. doi:https://doi.org/10.4103/ijd.IJD_115_17.
28. Prasad PV, George RV, Kaviarasan PK, Viswanathan P, Tippoo R, Anandhi C. Fine needle aspiration cytology in leprosy. Indian J Dermatol Venereol Leprol 2008 Jul-Aug 2008;74(4):352–356. doi:https://doi.org/10.4103/0378-6323.42902.
29. Jaswal TS, Jain VK, Jain V, Singh M, Kishore K, Singh S. Evaluation of leprosy lesions by skin smear cytology in comparison to histopathology. Indian J Pathol Microbiol. 2001;44(3):277–81.
30. Mehdi G, Maheshwari V, Ansari HA, Saxena S, Sharma R. Modified fine-needle aspiration technique for diagnosis of granulomatous skin lesions with special reference to leprosy and cutaneous tuberculosis. Diagn Cytopathol. 2010;38(6):391–6. https://doi.org/10.1002/dc.21207.
31. Chan TV, Spiegel JH. Klebsiella rhinoscleromatis of the membranous nasal septum. J Laryngol Otol. 2007;121(10):998–1002. https://doi.org/10.1017/s0022215107006421.
32. Umphress B, Raparia K. Rhinoscleroma. Arch Pathol Lab Med. 2018;142(12):1533–6. https://doi.org/10.5858/arpa.2018-0073-RA.
33. Bailhache A, Dehesdin D, Francois A, Marie JP, Choussy O. Rhinoscleroma of the sinuses. Rhinology Dec 2008;46(4):338–341.
34. Sood N, Sood S, Arora S, Deepika. Cytohistological features of rhinoscleroma. Indian J Pathol Microbiol. 2011;54(4):806–8. https://doi.org/10.4103/0377-4929.91523.
35. Ahmed AR, El-Badawy ZH, Mohamed IR, Abdelhameed WA. Rhinoscleroma: a detailed histopathological diagnostic insight. Int J Clin Exp Pathol. 2015;8(7):8438–45.
36. Laudien M. Orphan diseases of the nose and paranasal sinuses: Pathogenesis - clinic - therapy. *GMS Curr Top Otorhinolaryngol Head Neck Surg*. 2015;14:Doc04. doi:10.3205/cto000119.
37. Nabet C, Belzunce C, Blanchet D, et al. Histoplasma capsulatum causing sinusitis: a case report in French Guiana and review of the literature. BMC Infect Dis. 2018;18(1):595. https://doi.org/10.1186/s12879-018-3499-5.
38. Elansari R, Abada R, Rouadi S, Roubal M, Mahtar M. Histoplasma capsulatum sinusitis: possible way of revelation to the disseminated form of histoplasmosis in HIV patients: case report and literature review. Int J Surg Case Rep. 2016;24:97–100. https://doi.org/10.1016/j.ijscr.2016.03.010.
39. Drak Alsibai K, Couppié P, Blanchet D, et al. Cytological and histopathological Spectrum of histoplasmosis: 15 years of experience in French Guiana. Front Cell Infect Microbiol. 2020;10:591974. https://doi.org/10.3389/fcimb.2020.591974.
40. Huna-Baron R, Warren FA, Miller W, Jacobs J, Green J, Kupersmith MJ. Mucosal leishmaniasis presenting as sinusitis and optic neuropathy. Arch Ophthalmol. 2000;118(6):852–4.
41. Gul HC, Tosun F, Karakas A, et al. A case of mucosal leishmaniasis: mimicking intranasal tumor with perforation of septum. J Microbiol Immunol Infect. 2016;49(4):604–7. https://doi.org/10.1016/j.jmii.2013.11.007.
42. Bandyopadhyay A, Bose K. A rare case of cutaneous Leishmaniasis presenting as Rhinophyma. Iran J Pathol. 2015;10(2):155–9.
43. ul Bari A, Ejaz A. Rhinophymous leishmaniasis: A new variant. Dermatol Online J. 2009;15(3)
44. Mitropoulos P, Konidas P, Durkin-Konidas M. New World cutaneous leishmaniasis: updated review of current and future diagnosis and treatment. J Am Acad Dermatol. 2010;63(2):309–22. https://doi.org/10.1016/j.jaad.2009.06.088.
45. Baughman RP, Teirstein AS, Judson MA, et al. Clinical characteristics of patients in a case control study of sarcoidosis. Am J Respir Crit Care Med. 2001;164(10 Pt 1):1885–9. https://doi.org/10.1164/ajrccm.164.10.2104046.
46. Hardt J, Doyon F, Klinger C, Buhr HJ, Post S. MTL, a composite measure for objectively profiling hospitals on surgical performance

in colorectal cancer surgery. Int J Color Dis May 2019;34(5):889–898. doi:https://doi.org/10.1007/s00384-019-03273-7.
47. Edriss H, Kelley JS, Demke J, Nugent K. Sinonasal and Laryngeal Sarcoidosis-An Uncommon Presentation and Management Challenge. Am J Med Sci. 2019;357(2):93–102. https://doi.org/10.1016/j.amjms.2018.11.007.
48. Baum ED, Boudousquie AC, Li S, Mirza N. Sarcoidosis with nasal obstruction and septal perforation. Ear Nose Throat J. 1998;77(11):896–8. 900–2
49. Frable MA, Frable WJ. Fine-needle aspiration biopsy: efficacy in the diagnosis of head and neck sarcoidosis. Laryngoscope. 1984;94(10):1281–3.
50. Hoffman GS, Kerr GS, Leavitt RY, et al. Wegener granulomatosis: an analysis of 158 patients. Ann Intern Med. 1992;116(6):488–98. https://doi.org/10.7326/0003-4819-116-6-488.
51. Langford CA, Hoffman GS. Rare diseases.3: Wegener's granulomatosis. Thorax. 1999;54(7):629–37. https://doi.org/10.1136/thx.54.7.629.
52. Michael CW, Flint A. The cytologic features of Wegener's granulomatosis. Am J Clin Pathol. 1998;110(1):10–5. https://doi.org/10.1093/ajcp/110.1.10.
53. Dalia S, Sagatys E, Sokol L, Kubal T. Rosai-Dorfman disease: tumor biology, clinical features, pathology, and treatment. Cancer Control. 2014;21(4):322–7. https://doi.org/10.1177/107327481402100408.
54. Niu Y, Li Y, Wang J, et al. Laryngeal Rosai-Dorfman disease (sinus Histiocytosis with massive lymphadenopathy): a retrospective study of 5 cases. Biomed Res Int. 2017;2017:8521818. https://doi.org/10.1155/2017/8521818.
55. Hussain A, Tandon A, Prayaga AK, Paul TR, Narendra AM. Cytomorphology and histology correlation of Rosai-Dorfman disease: A 15-year study from a tertiary referral Centre in South India. Acta Cytol. 2017;61(1):55–61. https://doi.org/10.1159/000449460.
56. Rajyalakshmi R, Akhtar M, Swathi Y, Chakravarthi R, Bhaskara Reddy J, Beulah PM. Cytological diagnosis of Rosai-Dorfman disease: A study of twelve cases with emphasis on diagnostic challenges. J Cytol. 2020;37(1):46–52. https://doi.org/10.4103/JOC.JOC_4_19.
57. Shalley S, Chand N, Aggarwal A, Garg LN, Yadav V, Yadav A. Diagnostic accuracy of fine needle aspiration cytology in lesions of Oral cavity and salivary glands: A Clinico-pathological study. Open Dent J. 2018;12:782–90. https://doi.org/10.2174/1745017901814010782.
58. De Las Casas LE, Bardales RH. Fine-needle aspiration cytology of mucous retention cyst of the tongue: distinction from other cystic lesions of the tongue. Diagn Cytopathol. 2000;22(5):308–12. https://doi.org/10.1002/(sici)1097-0339(200005)22:5<308::aid-dc10>3.0.co;2-h.
59. Layfield LJ, Gopez EV. Cystic lesions of the salivary glands: cytologic features in fine-needle aspiration biopsies. Diagn Cytopathol. 2002;27(4):197–204. https://doi.org/10.1002/dc.10168.
60. Mills SE, Stelow EB, Hunt JL. Tumors of the upper Aerodigestive tract and ear. In: AFIP atlas of tumor pathology, series 4, vol. 17. ARP Press; 2012.
61. Handa U, Chhabra S, Mohan H. Epidermal inclusion cyst: cytomorphological features and differential diagnosis. Diagn Cytopathol D2008;36(12):861–863. doi:https://doi.org/10.1002/dc.20923.
62. Baschinsky D, Hameed A, Keyhani-Rofagha S. Fine-needle aspiration cytological features of dermoid cyst of the parotid gland: a report of two cases. Diagn Cytopathol. 1999;20(6):387–8. https://doi.org/10.1002/(sici)1097-0339(199906)20:6<387::aid-dc13>3.0.co;2-0.
63. Thompson LDR. Sinonasal carcinomas. Curr Diagn Pathol. 2006;2006(12):40–53.
64. Bishop JA, Guo TW, Smith DF, et al. Human papillomavirus-related carcinomas of the sinonasal tract. Am J Surg Pathol. 2013;37(2):185–92. https://doi.org/10.1097/PAS.0b013e3182698673.
65. El-Mofty SK, Lu DW. Prevalence of high-risk human papillomavirus DNA in nonkeratinizing (cylindrical cell) carcinoma of the sinonasal tract: a distinct clinicopathologic and molecular disease entity. Am J Surg Pathol. 2005;29(10):1367–72. https://doi.org/10.1097/01.pas.0000173240.63073.fe.
66. Larque AB, Hakim S, Ordi J, et al. High-risk human papillomavirus is transcriptionally active in a subset of sinonasal squamous cell carcinomas. Mod Pathol. 2014;27(3):343–51. https://doi.org/10.1038/modpathol.2013.155.
67. Lewis JS. Sinonasal squamous cell carcinoma: A review with emphasis on emerging histologic subtypes and the role of human papillomavirus. Head Neck Pathol. 2016;10(1):60–7. https://doi.org/10.1007/s12105-016-0692-y.
68. Chute DJ, Stelow EB. Cytology of head and neck squamous cell carcinoma variants. Diagn Cytopathol. 2010;38(1):65–80. https://doi.org/10.1002/dc.21134.
69. Grossl N, Tadros TS, Naib ZM. Sarcomatoid carcinoma of the larynx with neck and distant subcutaneous metastases. A case report with fine needle aspiration cytology. Acta Cytol. 1996;40(4):756–60. https://doi.org/10.1159/000333953.
70. Jayaram G, Elsayed EM. Carcinosarcoma of the palate: report of a case with a diagnosis of sarcomatoid metastasis by fine needle aspiration cytology. Acta Cytol 2005 5;49(5):520–524. doi:https://doi.org/10.1159/000326198.
71. Schantz HD, Ramzy I, Tio FO, Buhaug J. Metastatic spindle-cell carcinoma. Cytologic features and differential diagnosis. Acta Cytol. 1985;29(3):435–41.
72. Lewis JS, Ritter JH, El-Mofty S. Alternative epithelial markers in sarcomatoid carcinomas of the head and neck, lung, and bladder-p63, MOC-31, and TTF-1. Mod Pathol. 2005;18(11):1471–81. https://doi.org/10.1038/modpathol.3800451.
73. Lim SJ, Kim JY, Park KM. Fine needle aspiration cytology of Lymphoepithelial carcinoma of parotid gland: A case report. The Korean Journal of Cytopathology. 2002;13(2):74–44.
74. Seok JY, Lee KG. Cytologic features of metastatic lymphoepithelial carcinoma in pleural fluid: a case report. Acta Cytol. 2009;53(2):215–8. https://doi.org/10.1159/000325128.
75. El-Nagger AK, Chan JKC, Grandis JR, Takata T, Slootweg PJ. WHO classification of head and neck Tumours. 4th ed. World Health Organization Classification of Tumours. IARC; 2017.
76. Kanjanavirojkul N, Kularbkaew C, Yutanawiboonchai W. Fine needle aspiration in a malignant lymphoepithelial lesion: a case report. Acta Cytol 2008 2008;52(3):369–372. doi:https://doi.org/10.1159/000325526.
77. Agaimy A, Hartmann A, Antonescu CR, et al. SMARCB1 (INI-1)-deficient Sinonasal carcinoma: A series of 39 cases expanding the morphologic and Clinicopathologic Spectrum of a recently described entity. Am J Surg Pathol. 2017;41(4):458–71. https://doi.org/10.1097/PAS.0000000000000797.
78. Bishop JA, Antonescu CR, Westra WH. SMARCB1 (INI-1)-deficient carcinomas of the sinonasal tract. Am J Surg Pathol Sep 2014;38(9):1282–1289. doi:https://doi.org/10.1097/PAS.0000000000000285.
79. Bell D, Hanna EY, Agaimy A, Weissferdt A. Reappraisal of sinonasal undifferentiated carcinoma: SMARCB1 (INI1)-deficient sinonasal carcinoma: a single-institution experience. Virchows Arch. 2015;467(6):649–56. https://doi.org/10.1007/s00428-015-1853-1.
80. Allard FD, Bell D, Stelow EB. Cytopathologic features of SMARCB1 (INI-1)-deficient sinonasal carcinoma. Cancer Cytopathol. 2018;126(8):567–74. https://doi.org/10.1002/cncy.22020.

81. Dutta R, Nambirajan A, Mittal S, Roy-Chowdhuri S, Jain D. Cytomorphology of primary pulmonary NUT carcinoma in different cytology preparations. Cancer Cytopathol. 2021;129(1):53–61. https://doi.org/10.1002/cncy.22342.
82. Kuroda S, Suzuki S, Kurita A, et al. Cytological features of a variant NUT midline carcinoma of the lung harboring the NSD3-NUT fusion gene: A case report and literature review. Case Rep Pathol. 2015;2015:572951. https://doi.org/10.1155/2015/572951.
83. Bellizzi AM, Bruzzi C, French CA, Stelow EB. The cytologic features of NUT midline carcinoma. Cancer. 2009;117(6):508–15. https://doi.org/10.1002/cncy.20044.
84. Lee T, Choi S, Han J, Choi YL, Lee K. Abrupt Dyskeratotic and Squamoid cells in poorly differentiated carcinoma: case study of two thoracic NUT midline carcinomas with Cytohistologic correlation. J Pathol Transl Med. 2018;52(5):349–53. https://doi.org/10.4132/jptm.2018.07.16.
85. Bellizzi AM, Bourne TD, Mills SE, Stelow EB. The cytologic features of sinonasal undifferentiated carcinoma and olfactory neuroblastoma. Am J Clin Pathol. 2008;129(3):367–76. https://doi.org/10.1309/C00WN1HHJ9AMBJVT.
86. Rama Reddy B, Rajeswari R, Das B, Uppada R, Sreedhar T, Parankusa N. Fine Needle Aspiration Cytology of Spectrum of Sinonasal Lesions with Histopathological Correlation. *Journal of Dental and Medical Sciences*. 2015;14(2):75–82.
87. Kak I, Perez-Ordonez B. Sinonasal tract pathology: an updated review of select entities. Diagn Histopathol. 2019;25(7):265–73.
88. Tummidi S, Kothari K, Patil R, Singhal SS, Shah V. Sinonasal adenoid cystic carcinoma-role of on-site FNAC: a case report. BMC Ear Nose Throat Disord. 2018;18:6. https://doi.org/10.1186/s12901-018-0053-4.
89. Buch AC, Panicker N, Sarawagi S, Anwekar S, Kharat AT. Fine needle aspiration cytology diagnosis of paravertebral extraosseus Ewing's sarcoma. J Cytol. 2010;27(4):146–8. https://doi.org/10.4103/0970-9371.73304.
90. Bordia S, Meena S, Meena BK, Rajak V. Fine-needle aspiration cytology of Ewing's sarcoma of thoracic spine with extension into the Intradural space. Case Rep Oncol Med. 2014;2014:351386. https://doi.org/10.1155/2014/351386.
91. Miller DL, Roy-Chowdhuri S, Illei P, James A, Hruban RH, Ali SZ. Primary pancreatic Ewing sarcoma: a cytomorphologic and histopathologic study of 13 cases. J Am Soc Cytopathol. 2020;9(6):502–12. https://doi.org/10.1016/j.jasc.2020.04.013.
92. Fröstad B, Tani E, Brosjö O, Skoog L, Kogner P. Fine needle aspiration cytology in the diagnosis and management of children and adolescents with Ewing sarcoma and peripheral primitive neuroectodermal tumor. Med Pediatr Oncol. 2002;38(1):33–40. https://doi.org/10.1002/mpo.1260.
93. Thompson LD. Small round blue cell tumors of the sinonasal tract: a differential diagnosis approach. *Mod Pathol*. 2017;30(s1):S1–S26. doi:https://doi.org/10.1038/modpathol.2016.119.
94. Saleh HA, Clayman L, Masri H. Fine needle aspiration biopsy of intraoral and oropharyngeal mass lesions. Cytojournal. 2008;5:4. https://doi.org/10.1186/1742-6413-5-4.
95. Stamatakos MD, Houston GD, Fowler CB, Boyd E, Solanki PH. Diagnosis of ameloblastoma of the maxilla by fine needle aspiration. A case report. Acta Cytol. 1995;39(4):817–20.
96. Philip JK, Al-Jassar A, Naquib IS, Usmani S, El-Kabani M, Refaat SM. Primary non-Hodgkin lymphoma of frontal sinus diagnosed by fine needle aspiration cytology. Gulf J Oncolog. 2013;1(13):92–5.
97. Liu CY, Tsai HC. Comparison of diagnostic Cytomorphology of natural killer/T-cell lymphoma (nasal type) in conventional smears, liquid-based preparations, and histopathology. Case Rep Pathol. 2018;2018:6264810. https://doi.org/10.1155/2018/6264810.
98. Ng WK, Lee CY, Li AS, Cheung LK. Nodal presentation of nasal-type NK/T-cell lymphoma. Report of two cases with fine needle aspiration cytology findings. Acta Cytol. 2003;47(6):1063–8. https://doi.org/10.1159/000326648.
99. Kishimoto K, Kitamura T, Hirayama Y, Tate G, Mitsuya T. Three cases of extranodal NK/T-cell lymphoma of the nasal type diagnosed by nasal brush cytology. Diagn Cytopathol. 2007;35(2):125–9. https://doi.org/10.1002/dc.20604.
100. Kaur K, Kakkar A, Bhardwaj N, et al. Spectrum of cytomorphological features of extranodal NK/T-cell lymphoma, nasal type. Cytopathology. 2019;30(4):393–401. https://doi.org/10.1111/cyt.12705.

Infective Pathology of the Sinonasal Tract

5

Aanchal Kakkar

5.1 Introduction

Rhinosinusitis, or inflammation of the mucosa of the nasal cavity and paranasal sinuses, is the most common disease of the sinonasal tract. Based on the duration of symptoms and signs, it is classified as acute, sub-acute, or chronic. The sinonasal tract plays host to a variety of viral, bacterial, fungal, and parasitic infections, many of which are endemic in tropical countries and are increasingly being reported from non-endemic regions due to global travel. Barring viral rhinosinusitis, most of these infections are rare, and have non-specific clinical presentations, resulting in delayed diagnosis and considerable morbidity. Sinonasal infectious diseases and their causative organisms are summarized in Table 5.1.

Table 5.1 Sinonasal infectious diseases and their causative organisms

Causative organism	Infective disease
Viruses	
Rhinovirus Adenovirus Influenza and parainfluenza viruses Respiratory syncytial virus Enterovirus	Acute rhinosinusitis
Bacteria	
S. pneumoniae H. Influenzae M. Catarrhalis	Bacterial rhinosinusitis
Klebsiella rhinoscleromatis	Rhinoscleroma
Mycobacterium tuberculosis	Tuberculosis
Mycobacterium leprae	Leprosy
Pseudomonas aeruginosa, Staphylococcus aureus, Proteus spp., Escherichia spp.	Botryomycosis
Treponema pallidum	Syphilis
Fungi	
Aspergillus sp. Dematiaceous fungi (*Bipolaris*, *Curvularia*, *Alternaria)*	Allergic fungal sinusitis Mycetoma or fungal ball
Aspergillus sp. Mucorales (*Rhizopus*, *Mucor*, *Rhizomucor*)	Invasive fungal sinusitis
Entomophthorales (*Conidiobolus coronatus*)	Rhinofacial entomophthoromycosis
Histoplasma capsulatum	Histoplasmosis
Cryptococcus neoformans	Cryptococcosis
Protozoa	
Leishmania	Leishmaniasis
Mesomycetozoea	
Rhinosporidium seeberi	Rhinosporidiosis

5.2 Acute and Chronic Rhinosinusitis

Acute rhinosinusitis refers to an inflammatory process with symptoms that last up to 4 weeks. It is typically of infectious etiology, with viral infection accounting for more than 95% of cases. The common causative viruses include rhinovirus, adenovirus, influenza and parainfluenza viruses, respiratory syncytial virus, and enterovirus. Bacterial rhinosinusitis may rarely occur as a primary infection, but more often occurs as a secondary infection superimposed on viral rhinosinusitis. S. pneumoniae, H. influenzae, M. catarrhalis and, less commonly, S. pyogenes and S. aureus are implicated as the causative organisms.

Patients with acute rhinosinusitis present with nasal obstruction and watery nasal discharge; bacterial rhinosinusitis is associated with a purulent discharge.

Imaging shows mucosal thickening and air fluid levels within the sinuses. Although not frequently sampled for histological examination, the sinonasal mucosa shows an acute inflammatory cell infiltrate, with neutrophils being more prominent in bacterial rhinosinusitis. Stroma edema is also present. Treatment for acute viral rhinosinusitis is

A. Kakkar (✉)
Department of Pathology, All India Institute of Medical Sciences, New Delhi, India
e-mail: draanchalkakkar@aiims.edu

D. Jain, J. A. Bishop (eds.), *Atlas of Sinonasal Tract Pathology*, https://doi.org/10.1007/978-981-19-7315-4_5

symptomatic, while bacterial rhinosinusitis is managed with antibiotics.

Rhinosinusitis is considered chronic when symptoms last longer than 12 weeks. It is most frequently of allergic etiology, seen in atopic individuals. On endoscopic examination, the sinonasal mucosa appears edematous and bluish. Inflammatory nasal polyps may or may not be present. On histological examination, there is marked stromal edema, along with a mixed inflammatory infiltrate consisting of lymphocytes, plasma cells, histiocytes, and few eosinophils and neutrophils. Eosinophils are prominent in chronic allergic rhinosinusitis. Variable squamous metaplasia and goblet cell hyperplasia may be present. Long-standing cases may show epithelial hyperplasia thrown into papillary folds, i.e., hyperplastic papillary sinusitis.

5.3 Sinonasal Fungal Infections

Fungi are ubiquitously present in the environment, making exposure to them unavoidable. The extent of involvement of the sinonasal tract by fungal infections is therefore determined by the immune status of the host, ranging from an indolent colonization to aggressively invasive rhino-orbito-cerebral infections. Several conditions predispose individuals to sinonasal fungal infections by resulting in an immunocompromised state, including diabetes mellitus, HIV infection, and chemotherapy. While this holds true for the commoner fungal infections of the sinonasal tract, e.g., mucormycosis, rare infections like entomophthoromycosis occur in immunocompetent individuals, with no known predisposing factors. Sinonasal fungal infections are broadly classified into invasive and non-invasive rhinosinusitis. Non-invasive fungal sinusitis usually occurs in immunocompetent individuals, and includes mycetoma or fungal ball, and allergic fungal sinusitis. Invasive fungal sinusitis is frequent in immunocompromised patients.

Mycetoma or fungal ball presents with nasal obstruction and/or facial pain and heaviness. Fungal spores are inhaled from the environment, enter the sinuses through the ostia, where static secretions due to deficient mucociliary clearance provide an anaerobic environment favorable for their reproduction. Often, a single sinus is involved, with the maxillary sinus being involved most frequently, followed by the sphenoid and ethmoid sinuses. On imaging, the sinus appears opacified, and may or may not show calcification. Histological examination shows aggregates of fungal hyphae that are entangled together and enmeshed in fibrin (Fig. 5.1). Sporangia and conidia, commonly known as fruiting bodies, and fungal spores may be seen. Mucosa that is sampled does not show the presence of fungi, and there is minimal inflammatory reaction. Aspergillus is the most common genus to be isolated; however, Mucorales and dematiaceous fungi can also cause a fungal ball.

Allergic fungal rhinosinusitis (AFRS) is an IgE-mediated hypersensitivity reaction to antigens of fungal organisms that have colonized the sinonasal passages. It affects immunocompetent individuals particularly those with history of atopy and asthma, involving multiple sinuses bilaterally. Patients present with nasal obstruction and discharge, and facial heaviness and swelling. In severe cases, proptosis and facial deformity can occur. On endoscopy, the sinuses contain thick, tenacious fungal muck, with a consistency described as clay-like, or akin to peanut butter. Peripheral blood examination may show increased eosinophils and elevated serum IgE.

On microscopy (Fig. 5.2), abundant allergic mucin is seen, separate from mucosal fragments. It characteristically displays an alternating pattern of laminations, imparting a rippled, tigroid, or "tree-ring" appearance. Viable and degranulated eosinophils are enmeshed in mucin, giving the reddish-pink hue to alternate laminae, while nuclear debris from the inflammatory cells aggregates to form the blue laminae. Needle shaped or bipyramidal Charcot–Leyden crystals, a degradation product of eosinophils, are a frequent finding. Fungal hyphae are rarely appreciated on HE staining; however, PAS-D and Gomori methenamine silver highlight fungal hyphae, which are often distorted or fragmented. Importantly, the demonstration of fungal elements is not a requisite for making a diagnosis of allergic fungal rhinosi-

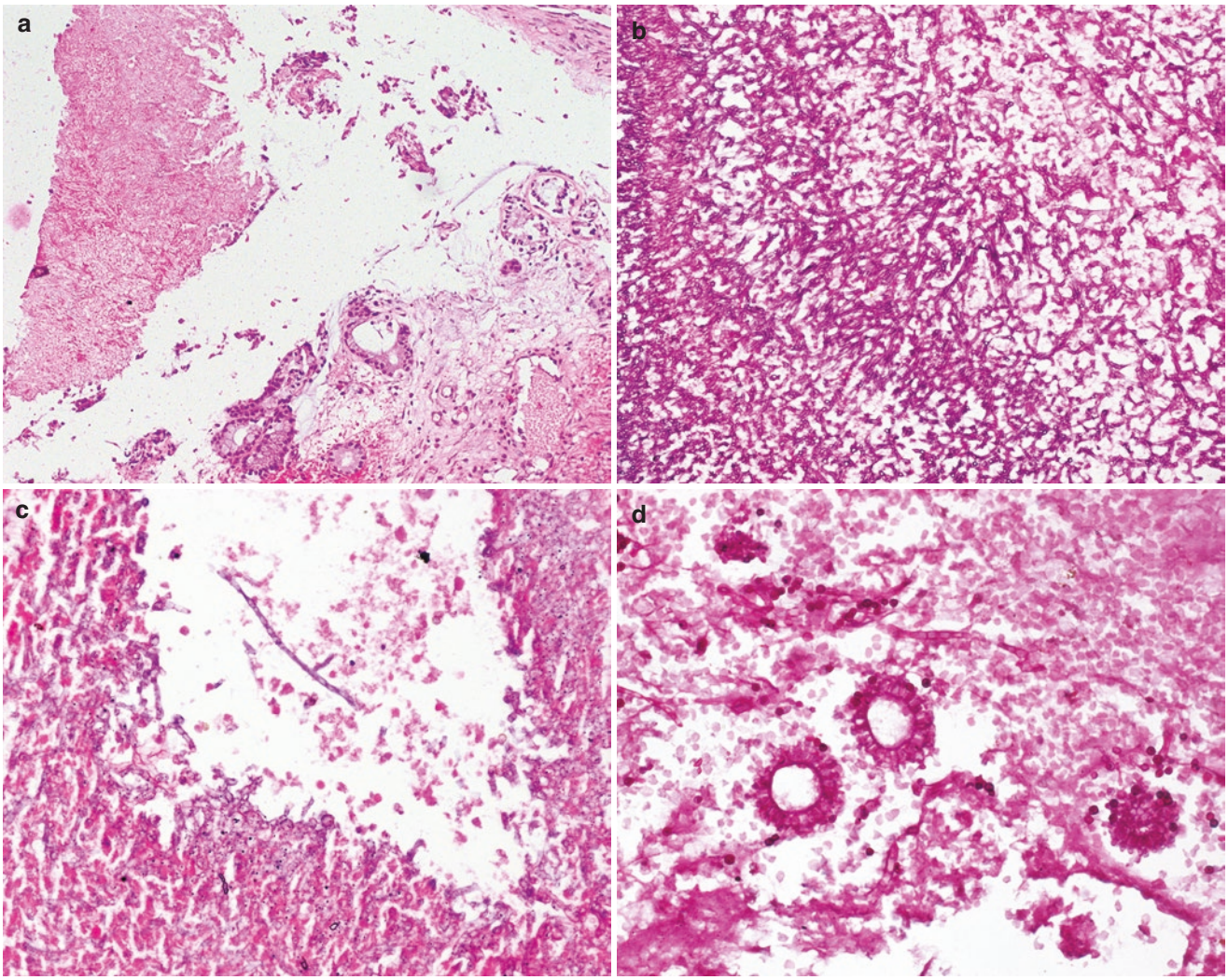

Fig. 5.1 Aggregate of Aspergillus fungal hyphae separate from the nasal mucosa forming a fungal ball (**a**, HE, 4x; **b**, Periodic acid–Schiff [PAS], 10X); acute-angled branching and septa are evident (**c**, HE, 20X); fruiting bodies with a central vesicle, radiating phialides, and scattered brownish pigmented spores may be seen (**d**, PAS, 40X)

nusitis. Mucosal fragments, when present, may show a subepithelial inflammatory infiltrate, but abscesses, necrosis, and fungal hyphae are not seen.

Majority of AFRS are attributed to *Aspergillus* spp. Other causative fungi include dematiaceous fungi, i.e., *Bipolaris*, *Curvularia*, *Alternaria, Exserohilum,* and *Phialophora*. Fungal hyphae of *Aspergillus* spp. show acute-angled dichotomous branching, i.e., two equal branches forming from the division of one hyphal stem. Septations are easily identified. Conidia or fruiting bodies may be seen in a fungal ball and consist of a central vesicle with attached radiating phialides and chains of spores.

The hyphae of dematiaceous fungi (Fig. 5.3) show septae with constrictions [1]. They appear brown in color due to the presence of melanin, which can be demonstrated by Fontana Masson staining if not evident on HE stain. Conidia, which are thick-walled vesicular swellings with internal septations, may be seen in fungal balls. Hyphae and yeast forms may be seen in non-invasive and invasive infections, being present within necrotic foci and multinucleated giant cells in the latter.

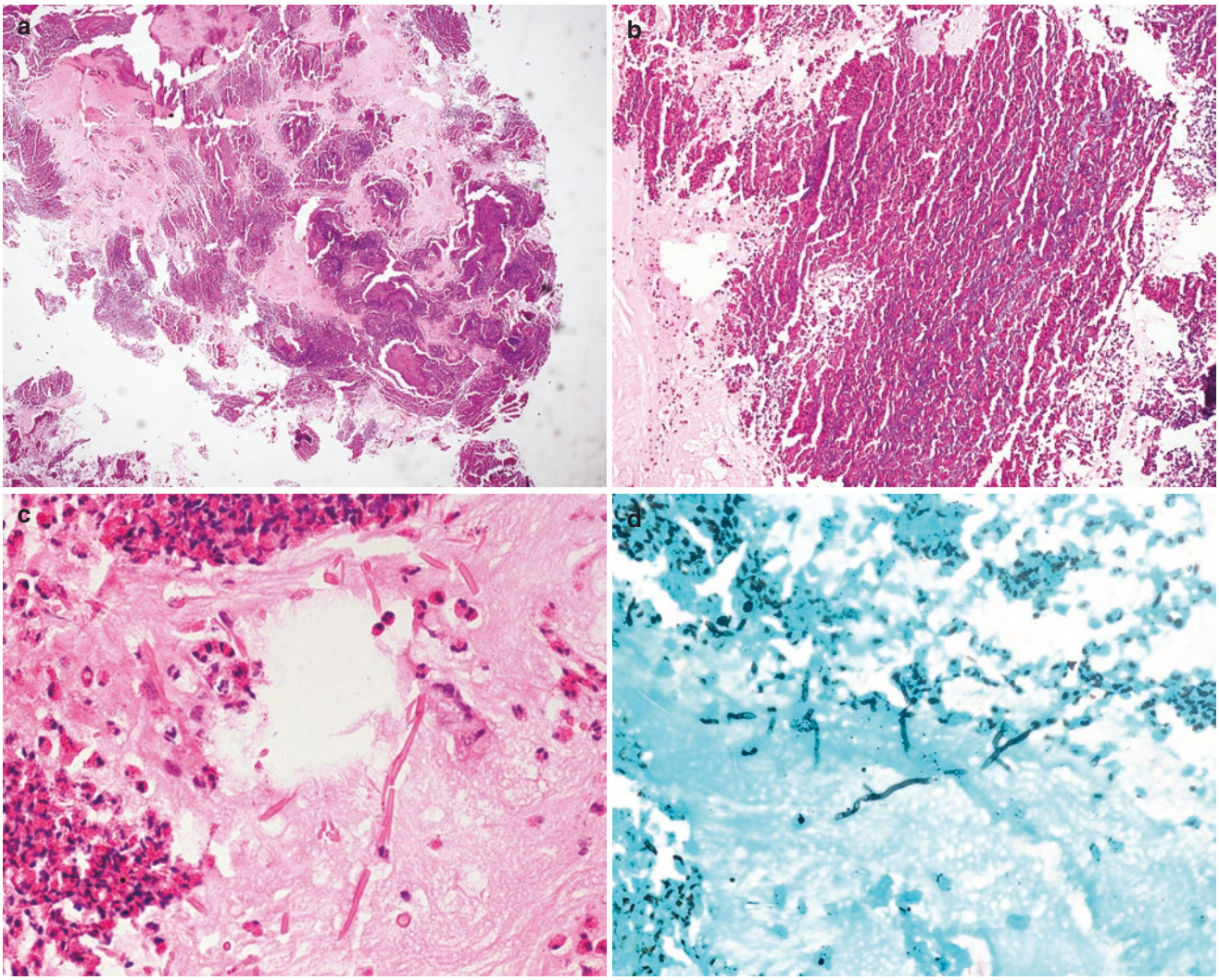

Fig. 5.2 Allergic fungal rhinosinusitis: Abundant allergic mucin (**a**, HE, 2X) with an alternating pattern of laminations (**b**, HE, 10X), showing numerous viable and degranulated eosinophils along with few needle-shaped or bipyramidal Charcot–Leyden crystals (**c**, HE, 40X). GMS shows fungal hyphae with acute-angled branching morphologically suggestive of Aspergillus sp. (**d**, Gomori methenamine silver [GMS], 40X)

5.3.1 Invasive Fungal Sinusitis

Invasive fungal sinusitis is a potentially lethal infection with extensive tissue destruction and an aggressive clinical course. It is defined by the presence of fungal hyphae within the mucosa and submucosa, with or without angioinvasion. It is of two types, acute invasive or chronic invasive fungal sinusitis; the latter may or may not show a granulomatous tissue response. Acute invasive fungal sinusitis is chiefly seen in immunocompromised persons, particularly those with hematological malignancies, post-transplant, and diabetics. *Aspergillus* is the most common causative species. The disease progresses rapidly to involve the orbit, leading to loss of vision. Surgical debridement of involved tissues is often required, with intraoperative frozen section to evaluate tissues for the presence or absence of fungal hyphae.

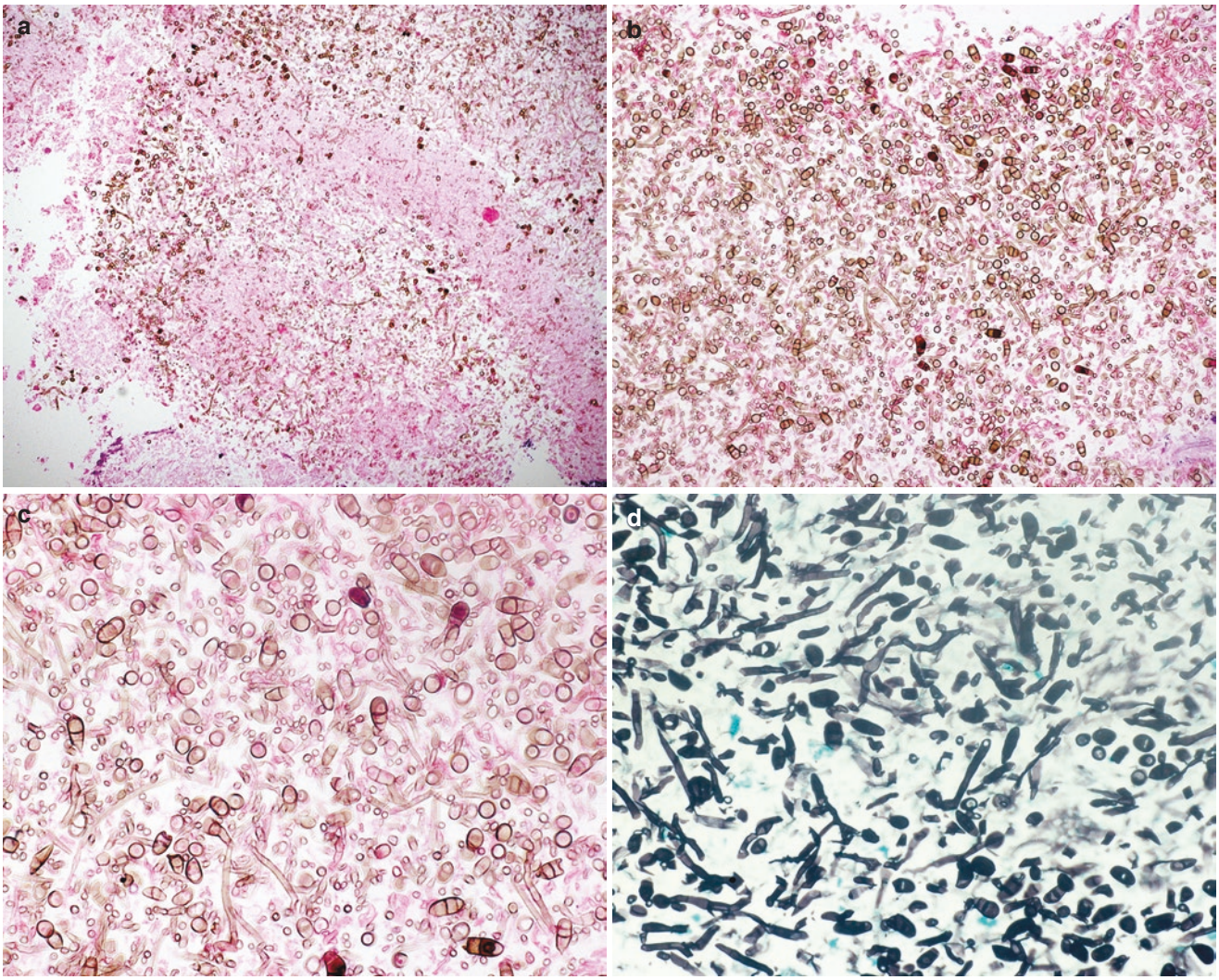

Fig. 5.3 Narrow brown pigmented and non-pigmented hyphae (**a**, HE, 10X) showing septae with constrictions (**b**, HE, 20X). Many conidia with thick walls and internal septations are seen (**c**, HE, 40X). GMS stain highlights the constrictions (**d**, GMS, 40X). Curvularia sp. was grown on culture

Histologically (Fig. 5.4a–c), necrosis is present; however, inflammatory infiltrate is sparse. Fungal hyphae can be identified with the aid of GMS and PAS stains. Angioinvasion with or without bone invasion may be present. Serum galactomannan assay has been used as a surrogate marker of tissue invasion. The main differential diagnosis is mucormycosis; the morphology of fungal hyphae (detailed below) can distinguish between the two.

Chronic invasive fungal sinusitis is seen in immunocompetent or immunocompromised patients, who present with features of chronic rhinosinusitis. It is most commonly caused by *Aspergillus spp.* Fungal hyphae are identified in the submucosa, accompanied by a mixed inflammatory infiltrate, but angioinvasion is infrequent. Chronic granulomatous fungal rhinosinusitis (Fig. 5.4d–h) is characterized by the presence of submucosal well-defined granulomas with prominent fibrosis; variable mixed inflammatory cell infiltrate, necrosis, and vasculitis may be present. Fungal hyphae are few, usually identified within the granulomas and multinucleated giant cells with the help of histochemical stains.

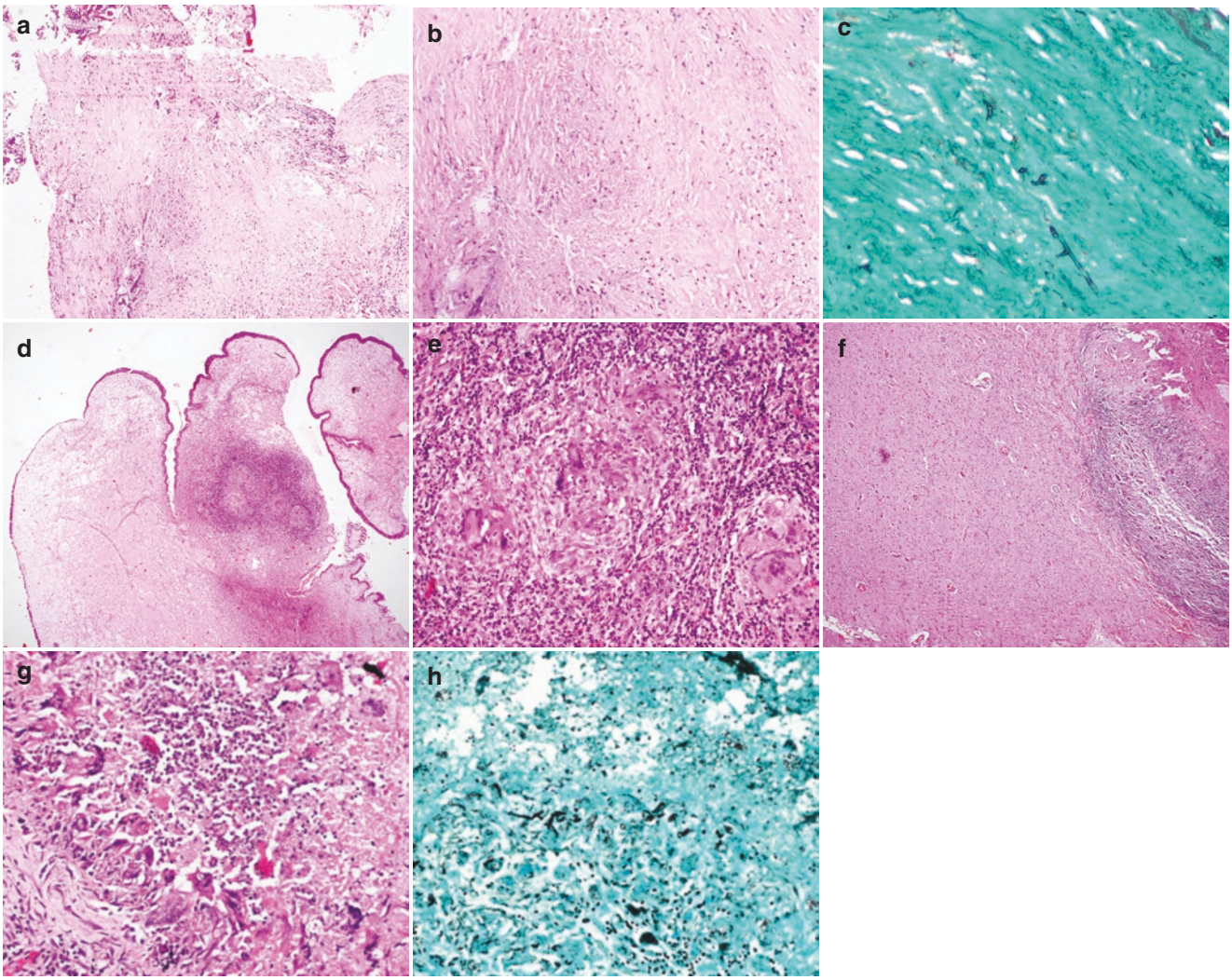

Fig. 5.4 Acute invasive fungal sinusitis shows necrosis of nasal mucosa (**a**, HE, 4X) with sparse inflammation (**b**, HE, 10X); GMS highlights hyphae of Aspergillus within the necrosis (**c**, GMS, 20X). Chronic granulomatous fungal sinusitis: Edematous and polypoid nasal mucosa with submucosal well-defined granulomas (**d**, HE, 2X) composed of epithelioid histiocytes and multinucleated giant cells (**e**, HE, 20X); brain involvement with granulomas (**f**, HE, 4X) showing central necrosis (**g**, HE, 20X); GMS highlights slender fungal hyphae within the granulomas (**h**, GMS, 20X)

Differential diagnosis includes eosinophilic angiocentric fibrosis (EAF), a rare chronic inflammatory and fibrosing disorder that affects the nasal cavity, particularly the septum, and presents as slowly progressive nasal obstruction. Biopsies show features of eosinophilic angiitis in the early stages, while dense perivascular onion-skin fibrosis with hyalinization is seen later in the disease process [2]. A mixed inflammatory cell infiltrate is present; IgG4-positive plasma cells are increased. While the presence of eosinophils may raise concern for fungal infection, necrosis, granulomas, fungal hyphae, and vascular thrombosis are not seen.

5.3.2 Sinonasal Mucormycosis

Sinonasal mucormycosis is an acute, rapidly progressive fungal infection caused by the order *Mucorales* that belongs to the subphylum *Mucoromycotina.* Among Mucorales, the genera *Rhizopus*, *Mucor,* and *Rhizomucor* are responsible for most infections in humans. Spores which are ubiquitous in the environment cause disease when inhaled, particularly in immunocompromised individuals. Diabetes mellitus, particularly diabetic ketoacidosis, is the most common risk factor for development of sinonasal mucormycosis. Glucose-

regulated protein 78 (GRP78) is an endoplasmic reticulum chaperone that acts as a cellular receptor to which the COTH3 spore coat protein antigen of Mucorales binds. Other risk factors include the use of systemic steroids, neutropenia, hematological malignancies, and stem cell transplant. The recent COVID-19 pandemic has seen a surge in cases of sinonasal mucormycosis [3]; however, the pathogenetic mechanisms remain to be elucidated. Mucosa appears necrotic with a blackish discoloration due to angioinvasion and vascular thrombosis. If untreated, sinonasal infection rapidly progresses to involve the orbit and brain, resulting in complete loss of vision and even death.

The histological picture is dominated by necrosis (Fig. 5.5) which has been termed bland or infarct-like, as cellular outlines are not seen within it. Initially, acute suppurative inflammation is present, with a dirty blue-gray appearance of necrosis with a neutrophilic infiltrate. Neutrophil micro-abscesses may be seen. The necrotic foci often show round to ovoid eosinophilic deposits with a peripheral basophilic rim, accompanied by light brownish colored, refractile deposits of similar size and shape. The latter are strongly birefringent on polarized microscopy. In chronic disease, ill-defined granulomas are formed (Fig. 5.6), with a central neutrophilic micro-abscess surrounded by histiocytes, lymphocytes, and multinucleated foreign body giant cells. Well-defined granulomas are less common. Angioinvasion and neural invasion by fungal hyphae are frequent findings.

Mucorales (Fig. 5.7) are characterized by broad (6 to 50 μm), pauciseptate, thin-walled, amphophilic hyphae that appear translucent on HE staining. The hyphae are folded upon themselves, imparting a ribbon-like appearance, and show branching at various angles, ranging from 45° to 90°. Fungal balls may be seen alongside invasive infections, particularly within the necrotic contents of the maxillary sinus. These may contain sporangia, thick-walled sacs 50 to 300 microns in diameter, which contain sporangiospores, which range from 4 to 8 μm in diameter, and show a Maltese cross

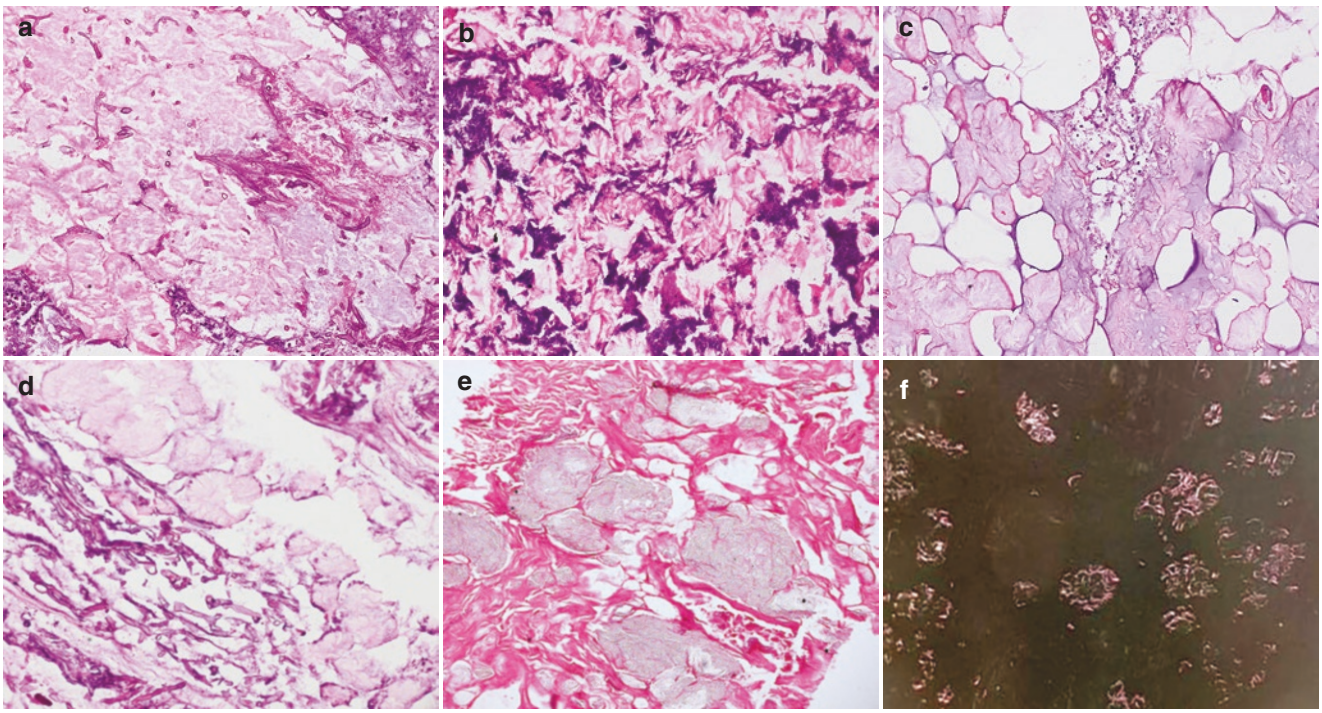

Fig. 5.5 Mucormycosis: Bland necrosis lacking cellular outlines (**a**, HE, 20X), initially with a dirty blue appearance due to neutrophilic debris (**b**, HE, 20X); fungal hyphae are usually found within or close to round to ovoid eosinophilic deposits with peripheral basophilic rim (**c**, HE, 20X), made conspicuous on PAS stain (**d**, PAS, 20X); pale brown refractile crystalline deposits are also frequent (**e**, HE, 10X) and are birefringent on polarized microscopy (**f**, HE, 4X)

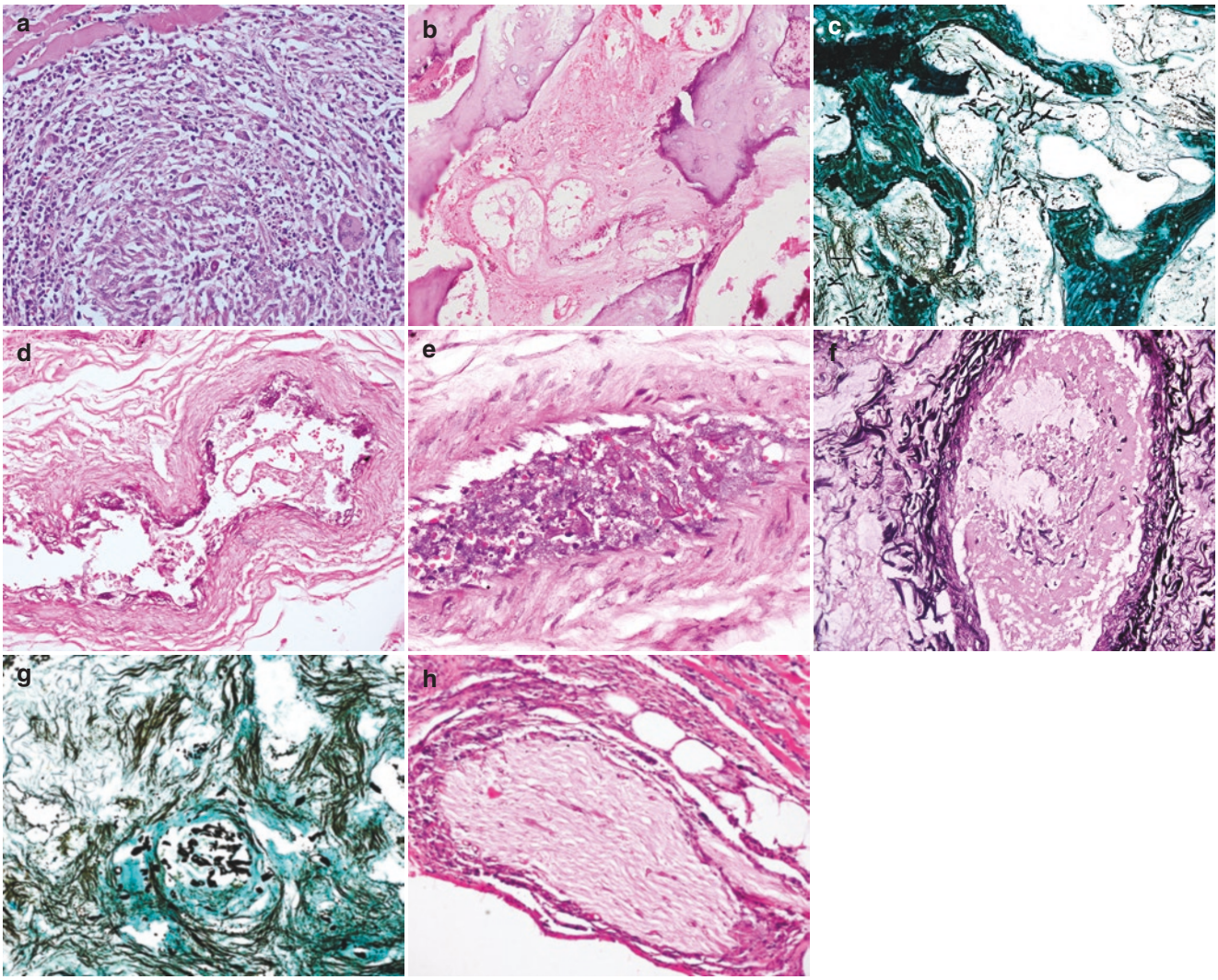

Fig. 5.6 Mucormycosis: Suppurative granuloma in soft tissue (**a**, HE, 20X); necrotic bone and intertrabecular spaces (**b**, HE, 20X) showing fungal hyphae on GMS (**c**, GMS, 10X); fungal hyphae invading vessel walls (**d**, HE, 20X) and seen in the vascular lumen (**e**, HE, 40X) highlighted on special stains (**f**, PAS, 20X; **g**, GMS, 20X); neural invasion (**h**, HE, 20X)

appearance on polarization. The sporangia are attached to a long, broad, relatively rigid unbranched hyphal structure known as a sporangiophore. The sporangia, sporangiophores, and sporangiospores may show brownish pigmentation [4].

Differential diagnosis includes granulomatosis with polyangiitis (GPA), previously known as Wegener granulomatosis, which is a systemic immune-mediated vasculitis of unknown etiology that affects the head and neck region, particularly the sinonasal tract, the kidneys, and lungs. The head and neck is involved in up to 80% of cases [5]. Rarely, only the sinonasal tract is involved, sparing other organs. Histologically, GPA is characterized by the classic triad of vasculitis, granulomatous inflammation, and ischemic geographic necrosis. Granulomatous inflammation takes the form of scattered multinucleated giant cells rather than well-formed granulomas with epithelioid histiocytes. Vasculitis involves small- and medium-sized arteries. The necrosis, variably termed biocollagenolytic or necrobiotic, has a smudgy basophilic appearance. In most cases, all three features are rarely encountered. Serological testing for elevated c-ANCA and proteinase 3 (PR3) aids in diagnosis.

Combined fungal infections (Fig. 5.8) such as mucormycosis with aspergillosis, and mucormycosis with candida do

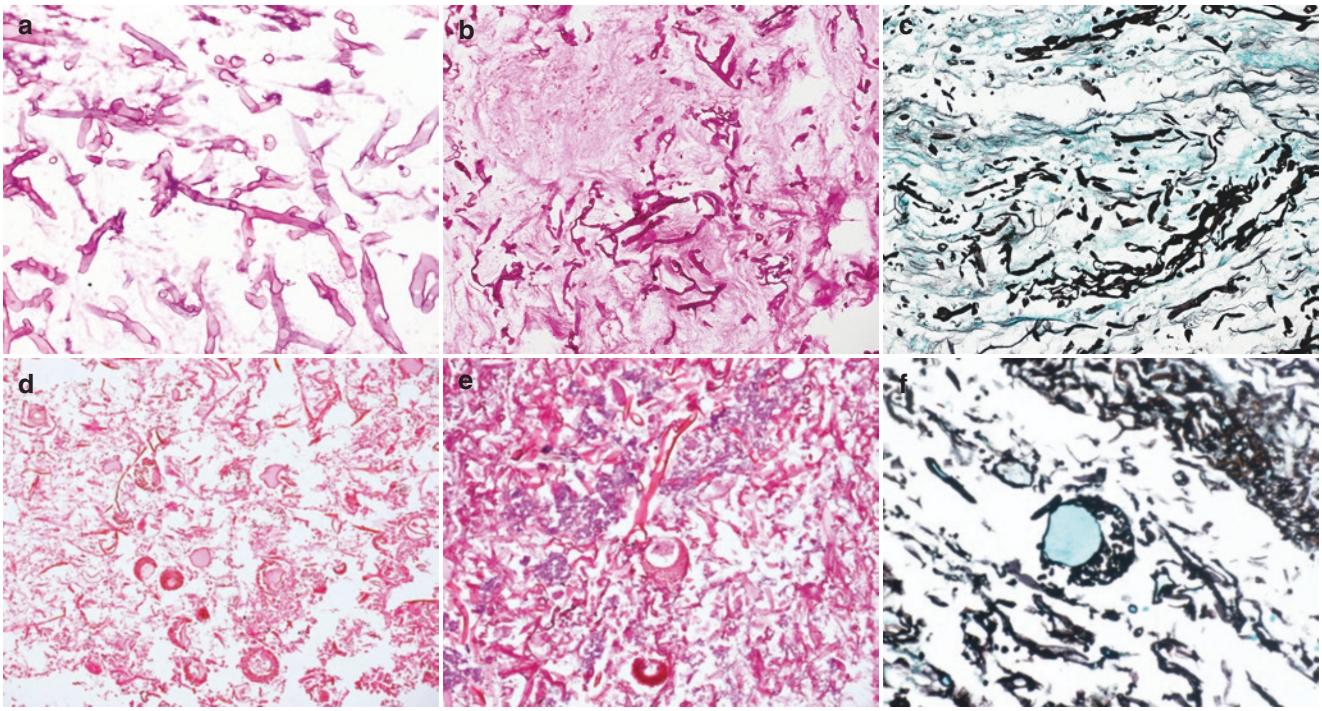

Fig. 5.7 Mucorales: Broad, ribbon-like hyphae with non-parallel walls and variable-angle branching, folded upon themselves (**a**, HE, 40X) stained with PAS (**b**, PAS, 20X) and GMS (**c**, GMS, 20X); fungal ball with sporangia, spores, and sporangiophores (**d**, HE, 10X); sporangia are thick-walled sac-like structures that contain spores 4–8 microns in diameter (**e**, HE, 20X; **f**, GMS, 40X)

occur on occasion, and a high index of suspicion is necessary to diagnose them. Broad pauciseptate hyphae that stain lightly with GMS are indicative of mucormycosis; abundant septations and acute-angled branching identify aspergillosis; presence of yeasts and pseudohyphae indicates *Candida. In-situ* hybridization and PCR-based techniques are useful in establishing the presence of dual infections.

5.3.3 Entomophthoromycosis

Entomophthoromycosis, or entomophthoramycosis, is a rare chronic mucocutaneous infection caused by fungal organisms of the subphylum *Mucoromycotina* and order Entomophthorales, which encompasses two genera that cause infection in humans viz. *Conidiobolus coronatus* and *Basidiobolus ranarum.* The former is responsible for causing rhinofacial conidiobolomycosis, endemic in tropical countries such as Africa, Central America, and India. Infection occurs in immunocompetent individuals, when fungal spores ubiquitously present in soil and dust are inhaled and cause traumatic inoculation of the nasal mucosa. Slow-growing, firm to hard, locally invasive masses develop, which simulate granulomatous diseases and even malignancy.

A high index of suspicion is required to make the diagnosis of rhinofacial entomophthoromycosis on histological examination. Biopsies (Fig. 5.9) show densely eosinophilic antigen-antibody complexes, i.e., Splendore–Hoeppli phenomenon radiating around fungal hyphae, which are often seen in cross section rather than along their length. A mixed inflammatory cell infiltrate, often rich in eosinophils, is seen. Vague granulomas and foreign body giant cells are present; however, necrosis is rare. Fungal hyphae, not easily evident on HE staining but better appreciated on GMS and PAS stains, are broad with a diameter of 10–20 μm, have non-parallel walls, and are pauciseptate [6]. When seen in transverse section, they appear to be surrounded by a slightly refractile envelope. Local destruction of tissues is evident; however, angioinvasion, infarction, and necrosis are uncommon. Potassium hydroxide preparation (KOH mount) may demonstrate fungal hyphae, but fungal cultures are often negative, making histological examination the only reliable diagnostic modality. PCR-based assays may be useful, if available. Diagnosis of rhinofacial entomophthoromycosis is

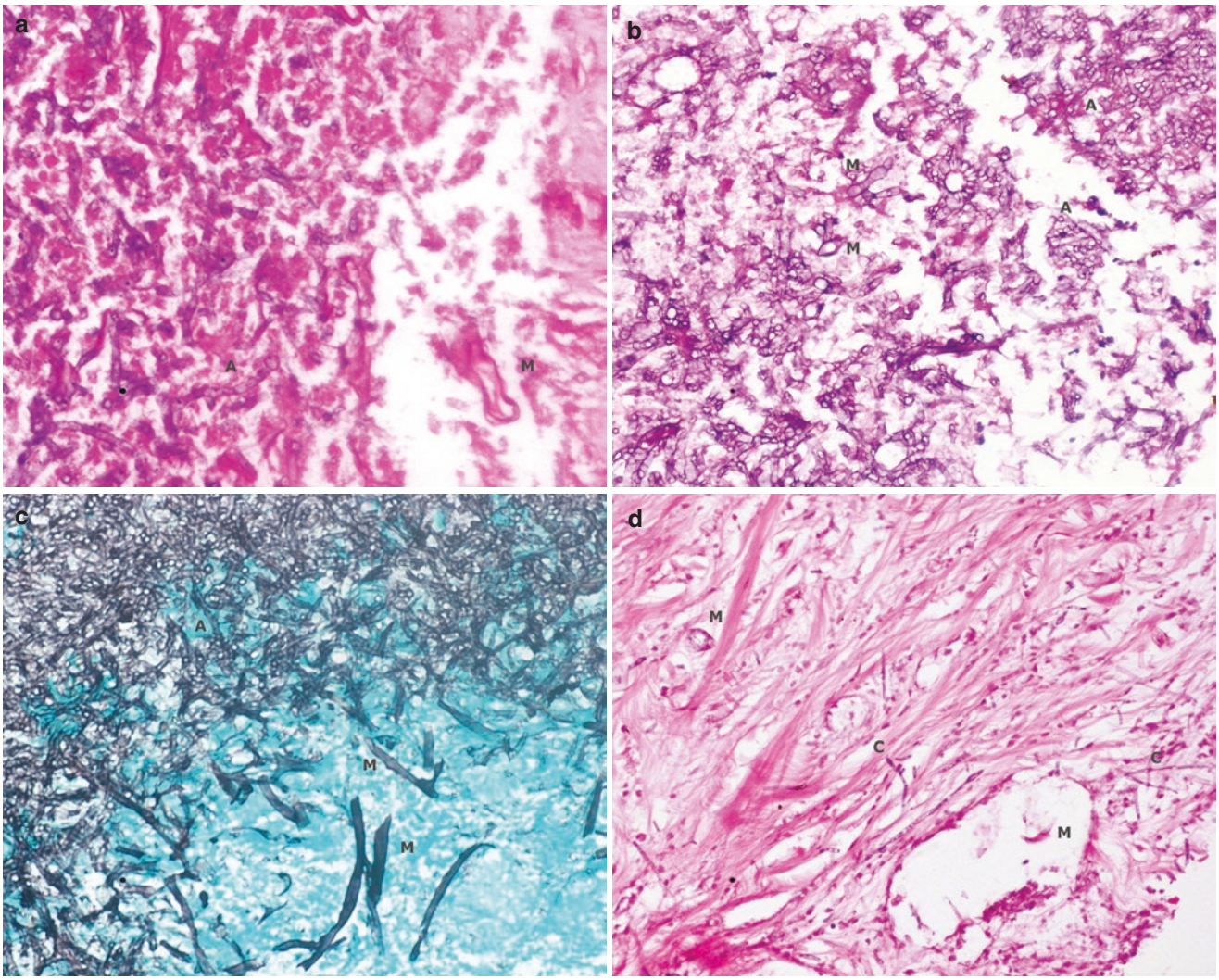

Fig. 5.8 Combined fungal infections: Mucor (M) and aspergillus (A) (**a**, HE, 40X; **b**, PAS, 20X; **c**, GMS, 40X); mucor with candida (C) (**d**, HE, 20X)

critical, as the antifungal treatment differs from that of the commoner invasive aspergillosis and mucormycosis.

5.3.4 Other Rare Fungal Infections

Infections like Histoplasmosis, cryptococcosis, sporotrichosis, blastomycosis, and coccidioidomycosis may extremely rarely involve the sinonasal tract. Histoplasmosis and cryptococcosis can involve the nasal vestibule and nasal mucosa adjacent to it as an extension of facial cutaneous disease, which is more conspicuous than the nasal manifestations, or in disseminated disease in immunocompromised persons. Biopsies show a mixed inflammatory infiltrate with many histiocytes and multinucleated giant cells. The overlying squamous epithelium often shows pseudoepitheliomatous hyperplasia. Special stains demonstrate the organisms within histiocytes and giant cells. Histoplasmosis (Fig. 5.10), caused by *H. capsulatum*, is characterized by the presence of yeasts 2–4 μm in diameter, seen in clusters within macrophages. Their cytoplasm is separated from the surrounding tissue by a clear cell wall. They stain positively with PAS and GMS. Narrow based budding can be present but is difficult to discern.

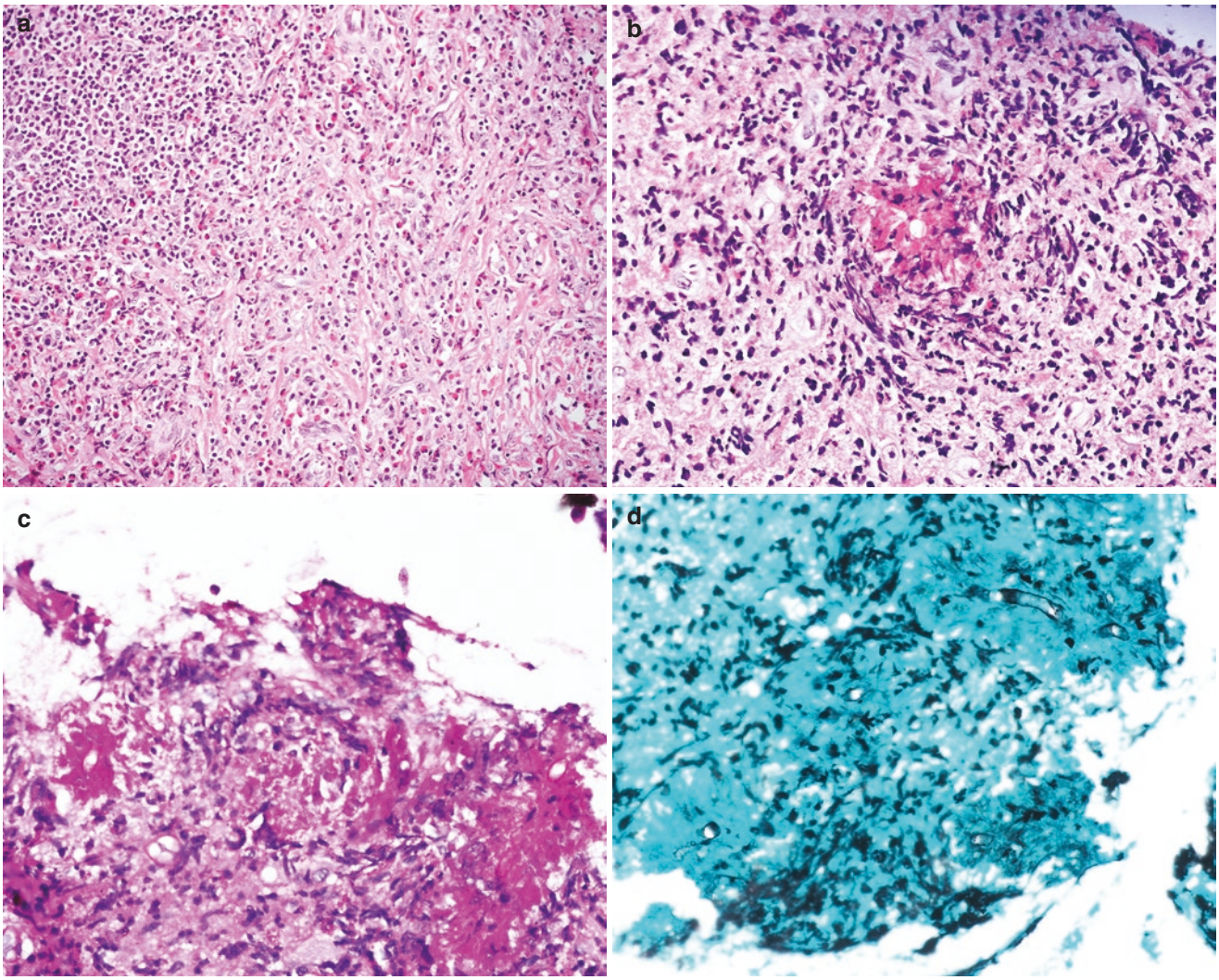

Fig. 5.9 Entomophthoromycosis: Eosinophil rich inflammatory infiltrate (**a**, HE, 20X) with interspersed densely eosinophilic Splendore–Hoeppli phenomenon around fungal hyphae seen in cross section (**b**, HE, 40X; **c**, PAS, 40X); the broad, pauciseptate hyphae with non-parallel walls are rarely seen along their length (**d**, GMS, 40X)

Cryptococcus neoformans, the causative organisms of cryptococcosis (Fig. 5.11), are encapsulated spherical to ovoid yeasts, varying from 5 to 10 μm in diameter; narrow based budding is often evident. The organisms are surrounded by a thick polysaccharide capsule which stains brightly with mucicarmine and Alcian blue, while the cell wall stains with PAS and GMS. Cryptococci also stain with Fontana-Masson due to the presence of melanin. Well-formed epithelioid cell granulomas and fibrosis may be seen. When the yeasts produce lesser amount of polysaccharide capsule, they may resemble other yeasts including Candida and Histoplasma.

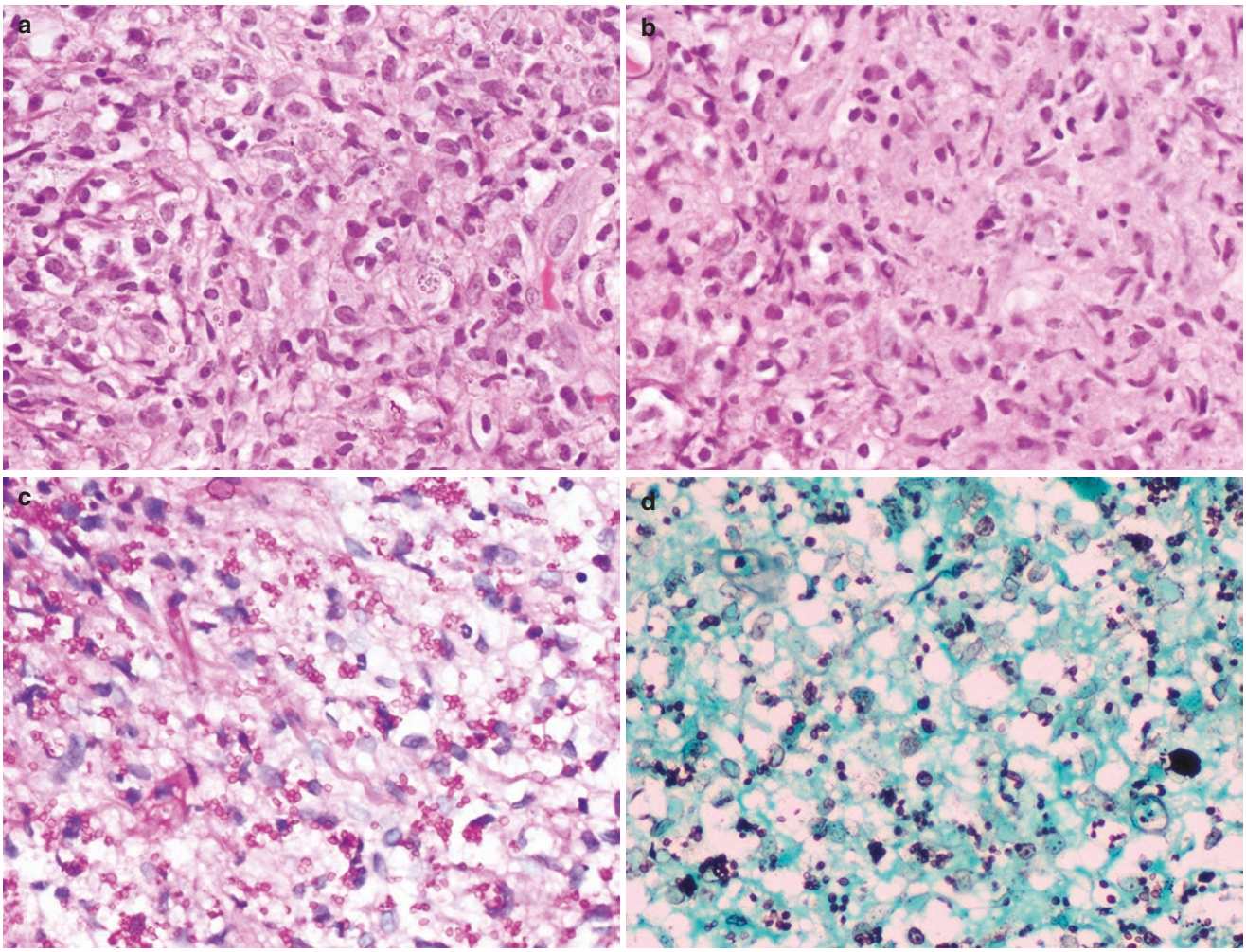

Fig. 5.10 Histoplasmosis: Histiocyte rich inflammatory infiltrate with numerous refractile organisms (**a**, HE, 20X), seen as basophilic yeasts surrounded by a clear cell wall (**b**, HE, 20X), better appreciated on PAS (**c**, 40X) and GMS (**d**, 40X) stains

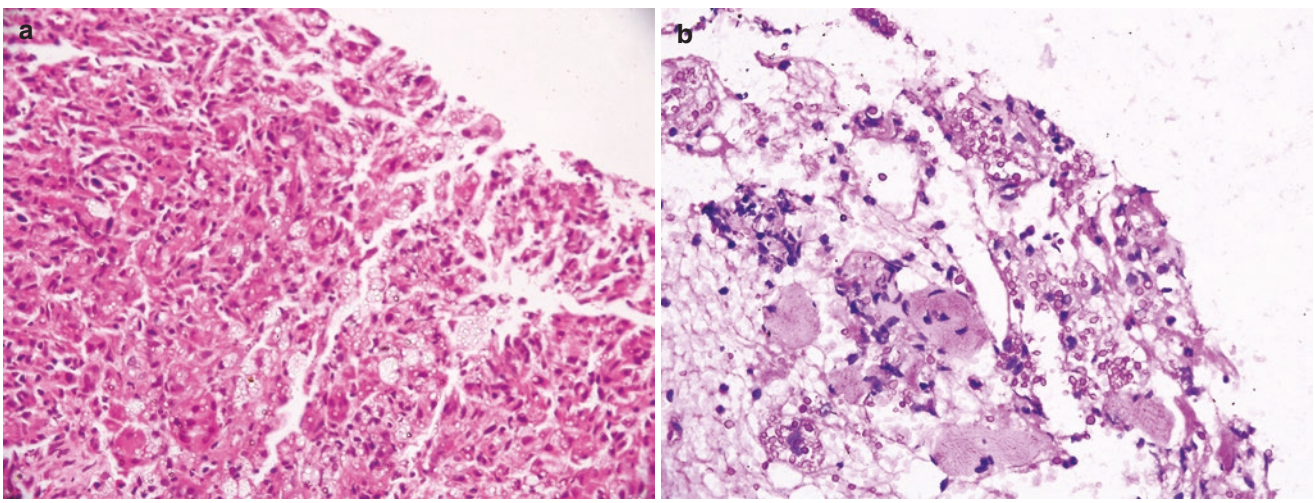

Fig. 5.11 Cryptococcosis reveals yeasts with a refractile capsule in a mixed inflammatory cell infiltrate (**a**, HE, 10X); the cell wall stains with PAS (**b**, PAS, 40X)

5.4 Sinonasal Bacterial Infections

5.4.1 Rhinoscleroma

Rhinoscleroma is a rare chronic infectious granulomatous disease caused by *Klebsiella rhinoscleromatis*, a gram-negative bacterium, that is endemic to tropical and subtropical countries in Africa, tropical and subtropical Asia, Central and South America, and parts of Eastern Europe [5].

Young adults are most frequently affected. Malnutrition, poor hygiene, and overcrowding are socioeconomic factor that contribute to the disease. Cases of rhinoscleroma in non-endemic regions are most often related to travel. The spread of infection is by the airborne route. The nasal mucosa is affected in nearly all cases, and may be accompanied by involvement of the nasopharynx, and, rarely, larynx, trachea, bronchi, and nasolacrimal duct.

Clinically, three progressive stages of the disease are recognized: catarrhal, rhinitic or exudative stage, the proliferative, florid, granulomatous or hypertrophic stage, and the fibrotic, sclerotic or cicatricial stage [7].

The histological features (Fig. 5.12) correlate well with the clinical stages of the disease. In the catarrhal stage, the nasal mucosa undergoes squamous metaplasia and shows a neutrophilic infiltrate. The hypertrophic stage shows the pathognomonic Mikulicz cells, which are large, mononuclear cells with vacuolated or foamy appearing cytoplasm and peripheral nuclei. These cells are often arranged in a nested pattern, surrounded by a rich plasma cell infiltrate in the richly vascularized submucosa. Russell bodies are easily identified. Lymphocytes are also present; however, neutrophils are less prominent. The fibrotic stage is associated with extensive fibrosis and chronic inflammation, but Mikulicz cells are rarely present. Gram stain, Giemsa and Warthin Starry stain are used to demonstrate the Gram-negative Klebsiella bacilli within the cytoplasm of Mikulicz cells. Klebsiella antigens can also be detected immunohistochemically.

Differential diagnosis includes histiocytic lesions, as well as neoplasms with clear cells. Extranodal Rosai–Dorfman disease (RDD) (Fig. 5.13) may involve the nasal cavity, presenting with nasal obstruction and a mass, and a histiocyte- and plasma cell rich infiltrate raises this possibility. Emperipolesis, characteristically seen in RDD, is less prominent at extranodal sites than in lymph nodes and has also been described in rhinoscleroma [8]. However, the histiocytes in Rosai–Dorfman disease are immunopositive for S-100, unlike Mikulicz cells which are S-100 negative and CD68 positive. The latter, accompanied by negativity for cytokeratins, helps to distinguish them from clear cell neoplasms such as myoepithelioma, hyalinizing clear cell carcinoma, and mucoepidermoid carcinoma.

Rhinophyma is a severe form of rosacea that presents clinically with bulbous enlargement of the nose, which on

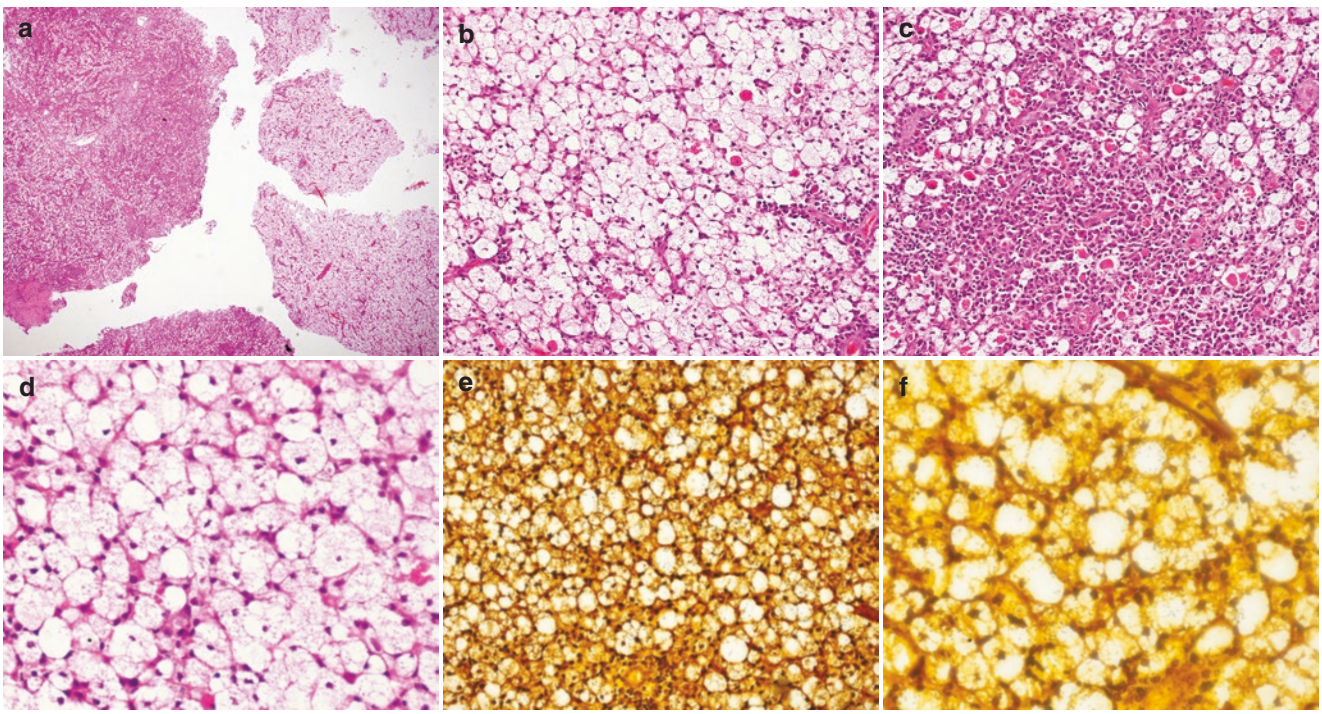

Fig. 5.12 Rhinoscleroma: Mottled appearance of mucosa (**a**, HE, 2X) due to variable admixture of sheets and nests of Mikulicz cells (**b**, HE, 20X) and plasma cells with many Russel bodies (**c**, HE, 20X). Mikulicz cells are large, mononuclear, with vacuolated or foamy cytoplasm (**d**, HE, 40X). Warthin Starry stain reveals numerous bacilli within the foamy cells (**e**, 20X; **f**, 40X)

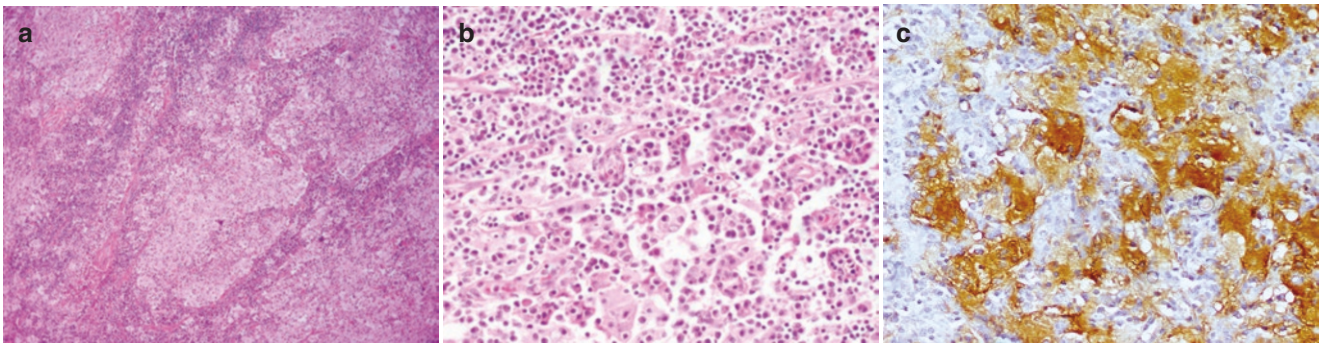

Fig. 5.13 Rosai–Dorfman disease has a similar mottled appearance, with basophilic lymphocyte-rich areas and eosinophilic histiocytes-rich areas (**a**, HE, 10X); large histiocytes demonstrating emperipolesis are easily appreciated in this example (**b**, HE, 20X), and stain positively with S100 (**c**, immunohistochemistry, 10x)

microscopy shows hyperplastic sebaceous glands with surrounding lympho-plasmacytic infiltrate; however, the sebaceous cells with abundant foamy vacuolated cytoplasm show maintained lobular architecture and association with hair follicles which are often plugged, making it easy to distinguish them from the histiocytes in rhinoscleroma.

In difficult cases, culture studies, PCR-based assays, and 16 s rRNA gene sequencing can be used to identify the organism in tissue culture or nasal swabs for confirmation of diagnosis of rhinoscleroma. Treatment involves systemic antibiotic therapy and surgical debridement. Recurrences may occur, and therefore a diagnosis of rhinoscleroma necessitates long-term follow-up.

5.4.2 Tuberculosis

Tuberculosis is a chronic granulomatous infection caused by *Mycobacterium spp.*, primarily by *M. tuberculosis.* Extranodal head and neck tuberculosis (TB) accounts for <1% of all extrapulmonary TB. The sinonasal tract is the most resistant to infection by mycobacteria among all head and neck mucosal sites, due to mucociliary clearance and bactericidal effect of secretions. Sinonasal TB is therefore extremely rare. The nasal septum and inferior turbinate are involved in most cases. It usually occurs secondary to pulmonary TB, often in immunocompromised patients, and those of low socioeconomic status. The route of sinonasal infection is through coughing and sneezing of infective material, or by hematogenous spread. The nasal mucosa appears thickened, with ulceration and crusting; septal perforation may occur. Histopathology (Fig. 5.14) shows necrotizing epithelioid cells granulomas with Langhans giant cells. Ziehl–Neelsen stain may not always demonstrate acid-fast bacilli. Nasal secretions and swabs also have a low yield of mycobacteria. Serological and molecular tests are therefore useful to supplement the histological diagnosis. Response to anti-tubercular treatment is probably the best confirmation of the diagnosis.

Atypical mycobacteria may present with involvement of the sinonasal tract in immunocompromised individuals. Biopsies do not show granulomas, but necrosis is present. A high index of suspicion is required to order acid-fast staining, which reveals numerous bacilli.

5.4.3 Leprosy

Leprosy is a chronic infectious disease caused by *Mycobacterium leprae*, that involves skin, nerves, and mucosae. The nasal cavity provides a cool environment required by the organisms; thus, nasal involvement is frequent in the disease, although rarely the isolated presentation. It plays a significant role in transmission of the disease, as nasal secretions harbor numerous bacilli. The nasal mucosa appears pale and thickened, with nodular infiltrates, which later progress to ulceration, crusting, and destruction of bone and cartilage, causing facial deformity. Tuberculoid leprosy is seen in patients with high cell-mediated immune response, which on biopsy shows epithelioid cell granulomas with giant cells and lymphocytes in the submucosa, and overlying pseudoepitheliomatous hyperplasia; necrosis is absent. Lepromatous leprosy (Fig. 5.15), the other end of the spectrum in patients with reduced cell-mediated immune response, shows sheets of foamy histiocytes admixed with lymphocytes, while well-formed granulomas are absent. Modified acid-fast staining reveals numerous bacilli in lepromatous leprosy, while they are rare in the tuberculoid form. Treatment is with long-term antibiotics which include rifampicin and dapsone.

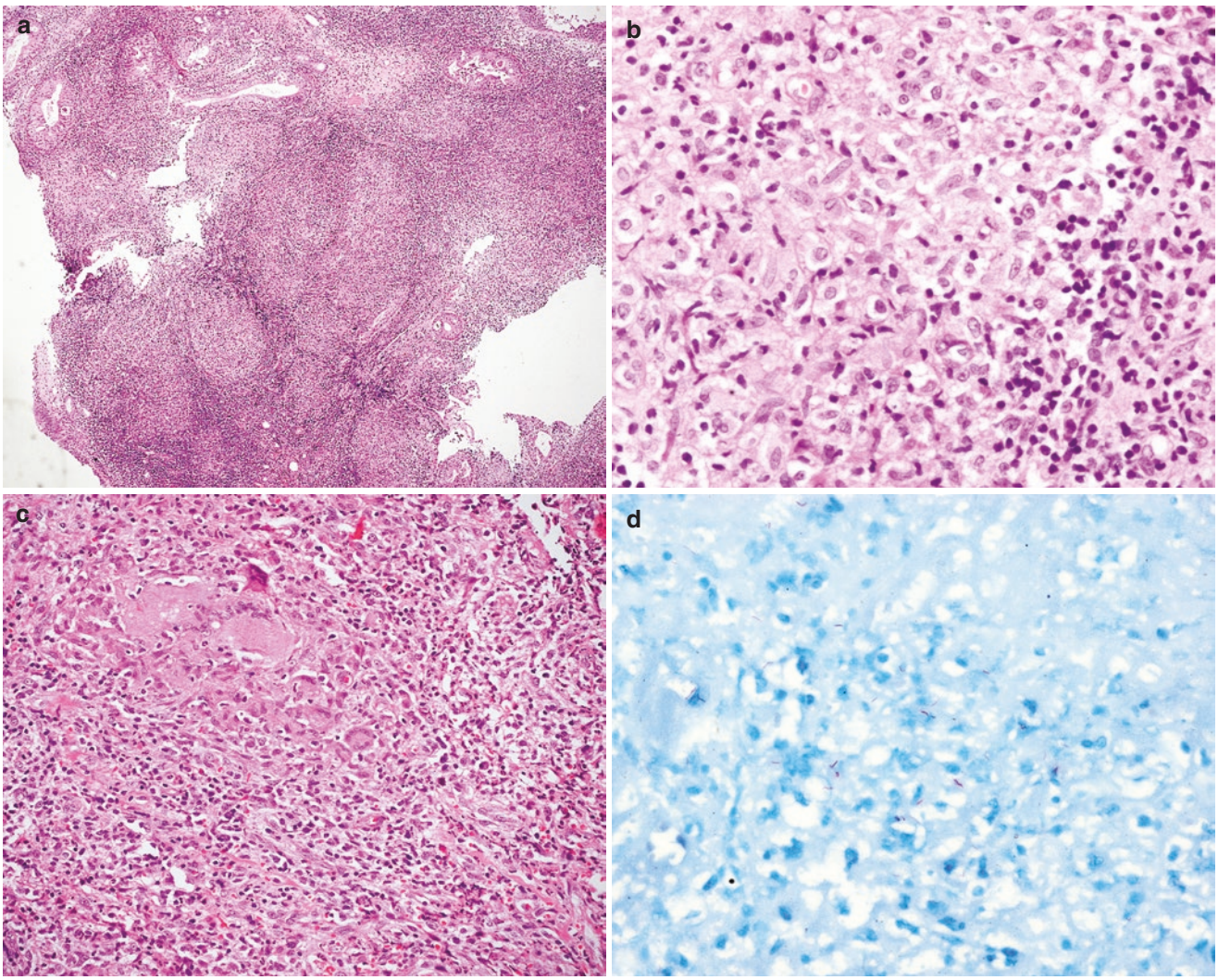

Fig. 5.14 Tuberculosis: Inflamed nasal mucosa (**a**, HE, 4X) with epithelioid cell granulomas (**b**, HE, 40X) and giant cells (**c**, HE, 20X); Ziehl–Neelsen [ZN] stain shows acid-fast bacilli (**d**, 60X)

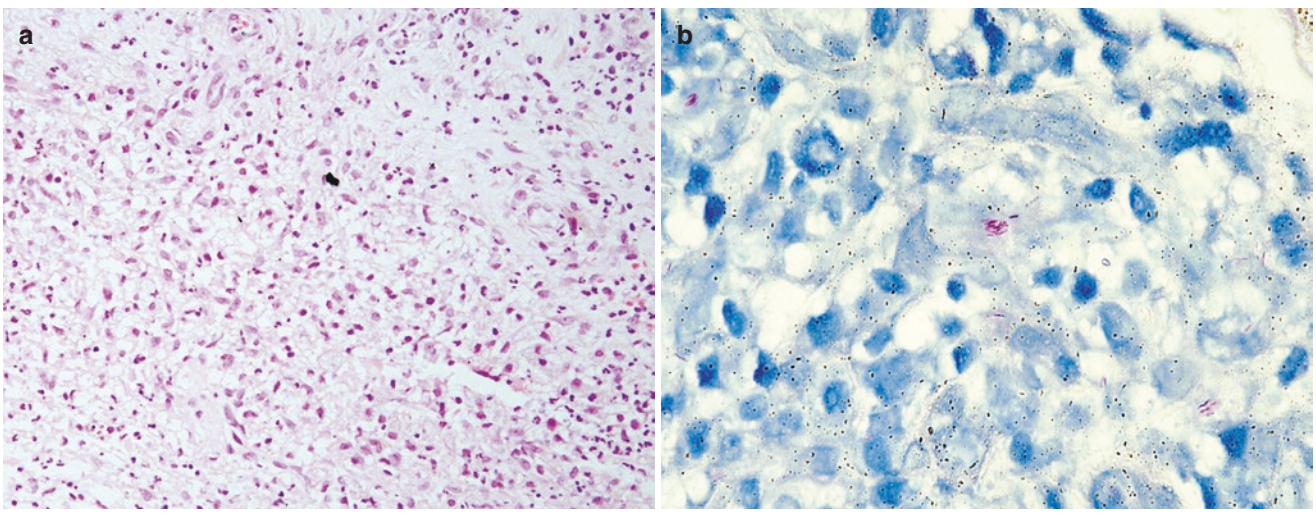

Fig. 5.15 Leprosy: Foamy and few epithelioid histiocytes (**a**, HE, 20X), some of which contain aggregates of acid-fast bacilli, i.e., globi (**b**, Modified ZN, 60X)

5.4.4 Botryomycosis

Botryomycosis, also known as bacterial pseudomycosis, is a chronic granulomatous suppurative infectious disease that involves skin and viscera, rarely involving the sinonasal or pharyngeal mucosae and simulating a neoplasm. The term botryomycosis is derived from the Greek words "botrys" = bunch of grape and "mycosis" = fungal infection, as it was initially presumed to be a fungal infection. Infection may occur in immunocompetent as well as immunodeficient hosts. Patients present with features of sinusitis; radiology shows a soft tissue mass in the sinus, with erosion of the bony walls [9].

Histological examination shows abundant amorphous, acellular debris along with eosinophilic granules which are aggregates of bacteria surrounded by neutrophils. Splendore–Hoeppli phenomenon may be present. The causative organisms on culture include *Pseudomonas aeruginosa*, *Staphylococcus aureus*, *Proteus spp.,* and *Escherichia spp.* The infection is often resistant to antibiotic treatment as the organisms are walled off within the compact granules.

5.4.5 Syphilis

Syphilis, a sexually transmitted infection, is caused by the spirochete *Treponema pallidum.* The primary infection, if untreated, progresses to chronic secondary, latent, and tertiary stages. Secondary syphilis is associated with mucocutaneous rash, while tertiary syphilis demonstrates gummas, which are nodular granulomatous lesions. The nasal mucosa is involved in tertiary syphilis, and shows ulceration, or features of atrophic rhinitis; destruction of the nasal septum leads to external deformity, i.e., saddle nose. If untreated, the disease progresses to nasal stenosis and atresia. Biopsies show a submucosal inflammatory cell infiltrate rich in plasma cells. The organisms, filamentous spiral bacteria 15–20 μm in length, can be demonstrated by Warthin–Starry staining, immunohistochemistry, or direct fluorescent antibody techniques [10]. Serological testing is, however, the mainstay of diagnosis.

5.5 Protozoal Parasites

5.5.1 Leishmaniasis

Mucocutaneous leishmaniasis is mainly caused by Leishmania, an obligate intracellular protozoan parasite transmitted by sandflies, and occurs several years after exposure. The involved nasal mucosa is edematous, erythematous, and nodular; necrosis and destruction of cartilage may be seen. On histological examination (Fig. 5.16), the tissue reaction consists of a mixed inflammatory infiltrate with histiocytes, lymphocytes, and plasma cells. Ulceration, suppuration, necrosis, granulomatous reaction, and pseudoepitheliomatous hyperplasia may also occur. The amastigote forms of the organism are round to oval, 2–4 μm in size, with a conspicuous nucleus and a rod-shaped kinetoplast. They are seen within histiocytes lined up against the cell membrane giving a "marquee" appearance akin to lightbulbs around a mirror, and extracellularly. Giemsa stains the cytoplasm pale blue, and the nucleus and kinetoplast pink-red or violet. GMS and PAS are negative, helping to distinguish from similar sized fungal yeast forms, in addition to the absence of a capsule. PCR may aid in accurate diagnosis.

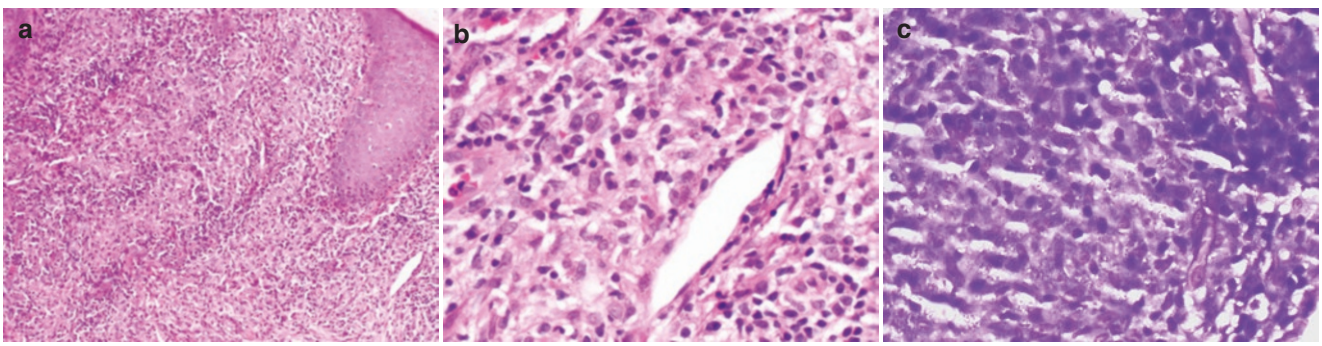

Fig. 5.16 Leishmaniasis: Metaplastic squamous mucosa with subepithelial histiocytes, lymphocytes, and plasma cells (**a**, HE, 10X); intracellular organisms with a distinct nucleus are seen within histiocytes (**b**, HE, 40X) and highlighted on Giemsa stain (**c**, 40X)

5.6 Rhinosporidiosis

Rhinosporidiosis is a chronic zoonotic infection caused by *Rhinosporidium seeberi*, an organism whose phylogenetic origin remained in question until recently. It has now been established as a eukaryotic parasite belonging to the class Mesomycetozoea, which consists of organisms situated between the animal-fungal divergence, including parasites of fish and other animals [11, 12]. The disease is endemic in tropical countries such as India, Sri Lanka, Bangladesh, and Brazil, and infects males more frequently [12]. The most accepted mode of transmission is via epithelial transmigration of endospores present in stagnant water or dust [13]. In the submucosa, the endospores mature into sporangia which contain numerous sporangiospores (endospores). The sporangia rupture, releasing the sporangiospores into the surrounding tissue, i.e., autoinoculation, which then transform from juvenile through intermediate to mature sporangia.

Rhinosporidiosis affects the mucosa of the upper respiratory tract including the nasal cavity, nasopharynx, and oropharynx, and may also involve the oral cavity, larynx, trachea, bronchi, esophagus, and the conjunctiva [13]. Clinically, nasal rhinosporidiosis presents as slow growing, vascular, friable, polypoid masses with a reddish, granular appearance often speckled with whitish spores, imparting an appearance akin to a strawberry or mulberry. In the nasal cavity, the polyps often arise from the inferior turbinate and the floor. Patients frequently complain of unilateral nasal obstruction, rhinorrhea, and epistaxis.

The distinct diagnostic histological feature (Fig. 5.17) of rhinosporidiosis is the presence of spherical cystic structures with a mucoid interior, i.e., sporangia, ranging from 100 μm to 450 μm in diameter, within the epithelium and submucosa. The sporangia contain sporangiospores that are 2–15 microns in diameter. Zonation of spores may be seen within sporangia, with the larger ones towards the center and smaller ones at the periphery. Empty cystic structures with a thick, eosinophilic chitinous wall that are known as trophocytes may be seen, which represent juvenile sporangia. The surrounding tissue shows an inflammatory infiltrate consisting of lymphocytes, plasma cells, and eosinophils. Foreign body giant cells and granulomas may also be seen. The overlying epithelium often shows squamous metaplasia.

Differential diagnosis includes sinonasal oncocytic papillomas with prominent microcysts containing mucin and neutrophils, which may resemble sporangia of rhinosporidiosis on low power. However, microcysts are only seen in the epithelium in sinonasal papillomas, and not in the submucosa. Sporangia of *Coccidioides immitis* (albeit two geographically different diseases) are smaller in diameter than those of *Rhinosporidium seeberi*, and do not stain for mucin. Surgical

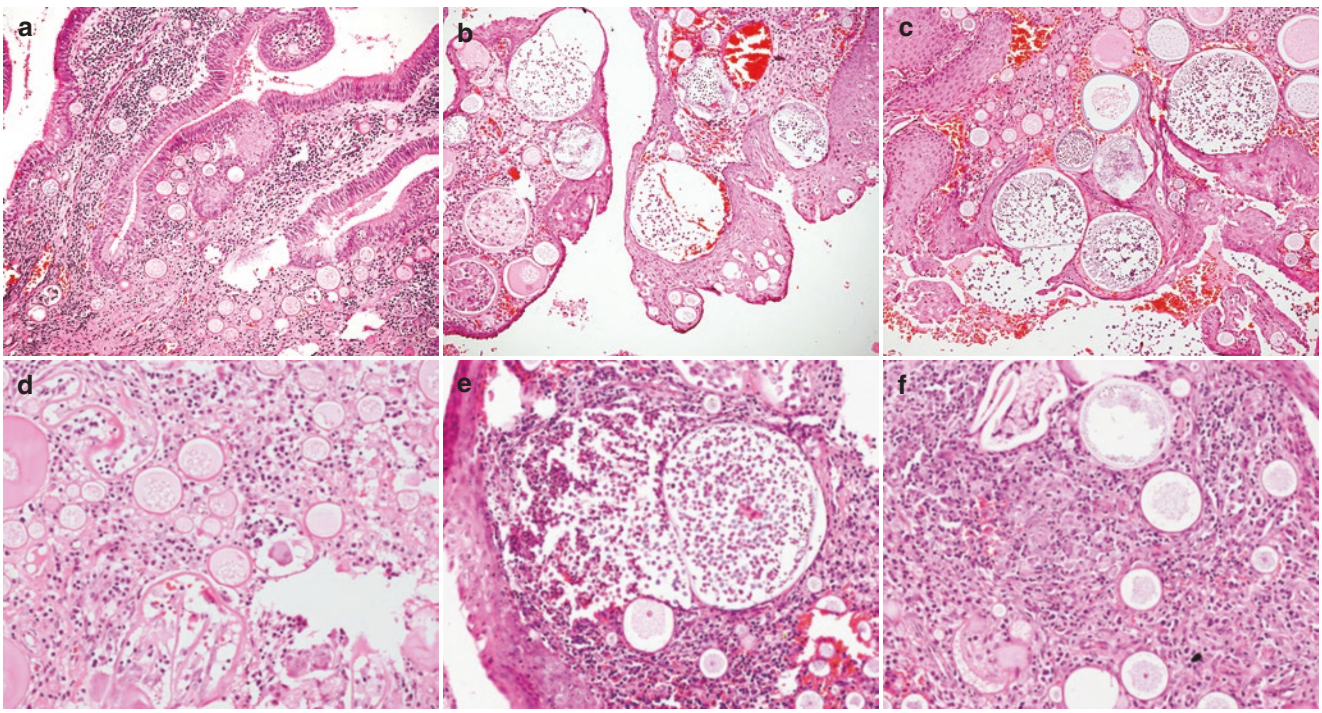

Fig. 5.17 Rhinosporidiosis: Numerous spherical cystic structures viz. sporangia are seen in the nasal mucosa and submucosa (**a**, HE, 10X) which shows squamous metaplasia (**b**, HE, 10X). Sporangia show various stages of maturation (**c**, HE, 10X): juvenile forms, i.e., trophocytes are empty cystic structures with a thick, eosinophilic chitinous wall (**d**, HE, 20X); mature sporangia contain sporangiospores showing zonation, i.e., larger ones towards the center (**e**, HE, 40X); lymphocytes, histiocytes, and plasma cells infiltrate the submucosa (**f**, HE, 20X)

excision with electrocauterization of the base of the polyp is the treatment of choice. Recurrences may occur in a small proportion of patients.

5.7 Conclusion

Infective diseases of the sinonasal tract often have non-specific clinical presentations. On occasion, they may present as mass forming lesions mimicking neoplasms. Microbiological techniques are not always sufficient to detect the causative organisms, underscoring the importance of histological examination. Identification of characteristic patterns of tissue response and highlighting the causative organisms with the use of appropriate histochemical stains are critical to distinguish these infective diseases from non-infectious inflammatory disorders, and making an accurate diagnosis.

References

1. Guarner J, Brandt ME. Histopathologic diagnosis of fungal infections in the 21st century. Clin Microbiol Rev. 2011;24(2):247–80.
2. Thompson LDR. Algorithmic approach to Fibroinflammatory Sinonasal tract lesions. Head Neck Pathol. 2021;15(1):120–9.
3. Sood A, Nayyar V, Mishra D, Kakkar A, Priya H. Post-COVID mucormycosis: ascertainment of the pathological diagnostic approach. J Oral Maxillofac Pathol. 2021;25:219–22.
4. Kakkar A, Kaur K. Histopathological diagnosis of rhino-Orbito-cerebral Mucormycosis. In: Gupta N, Honavar SG, editors. Rhino-orbito-cerebral mucormycosis. Singapore: Springer; 2022. p. 65–78.
5. Laudien M. Orphan diseases of the nose and paranasal sinuses: Pathogenesis - clinic - therapy. GMS Curr Top Otorhinolaryngol Head Neck Surg. 2015;14:Doc04.
6. El-Shabrawi MH, Arnaout H, Madkour L, Kamal NM. Entomophthoromycosis: a challenging emerging disease. Mycoses. 2014;57 Suppl 3:132–37.
7. Umphress B, Raparia K. Rhinoscleroma. Arch Pathol Lab Med. 2018;142(12):1533–6.
8. Chou TC, Tsai KB, Lee CH. Emperipolesis is not pathognomonic for Rosai-Dorfman disease: rhinoscleroma mimicking Rosai-Dorfman disease, a clinical series. J Am Acad Dermatol. 2013;69(6):1066–7.
9. Wenig BM, Smirniotopoulos JG, Heffner DK. Botryomycosis ('bacterial ball') of the sinonasal tract caused by Pseudomonas aeruginosa. Arch Pathol Lab Med. 1996;120(12):1123–8.
10. Sakthivel P, Kakkar A, Sharma SC, Panda S. Mucocutaneous secondary syphilis: 'The great Imitator'. Am J Med. 2018;131(2):e57–8.
11. Fredricks DN, Jolley JA, Lepp PW, et al. Rhinosporidium seeberi: a human pathogen from a novel group of aquatic Protistan parasites. Emerg Infect Dis. 2000;6(3):273–82.
12. Töz S. Rhinosporidium seeberi: is it a fungi or parasite? Turkiye Parazitol Derg. 2020;44(4):258–60.
13. Gupta RK, Singh BP, Singh BR. Rhinosporidiosis in Central India: a cross-sectional study from a tertiary care hospital in Chhattisgarh. Trop Parasitol. 2020;10(2):120–3.

Tumor-Like Lesions of Sinonasal Tract

6

Alessandro Franchi and Cecilia Taverna

6.1 Introduction

Sinonasal tumor-like lesions represent a heterogeneous group of non-neoplastic growths that may clinically and/or histologically mimic a tumor. They are generally treated with limited surgery and for some entities spontaneous healing can be expected and no treatment is necessary. Thus, careful differential diagnosis is needed to separate these lesions from benign and malignant sinonasal tumors in order to avoid overtreatment. Sinonasal tumor-like lesions occur over a wide age range, involving pediatric patients as well as adults. Their pathogenesis is mainly related to developmental anomalies and inflammatory disorders, but based on recent evidence, some entities may represent true neoplastic processes.

6.2 Sinonasal Cysts

Sinonasal cysts are a group of rare and benign entities that comprises dermoid cysts and surgical ciliated cyst. Dermoid cyst originates from developmental anomalies related to the midline closure events [1]. They are more commonly seen in children, but they can be found also in the adult population. They are generally located in the nasal root [1, 2].

Surgical ciliated cyst, also called postoperative maxillary cyst, paranasal cyst, or respiratory implantation cyst, is a benign lesion of adult age that occurs after surgery or trauma that involve the Schneiderian membrane, and it is mainly located in the maxillary sinus [3, 4].

A. Franchi (✉) · C. Taverna
Department of Translational Research, University of Pisa, School of Medicine, Pisa, Italy
e-mail: alessandro.franchi@unipi.it; cecilia.taverna@phd.unipi.it

Pathological Features

Microscopically, dermoid cyst is lined by keratinizing squamous cell epithelium in association with sebaceous glands and hair follicles (Fig. 6.1). A neural component is absent. Possible erosion of the surrounding bone tissue can be present.

Surgical ciliated cyst is lined by cuboidal to columnar ciliated pseudostratified epithelium with scattered mucous cells and presents a fibrous connective tissue underlying the epithelium (Fig. 6.2). For the possible overlap of infections, dermoid cysts and surgical ciliated cysts can show various degrees of acute and chronic inflammation in the stroma surrounding the epithelial layer.

Differential Diagnosis

Dermoid cyst has to be differentiated from teratoma, which may present cystic architecture, but it also shows tissues of endodermal origin. Surgical ciliated cyst has to be differentiated from mucous retention cyst and maxillary pseudocyst [5, 6].

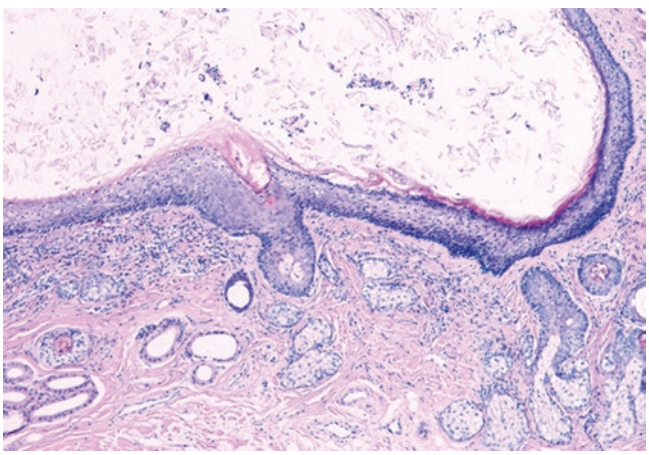

Fig. 6.1 Dermoid cyst is lined by keratinizing squamous cell epithelium in association with sebaceous glands and hair follicles

D. Jain, J. A. Bishop (eds.), *Atlas of Sinonasal Tract Pathology*, https://doi.org/10.1007/978-981-19-7315-4_6

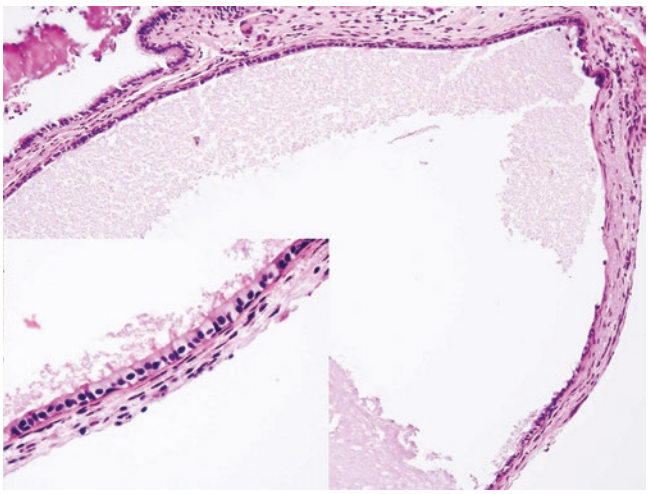

Fig. 6.2 Surgical ciliated cyst of the maxilla. Low power view showing the cyst wall lined by cuboidal to columnar epithelium. The inset shows the ciliated epithelial lining at higher power

6.3 Inflammatory Polyp

Inflammatory polyps (IPs) are non-neoplastic growth of the sinonasal mucosa due to the accumulation of edematous fluid and inflammation. They occur at all ages, being most common over 20 years. IPs are associated with several conditions including allergy, vasomotor rhinitis, infections, cystic fibrosis, Kartagener syndrome, diabetes mellitus, aspirin intolerance, and nickel exposure. The combination of nasal IPs with eosinophils, aspirin intolerance, and asthma is known as Samter triad or aspirin exacerbated respiratory disease (AERD) [7]. IPs occur as single and unilateral or as multiple and bilateral lesions, and most commonly arise from the middle meatus and ethmoid sinuses. Presenting symptoms include nasal obstruction, headaches, rhinorrhea, and epistaxis.

Pathologic Features

Grossly, IPs appear as translucent and soft lesions, measuring from few millimeters to several centimeters. Histologically, the core of the polyp consists of myxoid edematous stroma with pseudocysts containing eosinophilic proteinaceous fluid and a variably cellular infiltrate of inflammatory cells, usually rich in eosinophils, accompanied by variable number of lymphocytes, plasma cells, and some mast cells (Fig. 6.3). Seromucous glands are usually absent or displaced by the stromal edema. IPs are covered by respiratory type epithelium, often with goblet cell hyperplasia, but areas of squamous metaplasia may also be present (Figs. 6.4, 6.5, and 6.6). The basement membrane is thickened and hyaline (Fig. 6.4).

A number of secondary changes may occur in sinonasal IP, and some of these may cause concern for malignancy at histologic examination or create problems of differential diagnosis. The presence of atypical stromal cells is a well-recognized occurrence (Figs. 6.7, 6.8, and 6.9). These are large, bizarre spindle or stellate cells, with hyperchromatic, often angulated nuclei and prominent nucleoli. Multinucleated elements can also be present, but there is no evidence of mitotic activity. These atypical cells are often associated with areas showing reactive changes including necrosis, hemorrhage, vascular thrombosis, fibrosis, or ulceration and represent reactive fibroblasts/myofibroblasts [8]. The presence of atypical stromal cells may lead to consider a diagnosis of sarcoma, including rhabdomyosarcoma and angiosarcoma. However, in IP these atypical cells are localized in limited areas of the lesion, do not group together and do not present mitotic figures. Since stromal elements may seldom be positive for cytokeratins, spindle cell squamous cell carcinoma may also be considered in the differential diagnosis.

As a result of torsion of the stalk, hemorrhage and ischemia, with markedly dilated vascular spaces and fibrin accumulation, may relevantly change the usual appearance of IP, resulting in mimicry of a vascular neoplasm (so-called "angiomatous" IP). Such angiomatoid changes consist of a conspicuous proliferation of capillaries within the myxoid background of the polyp stalk, often with vessel thrombosis, fibrin deposition, foci of necrosis, hemorrhage, and presence of atypical stromal cells, that may simulate the appearance of an angiosarcoma [9–12].

Other secondary changes include fibrosis, ulceration of the surface epithelium, stromal deposition of amyloid-like material, osseous or cartilaginous metaplasia. Granulomas may be seen in polyps treated with intranasal injection, application of steroids, or other oily medications, as well as for rupture of mucous cysts.

Differential Diagnosis

Sinonasal papilloma frequently shows an inflammatory background with edema, and may be confused with IP, especially when the latter presents extensive areas of squamous metaplasia. However, sinonasal papillomas are unilateral lesions, lack the soft mucoid gross appearance of IP, and present a thick epithelium with transmigrating neutrophils, mucous cysts, and microabscesses, that are not seen in IP. Goblet cell hyperplasia, sometimes resulting in papillary outgrowths, as well as the presence of mucous accumulation may mimic the appearance of a well-differentiated adenocarcinoma. The presence of a thickened basement membrane, the multilayering of the epithelium, and the absence of atypia are features that support the diagnosis of IP. Limited areas of hyperplasia with ingrowth of the surface epithelium may cre-

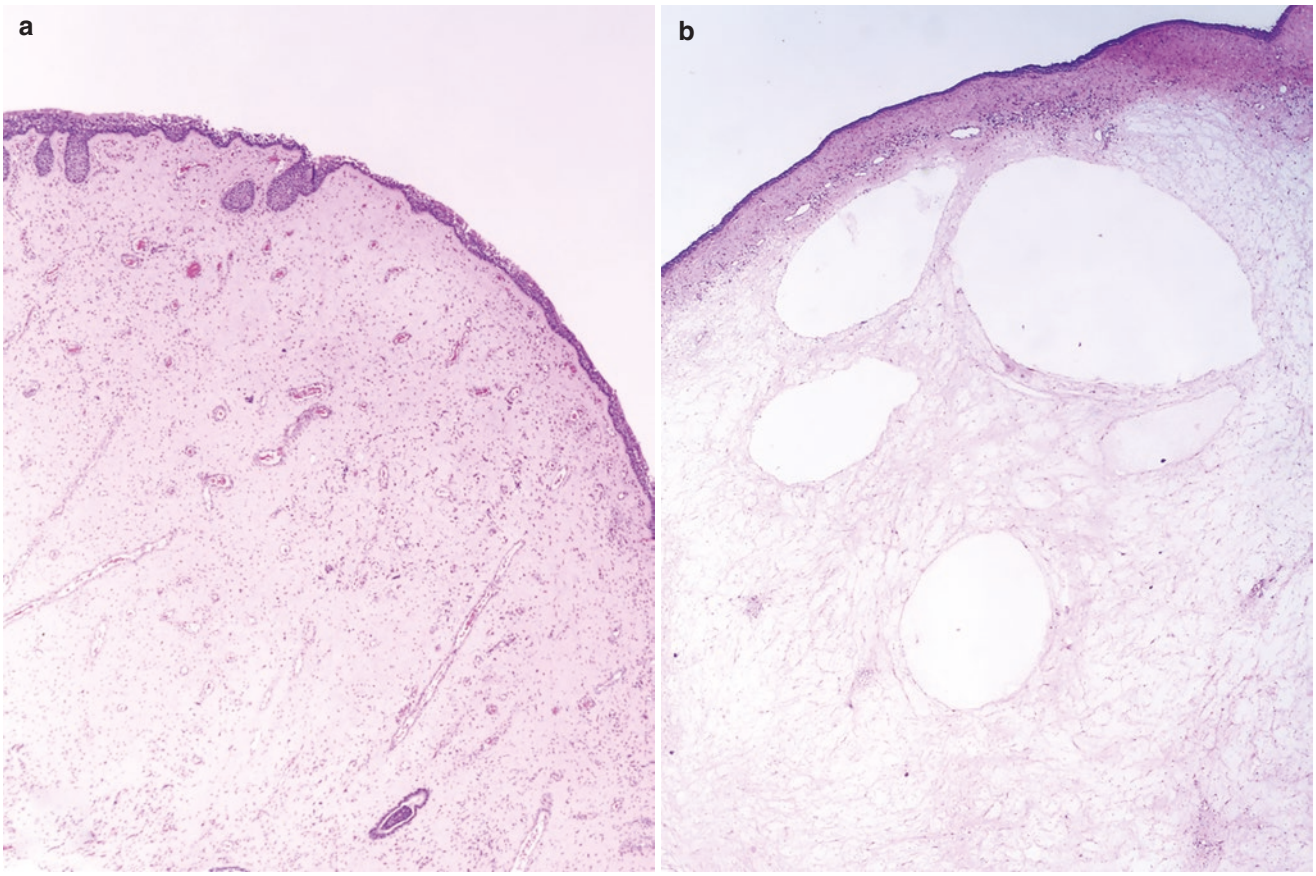

Fig. 6.3 Low power view of an inflammatory polyp to show the myxoid edematous stroma (**a**). Fluid accumulation may result in pseudocyst formation (**b**)

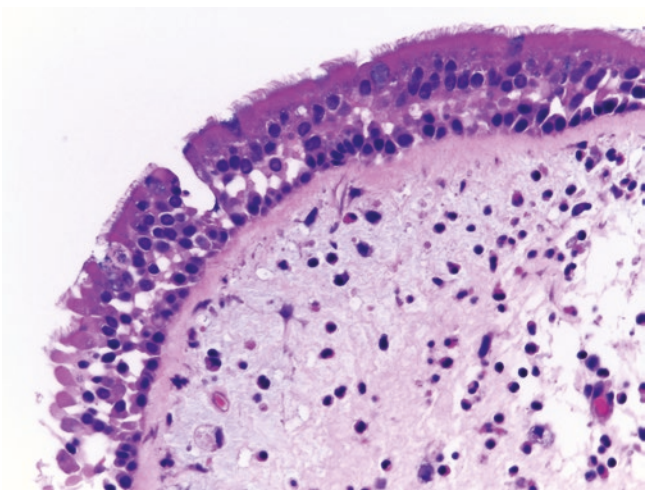

Fig. 6.4 Inflammatory polyps are covered by respiratory type epithelium that lies on a thickened and hyaline basement membrane

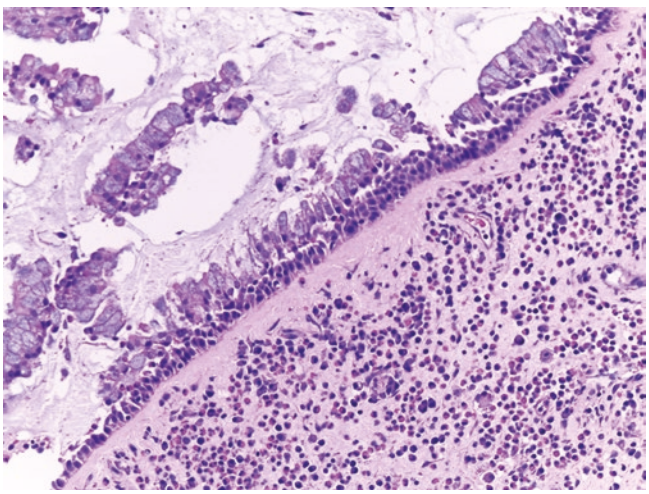

Fig. 6.5 In this inflammatory polyp, the epithelium shows hyperplasia of mucous producing cells

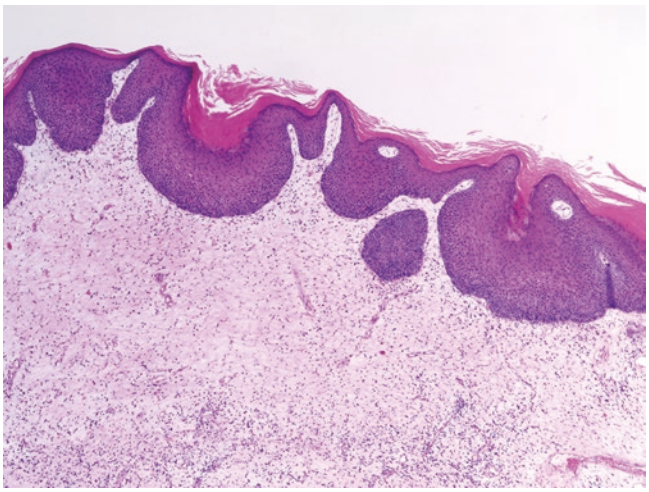

Fig. 6.6 Areas of squamous metaplasia of the surface epithelium may occasionally be present

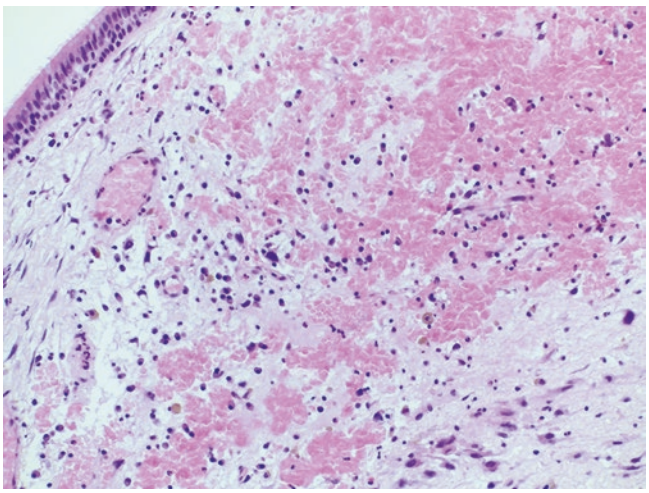

Fig. 6.8 Atypical stromal cells are often associated with areas of hemorrhage

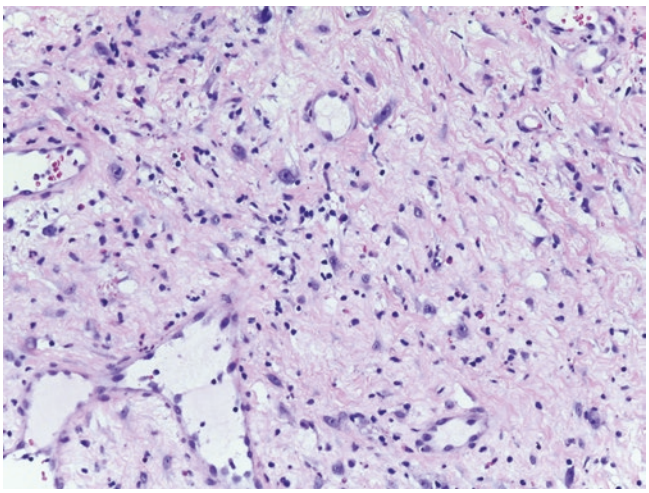

Fig. 6.7 Inflammatory polyp with atypical stromal cells showing enlarged nuclei and prominent nucleolus

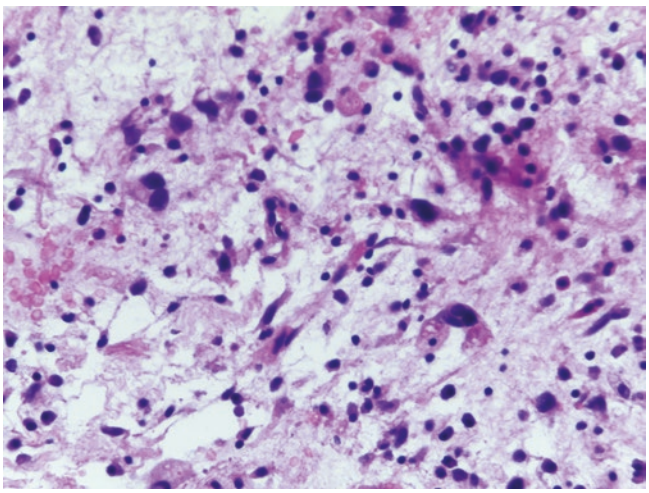

Fig. 6.9 Multinucleated atypical cells with enlarged hyperchromatic nuclei

ate an appearance that resembles respiratory epithelial adenomatoid hamartoma (REAH). Although REAH and IP may coexist in the same lesion, such limited and superficial areas of surface epithelial proliferation should not be interpreted as evidence of co-existing REAH.

6.3.1 Antrochoanal Polyp

Antrochoanal polyp (AP) takes origin from the maxillary sinus and extends through the middle meatus into the nasal cavity, with frequent posterior extension into the choana. It occurs at a younger age in comparison with IP and develops more frequently in male subjects, being often associated with chronic rhinosinusitis and allergy [13].

Pathologic Features

AP presents a smooth surface and a long and thin stalk that originates from the mucosa of the maxillary antrum. Microscopically, it is similar to a conventional IP, but the background is more fibrous and collagenized and the inflammatory infiltrate usually lacks a marked eosinophilic infiltrate (Fig. 6.10). Atypical stromal cells are present as well, often with other reactive changes, such as hemorrhage and necrosis due to torsion of the long stalk [14] (Fig. 6.11).

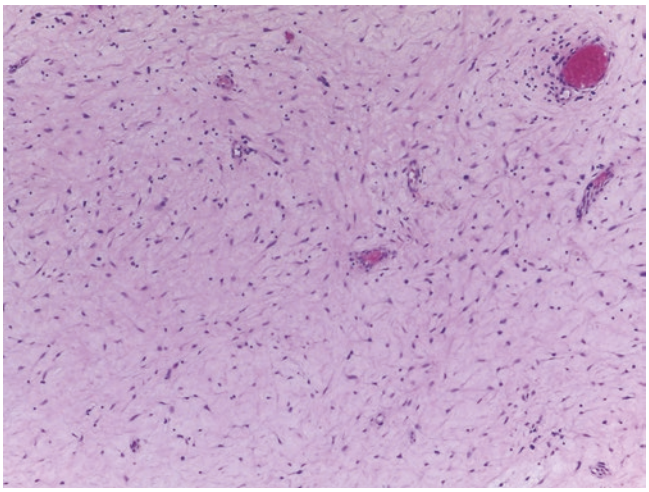

Fig. 6.10 The stroma of the antrochoanal polyp is richer in collagen

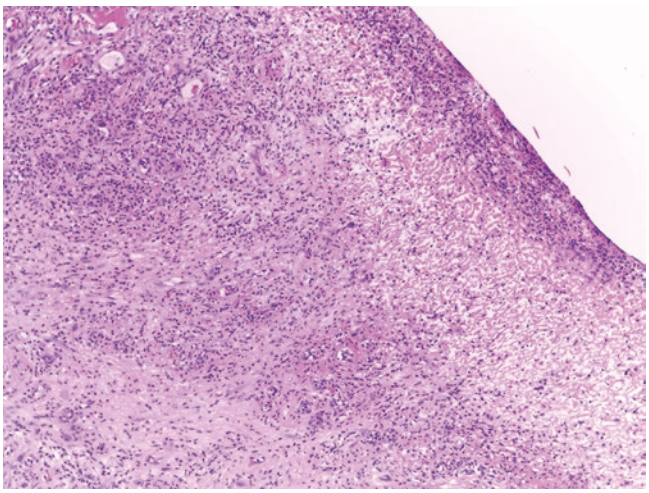

Fig. 6.11 In this antrochoanal polyp, the surface epithelium is ulcerated

Differential Diagnosis

The differential diagnosis is similar to that of IP and includes sarcomas, mainly for the presence of atypical stromal cells, and benign epithelial tumors like inverted papilloma.

6.4 Sinonasal Hamartomas

Hamartomas are rare, benign lesions composed of excessive, haphazard and disorganized proliferation of tissue normally present in the affected location. According to the fifth edition of the World Health Organization (WHO) Classification of Head and Neck Tumors, they can be divided into epithelial and mesenchymal hamartomas [15–17]. The group of epithelial hamartomas comprises *respiratory epithelial adenomatoid hamartoma* (REAH), which is the most frequent type, and *seromucinous hamartoma* (SH). *Nasal chondromesenchymal hamartoma* (NCMH) is a purely mesenchymal lesion. For the overlapping features often seen in REAH and SH, as well as for the existence of hybrid lesions known as chondro-osseous respiratory epithelial adenomatoid hamartoma (COREAH), sinonasal hamartomas more likely represent a spectrum of lesions rather than separate entities. Finally, *olfactory epithelial hamartoma* (OEH) has been recently reported as a new variant which shares some features with SH, in addition to the presence of olfactory epithelium [18].

The origin of epithelial sinonasal hamartomas is still under debate, as some authors consider them as developmental disorder related lesions, while others believe that they are reactive lesions related to chronic inflammatory processes and atopy [19, 20]. The presence of high levels of fractional allelic loss compared to polypoid sinus tissue suggests that REAH may be a benign neoplastic process [21]. HUMARA analysis demonstrated monoclonality in 1 case of SH, supporting the neoplastic nature of this lesion [22]. NCMH is strictly related to DICER1 mutation, which is associated with an increased risk of developing pleuropulmonary blastoma, ovarian sex-cord tumors, Sertoli-Leydig cell tumors, juvenile granulosa cell tumor, and gynandroblastoma, especially in young patients [23, 24].

REAH and SH arise in adult patients; males are 7 times more frequently affected than women [25], while NCMH often occurs in pediatric population [24].

REAH and SH are usually unilateral [26, 27]. REAH occurs in nasal cavity, often in the posterior nasal septum and SH can arise in nasal septum, nasopharynx, lateral nasal wall or paranasal sinuses [28]. In some cases, massive sinus involvement, bone erosion, or intracranial extension is reported [27]. NCMH is more commonly found in paranasal sinuses [24, 29]. OEH typically arise in olfactory cleft [18].

Pathologic Features

Macroscopically, sinonasal hamartomas appear as polypoid masses, with variable size [18, 30]. REAH and SH are firm, sometimes multinodular, with color ranging from yellow to gray and white, to tan-pink [30, 31], while NCMH has a typical rubbery consistency and blue-gray color [32].

Histologically, REAH is composed of pseudo-glandular structures invaginating from the surface epithelium, that are covered by multiple layers of ciliated respiratory cells with scattered mucous producing cells (Fig. 6.12). These pseudo-glands can be filled with mucinous or amorphous material

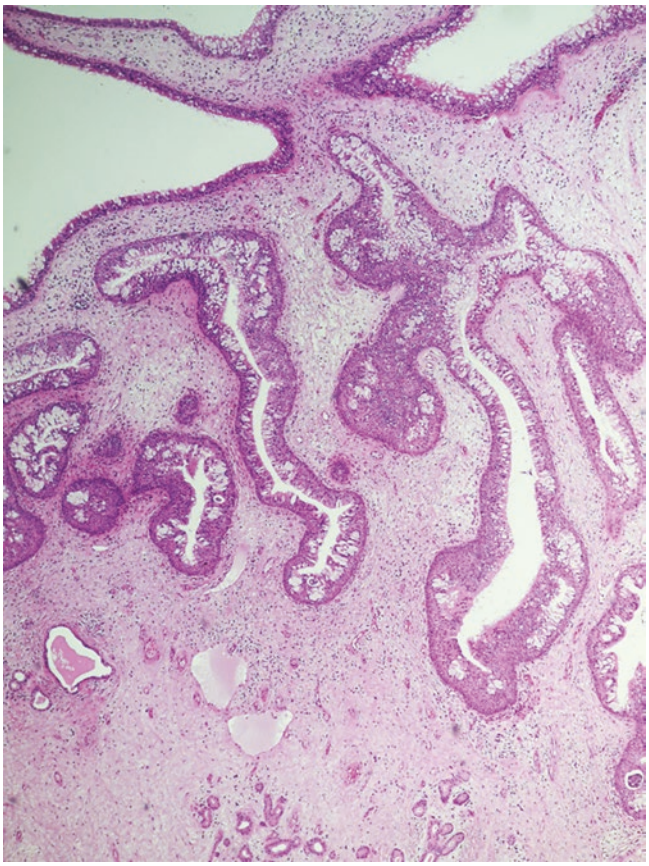

Fig. 6.12 Respiratory epithelial adenomatoid hamartoma consists of pseudo-glandular structures invaginating from the surface epithelium, that are covered by multiple layers of ciliated respiratory cells with scattered mucous producing cells

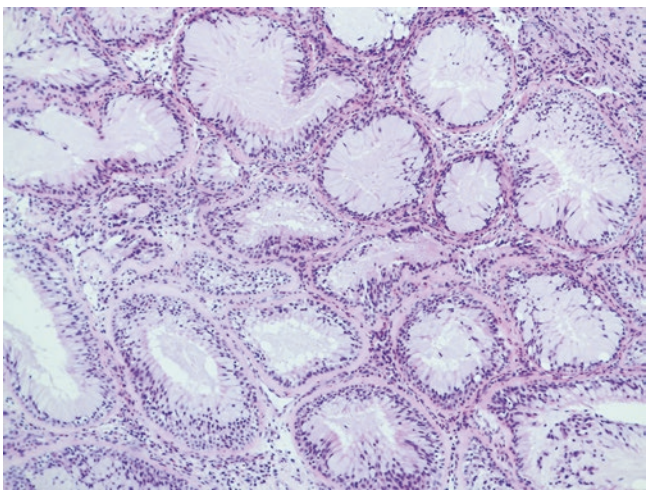

Fig. 6.13 Pseudo-glands of respiratory epithelial adenomatoid hamartoma can be lined by mucous producing cells

(Fig. 6.13). A peculiar feature is the presence of a thick, eosinophilic, often hyalinized basement membrane surrounding the pseudo-glandular elements (Fig. 6.14). Foci of squamous metaplasia are occasionally present [33].

SH presents with a variable histologic appearance and consists of invaginated respiratory epithelium, cysts lined by low cuboidal to flat cells and serous elements represented by small sized, round to angulated, often branching glands, pseudo-glands, and tubules arranged in clusters or with lobular haphazard architecture (Figs. 6.15 and 6.16). As seen in REAH, a thick fibrous basement membrane can be present, surrounding both the invaginated pseudo-glands and the typical serous component. Serous glands can be filled with dense eosinophilic mucin. Occasionally clear cells in the serous component and squamous metaplasia of the invaginated epithelium are observed [34]. Polypoid lesions with histologic features of both REAH and SH are occasionally observed (Fig. 6.17).

Myoepithelial/basal cells are present in the pseudo-glands of REAH, as well as in areas of squamous metaplasia. Given

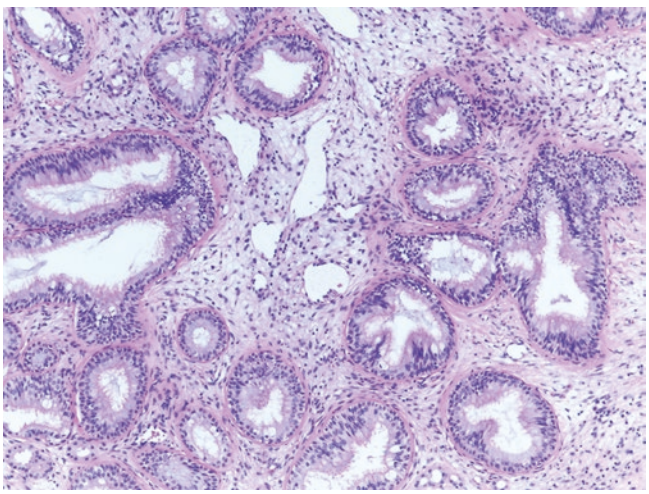

Fig. 6.14 A thick, eosinophilic hyaline basement membrane surrounds the pseudo-glandular elements

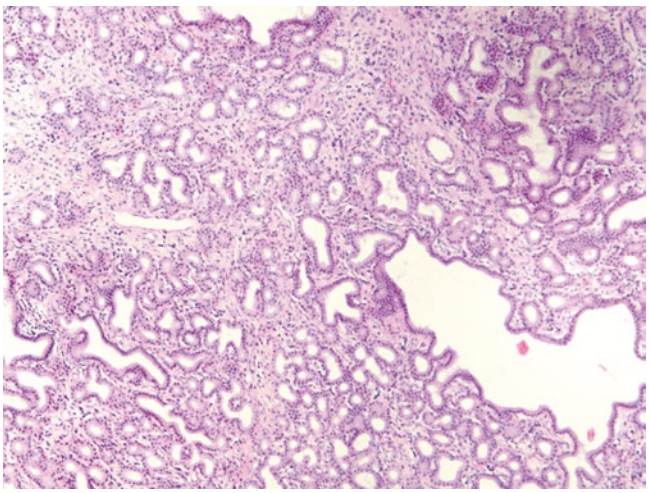

Fig. 6.15 Seromucinous hamartoma consists of branching glands and tubules with lobular arrangement lined by cuboidal cells. Some elements appear to be cystically dilated

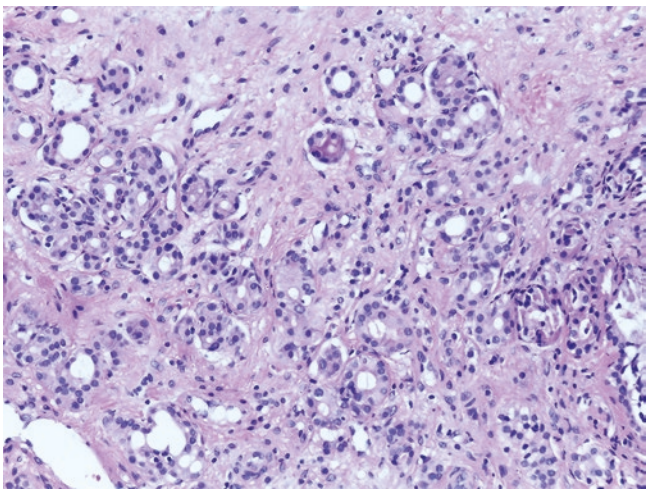

Fig. 6.16 The small serous glands, ducts, and tubules are lined by a single layer of bland-looking cuboidal cells

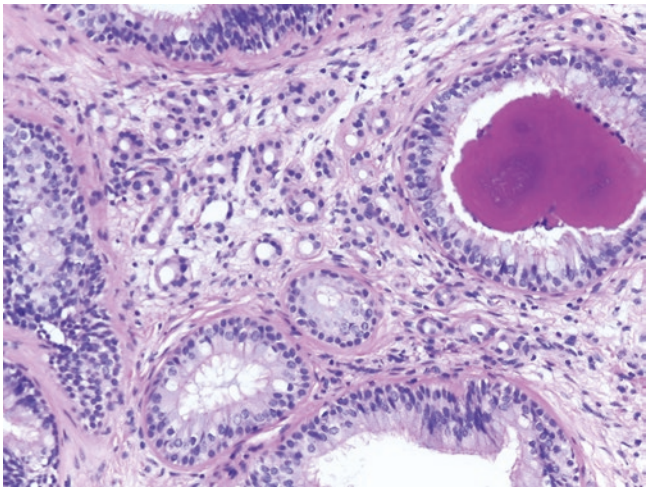

Fig. 6.17 In this lesion, the small ducts and tubules of seromucinous hamartoma are seen next to pseudo-glands lined by respiratory epithelium of respiratory epithelial adenomatoid hamartoma

their immunohistochemistry profile, with positivity for p63 and 34betaE12, and negativity for S100, smooth muscle actin, or calponin, they are more probably basal cells and not myoepithelial cells [35]. SH are usually negative for myoepithelial/basal markers [31, 34], even though Fleming et al. [36] reported the presence of scattered elements in the outer basal layer of serous gland positive to p63, smooth muscle actin, and calponin, so that the complete absence of a myoepithelial/basal cell layer is not a strict criterion to make the diagnosis of SH (Fig. 6.18).

REAH and SH share similar features of the stromal compartment, which is often edematous and can be filled by small to moderate amount of inflammatory cells. SH stroma typically lacks eosinophils.

NCMH is covered by respiratory epithelium and shows a submucosal proliferation of irregular nodes of cartilage in a background of stromal spindle cells. These nodules are usually well demarcated, even though in some cases they can be admixed with the stromal component mimicking a pseudo invasive process. Chondroid tissue displays both mature and immature features. In association with the main chondroid population, fragmented trabecular bone can be found, together with multinucleated cells with osteoclast-like features and adipose tissue. The stroma can display various proportion of vascular proliferation, with aneurysmal spaces and well-formed arterioles. In some cases, perivascular hyalinization is present, especially near areas of dense and keloidal collagen.

OEH has features that resemble both REAH and SH. It is usually covered by ciliated pseudostratified respiratory epithelium which invaginates in the submucosa forming gland-like structures, cysts and ducts. The main feature of this lesion is the presence of areas of olfactory epithelium, that can be seen both at the surface and in the invaginated gland-like structures. The olfactory epithelium consists of three populations of cells, basal, sustentacular, and olfactory receptor cells, that can be found in various combination in the pseudo-glandular spaces. When all of them are present, three layers of nuclei are visible: small and round nuclei at the basal aspect, an intermediate row of round and clear nuclei with visible nucleolus, and a superficial layer of palisading round to elongated nuclei. Olfactory receptor cells of the apical part of the superficial layer present small protrusions, which are probably olfactory vesicles. Sometimes only two rows of nuclei can be recognized. A filamentous component, consisting of thin eosinophilic cell processes is focally found, both above the basal layer or between the epithelium and the basement membrane. Occasionally, foci of squamous metaplasia can be seen. Stroma can be from dense to loose and edematous with mild to moderate inflammatory cells and eosinophils. Occasionally, stroma can contain benign spindle cells or fragmented bone trabeculae [18].

Immunohistochemistry has a limited role in the diagnosis of hamartomas, as the findings are often not specific. In REAH the glands show positive stain for cytokeratin 7 and negativity for CDX2 and CK20, while the basal cell layer is positive for p63 and p40 and negative for smooth muscle actin, calponin, and S100.

SH has a similar immunohistochemical profile, with invaginated surface epithelium being positive for CK7 and CK19, the serous component being positive for S100, and negativity for CK20. The occasional basal/myoepithelial cells stain positive for p63, smooth muscle actin, and calponin. Laminin highlights the basal membrane.

The cartilaginous component of NCMH stains for S100, while the stromal spindle cells are positive for smooth muscle actin and common muscle actin.

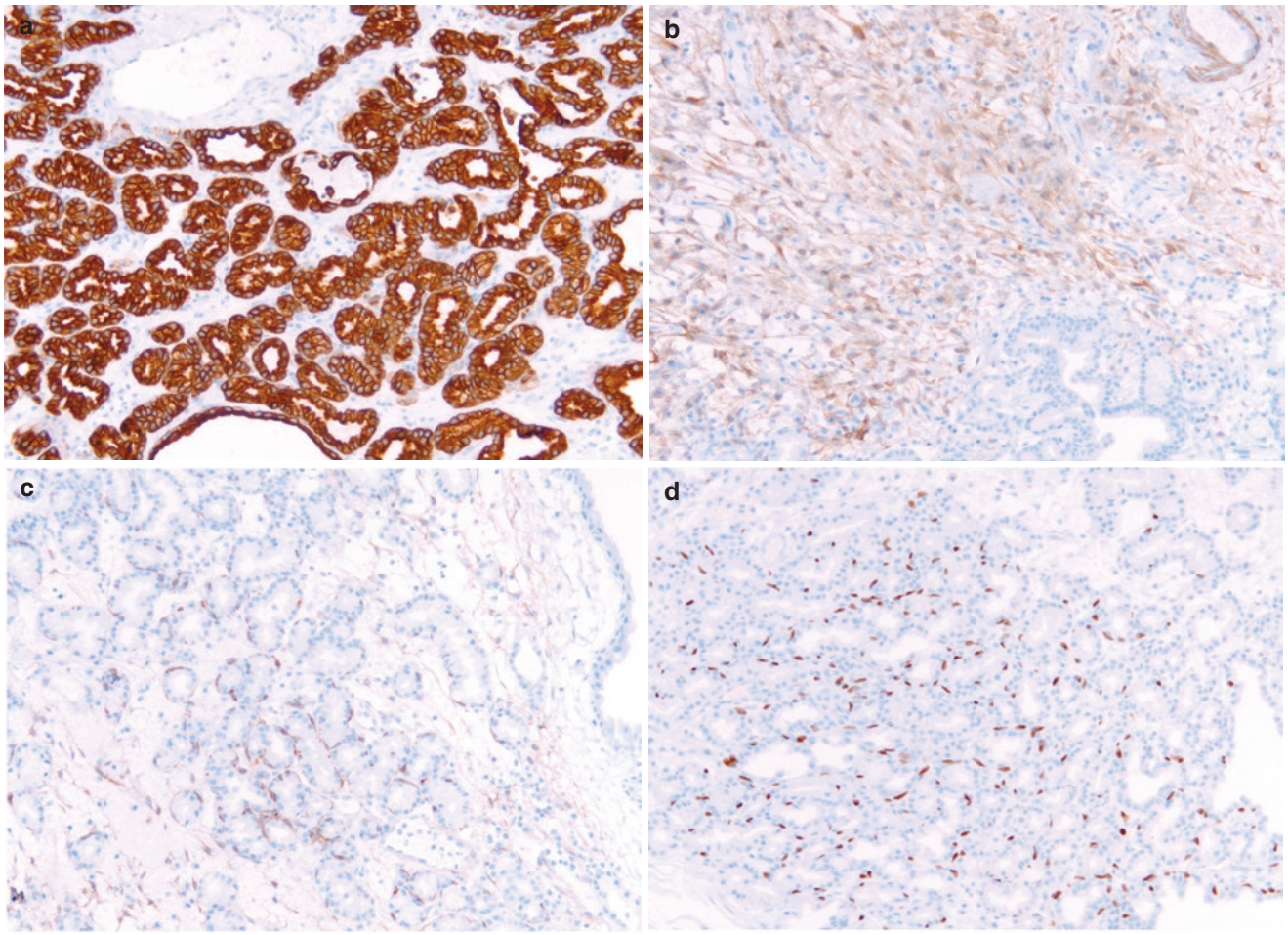

Fig. 6.18 Immunohistochemical findings in seromucinous hamartoma. (**a**) The serous gland proliferation is positive for cytokeratin 7. (**b**) The stroma contains calponin positive myofibroblasts. (**c**, **d**) Although most seromucinous hamartomas lack myoepithelial cells around glands, this example shows scattered myoepithelial/basal cells positive for calponin (**c**) and p63 (**d**)

OEH triple cell population expresses different immunohistochemical markers. Indeed, basal and sustentacular cells are positive for epithelial markers, which are negative in olfactory receptors cells; in addition, basal cells express p63 and CD56. Olfactory receptor cells stain positive to CD56 and occasionally to chromogranin and synaptophysin, with a typical dot-like, often supranuclear pattern. Interestingly, some mucinous cells of respiratory areas stain positive to CD56. Neuroendocrine markers are also found in intraepithelial filamentous aggregates. Seromucinous gland can be positive for S100 and chromogranin, while stromal spindle cells often seen in the background express smooth muscle actin [18].

Differential Diagnosis

Among benign lesions, REAH has to be differentiated from inflammatory polyps. Clinical presentation can be useful in the distinction, as usually inflammatory polyps are bilateral lesions often arising in the middle meatus, while REAH are frequently solitary lesions and occur in posterior nasal septum. On histological examination, few features can help distinguish the two lesions. Inflammatory polyps present a typical thick basement membrane of the surface epithelium, while in REAH the thick hyaline basement membrane characteristically envelopes the proliferative glands**.** In some cases, inflammatory polyps can present limited areas of surface epithelial invaginations similar to those seen in REAH [30, 37, 38]. However, pseudo-glandular spaces seen in inflammatory polyps are more irregular than those seen in REAH. In addition, the stromal component of inflammatory polyp is paucicellular and more loosely edematous than the stroma found in REAH.

Another benign lesion that has to be considered in the differential diagnosis of REAH is inverted sinonasal papilloma [39]. Clinically, they have a similar localization, even though sinonasal papillomas are usually more aggressive lesions, with possible bone erosion, extension in the adjacent tissues, and local recurrences. Moreover, malignant transformation is possible [40]. Inverted papillomas are characterized by an endophytic growth of the epithelium into the stroma. The

basement membrane is continuous, intact, and thin. The diagnosis, however, is straightforward when comparing the proliferative component of REAH and sinonasal papillomas, as in the latter the epithelium is transitional or non-keratinizing, with only intermixed respiratory elements and in some cases pseudocystic dilatations.

Both REAH and SH should be differentiated from sinonasal adenocarcinomas, especially from low-grade non-intestinal adenocarcinomas (LGA) and well-differentiated intestinal-type adenocarcinomas (ITAC) (Table 6.1). When LGA arises from the surface epithelium, it can be difficult to separate it from REAH with florid mucinous metaplasia, particularly when these features are seen in small biopsies [39]. Moreover, while the epithelial component of REAH and SH is negative for S100 and SOX10, the eosinophilic serous epithelial buds originated in respiratory epithelial invagination of low-grade adenocarcinoma are positive [22]. Adenocarcinomas, however, display complex and back-to-back architecture, with atypical cells and increased mitotic activity, while REAH shows bland-looking pseudoglands surrounded by the typical eosinophilic basement membrane.

Well-differentiated ITAC are composed of invasive branching, complex and fused glandular structures, often in cribriform or back-to-back architecture, without the presence of intervening benign stromal component. Cells display mild to moderate atypia and mitoses can be present. Immunohistochemistry shows positive stain for CK20 and CDX2 [39].

Absence of myoepithelial/basal cells is a feature of SH, REAH, and adenocarcinomas, so it is not useful in the differential diagnosis [35].

Biphenotypic sinonasal sarcoma can present invagination and hyperplasia of the surface epithelium similar to epithelial sinonasal hamartomas, but it is composed of spindle cells and it has a typical mixed neural and myogenic differentiation [41].

NCMH has to be differentiated from a number of entities that show some degrees of morphological overlap with its components. For the presence of cartilage elements, it has to be differentiated from chondroma, chondromyxoid fibroma, and chondrosarcoma [42].

6.5 Paranasal Sinus Mucocele

Paranasal sinus mucocele (PSM) is a cystic lesion lined by non-neoplastic epithelium that contains usually sterile mucus. It is the result of an expansion of the sinus cavity and bony walls due to the obstruction of sinus ostia for a chronic inflammatory process (including inflammatory polyps), a benign tumor, trauma, or prior surgery. Mucus accumulation determines an increase in sinus pressure and the progressive enlargement of the lesion with erosion of the bony wall.

PSM occurs at any age [43]. The frontal sinus is the most commonly affected, followed by the ethmoid sinuses, with 70 to 90% of PSM occurring in these locations [43, 44].

Pathologic Features

The histologic features of PSM include a respiratory mucosa lined by pseudostratified ciliated columnar epithelium with variable chronic inflammatory infiltrate. The surrounding bone presents reactive changes. In addition, cholesterol crys-

Table 6.1 Differential diagnosis of sinonasal epithelial hamartomas and adenocarcinomas

Lesion	Salient Histopathologic Features	Immunohistochemistry	Molecular changes
Respiratory Epithelial Adenomatoid Hamartoma (REAH)	Back-to-back glands lined by ciliated columnar cells, periglandular hyalinization; occasional mucinous change of proliferating epithelium	CK7+, CK20−, CDX2−, p63+ in the basal compartment, S100−	NA
Seromucinous Hamartoma	Lobular growth of small serous glands, uncommon mucinous glands; areas resembling REAH occasionally seen	S100+, CK7+, CK20−, CDX2−, myoepithelial markers−	*EGFR::ZNF267* fusion detected in 1 case
Intestinal-type Adenocarcinoma (ITAC)	Columnar cells, goblet cells, signet ring cells; papillary, glandular, solid and alveolar-mucinous architecture	CK20+, CK7 variably positive, CDX2+	*TP53* frequently mutated; activating mutations of *KRAS* and *BRAF* rarely seen; *EGFR* amplification in a subset of cases
Low Grade non ITAC	Different growth patterns, more frequently tubulo-papillary, cribriform, clear cell; back-to-back glands, mild atypia, low mitotic activity, infiltration of mucosa and bone	CK7+, CK20−, CDX2−; myoepithelial markers, DOG1, and SOX10 + in some cases; CAIX + in sinonasal renal cell-like adenocarcinoma	*ETV6::NTRK3, PRKAR1A::MET, FN1::NRG1,* and *DNAJB1::PRKACA* fusions; *CTNNB1, BRAF p.V600E and AKT1* mutations
High Grade non ITAC	Predominantly solid growth pattern, poorly formed glands, marked atypia, pleomorphism, necrosis, brisk mitotic activity	CK7+, CK20−, CDX2−	SMARCB1 loss in rare cases

tals, hemorrhage, fibrosis, granulation tissue and squamous metaplasia of the surface epithelium may be associated. These histopathologic findings are non-specific and not sufficient for the diagnosis that requires correlation with the clinical and radiologic findings (CT scan and MRI).

6.6 Necrotizing sialometaplasia

Necrotizing sialometaplasia (NSM) is a benign reactive change of seromucous glands that undergo coagulative necrosis and squamous metaplasia. Although it usually involves the minor salivary glands of the palate, it may also occur in the sinonasal mucosa [45–49]. It is likely due to an ischemic event and it is commonly associated with trauma or surgical procedures. In the nasal cavities, it may also occur in association with sinusitis [50]. The lesion is generally unilateral, even though bilateral or midline cases are reported [51, 52], and it presents as a localized swelling that becomes ulcerated.

Pathologic Features

Histologically, it is characterized by necrosis of the gland acini and extensive squamous metaplasia of the ducts (Fig. 6.19). Importantly, glandular lobular architecture is maintained, although squamous elements can be arranged in small groups in both ducts and acini, sometimes completely filling these structures to form solid nests, in which a basal layer is still recognizable (Fig. 6.20). Some acini and ducts can present mucinous elements admixed with squamous metaplasia as well as mucin-containing microcysts. The adjacent tissue can show "mucus escape reaction," mostly seen near areas of infarcted glands, due to their coalescence, with the presence of organized mucinous pools. The overlying epithelium can show pseudoepitheliomatous hyperplasia. However, dysplastic changes and abnormal mitotic figures are not observed. Scattered mitotic figures may be seen in areas of regenerating epithelium.

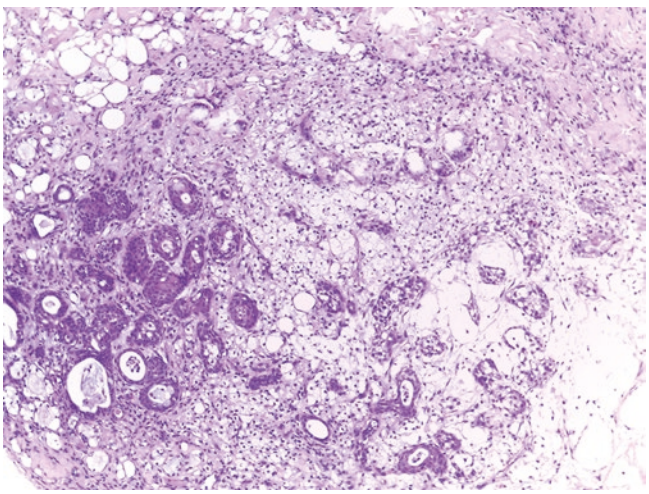

Fig. 6.19 Necrotizing sialometaplasia. Low power view to show the infarcted minor salivary gland on the right and the squamous metaplastic changes of residual ducts and acini on the left

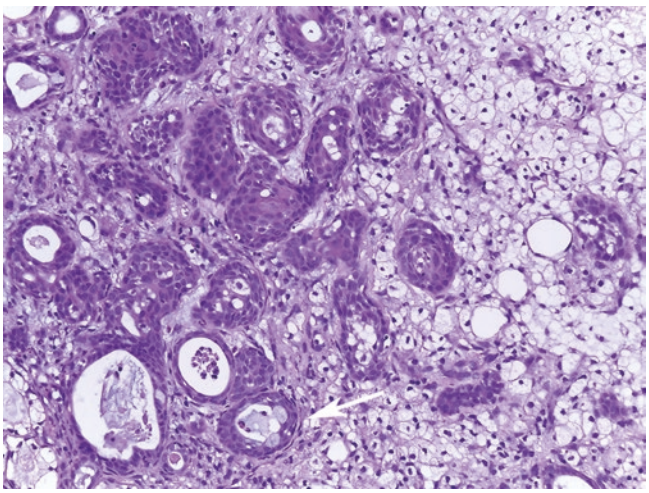

Fig. 6.20 The squamous elements lack cytologic atypia and lobular architecture of the gland is maintained. Few mucous cells are also present (arrow). An inflammatory infiltrate rich in foamy histiocytes infiltrates the metaplastic gland

Differential Diagnosis

The most important entities to be considered are squamous cell carcinoma and mucoepidermoid carcinoma. This differential diagnosis is particularly important because in NSM treatment is not necessary as the lesion heals spontaneously. The presence of metaplastic squamous nest in the stroma may mimic invasive squamous carcinoma. However, the lobular architecture of the salivary gland is maintained, the squamous nests are round to oval and present a smooth contour, and there is no cytologic atypia. NSM may also be present in association with sinonasal squamous carcinoma [53].

6.7 Organized Hematoma

Organized hematoma (OH) is a rare non-neoplastic lesion that due to its expansive and destructive nature may be clinically confused with a malignant process [54]. Patients are more frequently males with a mean age of 45 years. The most common presenting symptoms are epistaxis, nasal obstruction, cheek pain, cheek swelling, and bloody rhinorrhea [54–56]. Association with hypertension, previous sinonasal surgery, and bleeding disorders, including coagulation factor deficiency, end stage renal failure, liver cirrhosis, or use of anticoagulation agents, is well documented [54]. Most cases involve the maxillary sinus unilaterally and present as an expansile mass that extends into the nasal cavity.

OH may have an aggressive appearance on CT scans due to bone remodeling and destruction, thus requiring differential diagnosis with a malignant tumor. However, MRI findings are usually indicative of hemorrhage and neovascularization, thus helping in the distinction [56].

Pathologic Features

Grossly, the specimen consists more frequently of hemorrhagic fragments and clotted blood. Otherwise, the lesion may appear as a cyst with a thick fibrous wall containing clotted blood. Histologically, there is abundant deposition of fibrinoid amorphous eosinophilic material, mixed with extravasated erythrocytes, fragments of dense fibrous tissue with hemosiderin deposition, and dilated vessels (Figs. 6.21 and 6.22) [57, 58].

Differential Diagnosis

The histologic diagnosis is usually straightforward if the clinical presentation and the imaging features are known. Vascular tumors are the main differential diagnosis.

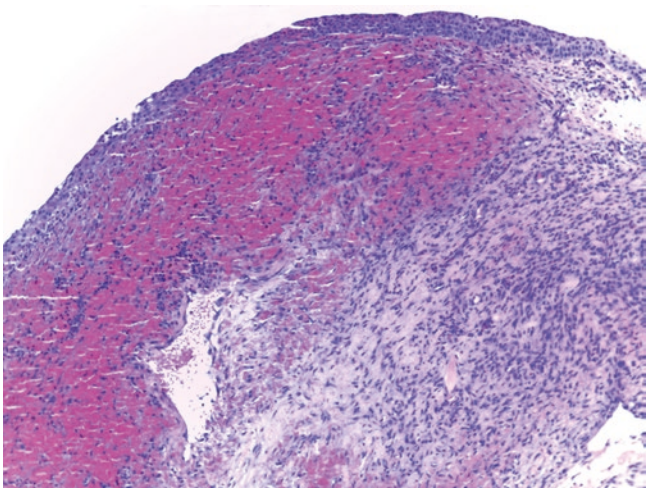

Fig. 6.21 Organized hematoma. Fragment of nasal mucosa with extravasated erythrocytes, fibrous tissue with hemosiderin deposition, and dilated vessels

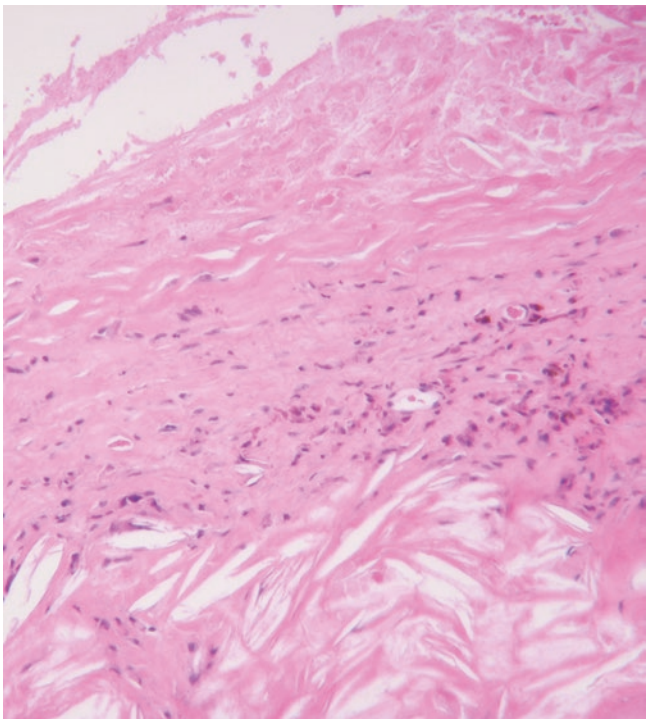

Fig. 6.22 The wall of the lesion consists of hyaline stroma with scattered lymphocytes and histiocytes, and deposition of cholesterol crystals

6.8 Amyloidosis

Localized amyloid deposition in the sinonasal mucosa is very rare, with about 20 cases reported in the English literature [59–62]. In some cases, the clinical presentation may resemble that of a sinonasal malignancy, with nasal obstruction, nasal discharge, and epistaxis [62]. Facial pain may also be present, and it is often associated with significant bony erosion of the walls of the sinonasal tract and of the skull [61]. The most common site of origin is the nasal cavity.

Pathologic Features

Histologically, deposits of amorphous eosinophilic material are present in the stroma, around blood vessels (Fig. 6.23) and around ducts of seromucous glands. They are often associated with diffuse chronic inflammation and foreign body granulomatous reaction (Fig. 6.24). Occasionally, amyloid deposits may appear as multiple globular eosinophilic deposits with a lamellar appearance reminiscent of corpora amylacea, which may be partially calcified [62]. Amyloid stains orange with Congo red and is typically apple-green birefringent at polarized light examination. The Congophilia is lost after pretreatment of the tissue with potassium permanganate in cases of AA, beta 2 microglobulin, or apolipoprotein amyloid. Immunohistochemistry may help to identify the type of amyloid deposition. In the head and neck, most cases are of the primary (AL) type and therefore they are positive for kappa or lambda light chain. Other protein constituents of systemic amyloid can be tested by immunohistochemistry [63].

Differential Diagnosis

Amyloid deposits may be overlooked and/or confused with fibrosis or sclerotic changes of the mucosa.

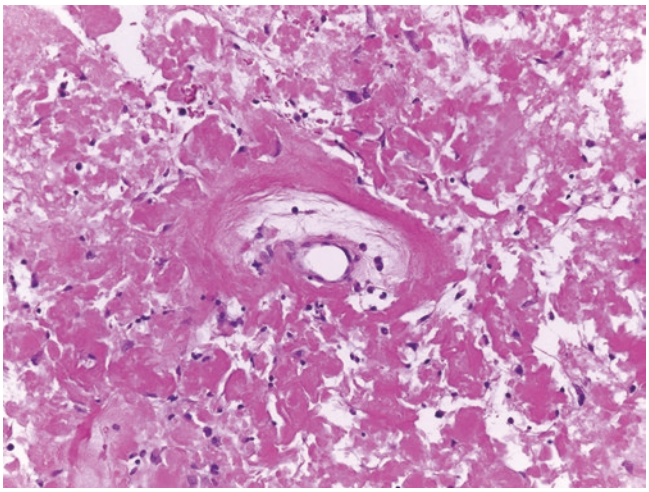

Fig. 6.23 Amyloid deposition around a blood vessel

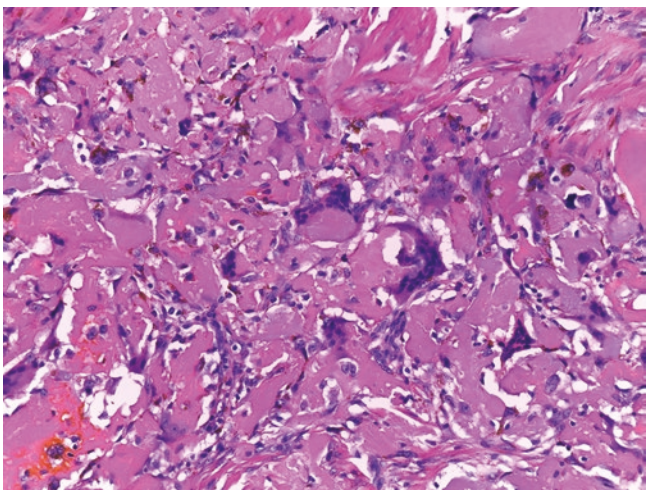

Fig. 6.24 Amyloid deposition with foreign body giant cell reaction. Focal deposits of hemosiderin are also present

6.9 Conclusion

Sinonasal tumor-like lesions represent a heterogeneous group of non-neoplastic growths that may clinically and/or histologically mimic a tumor, thus requiring careful histologic examination for the correct diagnosis and to avoid overtreatment.

References

1. Vaghela H, Bradley P. Nasal dermoid sinus cysts in adults. J Laryngol Otol. 2004;118:955–62.
2. Ni K, Li X, Zhao L, Wu J, Liu X, Shi H. Diagnosis and treatment of congenital nasal dermoid and sinus cysts in 11 infants: a consort compliant study. Medicine (Baltimore). 2020;99:e19435.
3. Golaszewski J, Muñoz R, Barazarte D, Perez L. Surgical ciliated cyst after maxillary orthognathic surgery: a literature review and case report. Oral Maxillofac Surg. 2019;23:281–4.
4. Ramakrishnan DS, Abdul Wahab PU, Dhasarathan P, Madhulaxmi M, Kandamani J. Surgical ciliated cyst of the left maxilla - a case report of unusual pathogenesis. Ann Maxillofac Surg. 2020;10:479–83.
5. Amin M, Witherow H, Lee R, Blenkinsopp P. Surgical ciliated cyst after maxillary orthognathic surgery: report of a case. J Oral Maxillofac Surg. 2003;61:138–14.
6. Leung YY, Wong WY, Cheung LK. Surgical ciliated cysts may mimic radicular cysts or residual cysts of maxilla: report of 3 cases. J Oral Maxillofac Surg. 2012;70:e264–9.
7. Walgama ES, Hwang PH. Aspirin-exacerbated respiratory disease. Otolaryngol Clin N Am. 2017;83-94:83.
8. Nakayama M, Wenig BM, Heffner DK. Atypical stromal cells in inflammatory nasal polyps: immunohistochemical and ultrastructural analysis in defining histogenesis. Laryngoscope. 1995;105:127–34.
9. Hadravsky L, Skalova A, Kacerovska D, et al. Angiomatoid change in polyps of the nasal and paranasal regions: an underrecognized and commonly misdiagnosed lesion. Report of 45 cases. Virchows Arch. 2012;460:203–9.
10. Heffner DK. Sinonasal angiosarcoma? Not likely (a brief description of infarcted nasal polyps). Ann Diagn Pathol. 2010;14:233–4.
11. Yfantis HG, Drachenberg CB, Gray W, Papadimitriou JC. Angiectatic nasal polyps that clinically simulate a malignant process. Report of 2 cases and a review of the literature. Arch Pathol Lab Med. 2000;124:406–10.
12. Sheahan P, Crotty PL, Hamilton S, Colreavy M, McShane D. Infarcted angiomatous polyps. Rhinology. 2004;262:225–30.
13. Lee DH, Yoon TM, Lee JK, Lim SC. Difference of antrochoanal polyp between children and adults. Int J Pediatr Otorhinolaryngol. 2016;84:143–6.
14. Choudhury N, Hariri A, Saleh H, Sandison A. Diagnostic challenges of antrochoanal polyps: a review of sixty-one cases. Clin Otolaryngol. 2018;43:670–4.
15. Wenig BM, Franchi A, Ro JY. Tumours of the nasal cavity, paranasal sinuses and skull base: respiratory epithelial adenomatoid hamartoma. In: El-Naggar AK, Chan JKC, Grandis JR, Takata T, Slootweg PJ, editors. World Health Organization classification of head and neck tumours. 4th ed. Lyon: IARC Press; 2017.
16. Ro JY, Franchi A. Tumours of the nasal cavity, paranasal sinuses and skull base: seromucinous hamartoma. In: El-Naggar AK, Chan JKC, Grandis JR, Takata T, Slootweg PJ, editors. World Health Organization classification of head and neck tumours. 4th ed. Lyon: IARC Press; 2017.
17. Toner M, Hunt JL. Tumours of the nasal cavity, paranasal sinuses and skull base: chondromesenchymal hamartoma. In: El-Naggar AK, Chan JKC, Grandis JR, Takata T, Slootweg PJ, editors. World Health Organization classification of head and neck tumours. 4th ed. Lyon: IARC Press; 2017.
18. Kossai M, El Zein S, Wassef M, Guichard JP, Pouliquen C, Herman P, et al. Olfactory epithelial hamartoma: a new subtype of Sinonasal hamartoma. Am J Surg Pathol. 2018;42(1):9–17.
19. Delbrouck C, Fernandez Aguilar S, Choufani G, Hassid S. Respiratory epithelial adenomatoid hamartoma associated with nasal polyposis. Am J Otolaryngol. 2004;25(4):282–4.
20. Schertzer JS, Levy JM, Wise SK, Magliocca KR, DelGaudio JM. Is respiratory epithelial Adenomatoid hamartoma related to central compartment atopic disease? Am J Rhinol Allergy. 2020;34(5):610–7.
21. Ozolek JA, Hunt JL. Tumor suppressor gene alterations in respiratory epithelial adenomatoid hamartoma (REAH): comparison to sinonasal adenocarcinoma and inflamed sinonasal mucosa. Am J Surg Pathol. 2006;30(12):1576–80.
22. Baneckova M, Michal M, Laco J, Leivo I, Ptakova N, Horakova M, et al. Immunohistochemical and genetic analysis of respiratory epithelial adenomatoid hamartomas and seromucinous hamartomas: are they precursor lesions to sinonasal low-grade tubulopapillary adenocarcinomas? Hum Pathol. 2020;97:94–102.

23. Stewart DR, Messinger Y, Williams GM, Yang J, Field A, Schultz KA, et al. Nasal chondromesenchymal hamartomas arise secondary to germline and somatic mutations of DICER1 in the pleuropulmonary blastoma tumor predisposition disorder. Hum Genet. 2014;133(11):1443–50.
24. Mason KA, Navaratnam A, Theodorakopoulou E, Chokkalingam PG. Nasal Chondromesenchymal hamartoma (NCMH): a systematic review of the literature with a new case report. J Otolaryngol Head Neck Surg. 2015;44:28.
25. Bullock MJ. Low-grade epithelial proliferations of the Sinonasal tract. Head Neck Pathol. 2016;10(1):47–59.
26. Cao Z, Gu Z, Yang J, Jin M. Respiratory epithelial adenomatoid hamartoma of bilateral olfactory clefts associated with nasal polyposis: three cases report and literature review. Auris Nasus Larynx. 2010;37(3):352–6.
27. Seol JG, Livolsi VA, O'Malley BW Jr, Chen JY, Loevner LA. Respiratory epithelial adenomatoid hamartoma of the bilateral olfactory recesses: a neoplastic mimic? AJNR Am J Neuroradiol. 2010;31(2):277–9.
28. Baillie EE, Batsakis JG. Glandular (seromucinous) hamartoma of the nasopharynx. Oral Surg Oral Med Oral Pathol. 1974;38(5):760–2.
29. Golbin DA, Ektova AP, Demin MO, Lasunin N, Cherekaev VA. Nasal Chondromesenchymal hamartoma with Skull Base and orbital involvement: case presentation. Cureus. 2018;10(6):e2892.
30. Gauchotte G, Marie B, Gallet P, Nguyen DT, Grandhaye M, Jankowski R, et al. Respiratory epithelial adenomatoid hamartoma: a poorly recognized entity with mast cell recruitment and frequently associated with nasal polyposis. Am J Surg Pathol. 2013;37(11):1678–85.
31. Ambrosini-Spaltro A, Morandi L, Spagnolo DV, Cavazza A, Brisigotti M, Damiani S, et al. Nasal seromucinous hamartoma (microglandular adenosis of the nose): a morphological and molecular study of five cases. Virchows Arch. 2010;457(6):727–34.
32. Norman ES, Bergman S, Trupiano JK. Nasal chondromesenchymal hamartoma: report of a case and review of the literature. Pediatr Dev Pathol. 2004;7(5):517–20.
33. Ozolek JA, Carrau R, Barnes EL, Hunt JL. Nasal chondromesenchymal hamartoma in older children and adults: series and immunohistochemical analysis. Arch Pathol Lab Med. 2005;129(11):1444–50.
34. Weinreb I, Gnepp DR, Laver NM, Hoschar AP, Hunt JL, Seethala RR, et al. Seromucinous hamartomas: a clinicopathological study of a sinonasal glandular lesion lacking myoepithelial cells. Histopathology. 2009;54(2):205–13.
35. Ozolek JA, Barnes EL, Hunt JL. Basal/myoepithelial cells in chronic sinusitis, respiratory epithelial adenomatoid hamartoma, inverted papilloma, and intestinal-type and nonintestinal-type sinonasal adenocarcinoma: an immunohistochemical study. Arch Pathol Lab Med. 2007;131(4):530–7.
36. Fleming KE, Perez-Ordonez B, Nasser JG, Psooy B, Bullock MJ. Sinonasal seromucinous hamartoma: a review of the literature and a case report with focal myoepithelial cells. Head Neck Pathol. 2012;6(3):395–9.
37. Nguyen DT, Gauchotte G, Arous F, Vignaud JM, Jankowski R. Respiratory epithelial adenomatoid hamartoma of the nose: an updated review. Am J Rhinol Allergy. 2014;28(5):187–92.
38. Nguyen DT, Nguyen-Thi PL, Gauchotte G, Arous F, Vignaud JM, Jankowski R. Predictors of respiratory epithelial adenomatoid hamartomas of the olfactory clefts in patients with nasal polyposis. Laryngoscope. 2014;124(11):2461–5.
39. Sangoi AR, Berry G. Respiratory epithelial adenomatoid hamartoma: diagnostic pitfalls with emphasis on differential diagnosis. Adv Anat Pathol. 2007;14(1):11–6.
40. Re M, Gioacchini FM, Bajraktari A, Tomasetti M, Kaleci S, Rubini C, et al. Malignant transformation of sinonasal inverted papilloma and related genetic alterations: a systematic review. Eur Arch Otorhinolaryngol. 2017;274(8):2991–3000.
41. Carter CS, East EG, McHugh JB. Biphenotypic Sinonasal sarcoma: a review and update. Arch Pathol Lab Med. 2018;142(10):1196–201.
42. Thirunavukkarasu B, Chatterjee D, Mohindra S, Dass Radotra B, Prashant SJ. Nasal Chondromesenchymal hamartoma. Head Neck Pathol. 2020;14(4):1041–5.
43. Lee TJ, Li SP, Fu CH, et al. Extensive paranasal sinus mucoceles: a 15-year review of 82 cases. Am J Otolaryngol Head Neck Med Surg. 2009;30:234–8.
44. Scangas GA, Gudis DA, Kennedy DW. The natural history and clinical characteristics of paranasal sinus mucoceles: a clinical review. Int Forum Allergy Rhinol. 2013;3:712–7.
45. Johnston WH. Necrotizing sialometaplasia involving the mucous glands of the nasal cavity. Hum Pathol. 1977;8:589–92.
46. Maisel RH, Johnston WH, Anderson HA, Cantrell RW. Necrotizing sialometaplasia involving the nasal cavity. Laryngoscope. 1977;87:429–34.
47. Chen KT. Necrotizing sialometaplasia of the nasal cavity. Am J Otolaryngol. 1982;3:444–6.
48. Close LG, Cowan DF. Recurrent necrotizing sialometaplasia of the nasal cavity. Otolaryngol Head Neck Surg. 1985;93:422–5.
49. Abrams AM. Necrotizing sialometaplasia of the nasal cavity. Otolaryngol Head Neck Surg. 1986;94:416.
50. Granich MS, Pilch BZ. Necrotizing sialometaplasia in the setting of acute and chronic sinusitis. Laryngoscope. 1981;91:1532–5.
51. Keogh PV, O'Regan E, Toner M, Flint S. Necrotizing sialometaplasia: an unusual bilateral presentation associated with antecedent anaesthesia and lack of response to intralesional steroids. Case report and review of the literature. Br Dent J. 2004;196(2):79–81.
52. Daudia A, Murty GE. First case of full-thickness palatal necrotizing sialometaplasia. J Laryngol Otol. 2002;116(3):219–20.
53. Franchi A, Gallo O, Santucci M. Pathologic quiz case 1. Necrotizing sialometaplasia obscuring recurrent well-differentiated squamous cell carcinoma of the maxillary sinus. Arch Otolaryngol Head Neck Surg. 1995;121(584):586.
54. Choi SJ, Seo ST, Rha KS, Kim YM. Sinonasal organized hematoma: clinical features of seventeen cases and a systematic review. Laryngoscope. 2015;125(9):2027–33.
55. Pang W, Hu L, Wang H, et al. Organized hematoma: an analysis of 84 cases with emphasis on difficult prediction and favorable management. Otolaryngol Head Neck Surg. 2016;154:626–33.
56. Kim JS, Oh JS, Kwon SH. The increasing incidence of paranasal organizing hematoma: a 20-year experience of 23 cases at a single center. Rhinology. 2016;54:176–82.
57. Yokoi H, Arakawa A, Matsumoto F, Yokoi N, Ikeda K, Kohno N. Organized hematoma of the maxillary sinus: a clinicopathologic study of 5 cases. Ear Nose Throat J. 2014;93:E23–6.
58. Omura G, Watanabe K, Fujishiro Y, Ebihara Y, Nakao K, Asakage T. Organized hematoma in the paranasal sinus and nasal cavity--imaging diagnosis and pathological findings. Auris Nasus Larynx. 2010;37:173–7.
59. Mufarrij AA, Busaba NY, Zaytoun GM, Gallo GR, Feiner HD. Primary localized amyloidosis of the nose and paranasal sinuses. A case report with immunohistochemical observations and a review of the literature. Am J Surg Pathol. 1990;14:379–83.
60. Tsikoudas A, Martin-Hirsch DP, Woodhead CJ. Primary sinonasal amyloidosis. J Laryngol Otol. 2001;115:55–6.
61. Prasad D, Somayaji GK, Aroor R, Abdulla MN. Primary nasal amyloidosis. Int Jf Otorhinolaryngol. 2009;9:2.
62. Kumar B, Pant B, Kumar V, Negi M. Sinonasal Globular Amyloidosis Simulating Malignancy: A Rare Presentation. Head Neck Pathol. 2016;10:379–83.
63. Schönland SO, Hegenbart U, Bochtler T, et al. Immunohistochemistry in the classification of systemic forms of amyloidosis: a systematic investigation of 117 patients. Blood. 2012;119:488–93.

Benign Epithelial Tumors of Sinonasal Tract

7

Manish Mahadeorao Bundele

7.1 Introduction

Sinonasal papillomas (SP) are benign epithelial neoplasm of sinonasal tract. The ectodermally derived ciliated pseudostratified respiratory epithelium that lines the sinonasal tract (Schneiderian membrane), gives rise to three morphologically distinct sinonasal papillomas—inverted (ISP), exophytic (ESP), and oncocytic (OSP).

The lesion was first described by Ward in 1854; however, it was Hyams' exhaustive review of 315 cases from the AFIP archives in 1971, which provided clearer understanding of this entity [1, 2]. Barnes and Bedetti later elucidated truly oncocytic features (presence of abundant mitochondria resulting in eosinophilic granular cytoplasm) of OSP [3] and is recently linked to activating KRAS mutations [4].

WHO 2017 and 2022 classifications omitted the eponymous "Schneiderian" designation and reclassified this entity simply as "sinonasal papilloma." Although three subtypes of sinonasal papillomas share a number of findings, there are sufficient clinical and microscopic differences to regard them as three distinctive clinicopathologic entities and a precise diagnosis should be given when possible [5–7].

7.2 Clinical Features

SP are common epithelial neoplasms of the head and neck, that comprise 0.5 to 4% of all sinonasal tumors [1, 2, 8]. ISP is the most common form of sinonasal papilloma, followed by ESP and OSP is the rarest type [1, 6]. Clinicopathologic features of 3 subtypes of SP are summarized in Table 7.1 [1, 2, 5, 6, 9, 10].

All three types of SP can affect patients of any age. Bilateral papillomas of any type of SP are uncommon.

ISP rarely can involve sites such as ear, nasopharynx, lacrimal sac, and oropharynx, but these sites are usually involved secondarily from sinonasal tract disease. All sinonasal papillomas typically present non-specifically as nasal obstruction, headache, epistaxis, rhinorrhea with or without an evident mass.

M. M. Bundele (✉)
Department of Pathology, Tan Tock Seng Hospital, Singapore, Singapore
e-mail: manish_bundele@ttsh.com.sg

D. Jain, J. A. Bishop (eds.), *Atlas of Sinonasal Tract Pathology*, https://doi.org/10.1007/978-981-19-7315-4_7

Table 7.1 Clinicopathologic features of 3 subtypes of SP [1, 2, 5, 6, 9, 10]

	Inverted SP	Exophytic SP	Oncocytic SP
Age	Adults (mean fifth–sixth decade)	Adults (mean third–fifth decade)	sixth decade onwards
Sex ratio (male: Female)	2–3:1	10:1	1:1
Location	Lateral nasal wall and paranasal sinuses	Nasal septum—Commonly lower anterior	Lateral nasal wall and paranasal sinuses
Gross pathology features	Often bulky, firm, gray, tan polyps. Cerebriform appearance, non-translucent	Small, discrete, broad based, papillary or warty; gray, pink, or tan; non-translucent	Often bulky, firm, tan or reddish polyps. Cerebriform appearance, non-translucent
Histopathology features	Prominent endophytic growth from the surface epithelium. Multi-layered epithelium; variably squamous, squamoid/transitional, or ciliated columnar	Exophytic growth pattern with finger-like projections. Multi-layered epithelium usually squamous; Koilocytosis	Exophytic and endophytic growth pattern. Multi-layered epithelium with oncocytic cells
Differential diagnosis	Sinonasal inflammatory polyp, papillary rhinosinusitis, REAH, carcinoma	Cutaneous squamous papilloma, inflammatory nasal polyp, Papillary (nonkeratinizing) squamous cell carcinoma	Rhinosporidiosis, low-grade papillary sinonasal adenocarcinoma
Rate of malignant transformation	5–15%	Close to 0	4–17%
Molecular alterations	*EGFR* mutations	None	*KRAS* mutations
Association with HPV	Unclear association. A minority have been reported to harbor low-risk or high-risk HPV types, with a possible increase in those with dysplasia or carcinomatous transformation	Most caused by low-risk HPV types	None

REAH Respiratory epithelial adenomatoid hamartoma, *HPV* Human Papilloma Virus

Radiologically, all SP appear as a soft-tissue density, with a "septate, striated" appearance classically seen on magnetic resonance imaging [5, 6, 11]. SP present as pink, gray, or tan polypoid tumor masses, and, in contrast to sinonasal polyps, are often less or non-translucent. On palpation, papillomas often have a firmer texture than inflammatory polyps.

7.3 Histopathology

All three types of SP share the features of epithelial thickening, scattered mucous cells or cysts, and intraepithelial neutrophils with microabscesses formation. When evaluating the epithelial thickness, it is helpful to note the thickness of normal "Schneiderian," i.e., ciliated pseudostratified columnar epithelium.

ISP features prominent downward growth of rounded, elongated and anastomosing epithelial nests from the surface epithelium, surrounded by an intact basement membrane (Figs. 7.1, 7.2, 7.3, 7.4, 7.5, 7.6, 7.7, and 7.8). The ISP epithelium (up to 30 cells thick) may be variably squamous, squamoid/transitional, or less commonly with retained surface ciliated columnar epithelium. Mitoses are sparse and confined to the basal/parabasal layers. Distinct cell borders with clearing of cytoplasm (glycogenation) are a frequent finding. Background stroma is edematous, myxoid or fibrous with absence of seromucinous glands.

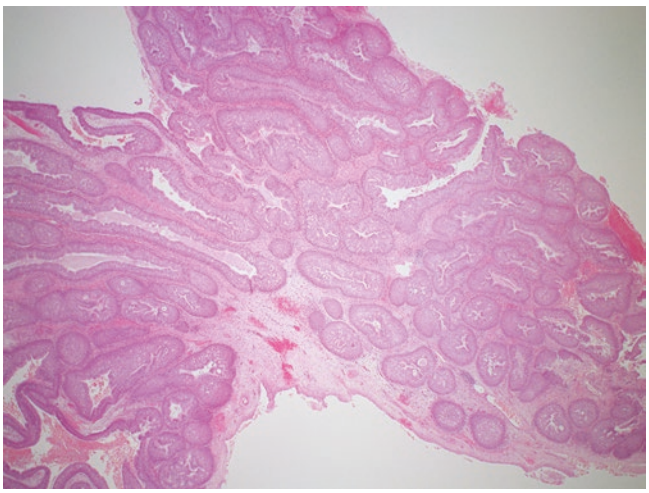

Fig. 7.1 HE x 20 ISP showing prominent deep inverted growth of rounded, elongated, and anastomosing epithelial nests from the surface epithelium, surrounded by an intact basement membrane. Seromucinous glands are not seen

In a fragmented specimen, the presence of thickened epithelium/epithelial nests surrounded by a well-defined basement membrane with adjacent delicate fibrous stroma

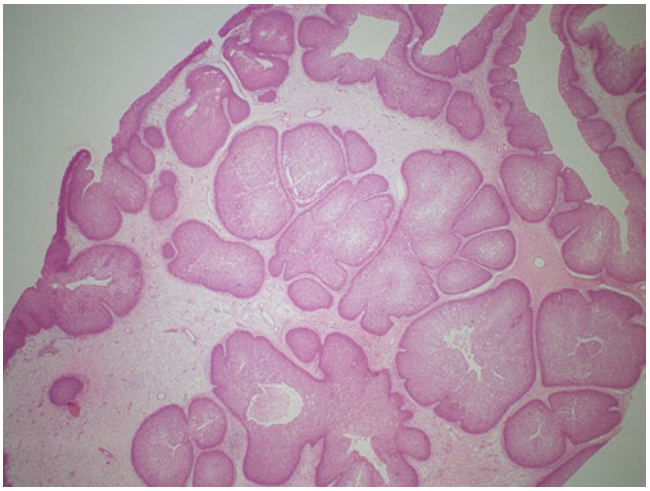

Fig. 7.2 HE x 20. ISP showing prominent deep inverted growth of rounded, elongated, and anastomosing epithelial nests from the surface epithelium, surrounded by an intact basement membrane. Seromucinous glands are not seen

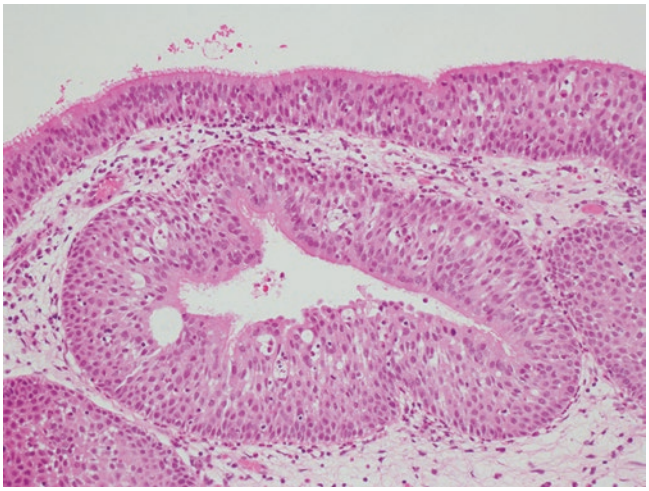

Fig. 7.4 HE x 200. This example of ISP showing retained surface ciliated columnar epithelium. Note the maintained cell polarity in the thickened epithelium

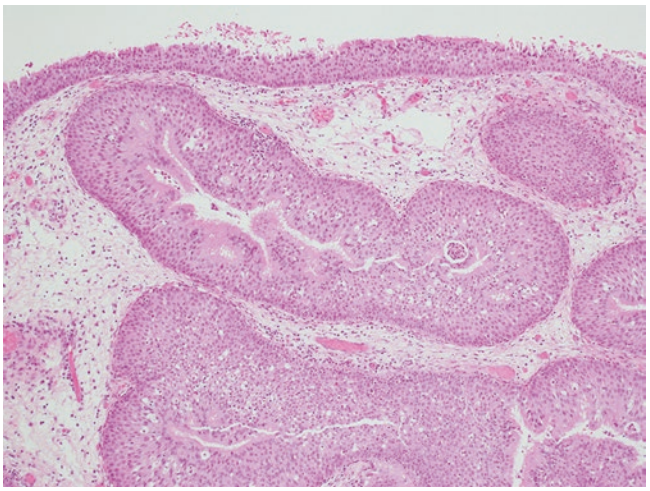

Fig. 7.3 HE x 100. ISP showing thickened transitional/squamoid epithelium with intraepithelial neutrophils and microcysts

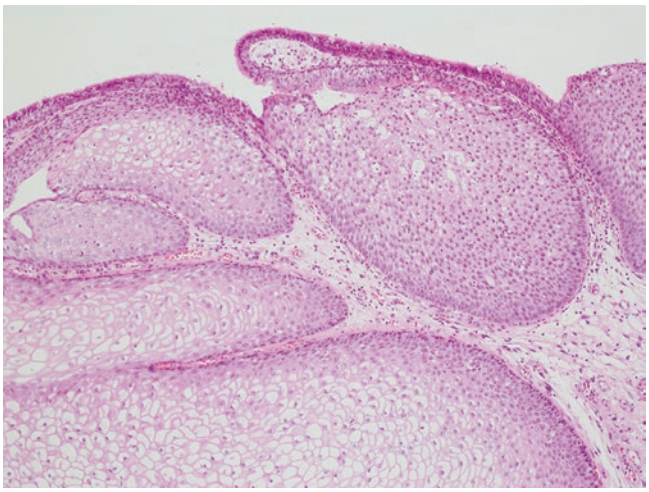

Fig. 7.5 HE x 100. This example shows transition of normal surface epithelium to ISP with thickened variably squamoid/transitional epithelium in the top right and more mature, glycogenated squamous epithelium towards the bottom with distinct cell border. Fewer transmigrating neutrophils are seen in squamous areas

suggests an endophytic growth pattern, consistent with an ISP [5]. Occasionally, ISP can be seen with polyps or hamartomas.

Locally aggressive infiltrative growth pattern of ISP may be seen but this does not imply malignancy on its own without accompanying cytomorphology. When carcinoma is present, it is synchronous in the majority (70%) of cases [1, 9].

ESP shows broad, branching fronds/papillae of epithelium with central fibrovascular cores (Figs. 7.9, 7.10, 7.11, 7.12, and 7.13). Most often lining is well-differentiated squamous epithelium (up to 20 cells thick) but it can be variably squamous, transitional, and columnar with mucous/goblet cells. Koilocytic atypia may be seen. ESP lack the endophytic growth patterns of ISP. Malignant transformation is exceptional [12].

OSP typically demonstrates both inverted and exophytic growth pattern (Figs. 7.14, 7.15, 7.16, 7.17, 7.18, and 7.19). The lining is pseudostratified with tall, columnar cells featuring centrally located ovoid nuclei. The cells have abundant eosinophilic and granular cytoplasm. They are also frequently interspersed with intraepithelial microabscesses

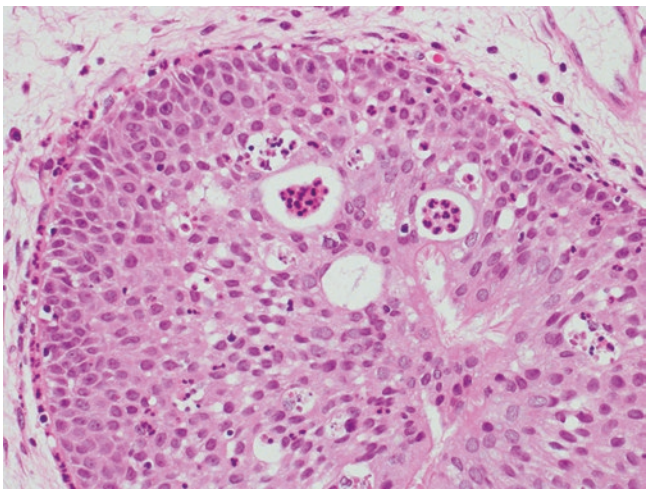

Fig. 7.6 HE x 400. Higher magnification of an inverted nest of ISP shows mucinous cells and a large number of transmigrating neutrophils forming small microabscesses

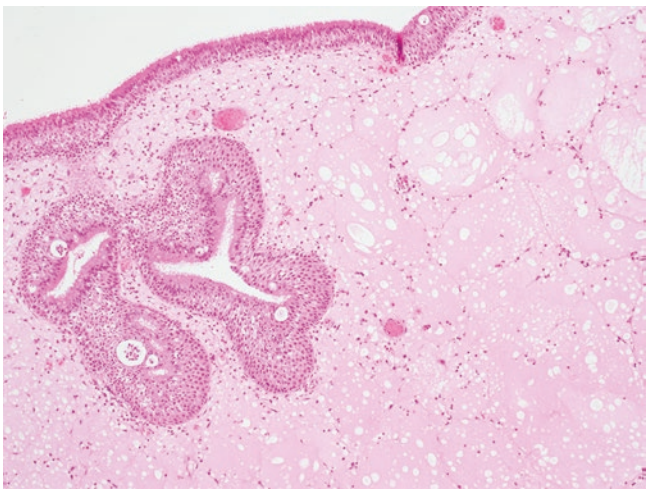

Fig. 7.8 HE x 100. Showing concurrent inflammatory polyp with normal thickness surface epithelium and submucosal edematous stroma, adjacent to ISP on the left featuring thickened epithelium and inverted growth pattern

Fig. 7.7 HE x 40. Showing concurrent inflammatory polyp with normal thickness surface epithelium and submucosal edematous stroma, adjacent to ISP on the left featuring thickened epithelium and inverted growth pattern

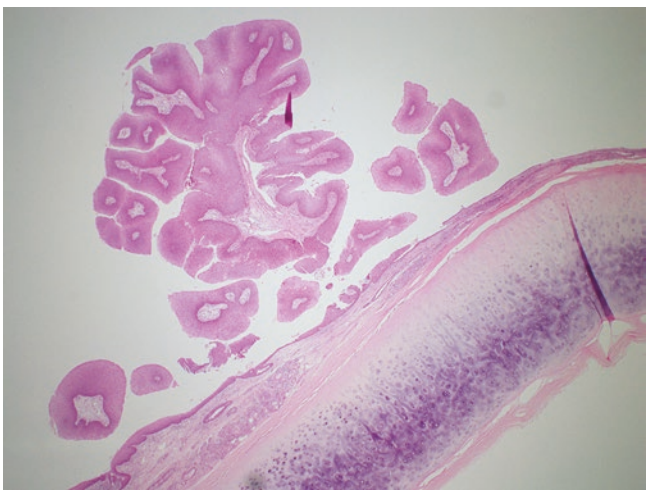

Fig. 7.9 HE x 20. Scanner view showing nasal septum with ESP featuring exophytic/complex papillary architecture

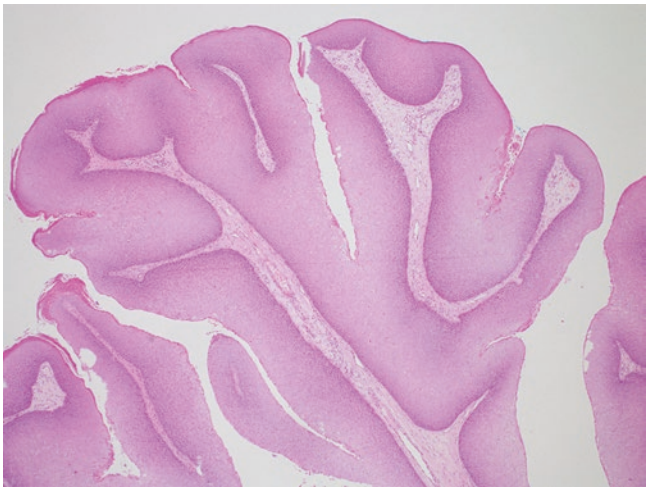

Fig. 7.10 HE x 40. ESP showing papillae with fibrovascular core lined by markedly thickened well-differentiated squamous epithelium. Focal surface parakeratosis is seen

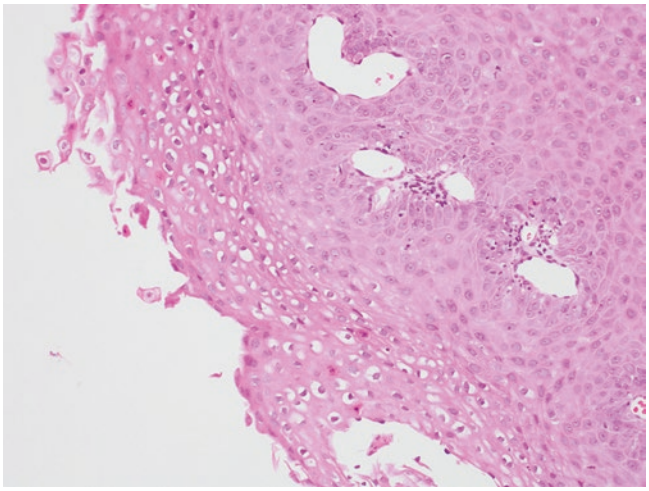

Fig. 7.12 HE x 200. ESP showing squamous epithelium with focus of koilocytotic atypia featuring raisinoid nuclei and perinuclear clearing of cytoplasm

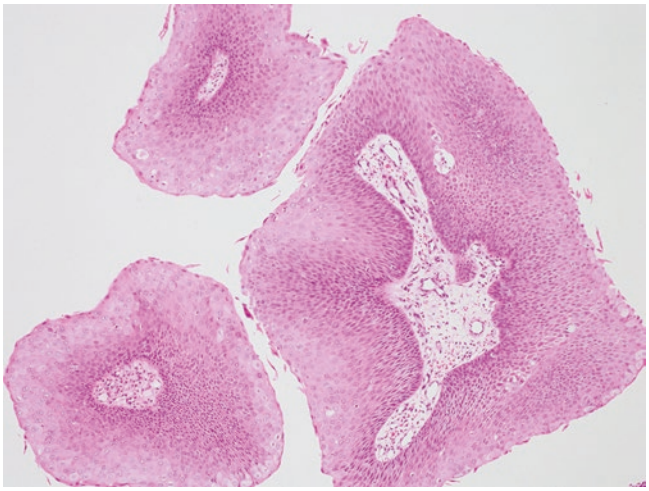

Fig. 7.11 HE x 100. ESP showing papillae lined by predominant squamous epithelium with occasional mucous cells and transmigrating neutrophils

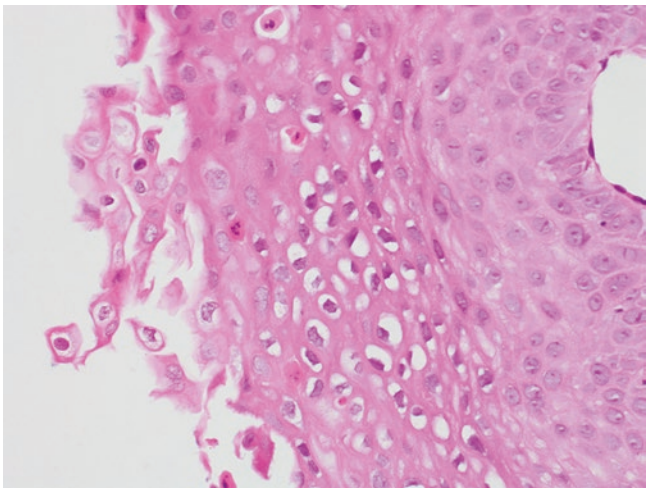

Fig. 7.13 HE x 400. ESP showing squamous epithelium with focus of koilocytotic atypia featuring raisinoid nuclei and perinuclear clearing of cytoplasm

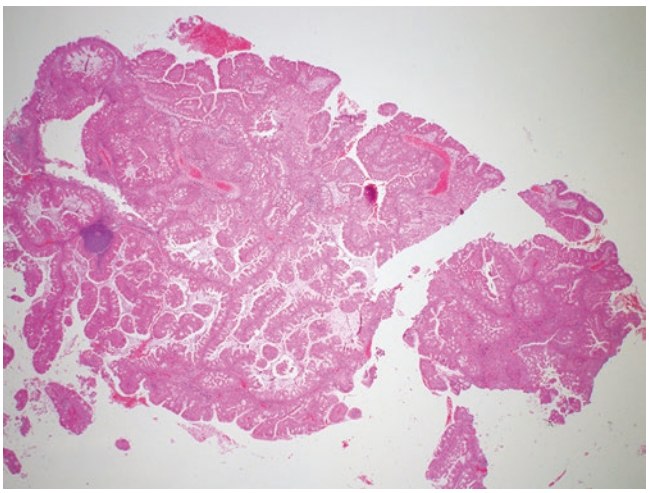

Fig. 7.14 HE x 20. Scanner views showing OSP with predominant exophytic/papillary component with long delicate fibrovascular cores and focal endophytic/inverted component

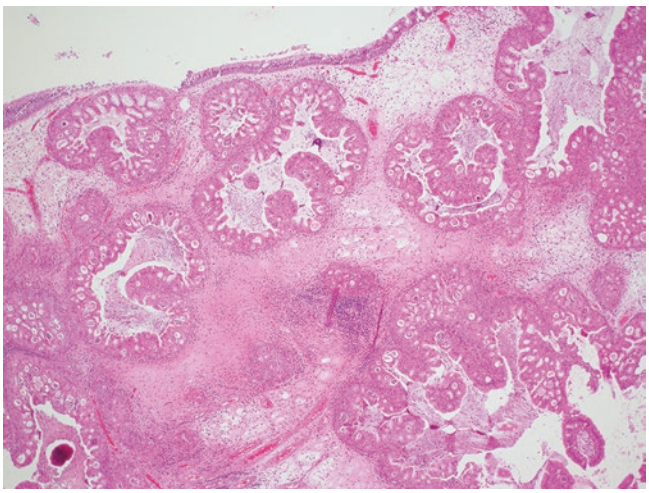

Fig. 7.15 HE x 40. OSP with areas of prominent endophytic/inverted component beneath the normal surface ciliated mucosa

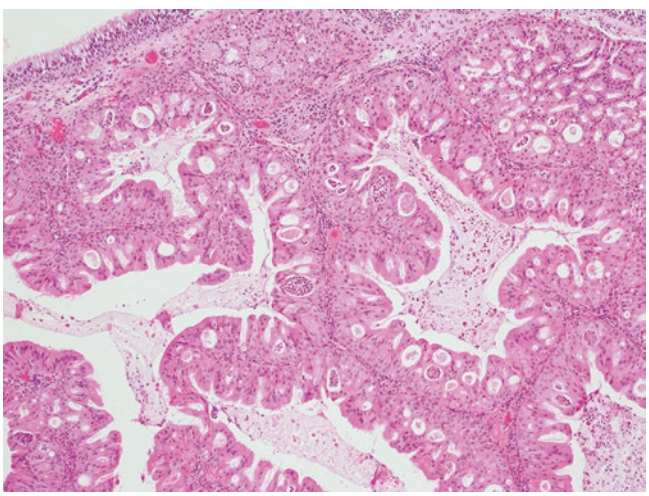

Fig. 7.16 HE x 100. OSP with areas of prominent endophytic/inverted component beneath the normal surface ciliated mucosa

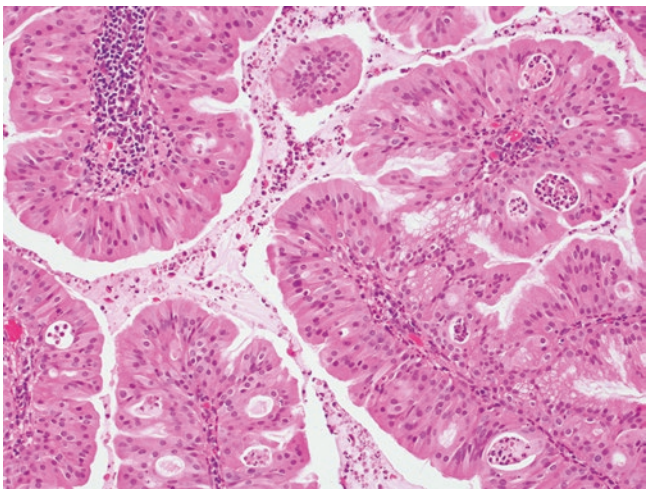

Fig. 7.17 HE x 200. OSP featuring multilayered columnar or oncocytic epithelium and associated with transmigrating neutrophils and intraepithelial microcysts

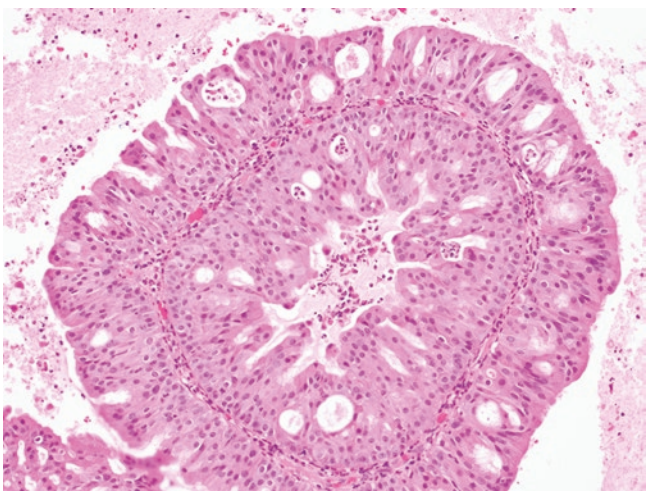

Fig. 7.18 HE x 200. OSP featuring multilayered columnar or oncocytic epithelium and associated with transmigrating neutrophils and intraepithelial microcysts

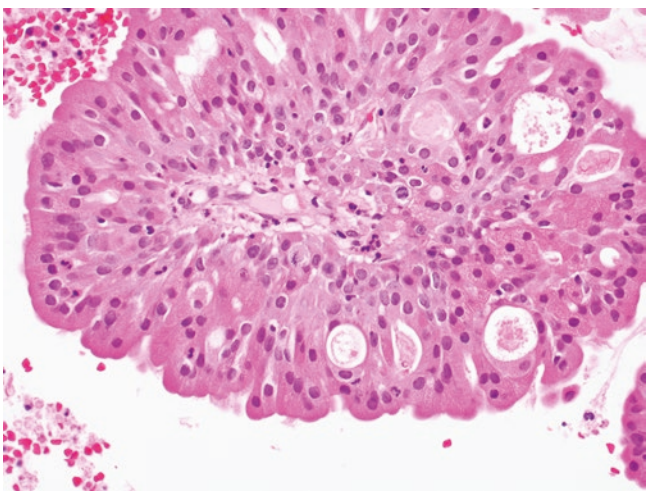

Fig. 7.19 HE x 400. The individual tumor cells show abundant eosinophilic or granular oncocytic cytoplasm. The nuclei are round, centrally located, and uniform

containing both neutrophils and mucin. The surface cells frequently show cilia. Mitotic figures are uncommon in OSP.

Occasionally, SP can show mixed features and, in these cases, the presence of ISP/OSP should be highlighted given the increased risk of subsequent malignant transformation.

7.4 Differential Diagnosis

Inflammatory polyps, a common entity of the sinonasal tract, may also endoscopically appear similar to SP. However, inflammatory polyps consist of thin surface ciliated epithelium overlying an edematous and vascularized stroma. The presence of marked epithelial thickening and intraepithelial microcysts are the key features of SP, and are not seen in an inflammatory polyp (see Chap. 6 for details).

Respiratory epithelial adenomatoid hamartomas (REAH) are downward glandular proliferations arising from the epithelium of the sinonasal tract. Grossly, REAH may appear similar to an ISP; however, it shows circumscribed growth. Although ISP has an intact, well-defined basement membrane, REAH demonstrate a dense, pink, hyalinized basement membrane that should be readily identifiable on low power. REAH also show abundant mucous cells, but no squamous hyperplasia or transmigrating neutrophils of ISP [5, 13] (see Chap. 6 for details).

Occasionally, papillary rhinosinusitis may come into differential; however, it lacks epithelial thickening and does not show inverted growth pattern and typical cytomorphology of SP.

Nonkeratinizing squamous cell carcinomas of the sinonasal tract commonly show inverted, ribbon-like growth pattern and are differentiated from ISP based on malignant cytomorphology. These carcinomas should not be presumed to have arisen from an ISP without evidence of preceding or concurrent benign ISP component (Figs. 7.20, 7.21, 7.22, 7.23, 7.24, 7.25, 7.26, and 7.27).

Recently recognized subtype of sinonasal nonkeratinizing squamous cell carcinomas harboring recurrent fusions between the *DEK* gene and the *AFF2* gene shows striking resemblance with sinonasal papillomas (see Chap. 8) [14].

Cutaneous squamous papilloma can involve nasal vestibule and may be confused with ESP; however, it lacks mucous/ goblet cells, ciliated or transitional epithelium and shows presence of dermal adnexal structures with absence of seromucinous glands.

OSP can be confused with low-grade sinonasal adenocarcinoma since both lesions show bland cytomorphology.

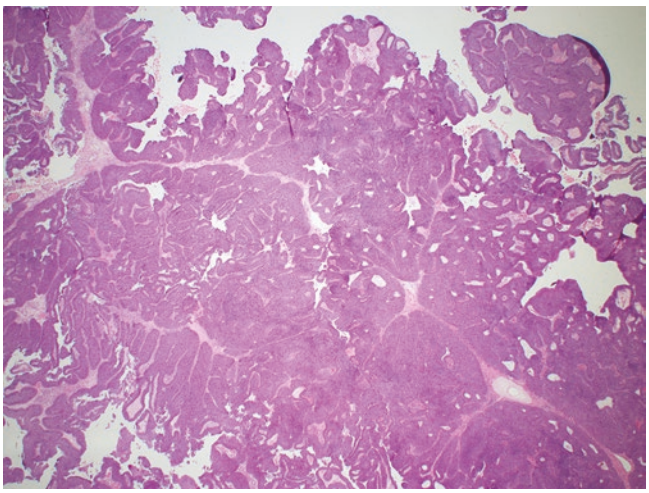

Fig. 7.20 HE x 20 Nonkeratinizing SCC. Scanner view showing complex architecture featuring deep inverted anastomosing nests with scant to no intervening stroma and focal surface exophytic component on right

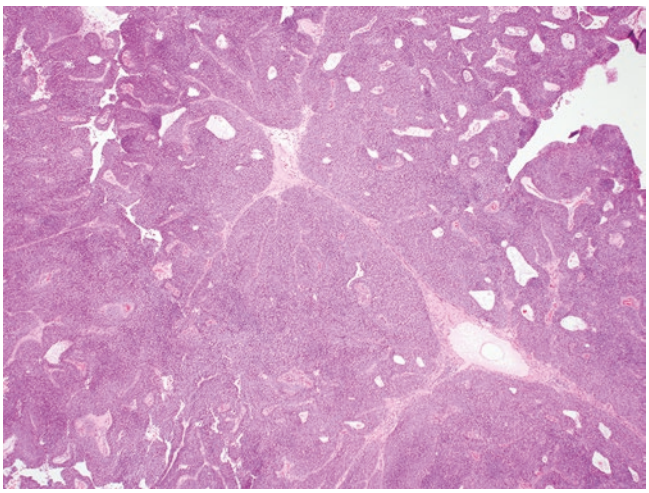

Fig. 7.21 HE x 40. Nonkeratinizing SCC

However, OSP show stratified lining epithelium while low-grade sinonasal adenocarcinoma shows infiltrative growth, with confluent acinar (back-to-back glands with a single layer of cuboidal cells), cystic, or trabecular pattern [3].

Although rhinosporidiosis has been considered a differential of OSP historically, it is a rare zoonotic disease, does not show oncocytic epithelial alterations, its spores are variably sized, located in the submucosal stroma versus uniform intraepithelial microcysts of OSP [2, 3].

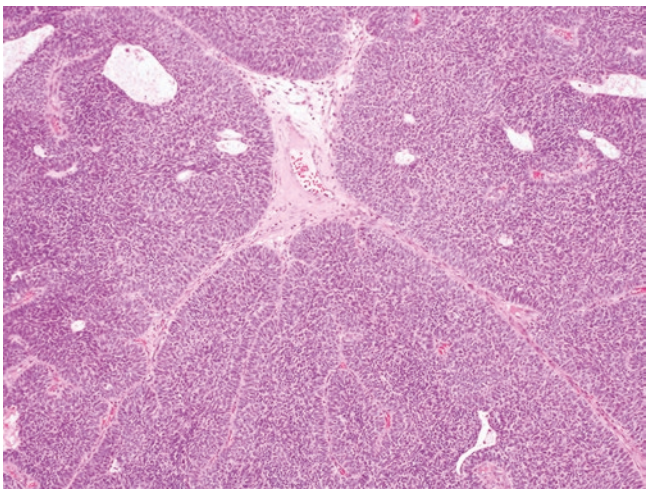

Fig. 7.22 HE x100. Nonkeratinizing SCC showing deep infiltrative basaloid nonkeratinizing nests

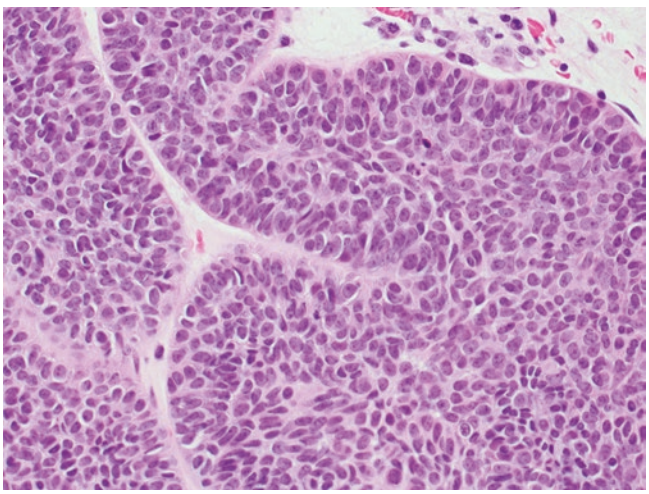

Fig. 7.23 HE x 400. Deeper infiltrative nests with marked cytologic atypia featuring nuclear enlargement and crowding, variable prominence of nucleoli, scattered apoptotic bodies, and scant to moderate cytoplasm

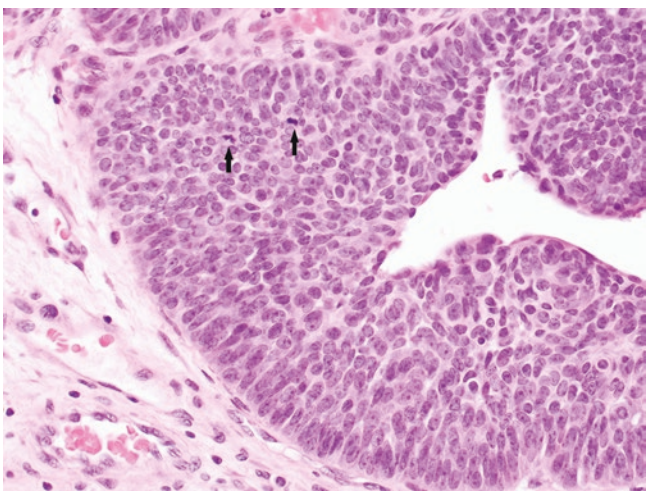

Fig. 7.24 HE x 400. Deeper infiltrative nests with marked cytologic atypia and scattered mitotic activity (arrows)

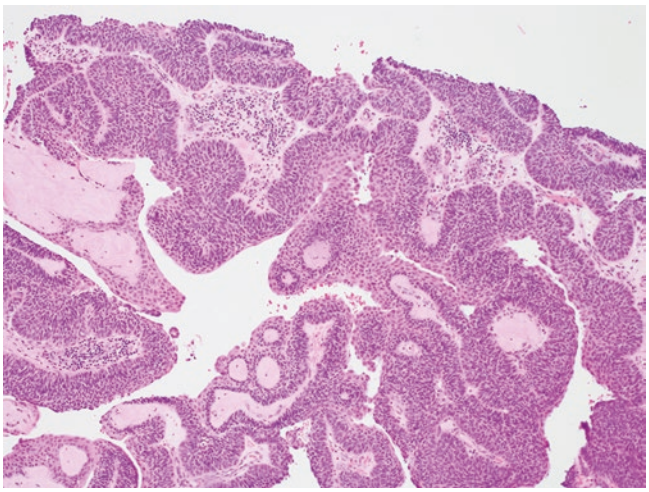

Fig. 7.25 HE x 400. Focal surface predominantly exophytic/papillary component shows squamoid appearance with bland cytology with transition from deeper infiltrative tumor

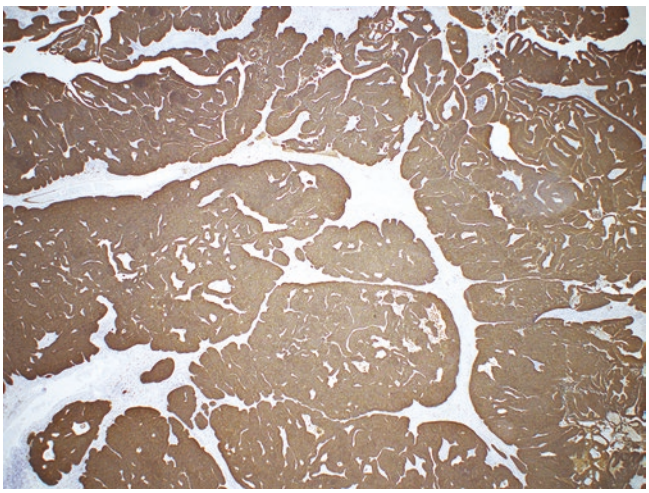

Fig. 7.26 Pancytokeratin AE1/3 x 20 shows diffuse positive staining including deeper infiltrative component

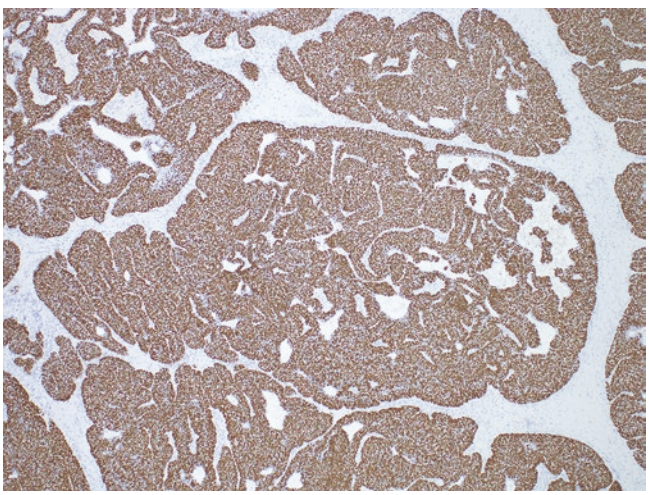

Fig. 7.27 p63 x 40 showing diffuse positive staining including deeper infiltrative component

7.5 Molecular Pathology

Most ISPs (88%) and carcinomas arising from ISPs (77%) harbor activating EGFR mutations [15].

ESP is caused by low-risk HPV types. OSP harbor activating KRAS mutations, are negative for EGFR mutations, and are not associated with HPV infection [1, 4].

7.6 Dysplasia and Carcinoma Ex-Sinonasal Papilloma

In order to exclude dysplasia or carcinoma, thorough histologic examination of SP is recommended.

A progressive spectrum of squamous metaplasia with increasing dysplasia to carcinoma *in-situ* (CIS) to frank invasion is often observed with malignant transformation of SP into SCC and suggests a multi-step pathogenesis.

Two types of dysplasia occur in sinonasal papillomas, keratinizing and nonkeratinizing.

Dyskeratosis, surface keratinization, increased epithelial pleomorphism, and loss of polarity suggest keratinizing dysplasia. Nonkeratinizing dysplasia in a sinonasal papilloma is often subtle and most frequently features loss of transmigrating neutrophils, with associated increased mitotic activity, increased cytologic atypia, and nuclear pleomorphism [16]. In practice, since strict criteria are lacking, atypical cellular changes that fall short of overt carcinoma are often regarded as dysplasia (Figs. 7.28, 7.29, 7.30, and 7.31).

Carcinomas are recognized by the malignant cytomorphology and may feature atypical mitoses and necrosis. Typically, the transition between the SP and carcinoma is very abrupt. Given its inverted pattern, it can be difficult to determine whether a carcinoma arising within an ISP/OSP is truly invasive. Irregular nests with a desmoplastic stromal reaction point to true invasion, and lymphovascular or perineural invasion are diagnostic (Figs. 7.32 and 7.33) [5].

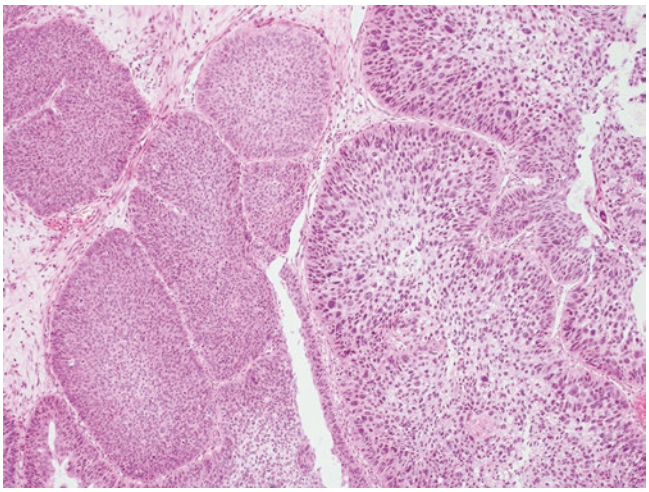

Fig. 7.28 HE x 100. ISP on left shows loss of transmigrating neutrophils, and minimal degree of atypia however the polarity still appears maintained. However, there is abrupt transition to the right of the image featuring nests with marked cytologic atypia with pleomorphic nuclei, loss of polarity and is in keeping with dysplasia arising in an ISP

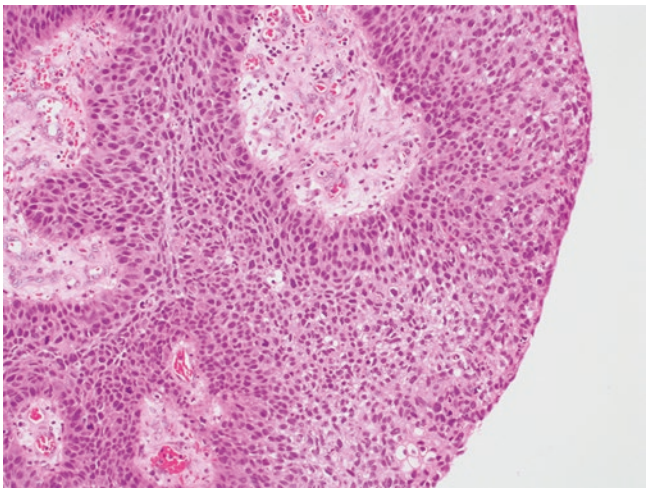

Fig. 7.29 HE x 200. This example of SP shows surface with marked cytologic atypia with pleomorphic nuclei, scattered mitotic activity, loss of polarity and is in keeping with dysplasia arising in a SP

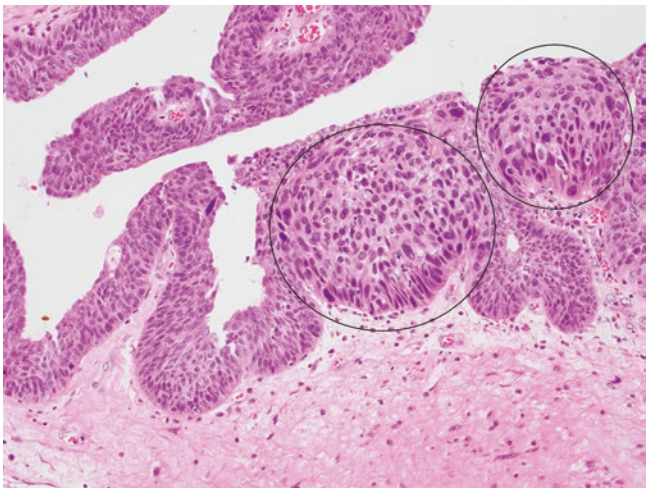

Fig. 7.30 HE x 100. This example of SP shows abrupt transition to dysplasia with marked cytologic atypia at the two marked circular areas. The circular area on the right shows almost full thickness involvement akin to carcinoma *in-situ*

Decreased transmigrating neutrophils, dyskeratosis, paradoxical maturation, atypical mitoses, desmoplasia, lymphovascular invasion, bone invasion, increased Ki-67 expression, and p53 expression in >25% of cells are among the most important features of carcinoma ex-ISP/OSP [9].

Although some studies implicated infection by high-risk HPV subtypes in malignant progression of sinonasal papillomas [8, 17], other studies found that transcription-

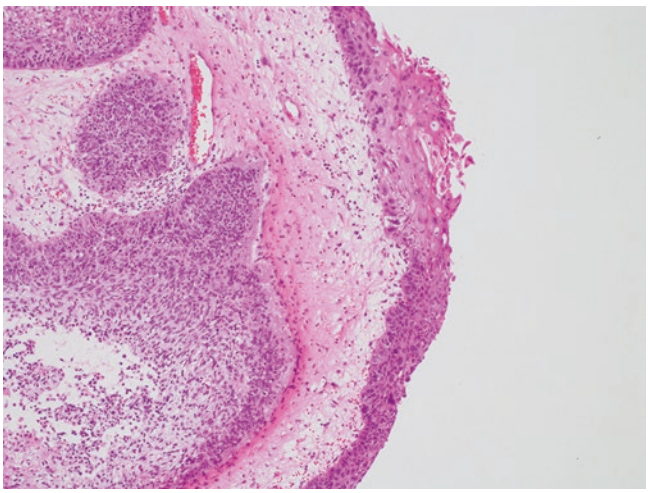

Fig. 7.31 HE x 100. This example of ISP shows keratinizing dysplasia featuring prominent surface keratosis, marked cytologic atypia, and loss of polarity

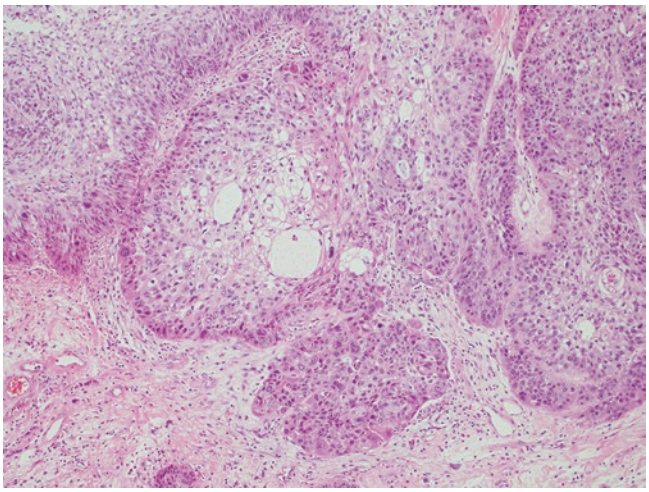

Fig. 7.32 HE x 100 & 7.33 HE x 200. ISP with dysplasia shows irregular infiltrating nests with stromal desmoplasia in keeping with carcinoma arising in an ISP

ally active high-risk HPV does not play a common role either in the development of ISP or in its transformation into carcinoma [18]. TP53 and/or CDKN2A alterations are likely early events in sinonasal papilloma-associated carcinomas. These carcinomas are molecularly distinct from other aerodigestive tract squamous cell carcinomas (SCC), exhibiting frequent EGFR and KRAS mutations that are only exceptionally seen at other anatomic sites [4, 15, 19]. SCC is the most common carcinoma ex-SP. Rarely, other carcinoma subtypes such as sinonasal undifferentiated carcinoma, small cell neuroendocrine carcinoma, and verrucous carcinoma are seen [5, 20].

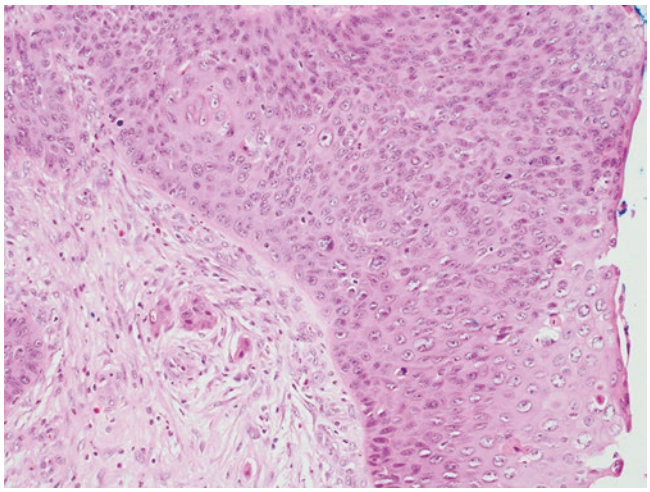

Fig. 7.33 HE x 200. ISP with dysplasia shows irregular infiltrating nests with stromal desmoplasia in keeping with carcinoma arising in an ISP

7.7 Prognosis

All types of SP are treated with complete surgical excision. The long-term prognosis of SP without *in-situ* or invasive carcinoma is excellent; however, all are prone to recur (20–30%) following incomplete excision. Recurrences can be multiple, are more common for ISP/OSP, and usually develops within 5 years of initial presentation. Prognosis for carcinoma is similar to SCC with a 5-year mortality approaching 40% [6, 9, 12, 21].

7.8 Conclusion

Recent developments in molecular studies have confirmed the uniqueness of three subtypes of SP. ISP arises in the lateral nasal wall and paranasal sinuses, but harbors activating EGFR mutation and an unclear relationship to HPV. ISP undergoes malignant transformation in 5–15% of cases. ESP is a tumor driven by low-risk HPV that typically arises in the nasal septum and does not undergo malignant transformation. OSP is a rare tumor, shares clinical features with ISP, is not HPV related, harbors activating KRAS mutations, and undergoes malignant transformation in 4–17% of cases.

References

1. Barnes L. Schneiderian papillomas and nonsalivary glandular neoplasms of the head and neck. Modern Pathol. 2002;15(3):279–97. https://doi.org/10.1038/modpathol.3880524.

2. Hyams VJ. Papillomas of the nasal cavity and paranasal sinuses. A clinicopathological study of 315 cases. Ann Otol Rhinol Laryngol. 1971;80(2):192–206. https://doi.org/10.1177/000348947108000205.
3. Barnes L, Bedetti C. Oncocytic Schneiderian papilloma: a reappraisal of cylindrical cell papilloma of the sinonasal tract. Hum Pathol. 1984;15(4):344–51. https://doi.org/10.1016/s0046-8177(84)80033-7.
4. Udager AM, McHugh JB, Betz BL, Montone KT, Livolsi VA, Seethala RR, et al. Activating KRAS mutations are characteristic of oncocytic sinonasal papilloma and associated sinonasal squamous cell carcinoma. J Pathol. 2016;239(4):394–8. https://doi.org/10.1002/path.4750.
5. Bishop JA. OSPs and ESPs and ISPs, oh my! An update on Sinonasal (Schneiderian) Papillomas. Head Neck Pathol. 2017;11(3):269–77. https://doi.org/10.1007/s12105-017-0799-9.
6. Hunt J, Bell D, Sarioglu S, Schneiderian papillomas. World Health Organization classification of head and neck tumours. IARC Press; 2017. p. 28–31.
7. Bishop JA, Thomson LDR, et al. editors. Chapter 2. Nasal cavity, paranasal sinuses and skull base. In: WHO Classification of Tumours Editorial Board. Head and neck tumours. Lyon (France): International Agency for Research on Cancer; forthcoming. (WHO classification of tumours series, 5th ed.; vol. 9). https://publications.iarc.fr.
8. Lawson W, Schlecht NF, Brandwein-Gensler M. The role of the human papillomavirus in the pathogenesis of Schneiderian inverted papillomas: an analytic overview of the evidence. Head Neck Pathol. 2008;2(2):49–59. https://doi.org/10.1007/s12105-008-0048-3.
9. Nudell J, Chiosea S, Thompson LD. Carcinoma ex-Schneiderian papilloma (malignant transformation): a clinicopathologic and immunophenotypic study of 20 cases combined with a comprehensive review of the literature. Head Neck Pathol. 2014;8(3):269–86. https://doi.org/10.1007/s12105-014-0527-7.
10. Vorasubin N, Vira D, Suh JD, Bhuta S, Wang MB. Schneiderian papillomas: comparative review of exophytic, oncocytic, and inverted types. Am J Rhinol Allergy. 2013;27(4):287–92. https://doi.org/10.2500/ajra.2013.27.3904.
11. Anari S, Carrie S. Sinonasal inverted papilloma: narrative review. J Laryngol Otol. 2010;124(7):705–15. https://doi.org/10.1017/s0022215110000599.
12. Christensen WN, Smith RR. Schneiderian papillomas: a clinicopathologic study of 67 cases. Hum Pathol. 1986;17(4):393–400. https://doi.org/10.1016/s0046-8177(86)80463-4.
13. Udager AM, McHugh JB. Human papillomavirus-associated neoplasms of the head and neck. Surg Pathol Clin. 2017;10(1):35–55. https://doi.org/10.1016/j.path.2016.10.007.
14. Kuo YJ, Lewis JS Jr, Zhai C, Chen YA, Chernock RD, Hsieh MS, Lan MY, Lee CK, Weinreb I, Hang JF. DEK-AFF2 fusion-associated papillary squamous cell carcinoma of the sinonasal tract: clinicopathologic characterization of seven cases with deceptively bland morphology. Mod Pathol. 2021;34(10):1820–30.
15. Udager AM, Rolland DCM, McHugh JB, Betz BL, Murga-Zamalloa C, Carey TE, et al. High-frequency targetable EGFR mutations in Sinonasal squamous cell carcinomas arising from inverted Sinonasal papilloma. Cancer Res. 2015;75(13):2600–6. https://doi.org/10.1158/0008-5472.can-15-0340.
16. Weindorf SC, Brown NA, McHugh JB, Udager AM. Sinonasal Papillomas and carcinomas: a contemporary update with review of an emerging molecular classification. Arch Pathol Lab Med. 2019;143(11):1304–16. https://doi.org/10.5858/arpa.2019-0372-RA.
17. Vor P, der Holte A, Fangk I, Glombitza S, Wilkens L, Welkoborsky HJ. Impact of human papillomaviruses (HPV) on recurrence rate and malignant progression of sinonasal papillomas. Cancer Med. 2021;10(2):634–41. https://doi.org/10.1002/cam4.3642.
18. Rooper LM, Bishop JA, Westra WH. Transcriptionally active high-risk human papillomavirus is not a common etiologic agent in the malignant transformation of inverted Schneiderian Papillomas. Head Neck Pathol. 2017;11(3):346–53. https://doi.org/10.1007/s12105-017-0779-0.
19. Brown NA, Plouffe KR, Yilmaz O, Weindorf SC, Betz BL, Carey TE, et al. TP53 mutations and CDKN2A mutations/deletions are highly recurrent molecular alterations in the malignant progression of sinonasal papillomas. Modern Pathol. 2020; https://doi.org/10.1038/s41379-020-00716-3.
20. Nakamura Y, Suzuki M, Ozaki S, Yokota M, Nakayama M, Hattori H, et al. Sinonasal inverted papilloma associated with small cell neuroendocrine carcinoma: a case report and literature review of rare malignancies associated with inverted papilloma. Auris Nasus Larynx. 2019;46(4):641–50. https://doi.org/10.1016/j.anl.2018.10.009.
21. Healy DY Jr, Chhabra N, Metson R, Holbrook EH, Gray ST. Surgical risk factors for recurrence of inverted papilloma. Laryngoscope. 2016;126(4):796–801. https://doi.org/10.1002/lary.25663.

Malignant Epithelial Tumors of Sinonasal Tract

8

Deepali Jain and Justin A. Bishop

8.1 Introduction

Malignant epithelial tumors of sinonasal tract have seen a major improvement in understanding of their pathogenesis due to advances in molecular pathology during the last decade or so resulting into introduction of many new distinct tumor entities.

WHO 2022 classification of tumors of nasal cavity and paranasal sinuses has integrated clinical, radiological, and molecular pathology features of each of these tumors (Table 8.1) for better diagnosis and management of patients [1].

Table 8.1 WHO 2022 classification of malignant epithelial tumors of nasal cavity and paranasal sinuses

Categories	Subtypes
Carcinomas	Keratinizing squamous cell carcinoma Non-keratinizing squamous cell carcinoma NUT carcinoma SWI/SNF complex (SMARCB1 and SMARCA4) deficient sinonasal carcinoma Sinonasal lymphoepithelial carcinoma Sinonasal undifferentiated carcinoma Teratocarcinosarcoma HPV-related multiphenotypic sinonasal carcinoma
Adenocarcinoma	Intestinal-type adenocarcinoma Non-intestinal-type adenocarcinoma
Neuroendocrine tumors	Well-differentiated epithelial neuroendocrine neoplasms/neuroendocrine tumors
Neuroendocrine carcinomas	Small cell carcinoma Large cell neuroendocrine carcinoma
Emerging entities	*DEK*::*AFF2* fusion associated squamous cell carcinomas *IDH*-mutant sinonasal undifferentiated carcinoma SMARCB1 deficient sinonasal adenocarcinoma

D. Jain (✉)
Department of Pathology, All India Institute of Medical Sciences, New Delhi, India
e-mail: deepalijain76@aiims.edu

J. A. Bishop
Department of Pathology, UT Southwestern Medical Center, Dallas, TX, USA

8.2 Squamous Cell Carcinoma

Keratinizing squamous cell carcinoma (KSCC) is a surface epithelial malignancy with squamous differentiation and keratinization (Fig. 8.1).

About half of sinonasal (SN) tract malignancies are KSCCs. Genomically *p53*, *KRAS*, and *EGFR* mutations have been identified in them. *EGFR* exon 20 mutation has been detected in tumors arising from inverted papillomas. Human papilloma virus (HPV) infection is not implicated in pathogenesis of most of KSCC [1, 2].

Non-keratinizing squamous cell carcinoma (NKSCC) is another subtype of surface SCC with no or minimal keratinization (Figs. 8.2, and 8.3).

WHO 2022 classification subtyped NKSCC, based on molecular etiopathogenesis, into two subtypes: HPV-associated squamous cell carcinoma and *DEK*::*AFF2* carcinoma [1, 3, 4].

HPV association varies in different ethnicities being highest in Western countries and a low frequency in Asia [5]. Most of HPV negative NKSCC of SN tract have been shown to carry fusions between the *DEK* gene on chromosome 6p22.3 and the *AFF2* gene on chromosome Xq28 [6].

Morphologically, NKSCC show surface proliferation with downward pushing invasion of tumor cell nests without much desmoplasia [1].

Other variants of SCC such as acantholytic, adenosquamous, basaloid, spindle, and verrucous are rare in SN tract in comparison to other head and neck sites. Papillary subtype needs to be tested for HPV and *DEK*::*AFF2* fusion as these tend to show papillary exophytic growth pattern (Fig. 8.4).

The *DEK*::*AFF2* fusion carcinomas show bland cytomorphology with exophytic and endophytic proliferation. The tumor cells are oval to fusiform in some examples with monotonous appearance [4, 6] (Figs. 8.5, 8.6, and 8.7). Some reported cases show prominent neutrophilic infiltration which brings NUT carcinoma in differential; however, cytomorphology of NUT carcinoma is high grade.

D. Jain, J. A. Bishop (eds.), *Atlas of Sinonasal Tract Pathology*, https://doi.org/10.1007/978-981-19-7315-4_8

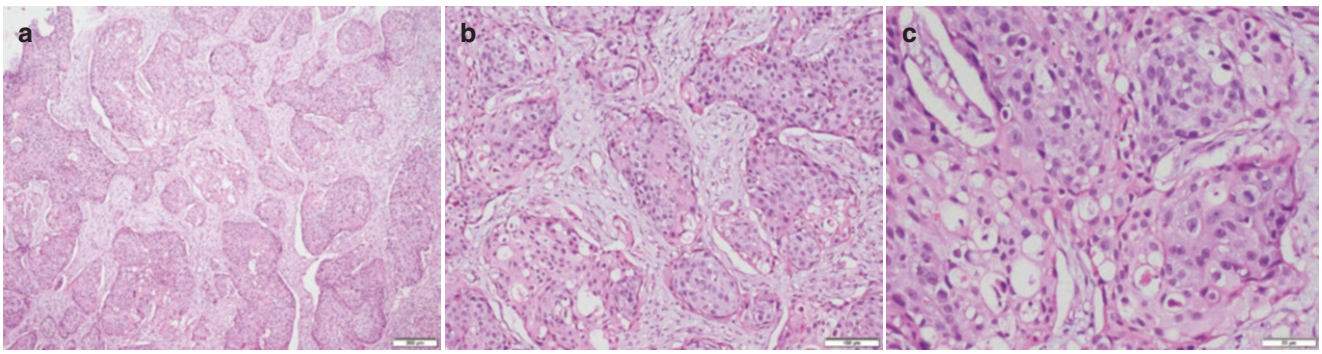

Fig. 8.1 Infiltrating nests and lobules of tumor with desmoplastic stroma (**a**). The tumors cells are polygonal and show intracellular keratinization (**b**). Cytoplasmic vacuolation and pseudoglandular spaces are evident (**c**). Tumor is positive for p40 (not shown here)

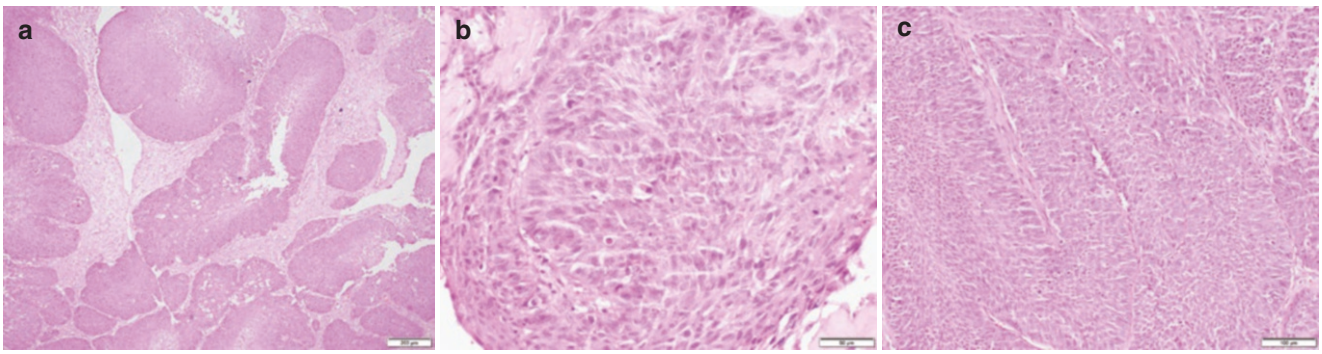

Fig. 8.2 Inverted papilloma with epithelial dysplasia (**a**), carcinoma *in-situ* (**b**) and interconnecting fronds of non-keratinizing squamous cell carcinoma (**c**)

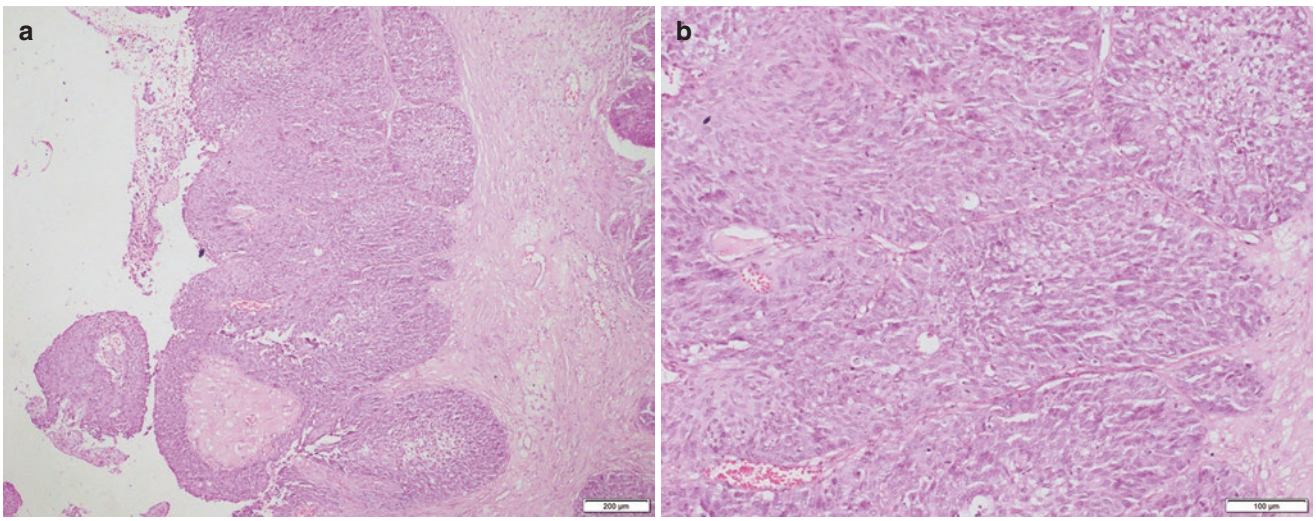

Fig. 8.3 The tumor nests at advancing edge show a smooth contour (**a**). Striking nuclear atypia and mitotic activity is noted (**b**)

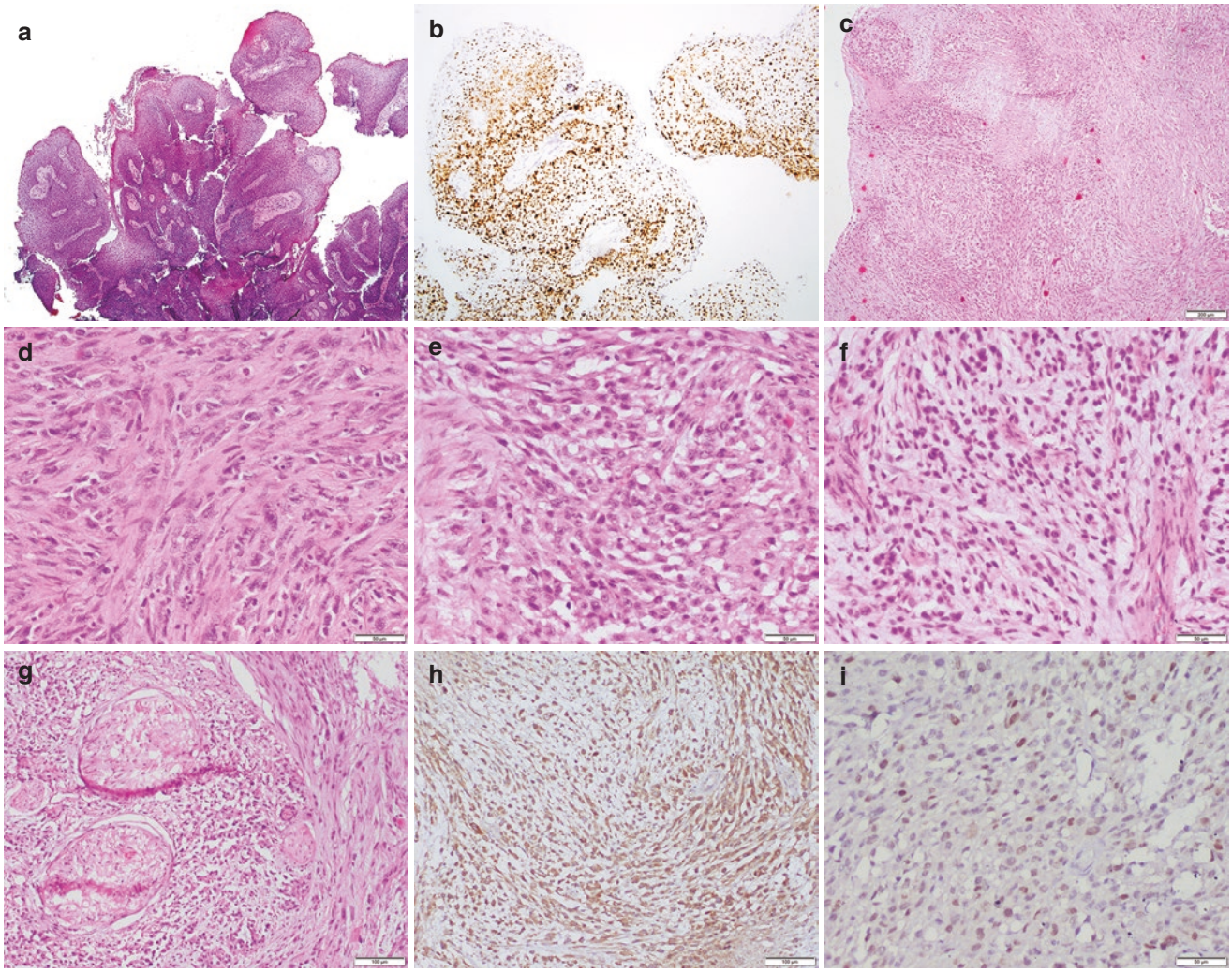

Fig. 8.4 Proliferating fronds of squamous epithelium with fibrovascular cores (**a**) positive for RNA *in-situ* hybridization for human papilloma virus (HPV) (**b**). Clinically, it was a soft tissue density mass in maxillary antrum with bone destruction. A case of spindle cell carcinoma with surface ulceration, geographic areas of necrosis and myxoid change (**c**). Pleomorphic epithelioid oval to spindle cells (**d**–**f**) show perineural invasion (**g**); positive for epithelial membrane antigen (EMA) (**h**) and p40 (**i**)

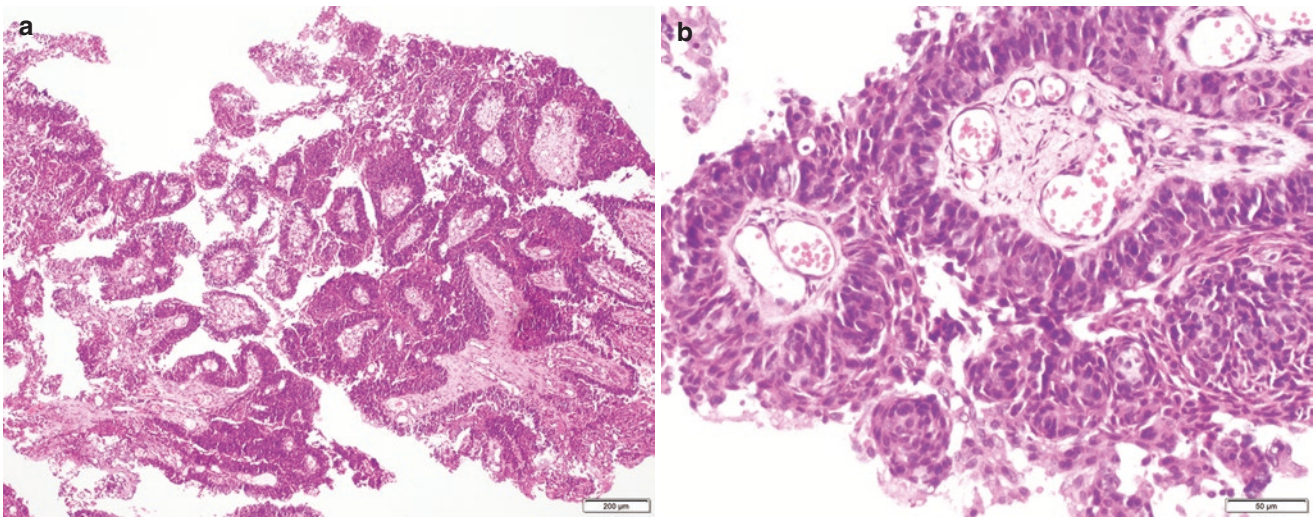

Fig. 8.5 (**a**) Low power view shows a complex papillary pattern of tumor which on higher magnification shows mild nuclear atypia (**b**)

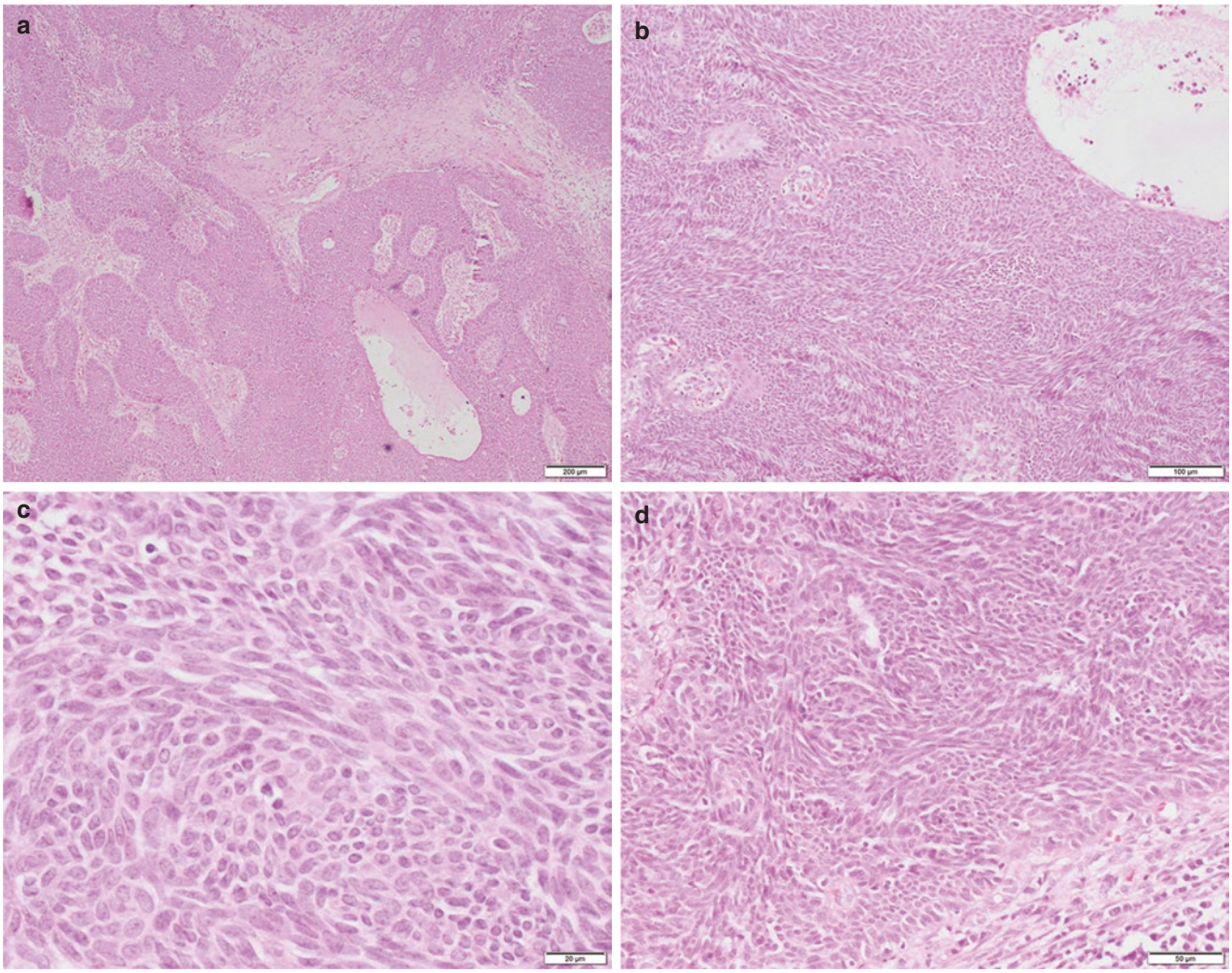

Fig. 8.6 Same case on recurrence shows predominantly endophytic growth with intercommunicating cords, nests, and papillae (**a**). Tumor cells appear transitional and have monomorphic oval to fusiform bland nuclei (**b**, **c**). Smooth transitioning to stroma is seen (lower right) (**d**)

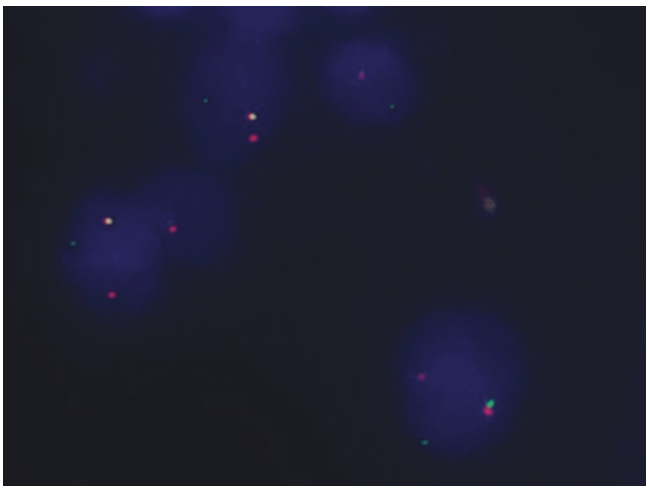

Fig. 8.7 *DEK* breakapart fluorescence *in-situ* hybridization shows break apart of *DEK* gene

Similar to squamous cell carcinoma of other body sites, all variants and subtypes are immunopositive for high molecular weight keratins, p40 and p63.

8.3 Sinonasal Lymphoepithelial Carcinoma

Sinonasal lymphoepithelial carcinoma (SNLEC) is an undifferentiated variant of squamous cell carcinoma, mostly occur in Asia in endemic form, associated with Epstein–Barr Virus (EBV) infection.

Tumor grows in syncytial appearance and tumor cells show abundant eosinophilic to amphophilic cytoplasm. The tumor cells show round nuclei with vesicular chromatin and prominent nucleoli. Although lymphoplasmacytic infiltrate

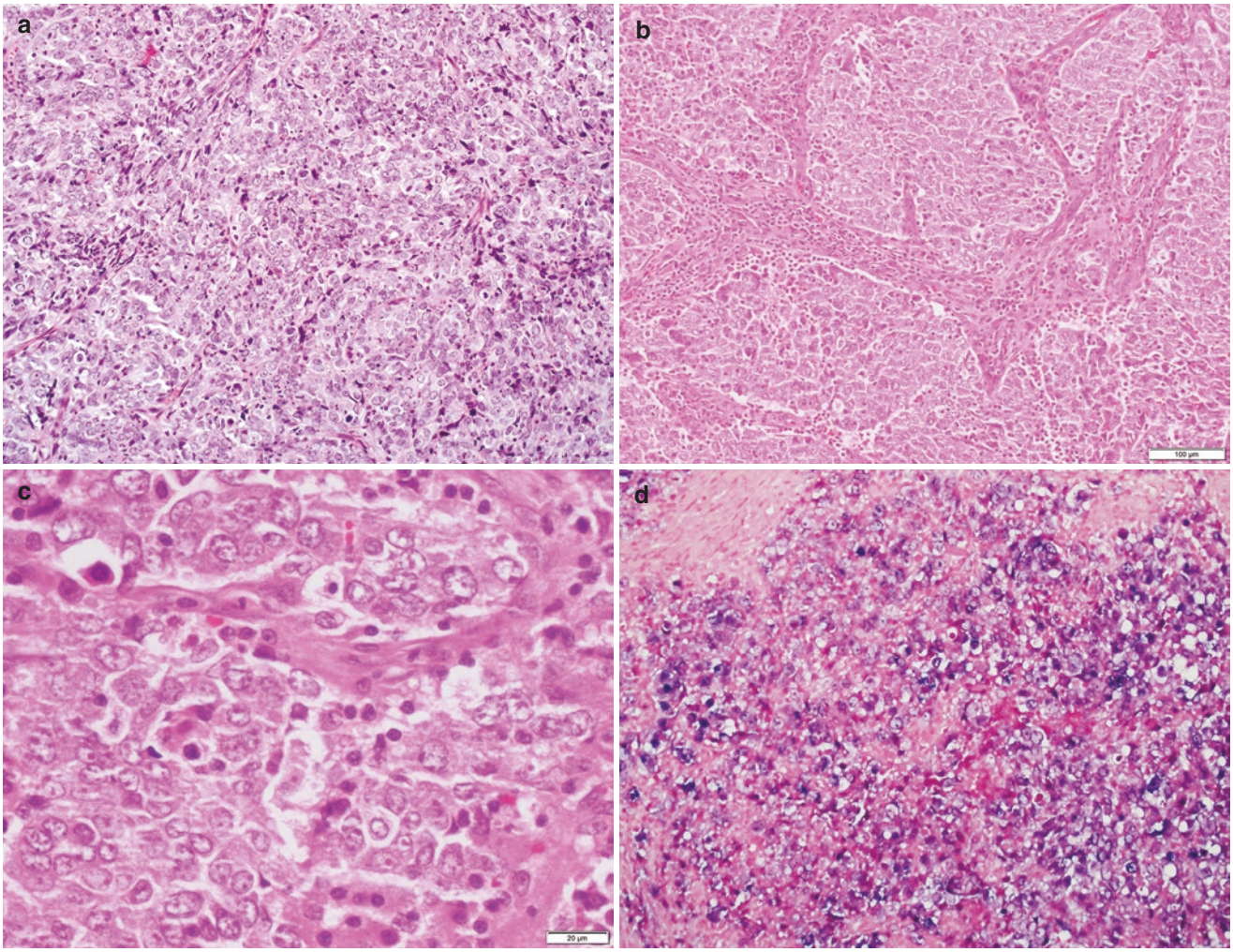

Fig. 8.8 (**a**–**c**) Syncytium of large undifferentiated cells with vesicular chromatin and prominent nucleoli. Prominent lymphoplasmacytic infiltrate is integral component of the tumor present within the stroma separating tumor lobules seen in (**b**). Tumor shows positive EBV-encoded small RNA (EBER) by *in-situ* hybridization (**d**)

is diagnostic, it is less prominent in SN tract in comparison to the nasopharyngeal counterpart (Fig. 8.8).

Keratin, p63, p40 and *in-situ* hybridization for EBV-encoded small RNA (EBER) is positive especially in endemic form [7, 8].

8.4 NUT Carcinoma

NUT (Nuclear protein in testis) carcinoma is a poorly differentiated carcinoma with squamous differentiation which is characterized by translocation/fusion involving the *NUTM1* gene on chromosome 15q14 with various partner genes, commonly BRD4 [t (15;19)], leading to formation of an oncoprotein [9].

NUT carcinoma is a high-grade tumor with "malignant small round blue" cell morphology comprising of sheets of primitive appearing undifferentiated cells. The cells possess uniform vesicular nuclei and prominent nucleoli. Foci of abrupt keratinization (keratinized squamous cells with or without keratin pearls and cytoplasmic clearing) are classical and can be seen in about a third of NUT carcinoma cases.

Immunohistochemistry with the NUT antibody is specific for the diagnosis only with diffuse (>50% of tumor cells) granular/speckled positivity. The tumor cells are immunopositive for pancytokeratin, p40 and p63 (more sensitive than p40) (Figs. 8.9, 8.10, 8.11, 8.12, 8.13, and 8.14). These tumors have an aggressive clinical course with a mean survival of 12 months [10].

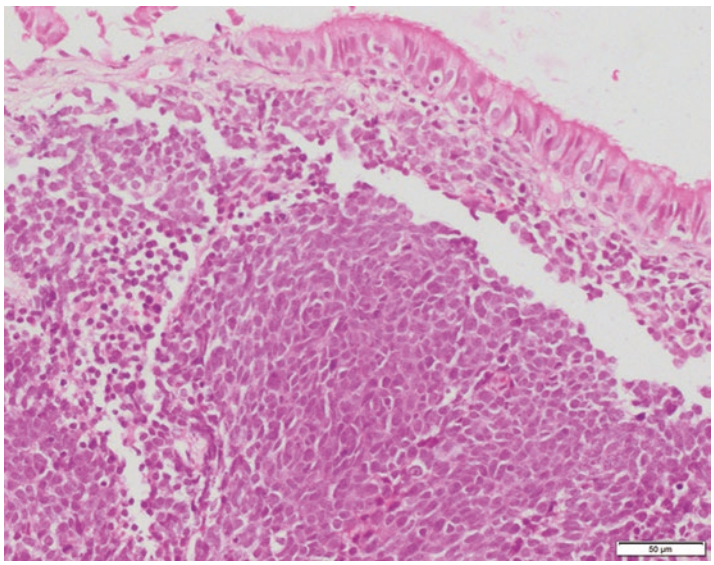

Fig. 8.9 A highly cellular tumor with overlying normal respiratory epithelium. Majority of tumor cells are round with hyperchromatic nuclei. Here the differential diagnoses cover spectrum of malignant small round cell tumors

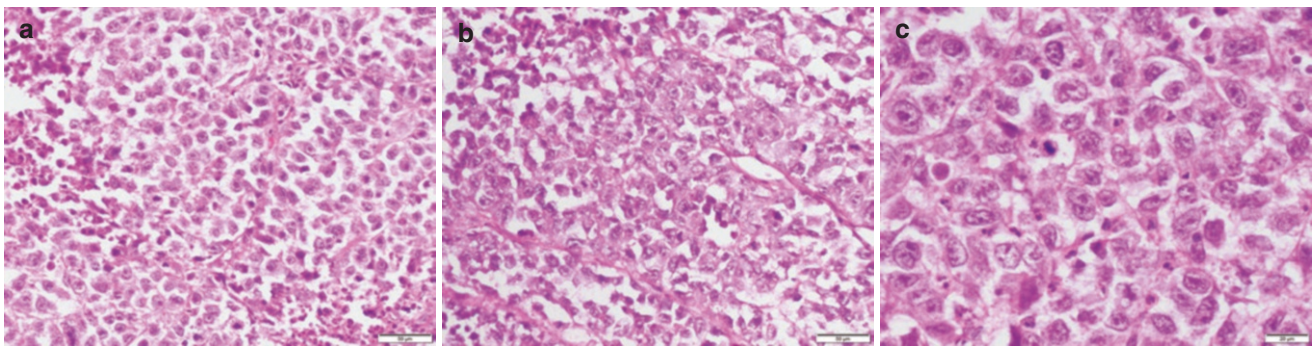

Fig. 8.10 (**a**–**c**) Another case on higher magnification shows perfectly round basaloid/undifferentiated tumor cells with stippled chromatin and prominent nucleoli. Necrosis and microabscesses are present (left upper and right lower-**a**)

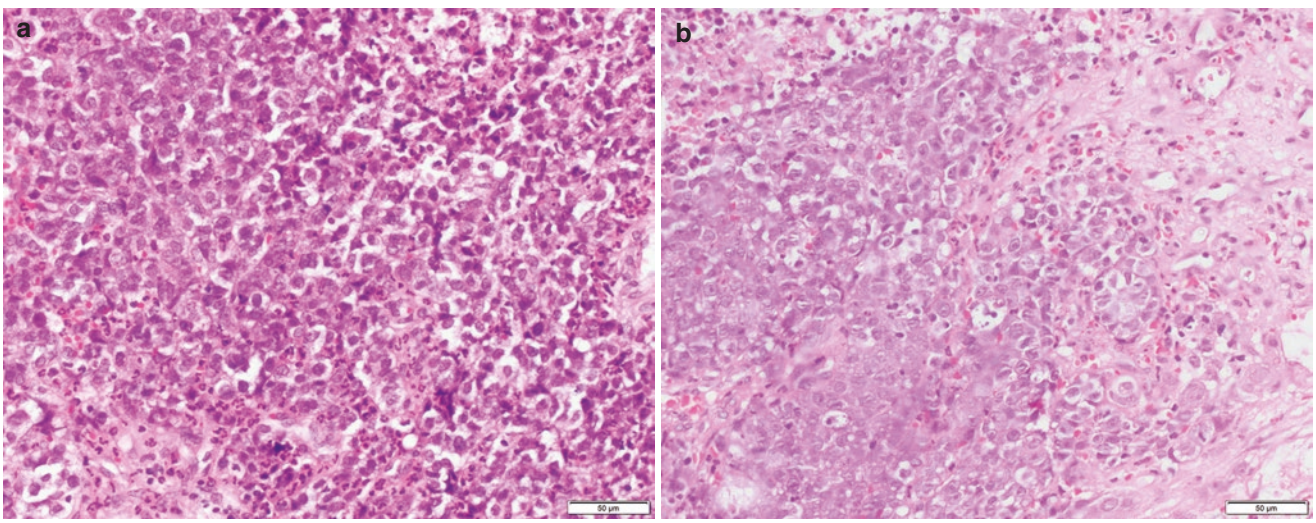

Fig. 8.11 (**a**, **b**) Tumor is heavily infiltrated by polymorphs (a helpful diagnostic clue of NUT carcinoma)

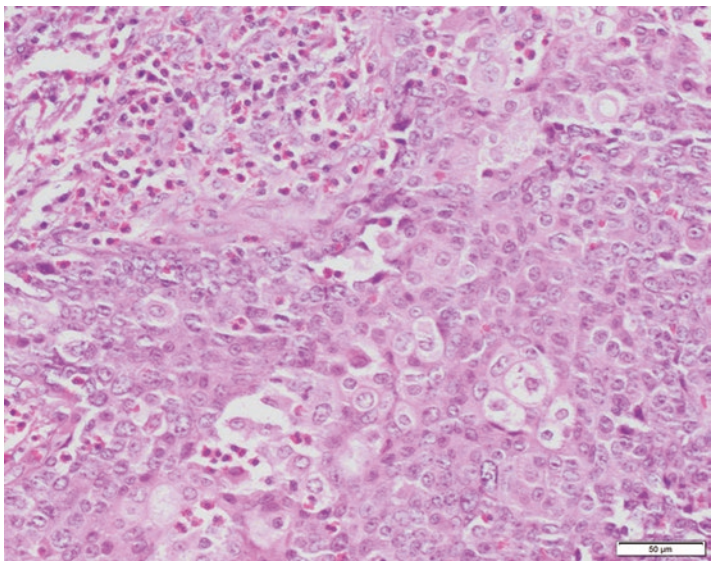

Fig. 8.12 This examples shows infiltration of tumor by eosinophils (possibly due to tumor released cytokines)

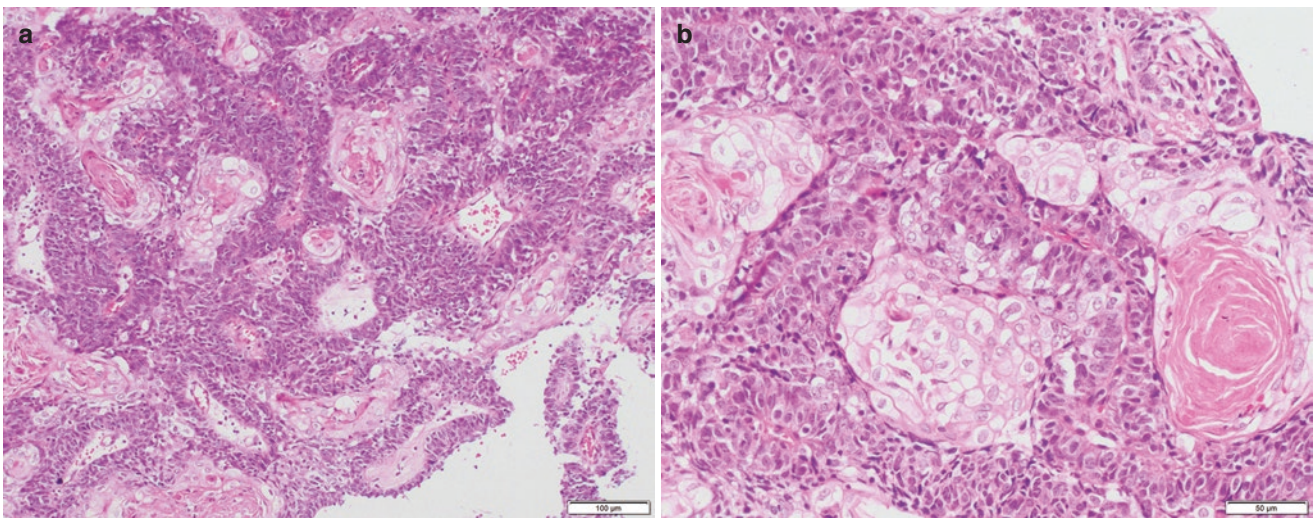

Fig. 8.13 (**a**, **b**) Abrupt keratinization with keratin pearls and surrounding clear squamous cells seen in about a third of NUT carcinoma, a diagnostic feature of NUT carcinoma

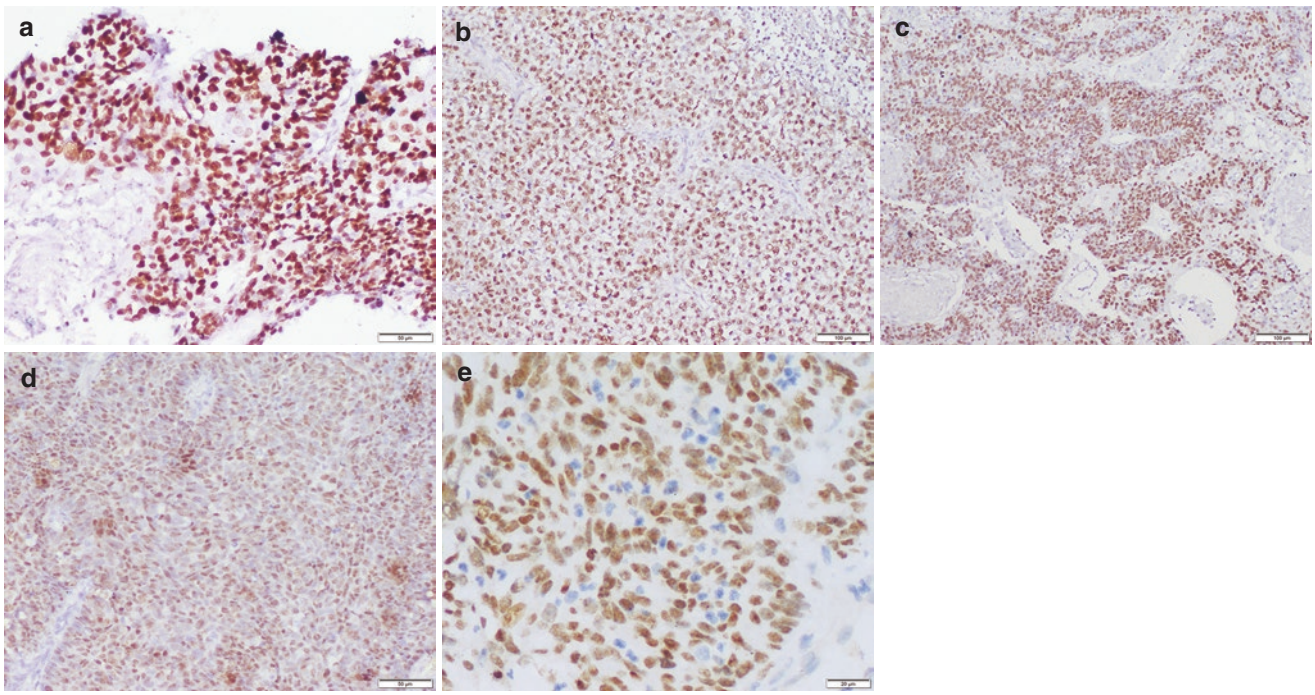

Fig. 8.14 p40 (**a**), p63 (**b**, **c**), and NUT immunohistochemistry (**d**, **e**) are diffuse and strong nuclear positive. p63 is more consistently positive than p40 in NUT carcinomas. NUT shows speckled nuclear pattern

8.5 HPV-Related Multiphenotypic Sinonasal Carcinoma (HMSC)

As the name indicates, this tumor is characterized by morphological and immunophenotypical characteristics of a salivary type carcinoma (ductal and myoepithelial differentiation) and squamous cell carcinoma. HMSC is limited to sinonasal tract.

Histology resembles solid to cribriform areas reminiscent of adenoid cystic carcinoma. The surface respiratory epithelium shows dysplasia. Immunohistochemistry shows p16 positivity, though HPV association needs to be confirmed by molecular methods. Transcriptionally active high-risk HPV type 33 is implicated in pathogenesis in most of the cases. The presence of high-risk HPV and absence of MYB gene fusion distinguishes it from the close differential of adenoid cystic carcinoma (Fig. 8.15, 8.16, 8.17, and 8.18).

These tumors behave indolently without much frequency of distant metastasis and tumor-related deaths [11].

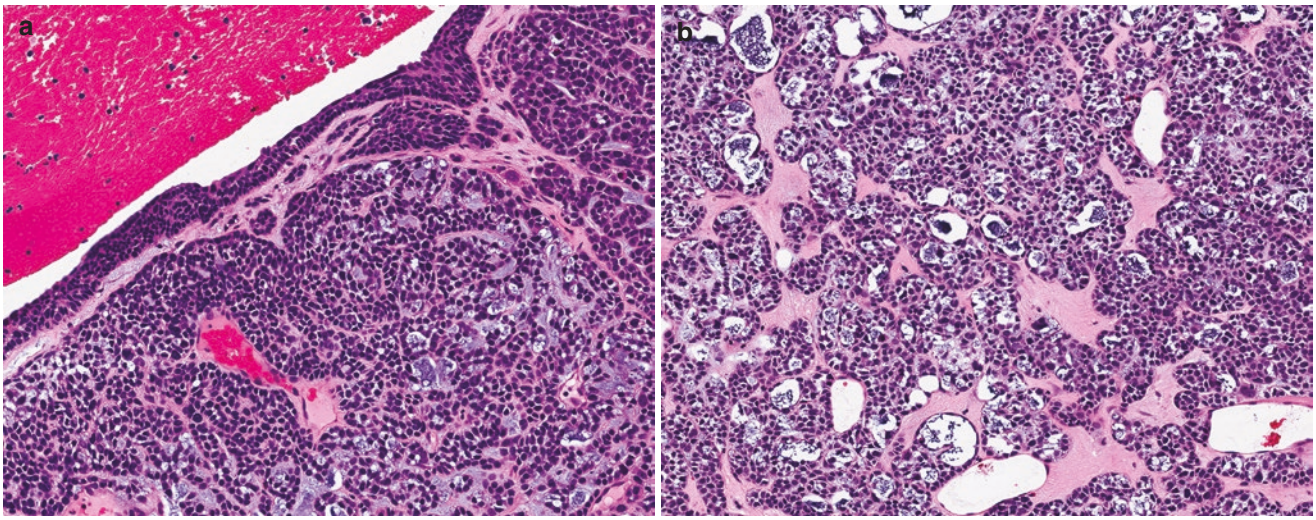

Fig. 8.15 A tumor with basaloid cells arranged in solid nests and cribriform pattern mimicking adenoid cystic carcinoma. Note the surface squamous epithelium with dysplasia (**a**). The cribriform spaces are filled with myxoid appearing basophilic material. The stroma is densely hyalinized (**b**)

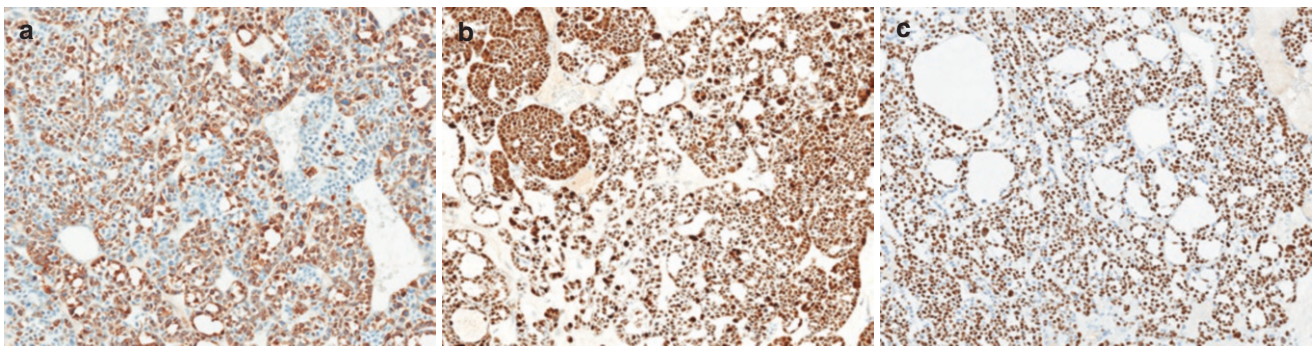

Fig. 8.16 One of the multiphenotypic lineage is myoepithelial cell differentiation which is shown by smooth muscle actin (cytoplasmic) (**a**), S100 (nuclear and cytoplasmic) (**b**), and p40 (nuclear) (**c**) staining in tumor cells

Fig. 8.17 CD117 highlights ductal differentiation; however, MYB gene rearrangement is negative in these tumors in contrast to adenoid cystic carcinomas

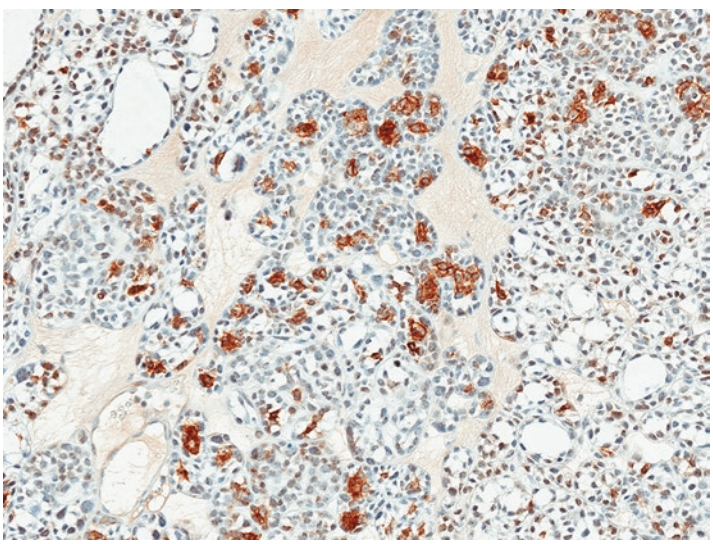

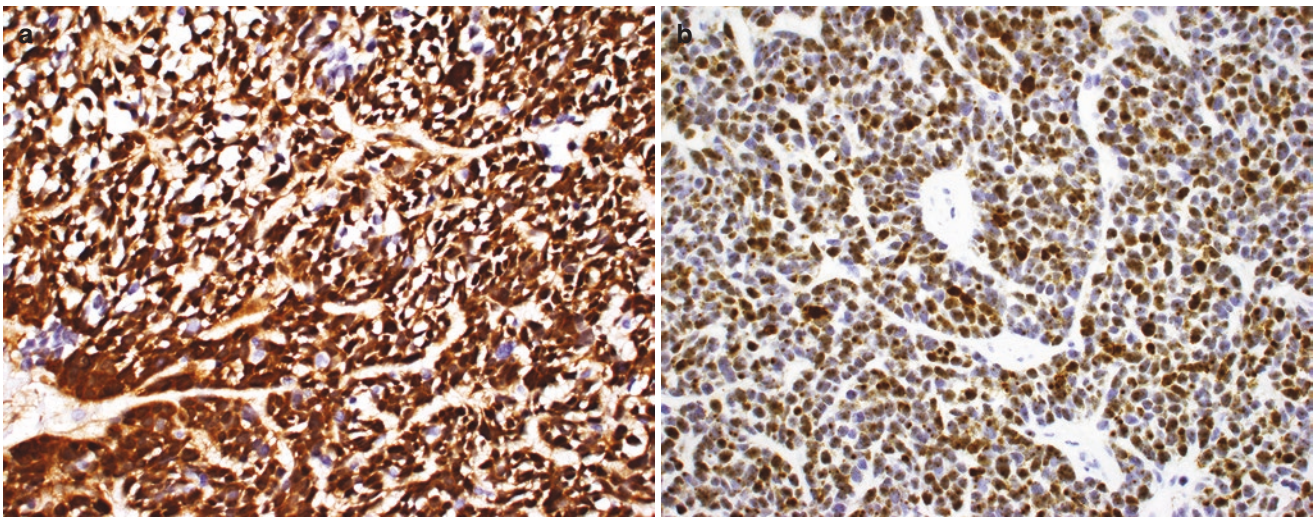

Fig. 8.18 Although p16 is a poor surrogate marker for HPV infection, it is consistently positive (diffuse, strong, nuclear, and cytoplasmic) (**a**). RNA *in-situ* hybridization for high-risk HPV is diffusely positive (**b**)

8.6 Adenocarcinoma

Sinonasal adenocarcinomas (showing glandular differentiation) can be salivary type (see Chap. 9) and non-salivary adenocarcinomas. The latter are further subdivided into intestinal and non-intestinal-type adenocarcinomas.

8.6.1 Intestinal-Type Adenocarcinomas (ITAC)

This group of tumors resembles the adenocarcinoma/adenoma of the intestine or rarely normal intestinal mucosa. ITAC originate from intestinal metaplasia of surface epithelium. Exposure to wood and leather dust are implicated occupational risk factors. These tumors commonly involve the ethmoid sinuses and nasal cavity.

Histologically, tumors range from well-differentiated papillary adenocarcinomas to poorly differentiated/solid and mucinous carcinomas (Figs. 8.19 and 8.20).

On immunohistochemistry, these tumors are positive for CK20, CDX2, SATB2, and villin and variably positive for CEA and CK7 [12].

Genomically, ITAC show frequent p53 mutations.

Clinical course is aggressive with frequent local recurrences, metastasis, and death.

8.6.2 Non-intestinal-Type Adenocarcinomas

This group includes tumors that does not show characteristics of minor salivary gland or intestinal-type adenocarcinomas. Unlike ITAC there are no known occupational risk factors. Nasal cavity and maxillary sinuses are commonly involved. These are further subdivided into low-grade and high-grade tumors.

On immunohistochemistry, these tumors are immunonegative for CK20, CDX2, and villin.

Markers of seromucinous differentiation, S100, DOG1, and SOX10, are expressed in the majority of non-intestinal-type adenocarcinomas [1, 13].

Low-grade non-intestinal-type adenocarcinomas show a back to back arrangement of uniform glands lined by single layer of cuboidal or columnar cells. Low-grade tumors may arise in association with benign lesions (sinonasal papillomas and respiratory epithelial adenomatoid hamartomas) [2] (Fig. 8.21).

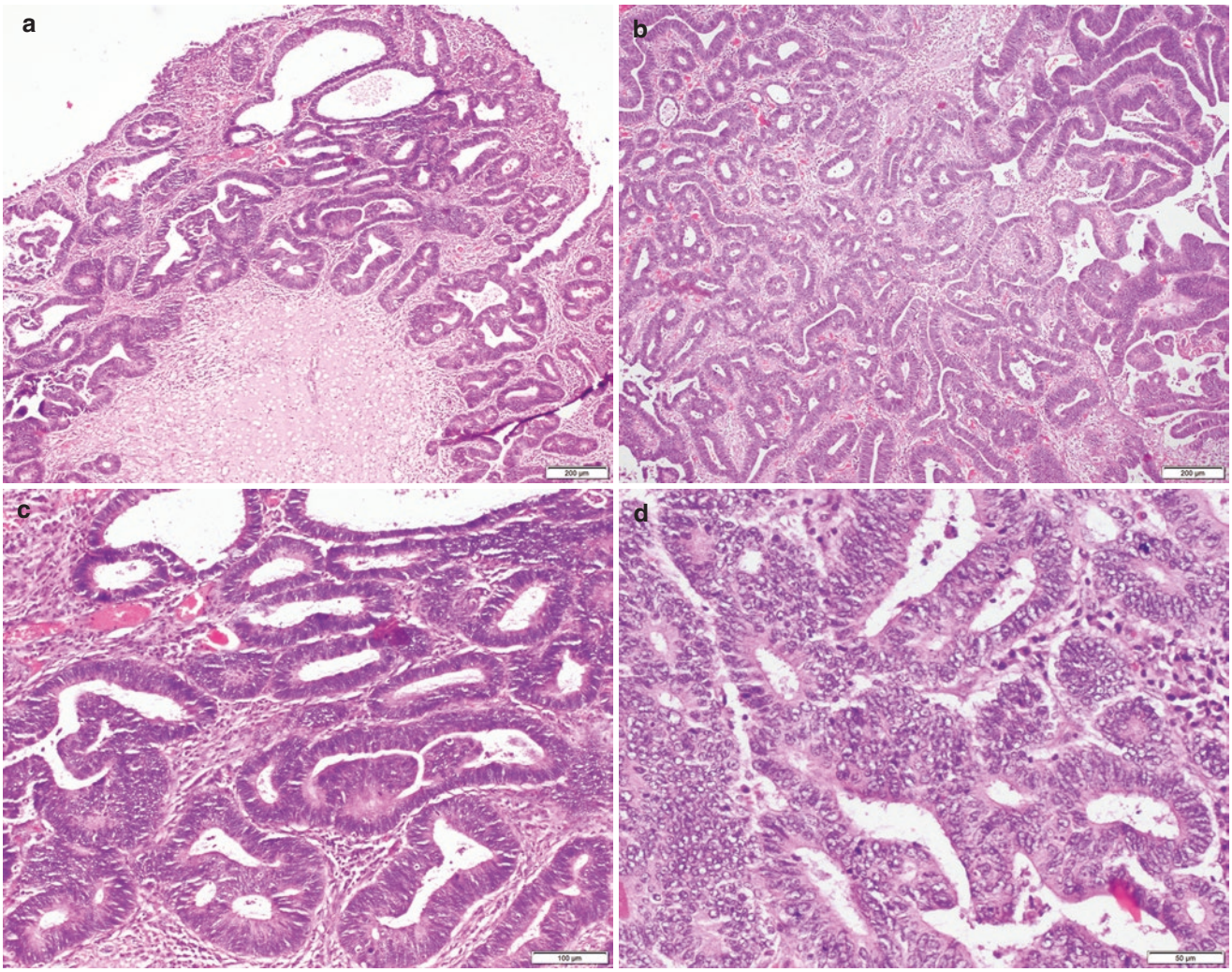

Fig. 8.19 A polypoidal tumor appears as a tubular adenoma of colon with overlying respiratory epithelium (**a**). This tumor shows complex tubulopapillary growth with branching and intercommunicating glands lined by tall columnar ("cigar shaped nuclei") epithelium (**b**). High-grade nuclear features are seen (**c**, **d**)

High-grade tumors show solid growth pattern with nuclear pleomorphism or malignant infiltrating glands with atypical mitoses in desmoplastic stroma [1, 2] (Fig. 8.22).

A subset of low-grade carcinomas show uniform population of cuboidal to columnar cells with glycogen-rich clear cytoplasm which is reminiscent of renal cell carcinoma and have been named as sinonasal renal cell-like adenocarcinoma. Renal cell-like adenocarcinoma expresses CK7, CAIX, and CD10, whereas negative for vimentin, RCCMa (renal cell carcinoma marker), and PAX8 (Fig. 8.23) (Table 8.2).

A subset of low-grade tumors carry ETV6::NTRK3/RET fusions. Interestingly, most cases of secretory carcinomas show same translocation involving ETV6 and NTRK3 genes. However, secretory carcinomas rarely involve sinonasal tract (Fig. 8.24). Rarely, CTNNB1 and BRAF mutations are reported [14].

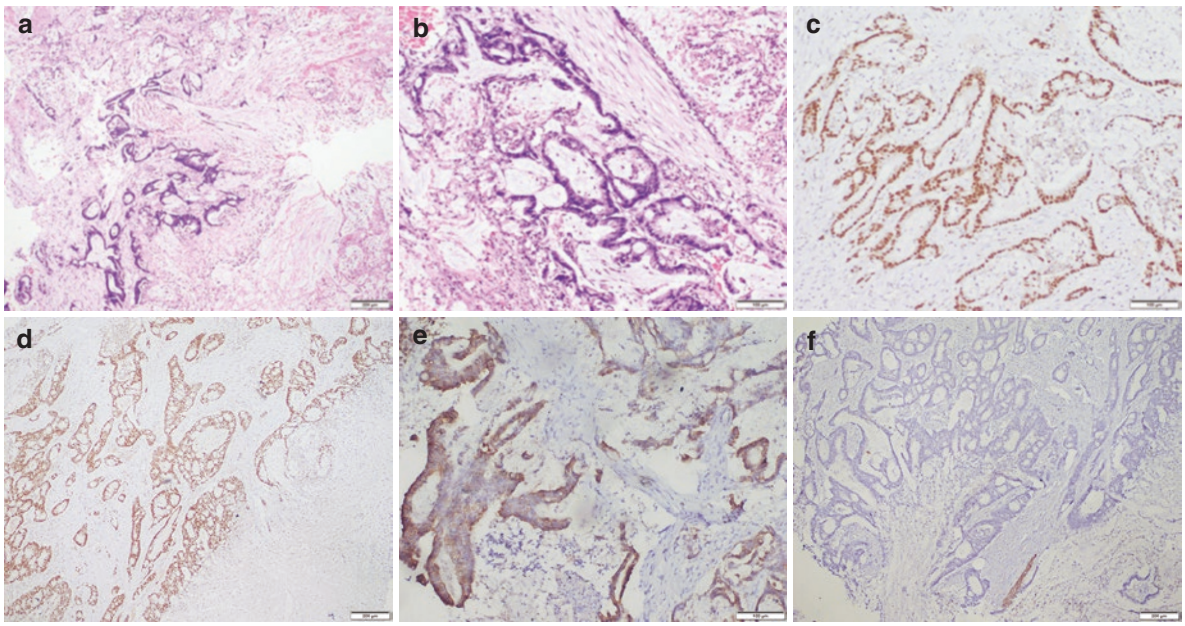

Fig. 8.20 Another example of ITAC shows abundant mucin, necrotic exudate, and abnormal malignant glands (**a**, **b**) which show nuclear positivity for CDX2 (**c**), SATB2 (**d**), and CK20 (**e**). CK 7 is negative (**f**)

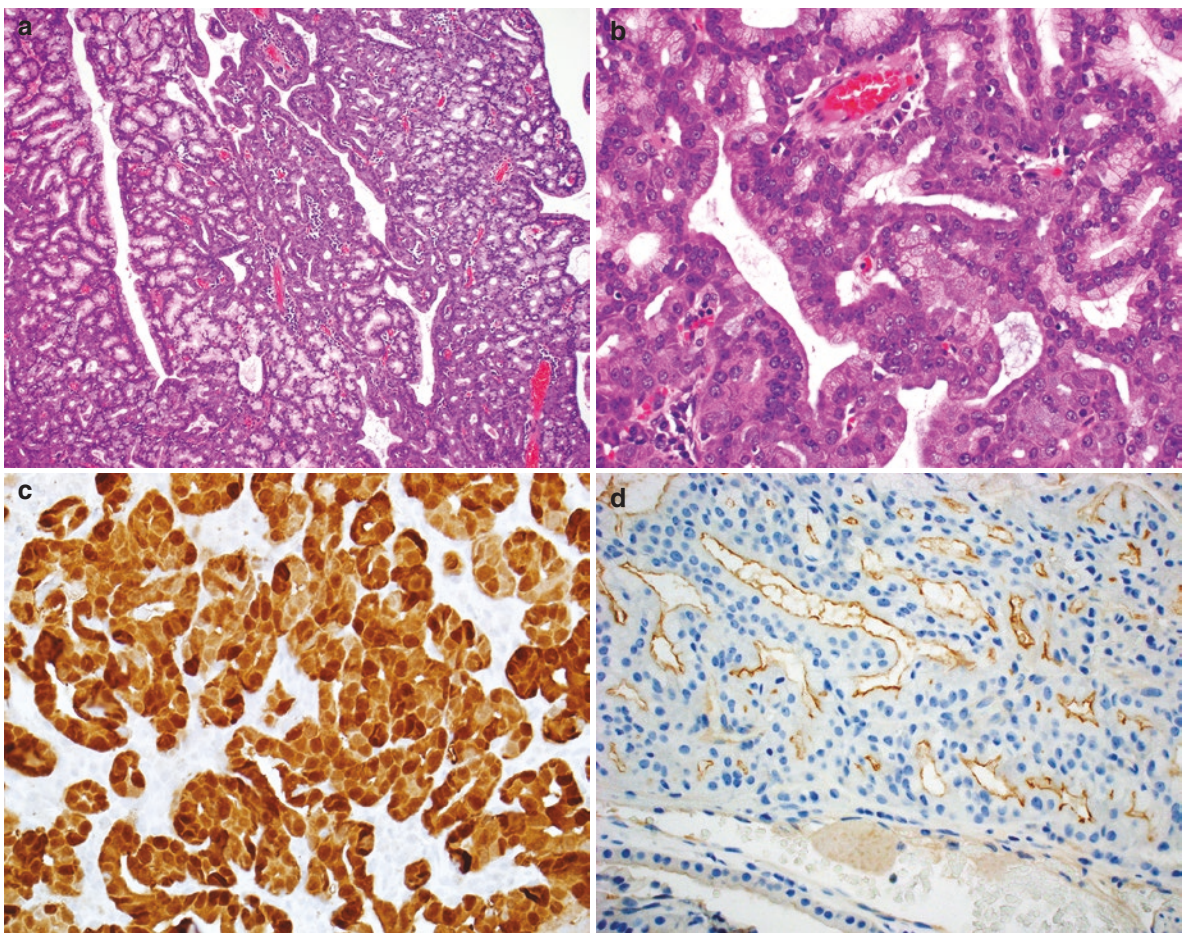

Fig. 8.21 (**a**, **b**) Low-grade non-intestinal adenocarcinoma: an exophytic tumor with tubulopapillary pattern where glands are placed back to back. The glands are low-grade seromucinous, lined by single layer of cuboidal epithelium with mild atypia. The tumor cells are diffusely positive for S-100 (**c**). DOG1 shows apical luminal staining (**d**)

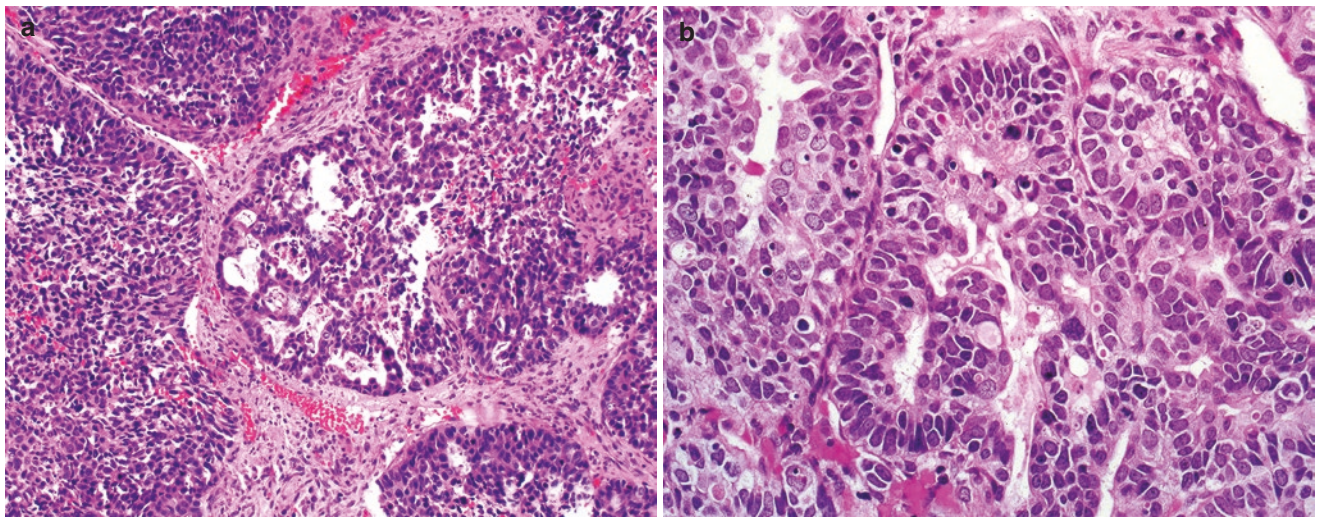

Fig. 8.22 (**a**, **b**) High-grade non-intestinal adenocarcinoma: Nested growth of an adenocarcinoma with solid and cribriform architecture. Note high-grade nuclear atypia (in comparison to Fig. 8.21b) with necrosis and mitosis

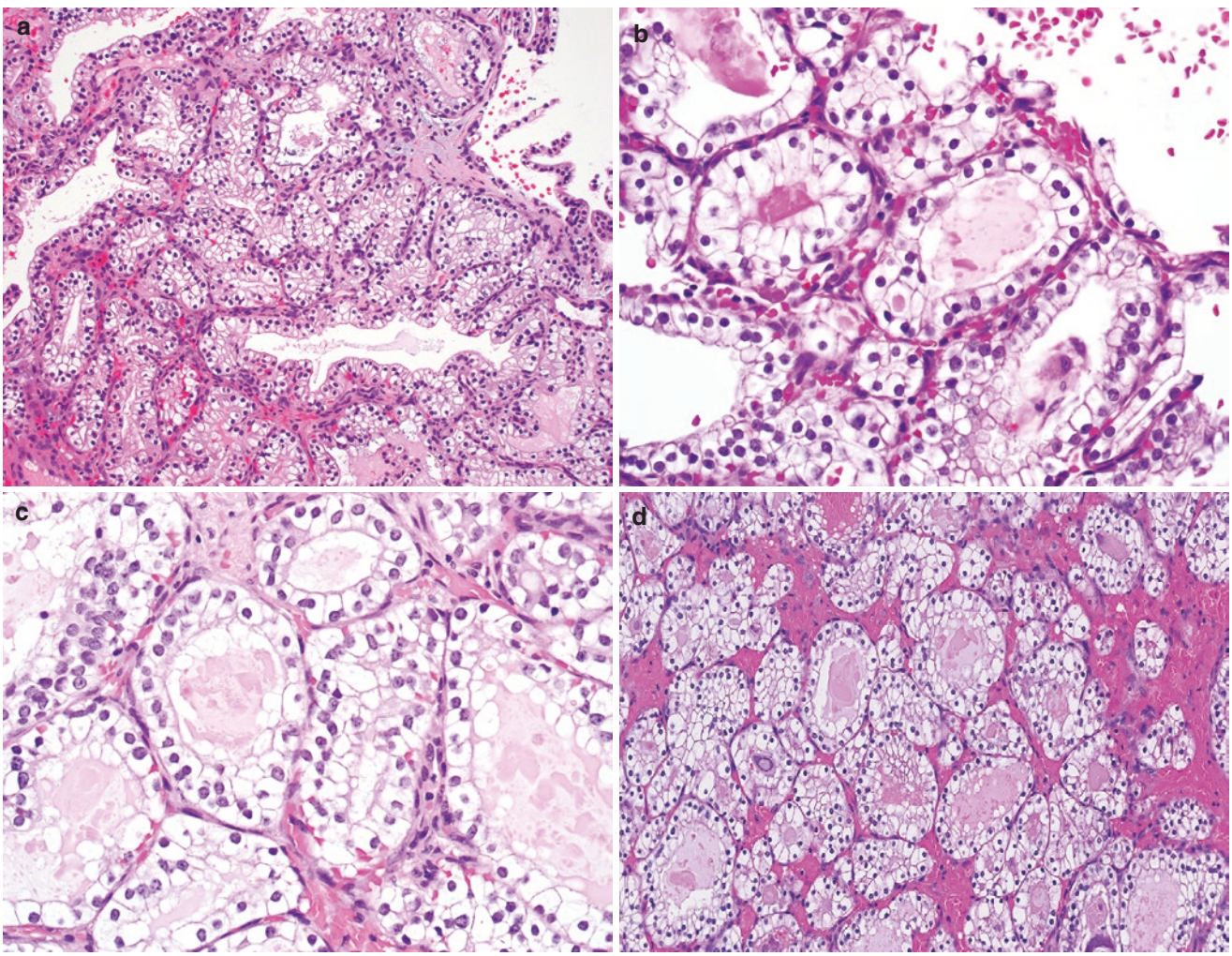

Fig. 8.23 (**a**–**d**) This variant shows remarkable degree of cytoplasmic clearing quite reminiscent of metastatic renal cell carcinoma. Like other low-grade sinonasal adenocarcinomas, some sinonasal renal cell-like adenocarcinomas are positive for S100 (**e**)

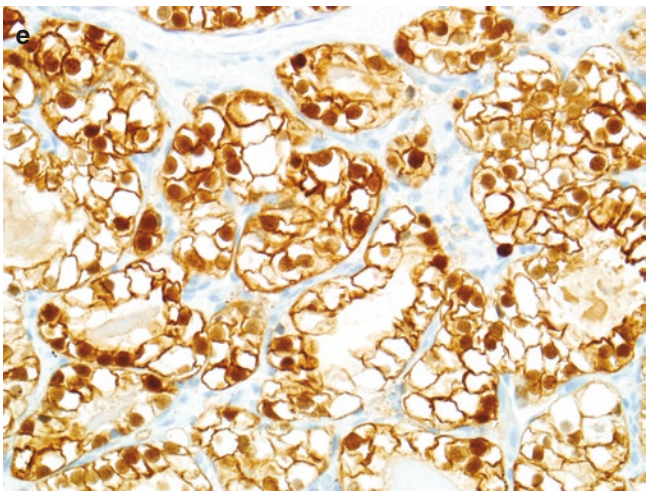

Fig. 8.23 (continued)

Table 8.2 Differences between sinonasal renal cell-like adenocarcinoma and metastatic renal cell carcinoma to sinonasal tract

Features	Sinonasal renal cell-like adenocarcinoma	Metastatic renal cell carcinoma
Location	Nasal cavity, paranasal sinuses, nasopharynx	Anywhere in the head and neck, including sinonasal tract
Histological features	• Acini and follicles of large polyhedral cells with abundant clear cytoplasm. • Follicles filled with thin eosinophilic material and sometimes hemorrhage. • Subtle nuclear atypia low mitotic rate, no necrosis.	• Alveolar and acinar pattern with prominent, arborizing capillary network. • Cells have optically clear abundant cytoplasm. • Nuclear pleomorphism, high mitotic rate, and necrosis are seen in high-grade tumors.
Immunohistochemistry	Positive for CK7, variably positive for S100 and CD10, negative for RCCMa, PAX8, and vimentin	Positive for PAX-8, RCCMa, CD10, and vimentin. CK7 is negative in clear cell type

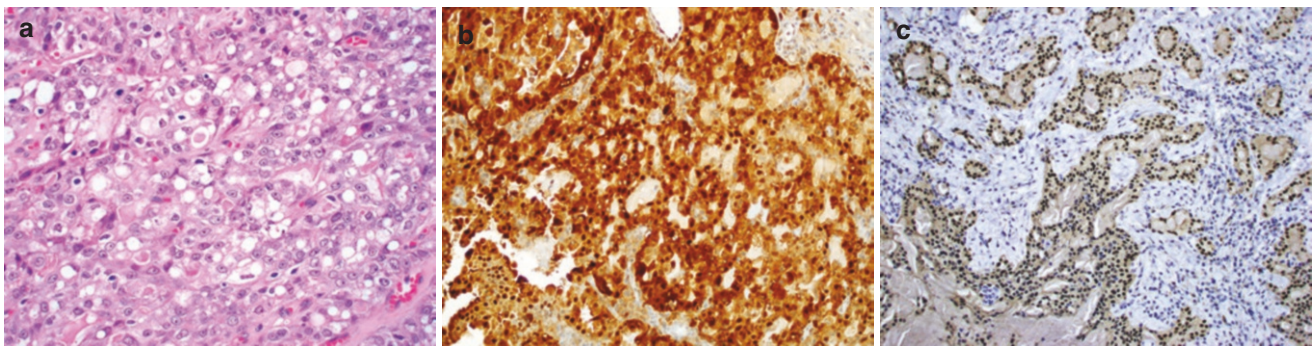

Fig. 8.24 The tumor is arranged in compact back-to-back tubules with intraluminal pink secretions. The tumor cells are round to polygonal in shape and have abundant eosinophilic to vacuolated cytoplasm. Nuclei are vesicular and show distinct nucleoli (**a**) S-100 (**b**) and pan-TRK (**c**) are diffusely positive. TRK expression suggests ETV6::NTRK rearrangement

8.7 SWI/SNF Complex Deficient Sinonasal Carcinoma

The SWI/SNF complex is a family of chromatin remodelling genes that function as tumor suppressors. Inactivating mutations lead to four distinct categories of tumors—SMARCB1(INI-1) deficient carcinoma, SMARCB1 deficient adenocarcinoma, SMARCA4 deficient carcinoma, and SMARCA4 deficient sinonasal teratocarcinosarcoma.

8.7.1 SMARCB1 Deficient Sinonasal Carcinoma

SMARCB1 (INI-1) deficient sinonasal carcinoma is a type of undifferentiated carcinoma with definitional inactivation of the *SMARCB1* gene on chromosome 22q11 due to biallelic deletion of *SMARCB1* gene in most of the cases. Monoallelic deletion or mutations occur in minority of cases. These tumors usually involve paranasal sinuses (ethmoids).

Histology shows mostly basaloid morphology with or without scattered rhabdoid cells. The other cytomorphologic subtype is oncocytoid/ plasmacytoid in which tumor cells possess abundant dense eosinophilic cytoplasm with central to eccentrically placed nuclei. This pattern can be present in solid sheets or complex tubuloglandular pattern which lead to diagnosis of SMARCB1 deficient adenocarcinoma. Rarely tumors show yolk-sac like patterns along with variable yolk-sac carcinoma immunophenotype in the form of SALL-4, glypican 3, and hep-par 1 positivity [14–16].

Immunohistochemistry for INI-1(SMARCB1) shows loss of expression in all variants while it is expressed in the nuclei of normal cells such as stromal fibroblasts, endothelial cells, and inflammatory cells. The tumor cells show immunopositivity for pankeratin with variable immunoreactivity for p63, p40, and neuroendocrine markers (Figs. 8.25, 8.26, and 8.27).

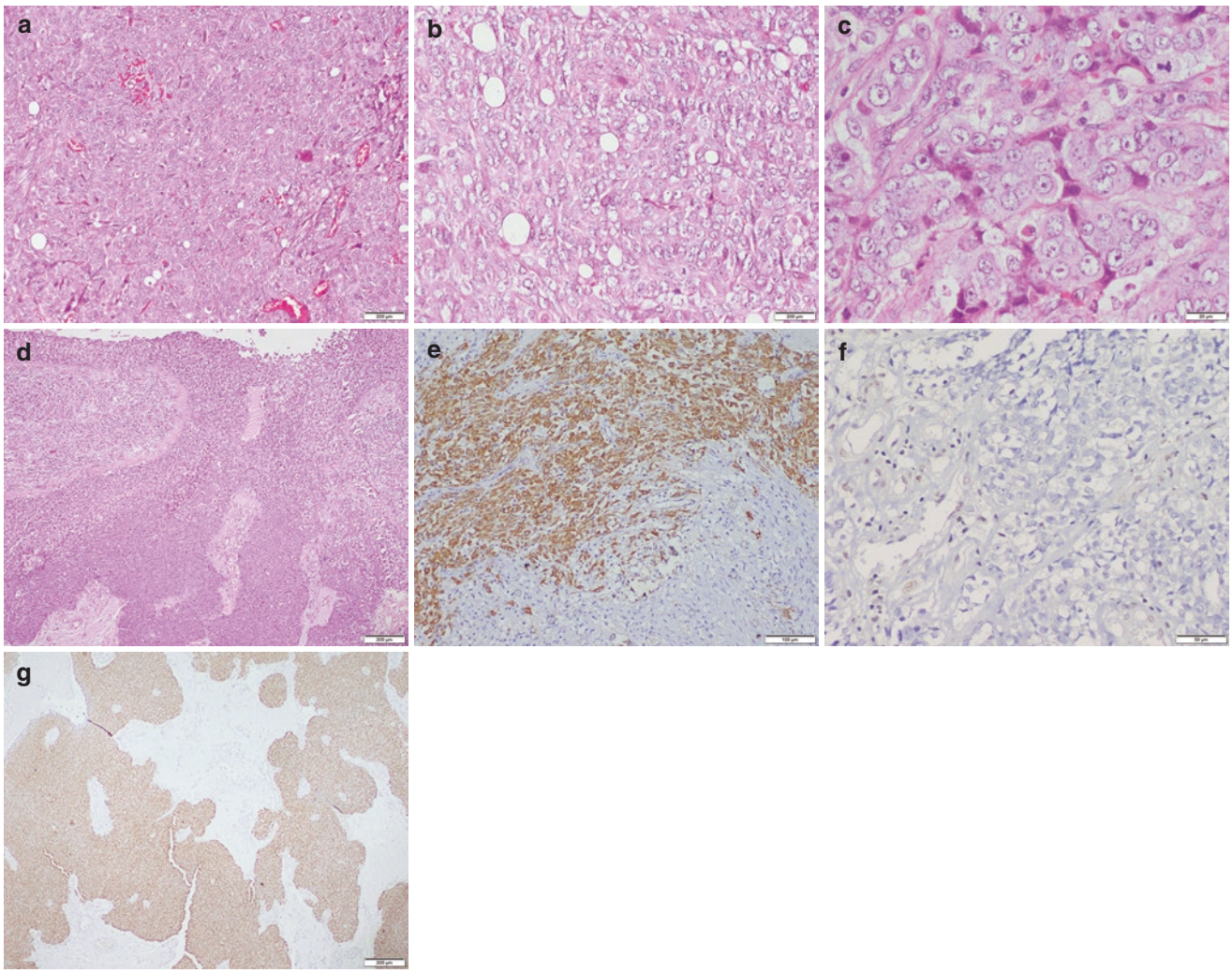

Fig. 8.25 Blue (basaloid) cell appearance. Cytologically monomorphic high-grade medium sized basaloid cells. Note empty vacuoles scattered throughout tumor (**a**, **b**). The nuclei have vesicular chromatin and pinpoint prominent nucleoli (**c**). The basaloid cells growing inwards from surface epithelium in expansile fashion mimicking inverted papilloma pattern. Entire epithelium is replaced by tumor cells (**d**). Tumor cells are diffusely positive for keratin (**e**) and show loss of SMARCB1 (INI1) protein in tumor cells (**f**). p40 shows positivity (**g**) (squamous markers show positivity in >50% cases)

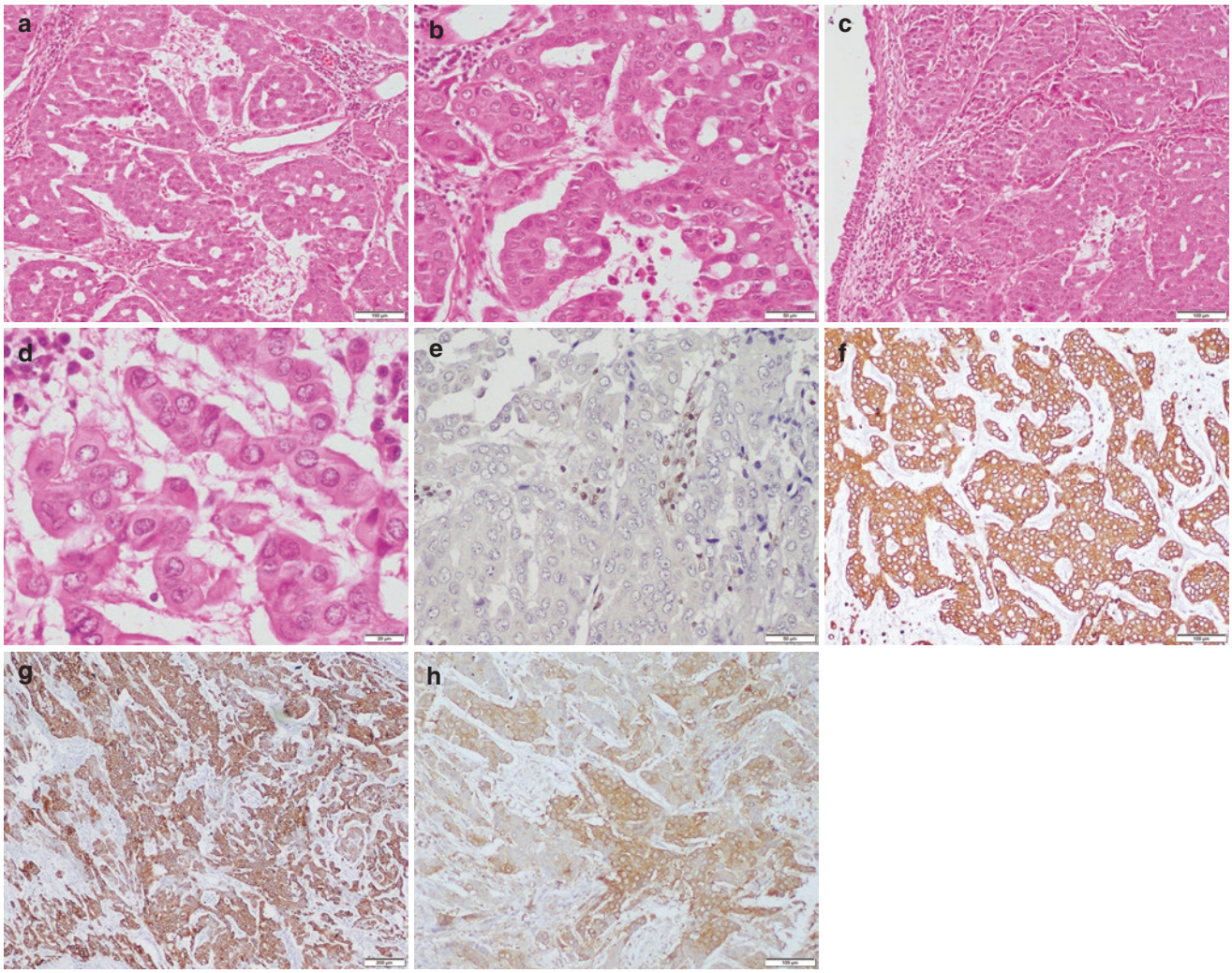

Fig. 8.26 Pink (oncocytoid) cell appearance. The tumor is arranged in complex tubular pattern with cribriforming suggestive of adenocarcinoma pattern. In contrast to basaloid variant, the cells have more cytoplasm which is dense eosinophilic throughout. The cellular monomorphism exists in this variant also. The nuclei are round and have fine chromatin (**a**–**d**). Overlying respiratory epithelium is identified which shows pagetoid spread of tumor cells in (**c**). The tumor here is arranged in solid sheets without glandular differentiation. The tumor cells show complete loss of SMARCB1 (INI1) protein from the tumor cells. Normal lymphocytes serve as control and retain brown nuclear staining (**e**). Keratin (**f**) and CK7 (**g**) are diffusely positive. Synaptophysin is also positive (**h**). About a third of tumors show positivity for neuroendocrine markers

8.7.2 SMARCA4 Deficient Sinonasal Carcinoma

The SMARCA4 gene is located on chromosome 19p13.2, inactivation of which leads to a group of aggressive carcinomas. SMARCA4 deficient SN carcinomas are also poorly to undifferentiated carcinomas with morphologic resemblance to neuroendocrine (NE) carcinomas. Similar to high-grade NE carcinomas, the tumor cells show nuclear molding, spindling, crushing, and stippled chromatin (small cell carcinoma phenotype). Some tumors show more cytoplasm, squared off edges, and prominent nucleoli and thus resemble large cell neuroendocrine carcinoma. Rare rhabdoid cells can be recognized on close search of tumor specimens. A characteristic cytologic monomorphism is maintained in these tumors also which is a diagnostic feature of all SWI/SNF family of tumors [17, 18] (Figs. 8.28, 8.29, 8.30, and 8.31).

A variation on this theme is identified in sinonasal teratocarcinosarcomas (TCS) which exhibit complete or partial loss of SMARCA4 (BRG1 protein) in about 70% of cases. SMARCA4 deficient or proficient tumors show *CTNNB1* mutations in a subset of cases. TCS are an admixture of carcinoma (epithelial), sarcoma (mesenchymal), and primitive neuroepithelium [19, 20] (Figs. 8.32, 8.33, 8.34, and 8.35).

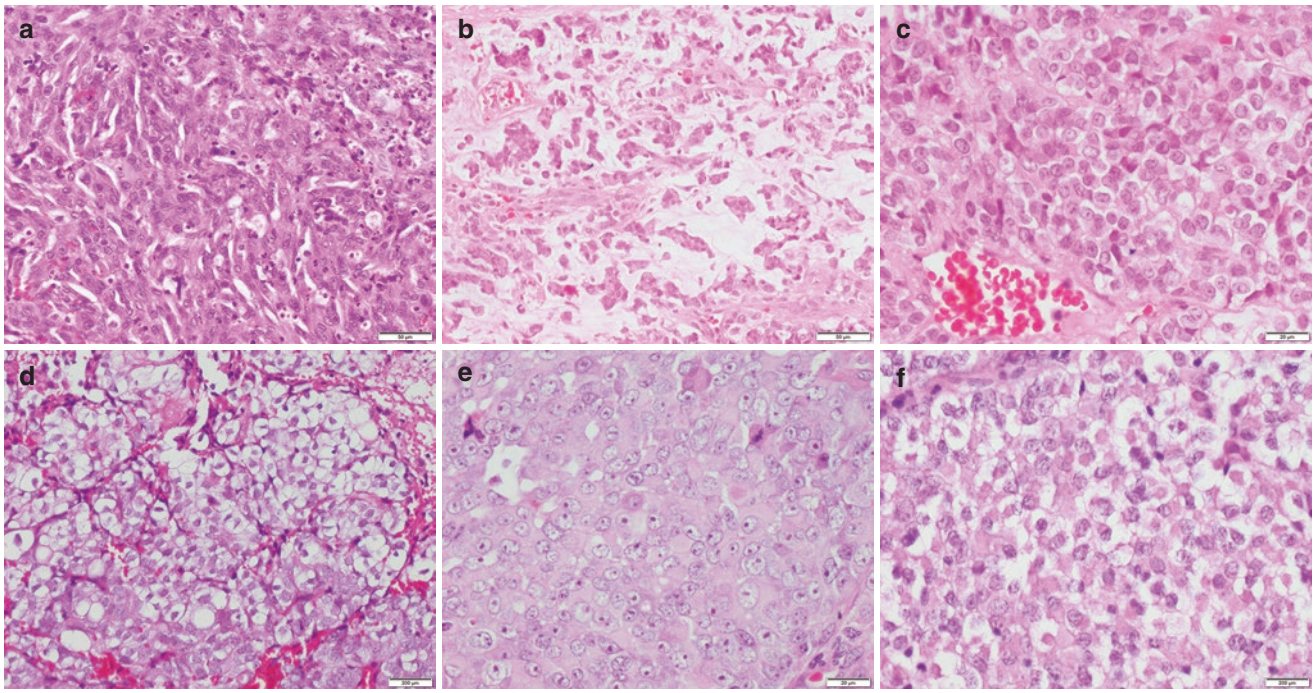

Fig. 8.27 Some tumors do not fall into strict basaloid or oncocytoid categories and show epithelioid tumor cells arranged in sheets with moderate amount of cytoplasm. Polymorphonuclear leukocytes are infiltrating into the tumor (right side) (**a**). Tumor cells in groups and nests are floating in myxoid stroma (**b**) and sometimes show abundant clear cytoplasm (**c**, **d**) and prominent rhabdoid appearance (**e**, **f**). Occasionally tumors show yolk-sac like morphology and immunophenotype (not shown here)

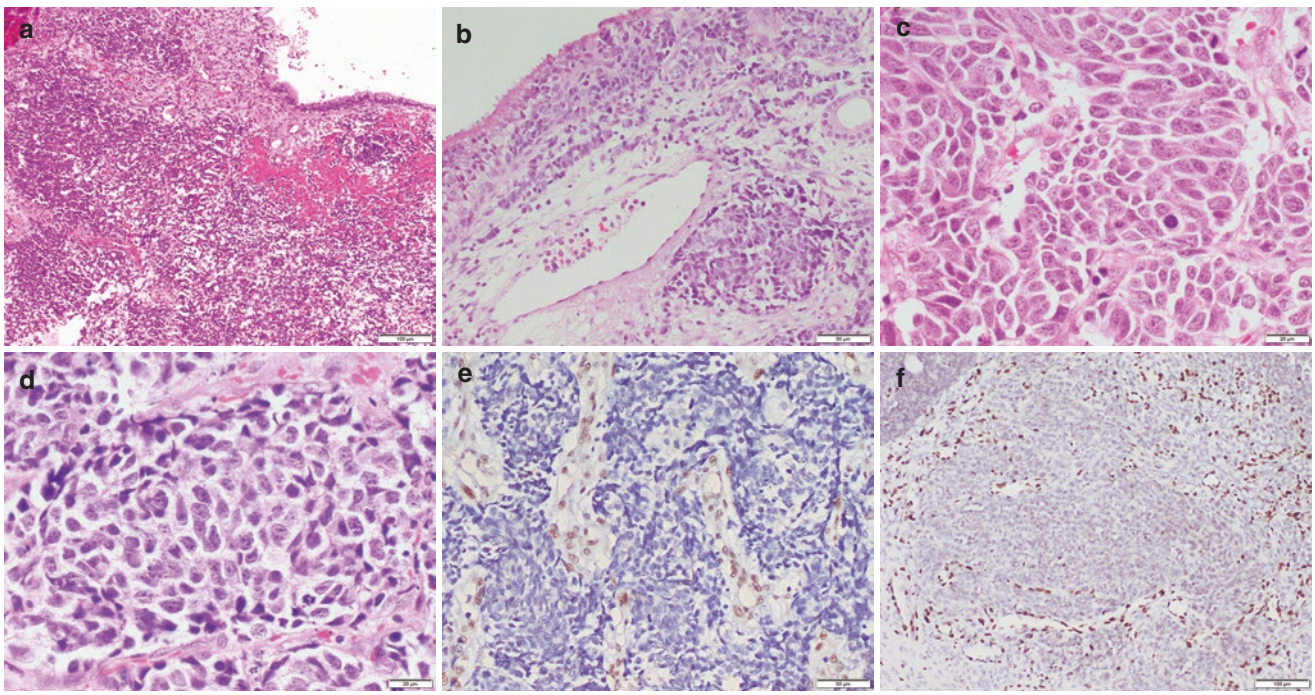

Fig. 8.28 Small cell carcinoma (SCC) phenotype: A highly cellular "blue" tumor present in sheets beneath respiratory epithelium. The tumor cells are round to fusiform and the stroma is richly vascular (**a**). Pagetoid spread of these undifferentiated tumor cells can be seen (upper part of **b**). The tumor cells are oval to fusiform with high N/C ratio, stippled "salt and pepper" chromatin and multiple chromocenters reminiscent of SCC. Frequent mitotic figures are seen (**c**, **d**). The tumor cells show loss of SMARCA4 (BRG1) protein against the background endothelial cells which retain normal immunoexpression of protein (**e**). This example demonstrates reduced (dim) expression of BRG1 in comparison to normal control of endothelial cells (**f**). Tumor cells spread through entrapped surface epithelium which retains BRG1 expression (**g**). Same is depicted by p40 stain which is negative in tumor cells (**h**). Retinoblastoma protein is retained (not lost as in SCC) in tumor cells (**i**). Chromogranin is focally positive (**j**)

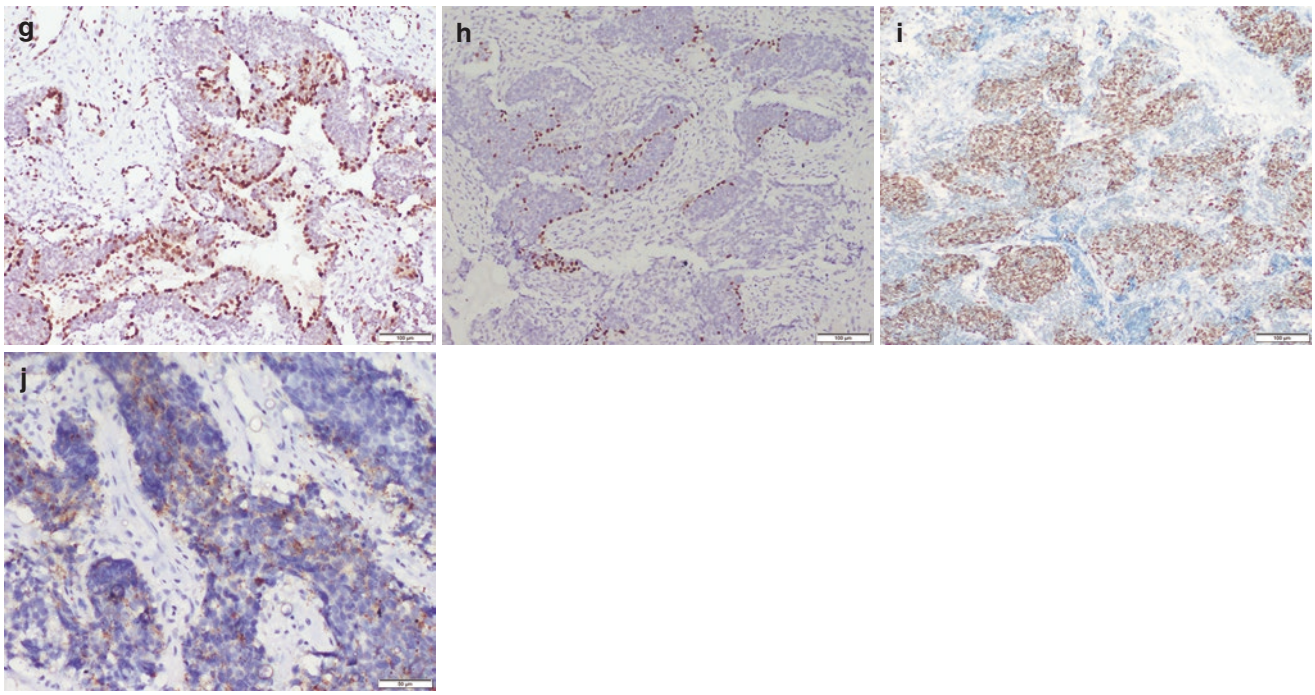

Fig. 8.28 (continued)

Fig. 8.29 Cytology of lymph node metastasis of a known case of SMARCA4 deficient carcinoma shows undifferentiated tumor cells mimicking small cell carcinoma

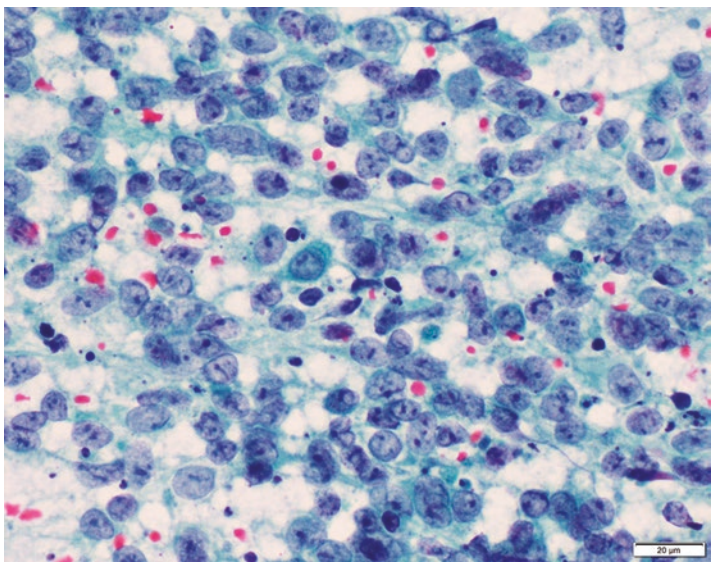

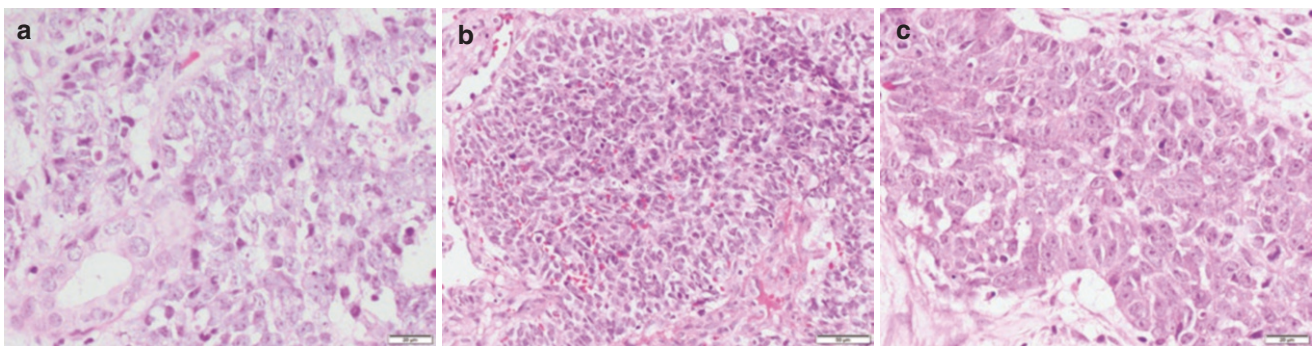

Fig. 8.30 Large cell neuroendocrine carcinoma (LCNEC) phenotype: The tumor cells show high nuclear/cytoplasmic ratio with finely stippled chromatin and conspicuous multiple nucleoli. A normal gland is entrapped in the tumor (left lower -**a**). A large tumor nest shows peripheral palisading. Note prominent nucleoli and moderate cytoplasm (**b**, **c**)

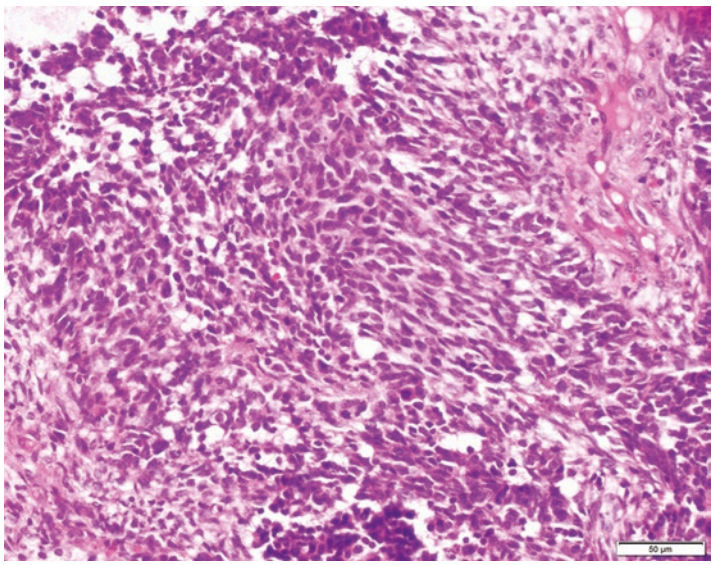

Fig. 8.31 Sometimes tumor shows prominent spindling

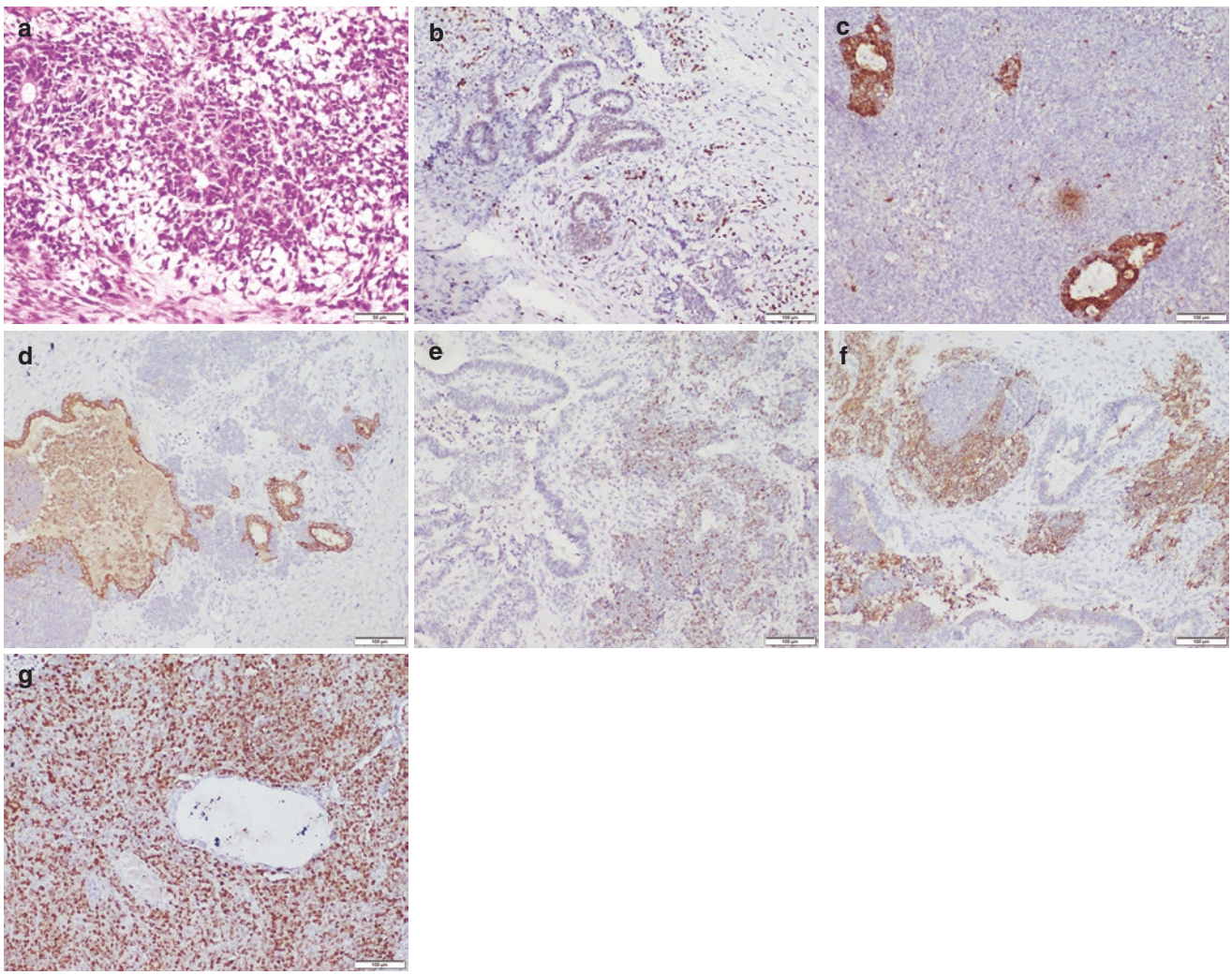

Fig. 8.32 A teratocarcinosarcoma shows primitive neuroepithelium (NE) arranged in rosettes. Malignant stromal cells are seen in left lower corner (**a**). BRG1 expression is reduced to absent in rosettes and background malignant stroma (**b**). Pan-Keratin (**c**) and CK7 (**d**) highlight glandular component of TCS while NE component is negative. On the other hand, INSM1 (**e**) and synaptophysin (**f**) are positive in NE component. These tumors are high-grade and show prolific KI67 labelling index (**g**)

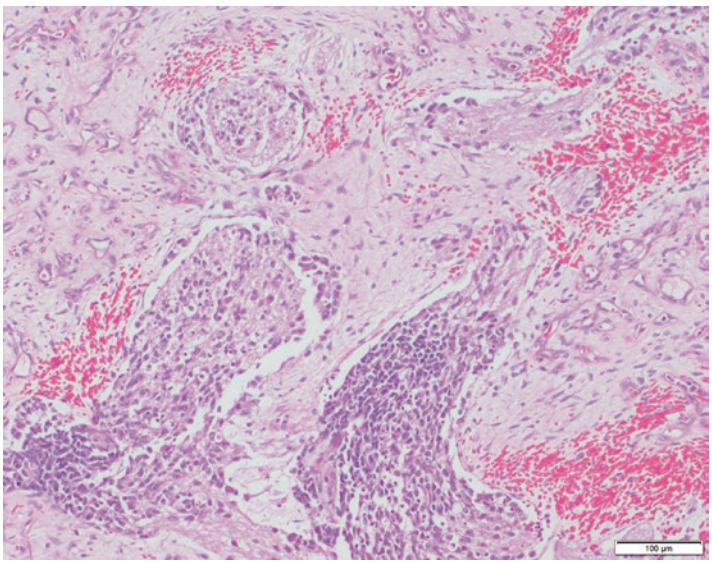

Fig. 8.33 Another case of TCS shows neurofibrillary background and undifferentiated primitive NE component

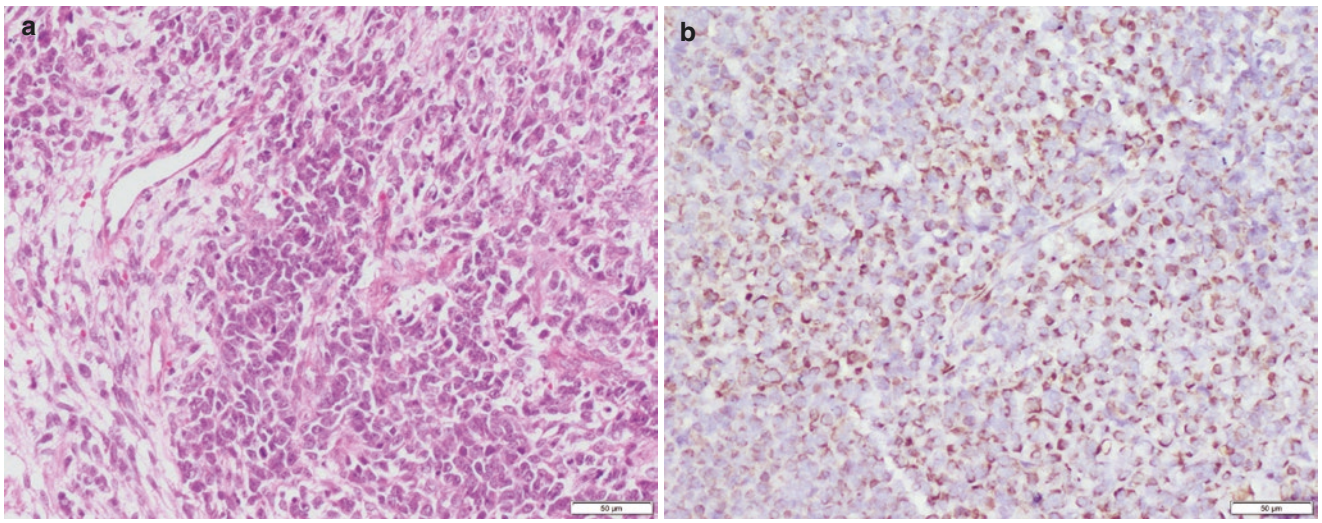

Fig. 8.34 TCS with rhabdomyoblastic differentiation (center) is seen in malignant stroma (**a**). Desmin is diffusely positive in stroma (**b**)

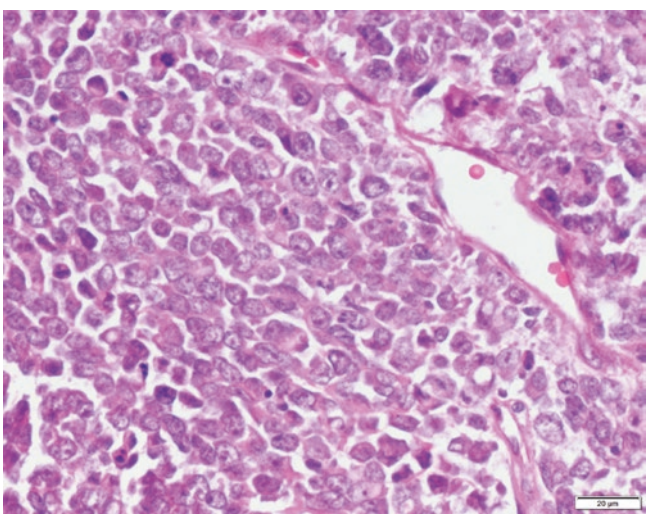

Fig. 8.35 This example of SMARCA4 deficient carcinoma shows high-grade morphology with prominent rhabdoid cells

IHC of SMARCA4 deficient carcinoma shows BRG1 loss with retention of other family proteins viz. SMARCA2 (BRM) and SMARCB1 (INI1). Focal reactivity to neuroendocrine markers is present.

TCS show positivity for keratins, p40 and p63 in epithelial component, NE markers in NE elements and mesenchymal component stains according to type of differentiation. When present, the degree of BRG1 loss may vary in the three components.

8.8 Sinonasal Undifferentiated Carcinomas (SNUC)

Sinonasal undifferentiated carcinomas are a diagnoses of exclusion where tumors do not show any lineage commitment either on morphology or on immunophenotyping.

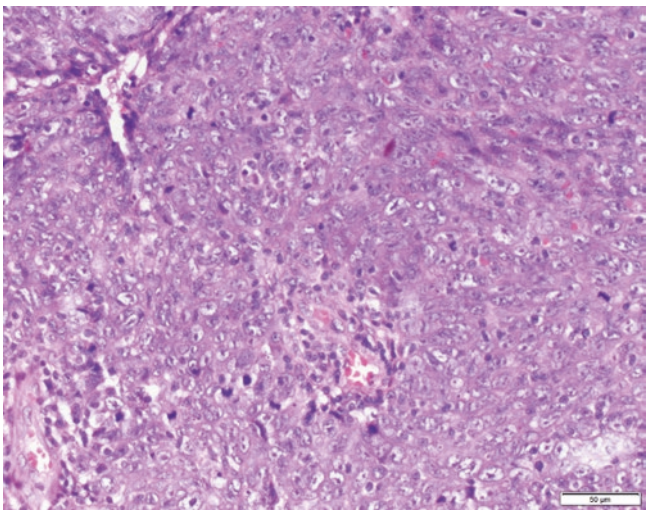

Fig. 8.36 Tumor nests show high-grade morphology with undifferentiated tumor cells. Immunophenotypically null cell type

Morphologically these tumors are undifferentiated high-grade tumors with frequent necrosis and mitosis (Fig. 8.36). Aside from simple keratins and epithelial membrane antigen (EMA), they do not show any consistent immunophenotype. No viral associations are reported. Differential diagnoses on morphology range from basaloid carcinoma, NUT carcinoma, SWI/SNF deficient tumors to high-grade neuroendocrine carcinomas [2].

Pathogenetically, *IDH2* hotspot mutations are identified in a significant number of SNUC cases (Fig. 8.37). Although IDH1/2 mutation-specific IHC is available, it is neither sensitive nor specific to identify all reported variants. Sequencing or PCR-based testing is suitable for mutation testing [21, 22].

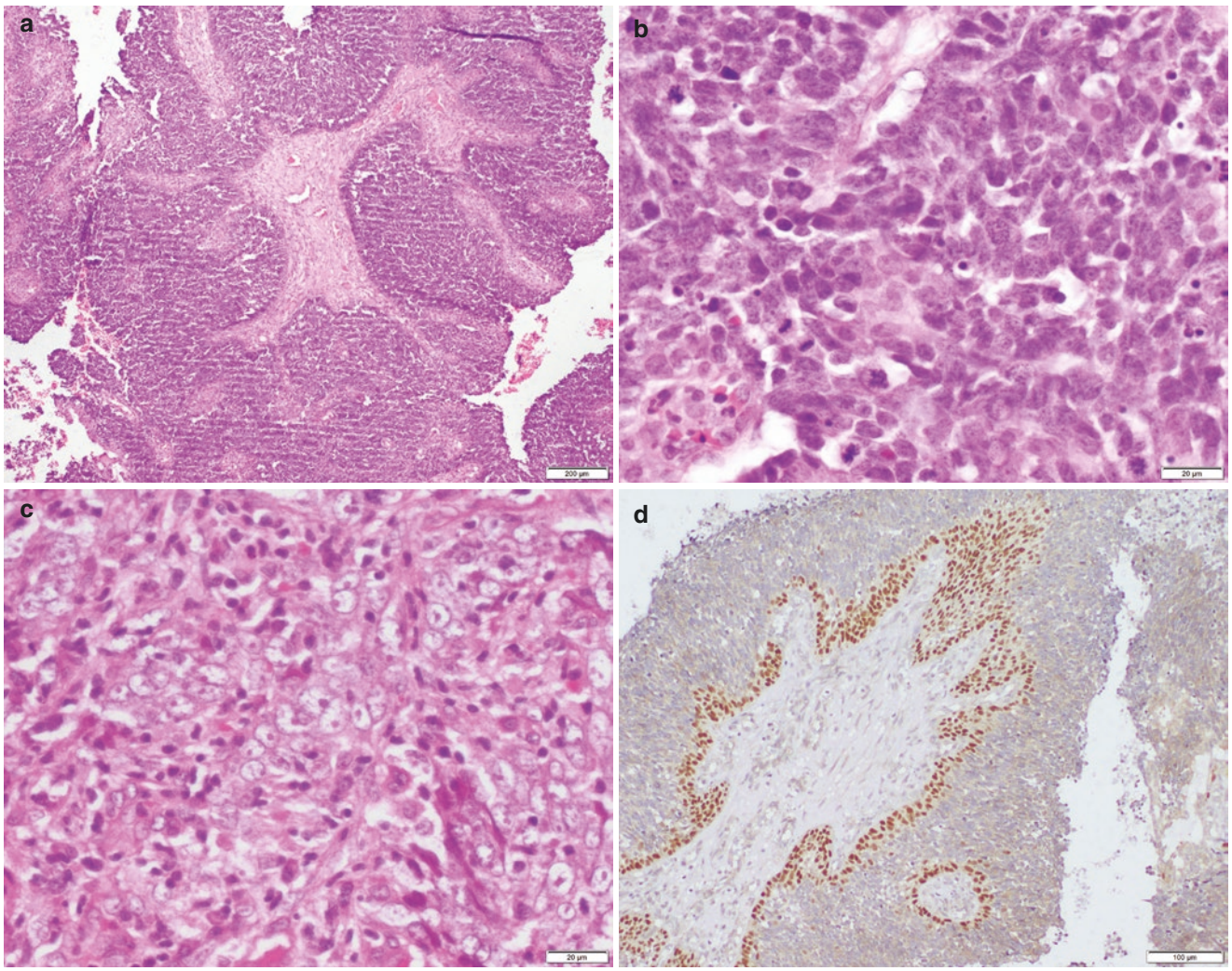

Fig. 8.37 Sheets and nests of undifferentiated tumor cells arising from epithelium and invading downwards with peripheral palisading reminiscent of inverted papilloma pattern (**a**) Higher magnification shows hyperchromatic nuclei with condensed chromatin (**b**) and vesicular nuclei with prominent nucleoli (**c**). Many mitotic figures are seen in (**b**). Tumor spreads through the entire thickness of epithelium with intact basal layer highlighted by p40 stain (**d**). IDH1/2 mutation specific IHC strongly positive in a IDH2 mutation positive case (**e**)

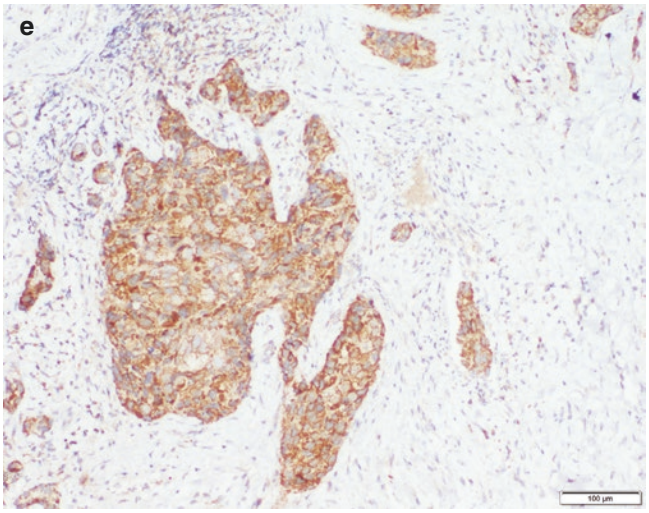

Fig. 8.37 (continued)

8.9 Sinonasal Neuroendocrine Tumors

WHO 2022 classification of head and neck tumors has unified the grading and nomenclature of neuroendocrine tumors at different sites. Sinonasal neuroendocrine tumors are subdivided into:

Grade 1: lack necrosis and have <2 mitoses per 2mm^2.

Grade 2: necrosis (often punctate or coagulative) and/or 2–10 mitoses per 2mm^2.

The use of Ki67 proliferation index is encouraged which is generally <20% in low-grade tumors. These tumors do not show abnormal p53 staining indicative of p53 mutation and retain rb (retinoblastoma protein) immunoexpression.

Neuroendocrine carcinomas can have small cell or large cell morphology with mitoses >10/2 mm2, and Ki-67 > 20% (Fig. 8.38).

Morphology of these tumors is same as at any other body site. It is important to exclude SMARCA4 deficient SN carcinomas if neuroendocrine markers are focal, weak and not consistent in an otherwise morphologically compatible NE carcinoma [1, 18].

Table 8.3 summarizes all basaloid (malignant blue cell morphology) appearing carcinomas of sinonasal tract.

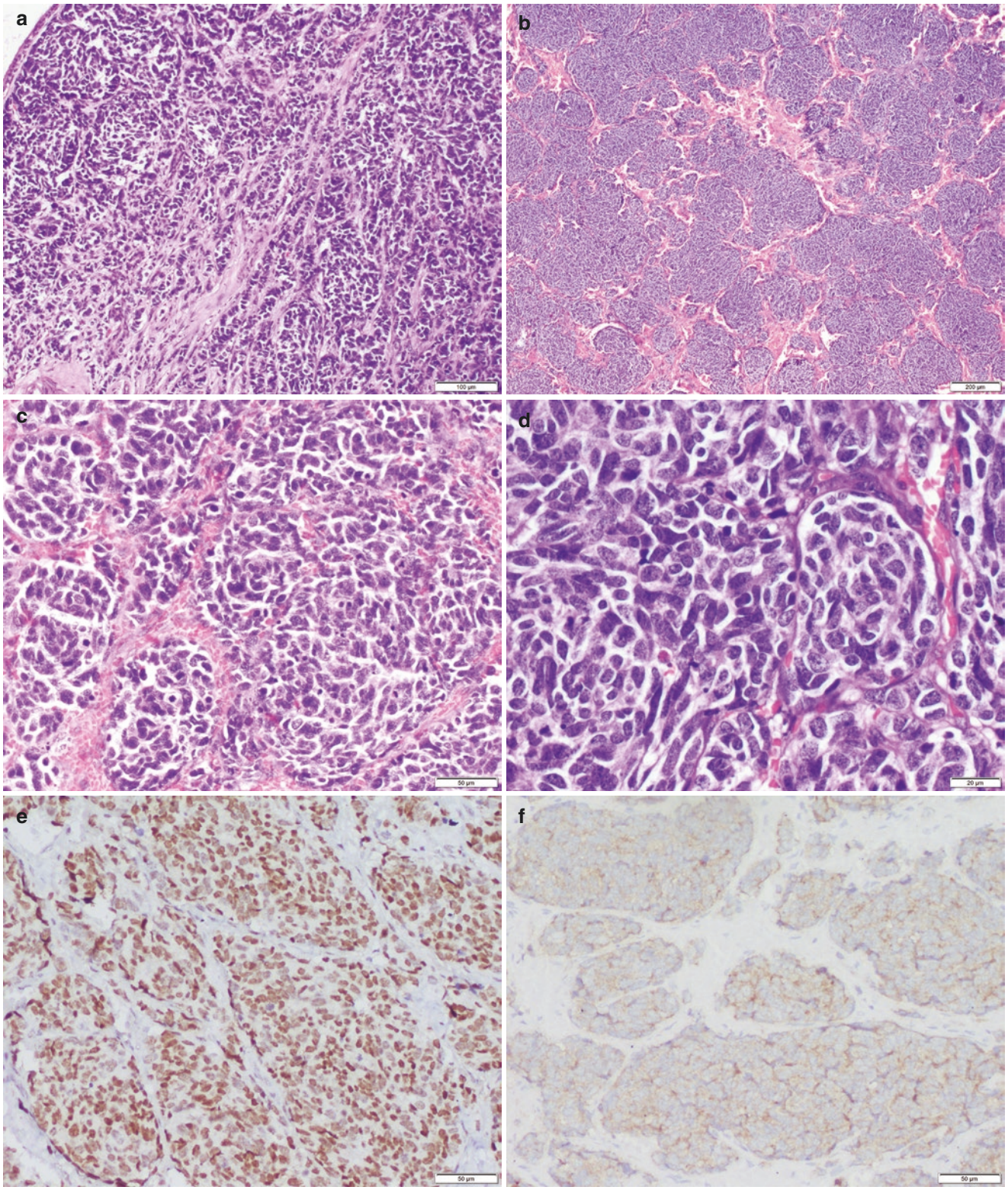

Fig. 8.38 A hypercellular "blue" tumor with overlying respiratory epithelium (left upper corner) (**a**). The tumor is arranged in swirling round nests and clusters (**b**). Individual cells are epithelioid round to oval shaped with stippled chromatin (**c**, **d**). Tumor is intensely positive for INSM1 (**e**) and synaptophysin (**f**). Retinoblastoma protein is lost in tumor cells. Normal endothelial cells around tumor nests serve as internal control (**g**)

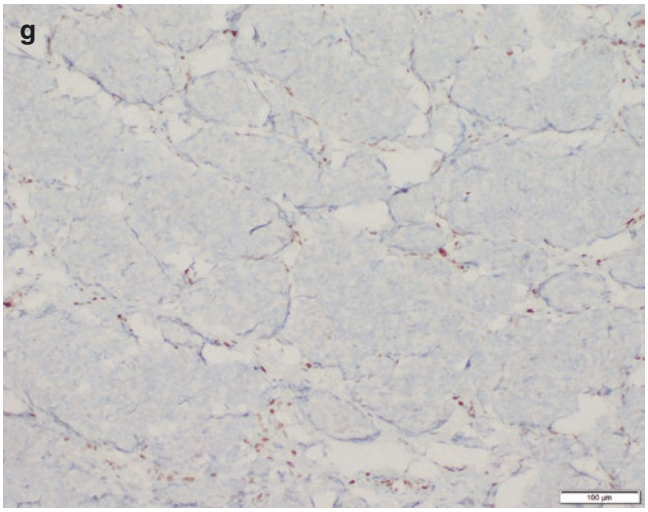

Fig. 8.38 (continued)

Table 8.3 Differential diagnoses of malignant "round blue cell" sinonasal carcinomas

	Morphologic hints	Initial IHC panel	Extended IHC panel	Other tests
Basaloid squamous cell carcinoma	Palisading of tumor nests, cohesiveness of tumor cells, subtle squamous phenotype	Keratin, p40 positive	NUT negative p16 ±	HPV ISH ±
NUT carcinoma	Undifferentiated cells with prominent nucleoli, neutrophils, abrupt keratinization	Keratin, p40, p63, NUT positive		NUT FISH, if available, positive for rearrangement
Lymphoepithelial carcinoma	Syncytium of cells, prominent nucleoli, stroma containing lymphocytes and plasma cells	Keratin, p40 positive, NUT negative	EBV LMP ±	EBER ISH positive
SMARCB1 (INI-1) deficient carcinoma	Basaloid cells, scattered rhabdoid cells, nondescript morphology not fitting in any other diagnoses	Keratin positive, p40, p63, NUT, NE markers negative[a]	INI-1 loss	
SMARCA4 deficient carcinoma	Small cell carcinoma or LCNEC morphology, rhabdoid cells	Keratin positive, NE markers focal, patchy, not consistent, p40, p63 negative	SMARCA4 (BRG1) loss, INI-1, SMARCA2 (BRM) and RB retained	
TCS (in biopsy specimens when only primitive neuroepithelial component is sampled)	Rosettes, nuclear molding, fine stippled chromatin	Keratin, CD99, NKX2.2 negative, NE markers positive	SMARCA4 (BRG1) loss	Repeat sampling if possible
Neuroendocrine carcinoma	NE phenotypic features	Keratin dot like (usually), NE markers positive	Rb deleted	
Solid adenoid cystic carcinoma	Solid basaloid cells, subtle basophilic secretions, cribriforming	Keratin positive, p40, p63 positive in myoepithelial cells	CK7, CD117 positive	*MYB* rearrangement
HMSC (in biopsy specimens if only solid component is sampled)	Surface dysplasia, subtle basophilic secretions, cribriforming	Keratin positive, p40, p63 positive in myoepithelial and squamous components	CD117, p16 positive	HPV ISH
SNUC	If no clue	Only keratin positive All other markers negative	IDH 1/2 ±	*IDH1/2* mutation testing by PCR based or sequencing methods

NE Neuroendocrine, *LCNEC* Large cell neuroendocrine carcinoma, *SNUC* Sinonasal undifferentiated carcinomas, *HMSC* HPV-related Multiphenotypic Sinonasal Carcinoma, *TCS* Teratocarcinosarcoma

[a] p40 and NE markers can come positive

8.10 Conclusion

Sinonasal carcinomas are an important category of tumors which needs thorough workup of cases to establish a correct diagnosis. Before labelling a case as SNUC, a battery of ancillary testing needs to be performed to provide a correct diagnosis as it has significant clinical implications.

Acknowledgement The authors thank Dr. Divya Kannan for help with the images in Fig. 8.1.

References

1. WHO Classification of Tumours Editorial Board. Head and neck tumours [Internet; beta version ahead of print]. Lyon (France): International Agency for Research on Cancer; 2022 [cited 2022 July 13]. (WHO classification of tumours series, 5th ed.; vol. 9). Available from: https://tumourclassification.iarc.who.int/chapters/52.
2. Franchi A. In: Franchi A, editor. Epithelial tumors. In pathology of sinonasal tumors and tumor-like lesions. Cham: Springer Nature; 2020. p. 85–146.
3. Jiromaru R, Yamamoto H, Yasumatsu R, Hongo T, Nozaki Y, Hashimoto K, Taguchi K, Masuda M, Nakagawa T, Oda Y. HPV-related Sinonasal carcinoma: Clinicopathologic features, diagnostic utility of p16 and Rb immunohistochemistry, and EGFR copy number alteration. Am J Surg Pathol. 2020;44(3):305–15.
4. Kuo Y-J, Lewis JS, Zhai C, Chen Y-A, Chernock RD, Hsieh M-S, et al. DEK-AFF2 fusion-associated papillary squamous cell carcinoma of the sinonasal tract: clinicopathologic characterization of seven cases with deceptively bland morphology. Mod Pathol. 2021;34(10):1820–30.
5. Elgart K, Faden DL. Sinonasal squamous cell carcinoma: etiology, pathogenesis, and the role of human papilloma virus. Curr Otorhinolaryngol Rep. 2020;8(2):111–9.
6. Rooper LM, Agaimy A, Dickson BC, Dueber JC, Eberhart CG, Gagan J, et al. DEK-AFF2 carcinoma of the Sinonasal region and Skull Base: detailed Clinicopathologic characterization of a distinctive entity. Am J Surg Pathol. 2021;45(12):1682–93.
7. Jeng YM, Sung MT, Fang CL, Huang HY, Mao TL, Cheng W, Hsiao CH. Sinonasal undifferentiated carcinoma and nasopharyngeal-type undifferentiated carcinoma: two clinically, biologically, and histopathologically distinct entities. Am J Surg Pathol. 2002 Mar;26(3):371–6.
8. Wenig BM. Lymphoepithelial-like carcinomas of the head and neck. Semin Diagn Pathol. 2015 Jan;32(1):74–86.
9. Bishop JA, Westra WH. NUT midline carcinomas of the sinonasal tract. Am J Surg Pathol. 2012;36(8):1216–21.
10. Kakkar A, Antony VM, Irugu DVK, Adhikari N, Jain D. NUT midline carcinoma: a series of five cases, including one with unusual clinical course. Head Neck Pathol. 2018 Jun;12(2):230–6.
11. Bishop JA, Andreasen S, Hang JF, Bullock MJ, Chen TY, Franchi A, Garcia JJ, Gnepp DR, Gomez-Fernandez CR, Ihrler S, Kuo YJ, Lewis JS Jr, Magliocca KR, Pambuccian S, Sandison A, Uro-Coste E, Stelow E, Kiss K, Westra WH. HPV-related multiphenotypic Sinonasal carcinoma: an expanded series of 49 cases of the tumor formerly known as HPV-related carcinoma with adenoid cystic carcinoma-like features. Am J Surg Pathol. 2017;41(12):1690–701.
12. Leivo I. Sinonasal adenocarcinoma: update on classification, Immunophenotype and molecular features. Head Neck Pathol. 2016;10(1):68–74.
13. Purgina B, Bastaki JM, Duvvuri U, Seethala RR. A subset of Sinonasal non-intestinal type adenocarcinomas are truly Seromucinous adenocarcinomas: a morphologic and Immunophenotypic assessment and description of a novel pitfall. Head Neck Pathol. 2015;9(4):436–46.
14. Thompson LDR, Bishop JA. Update from the 5th Edition of the world health organization classification of head and neck tumors: nasal cavity, paranasal sinuses and skull base. Head Neck Pathol. 2022 Mar;16(1):1–18.
15. Shah AA, Jain D, Ababneh E, Agaimy A, Hoschar AP, Griffith CC, Magliocca KR, Wenig BM, Rooper LM, Bishop JA. SMARCB1 (INI-1)-Deficient adenocarcinoma of the sinonasal tract: a potentially under-recognized form of sinonasal adenocarcinoma with occasional yolk sac tumor-like features. Head Neck Pathol. 2020;14(2):465–72.
16. Kakkar A, Antony VM, Pramanik R, Sakthivel P, Singh CA, Jain D. SMARCB1 (INI1)-deficient sinonasal carcinoma: a series of 13 cases with assessment of histologic patterns. Hum Pathol. 2019;83:59–67.
17. Agaimy A, Jain D, Uddin N, Rooper LM, Bishop JA. SMARCA4-deficient Sinonasal carcinoma: a series of 10 cases expanding the genetic Spectrum of SWI/SNF-driven Sinonasal malignancies. Am J Surg Pathol. 2020;44(5):703–10.
18. Kakkar A, Ashraf SF, Rathor A, Adhya AK, Mani S, Sikka K, Jain D. SMARCA4/BRG1-deficient Sinonasal carcinoma: morphologic Spectrum of an evolving entity. Arch Pathol Lab Med. 2021;146:1122. https://doi.org/10.5858/arpa.2021-0001-OA.
19. Rooper LM, Uddin N, Gagan J, Brosens LAA, Magliocca KR, Edgar MA, Thompson LDR, Agaimy A, Bishop JA. Recurrent loss of SMARCA4 in Sinonasal Teratocarcinosarcoma. Am J Surg Pathol. 2020;44(10):1331–9.
20. Birkeland AC, Burgin SJ, Yanik M, Scott MV, Bradford CR, McHugh JB, McLean SA, Sullivan SE, Nor JE, McKean EL, Brenner JC. Pathogenetic analysis of Sinonasal Teratocarcinosarcomas reveal actionable β-catenin overexpression and a β-catenin mutation. J Neurol Surg B Skull Base. 2017;78(4):346–52.
21. Kakkar A, Rathor A, Ashraf SF, Singh V, Sikka K, Jain D. IDH1/2 mutations in Sinonasal undifferentiated carcinomas: previously undescribed IDH2 R172K and R140x variants. Am J Surg Pathol. 2022;46:1284. https://doi.org/10.1097/PAS.0000000000001912.
22. Dogan S, Frosina D, Geronimo JA, Hernandez E, Mohanty A, Bale T, Hechtman JF, Arcila ME, Hameed MR, Jungbluth AA. Molecular epidemiology of IDH2 hotspot mutations in cancer and immunohistochemical detection of R172K, R172G, and R172M variants. Hum Pathol. 2020;106:45–53.

Salivary Gland Tumors of the Sinonasal Tract

9

Nora Katabi and Maelle Saliba

9.1 Introduction

Minor salivary gland tumors of the sinonasal cavity represent a heterogeneous subgroup of neoplasms with significant heterogeneity in clinical behavior [1]. They are relatively rare, accounting for 4–8% of all sinonasal tumors and 15–23% of all salivary gland neoplasms [2, 3]. Inversely, 8% of minor salivary gland carcinomas occur in the sinonasal tract [3]. Although rare, they are nevertheless second in frequency to squamous cell carcinoma at this site [4]. They tend to arise in paranasal sinuses more commonly than in the nasal cavity, with the maxillary sinus being the most common site of origin [2]. The majority of patients will present with advanced disease, as tumors are unlikely to present with early symptoms [5]. Complaints are generally delayed until the tumor reaches one of the cortical plates and invades bone [6]. Overall, benign sinonasal salivary gland neoplasms are much less frequent than malignant neoplasms, and are mainly represented by pleomorphic adenomas [7]. Adenoid cystic carcinoma is, by far, the most common salivary gland carcinoma of the sinonasal tract, followed by mucoepidermoid carcinoma [2, 7, 8].

The subtyping and grading of sinonasal salivary gland tumors is faced with many challenges. As for other sinonasal tumors, specimen gross inspection provides limited information, seeing as diagnostic tissue material is often obtained by endoscopic procedures or polypectomies [1]. Furthermore, salivary gland tumors are notorious for their degree of histologic and immunohistochemical overlap. Immunohistochemical staining for ductal (e.g., CEA, EMA, CK7, and CD117) and myoepithelial markers (S100, SOX10, p40, p63, GFAP, SMA, calponin, and CD10) is seen in all tumors that harbor these cell lines [9, 10]. Finally, the multitude of grading systems adopted for each salivary gland tumor histotype makes it difficult to unify and comment on the prognostic effect of tumor grade [3].

Complete surgical resection with or without postoperative radiotherapy is the treatment of choice for most sinonasal salivary gland tumors [2, 4, 11, 12]. Inopportunely, in view of the complex anatomy, clear resection margins are not always achievable for sinonasal tumors, especially for those that arise in the paranasal location [2, 12–14]. Tumor American Joint Committee on Cancer (AJCC) stage and histologic subtype are the most predictive variables of survival and recurrence [3]. Therefore, sinonasal minor salivary gland tumors ought to be distinguished from one another and from other lesions in the differential diagnosis owing to the prognostic and possible therapeutic difference for these lesions. This chapter explores the variety of benign and malignant salivary-type glandular tumors that are most likely to be encountered in the sinonasal tract.

9.2 Pleomorphic Adenoma

Pleomorphic adenoma (PA), or mixed tumor, is defined as a benign salivary gland tumor with ductal, myoepithelial, and stromal components [9]. Sinonasal PAs are rare, with most cases affecting women and presenting in the third to sixth decade of life [1, 9, 15]. The nasal cavity is the most common primary sinonasal location with about 80% of cases arising from the bony or cartilaginous nasal septum [9, 15]. Grossly, the tumor typically consists of a single, firm, polypoid or exophytic mobile nodule, usually causing no destruction of the surrounding tissue [1, 9].

Histology

PAs arising from minor salivary glands such as those in the sinonasal tract are less frequently encapsulated than those arising from major salivary glands [16, 17]. Instead of a fibrous capsule, they tend to display nodular or bosselated borders, creating an added layer of diagnostic difficulty on

N. Katabi (✉) · M. Saliba
Department of Pathology, Memorial Sloan Kettering Cancer Center, New York, NY, USA
e-mail: Katabin@mskcc.org; ms6393@cumc.columbia.edu

D. Jain, J. A. Bishop (eds.), *Atlas of Sinonasal Tract Pathology*, https://doi.org/10.1007/978-981-19-7315-4_9

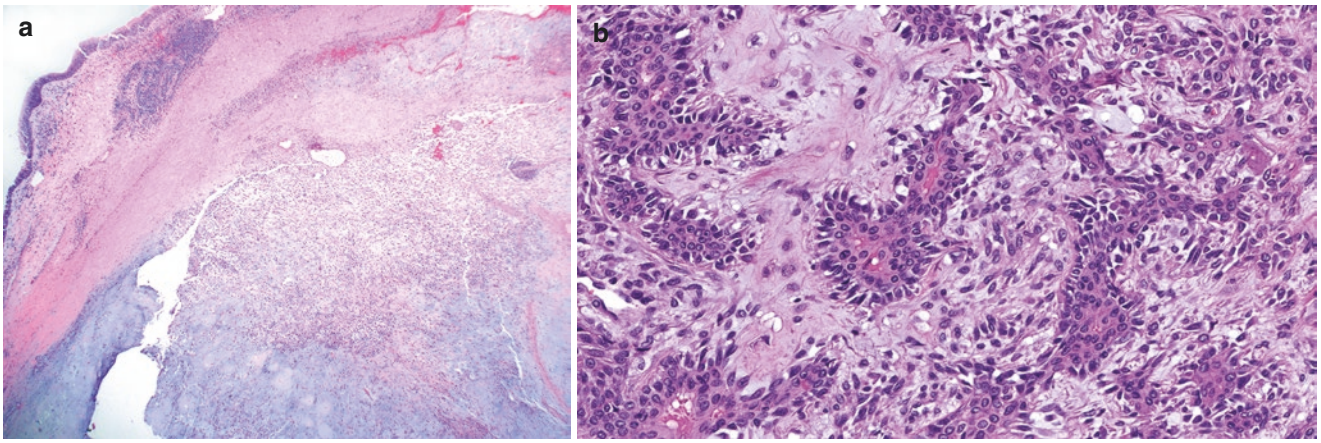

Fig. 9.1 (**a**) Pleomorphic adenoma (H&E, 10x): Low-power view of a pleomorphic adenoma showing a well-circumscribed however unencapsulated border. The identification of a chondromyxoid stroma facilitates the diagnosis of pleomorphic adenoma. (**b**) Pleomorphic adenoma (H&E, 20x): Pleomorphic adenomas harbor a mixture of epithelial cells, usually seen lining ductal spaces, and myoepithelial cells, seen here with a spindled clear cytoplasm. Both type of cells are embedded within a myxoid to hyaline stroma

limited biopsy material (Fig. 9.1a) [17]. PAs characteristically display unique arrangement of epithelial, myoepithelial, and stromal elements set in a variety of architectural patterns [1, 9, 17]. The stroma can be myxoid, chondromyxoid, or hyalinized. The epithelial cells typically form ductal structures (Fig. 9.1b). The myoepithelial cells may show a spectrum of appearances including spindled, epithelioid, and plasmacytoid morphologies [1, 9]. Tumors can be traiged into three main groups: 1-myxoid cases or "stroma-rich" showing 80% stroma, 2-cellular cases or "myoepithelial predominant" showing 80% cellularity and 3-mixed cases (classic), with the myxoid cases or "stroma-rich" variant being more prone to recurrence (Fig. 9.2 a, b) [1]. Tumors arising in the nasal cavity tend to be more cellular, showing less stromal component compared to PAs of major salivary glands [9]. The diagnosis can be further complicated by the presence of adipocytes, sebaceous cells, as well as oncocytic, mucinous, and squamous metaplasia [1, 16].

Ancillary Testing

Cytokeratins (e.g., CK7) are strongly reactive in ductal epithelial cells and variably reactive in the myoepithelial component. Myoepithelial markers S100, SOX10, p40, p63, GFAP, SMA, calponin, SMMH, and CD10 highlight the myoepithelial component (Fig. 9.2 c–f) [1]. Rearrangements involving Pleomorphic Adenoma Gene 1 (*PLAG1*) and High Mobility Group A2 (*HMGA2*) are the most common genetic alterations reported in PA of all locations [9].

Differential Diagnosis

Considering its diverse architectural and cytomorphologic features, PA can closely mimic other salivary gland tumors in the differential diagnosis, at least focally. Appreciating the circumscription of the tumor may prove to be challenging in unencapsulated tumors, especially in fragmented specimens [1]. The differential diagnosis thus includes malignant entities with less obviously infiltrative borders (e.g., epithelial-myoepithelial carcinoma, Table 9.1).

Treatment and Prognosis

Sinonasal PAs are treated with complete surgical excision. Recurrence rate is low, reported to be lower than that at the parotid site and is associated with incomplete excisions [20]. Malignant transformation (carcinoma ex-PA) has been reported in 2.4–10% of cases [9].

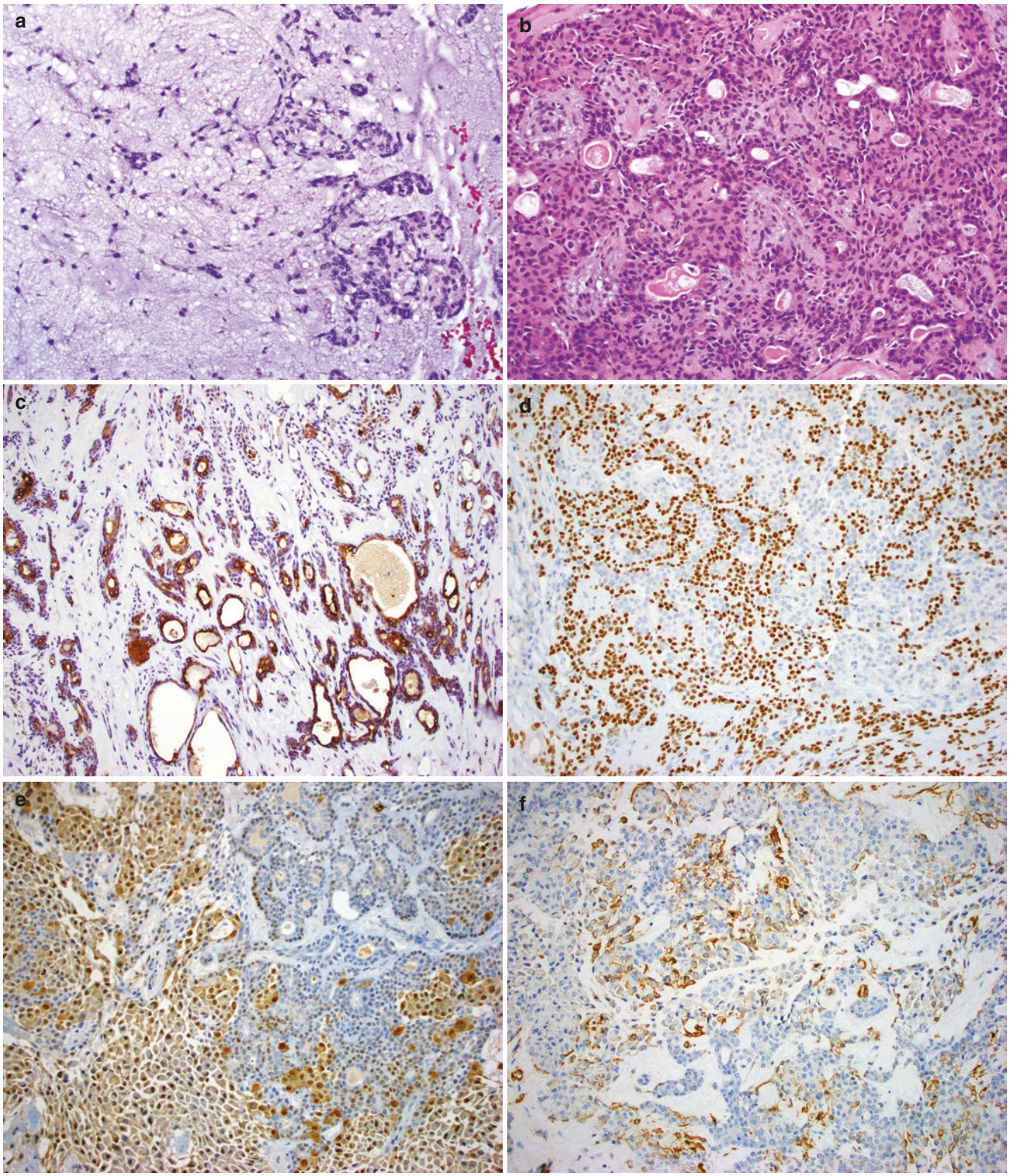

Fig. 9.2 (**a, b**) (H&E, 20x) Pleomorphic adenoma with stroma rich (**a**) and cellular morphology (**b**). (**c–f**) Pleomorphic adenoma shows positivity of CK 7 in ductal component (**c**) and p40 (**d**), S100 (**e**), and SMA (**f**) in myoepithelial cells. (Fig. 9.2a–f contributed by Justin Bishop)

Table 9.1 Histopathologic features of PA versus epithelial-myoepithelial carcinoma [9, 18, 19]

	Pleomorphic adenoma	Epithelial-myoepithelial carcinoma	Utility in differential diagnosis
Tumor Borders	Well-circumscribed, frequently encapsulated	Multinodular pushing borders with focal infiltrative growth	Low
Components	Epithelial and myoepithelial components set in a myxochondroid stroma	Biphasic epithelial and myoepithelial components	Intermediate, when the myxochondroid stroma is identified
Histology	Variable; "stroma-poor," cellular or classic forms	Classic tubular arrangement composed of inner layer of ductal cells surrounded by an outer layer of clear myoepithelial cells	Low, stroma-poor PA may resemble epithelial-myoepithelial carcinoma
High-grade features	Rarely shows increase in mitotic activity; no tumor necrosis	Usually low mitotic activity, no necrosis; perineural invasion may be present	High, if perineural invasion is identified
Immunohistochemistry	Epithelial and myoepithelial markers alternatively highlight both cell types	Epithelial and myoepithelial markers alternatively highlight both cell types	Low to none
Ancillary testing	*PLAG1* or *HMGA2* rearrangements	*PLAG1* or *HMGA2* rearrangements can be seen in epithelial-myoepithelial carcinoma ex pleomorphic adenoma	Low to none
Prognosis	Excellent with complete excision	Good; recurrences and metastases are uncommon	–

9.3 Adenoid Cystic Carcinoma

It is the most common sinonasal malignancy after squamous cell carcinoma, representing 10–18% of all malignant sinonasal tumors [2, 4, 8]. The tumor preferentially arises in the maxillary sinus, followed by the nasal cavity [21, 22]. It is believed to arise from the minor mucoserous glands present below the respiratory epithelium of the nasal and sinonasal mucosae [23]. Unlike ACC of other salivary gland sites, neurological symptoms and pain are not common in patients with sinonasal ACC [8, 24, 25].

Histology

ACC is a biphasic neoplasm composed of a dual population of ductal and myoepithelial cells [9, 17]. The ductal (luminal) cells are cuboidal and typically show an eosinophilic cytoplasm with round nuclei. The myoepithelial cells are peripheral (abluminal), exhibiting indistinct cell borders with angulated nuclei and scant, clear or basophilic cytoplasm [17, 20]. The stroma is often hyalinized or can be myxoid. Three main architectural arrangements characterize ACC: tubular, cribriform, and solid [9] (Fig. 9.3 a–c). The presence of increased mitoses (≥5/10 high power fields) and/or any solid-type histology portends worse survival and should be mentioned in the report [8, 26]. In contrast to nonsinonasal ACC, perineural invasion is only present in 54.7% of sinonasal ACC (Fig. 9.3d) [8]. High-grade transformation represents an aggressive phenomenon with severe nuclear atypia, high mitotic activity, extensive comedonecrosis, and loss of the biphasic ductal/myoepithelial differentiation (Fig. 9.4a) [26–29].

Ancillary Testing

Apart for solid-predominant ACC, immunohistochemistry highlights the biphasic ductal and myoepithelial cells (Fig. 9.3 e, f). Considering that there is no specific marker for ACC, and that the immunostaining pattern can be variable, it is important to perform a panel of stains that includes ductal (pan-cytokeratin, EMA, CK5/6, and CD117) and myoepithelial/basal markers (p63,p40, SMA, S100, GFAP, and calponin). Despite being negative for high-risk HPV, p16 immunohistochemical stain can show misleading positivity [30].

Fusions involving *MYB* family, specifically its translocation t(6;9) *MYB*::*NFIB*, are the most frequent genetic events in ACC of all anatomic locations [30–37]. *MYB*::*NFIB* fusion gene has been reported in 60–90% of ACC overall and up to 62% of sinonasal ACC (Fig. 9.4b) [9, 26, 38]. Of note, MYB immunohistochemistry has been shown to lack both sensitivity and specificity for ACC Table 9.2 [8, 26].

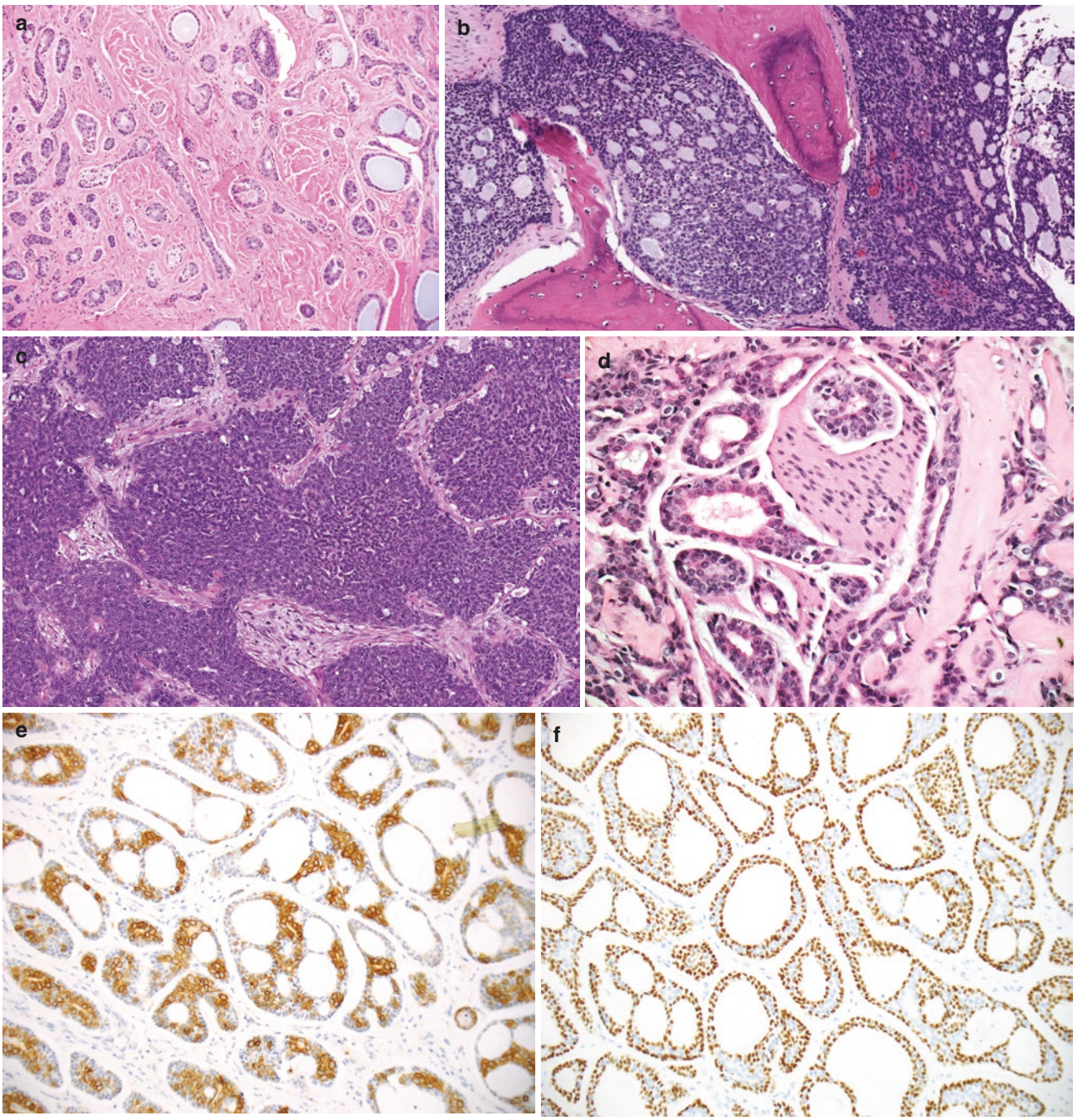

Fig. 9.3 (**a**) Adenoid cystic carcinoma(H&E, 10x): Adenoid cystic carcinoma with a predominantly tubular architecture consisting of duct-like structures depicted either perpendicularly or longitudinally depending on the plane of section. (**b**) Adenoid cystic carcinoma(H&E, 20x): Classic cribriform pattern of adenoid cystic carcinoma infiltrating bony trabeculae showing pseudocystic punched-out spaces filled with myxoid to hyaline basement membrane-like material. (**c**) Adenoid cystic carcinoma(H&E, 20x): Predominantly solid *MYB*-rearranged adenoid cystic carcinoma demonstrating loss of biphasic cellular differentiation and scarce luminal spaces. (**d**) Adenoid cystic carcinoma (H&E, 40x): Perineural invasion in adenoid cystic carcinoma showing evident biphasic populations. Cuboidal epithelial cells with scant eosinophilic cytoplasm are seen lining ductal spaces and are surrounded by myoepithelial cells with more abundant, pale cytoplasm and angulated hyperchromatic nuclei. (**e**) Adenoid cystic carcinoma (H&E, 40x): CD117, a ductal marker, stains the luminal ductal cells. (**f**) Adenoid cystic carcinoma (p63, 20x): p63 stains the outer abluminal myoepithelial cells

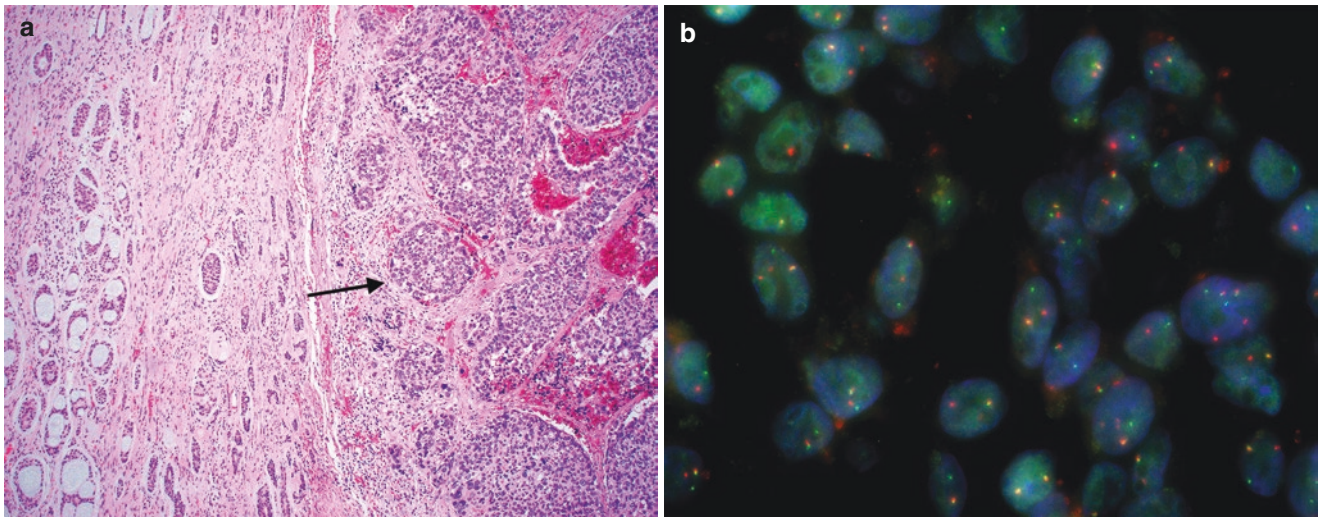

Fig. 9.4 (**a**) (H&E, 10x) shows high-grade transformation (arrow) in a cribriform patterned adenoid cystic carcinoma. (**b**) MYB gene break-apart on FISH. (Fig. 9.4a, b contributed by Justin Bishop)

Table 9.2 Immunohistochemical staining profile of adenoid cystic carcinoma

Immunohistochemical stain	Positive staining	Pattern of staining
Pan-cytokeratin	100%	Ductal and basal/ myoepithelial
CK7	100%	Ductal and basal/ myoepithelial
CK5/6	100%	Ductal and basal/ myoepithelial
EMA	95%	Focal ductal and basal/ myoepithelial
CD117	90%	Weak mostly ductal
S100	76%	Ductal and basal/ myoepithelial
p63	83%	Basal/myoepithelial
SMA	100%	Basal/myoepithelial
Calponin	83%	Basal/myoepithelial
GFAP	10%	Focal basal/myoepithelial

Differential Diagnosis

Sinonasal ACC may display a variety of morphologic appearances and can closely mimic several neoplasms, especially on small biopsy material. This is particularly true in solid ACC, where the tumor is basaloid and lacks the characteristic biphasic differentiation. In general, the differential diagnosis of sinonasal ACC is broad and includes many tumor entities, detailed in Table 9.3.

HPV-Related Multiphenotypic Sinonasal Carcinoma [39]

Initially called HPV-related carcinoma with adenoid cystic-like features, HPV-related multiphenotypic sinonasal carcinoma (HMSC) is a recently defined variant of sinonasal carcinoma that shows histologic features of ACC and has a strong association with high-risk HPV. The tumor is thought to have at least partial histologic and immunohistochemical salivary gland differentiation and is presumed to be exclusive to the sinonasal tract. Histologically, these tumors mimic the appearance of high-grade, predominantly solid ACC. The tumors typically grow in large lobules separated by thin fibrous bands and exhibit a mixture of myoepithelial, ductal, and squamous differentiation. The squamous component is represented by a dysplastic overlying squamous epithelium. The dysplasia is commonly accompanied by HPV signature "bizarre" cellular atypia with giant nuclei. Though the histologic and immunohistochemical features of this lesion vary broadly, one invariable defining feature is the presence of transcriptionally active high-risk HPV, most commonly HPV type 33. Therefore, reflex testing for p16 and high-risk HPV, i.e., high-risk HPV *in-situ* hybridization or polymerase chain reaction (PCR), can help confirm or infirm HMSC when faced with a sinonasal tumor exhibiting even focal high-grade "salivary like" features.

Treatment and Prognosis

ACC is characterized by relentless slow growth and a relatively elevated frequency of local and distal recurrences. While roughly 30% of patients develop distant metastases to the lungs and bones, nodal metastasis is not a common feature of sinonasal ACC.

Table 9.3 Key differences between adenoid cystic carcinoma and entities in the differential diagnosis [1, 3, 8, 9, 17, 20, 39–46]

	ACC	HMSC	Basaloid SCC	NUT carcinoma	ONB (High-grade)	SNUC	NEC (small cell or large cell types)	Sinonasal non-intestinal adenoca, high-grade
Definition and components	Biphasic salivary gland neoplasm with ductal and myoepithelial cell lines	Variable mixture of ductal and myoepithelial cells with dysplastic squamous surface epithelium	SCC variant with basaloid cells, may be high-risk HPV related	Genetically defined poorly differentiated carcinoma that often shows abrupt squamous differentiation	Malignant neoplasm arising from specialized sensory neuroepithelial olfactory cells	Highly aggressive undifferentiated carcinoma with no squamous or glandular differentiation	Heterogeneous group of malignant neoplasms with epithelial and neuroendocrine differentiation	Adenoca with no features of salivary gland tumors or intestinal-type adenoca
Tumor borders	Infiltrative, destructive growth	Infiltrative, destructive growth	Infiltrative, destructive growth	Infiltrative, destructive growth	Infiltrative, destructive growth	Infiltrative, widely destructive growth	Infiltrative, destructive growth	Infiltrative, destructive growth
Growth pattern	Classically tubular and cribriform with solid arrangement predominating in high-grade cases	Broad morphologic spectrum reminiscent of ACC: Most commonly solid, with large lobules and sheets separated by thin fibrous bands	• Typically grows in lobules and trabeculae • Can show growth patterns, myxoid stroma and BM-like material similar to ACC • Possible surface dysplasia	• Solid growth resembling poorly differentiated ACC • Abrupt squamous differentiation (absence of gradual differentiation)	• Lobules of cells with syncytial growth set in a fibrillary edematous neural matrix • Frequent pseudo and true rosettes • Sustentacular cells lining the lobules	Sheets and lobules of tumor cells lacking any squamous or glandular differentiation	• Various growth patterns including organoid, trabecular, ribbons, cribriform and solid patterns • Possible rosette formation	Usually arises from the mucosa and grow in a solid or sheet-like pattern
Cytomorphology	Isomorphic basaloid myoepithelial cells with angulated hyperchromatic nuclei surrounding scattered eosinophilic cuboidal ductal cells	• Similar to ACC except for more pronounced nuclear pleomorphism • Dysplastic overlying squamous epithelium shows bizarre atypia	Pleomorphic basaloid cells with peripheral palisading and abrupt squamous differentiation	• Monotonous small to medium-sized cells, with round to ovoid nuclei and clear to pale cytoplasm • Lack of significant pleomorphism	Small cells with scant cytoplasm, high N/C ratio, and uniform nuclei showing delicate, salt and pepper chromatin distribution	Pleomorphic cells with prominent nucleoli and scant cytoplasm	• Small cell NEC: Smaller cells with high N/C ratio, stippled (salt and pepper) chromatin and inconspicuous nucleoli • Large cell NEC: Larger cells with moderate amount of cytoplasm, and prominent nucleoli	High-grade cases have pleomorphic cells with eosinophilic to clear appearing cytoplasm

(continued)

Table 9.3 (continued)

	ACC	HMSC	Basaloid SCC	NUT carcinoma	ONB (High-grade)	SNUC	NEC (small cell or large cell types)	Sinonasal non-intestinal adenoca, high-grade
High-grade features	• Increased mitotic activity and necrosis, especially in high-grade cases • Frequent perineural invasion	Increased mitotic activity and necrosis	Increased mitotic activity with distinctive comedonecrosis	Can show increased mitotic activity and necrosis	Nuclear pleomorphism, mitoses, and necrosis present in high-grade tumors	Significantly increased mitotic activity (including atypical forms) with extensive necrosis and vascular invasion	• High mitotic rate, extensive necrosis, and apoptosis • Neurotropism and lymphovascular invasion common	Increased mitoses, necrosis, and perineural Invasion
Immunohistochemistry	Biphenotypic expression of luminal epithelial markers (e.g., CK7, C-kit) and abluminal myoepithelial markers (e.g., p40, p63, SMA, calponin, S100)	• Biphenotypic, as in ACC, with positive myoepithelial markers • Strong and diffuse p16 reactivity	• Diffuse positivity for squamous markers (p63/p40, CK5/6) • May show p16 positivity	• Positive staining for epithelial and squamous markers (CK-PAN, CK5/6, and p63) • Diffuse reactivity with antibodies to NUT protein	• Positive for neuroendocrine markers (chromogranin synaptophysin, CD56 and INSM1) and calretinin • S100 highlights peripheral sustentacular cells	• Positive for general epithelial markers • Negative for lineage-specific markers • Possible limited positivity for neuroendocrine markers • Potential staining for IDH2 IHC	• Dot-like positivity for cytokeratins • Strong and diffuse positivity for neuroendocrine markers (chromogranin synaptophysin, CD56, and INSM1)	• Positive for CK7 • Negative for CK20, CDX2, villin, and neuroendocrine markers • Possible limited S100 expression
Additional ancillary testing	*MYB*/*MYBL1*:: *NFIB* fusion	Positive for high-risk HPV *in-situ* hybridization/ PCR	Potentially positive for high-risk HPV *in-situ* hybridization/ PCR	Balanced chromosomal translocation t(15;19) resulting in BRD::NUTM1 oncogene	Chromosomal alterations of 19, 8q, 15q, 22q, 4q	Frequent *IDH2* mutations	Inactivating mutations in *TP53* and *RB1*	Not known
Most helpful in the differential diagnosis with ACC	Presence of *MYB* gene rearrangement	• Nuclear pleomorphism • Dysplastic surface • Positivity for p16 and high-risk HPV	• Nuclear pleomorphism • Squamous differentiation • Dysplastic surface • Potential positivity for p16 and high-risk HPV • Negative staining for myoepithelial markers	• Younger patient with midline presentation (classic cases) • Abrupt keratinization • Negative staining for myoepithelial markers • *NUT* gene rearrangement detected by IHC, FISH, or genetic testing	• Rosette formation • Positive staining for neuroendocrine markers and calretinin • Little to absent cytokeratin reactivity	• Nuclear pleomorphism • Lacks cribriform and tubular growth patterns, myxoid stroma, and basement membrane-like material deposition • Negative staining for myoepithelial markers	• Neuroendocrine chromatin distribution	• Nuclear pleomorphism

HMSC HPV-related multiphenotypic Sinonasal Carcinoma, *PA* Pleomorphic Adenoma, *EMCA* Epithelial-Myoepithelial Carcinoma, *MEC* Mucoepidermoid Carcinoma, *SCC* Squamous Cell Carcinoma, *SNUC* Sinonasal Undifferentiated Carcinoma, *ONB* Olfactory Neuroblastoma, *NEC* Neuroendocrine Carcinoma, *HMSC* HPV related Multiphenotypic Sinonasal Carcinoma, *adenoca* Adenocarcinoma, *N/C* Nuclear/Cytoplasmic, *BM* Basement Membrane, *IHC* Immunohistochemistry, *FISH* Fluorescence *In-Situ* Hybridization

9.4 Mucoepidermoid Carcinoma

While mucoepidermoid carcinomas (MEC) constitute the most frequent salivary gland tumor subtype in head and neck anatomic sites such as the oral cavity and the oropharynx, they account for only 8% of salivary gland tumors in the sinonasal cavity [3, 7]. Overall, sinonasal MECs account for less than 0.1% of all malignant sinonasal tract neoplasms and have a predilection for the nasal cavity [7]. Macroscopically, MEC presents as an unencapsulated, variably circumscribed mass with frequent cystic change [9]. High-grade tumors tend to be solid with foci of hemorrhage and necrosis.

Histology

Sinonasal MECs are invasive by definition, even in cases that demonstrate a relatively well-demarcated periphery [7]. They are predominantly composed of a variable mixture of epidermoid, mucous, and intermediate-type cells (Fig. 9.5a, b) [1]. They rarely show keratin pearl formation or dyskeratosis unless if adjacent to a previous biopsy or FNA site [1, 47]. Mucous cells (mucocytes) classically consist of a goblet-shaped cells with a small nucleus that is compressed to the side by abundant foamy to clear cytoplasm. Though mucocytes are present by definition, they can sometimes be so scanty that their identification requires the use of mucin stains such as mucicarmine or Alcian blue (Fig. 9.6a) [1, 7]. Intermediate cells are thought to represent a histologically uncommitted population of cells between small cuboidal basal cells and large polygonal epidermoid cells (Fig. 9.5b) [7, 17, 47]. Worth mentioning, focal to generalized oncocytic metaplasia resulting in the oncocytic variant of MEC is occasionally seen.

Ancillary Testing

Sinonasal MEC shows a similar immunohistochemical staining profile to that arising in major salivary glands [7]. Pankeratin, CK5/6, p40, and p63 typically show diffuse reactivity, while CEA and CK20 immunoreactivity is only noted in mucocytes (Fig. 9.6b) [7]. Though MEC is typically negative for myoepithelial markers, e.g., S100, SOX10, SMA, and calponin, few studies have reported focal expression of S100 [48]. In regard to cytogenetic and genomic testing, MEC is associated with translocations involving the *MAML2* and *CRTC1* or *CRTC3* genes. Detection of a *MAML2* rearrangement using break-apart FISH probes is helpful in confirming the diagnosis of MEC and ruling out other neoplasms in the differential diagnosis (Fig. 9.6c).

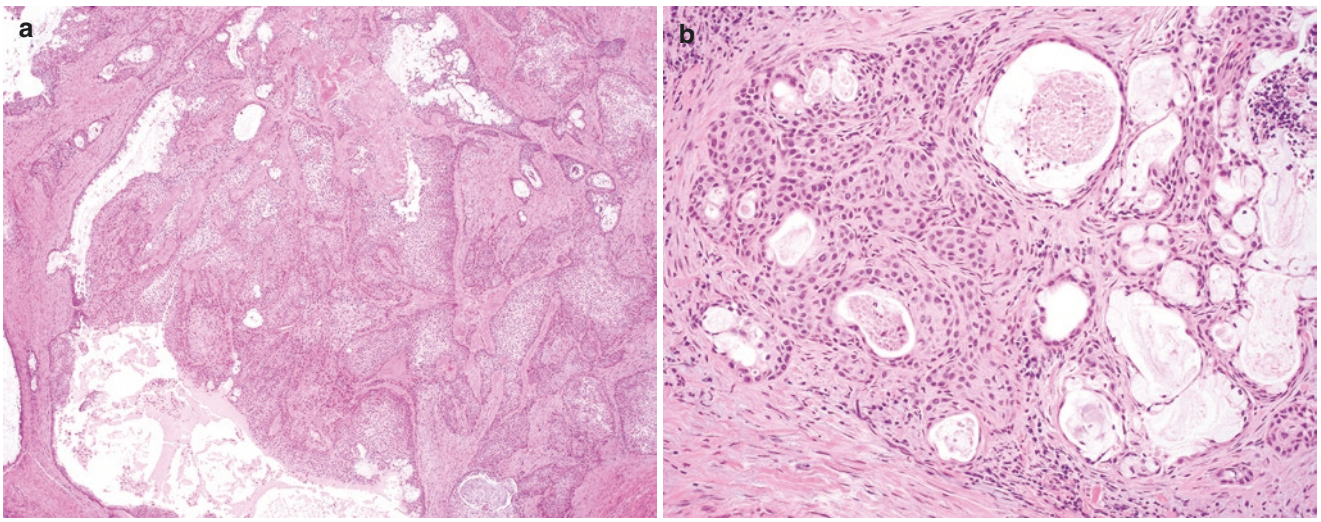

Fig. 9.5 (**a**) Mucoepidermoid carcinoma(H&E, 10x): Mucoepidermoid carcinoma imparts a low-power impression of a carcinoma with mixed squamoid and glandular features. Overt squamous differentiation and keratinization are not seen. (**b**) Mucoepidermoid carcinoma(H&E, 20x): The epidermoid cells of mucoepidermoid carcinoma are recognizable based on their abundant eosinophilic cytoplasm and distinct polygonal cell borders (center of the figure). Mucocytes can often be seen lining cystic spaces filled with mucin (right part of figure). Intermediate cells range in appearance from small, basal cells with scanty basophilic cytoplasm to larger, oval cells, with more abundant eosinophilic cytoplasm

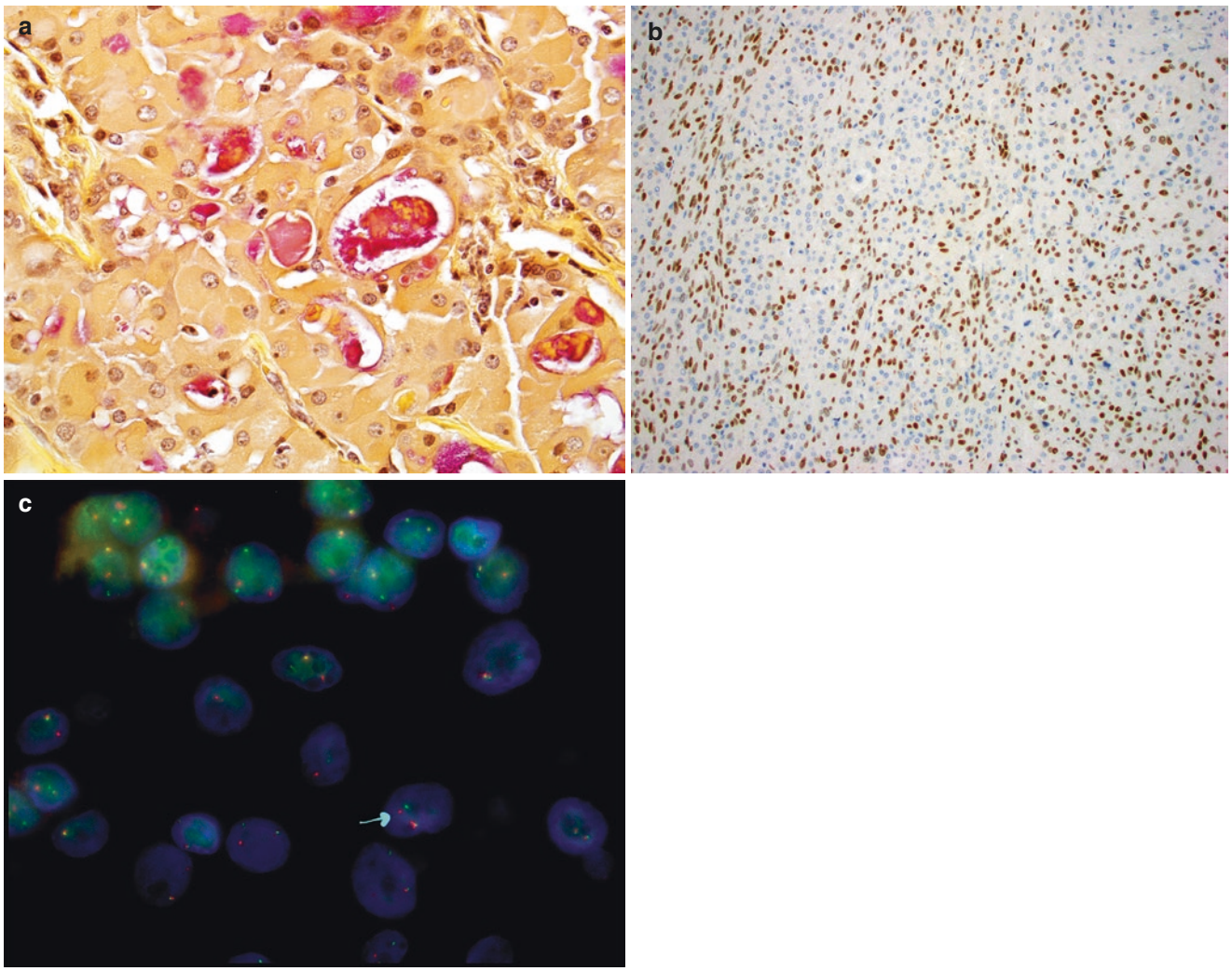

Fig. 9.6 (**a**) Mucicarmine stains positive in mucous cells. (**b**) p40 shows positivity in epidermoid cells. (**c**) MAML2 gene break-apart (arrow) on FISH. (Fig. 9.6a–c contributed by Justin Bishop)

Differential Diagnosis

Necrotizing sialometaplasia (NS) can mimic MEC by showing squamous proliferation with foci of mucocytic differentiation [1]. NS, however, has a lobular distribution, no demonstrable invasion and usually shows areas of transition from the ducts to the solid islands of squamous cells formed by intraductal regenerative hyperplasia (Fig. 9.7a) [1, 7]. High-grade MEC may also resemble nonkeratinizing SCC [1]. This differential is particularly relevant in the sinonasal cavity, where SCC constitutes the most prevalent malignancy [4]. Mucin stains can demonstrate the presence of scattered mucocytes. In addition, significant cytologic atypia, as well as well-defined "squamous" differentiation with overt keratinization (i.e., intercellular bridges, single cell keratinization, dyskeratosis, and keratin pearl formation) are not features of MEC [1, 7, 20]. Adenosquamous carcinoma (ASCC) can also mimic MEC considering that it also displays a mixture of squamoid and mucinous cells (Fig. 9.7b). A diagnosis of MEC can usually be reached based on the presence of blended cell types (epidermoid, mucous, and intermediate) rather than that of a distinct biphasic process seen in ASCC [7]. As for conventional SCC, the presence of overt squamous differentiation and nuclear pleomorphism favor the diagnosis of ASCC over that of MEC [7].

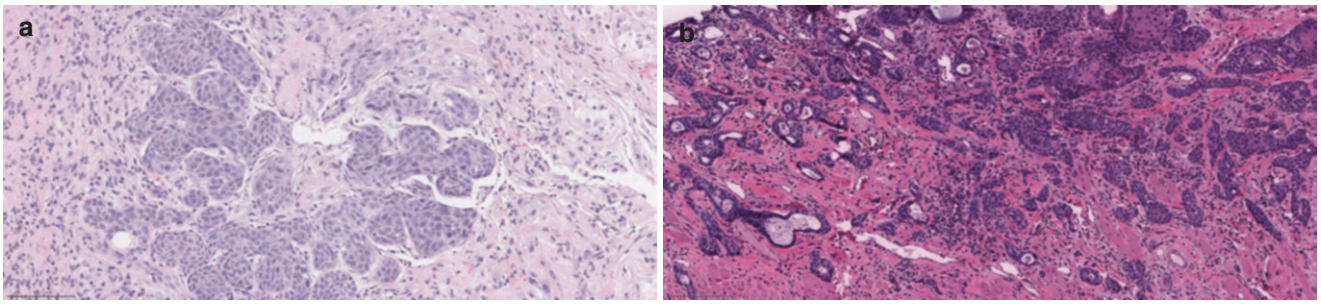

Fig. 9.7 (**a**) A case of sialometaplasia for comparison. (**b**) Adenosquamous carcinoma with squamous and glandular differentiation

Treatment and Prognosis

Wide excision with clear margins is usually the sole treatment of choice in sinonasal MEC, as the benefit of radiation therapy has yet to be demonstrated [7]. Recurrences develop in about one-third of patients, usually within 2 years [7]. Nodal metastases are more common in MEC than in ACC [7]. The 5-year survival for sinonasal MEC approximates 50% [49].

9.5 Others

Several other rarer subtypes of salivary gland tumors have been reported in the sinonasal tract. Some of these entities have an incidence rate that does not exceed that of a few case reports.

9.5.1 Polymorphous Adenocarcinoma

Polymorphous adenocarcinoma (PAC) is a rare salivary gland adenocarcinoma known to occur predominantly in minor salivary glands [17, 50]. A distinctive type of cribriform adenocarcinoma of minor salivary gland (CAMSG) has recently been included under the subheading of PAC which mostly occur in tongue.

Histology

As the name implies, PAC is characterized by a diversity of growth patterns that comprise fascicles, cords, tubules, trabeculae, pseudo-cribriform aggregates (due to the presence of true lumina), solid and "Indian-file" arrangements (Fig. 9.8a) [50, 51]. Typical features include a targetoid concentric growth around vessels and nerves and a blue-gray myxoid fibrous/hyalinized stroma (Fig. 9.8b) [51]. CAMSG, on the other hand, typically shows architectural uniformity with predominant cribriform and solid growth patterns (Fig. 9.9 a, b) [50].

Ancillary Testing

Both PAC and CAMSG have a similar immunohistochemical staining pattern characterized by reactivity for CK-PAN, S100, EMA, and CD117 [17]. PAC is also aberrantly positive for p63 while negative for p40, the latter being a more specific marker of basal and myoepithelial cells (Fig. 9.10 a–c) [52]. On the genomic front, PACs are characterized by hotspot point (E710D) mutations in the *PRKD1* gene, whereas CAMSGs are characterized by *PRKD1–3* translocation.

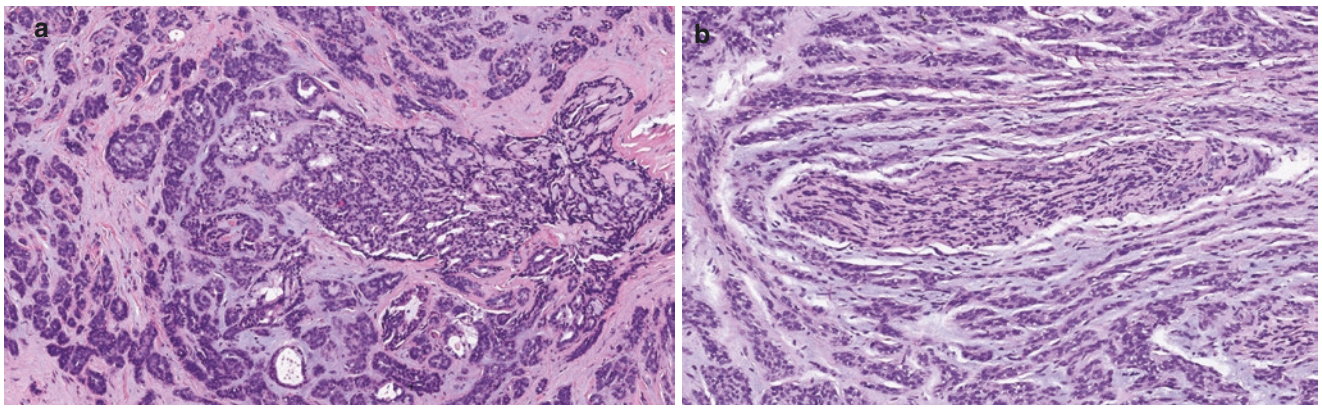

Fig. 9.8 (**a**) Polymorphous adenocarcinoma (H&E, 20x): Infiltrative salivary gland tumor showing diverse architectural growth patterns including fascicles, tubules, trabeculae, and pseudo-cribriform aggregates and belonging to the phenotypic spectrum of polymorphous adenocarcinoma. (**b**) Polymorphous adenocarcinoma (H&E, 20x): Classic targetoid concentric layering of tumor cells around nerves

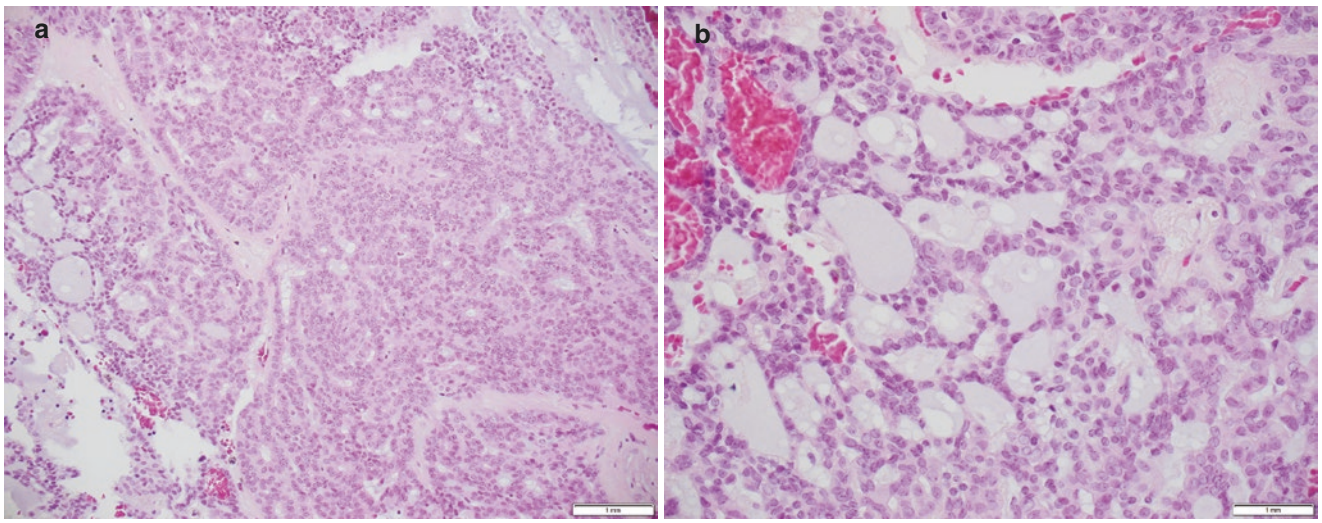

Fig. 9.9 (**a, b**) Cribriform adenocarcinoma of minor salivary gland to show predominantly cribriform arrangement

Differential Diagnosis

PAC has overlapping histologic features with cellular pleomorphic adenoma, considering both entities can show architectural diversity with a focally mucohyaline stroma [17, 52]. Fragmented and limited diagnostic material makes it difficult to distinguish between these two entities [48]. The presence of infiltrative borders and perineural invasion establishes the diagnosis of PAC over that of PA [17]. Both PAC and CAMSG can mimic adenoid cystic carcinoma [17]. Features in favor of ACC include the presence of angulated, hyperchromatic nuclei, the absence of a mucohyaline matrix, the presence of increased mitotic activity, and evidence of a dual cell population with immunohistochemical evidence of true myoepithelial differentiation [17, 20]. In addition, negative p40 immunostaining is a potential argument in favor of a PAC over that of both PA and ACC [52].

Treatment and Prognosis

Due to the infiltrative nature of PAC and its propensity for perineural invasion, patients usually have positive margins, even after radical resection [50]. The standard treatment comprises wide surgical excision, often with adjuvant radiotherapy [51]. While PAC only rarely metastasizes, CAMSG tends to be more aggressive and often shows metastases to the neck lymph nodes [51].

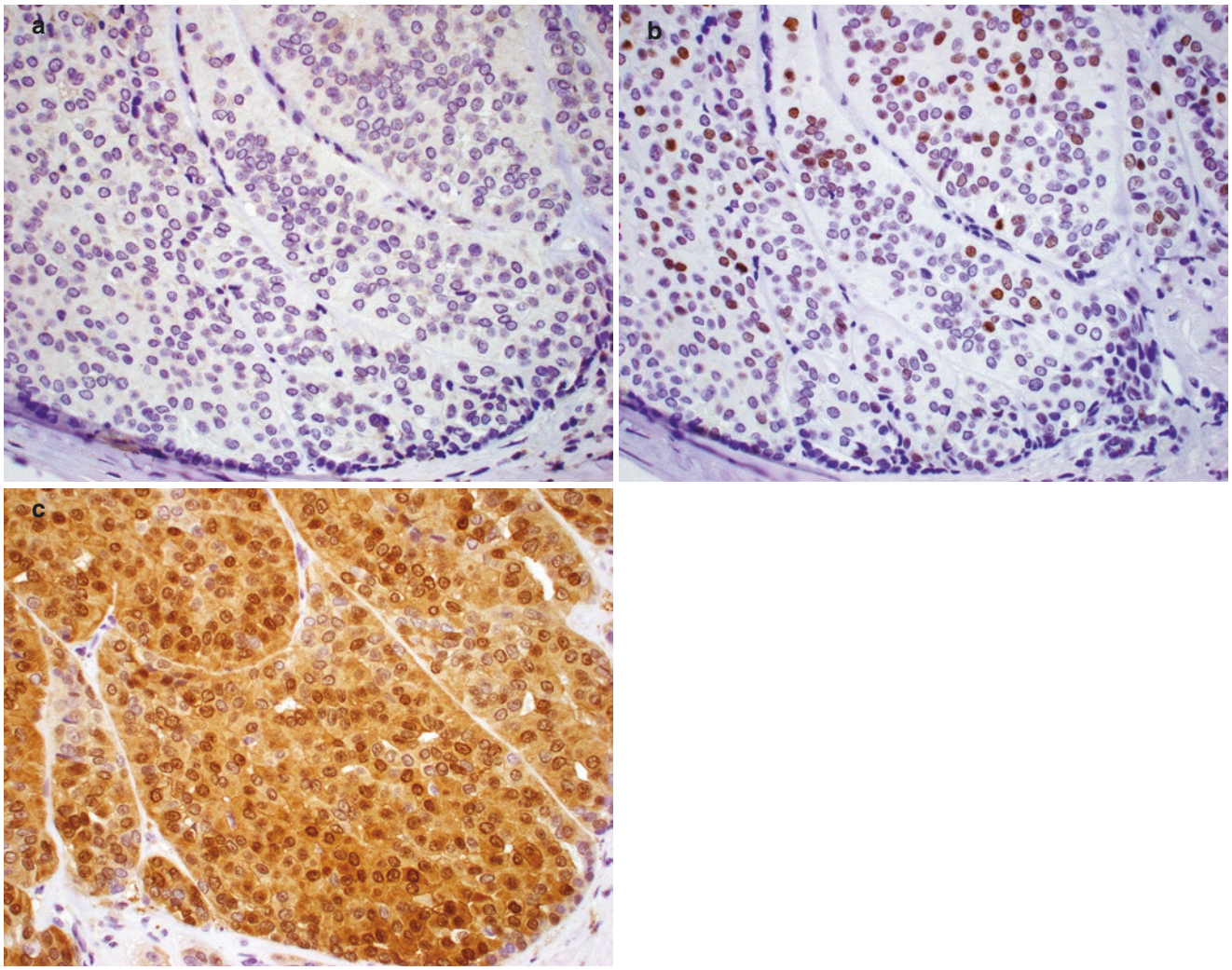

Fig. 9.10 (**a–c**) Polymorphous adenocarcinoma negative for p40 (**a**) whereas positive for p63 (**b**) and S-100 (**c**). (Fig. 9.10a–c contributed by Justin Bishop)

9.5.2 Epithelial-Myoepithelial Carcinoma

Sinonasal epithelial-myoepithelial carcinoma (EMCA) is exceedingly rare, with around 20 cases described in the literature [18]. The tumor shows a slight female preponderance with a mean age of occurrence estimated at 60 years [19, 53]. Most of the reported sinonasal EMCAs were centered in the maxillary sinus, with only anecdotal cases arising in the nasal cavity and frontoethmoidal sinus [18, 54, 55]. Most EMCAs are thought to have arisen from a preexisting PA (up to 80% of cases) [56]. Although rare high-grade cases have been reported, EMCAs are classically low-grade tumors that typically feature in the differential diagnosis with pleomorphic adenoma [18, 56].

Histology

EMCAs typically display a characteristic multinodular growth pattern and a pushing invasion front that could be mistaken for a noninvasive well-circumscribed border, especially on limited diagnostic material [19]. Most tumors show a classic biphasic tubular histology (Fig. 9.11a). The tubular structures are formed by an inner, single layer of epithelial cells lining the lumens and surrounded by a variable number of myoepithelial cells often showing cytoplasmic clearing (Fig. 9.11b) [20, 54]. Less common histologic features include oncocytic metaplasia, spindle cell myoepithelial overgrowth, and anaplasia with transformation to high-grade carcinoma (Fig. 9.12 a–c) [19, 55].

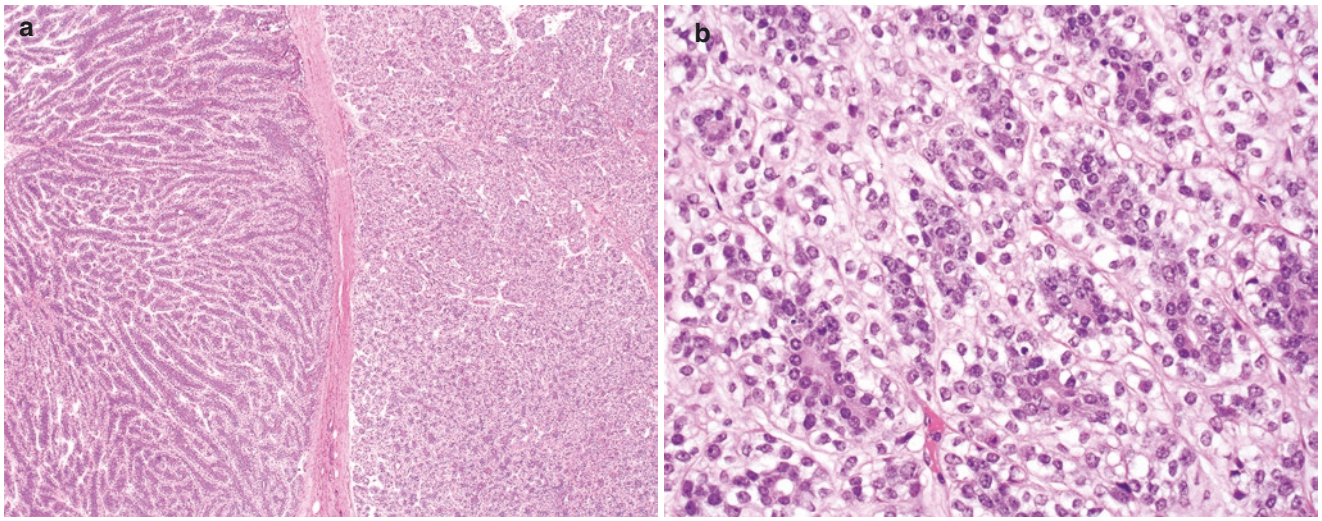

Fig. 9.11 (**a**) Epithelial-myoepithelial carcinoma (H&E, 10x): Multinodular growth of epithelial-myoepithelial carcinoma. (**b**) Epithelial-myoepithelial carcinoma (H&E, 20x): Epithelial-myoepithelial carcinoma shows a classic biphasic tubular histology consisting of an inner layer of cuboidal ductal cells with eosinophilic cytoplasm surrounded by outer myoepithelial cells with clear cytoplasm

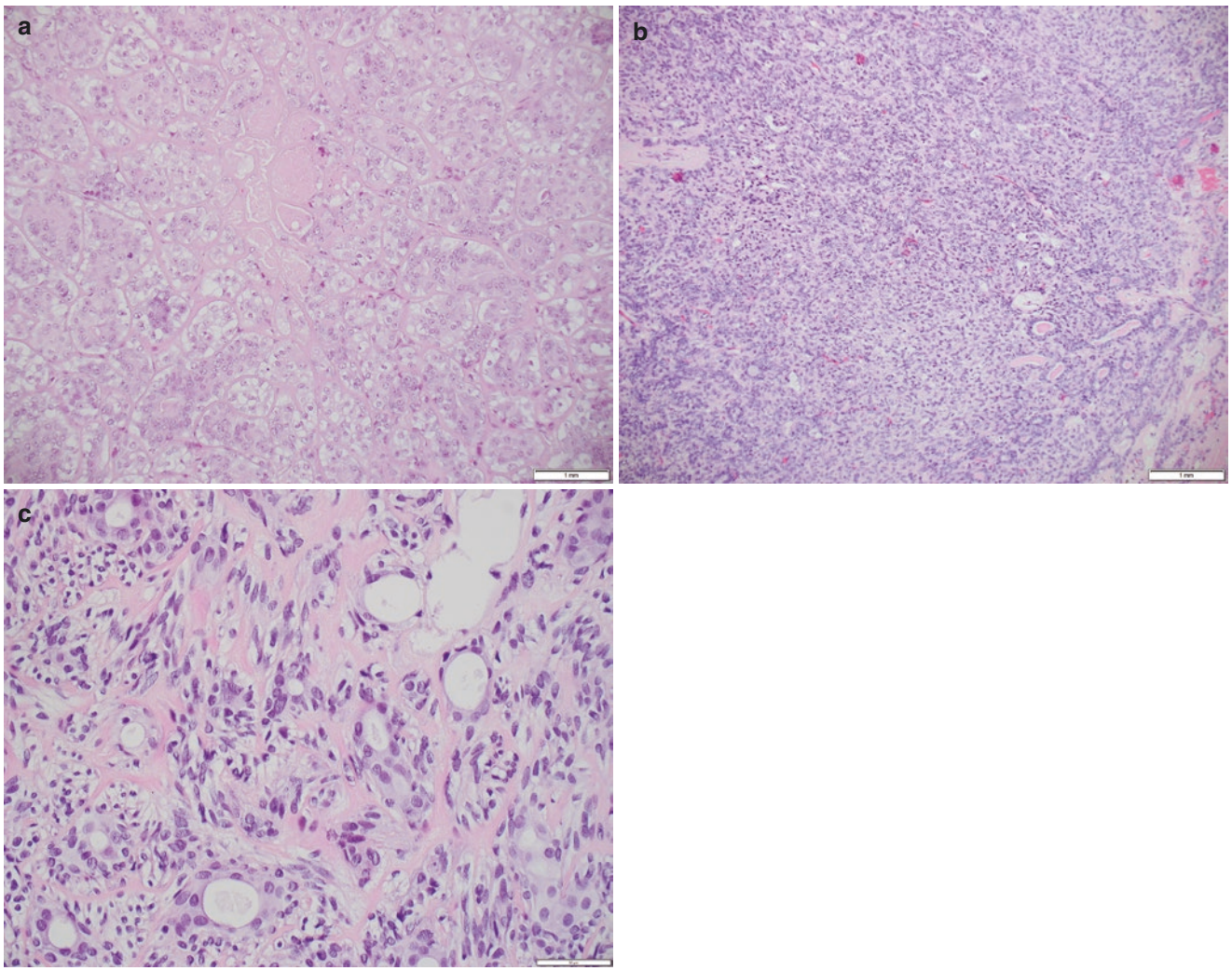

Fig. 9.12 (**a–c**) Epithelial-myoepithelial carcinoma with high-grade transformation in the form of nuclear atypia and necrosis (**a**), myoepithelial overgrowth (**b**), and spindling of tumor cells (**c**)

Ancillary Testing

Immunohistochemistry highlights the biphasic epithelial and myoepithelial constituents of EMCA: the luminal cells are positive for epithelial ductal markers such as CK7 and EMA, while the abluminal cells are immunoreactive for myoepithelial markers such as calponin, SMA, S-100, and p63 [54, 55]. *PLAG1* and *HMGA2* rearrangements are the most common genetic events in EMCA, reflecting the high rate of cases that originated from a preexisting PA (EMCA ex-PA) [56]. De novo carcinomas are negative for *PLAG1* and *HMGA2* [57].

Differential Diagnosis

The histological differential diagnosis of EMCA is mainly with pleomorphic adenoma (PA), the tubular variant of adenoid cystic carcinoma (ACC), and metastatic renal cell carcinoma [53, 54]. While the similarity with the first two entities consists of the double-layered, duct-like arrangement of epithelial and myoepithelial cells, the similarity with metastatic renal cell carcinoma lies in the cytoplasmic clearing that is common to both tumors [17].

Treatment and Prognosis

The treatment of EMCA is essentially surgical, considering that patients who underwent radiotherapy had no apparent added survival benefit [54, 58]. EMCA is typically a low-grade neoplasm that follows a relatively indolent clinical course with good prognosis.

9.5.3 Hyalinizing Clear Cell Carcinoma

Hyalinizing clear cell carcinoma (HCCC) is a rare, low-grade salivary gland tumor characteristically composed of a monomorphous population of clear cells that form cords and nests in a hyalinized stroma [59]. By definition, the tumor displays a squamoid phenotype and lacks features of other clear cell-rich salivary gland carcinomas [9]. It preferentially affects women in their fifth to eighth decade of life, and has a predilection to intraoral sites [9, 60]. Rare cases of primary HCCC confirmed to have the characteristic *EWSR1*::*ATF1* fusion have been reported to arise from the sinonasal tract [59, 60]. The tumor shows infiltrative borders, at least focally, and can show perineural invasion [17]. They typically display polygonal to round cells arranged in nests and separated by a hyalinized fibrous stroma (Fig. 9.13a) [60]. The cells have clear to lightly eosinophilic cytoplasm [9] (Fig. 9.13b). Mitotic figures and necrosis are uncommon [17]. Considering the presence of clear cells, immunohistochemical studies are needed to exclude myoepithelial differentiation as well as sinonasal renal cell-like adenocarcinoma [59]. HCCCs are positive for cytokeratins, p63, and p40 while negative for other myoepithelial markers (Fig. 9.14a, b) [9]. The tumor is classically a low-grade malignancy associated with an excellent prognosis after complete surgical excision.

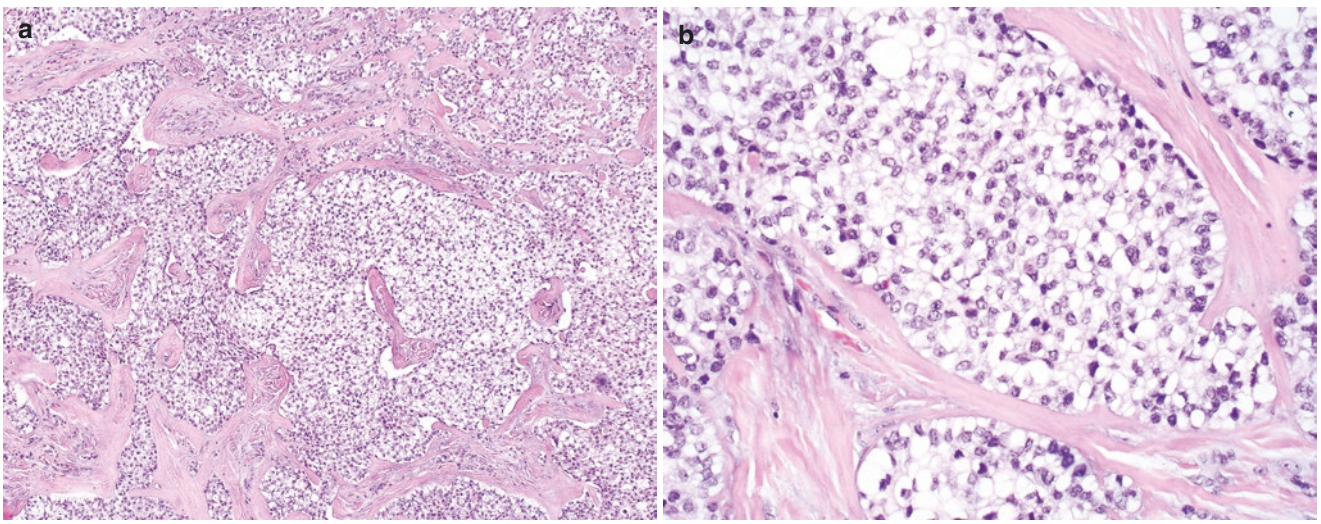

Fig. 9.13 (**a**) Hyalinizing clear cell carcinoma (H&E, 10x): Hyalinizing clear cell carcinoma arranged in interconnecting cords and trabeculae separated by a densely hyalinized stroma. (**b**) Hyalinizing clear cell carcinoma (H&E, 20x): High power examination shows a monotonous population of epithelial cells with abundant clear cytoplasm, well-defined borders, and eccentric nuclei

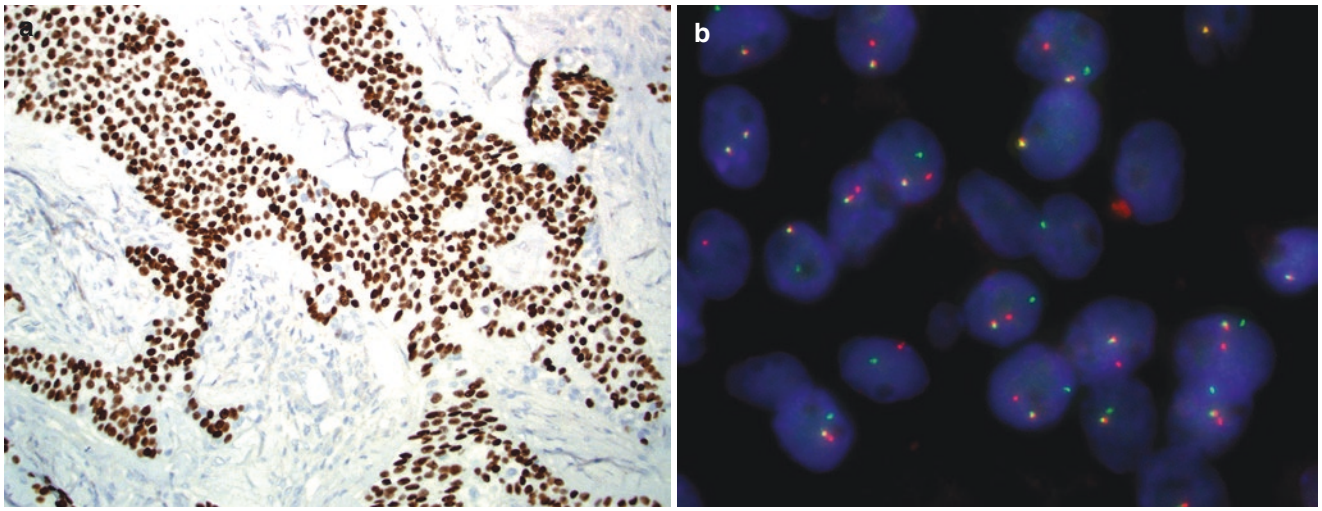

Fig. 9.14 (**a**) p40 is diffusely positive in HCCC. (**b**) *EWSR1* gene rearrangement on FISH. (Fig. 9.14 a, b contributed by Justin Bishop)

9.5.4 Salivary Duct Carcinoma

Salivary duct carcinoma (SDC) is exceedingly rare as a primary sinonasal tract malignancy. The tumor histologically resembles high-grade mammary duct carcinoma, frequently showing cribriform, papillary, or solid growth patterns, often with comedonecrosis [9, 61]. The tumor cells typically display apocrine features with abundant eosinophilic cytoplasm, large pleomorphic nuclei and conspicuous nucleoli (Fig. 9.15a) [9, 17]. Immunohistochemically, the tumor is characterized by strong and diffuse androgen receptor (AR) expression paired with positive staining for GATA3 or GCDFP-15 (Fig. 9.15b) [62]. CK5/6, p63, and p40 are negative [17, 63]. A subset of cases show human epidermal growth factor receptor 2 (HER2) overexpression by immunohistochemistry or HER2 amplification using FISH [62]. Evaluation of AR and HER2 status is needed to help guide treatment strategies [62, 64]. SDC is notorious for its high recurrence rate, aggressive local behavior, and poor prognosis [62, 65].

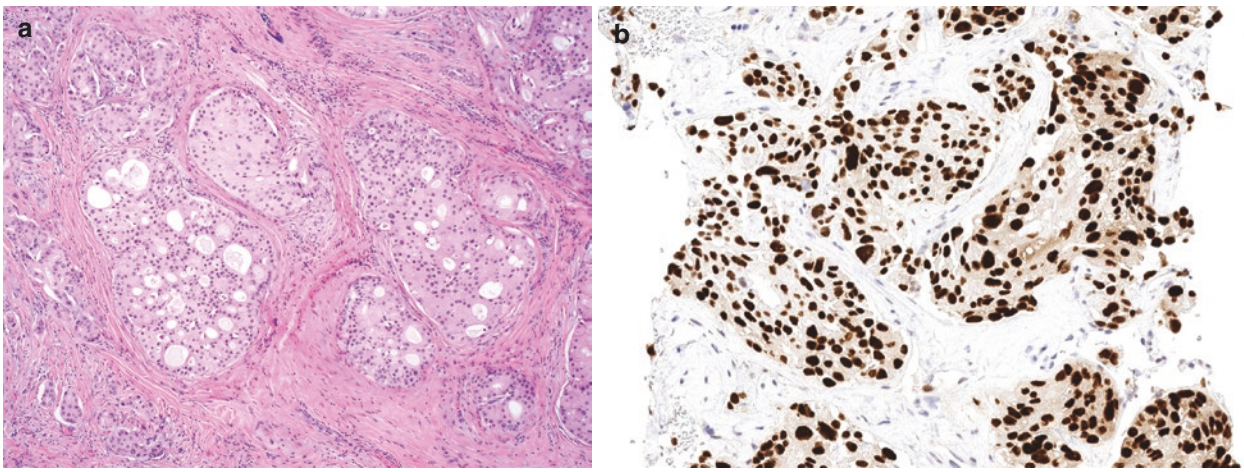

Fig. 9.15 (**a**) Salivary duct carcinoma (H&E, 10x): Salivary duct carcinoma is typically arranged in glandular and cribriform patterns with roman bridges reminiscent of those seen in mammary duct carcinoma. The tumor cells show characteristic apocrine features consisting of cells with abundant deeply eosinophilic cytoplasm. (**b**) Salivary duct carcinoma (Androgen Receptor IHC, 20x): Positivity for androgen receptor is a consistent finding in salivary duct carcinoma

9.6 Conclusion

Salivary gland tumors of the sinonasal cavity are relatively rare. Overall, benign tumors are much less frequent than malignant neoplasms. Adenoid cystic carcinoma is, by far, the most common salivary gland carcinoma of the sinonasal tract. Characteristic morphology, immunohistochemistry, and molecular studies in selected cases help in establishing a correct diagnosis.

References

1. Thompson L. In: Goldblum JR, editor. Head and neck pathology. 2nd ed. Elsevier Saunders; 2012.
2. Pantvaidya GH, Vaidya AD, Metgudmath R, Kane SV, D'Cruz AK. Minor salivary gland tumors of the sinonasal region: results of a retrospective analysis with review of literature. Head Neck. 2012;34(12):1704–10.
3. Hay AJ, Migliacci J, Karassawa Zanoni D, McGill M, Patel S, Ganly I. Minor salivary gland tumors of the head and neck-memorial Sloan Kettering experience: incidence and outcomes by site and histological type. Cancer. 2019;125(19):3354–66.
4. Lupinetti AD, Roberts DB, Williams MD, Kupferman ME, Rosenthal DI, Demonte F, et al. Sinonasal adenoid cystic carcinoma: the M. D Anderson Cancer Center experience. Cancer. 2007;110(12):2726–31.
5. Haerle SK, Gullane PJ, Witterick IJ, Zweifel C, Gentili F. Sinonasal carcinomas: epidemiology, pathology, and management. Neurosurg Clin N Am. 2013;24(1):39–49.
6. da Cruz Perez DE, Pires FR, Lopes MA, de Almeida OP, Kowalski LP. Adenoid cystic carcinoma and mucoepidermoid carcinoma of the maxillary sinus: report of a 44-year experience of 25 cases from a single institution. J Oral Maxillofac Surg. 2006;64(11):1592–7.
7. Wolfish EB, Nelson BL, Thompson LD. Sinonasal tract mucoepidermoid carcinoma: a clinicopathologic and immunophenotypic study of 19 cases combined with a comprehensive review of the literature. Head Neck Pathol. 2012;6(2):191–207.
8. Thompson LD, Penner C, Ho NJ, Foss RD, Miettinen M, Wieneke JA, et al. Sinonasal tract and nasopharyngeal adenoid cystic carcinoma: a clinicopathologic and immunophenotypic study of 86 cases. Head Neck Pathol. 2014;8(1):88–109.
9. El-Naggar AK, Chan JKC, Rubin Grandis J, Takata T, Slootweg PJ, International Agency for Research on C. WHO classification of head and neck tumours 2017.
10. Nagao T, Sato E, Inoue R, Oshiro H, Takahashi RH, Nagai T, et al. Immunohistochemical analysis of salivary gland tumors: application for surgical pathology practice. Acta Histochem Cytochem. 2012;45(5):269–82.
11. Lopes MA, Santos GC, Kowalski LP. Multivariate survival analysis of 128 cases of oral cavity minor salivary gland carcinomas. Head Neck. 1998;20(8):699–706.
12. Strick MJ, Kelly C, Soames JV, McLean NR. Malignant tumours of the minor salivary glands--a 20 year review. Br J Plast Surg 2004;57(7):624–631.
13. Tran L, Sidrys J, Horton D, Sadeghi A, Parker RG. Malignant salivary gland tumors of the paranasal sinuses and nasal cavity. The UCLA experience. Am J Clin Oncol. 1989;12(5):387–92.
14. Spiro RH, Huvos AG, Strong EW. Adenoid cystic carcinoma of salivary origin. A clinicopathologic study of 242 cases. Am J Surg. 1974;128(4):512–20.
15. Li W, Lu H, Zhang H, Lai Y, Zhang J, Ni Y, et al. Sinonasal/nasopharyngeal pleomorphic adenoma and carcinoma ex pleomorphic adenoma: a report of 17 surgical cases combined with a literature review. Cancer Manag Res. 2019;11:5545–55.
16. Nonitha S, Yogesh TL, Nandaprasad S, Maheshwari BU, Mahalakshmi IP, Veerabasavaiah BT. Histomorphological comparison of pleomorphic adenoma in major and minor salivary glands of oral cavity: a comparative study. J Oral Maxillofac Pathol. 2019;23(3):356–62.
17. Thompson LDR, Wenig BM. Diagnostic pathology: head and neck. 2nd ed. Elsevier; 2016.
18. Schuman TA, Kimple AJ, Edgerly CH, Ebert CS, Zanation AM, Thorp BD. Sinonasal epithelial-myoepithelial carcinoma: report of a novel subsite and review of the literature. Allergy Rhinol (Providence). 2018;9:2152656718764229.

19. Seethala RR, Barnes EL, Hunt JL. Epithelial-myoepithelial carcinoma: a review of the clinicopathologic spectrum and immunophenotypic characteristics in 61 tumors of the salivary glands and upper aerodigestive tract. Am J Surg Pathol. 2007;31(1):44–57.
20. Westra WH, Bishop JA. In: Epstein JI, editor. Head and Neck. 1st ed. Lippincott Williams & Wilkins; 2016.
21. Trope M, Triantafillou V, Kohanski MA, Kuan EC, Tong CCL, Patel NN, et al. Adenoid cystic carcinoma of the sinonasal tract: a review of the national cancer database. Int Forum Allergy Rhinol. 2019;9(4):427–34.
22. Unsal AA, Chung SY, Zhou AH, Baredes S, Eloy JA. Sinonasal adenoid cystic carcinoma: a population-based analysis of 694 cases. Int Forum Allergy Rhinol. 2017;7(3):312–20.
23. Gnepp DR, Heffner DK. Mucosal origin of sinonasal tract adenomatous neoplasms. Mod Pathol. 1989;2(4):365–71.
24. Rhee CS, Won TB, Lee CH, Min YG, Sung MW, Kim KH, et al. Adenoid cystic carcinoma of the sinonasal tract: treatment results. Laryngoscope. 2006;116(6):982–6.
25. Pommier P, Liebsch NJ, Deschler DG, Lin DT, McIntyre JF, Barker FG 2nd, et al. Proton beam radiation therapy for skull base adenoid cystic carcinoma. Arch Otolaryngol Head Neck Surg. 2006;132(11):1242–9.
26. Xu B, Drill E, Ho A, Ho A, Dunn L, Prieto-Granada CN, et al. Predictors of outcome in adenoid cystic carcinoma of salivary glands: a Clinicopathologic study with correlation between MYB fusion and protein expression. Am J Surg Pathol. 2017;41(10):1422–32.
27. Seethala RR, Hunt JL, Baloch ZW, Livolsi VA, Leon BE. Adenoid cystic carcinoma with high-grade transformation: a report of 11 cases and a review of the literature. Am J Surg Pathol. 2007;31(11):1683–94.
28. Cheuk W, Chan JK, Ngan RK. Dedifferentiation in adenoid cystic carcinoma of salivary gland: an uncommon complication associated with an accelerated clinical course. Am J Surg Pathol. 1999;23(4):465–72.
29. Hellquist H, Skálová A, Barnes L, Cardesa A, Thompson LD, Triantafyllou A, et al. Cervical lymph node metastasis in high-grade transformation of head and neck adenoid cystic carcinoma: a collective international review. Adv Ther. 2016;33(3):357–68.
30. Antony VM, Kakkar A, Sikka K, Thakar A, Deo SVS, Bishop JA, Jain D. p16 Immunoexpression in sinonasal and nasopharyngeal adenoid cystic carcinomas: a potential pitfall in ruling out HPV-related multiphenotypic sinonasal carcinoma. Histopathology. 2020;77(6):989–93.
31. Persson M, Andrén Y, Mark J, Horlings HM, Persson F, Stenman G. Recurrent fusion of MYB and NFIB transcription factor genes in carcinomas of the breast and head and neck. Proc Natl Acad Sci U S A. 2009;106(44):18740–4.
32. Brill LB 2nd, Kanner WA, Fehr A, Andrén Y, Moskaluk CA, Löning T, et al. Analysis of MYB expression and MYB-NFIB gene fusions in adenoid cystic carcinoma and other salivary neoplasms. Mod Pathol. 2011;24(9):1169–76.
33. Persson M, Andrén Y, Moskaluk CA, Frierson HF Jr, Cooke SL, Futreal PA, et al. Clinically significant copy number alterations and complex rearrangements of MYB and NFIB in head and neck adenoid cystic carcinoma. Genes Chromosomes Cancer. 2012;51(8):805–17.
34. Ho AS, Kannan K, Roy DM, Morris LG, Ganly I, Katabi N, et al. The mutational landscape of adenoid cystic carcinoma. Nat Genet. 2013;45(7):791–8.
35. Nordkvist A, Mark J, Gustafsson H, Bang G, Stenman G. Non-random chromosome rearrangements in adenoid cystic carcinoma of the salivary glands. Genes Chromosomes Cancer. 1994;10(2):115–21.
36. Brayer KJ, Frerich CA, Kang H, Ness SA. Recurrent fusions in MYB and MYBL1 define a common, transcription factor-driven oncogenic pathway in salivary gland adenoid cystic carcinoma. Cancer Discov. 2016;6(2):176–87.
37. Mitani Y, Liu B, Rao PH, Borra VJ, Zafereo M, Weber RS, et al. Novel MYBL1 gene rearrangements with recurrent MYBL1-NFIB fusions in salivary adenoid cystic carcinomas lacking t(6;9) translocations. Clin Cancer Res. 2016;22(3):725–33.
38. Moskaluk CA. Adenoid cystic carcinoma: clinical and molecular features. Head Neck Pathol. 2013;7(1):17–22.
39. Bishop JA, Andreasen S, Hang JF, Bullock MJ, Chen TY, Franchi A, et al. HPV-related multiphenotypic Sinonasal carcinoma: an expanded series of 49 cases of the tumor formerly known as HPV-related carcinoma with adenoid cystic carcinoma-like features. Am J Surg Pathol. 2017;41(12):1690–701.
40. Wieneke JA, Thompson LD, Wenig BM. Basaloid squamous cell carcinoma of the sinonasal tract. Cancer. 1999;85(4):841–54.
41. Thompson LD. Olfactory neuroblastoma. Head Neck Pathol. 2009;3(3):252–9.
42. Dogan S, Chute DJ, Xu B, Ptashkin RN, Chandramohan R, Casanova-Murphy J, et al. Frequent IDH2 R172 mutations in undifferentiated and poorly-differentiated sinonasal carcinomas. J Pathol. 2017;242(4):400–8.
43. Dogan S, Frosina D, Fayad M, de Oliveira TB, Alemar B, Rosenblum M, et al. The role of a monoclonal antibody 11C8B1 as a diagnostic marker of IDH2-mutated sinonasal undifferentiated carcinoma. Mod Pathol. 2019;32(2):205–15.
44. DeMonte F, Ginsberg LE, Clayman GL. Primary malignant tumors of the sphenoidal sinus. Neurosurgery. 2000;46(5):1084–91. discussion 91–2
45. Vedrine PO, Thariat J, Merrot O, Percodani J, Dufour X, Choussy O, et al. Primary cancer of the sphenoid sinus--a GETTEC study. Head Neck. 2009;31(3):388–97.
46. Rickman DS, Beltran H, Demichelis F, Rubin MA. Biology and evolution of poorly differentiated neuroendocrine tumors. Nat Med. 2017;23(6):664–73.
47. Coca-Pelaz A, Rodrigo JP, Triantafyllou A, Hunt JL, Rinaldo A, Strojan P, et al. Salivary mucoepidermoid carcinoma revisited. Eur Arch Otorhinolaryngol. 2015;272(4):799–819.
48. Zhu S, Schuerch C, Hunt J. Review and updates of immunohistochemistry in selected salivary gland and head and neck tumors. Arch Pathol Lab Med. 2015;139(1):55–66.
49. Triantafillou V, Maina IW, Kuan EC, Kohanski MA, Tong CC, Patel NN, et al. Sinonasal mucoepidermoid carcinoma: a review of the national cancer database. Int Forum Allergy Rhinol. 2019;9(9):1046–53.
50. Mimica X, Katabi N, McGill MR, Hay A, Zanoni DK, Shah JP, et al. Polymorphous adenocarcinoma of salivary glands. Oral Oncol. 2019;95:52–8.
51. Vander Poorten V, Triantafyllou A, Skálová A, Stenman G, Bishop JA, Hauben E, et al. Polymorphous adenocarcinoma of the salivary glands: reappraisal and update. Eur Arch Otorhinolaryngol. 2018;275(7):1681–95.
52. Rooper L, Sharma R, Bishop JA. Polymorphous low grade adenocarcinoma has a consistent p63+/p40- immunophenotype that helps distinguish it from adenoid cystic carcinoma and cellular pleomorphic adenoma. Head Neck Pathol. 2015;9(1):79–84.
53. Pradhan SA, Khannan R, Hazarika B, Desai M. Sinonasal epithelial-myoepithelial carcinoma-a rare entity. Indian J Otolaryngol Head Neck Surg. 2007;59(2):168–70.
54. Lee YS, Ha SM, Paik SW, Yang HJ, Jeon HJ, Park DJ, et al. Epithelial-myoepithelial carcinoma originating from a minor salivary gland in the nasal septum: a case report and literature review. Medicine (Baltimore). 2020;99(5):e19072.
55. Nguyen S, Perron M, Nadeau S, Odashiro AN, Corriveau MN. Epithelial myoepithelial carcinoma of the nasal cavity: clinical, histopathological, and Immunohistochemical distinction of a case report. Int J Surg Pathol. 2018;26(4):342–6.

56. El Hallani S, Udager AM, Bell D, Fonseca I, Thompson LDR, Assaad A, et al. Epithelial-myoepithelial carcinoma: frequent morphologic and molecular evidence of preexisting pleomorphic adenoma, common HRAS mutations in PLAG1-intact and HMGA2-intact cases, and occasional TP53, FBXW7, and SMARCB1 alterations in high-grade cases. Am J Surg Pathol. 2018;42(1):18–27.
57. Katabi N, Ghossein R, Ho A, Dogan S, Zhang L, Sung YS, et al. Consistent PLAG1 and HMGA2 abnormalities distinguish carcinoma ex-pleomorphic adenoma from its de novo counterparts. Hum Pathol. 2015;46(1):26–33.
58. Vázquez A, Patel TD, D'Aguillo CM, Abdou RY, Farver W, Baredes S, et al. Epithelial-myoepithelial carcinoma of the salivary glands: an analysis of 246 cases. Otolaryngol Head Neck Surg. 2015;153(4):569–74.
59. Lan J, Huang SC, Chen YH, Chen WC, Jin YT, Lu YC, et al. Primary paranasal sinus clear cell carcinoma with EWSR1-ATF1 fusion: report of 2 molecularly confirmed cases exhibiting unique histopathology. Hum Pathol. 2017;63:139–43.
60. AlAli BM, Alyousef MJ, Kamel AS, Al Hamad MA, Al-Bar MH, Algowiez RM. Primary paranasal sinus hyalinizing clear cell carcinoma: a case report. Diagn Pathol. 2017;12(1):70.
61. Higo R, Takahashi T, Nakata H, Harada H, Sugasawa M. Salivary duct carcinoma in the sinonasal tract. European Arch Otorhinolaryngol. 2007;264(5):561–3.
62. Nakaguro M, Tada Y, Faquin WC, Sadow PM, Wirth LJ, Nagao T. Salivary duct carcinoma: updates in histology, cytology, molecular biology, and treatment. Cancer Cytopathol. 2020;128(10):693–703.
63. Udager AM, Chiosea SI. Salivary duct carcinoma: an update on morphologic mimics and diagnostic use of androgen receptor immunohistochemistry. Head Neck Pathol. 2017;11(3):288–94.
64. Schmitt NC, Kang H, Sharma A. Salivary duct carcinoma: an aggressive salivary gland malignancy with opportunities for targeted therapy. Oral Oncol. 2017;74:40–8.
65. Müller S, Mantsopoulos K, Iro H, Agaimy A. Salivary duct carcinoma of the sinonasal cavity: a case report and review of the literature. Head Neck. 2016;38(8):E2464–6.

Benign and Borderline Sinonasal Mesenchymal Tumors

10

Somboon Keelawat and Andrey Bychkov

10.1 Introduction

Owing to the multiple types of tissues present in the sinonasal tract, this region may harbor a wide range of benign and borderline mesenchymal neoplasms. This chapter presents an illustrative overview of all these lesions.

10.2 Benign Mesenchymal Tumors

10.2.1 Leiomyoma

Leiomyomas are benign mesenchymal tumors with smooth muscle differentiation [1–4]. These tumors are extremely rare in the head and neck region, accounting for less than 1% of all leiomyomas. The lips are the most common location for these neoplasms, followed by the tongue, cheeks, palate, gingiva, and mandible [1]. Sinonasal tract leiomyomas are even rarer, with involvement of the nasal cavity in most of the cases. Three hypotheses have been proposed to explain smooth muscle tumors in the sinonasal tract: (1) they may be derived from aberrant undifferentiated mesenchymal cells; (2) may originate in smooth muscle elements in the walls of the blood vessels; and (3) in nasal vestibule leiomyomas, tumor may develop from erector pili of the nostril hair follicles [5].

Macroscopy

- On endoscopic examination, the tumors appear polypoid, grayish, glistening, and oftentimes filling the sinonasal cavity.
- Gross sectioning of the specimens shows sharply demarcated lesions with multilobular, firm white to tan trabecular and spongy cut surfaces.

Histopathology

- Tumors are unencapsulated and located at subepithelial areas.
- Mucosal ulceration may occur but is rather uncommon.
- Neoplastic cells have spindle shape with oval to elongated and blunt-ended (cigar-shaped) nuclei with eosinophilic cytoplasm. Tumor cells are arranged in interlacing bundles and whorls (Fig. 10.1a–d).
- Nuclear atypia and mitoses are absent.

Immunohistochemistry

- Leiomyomas express smooth muscle markers: α-SMA (Fig. 10.1e), MSA, desmin (Fig. 10.1f), and h-caldesmon.
- Estrogen and progesterone receptors (ER and PR) expression has been described in sinonasal leiomyoma and angioleiomyoma [6].

Differential Diagnosis

- Leiomyosarcoma and smooth muscle tumor of uncertain malignant potential (SMTUMP). In contrast to leiomyoma which has well-circumscribed border, low cellularity, and absence of nuclear pleomorphism with no mitotic figures, leiomyosarcoma reveals the presence of mitoses (> 4/10 HPF) including atypical ones, infiltrative growth, along with moderate to high cellularity and mild-to-marked pleomorphism accompanied by necrosis [5, 7–9] (Fig. 10.2a, b). SMTUMP shows low cellularity, mild-to-moderate pleomorphism and 1–4 mitotic figures/10 HPFs [9, 10].
- Benign metastasizing leiomyoma is a rare phenomenon of uterine or extrauterine ER/PR-dependent smooth muscle tumors that presents with indolent pulmonary tumors [11,

S. Keelawat (✉)
Department of Pathology, Faculty of Medicine, Chulalongkorn University, Bangkok, Thailand
e-mail: Somboon.Ke@chula.ac.th

A. Bychkov
Department of Pathology, Kameda Medical Center, Chiba, Japan
e-mail: bychkov.andrey@kameda.jp

D. Jain, J. A. Bishop (eds.), *Atlas of Sinonasal Tract Pathology*, https://doi.org/10.1007/978-981-19-7315-4_10

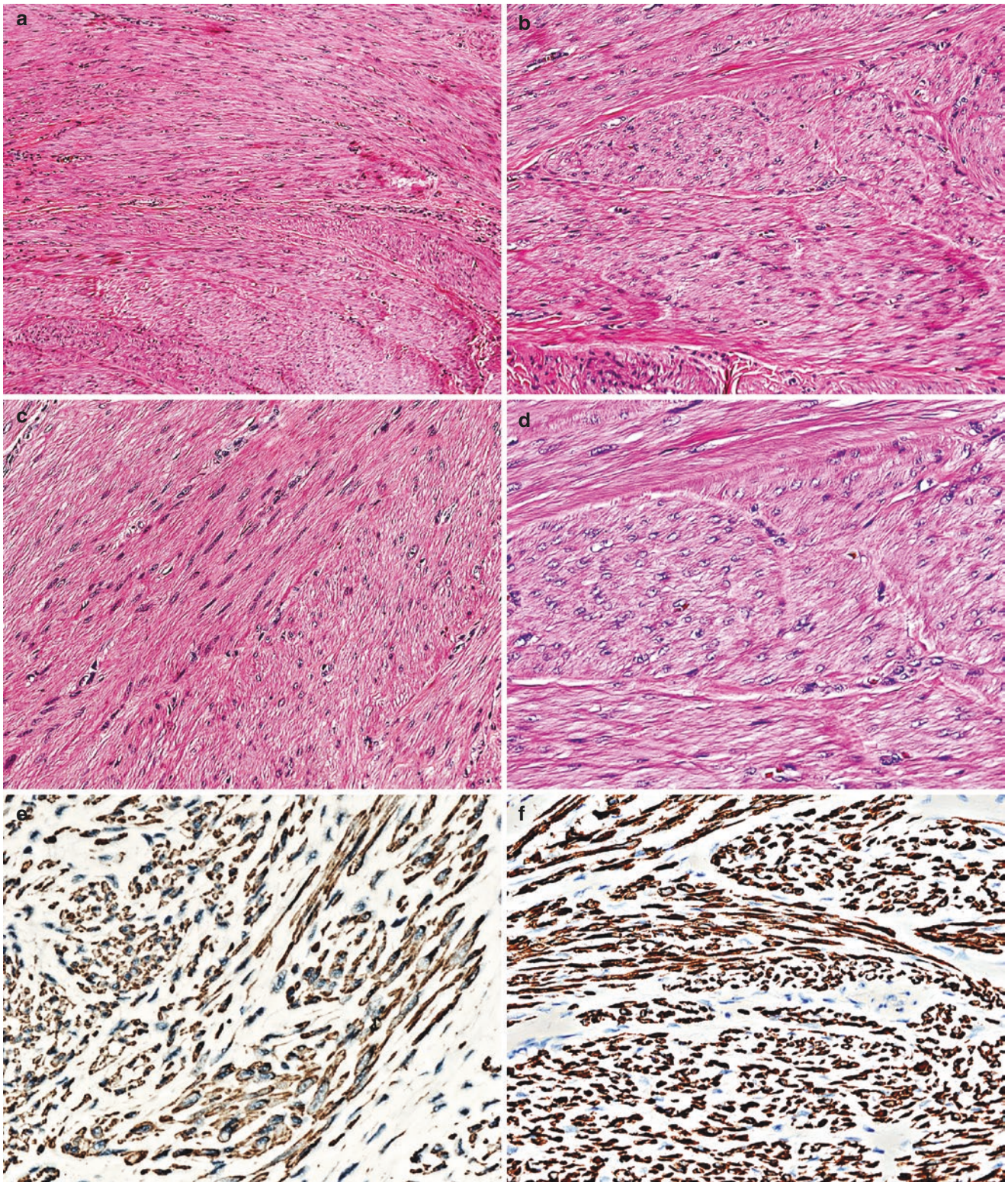

Fig. 10.1 Histology and immunohistochemistry of leiomyoma. Tumor arranged in intersecting fascicles (**a**–**d**). Neoplastic cells have cigar-shaped nuclei (**c**) with round-shaped appearance on cross-sectional plane (**d**). Tumor cells express SMA (**e**) and desmin (**f**)

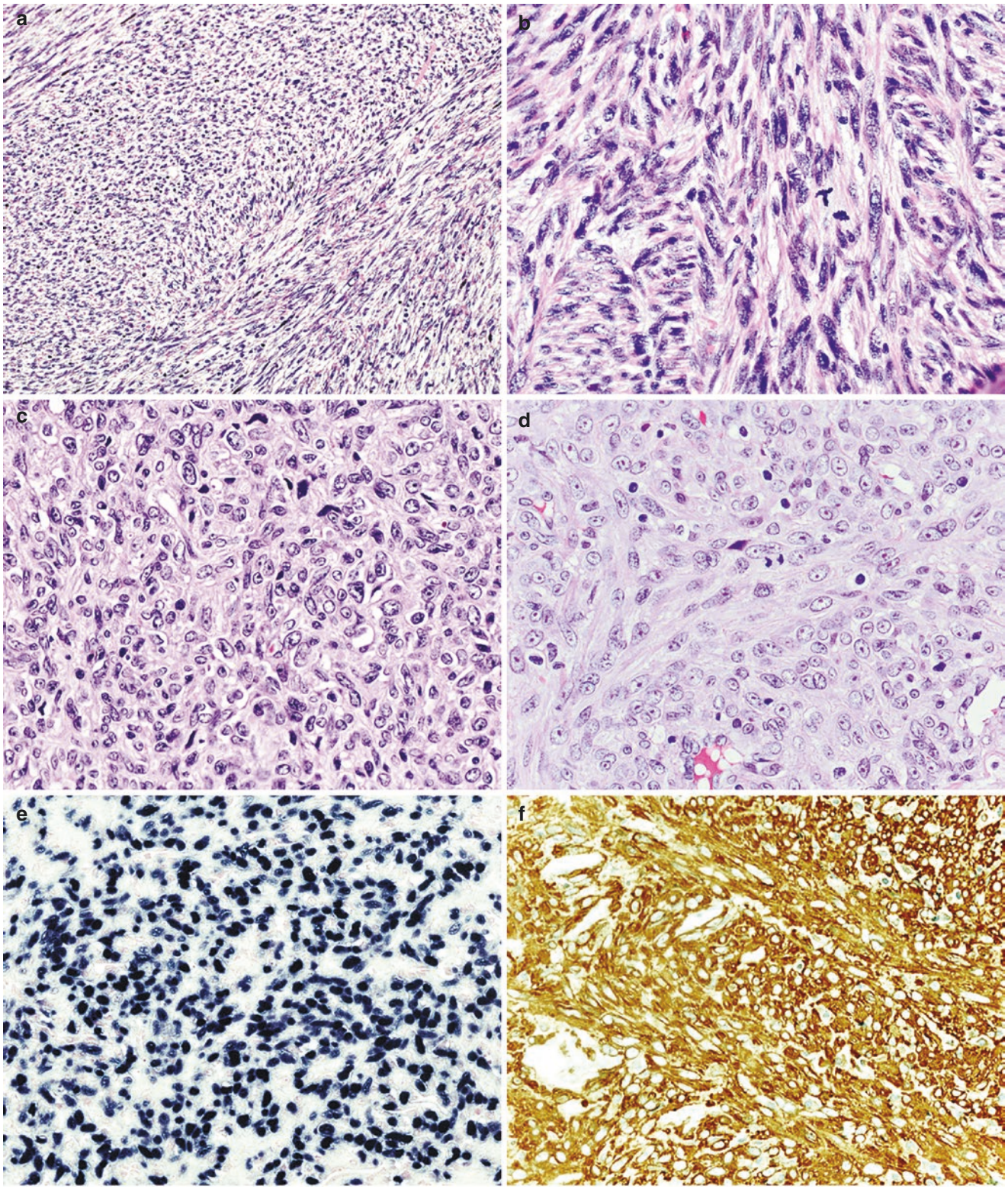

Fig. 10.2 Differential diagnosis of leiomyoma. Leiomyosarcoma with hypercellular fascicles (**a**) showing nuclear pleomorphism and high mitotic activity, including atypical mitoses (**b**). Epstein–Barr virus-associated smooth muscle tumor (**c**, **d**), positive for EBER (**e**) and smooth muscle actin (**f**)

12]. Sinonasal involvement has been reported, therefore, this condition should be included in the differential diagnosis in the lesions of the sinonasal tract. The only key information needed for making diagnosis of this entity is the history of uterine or extrauterine ER/PR-positive leiomyomas [13].

- Epstein–Barr virus-associated smooth muscle tumor (EBV-SMT). EBV-SMT is a special, rare subset of smooth muscle tumors (Fig. 10.2c, d) that occurs in immunosuppressed individuals, the majority of which are AIDS patients with solid organ transplant recipients being a minor subgroup [11]. In addition to smooth muscle markers (α-SMA, MSA, desmin, and h-caldesmon), EBER is the most useful study for diagnostic confirmation of these tumors (Fig. 10.2e, f).

Treatment and Prognosis

- Complete surgical resection is the treatment of choice for sinonasal leiomyomas.
- Recurrence is rare with only a few cases reported in literature [14].

10.2.2 Schwannoma

Schwannoma is a benign nerve sheath tumor arising from the Schwann cells of the peripheral nerve [15]. The most common locations are skin and subcutaneous tissue of the head and neck or along the flexor surfaces of the extremities [16]. Less than 4% of schwannomas arise from the nasal cavity and paranasal sinuses, of which the most preferred sites are the ethmoid followed by maxillary, nasal, sphenoid, and frontal sinus cavities [17].

Macroscopy

- Polypoid, well-circumscribed but non-encapsulated, globular, firm to rubbery, white to yellow-tan masses. Sectioning of the mass shows solid and cystic cut surfaces, occasionally with hemorrhage and myxoid change.
- Mean size—2.5 cm (up to 7 cm).

Histopathology

- Although, in general, schwannomas are encapsulated, the tumors of the sinonasal tract usually present with submucosal mass without discernible capsule (Fig. 10.3a).
- Tumor cells have elongated spindle and wavy shape with poorly defined, pale, fibrillar cytoplasm and bland oval nuclei with tapering ends, arranged in interlacing fascicles (Fig. 10.3b).
- The lesions are composed of two parts, namely hypercellular areas (Antoni A) alternating with hypocellular myxoid zones (Antoni B) (Fig. 10.3c).
- Verocay bodies, the characteristic features of the tumor, consist of a stacked arrangement of two rows of elongated palisading nuclei that alternates with acellular zones made up of cytoplasmic processes (Fig. 10.3d). These structures are occasionally found, particularly in the hypercellular Antoni A areas while perivascular hyalinization is a characteristic finding in Antoni B.
- Rare mitoses, no necrosis.
- Occasionally, tumor cells may exhibit degenerative nuclear atypia (so-called ancient change) [18] and some cases may contain melanin pigment (referred to as melanotic schwannoma) [19].

Immunohistochemistry

- Strong and diffuse reactivity for S100 (Fig. 10.3e) and SOX10 (Fig. 10.3f).
- Patchy positivity for GFAP.
- Focal AE1/AE3 immunoreactivity has been recorded as well as CD34, which are usually expressed in fibroblasts present in the Antoni B areas.
- Neurofilament (NF), actin, and desmin are negative.
- In melanotic variant, melanoma markers (e.g., HMB-45 and Melan A) can be expressed [19].

Differential Diagnosis

- Malignant peripheral nerve sheath tumor (MPNST). In contrast to schwannoma, MPNST shows marked nuclear atypia, tumor necrosis, and a high mitotic index including those with atypical shapes [20]. Decreased expression of S100 protein is another indicator used for the diagnosis of malignancy [18] (Fig. 10.4a–c).
- Solitary fibrous tumor (SFT). SFT shares some features with schwannoma including hypercellular and hypocellular areas. However, immunohistochemical studies can readily distinguish both tumors since schwannoma shows strong positivity for S100 protein and SOX10 while SFT exhibits STAT6 nuclear expression [21]. Also, hemangiopericytoma-like pattern is more frequently seen in SFT but is not a common feature of schwannoma [22].

Treatment and Prognosis

- Sinonasal schwannomas have a very low recurrence rate usually related to incomplete resection [17, 20].
- Malignant transformation almost never occurs but erosion of neighboring osseous structures due to pressure necrosis by tumor masses is possible [20].
- Local excision without the need for wide margins is considered as an appropriate primary treatment, with further surgery undertaken for those who develop local recurrence [18].
- Radiotherapy for patients who are medically unfit or unsuitable for surgery.

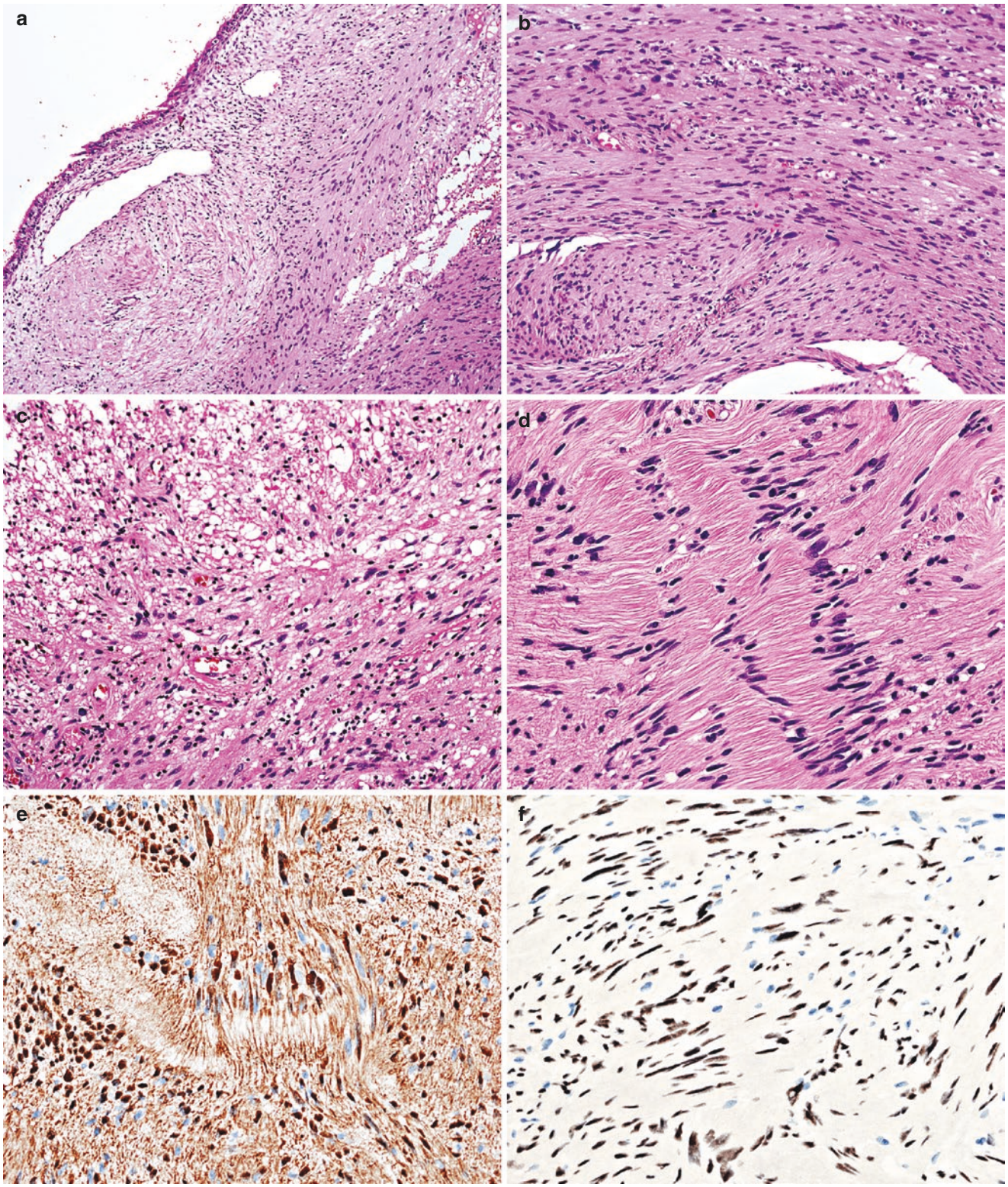

Fig. 10.3 Histology and immunohistochemistry of schwannoma. Unencapsulated submucosal mass (**a**) is composed of Antoni A (**b**) and Antoni B (**c**) patterns. Verocay body (**d**). Tumor cells express S-100 (**e**) and SOX-10 (**f**)

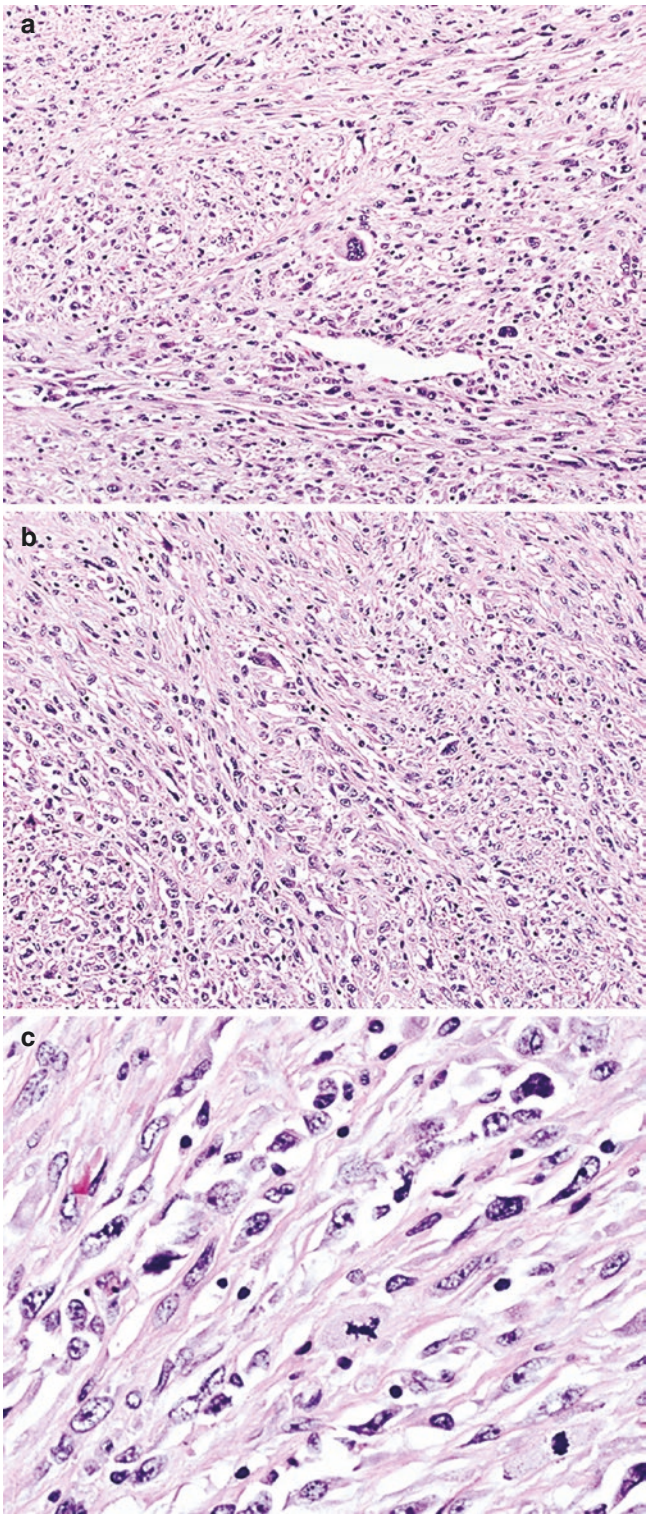

Fig. 10.4 Malignant peripheral nerve sheath tumor. Pleomorphic malignancy with marked nuclear atypia (**a**–**c**) and atypical mitotic figures (**c**)

10.2.3 Neurofibroma

Neurofibroma (NF) is a benign neoplasm derived from mixed cellular components of the nerve sheath, composed of Schwann cells, perineurial-like cells, fibroblasts of the connective tissue of the endoneurium and residual interspersed myelinated and unmyelinated axons embedded in extracellular matrix [23, 24]. These tumors can occur sporadically as solitary lesions which comprise the majority of cases and as multiple or numerous tumors in individuals with neurofibromatosis type 1 [24]. They are commonly found in the extremities and the head and neck regions. Of all the head and neck cases, only 4% occur in the sinonasal tract, with the most common site being the nasal vestibule, followed by the maxillary sinus [23]. About 10% of sinonasal NFs are associated with neurofibromatosis type 1. Sinonasal NF is believed to develop from the first and second branches of the trigeminal nerve that innervates various nasal and sinus cavity structures.

Macroscopy

- Non-encapsulated, occasionally polypoid, with firm, glistening, white and grayish cut surfaces.

Histopathology

- Unencapsulated tumors which typically demonstrate a blending of ovoid to spindled cells that contain curved, wavy, and pointed-end nuclei with thin cytoplasmic processes (Fig. 10.5a–c). Tumor cells are intermingled with collagen and myxoid stroma. Few mast cells can be identified.
- Nuclear palisading, a characteristic feature of schwannoma, is generally absent in NF.
- Pleomorphism, an increased cellularity and mitoses are extremely uncommon, which, if present (in particular, atypical mitoses) should raise concern of malignant transformation [23, 25]. No accompanying necrosis.

Immunohistochemistry

- Positive for various immunohistochemical markers due to mixed cellular composition.
- Positive for S100, which highlights Schwann cells (Fig. 10.5d), but labels less than half of tumor cells.
- Schwann cells may also show SOX10 (Fig. 10.5e) and neurofilament proteins immunoreactivity [25].
- EMA and GLUT1 are expressed by perineurial-like cells, whereas stromal fibroblasts are positive for CD34 [24] (Fig. 10.5f).

Differential Diagnosis

- Perineurioma is usually composed of slender spindle cells with wavy or tapering nuclei and characteristic delicate bipolar cytoplasmic processes. They are predominantly arranged in storiform growth pattern with other distinctive architectural features including whorled, Pacinian, or short fascicular arrangement [26]. Unlike NF, all perineuriomas are negative for S100 [26].

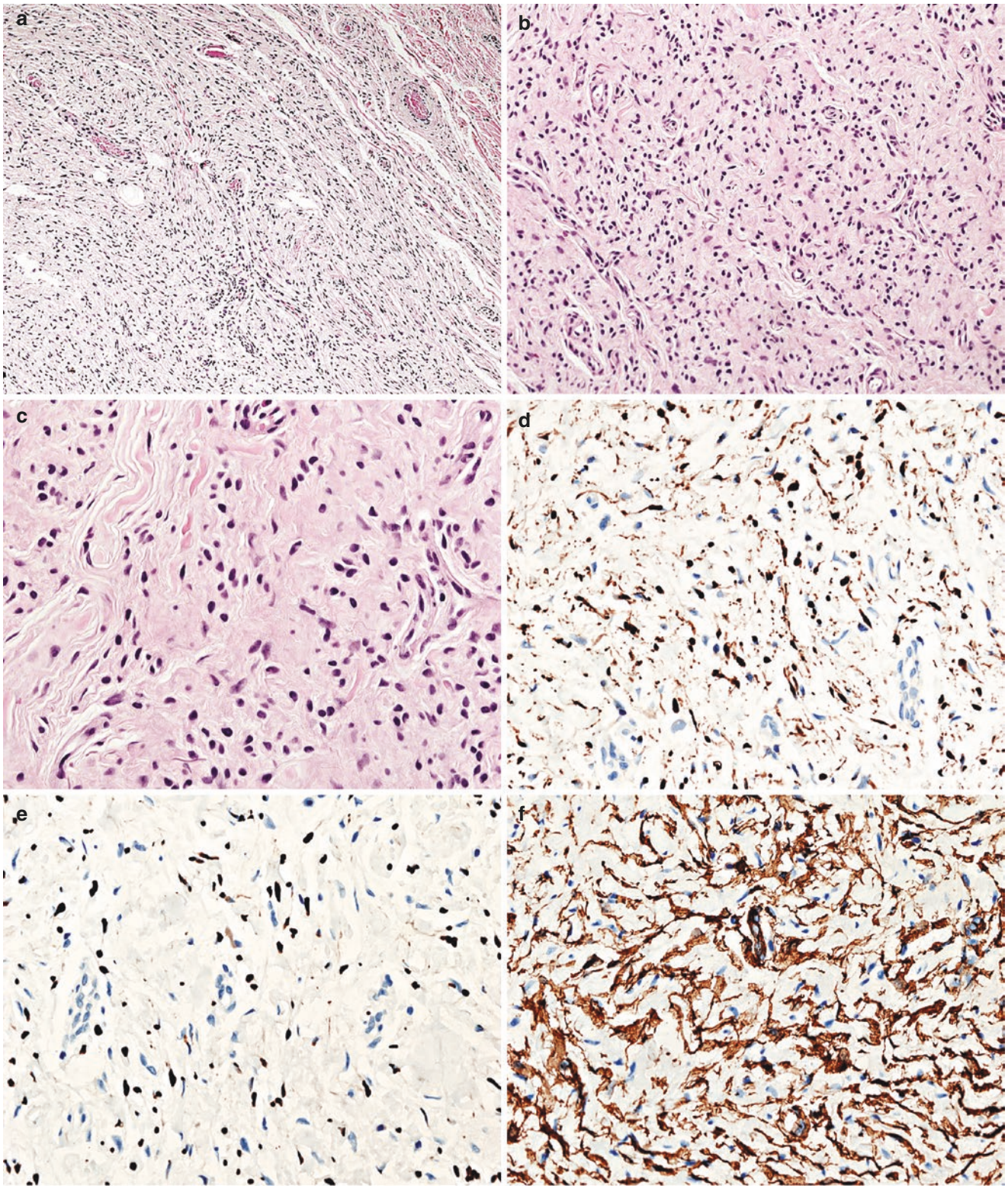

Fig. 10.5 Histology and immunohistochemistry of neurofibroma. The tumor is hypocellular and consists of ovoid to spindled cells with curved, wavy, and pointy nuclei on collagen tissue stroma (**a**–**c**). Tumor cells express S-100 (**d**), SOX-10 (**e**), and CD-34 (**f**)

- Fibromatosis. NF lacks infiltrative growth and collagen deposition making it distinctly different from fibromatosis [25]. Furthermore, β-catenin, which is positive in most cases of fibromatosis, is usually negative in NF [27].

Treatment and Prognosis

- Prognosis of NF is excellent with a recurrence rate of only 5% [17] likely due to incomplete excision.
- Malignant transformation is extremely rare.

10.2.4 Lobular Capillary Hemangioma

Lobular capillary hemangioma, also known as pyogenic granuloma, is a benign vascular neoplasm, characterized by capillary proliferation with a microscopically distinctive lobular arrangement that affects the skin and mucosa of the oral cavity and sinonasal region. Nasal mucosa involvement is less common and mostly found at the nasal septum, followed by turbinate and sinus [28, 29]. Lobular capillary hemangioma of the nasal cavity shows a female preponderance. A history of trauma was reported in 12% of cases while up to 15% of nasal pyogenic granulomas are related to pregnancy [30]. Furthermore, a higher incidence of this neoplasm has been reported to be associated with a use of oral contraceptives [28, 30, 31].

Macroscopy

- Polypoid, gray-white with purple to red areas (Fig. 10.6), frequently with surface ulceration.
- Usually, small lesion with the mean size <1 cm (occasionally up to 8 cm).

Histopathology

- A circumscribed lesion composed of proliferative capillaries with plump endothelial cells, encircled by pericytes, arranged in lobulated pattern (Fig. 10.7a), in the background of edematous and fibroblastic stroma. Within the

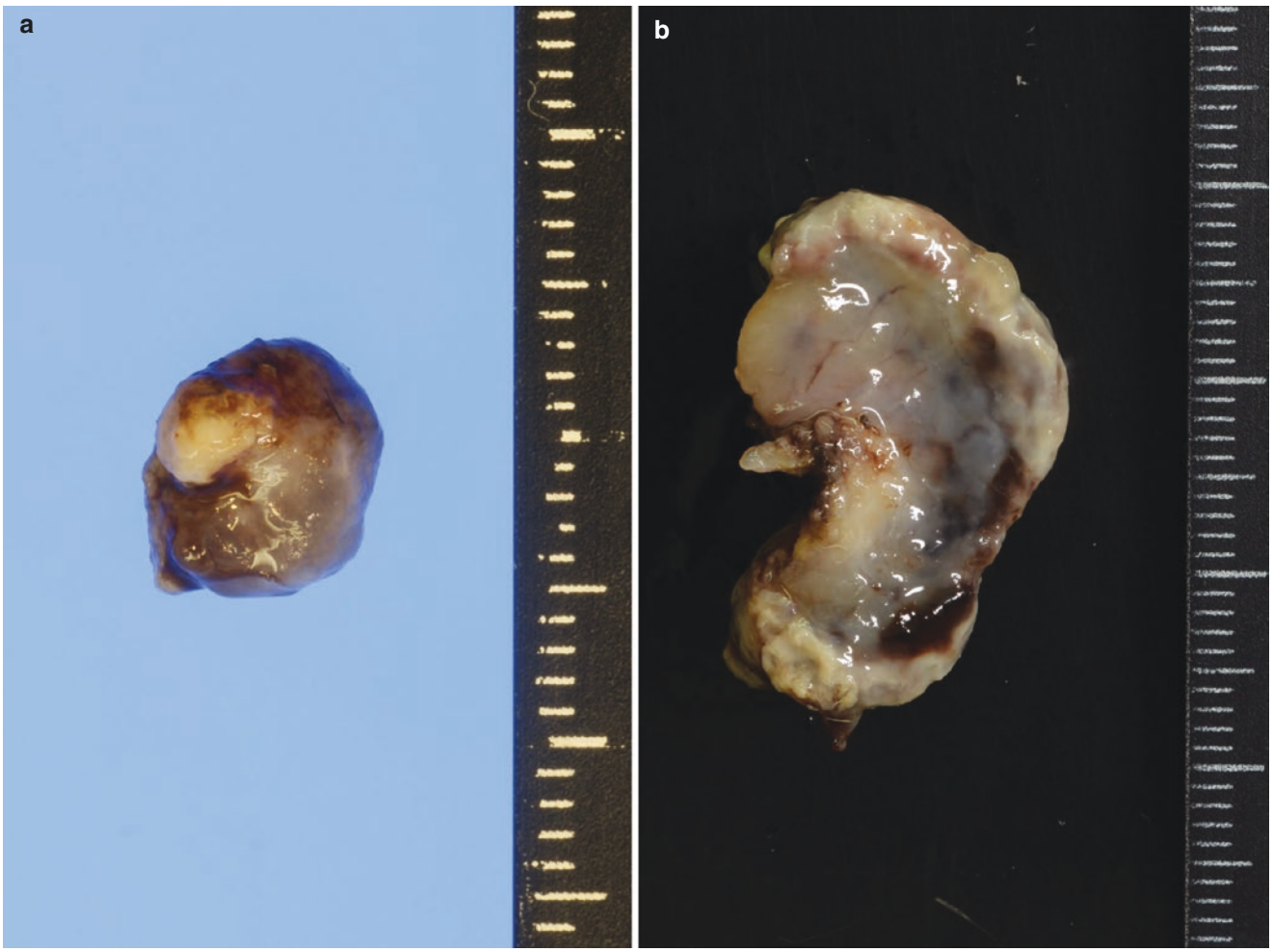

Fig 10.6 Gross appearance of lobular capillary hemangioma. Tumors are well-circumscribed, gray white to dark-red in appearance with superficial foci of hemorrhage (**a**, **b**)

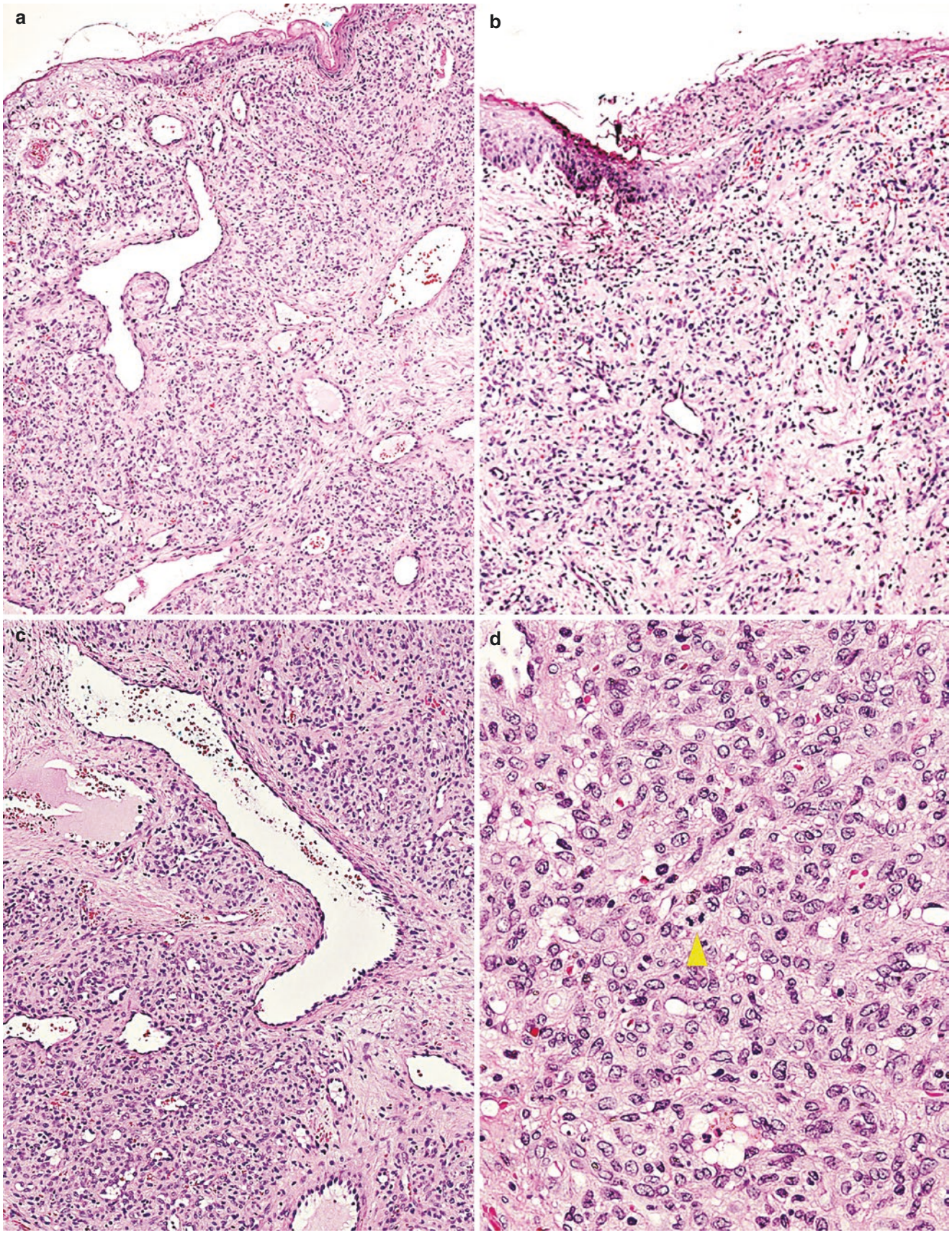

Fig. 10.7 Histology of lobular capillary hemangioma of the nasal vestibule. Circumscribed proliferation of capillaries, arranged in multiple lobules located beneath the epithelial mucosa (**a**). There are large veins (**a**, **c**) intervening among small capillaries within the lobules (**a**). Mucosal ulceration is present (**b**). Mitoses (arrowhead) are often identified (**d**)

lobules are large central veins intervening among small capillaries [29] (Fig. 10.7a, c).
- The overlying epithelium is usually atrophic and ulcerated in most cases (Fig. 10.7b).
- Mitoses are often identified (without atypical forms), up to 4/HPF [29, 30] (Fig. 10.7d).

Immunohistochemistry

- Positive for FLI1, CD34, CD31, and factor VIII-related antigen.
- Variable expression of ER and PR.

Differential Diagnosis

- Polypoid granulation tissue, which is lacking lobulated architecture of capillaries classical for pyogenic granuloma. Also, polypoid granulation tissue usually shows striking inflammation with stromal edema admixed with newly-formed capillaries that tend to radiate to the ulcerated mucosal surface (Fig. 10.8a, b).
- Angiosarcoma usually has infiltrative border and contains anastomosing vessels (Fig. 10.8c, d) that appear as tortuous, irregular channels dissecting the stroma with cleft-like spaces [29, 32]. Neoplastic endothelial cells demonstrate moderate to severe nuclear pleomorphism with coarse chromatin and prominent nucleoli. Necrosis and hemorrhage are common. Atypical mitotic figures are seen in most cases.

Treatment and Prognosis

- Surgical excision.
- Recurrence ranges from 0–42%, depending on the case series and the duration of follow-up.
- For pregnancy-related tumors, regression can occur after delivery.

10.2.5 Osteoma

Osteomas are benign, indolent, bone forming neoplasms that are limited almost exclusively to the craniofacial bones

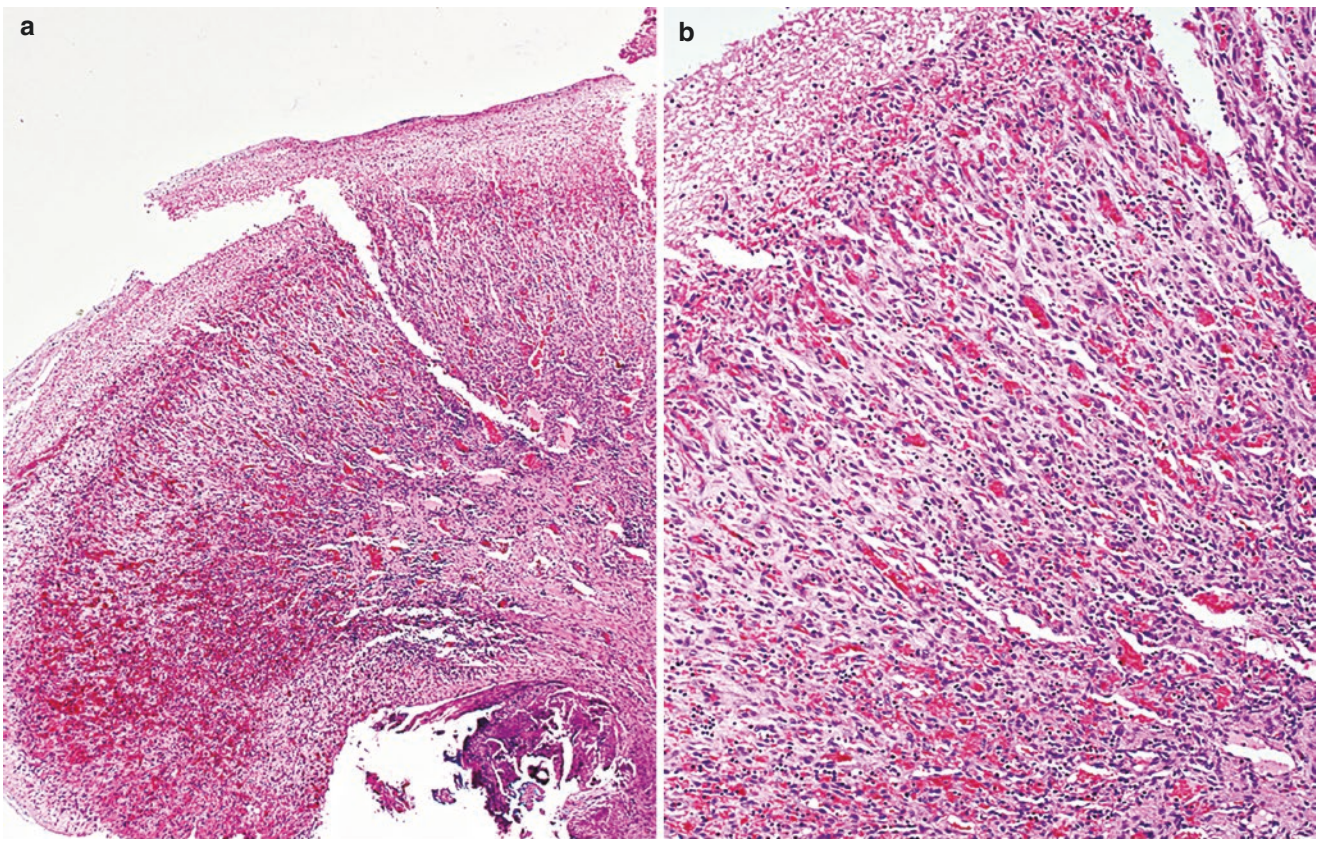

Fig. 10.8 Differential diagnosis of lobular capillary hemangioma. Polypoid granulation tissue with proliferating newly-formed capillaries radiating to the ulcerated mucosal surface (**a**, **b**). Angiosarcoma showing anastomosing vessels, lined by pleomorphic endothelial tumor cells (**c**, **d**)

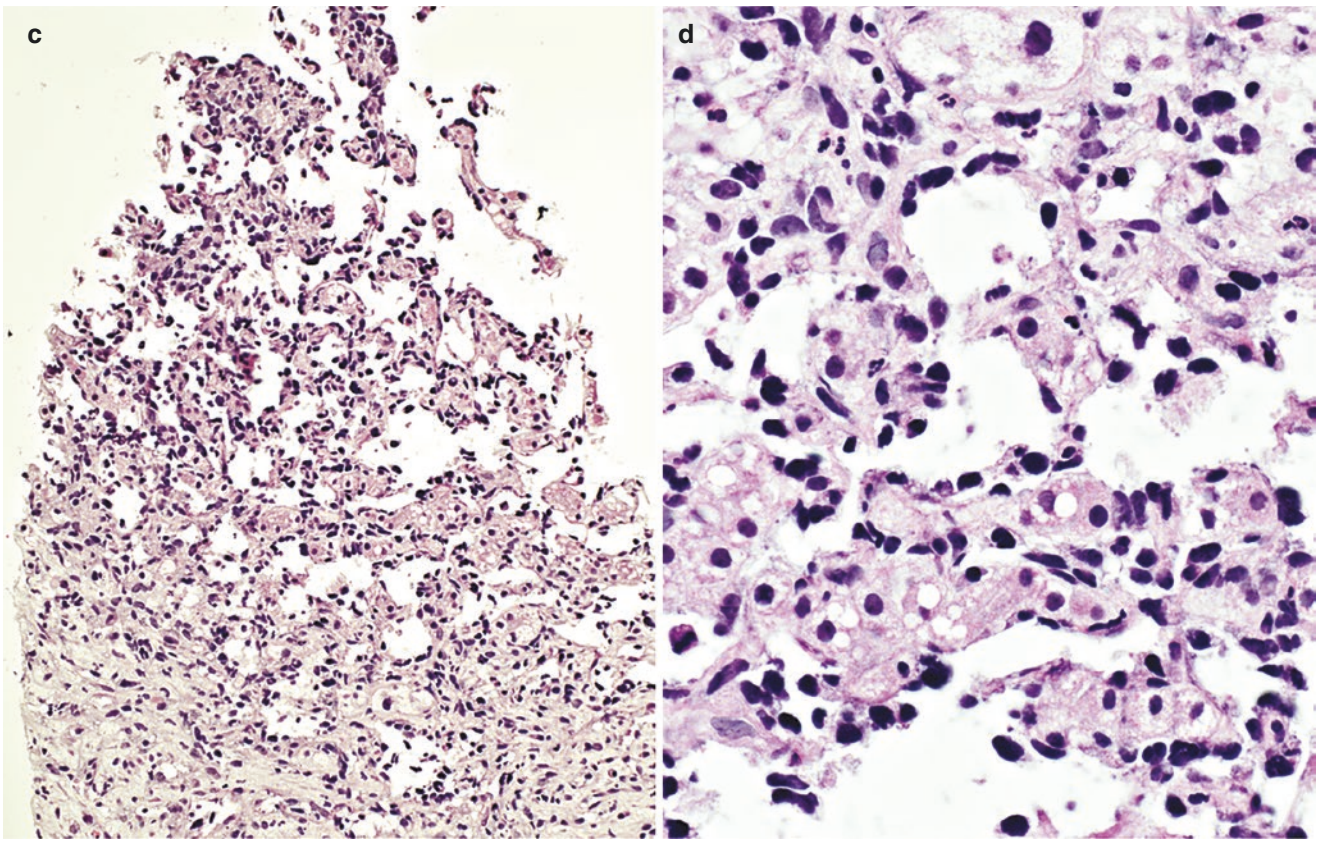

Fig. 10.8 (continued)

including cranial vault, mandible, external auditory canal, and the bones that define the paranasal sinuses, nasal cavity, and the orbit (so-called sino-orbital osteomas) [33, 34]. Among the sino-orbital lesions, frontal sinus is the most common site [33, 35].

Osteomas may also be one of the manifestations of Gardner's syndrome, an autosomal dominant disorder, characterized by adenomatous intestinal polyps, multiple osteomas in the skull, maxilla, mandible, multiple cutaneous and subcutaneous lesions (epidermoid cyst and desmoid tumor) and a mutation of the *APC* gene [33, 35]. So far, etiology of sporadic osteomas remains unclear although trauma, inflammation, and maldevelopment have been considered as possible causes [35].

Macroscopy

- Round or oval, hard, yellowish-white and well-circumscribed, usually with an attachment to the adjacent or underlying bone with a broad base or occasionally a thin stalk.
- Mean size 3.1 cm (range, 0.6–8 cm) [34].

Histopathology

- Sino-orbital osteomas are located beneath the respiratory epithelium and composed of lamellar bone, either of compact (dense) type with little fibrous stroma or trabecular bone with more fibrous tissue component, or a combination of them [33, 34]. Dense bony part usually defines the periphery of the mass where it has a rounded, sharply defined border (Fig. 10.9a–c).
- Tumor lesions may blend with or protrude from surface of the underlying bone.
- Occasionally, there are narrow anastomosing woven bone rimmed by osteoblasts and osteoclasts, the characteristic features of osteoblastoma, identified typically at the base of the tumor which is the site of attachment to the bone of origin. These changes indicate remodeling process within the lesion and have no correlation with a more aggressive clinical behavior [33].

Differential Diagnosis

- Osteoid osteoma and osteoblastoma are rarely found in sinonasal cavities. Compared to these two enti-

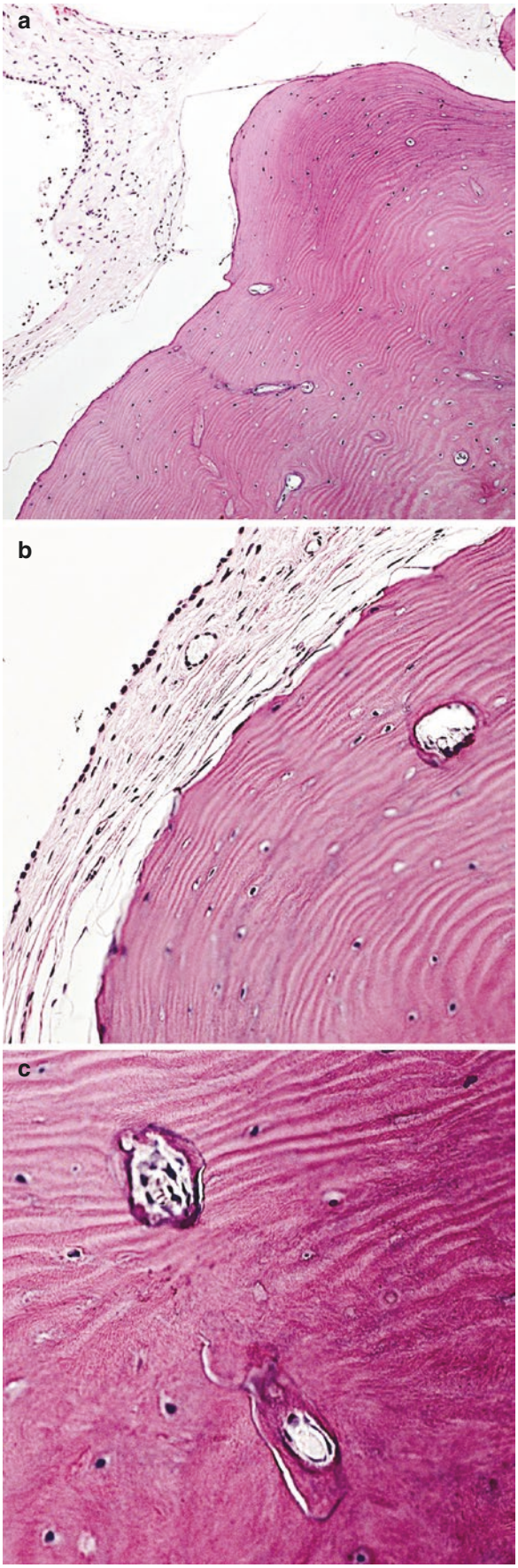

Fig. 10.9 Histology of osteoma. The tumor is located beneath the epithelium and composed of compact mature lamellar bone (**a**–**c**)

ties, osteoma has much more mature bone either in the form of compact and cancellous bone. The edge of an osteoma has a smooth rounded contour, often lined by respiratory mucosa, representing the outer surface of its polypoid growth within the sinus cavity. Osteoblastoma, in contrast, presents as an expansile intramedullary or periosteal bone lesion with much less mature bone.

- Fibro-osseous lesions, including ossifying fibroma and fibrous dysplasia. Unlike osteoma, ossifying fibroma (Fig. 10.10a–d) and fibrous dysplasia contain more woven bone and much less mature bone with prominent collagenous spindle cell stroma in the background.

Treatment and Prognosis

- Surgery for symptomatic osteomas. For asymptomatic cases, a conservative approach with regular radiological examination [36] is usually recommended. Surgery is reserved for those lesions involving >50% of the sinus volume, rapidly evolving osteomas (growth >1 mm/year), intracranial or intraorbital extension, frontal osteomas located in the frontal recess, and sphenoid osteomas [35].
- Recurrence is rare after excision.
- No malignant transformation has been reported [35].

10.2.6 Sinonasal Tract Angiofibroma

Sinonasal tract angiofibroma (STA) is a locally aggressive fibrovascular neoplasm arising from the posterolateral wall of the roof of the nasal cavity or lateral nasopharynx [37] and affecting exclusively adolescents and young male patients [38, 39]. This entity has been known as juvenile angiofibroma, juvenile nasopharyngeal angiofibroma, and nasopharyngeal angiofibroma and was previously classified as a soft tissue tumor of the nasopharynx in the previous WHO Classification of Head and Neck Tumours [38]. However, the 2022 WHO Classification of Head and Neck Tumours has revised this neoplasm as a mesenchymal tumor of the sinonasal tract [37].

Due to its predilection for adolescent males, the etiology of STA is believed to be related to sex hormones, particularly androgen [40]. In addition, since a somatic mutation in the ß-catenin encoding gene (*CTNNB1*) is seen in 75% of the cases, aberrant Wnt-signaling may play a central role in the pathogenesis of these tumors [41]. This hypothesis is also supported by the increased incidence in patients with familial adenomatous polyposis (FAP) [42–44]. Since the lesion occurs almost exclusively in males, hence, if diagnosed in females, they should be evaluated for testicular feminization [37].

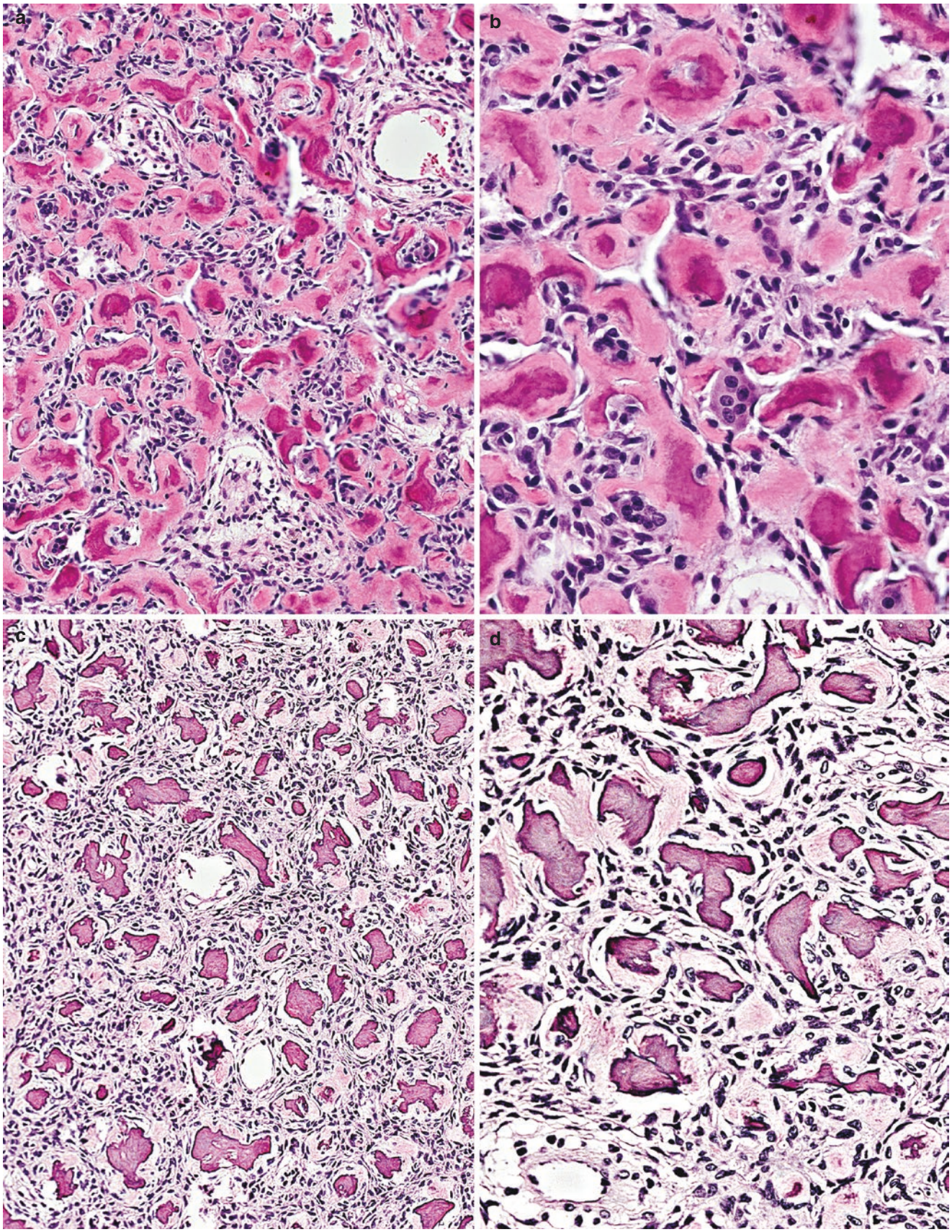

Fig. 10.10 Ossifying fibroma. Anastomosing trabeculae of immature bone and spindle cell stromal background (**a**, **b**). Closely packed spherical ossicles embedded in spindle cell stroma (**c**, **d**)

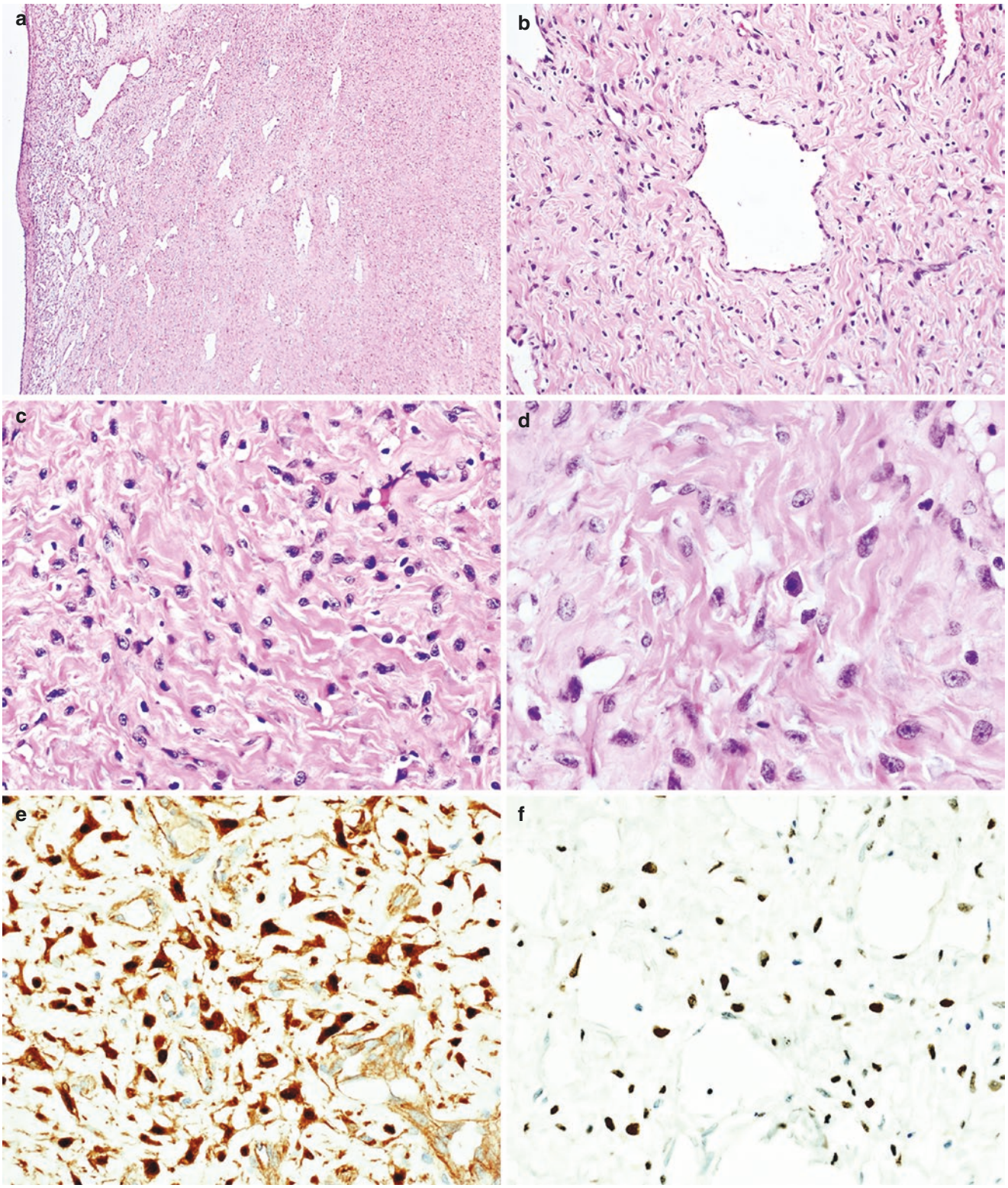

Fig. 10.11 Histology and immunohistochemistry of sinonasal tract angiofibroma. Tumor is composed of variable-sized and shaped thin-walled vascular spaces and collagenous stroma (**a**–**d**). Mast cells are occasionally seen (**d**). Neoplastic cells show positive nuclear staining to beta-catenin (**e**) and androgen receptor (**f**)

Macroscopy

- The tumor is firm, polypoid, and lobulated, often taking the shape of surrounding structures.
- Color varies from yellow to dark red.

Histopathology

- The tumors are composed of vascular spaces and collagenous stroma (Fig. 10.11a–d).
- The vascular component consists of variable-sized and shaped vessels, ranging from small rounded or slit-like capillaries to larger irregularly dilated and branching (staghorn-like) vessels. Their walls are thin and may be supported only by endothelial cells or encircled (focally or continuously) by smooth muscles of varying thickness.
- The stroma varies from loose, edematous to highly cellular (with fibroblasts or myofibroblasts) and densely collagenous.
- Mast cells are frequently found (Fig. 10.11d).
- Mitotic activity is usually absent.

Immunohistochemistry

- Endothelial cells are highlighted by CD31, CD34, and ERG, while the smooth muscles of the vascular wall are positive to SMA, HHF35, and h-caldesmon [39].
- Androgen receptor (AR) and beta-catenin show nuclear expression in stromal cells in 40–75% and > 90%, respectively [38, 39] (Fig. 10.11e–f).

Differential Diagnosis

- Vascular-rich nasal turbinate tissue. Due to its highly vascularized appearance, nasal turbinate tissue can be confused with angiofibroma. Aside from the anatomic location, there are certain histologic differences between these two lesions. Usually, the nasal turbinate tissue contains large-caliber blood vessels surrounded by thick smooth muscle walls (Fig. 10.12a–b). In contrast, angiofibroma typically consists of variable-sized thin wall vessels (with or without smooth muscle layers). In addition, nasal turbinate lacks hypercellular stroma of angiofibroma.
- Hemangioma. Unlike angiofibroma, hemangioma lacks cellular stroma (Fig. 10.12c). Also, compared to the former, the vascular channels in hemangioma appear relatively more homogeneous. Moreover, AR and beta-catenin are absent in hemangioma but positive in angiofibroma.

Treatment and Prognosis

- Although classified as a benign mesenchymal neoplasm, local recurrence occurs in 5–25% of cases [38]. Prognosis depends on the extent of the tumors and the adequacy of surgical resection.

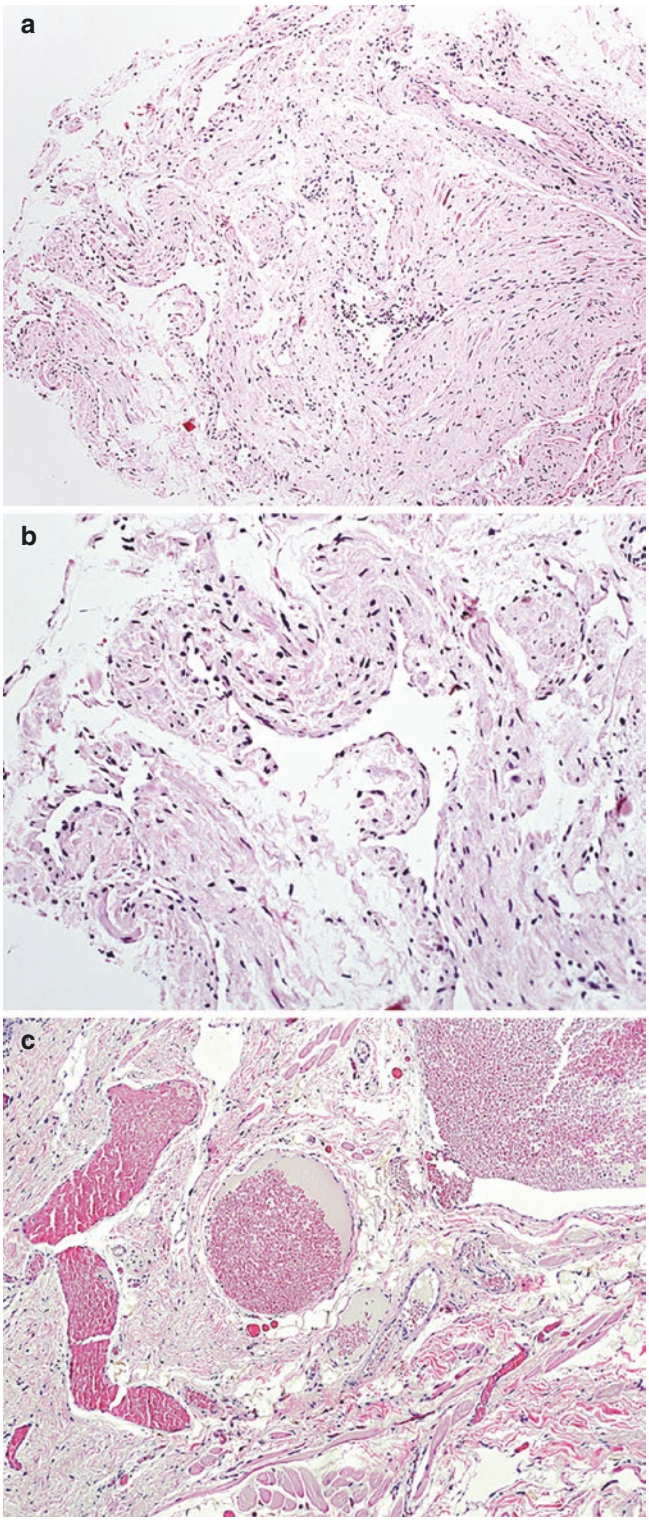

Fig. 10.12 Differential diagnosis of sinonasal tract angiofibroma. Vascular-rich nasal turbinate tissue showing vascularized tissue consisting of relatively thick walled blood vessels (**a**, **b**). Hemangioma with loose stroma containing vascular spaces filled with red blood cells (**c**)

- Malignant (sarcomatous) transformation is uncommon and, if present, usually associated with the previous radiotherapy [38].

- Complete surgical resection is considered the treatment of choice [39].
- The tumor also responds to estrogen therapy [45].

10.3 Borderline Mesenchymal Tumors

10.3.1 Desmoid-Type Fibromatoses

Desmoid-type fibromatoses, also known as aggressive fibromatoses or desmoid tumors, are non-metastasizing, locally aggressive, histologically bland-looking (myo)fibroblastic neoplasms that have a tendency toward recurrence [27, 46–48].

Overall, about 10–15% of fibromatoses occur in the head and neck [46]. However, in children, the occurrence of the tumors in these regions becomes greater than one-third of cases [47]. Of all neoplasms arising in these regions, soft tissues of the neck are most frequently affected followed by the face, while the paranasal sinuses, nasopharynx, orbit, and oral cavity are rarely involved [46, 47].

Macroscopy

- Desmoid-type fibromatosis tend to present as large bulky firm and gritty mass, typically 5–10 cm in size that locally infiltrates adjacent tissue structures [48].
- The cut surfaces are white or tan-white with coarsely trabeculated or whorled appearance resembling scar tissue.

Histopathology

- Poorly circumscribed, infiltrative growth (to soft tissues and/or bone) of low to moderate cellularity of spindle-shaped cells, which are arranged in fascicular pattern and set in the background of abundant collagenous or myxoid tissue (Fig. 10.13a–c) with occasional keloid-like areas.
- Cells have tapering to plump vesicular nuclei, small nucleoli, and indistinct cytoplasm.
- Pleomorphism is minimal with very rare mitoses.
- Atypical mitoses and necrosis are absent [46].
- Mucosal ulceration in some cases.

Immunohistochemistry

- Approximately 70–75% of desmoid-type fibromatosis cases show nuclear positivity for β-catenin (Fig. 10.13d), usually more often in cases associated with familial colorectal polyposis than in sporadic tumors [27].
- Cyclin D1 and calretinin expression is seen in approximately 70–100% and 75% of the tumors, respectively [49, 50].
- Variable immunostaining by MSA, α-SMA, and desmin.

Differential Diagnosis

- Fibrosarcoma: microscopically shows "herringbone" pattern and has more cellularity, with a greater degree of pleomorphism, mitotic activity, and more prominent necrosis. In addition, fibrosarcoma, unlike fibromatosis, is classically β-catenin negative (Fig. 10.14a, b).
- Reactive fibrosis (scar tissue) is less cellular and has no infiltrative or destructive growth as typically seen in fibromatosis (Fig. 10.14c, d). Long-standing history of recurrent rhinosinusitis including a history of trauma or surgical procedure at the affected sites may be another clue for distinguishing this process from desmoid tumor [47].
- Nodular fasciitis usually has areas of more loosely arranged, stellate and "tissue culture-like" cells, more common mitotic activity, and no β-catenin immunoreactivity (Fig. 10.14e, f).

Treatment and Prognosis

- Surgical resection.
- In patients with recurrent tumors or in whom complete surgical excision is not possible, chemotherapy or radiotherapy may be used as adjuvant treatment following surgery [47].
- The use of nonsteroidal anti-inflammatory and anti-estrogen drugs (tamoxifen) has also been suggested as the treatment for the recurrent desmoid tumors [51].

10.3.2 Sinonasal Glomangiopericytoma

Sinonasal glomangiopericytoma (SNGP) is a borderline/low-grade malignant sinonasal mesenchymal neoplasm that demonstrates a perivascular myoid differentiation [52]. SNGP is a rare tumor accounting for <0.5% of all sinonasal tract neoplasms, which occurs mainly in the sixth and seventh decades of life, with a slight female predominance [53]. Nasal cavity, either alone or with coexisting paranasal sinus involvement, is usually affected. Occasionally, isolated paranasal sinus disease may occur [52]. Of the paranasal sinuses, the ethmoid and sphenoid sinuses are most commonly involved. Most SNGPs harbor *CTNNB1* missense mutations resulting in accumulation of β-catenin and upregulation of cyclin D1, which leads to oncogenic activation [52].

Macroscopy

- Polypoid, smooth surfaced, red to red-brown or pink to pink-tan, soft, and fleshy to friable with homogenous cut surfaces usually showing focal hemorrhage.

Histopathology

- Unencapsulated proliferation of closely packed bland and uniform spindle cells with syncytial architecture (Fig. 10.15) below an intact or occasionally ulcerated epithelium separated by a subepithelial tumor-free zone.

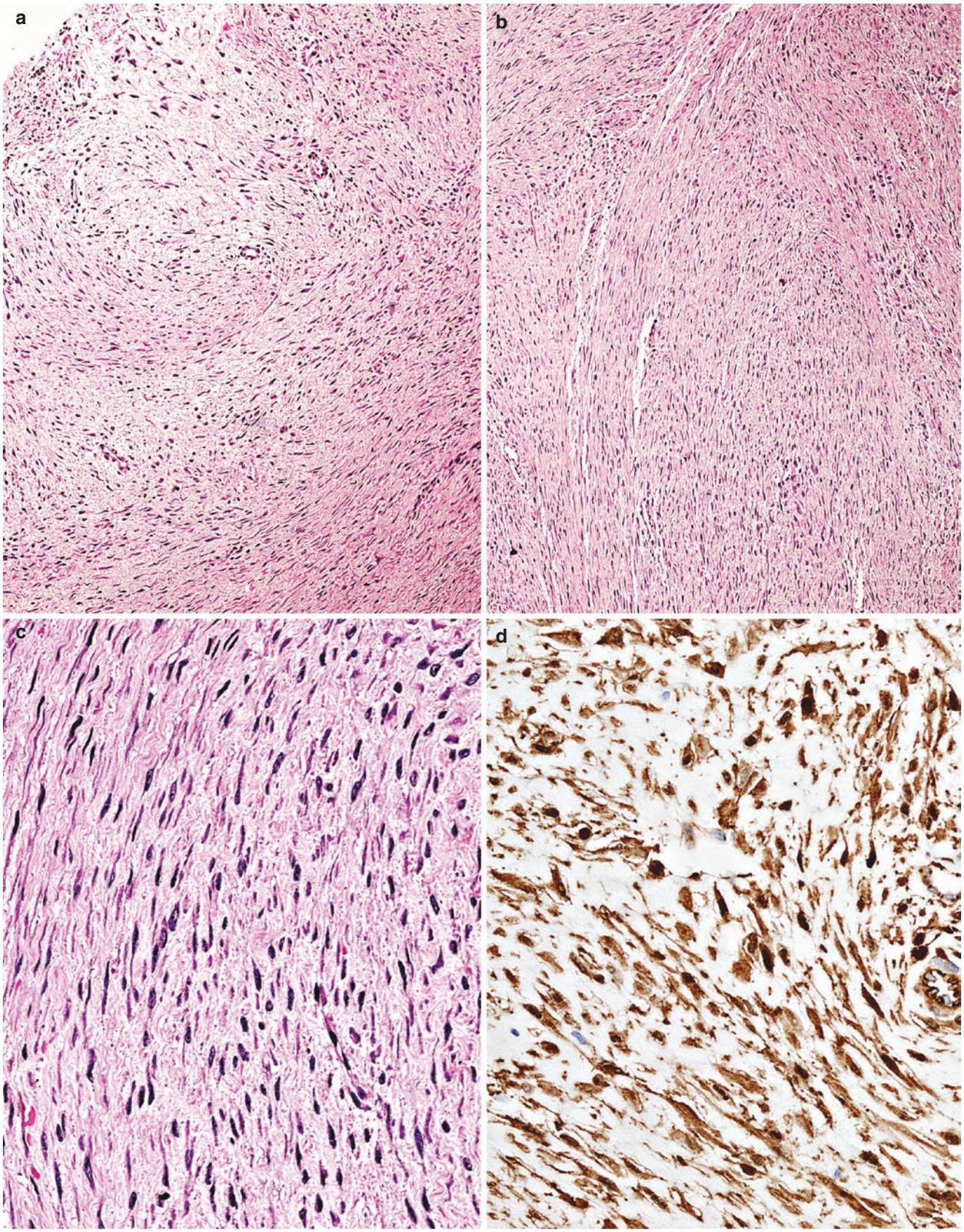

Fig. 10.13 Histology and immunohistochemistry of desmoid-type fibromatosis. The tumor lesion contains moderate cellularity of spindle-shaped cells with tapering nuclei and indistinct cytoplasm admixed with collagenous tissue, arranged in fascicular pattern (**a**–**c**). Areas with loose myxoid appearance. (**b**) Tumor cells express nuclear β-catenin (**d**)

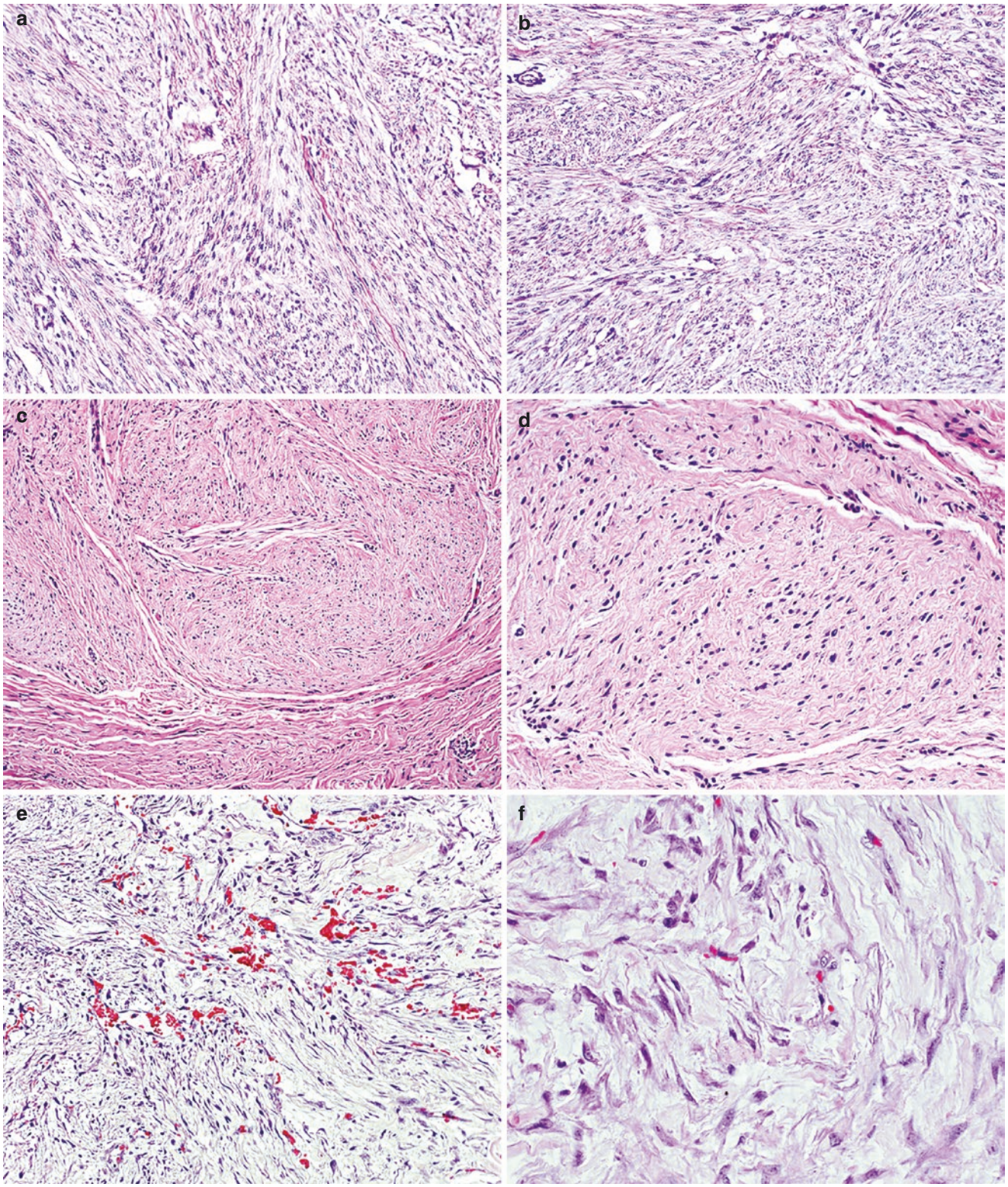

Fig. 10.14 Differential diagnosis of desmoid-type fibromatosis. Fibrosarcoma showing hypercellular spindle cells with fascicular arrangement and vague "herringbone" pattern (**a**, **b**). Fibrous scar showing rather well-circumscribed hypocellular fibrotic tissue (**c**, **d**). Nodular fasciitis with loosely arranged "tissue culture-like" fibroblasts (**e**, **f**)

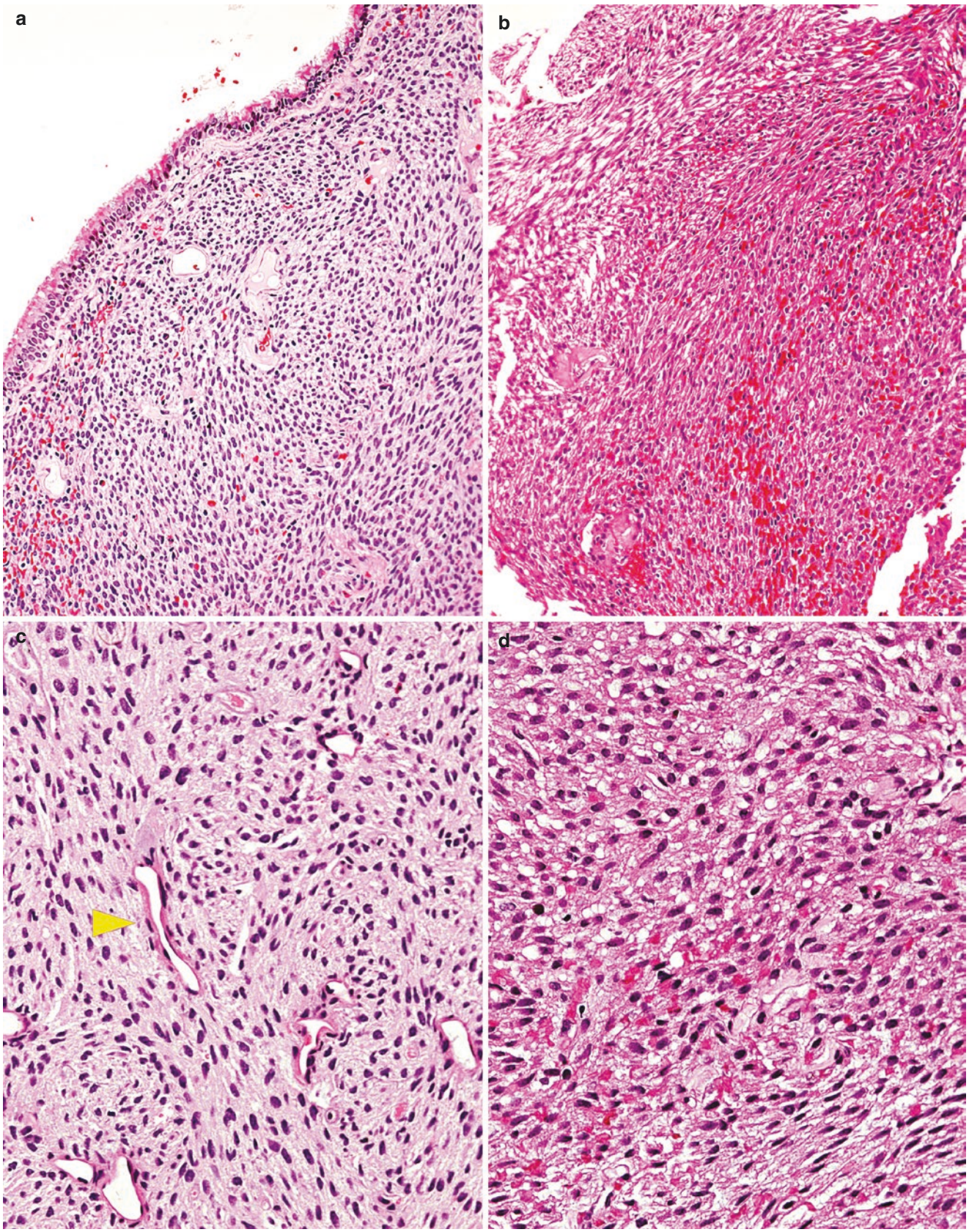

Fig. 10.15 Histology of sinonasal glomangiopericytoma. Unencapsulated submucosal proliferation of closely packed bland and uniform spindle cells (**a**) intervened with hemangiopericytoma-like vessels (**c**, arrowhead). Tumor contains areas of extravasated red blood cells (**b**, **d**)

- There is an admixture of different arrangement patterns, namely short fascicular, storiform and whorled, intervened with typical hemangiopericytoma-like vessels (Fig. 10.15c) which are commonly surrounded by thick acellular perivascular hyalinized materials.
- Tumor cells appear round, oval to spindle in shape and contain vesicular to hyperchromatic nuclei with inconspicuous nucleoli and eosinophilic cytoplasm with indistinct cell borders.
- Mitotic figures are occasionally detected but usually infrequent (< 3/10 HPF). Nuclear pleomorphism is generally absent or mild. No necrosis is present [52–54].
- Occasionally, areas of fibrosis and myxoid changes.
- Most tumors contain inflammatory cells (mostly eosinophils and mast cells) and areas of extravasated red blood cells (Fig. 10.15b, d).
- Features indicating malignancy include profound pleomorphism, invasion, necrosis, and increased mitoses (> 4 per 2 mm^2) [55].

Immunohistochemistry

- Positive for β-catenin (nuclear expression) (Fig. 10.16a), Factor XIIIa (Fig. 10.16b), cyclin D1 (Fig. 10.16c), α-SMA (Fig. 10.16d), and MSA (Fig. 10.16f) [52].
- In some cases, CD34 may be focally positive with weak to moderate intensity (Fig. 10.16e).

Differential Diagnosis

- Monophasic synovial sarcoma: usually positive for cytokeratin and EMA but negative for α-SMA, MSA, and cyclin D1.
- Glomus tumor: negative for *CTNNB1* mutations and, therefore, shows no nuclear β-catenin immunoreactivity.

Treatment and Prognosis

- Surgery is considered the treatment of choice while radiotherapy is chosen for inoperable cases, or metastases.
- SNGPs usually exhibit low malignant potential with exceedingly rare distant metastases.
- Recurrence rate is about 40% (range 7–50%) with an average time to relapse of 6–7 years [52, 56].

10.3.3 Solitary Fibrous Tumor

SFT is an uncommon tumor composed of spindled fibroblastic cells set within a branching vasculature [21, 57, 58] and chararcteristically shows *NAB2::STAT6* gene fusion [57]. The tumor may arise in any anatomic site, 50% of which are in the thoracic cavity [59]. Other regions that have been described include the liver, adrenal gland, skin, and head and neck area. The preferred sites for the head and neck tumors include orbit followed by nasal cavity and/or paranasal sinuses [21, 59].

Macroscopy

- Polypoid, white to pale tan with a firm consistency.
- Presence of extensive necrosis may suggest sarcomatous transformation [58].

Histopathology

- Unencapsulated tumor located at the submucosa.
- Combination of hyper- and hypocellular areas (Fig. 10.17a, b).
- The neoplastic cells are bland-looking, spindle in shape showing haphazard (patternless) growth with mostly fascicular (Fig. 10.17c) or storiform pattern.
- There is a collagenous background that may appear ropey, hyalinized, sometimes keloid-like, or amianthoid-looking [57].
- Dilated, branching or hemangiopericytoma-like vessels are usually present (Fig. 10.17d).
- Mitotic count is usually low, and necrosis is not common, which, if distinctly detected, should raise concern of high-grade sarcomatous transformation [58].

Immunohistochemistry

- STAT6 protein is the most reliable marker for a diagnosis of SFT [21] (Fig. 10.17e, f).
- CD34, Bcl-2, and CD99 are consistently expressed in SFT, but less specific due to overlap with other mesenchymal neoplasms.

Treatment and Prognosis

- Surgery is considered the treatment of choice and SFT is usually cured with complete excision. Yet, evaluation of margins is often difficult as tumors resected by endoscopic surgical approaches are received in fragments [21].
- When all anatomic sites are included, most SFTs are indolent. Malignant features can be found in 5–20% of thoracic SFTs but they are very rare in extrathoracic tumors particularly in the sinonasal region [59]. Among the reported sinonasal SFT with available follow-up data, there were no instances of metastasis or death due to disease [21]. However, it should always be kept in mind that a slight potential for recurrence from the sinonasal tract neoplasms does exist [21].
- Factors related to adverse clinical outcome include age > 55 years, tumor size >15 cm, necrosis, and mitotic count more than 4/10 HPF [57].

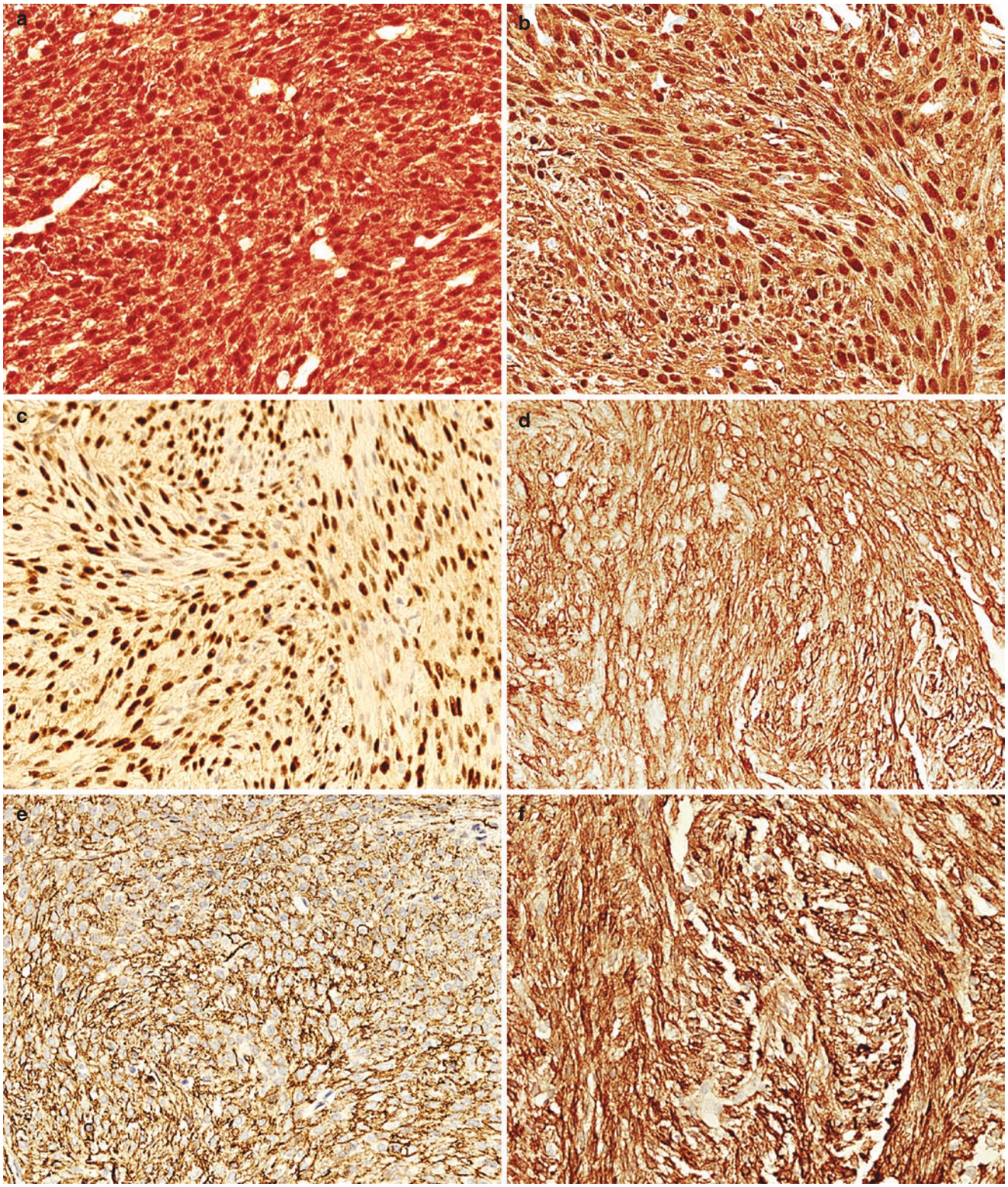

Fig. 10.16 Immunophenotype of SNGP. Positive for β-catenin (**a**), Factor XIIIa (**b**), Cyclin D1 (**c**), SMA (**d**), CD34 (**e**), and MSA (**f**)

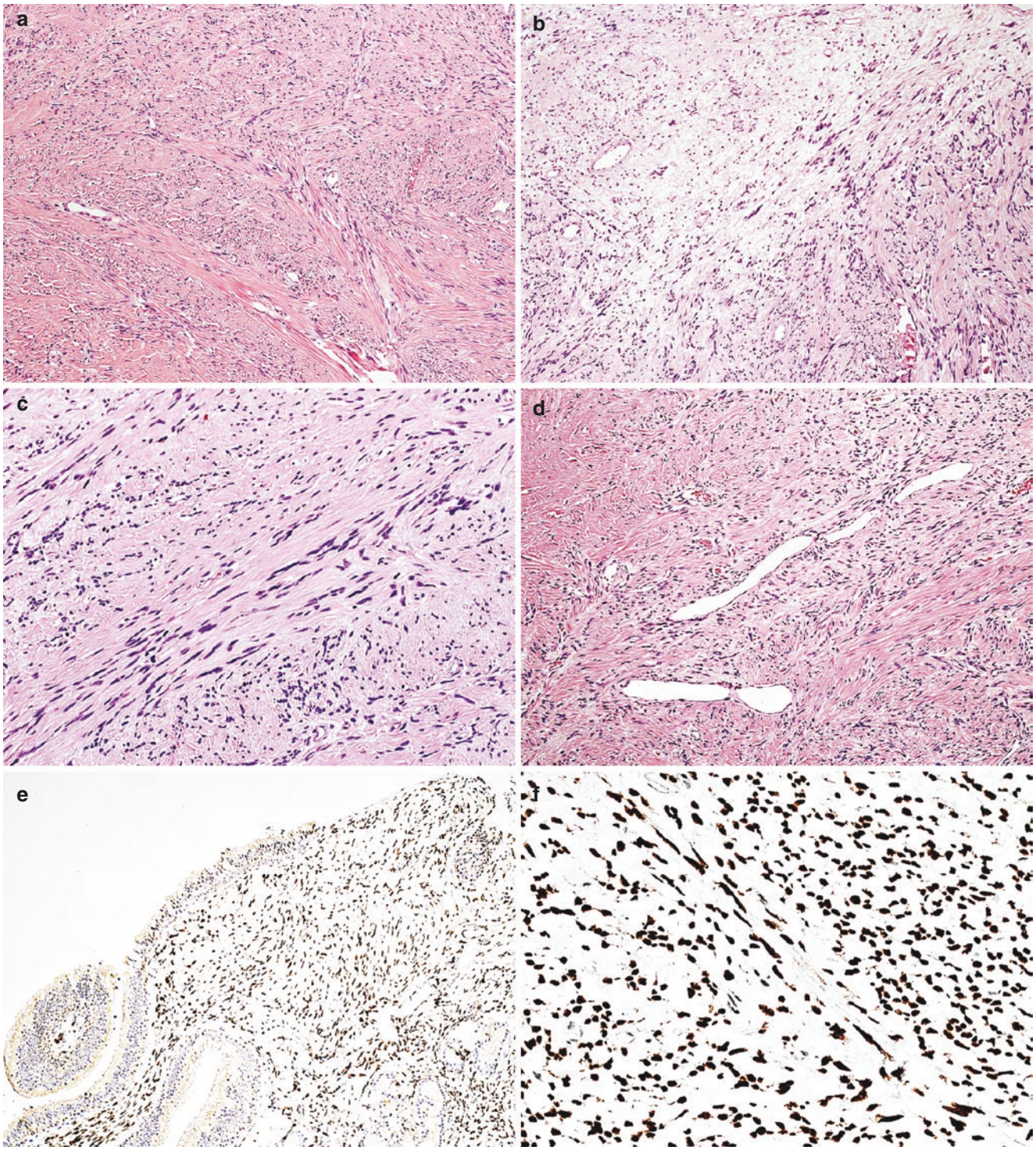

Fig. 10.17 Histology and immunohistochemistry of SFT. Bland-looking, spindle-shaped cells, arranged in haphazard pattern (**a**–**d**) admixed with collagenous tissue background and is composed of hyper- and hypocellular areas (**b**). There are dilated, staghorn shaped blood vessels (**d**). Tumor cells express nuclear STAT6, well appreciated on low power (**e**, subepithelial) and high power (**f**)

10.4 Conclusion

Sinonasal tract harbors a wide range of benign and borderline mesenchymal neoplasms. Majority of these tumors have no site-specific morphology. Knowledge of histopathology, immunohistochemistry, and differential diagnosis is important for the correct diagnosis.

References

1. Thompson LDR, Bullerdiek J, Flucke U, Franchi A. Benign soft tissue tumours. In: El-Naggar AK, Chan JKC, Grandis JR, Takata T, Slootweg PJ, editor. WHO Classification of Head and Neck Tumours. 4th ed. Lyon: IARC; 2017. p. 47.
2. Harcourt JP, Gallimore AP. Leiomyoma of the paranasal sinuses. J Laryngol Otol. 1993;107(8):740–1. PubMed PMID:8409732. Epub 1993/08/01
3. Rajasekar MKNS, Thrupthi S. A rare case report of nasal leiomyoma. International. J Sci Res. 2019;8(11)
4. Siddana SGMM, Ashwathappa DT, S. Leiomyoma of the maxilla: case report with review of literature. J Indian Acad Oral Med Radiol. 2014;26:331–4.
5. Agarwal AK, Bansal R, Singhal D. Sinonasal leiomyoma: report of 2 cases. ENT-Ear, Nose & Throat Journal. 2005;84(4):224–30. PubMed PMID:15929322
6. Zhu G, Xiao D, Sun P. Expression of estrogen and progesterone receptors in angioleiomyoma of the nasal cavity of six patients. Oncol Lett. 2016;11(4):2359–64. PubMed PMID: 27073480. Pubmed Central PMCID: PMC4812515. Epub 2016/04/14
7. Kuruvilla A, Wenig BM, Humphrey DM, Heffner DK. Leiomyosarcoma of the sinonasal tract. A clinicopathologic study of nine cases. Arch Otolaryngol Head Neck Surg. 1990;116(11):1278–86. PubMed PMID:2242259. Epub 1990/11/01
8. Lazar A EH, Shipley J. Smooth-muscle tumours. In: Fletcher CDM BJ, Hogendoorn PCW, Merents F, editor. WHO classification of Tumours of soft tissue and bone. Lyon: IARC; 2013. p. 111–113.
9. Huang HY, Antonescu CR. Sinonasal smooth muscle cell tumors: a clinicopathologic and immunohistochemical analysis of 12 cases with emphasis on the low-grade end of the spectrum. Arch Pathol Lab Med. 2003;127(3):297–304. PubMed PMID: 12653572. Epub 2003/03/26
10. Nayak DR, Ghanpur AD, Reddy AN, Sharma S. Smooth muscle tumour of uncertain malignant potential (SMTUMP) in the nasal cavity: an incidental finding. BMJ Case Rep. Nov 22;2016. PubMed PMID: 27879303. Pubmed Central PMCID: PMC5129059. Epub 2016/11/24.
11. Miettinen M. Smooth muscle tumors of soft tissue and non-uterine viscera: biology and prognosis. Mod Pathol. 2014;27(Suppl 1):S17–29. PubMed PMID: 24384850. Pubmed Central PMCID: PMC7662208. Epub 2014/01/05
12. Abramson S, Gilkeson RC, Goldstein JD, Woodard PK, Eisenberg R, Abramson N. Benign metastasizing leiomyoma: clinical, imaging, and pathologic correlation. AJR Am J Roentgenol. 2001;176(6):1409–13. PubMed PMID: 11373202. Epub 2001/05/25
13. Hanada TYH, Hanaya R, Kurono Y, Nagano H, Kitajima S, Hiraki T, Arita K. A patient with sinonasal leiomyoma presenting with exophthalmos: case report and review of the literature. Neurology Asia. 2013;18(3):327–30.
14. Purohit GN, Agarwal N, Agarwal R. Leiomyoma arising from septum of nose. Indian J Otolaryngol Head Neck Surg. 2011;63(Suppl 1):S64–S7.
15. Joshi R. Learning from eponyms: Jose Verocay and Verocay bodies, Antoni a and B areas, Nils Antoni and schwannomas. Indian. Dermatol Online J. 2012;3:215–9.
16. Antonescu CR, Perry, A, Woodruff, JM. Nerve sheath tumours. In: Fletcher CDM, Bridge JA, Hogendoorn PCW, Mertens F, editors. WHO Classification of Tumours of Soft Tissue and Bone. Lyon: IARC; 2013. p. 170–2.
17. Thompson LDR, Bullerdiek J, Flucke U, Franchi A. Benign soft tissue tumours. In: El-Naggar AK, Chan JKC, Grandis JR, Takata T, Slootweg PJ, editors. WHO Classification of Head and Neck Tumours. 4th ed. Lyon: IARC; 2017. p. 48–9.
18. Sheikh HY, Chakravarthy RP, Slevin NJ, Sykers AJ, Banerjee SS. Benign schwannoma in paranasal sinuses: a clinico-pathological study of five cases, emphasising diagnostic difficulties. J Laryngol Otol. 2008;122:598–602.
19. Mey KH, Buchwald C, Daugaard S, Prause JU. Sinonasal schwannoma--a clinicopathological analysis of five rare cases. Rhinology 2006;44(1):46–52. PubMed PMID: 16550950. Epub 2006/03/23.
20. Buob D, Wacrenier A, Chevalier D, Aubert S, Quinchon JF, Gosselin B, et al. Schwannoma of the sinonasal tract: a clinicopathologic and immunohistochemical study of 5 cases. Arch Pathol Lab Med. 2003;127(9):1196–9. PubMed PMID: 12946223. Epub 2003/08/30
21. Thompson LDR, Lau SK. Sinonasal tract solitary fibrous tumor: a Clinicopathologic study of six cases with a comprehensive review of the literature. Head Neck Pathol. 2018;12(4):471–80. PubMed PMID: 29282671. Pubmed Central PMCID: PMC6232205. Epub 2017/12/29
22. Seles MF, Srinivasa P, Ramadoss N. Schwannoma nasal cavity: a clinicopatholgoical case report. Int J Otorhinolaryngol Head Neck Surg. 2019;5(3):781–4.
23. Thompson LDR, Bullerdiek J, Flucke U, Franchi A. Benign soft tissue tumours. In: El-Naggar AK, Chan JKC, Grandis JR, Takata T, Slootweg PJ, editors. WHO Classification of Head and Neck Tumours. 4th ed. Lyon: IARC; 2017. p. 49–50.
24. Antonescu CR, Brems H, Legius E, Woodruff, JM. Nerve sheath tumours. In: Fletcher CDM, Bridge JA, Hogendoorn PCW, Mertens F, editors. WHO Classification of Tumours of Soft Tissue and Bone. 4th ed. Lyon: IARC; 2013. p. 174–6.
25. Azani AB, Bishop JA, Thompson LDR. Sinonasal tract Neurofibroma: a clinicopathologic series of 12 cases with a review of the literature. Head Neck Pathol. 2015;9(3):323–33. PubMed PMID: 25503638. Pubmed Central PMCID: PMC4542792. Epub 2014/12/17
26. Goldblum JR, Folpe AL, Weiss SW. Enzinger and Weiss' Soft Tissue Tumors. 6th ed. Beijing: Elsevier Saunders; 2014.
27. Goldblum JR, Fletcher JA. Desmoid-type fibromatosis. In: Fletcher CDM, Bridge JA, Hogendoorn PCW, Mertens F, editors. WHO Classification of Tumours of Soft Tissue and Bone. 4th ed. Lyon: IARC; 2013. p. 72–3.
28. Puxeddu R, Berlucchi M, Ledda GP, Parodo G, Farina D, Nicolai P. Lobular capillary hemangioma of the nasal cavity: a retrospective study on 40 patients. Am J Rhinol. 2006;20(4):480–4. PubMed PMID:16955784. Epub 2006/09/08
29. Thompson LDR, Bullerdiek J, Flucke U, Franchi A. Benign soft tissue tumors. In: El-Naggar AK, Chan JKC, Grandis JR, Takata T, Slootweg PJ, editors. WHO Classification of Head and Neck Tumours. 4th ed. Lyon: IARC; 2017. p. 47–8.
30. Smith SC, Patel RM, Lucas DR, McHugh JB. Sinonasal lobular capillary hemangioma: a clinicopathologic study of 34 cases characterizing potential for local recurrence. Head Neck Pathol. 2013;7(2):129–34. PubMed PMID:23184353. Pubmed Central PMCID: PMC3642257. Epub 2012/11/28
31. Nichols GE, Gaffey MJ, Mills SE, Weiss LM. Lobular capillary hemangioma: an immunohistochemical study including steroid hormone receptor status. Am J Clin Pathol. 1992;97(6):770–5.

32. Nelson BL, Thompson LD. Sinonasal tract angiosarcoma: a clinicopathologic and immunophenotypic study of 10 cases with a review of the literature. Head Neck Pathol. 2007;1(1):1–12. PubMed PMID: 20614274. Pubmed Central PMCID: PMC2807511. Epub 2007/09/01
33. Toner M, Allen CM, Castle J. Benign maxillofacial bone and cartilage tumours. In: El-Naggar AK, Chan JKC, Grandis JR, Takata T, Slootweg PJ, editors. WHO Classification of Head and Neck Tumours. 4th ed. Lyon: IARC; 2017. p. 246.
34. McHugh JB, Mukherji SK, Lucas DR. Sino-orbital osteoma: a clinicopathologic study of 45 surgically treated cases with emphasis on tumors with osteoblastoma-like features. Arch Pathol Lab Med. 2009;133(10):1587–93. PubMed PMID: 19792048. Epub 2009/10/02
35. Cheng KJ, Wang SQ, Lin L. Giant osteomas of the ethmoid and frontal sinuses: clinical characteristics and review of the literature. Oncol Lett. 2013;5(5):1724–30. PubMed PMID: 23759920. Pubmed Central PMCID: PMC3678544. Epub 2013/06/14
36. El-Mofty SK, Nelson B, Toyosawa S. Fibro-osseous and osteochondromatous lesions. In: El-Naggar AK, Chan JKC, Grandis JR, Takata T, Slootweg PJ., editors. WHO Classification of Head and Neck Tumours. 4th ed. Lyon: IARC; 2017. p. 251–2.
37. Thompson LDR, Agaimy A, Jo VY. Sinonasal tract angiofibroma. In: WHO Classification of Tumours Editorial Board Head and Neck Tumours [Internet; beta version ahead of print]. Lyon International Agency for Research on Cancer; 2022 [cited 2022, 06, 07]. (WHO classification of tumours series, 5th ed.; vol. 9). Available from: https://tumourclassification.iarc.who.int/chapters/52.
38. Prasad ML, Franchi A. Thompson LDR. Soft tissue tumours. In: El-Naggar AK, Chan JKC, Grandis JR, Takata T, Slootweg PJ, editors. WHO Classification of Head and Neck Tumours. 4th ed. Lyon: International Agency for Research on Cancer; 2017. p. 74–5.
39. Xu B. Nasopharyngeaal angiofibroma. PathologyOutlines.com. website. https://www.pathologyoutlines.com/topic/nasalangiofibroma.html. Accessed 7 June 2022.
40. Hwang HC, Mills SE, Patterson K, Gown AM. Expression of androgen receptors in nasopharyngeal angiofibroma: an immunohistochemical study of 24 cases. Mod Pathol. 1998;11(11):1122–6. PubMed PMID:9831211. Epub 1998/11/27
41. Abraham SC, Montgomery EA, Giardiello FM, Wu TT. Frequent beta-catenin mutations in juvenile nasopharyngeal angiofibromas. Am J Pathol. 2001;158(3):1073–8. PubMed PMID: 11238055. Pubmed Central PMCID: PMC1850353. Epub 2001/03/10
42. Giardiello FM, Hamilton SR, Krush AJ, Offerhaus JA, Booker SV, Petersen GM. Nasopharyngeal angiofibroma in patients with familial adenomatous polyposis. Gastroenterology. 1993;105(5):1550–2. PubMed PMID: 8224661. Epub 1993/11/01
43. Ferouz AS, Mohr RM, Paul P. Juvenile nasopharyngeal angiofibroma and familial adenomatous polyposis: an association? Otolaryngol Head Neck Surg. 1995;113(4):435–9. PubMed PMID: 7567017. Epub 1995/10/01
44. Waterhouse D. Nasopharyngeal angiofibroma: a manifestation of familial adenomatous polyposis. ANZ J Surg. 2013;83(5):387–8. PubMed PMID: 23614886. Epub 2013/04/26
45. Johns ME, MacLeod RM, Cantrell RW. Estrogen receptors in nasopharyngeal angiofibromas. Laryngoscope. 1980;90(4):628–34. PubMed PMID: 6244469 Epub 1980/04/01
46. Wenig BM, Flucke U, Thompson LDR. Borderline/low-grade malignant soft tissue tumours. In: El-Naggar AK, Chan JKC, Grandis JR, Takata T, Slootweg PJ, editors. WHO Classification of Head and Neck Tumours. 4th ed. Lyon: IARC; 2017. p. 43.
47. Gnepp DR, Henley J, Weiss S, Heffner D. Desmoid fibromatosis of the sinonasal tract and nasopharynx. A clinicopathologic study of 25 cases. Cancer. 1996;78(12):2572–9. PubMed PMID: 8952566. Epub 1996/12/15
48. Lakhan SE, Eager RM, Harle L. Aggressive juvenile fibromatosis of the paranasal sinuses: case report and brief review. J Hematol Oncol. 2008;28(1):3. PubMed PMID: 18577255. Pubmed Central PMCID: PMC2438440. Epub 2008/06/26
49. Andino L, Cagle PT, Murer B, Lu L, Popper HH, Galateau-Salle F, et al. Pleuropulmonary desmoid tumors: immunohistochemical comparison with solitary fibrous tumors and assessment of beta-catenin and cyclin D1 expression. Arch Pathol Lab Med. 2006;130(10):1503–9. PubMed PMID: 17090192. Epub 2006/11/09
50. Barak S, Wang Z, Miettinen M. Immunoreactivity for calretinin and keratins in desmoid fibromatosis and other myofibroblastic tumors: a diagnostic pitfall. Am J Surg Pathol. 2012;36(9):1404–9. PubMed PMID: 22531174. Pubmed Central PMCID: PMC7477945. Epub 2012/04/26
51. Hansmann A, Adolph C, Vogel T, Unger A, Moeslein G. High-dose tamoxifen and sulindac as first-line treatment for desmoid tumors. Cancer. 2004;100(3):612–20. PubMed PMID: 14745880. Epub 2004/01/28
52. Thompson LDR, Flucke U, Wenig BM. Borderline/low-grade malignant soft tissue tumours. In: El-Naggar AK, Chan JKC, Grandis JR, Takata T, Slootweg PJ, editors. WHO Classification of Head and Neck Tumours. 4th ed. Lyon: IARC; 2017. p. 44–5.
53. Obeidin F, Jennings LJ, Alexiev BA. Sinonasal glomangiopericytoma: A clinicopathologic study. Pathol Res Pract. 2019;215(5):983–7. PubMed PMID: 30739805. Epub 2019/02/12
54. Dandekar M, McHugh JB. Sinonasal glomangiopericytoma: case report with emphasis on the differential diagnosis. Arch Pathol Lab Med. 2010;134(10):1444–9. PubMed PMID: 20923298. Epub 2010/10/07
55. Thompson LDR, Jun, SY, Lai CK. Sinonasal glomangiopericytoma. In: WHO Classification of Tumours Editorial Board Head and Neck Tumours [Internet; beta version ahead of print]. Lyon: International Agency for Research on Cancer; 2022. [cited 2022, 06,07]. (WHO classification of tumours series, 5th ed.; vol.9). Available from: https://tumourclassification.iarc.who.int/chapters/52.
56. Oosthuizen JC, Kennedy S, Timon C. Glomangiopericytoma (sinonasal-type haemangiopericytoma). J Laryngol Otol. 2012;126(10):1069–72. PubMed PMID: 22992272. Epub 2012/09/21
57. Flucke U, Thompson LDR, Wenig BM. Borderline/low-grade malignant soft tissue tumours. In: El-Naggar AK, Chan JKC, Grandis JR, Takata T, Slootweg PJ, editors. WHO Classification of Head and Neck Tumours. 4th ed. Lyon: IARC; 2017. p. 45.
58. Smith SC, Gooding WE, Elkins M, Patel RM, Harms PW, McDaniel AS, et al. Solitary fibrous tumors of the head and neck: a multi-institutional Clinicopathologic study. Am J Surg Pathol. 2017;41(12):1642–56. PubMed PMID: 28877055. Pubmed Central PMCID: PMC5680135. Epub 2017/09/07
59. Ganly I, Patel SG, Stambuk HE, Coleman M, Ghossein R, Carlson D, et al. Solitary fibrous tumors of the head and neck: a clinicopathologic and radiologic review. Arch Otolaryngol Head Neck Surg. 2006;132(5):517–25. PubMed PMID: 16702568. Epub 2006/05/17

Malignant Mesenchymal Tumors of Sinonasal Tract

11

Deepali Jain and Justin A. Bishop

11.1 Introduction

World Health Organization (WHO) 2022 classification of head and neck tumors [1] divides mesenchymal tumors of sinonasal (SN) tract into benign and malignant tumors. The former includes sinonasal tract angiofibroma and sinonasal glomangiopericytoma (see Chap. 10), whereas the latter are biphenotypic sinonasal sarcoma and chordoma. In addition there are other malignant mesenchymal tumors of head and neck which are separately discussed in which there are few tumors which variably involve SN tract. These tumors are rhabdomyosarcoma (RMS) and Ewing sarcoma. Phosphaturic mesenchymal tumors are of uncertain behavior and comprise of benign and malignant subtypes. In this chapter all of these tumors are discussed.

11.2 Biphenotypic Sinonasal Sarcoma

These low grade sarcomas exclusively involve SN tract with neural and myogenic differentiation which is shown by S-100 and muscle actin immunostains. Cytogenetically, tumors harbor *PAX3* rearrangement commonly with partner gene *MAML3* [t(2;4)(q35;q31.1)] [2].

Clinically, women are frequently affected than men. These are locally infiltrative polyps or mass lesions which tend to recur after surgical excision.

Histopathologically, tumor is characterized by spindle cell proliferation in herringbone/fascicular arrangement without much atypia, mitotic activity, and necrosis.

Tumor infiltrates adjacent bone. Overlying respiratory epithelium is hyperplastic with or without squamous metaplasia and entrapped within the tumor cells. The stroma is variably collagenized and shows prominent vasculature [3].

Immunohistochemically, tumor cells show focal to diffuse S-100 positivity. Lack of SOX10 staining along with smooth muscle actin and variable desmin and other muscle markers differentiate them from nerve sheath tumors. Nuclear PAX3 and beta catenin staining is present along with nonspecific Pan TRK. NTRK-rearranged spindle cell tumors show S-100 positivity along with CD34; however, they show NTRK rearrangement on molecular testing instead of PAX3 fusions [4]. Experience of sinonasal NTRK-rearranged sarcomas is limited and not reported in literature (See Figs. 11.1, 11.2, 11.3, 11.4, 11.5, 11.6, 11.7, 11.8, 11.9, 11.10, 11.11, and 11.12).

D. Jain (✉) · J. A. Bishop
Department of Pathology, All India Institute of Medical Sciences, New Delhi, India

Department of Pathology, UT Southwestern Medical Center, Dallas, TX, USA
e-mail: deepalijain76@aiims.edu

D. Jain, J. A. Bishop (eds.), *Atlas of Sinonasal Tract Pathology*, https://doi.org/10.1007/978-981-19-7315-4_11

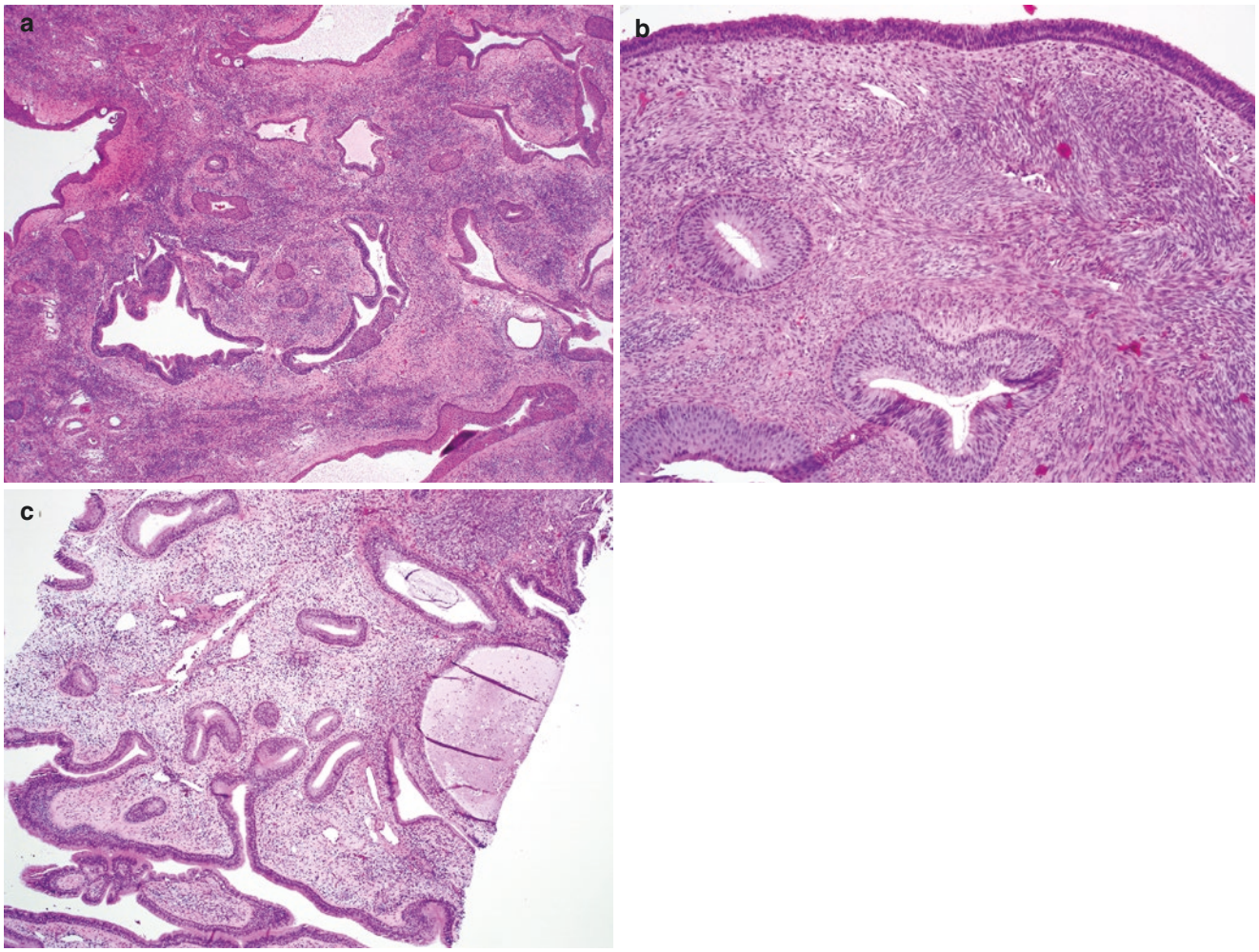

Fig. 11.1 Low magnification shows tumor cells insinuating between entrapped respiratory epithelium and cystically dilated glands (**a**–**c**)

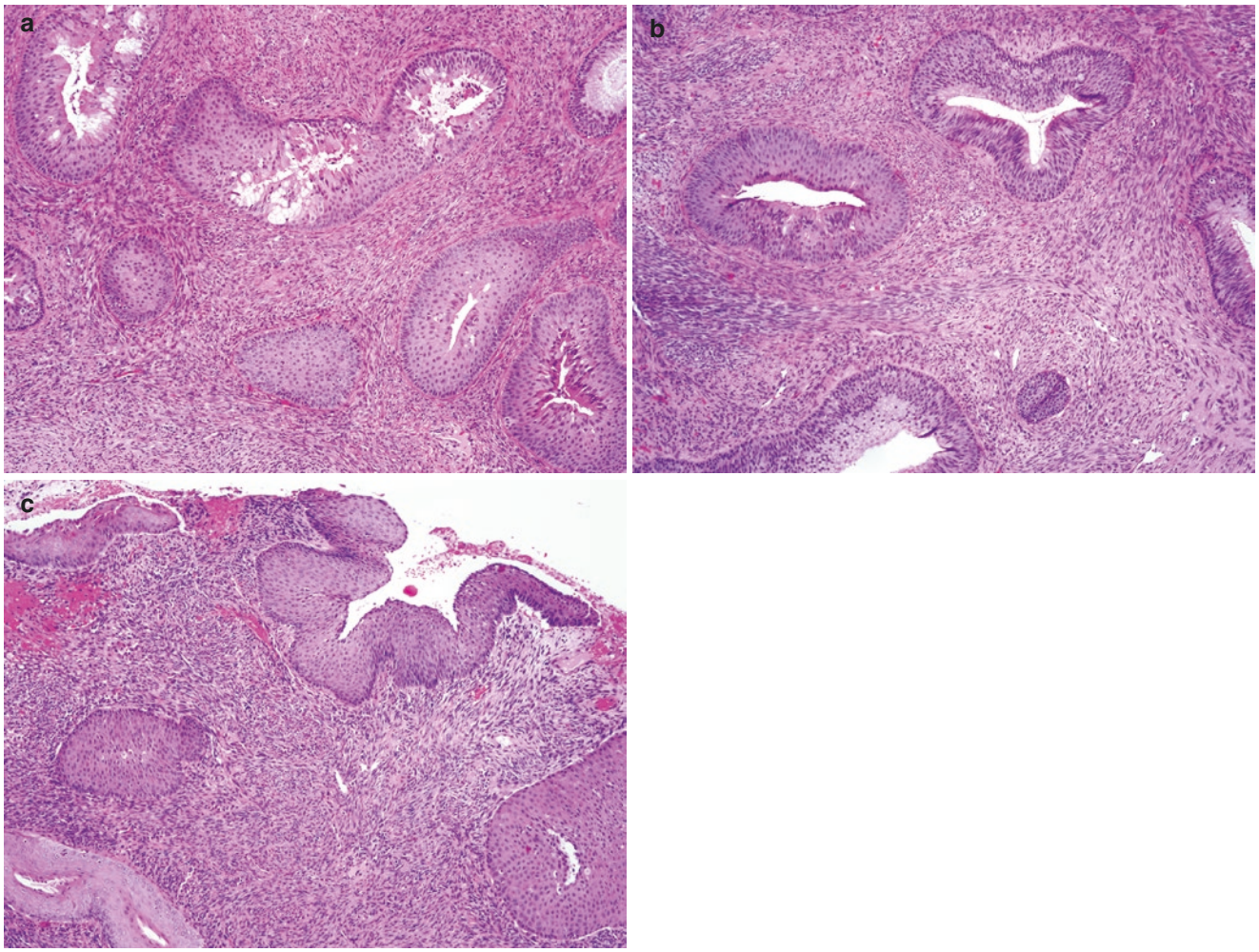

Fig. 11.2 Tumor is densely cellular with fascicular pattern of spindle cells. Entrapped epithelial foci show squamous metaplasia (**a**–**c**)

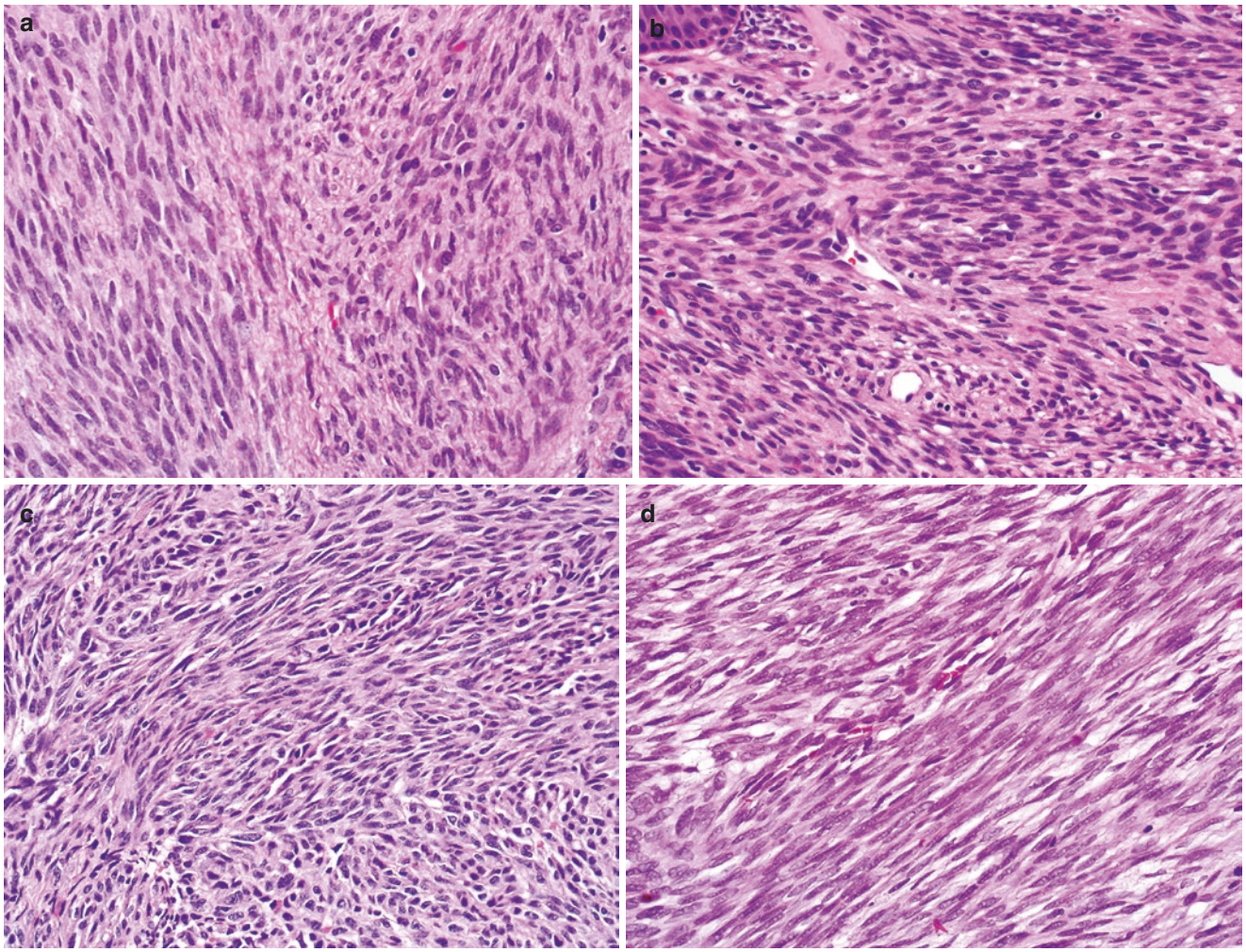

Fig. 11.3 Individual tumor cells on higher magnification show relatively monomorphic spindle cells with eosinophilic cytoplasm. Fine nuclear chromatin and absence of nucleoli with no mitotic activity and necrosis. Some of the nuclei show wavy nuclear membranes (**a–d**)

Fig. 11.4 Tumor is infiltrating into adjacent bone (right corner)

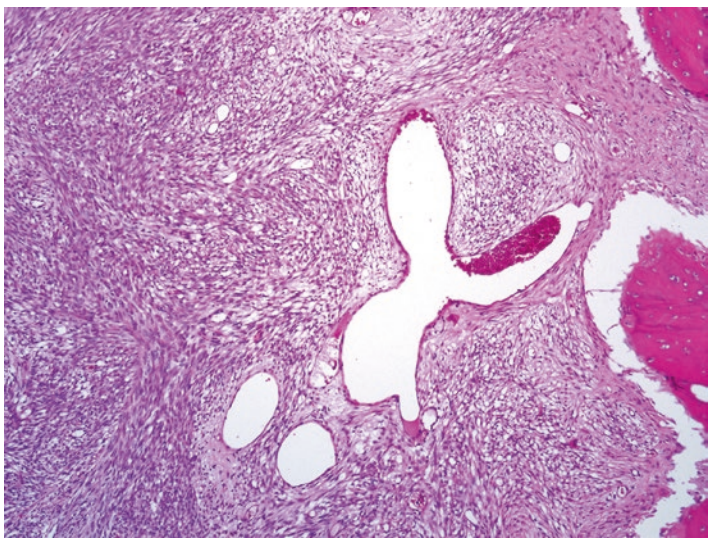

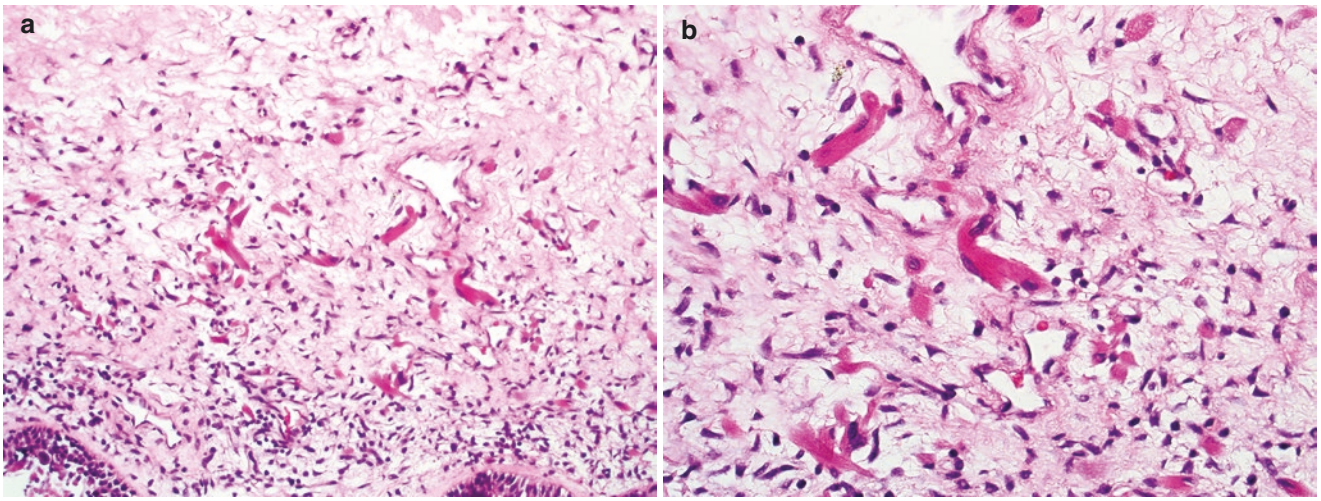

Fig. 11.5 Rhabdomyoblastic differentiation is noticed with abundant dense eosinophilic cytoplasm in few cells (strap cells) (**a**, **b**)

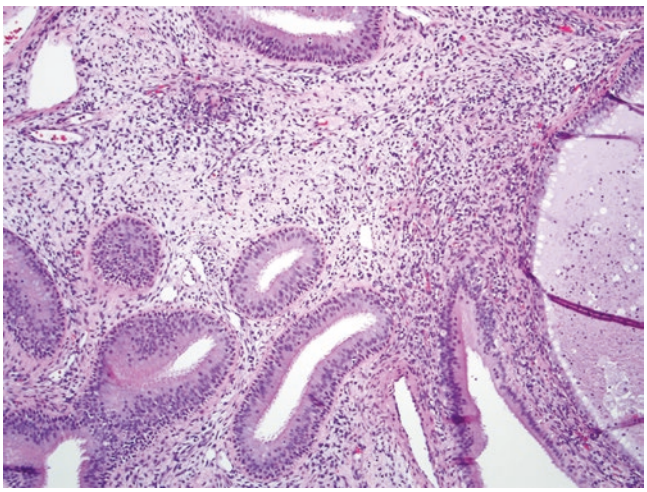

Fig. 11.6 At times tumor is subtle with sparse tumor cells which are misidentified as stromal cells

Fig. 11.7 Computerized tomography (CT) scan shows a large heterogeneously enhancing bilobed mass lesion in the nasal cavity and ethmoid sinuses

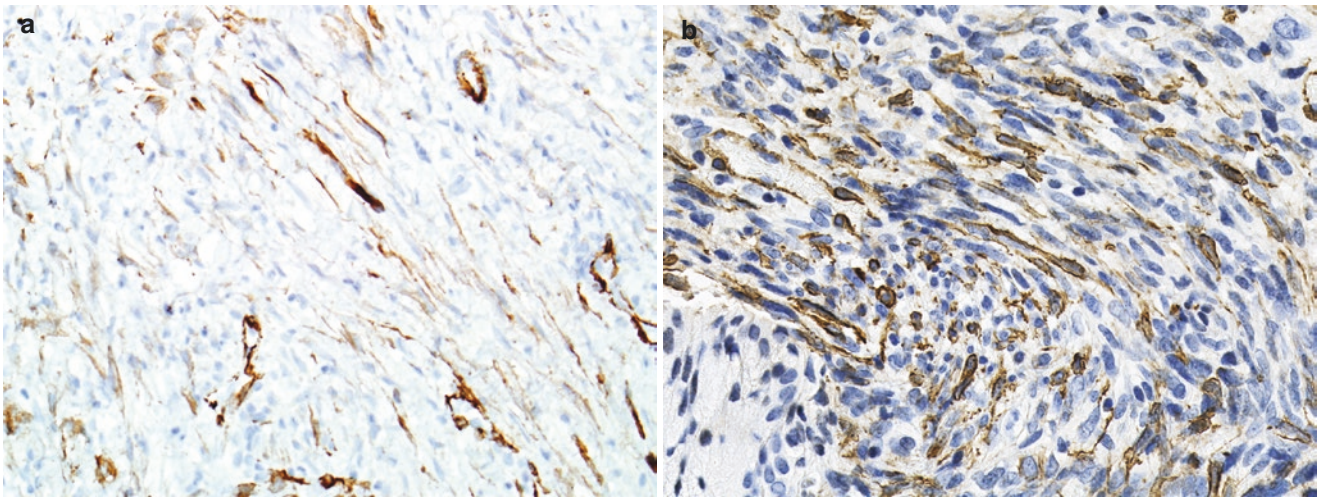

Fig. 11.8 Smooth muscle actin shows sparse to diffuse positivity in tumor cells (**a**, **b**)

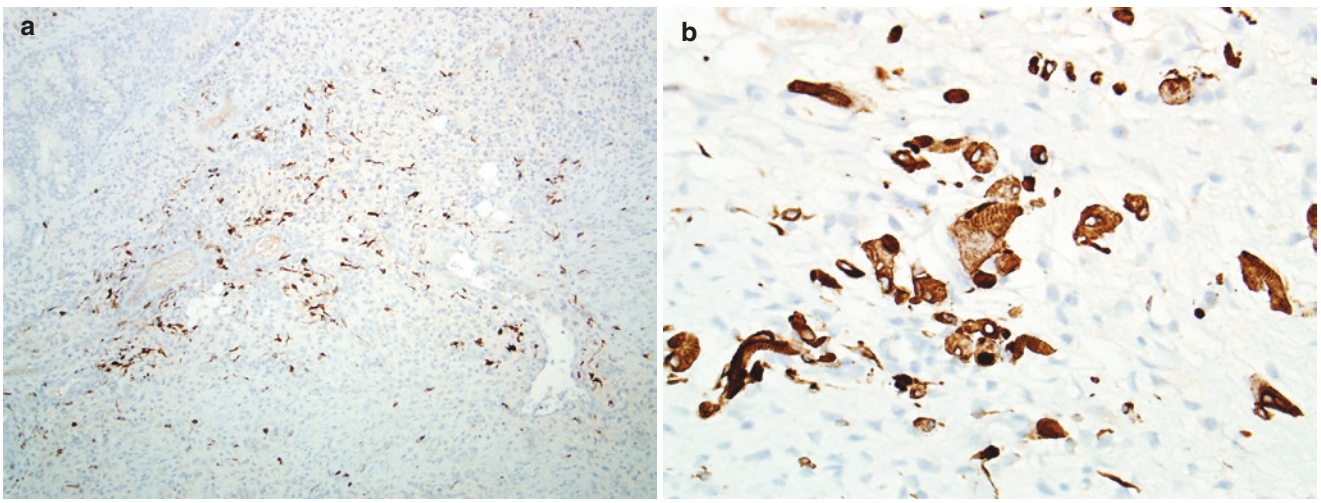

Fig. 11.9 Desmin stains few tumor cells (**a**) and strap cells (**b**)

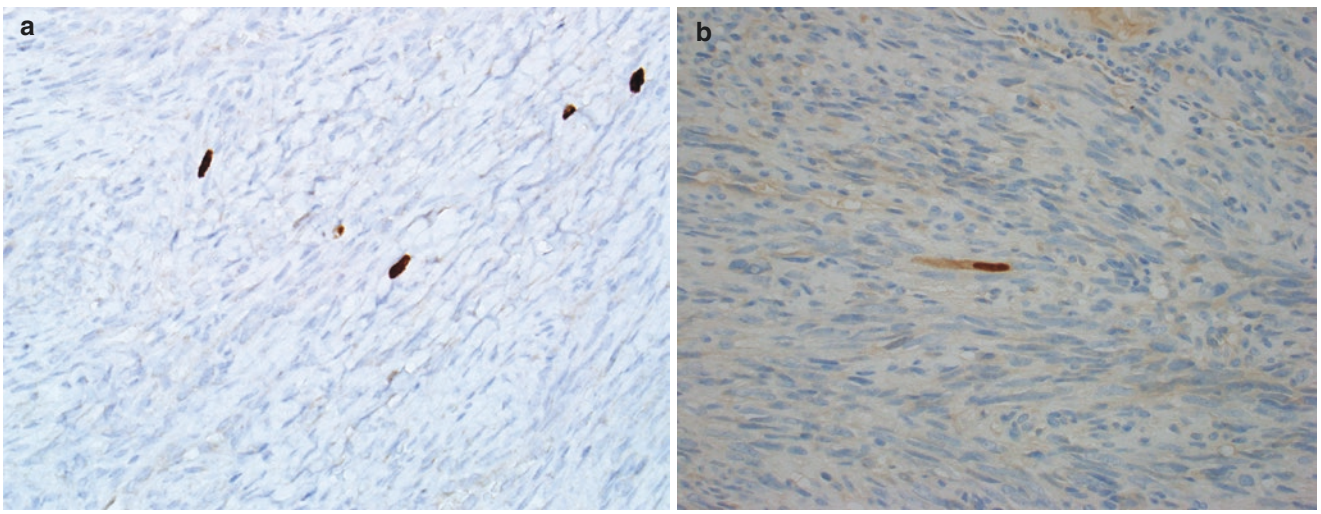

Fig. 11.10 Myogenin shows nuclear positivity in rare tumor cells (**a**, **b**)

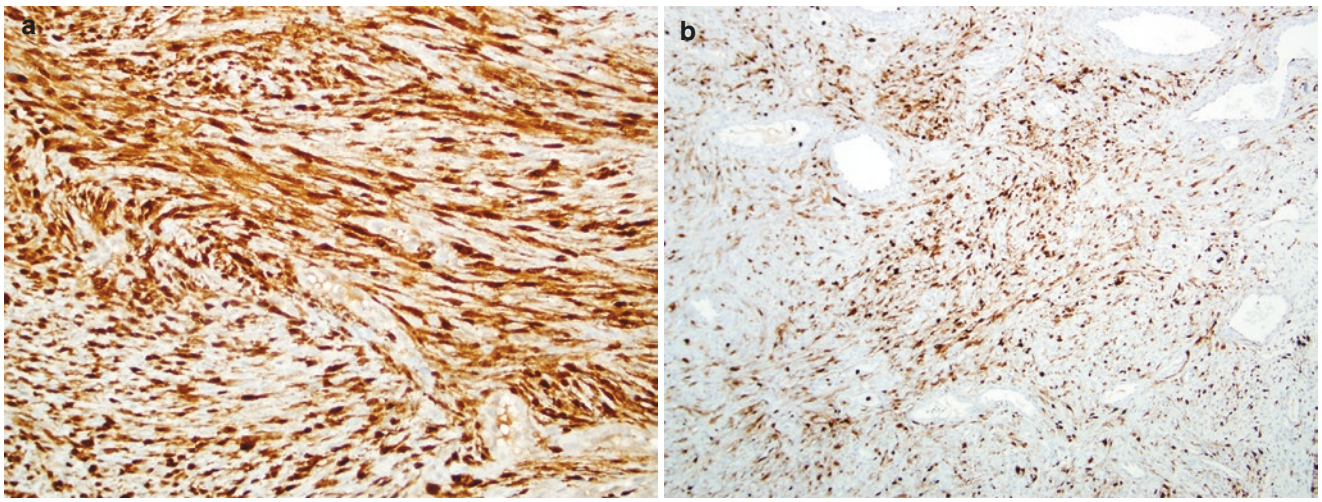

Fig. 11.11 S-100 diffusely positive (nuclear and cytoplasmic) in tumor cells (**a**, **b**)

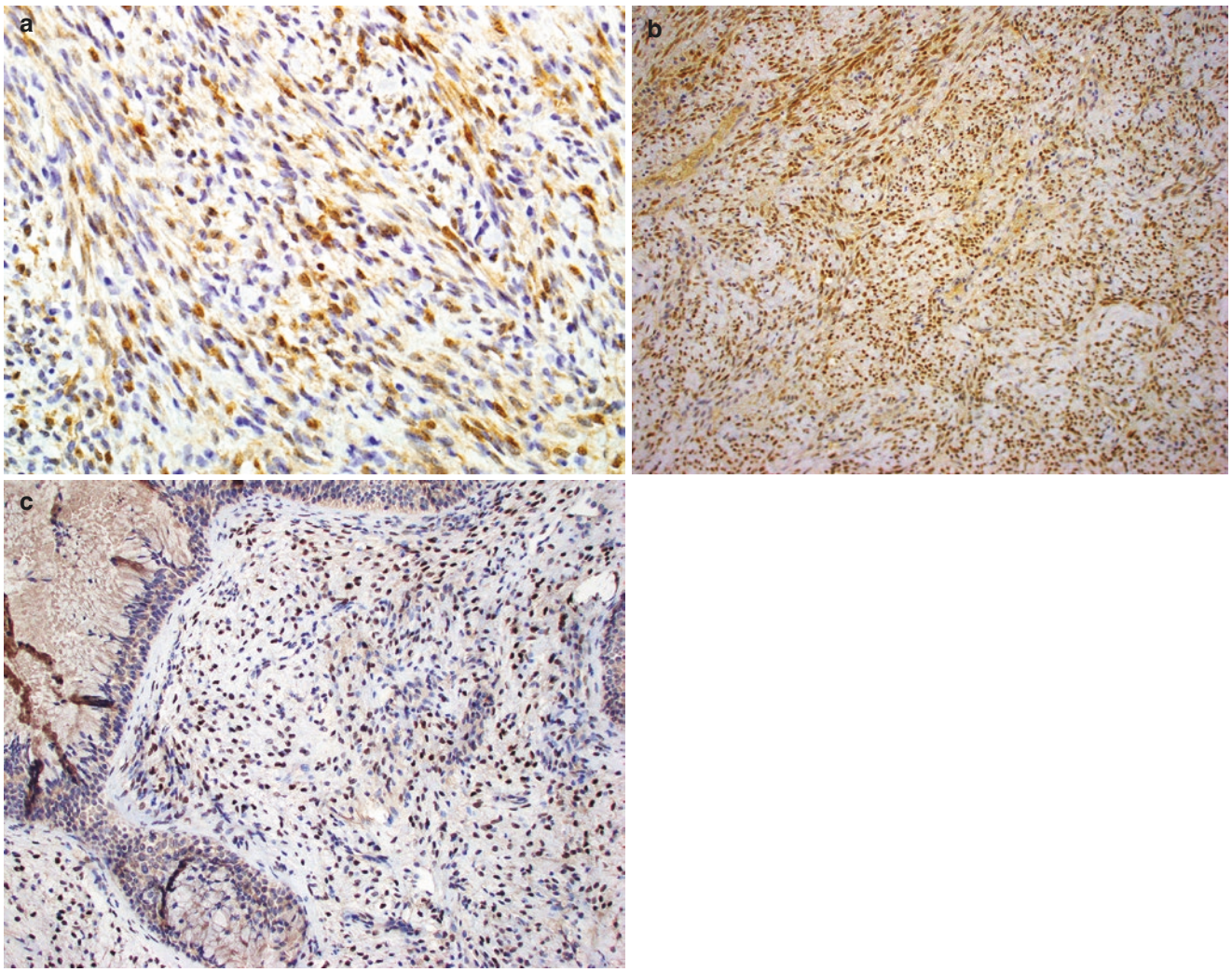

Fig. 11.12 Beta catenin (**a**) and PAX3 shows nuclear staining (**b**, **c**)

11.3 Chordoma

Chordomas are malignant tumors arising from remnants of notochord. Chordomas of nasal wall, nasopharynx, and paranasal sinuses are extra-axial tumors sometimes associated with a sinus tract extending from the clivus [5].

Grossly, tumors are lobulated gelatinous masses due to (chondro)myxoid stroma.

As the name indicates tumor cells are arranged mostly in cords which are embedded within a myxoid matrix. Scattered large physaliferous cells are present with abundant vacuolated/bubbly eosinophilic cytoplasm.

There are multiple subtypes of chordoma which are based on degree and type of differentiation of the tumor. These include chondroid, cellular, poorly differentiated and dedifferentiated types.

Irrespective of subtype, all chordomas are positive for epithelial markers (keratin and epithelial membrane antigen) with S100. Brachyury (*T-box transcription factor T or TBXT)*, a notochord differentiation protein, is a specific nuclear marker for chordoma; however, it is negative in dedifferentiated areas [6]. The most close differentials on morphology and on IHC of chordoma are metastatic mucin secreting carcinoma (due to epithelial marker expression), chondrosarcoma (due to S-100 positivity), and myoepithelial tumors (co-expression of epithelial markers with S100) (See Figs. 11.13, 11.14, 11.15, 11.16, 11.17, and 11.18).

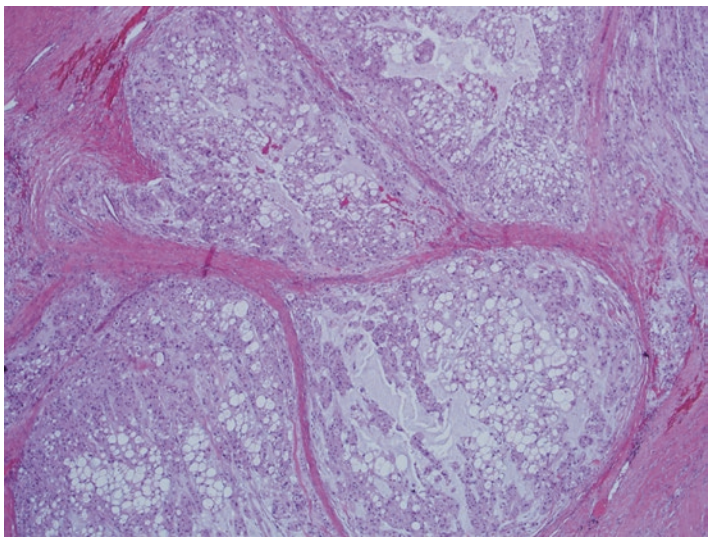

Fig. 11.13 Low power shows lobular architecture with fibrous septae separating tumor lobules

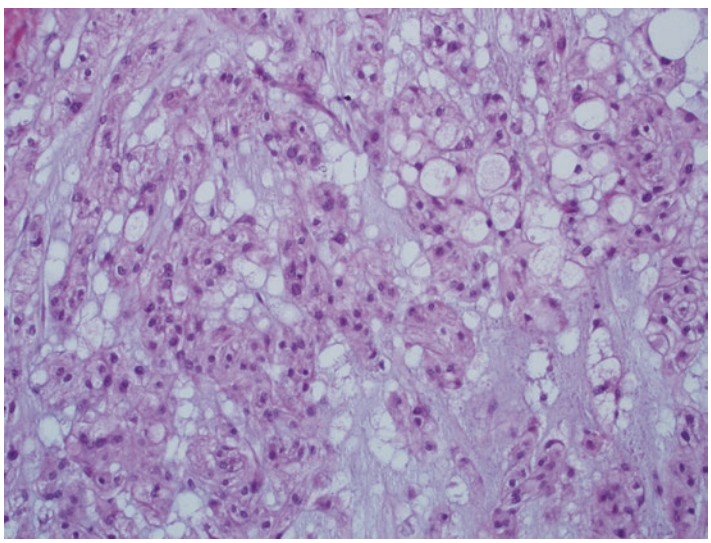

Fig. 11.14 Tumor cells forming short cords, nests, and groups of cells within extracellular myxoid matrix

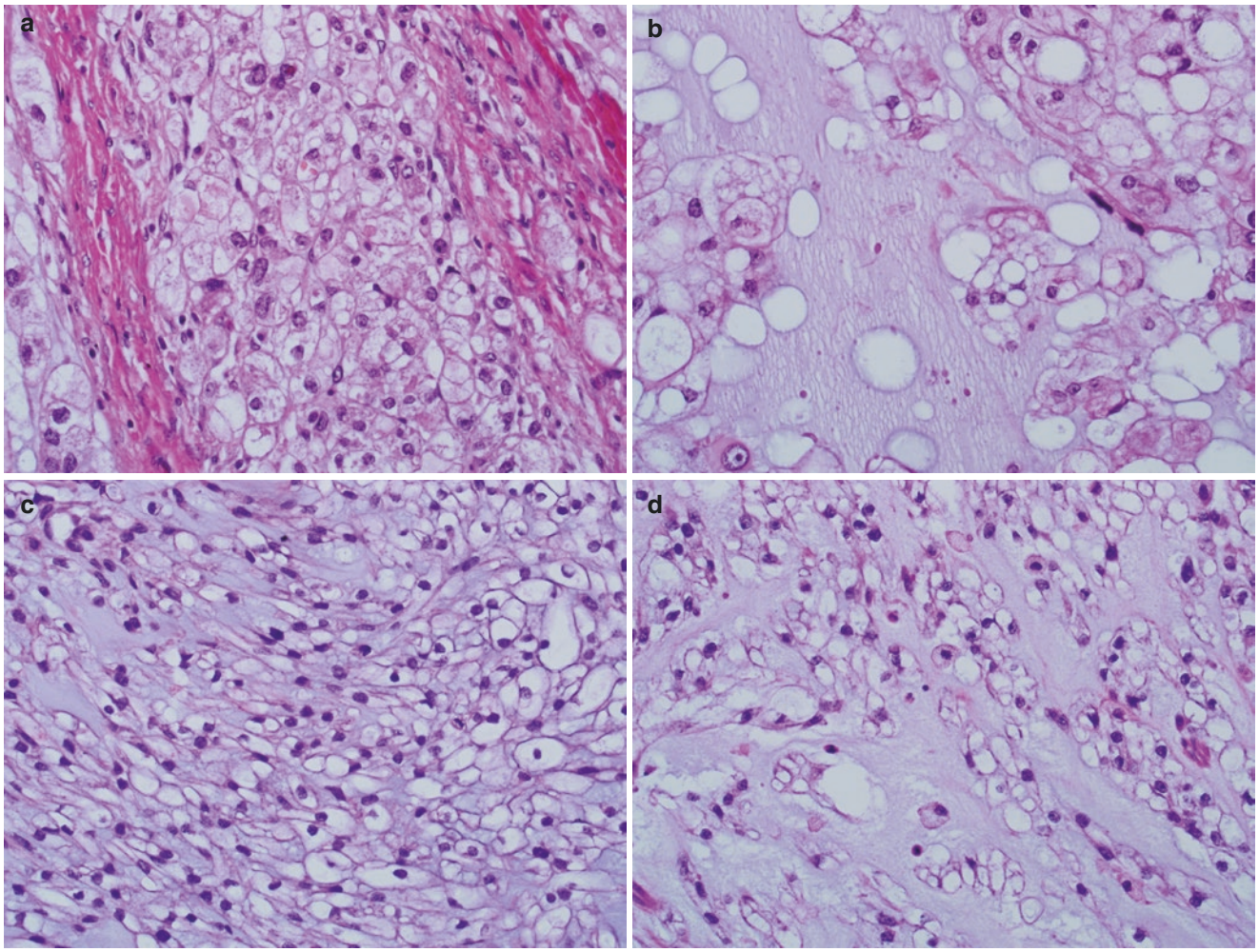

Fig. 11.15 Higher magnification shows individual tumor cells which are large and polygonal epithelioid cells with abundant bubbly or vacuolated to clear cytoplasm (**a**–**d**)

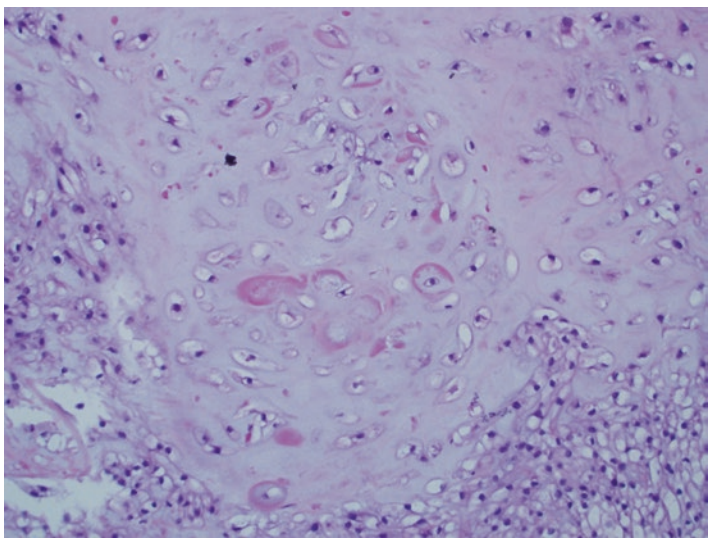

Fig. 11.16 Chondroid chordoma shows hyaline cartilage like matrix

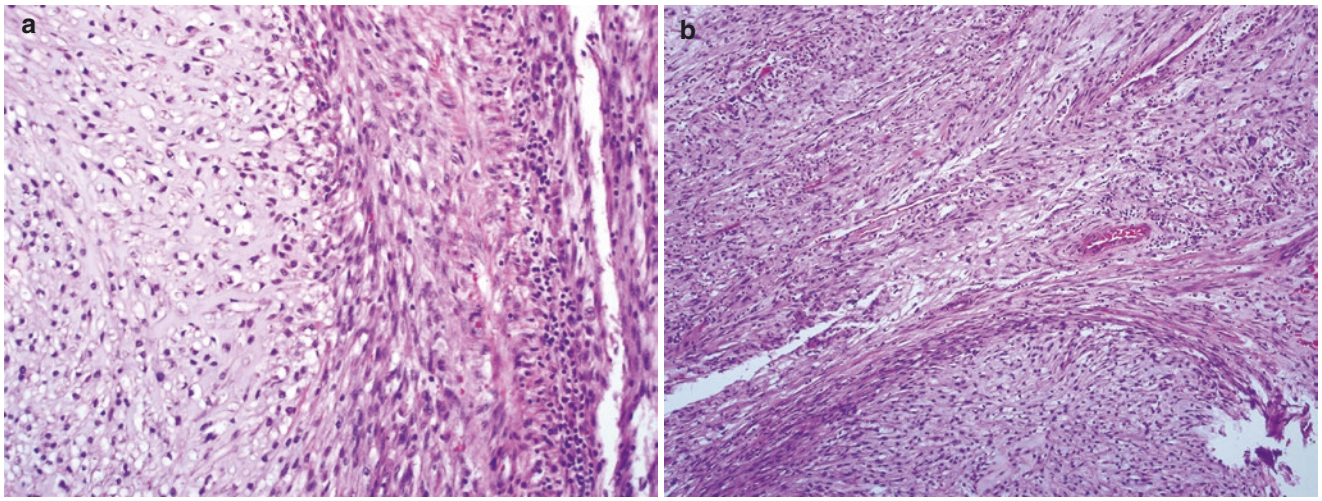

Fig. 11.17 Dedifferentiated chordoma shows biphasic tumor with juxtaposed chordoma (left) and undifferentiated sarcoma (right) (**a**); chordoma (lower) and sarcoma (upper) (**b**)

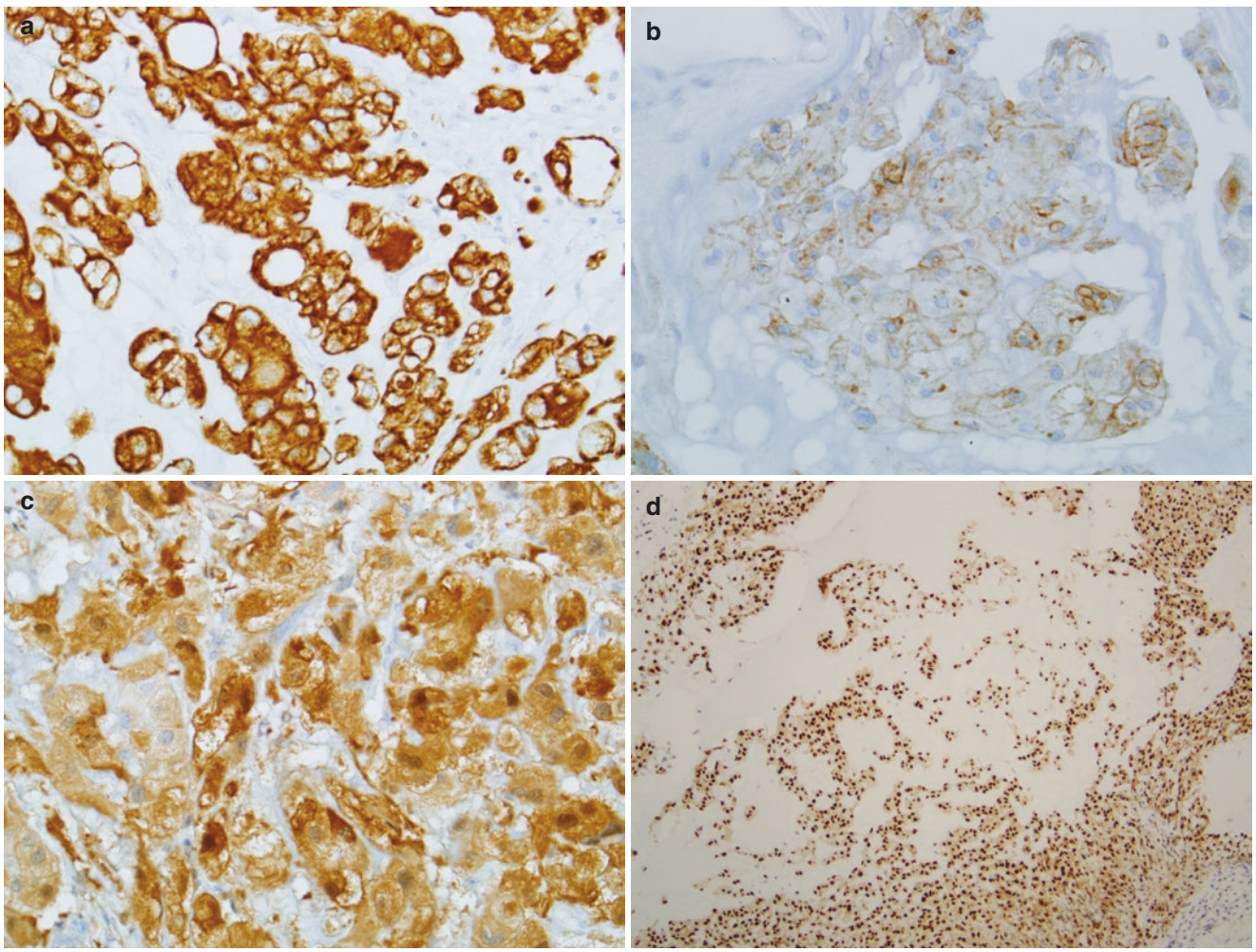

Fig. 11.18 IHC shows diffuse positivity for keratin (**a**), epithelial membrane antigen (**b**), S-100 (**c**) and Brachyury (**d**, **e**)

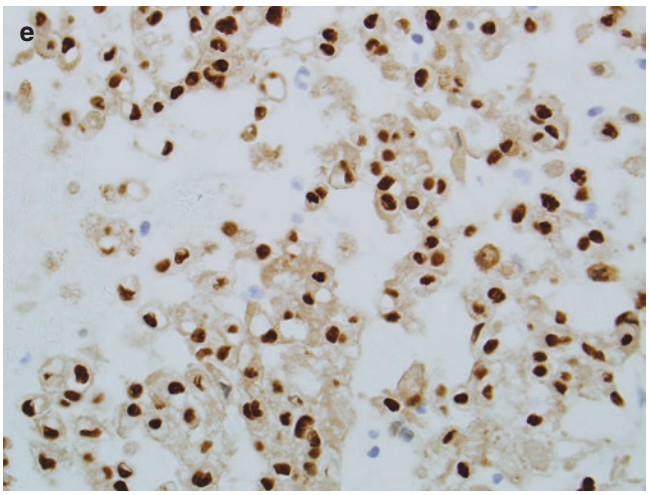

Fig. 11.18 (continued)

11.4 Phosphaturic Mesenchymal Tumor

Phosphaturic mesenchymal tumors are extremely rare soft tissue and bone tumors which belong to category of tumors of uncertain differentiation. Mostly these are benign to borderline clinically; however, rare malignant subtype occurs. Paranasal sinuses are frequent sites of involvement in head and neck area [7].

As its name suggests, patients are phosphaturic and present with osteomalacia. Laboratory examination shows severe hypophosphatemia due to elevated serum levels of fibroblast growth factor 23 (FGF23). Fibroblast growth factor receptor 1 (FGFR1) fusions result into upregulation of FGFR signalling pathways and tumorigenesis.

On morphology, the tumor is composed of nondescript to bland spindle cells which are present in richly vascularized stroma. The stroma is so overwhelming that the tumors mimic vascular neoplasms on cursory look. The vessels range from capillary sized to cavernous spaces and hemangiopericytoma like gaping vessels. These are variably thickened and sometimes show organizing thrombi. Another characteristic feature of tumor is variably hyalinized stroma with so-called smudgy matrix containing grungy calcification. Admixture of mature adipose tissue, woven bone, and histiocytes are other integral components of tumor. No mitosis or necrosis is seen.

Malignant PMTs show anaplastic features and resemble sarcomas.

IHC shows positivity for SATB2, CD56, ERG, and SSTR2A [8, 9] (See Figs. 11.19, 11.20, 11.21, 11.22, and 11.23).

RMS family of tumors are most common sarcomas of sinonasal tract especially in pediatric population. The salient features of RMS subtypes, which affect SN tract, are tabulated (Table 11.1) along with a close common differential diagnosis of Ewing sarcoma at the same site [10–12].

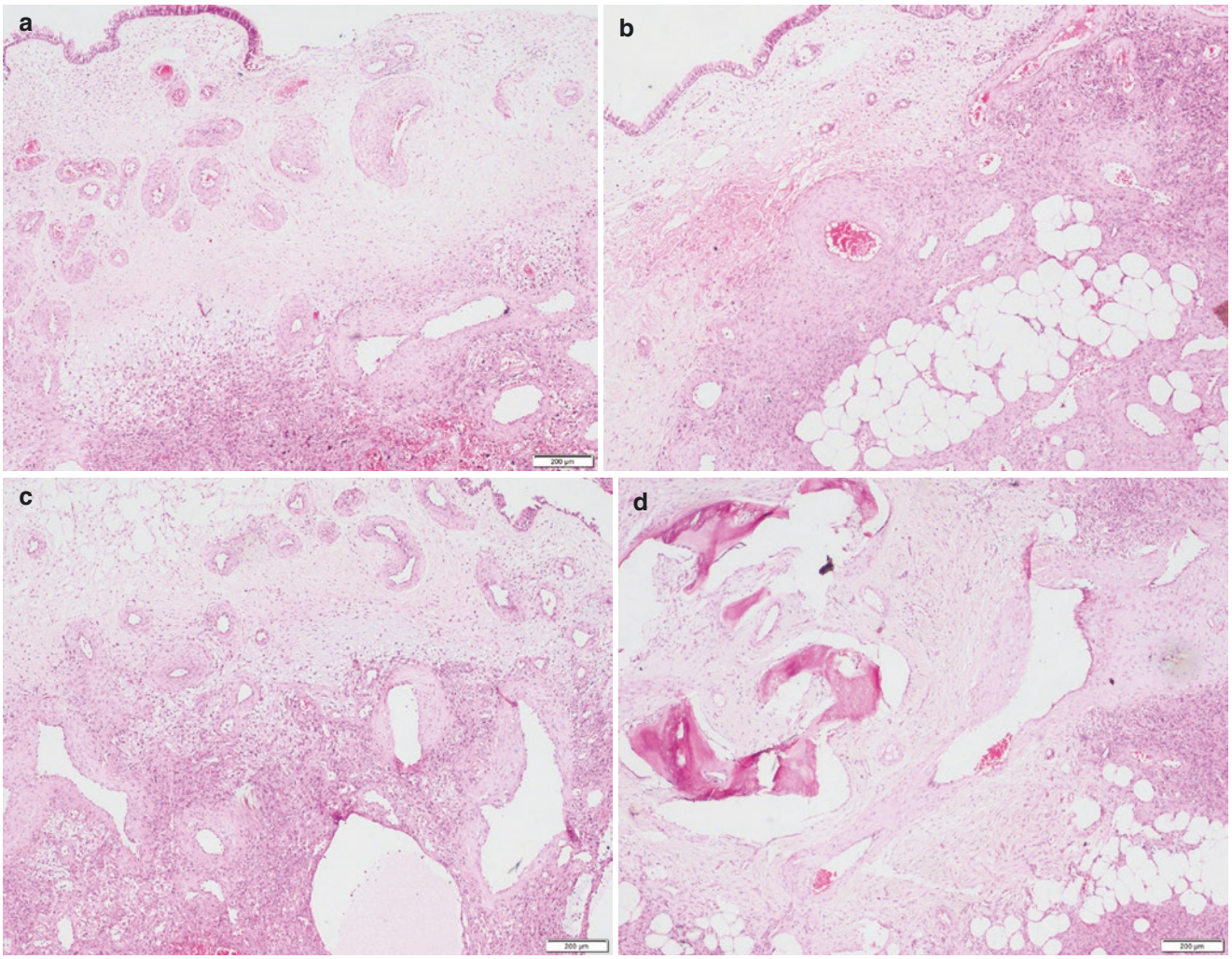

Fig. 11.19 This patient has high serum fibroblast growth factor (FGF) 23, hypophosphatemia, and tumor induced osteomalacia. Low magnification of a sinonasal PMT shows respiratory mucosa with an underlying tumor variably composed of abnormal shaped vessels, lobules of mature adipose tissue and nondescript spindle cells. Abnormally thickened large blood vessels with woven metaplastic bone and admixed fat (**d**). (**a**–**d**)

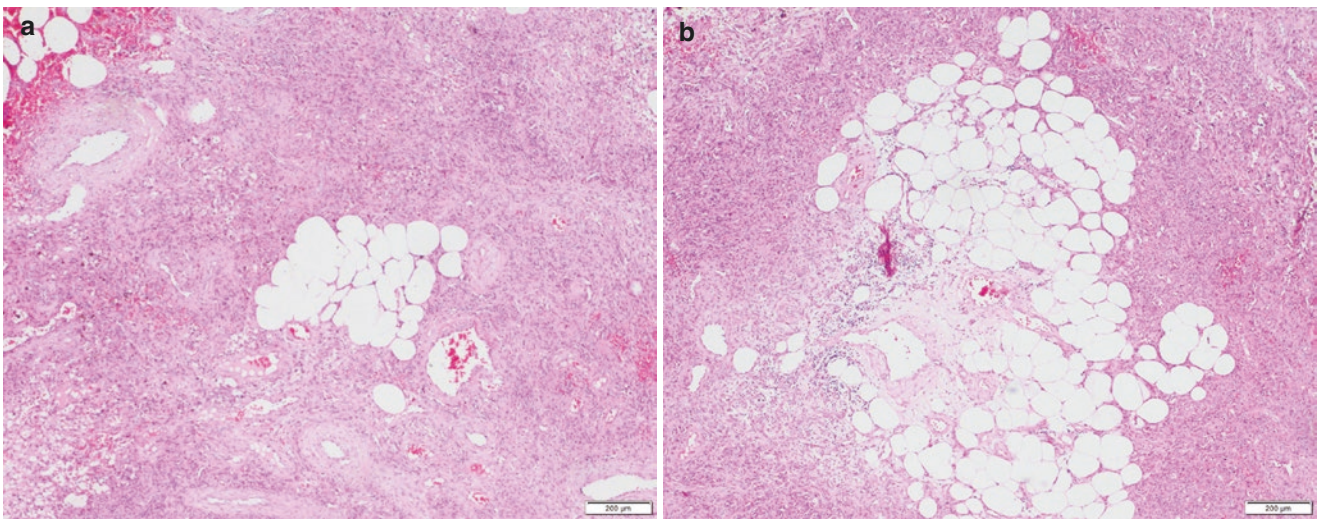

Fig. 11.20 Photomicrographs show bland hyperchromatic spindle cells arranged patternless and in small fascicles intricately admixed with fat and embedded in richly vascularized stroma (**a**, **b**)

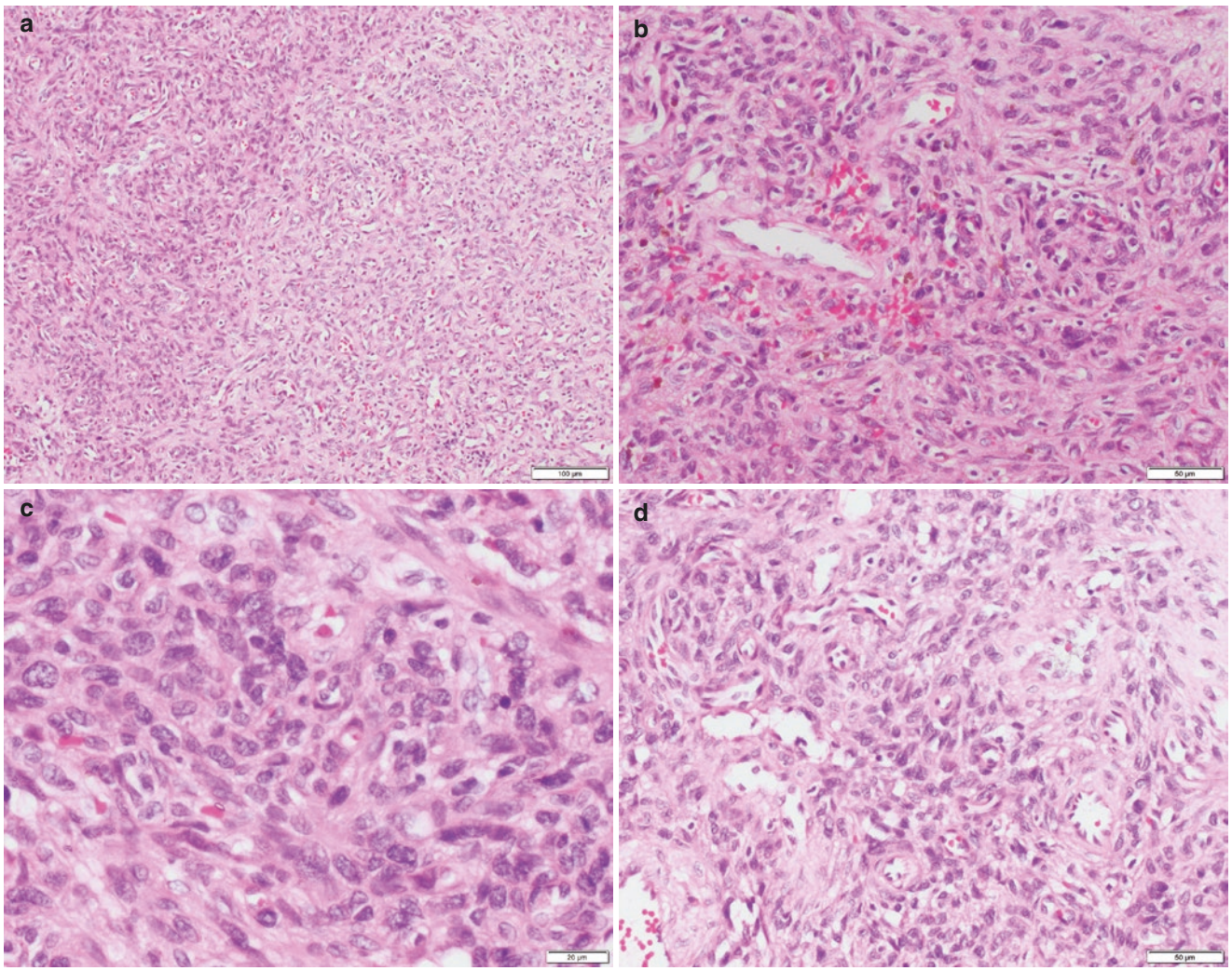

Fig. 11.21 Higher magnification shows bland spindle to stellate cells in majority and some oval-round cells without much atypia, mitosis/necrosis, and indistinct nucleoli. Hemosiderin pigment is seen (**b**) (**a**–**d**)

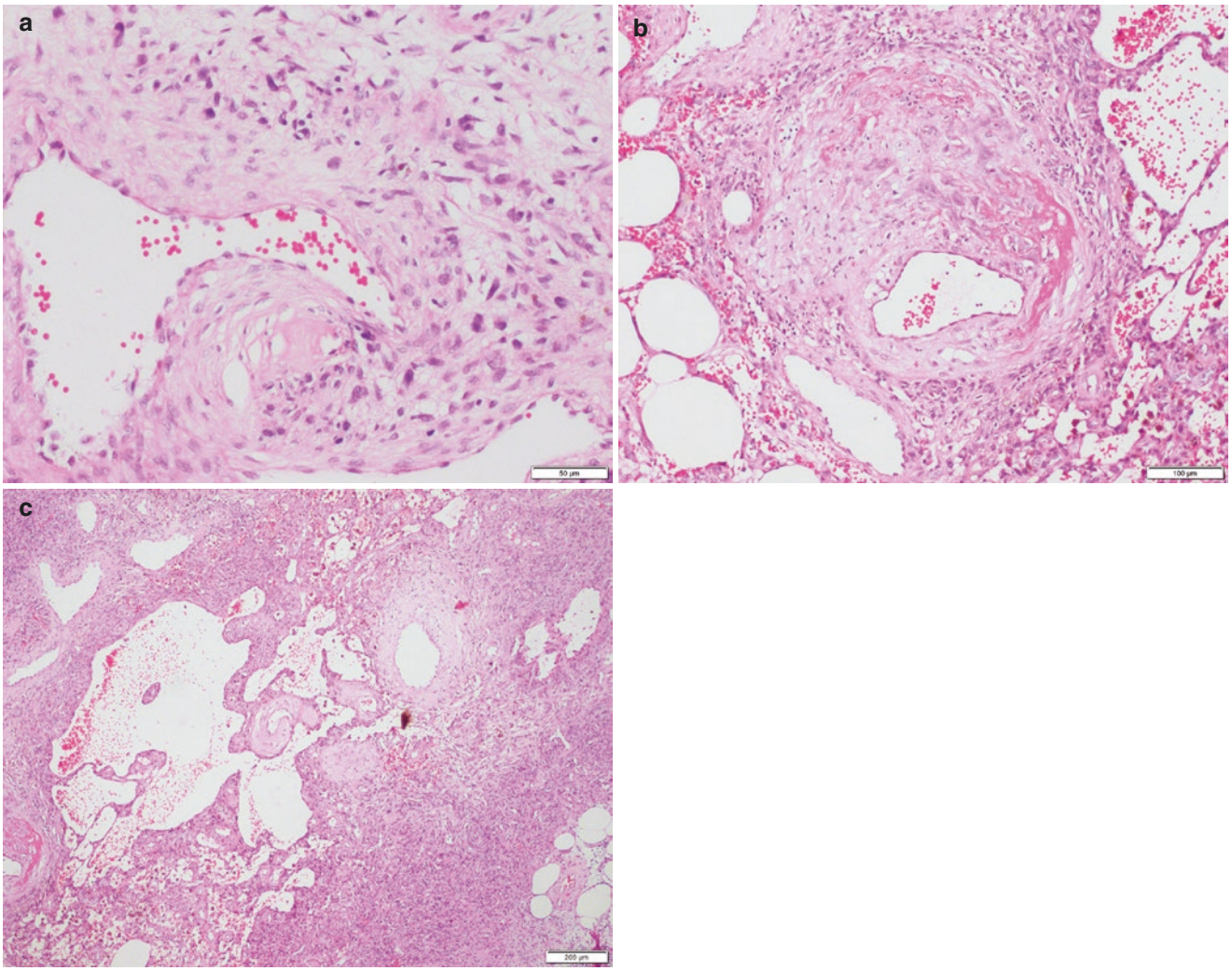

Fig. 11.22 Due to rich vascularity and odd shaped blood vessels, the differential diagnosis is vascular tumors. In this photograph, one of the thick walled large vessels shows tumor cells in the wall which are almost encroaching to the lumina (**a**). Another vessel shows organizing thrombus, fibrin and recanalization and surrounding hemosiderin suggesting chronic microhemorrhages (**b**). Abnormally branched cavernous shaped blood vessel with old hemorrhage (**c**). Note tumor cells are closely apposed to spindle shaped endothelial cells. Grungy calcification and giant cells are absent in this case

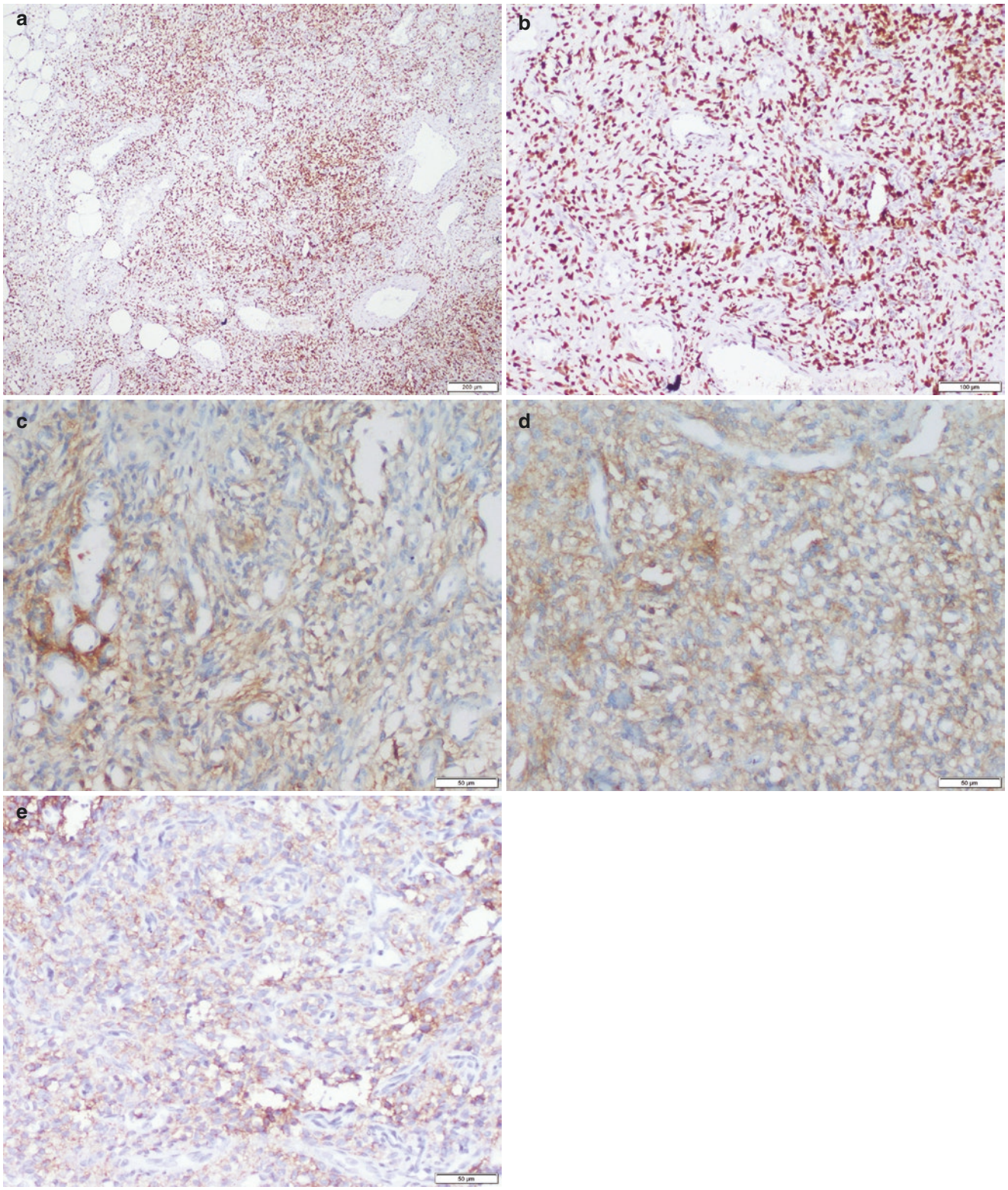

Fig. 11.23 Tumor cells diffusely positive for SATB2 (**a**, **b**), SSTR2 (Somatostatin receptor 2) (**c**, **d**), and CD56 (**e**)

Table 11.1 Salient features of different subtypes of RMS and Ewing sarcoma of SN tract

Features	Embryonal RMS (See Figs. 11.24, 11.25, 11.26, and 11.27)	Alveolar RMS (See Figs. 11.28, 11.29, 11.30, 11.31, 11.32, 11.33, and 11.34)	Spindle cell/Sclerosing RMS	Ewing Sarcoma (See Figs. 11.35, 11.36, 11.37, 11.38, 11.39, 11.40, and 11.41)
Location	Paranasal sinuses and nasal cavity (botryoid subtype)	Paranasal sinuses more than nasal cavity, also nasopharynx	Nasopharynx	Most often maxillary sinus and nasal fossa
Genetic alteration	Involvement of RAS pathway	*PAX3* or *PAX7* rearrangements, with partner gene *FOXO1*	A subset shows MyoD1 mutations Various gene fusions	*EWSR1* rearrangements, most commonly t(11;22) resulting in *EWSR1::FLI1* fusion
Histology	Primitive mesenchymal cells, stellate cells, tadpole or spider cells embedded within a loose, myxoid mesenchyme Botryoid subtype shows tight adherence of linear array of tumors cells to surface epithelial lining (cambium layer)	Solid to lobular architecture with central loss of cell cohesion gives rise to so-called alveolar pattern Round tumor cells with hyperchromatic nuclei, large nucleoli, and scant cytoplasm Rare multinucleated giant cells and rhabdomyoblasts with eosinophilic cytoplasm	Infiltrating sheets and fascicles of spindle to ovoid and fusiform cells with eosinophilic cytoplasm. Hyalinized and sclerotic stroma with cords of tumor cells Scattered primitive appearing round cells and rhabdomyoblasts are present	Solid to lobular and nest like architecture Round tumor cells with pale eosinophilic to clear scant cytoplasm Fine chromatin and indistinct nucleoli True or false rosettes rarely seen
IHC and cytogenetics	Desmin, MyoD1, Myogenin positive (all can be very focal and generally less diffuse than alveolar variant)	Diffusely positive for desmin and myogenin. Keratins can be positive Positive for *PAX3* or *PAX7* rearrangements, with partner gene *FOXO1*	Strong and diffuse positive for desmin and MyoD1 Myogenin focal positive	Membranous CD99 positivity, rare expression for neuroendocrine markers Positive for *EWSR1* rearrangements, usually with *FLI1* partner gene

For Ewing sarcoma and adamantinoma like Ewing sarcoma also see Chap. 13

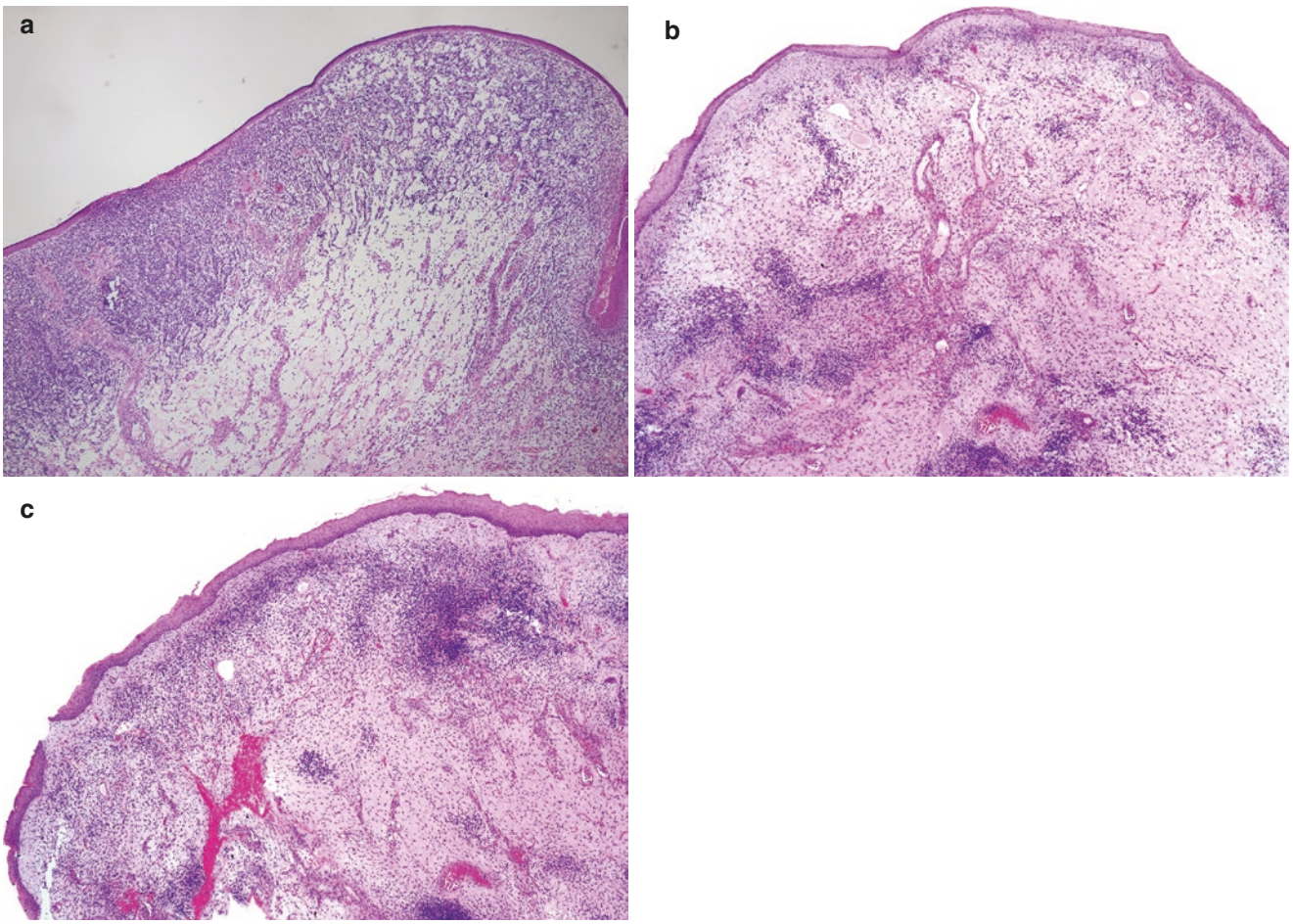

Fig. 11.24 Low power view of botryoid RMS in which polypoidal mucosal fragments are seen with a subepithelial cellular band of tumor infiltrate (**a**–**c**)

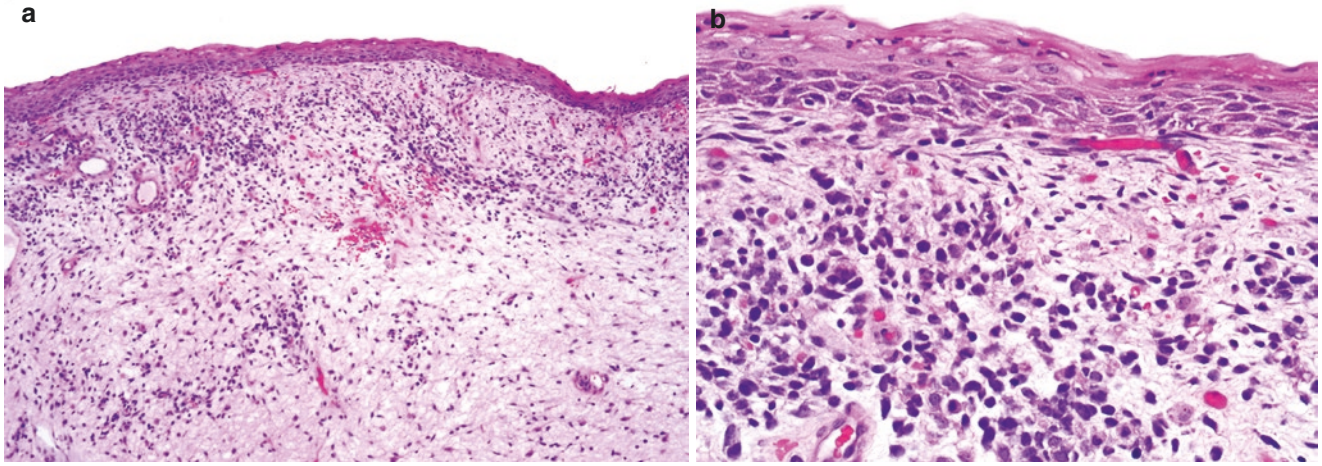

Fig. 11.25 Embryonal RMS. Higher magnification shows sparse cellular infiltrate of small hyperchromatic tumor cells in the edematous stroma (**a**, **b**)

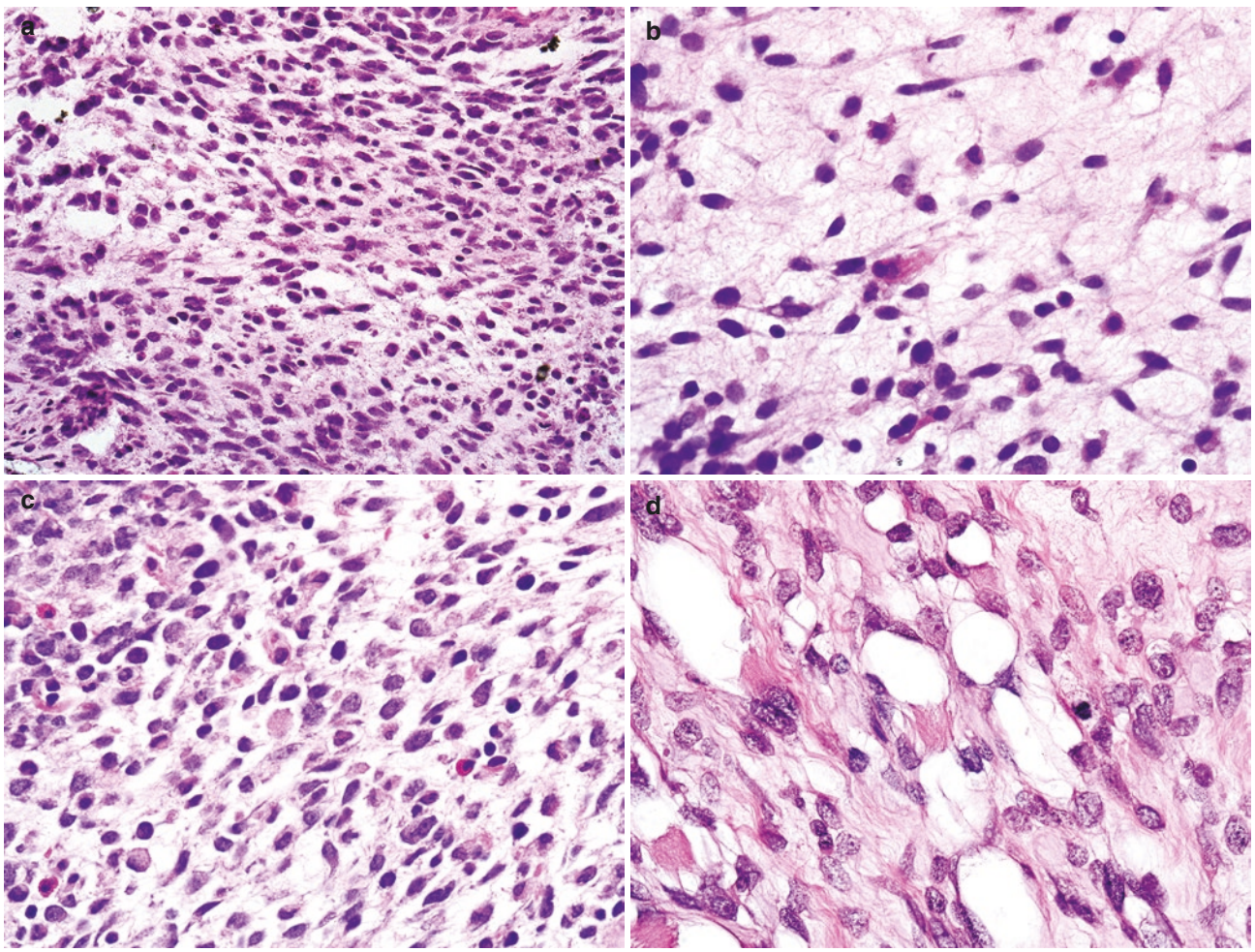

Fig. 11.26 Embryonal RMS. The tumor cells are round to spindle/fusiform in shape with condensed nuclear chromatin. Rhabdomyoblastic differentiation is seen (**b**–**d**) (**a**–**d**)

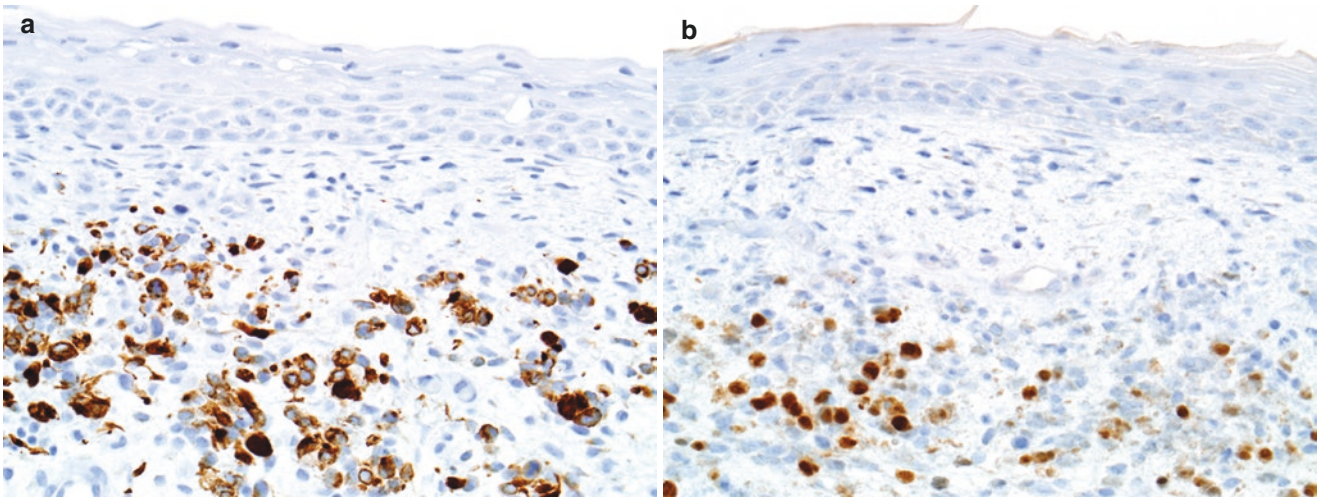

Fig. 11.27 Embryonal RMS. Desmin (diffuse, **a**) and myogenin (**b**) expression (in some tumor cells) is seen

Fig. 11.28 Alveolar RMS. Low magnification view shows a highly cellular tumor present in the subepithelium with stretched out overlying respiratory epithelium

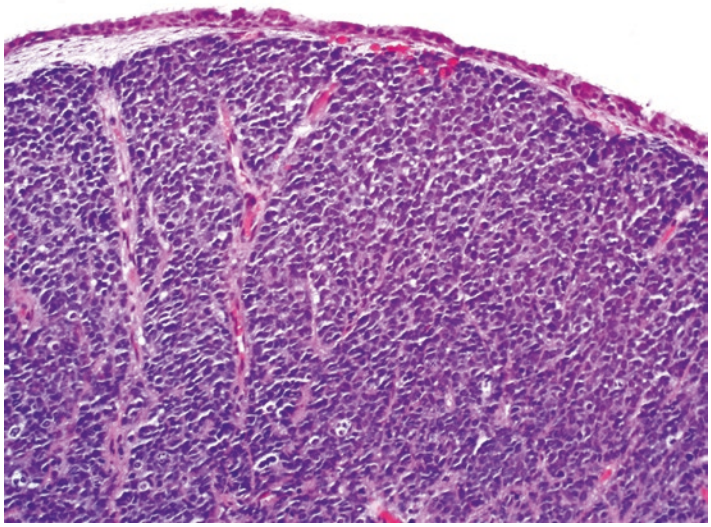

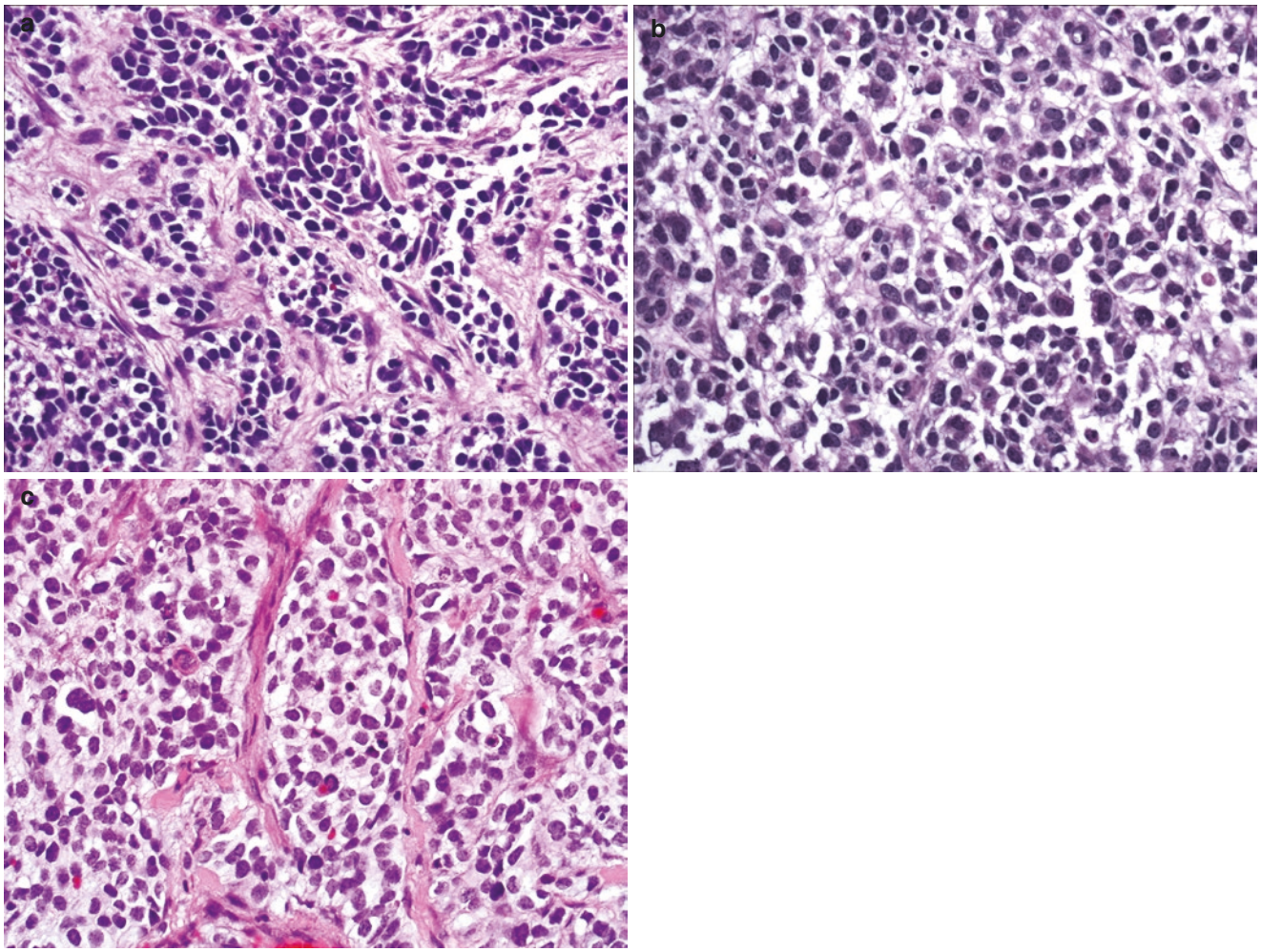

Fig. 11.29 Alveolar RMS. The tumor is arranged in nests and lobules separated by fibrous septae. Individual tumor cells are primitive appearing round cells with hyperchromatic nuclei and prominent nucleoli (**a**–**c**)

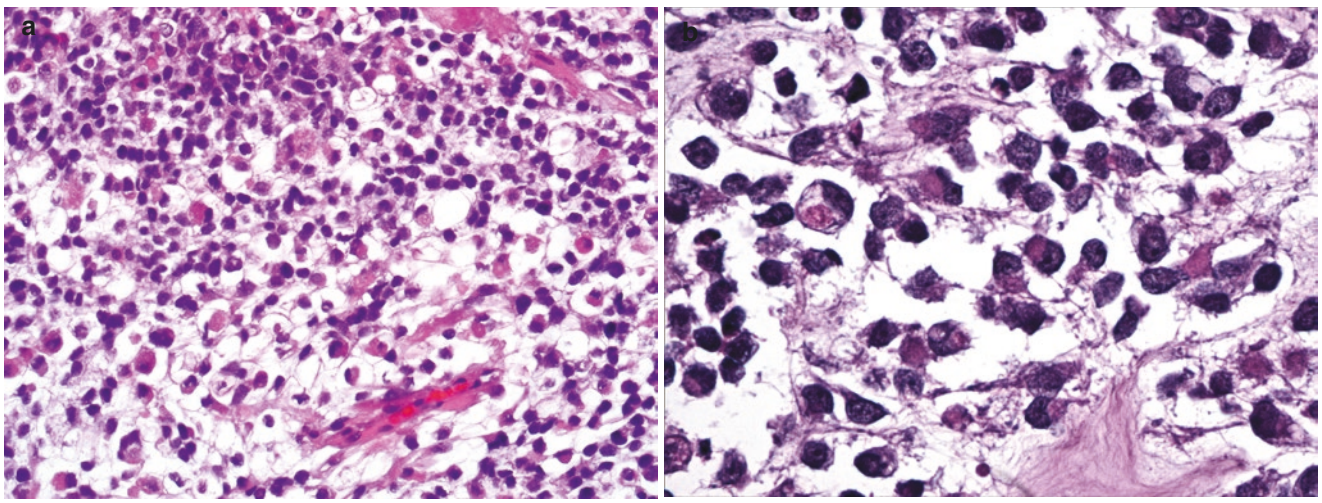

Fig. 11.30 Alveolar RMS. Tumor cells show scant to moderate amount of eosinophilic cytoplasm imparting plasmacytoid/rhabdoid appearance (rhabdomyoblastic differentiation) (**a**, **b**)

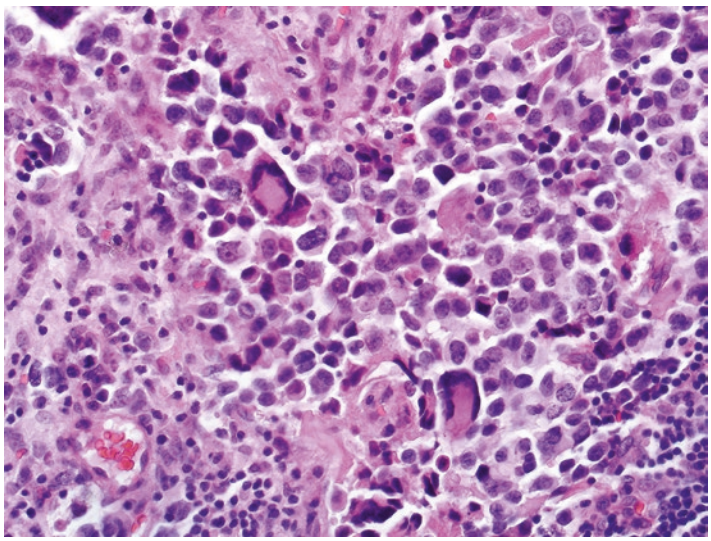

Fig. 11.31 Alveolar RMS. Scattered multinucleated giant cells are commonly seen

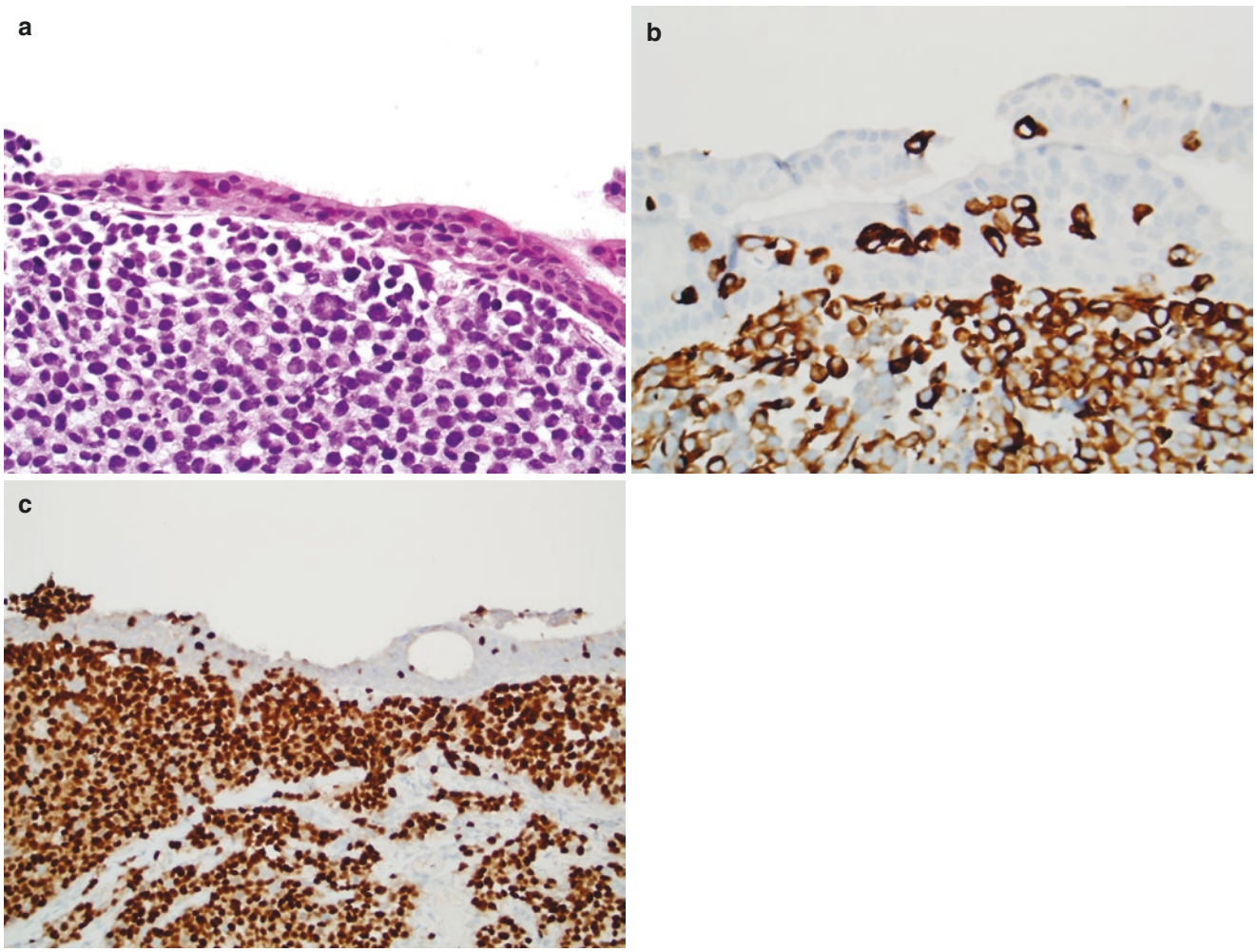

Fig. 11.32 Alveolar RMS. Pagetoid spread of tumor cells into overlying epithelium is seen which is highlighted by desmin (**b**) and myogenin (**c**) stains (**a**–**c**)

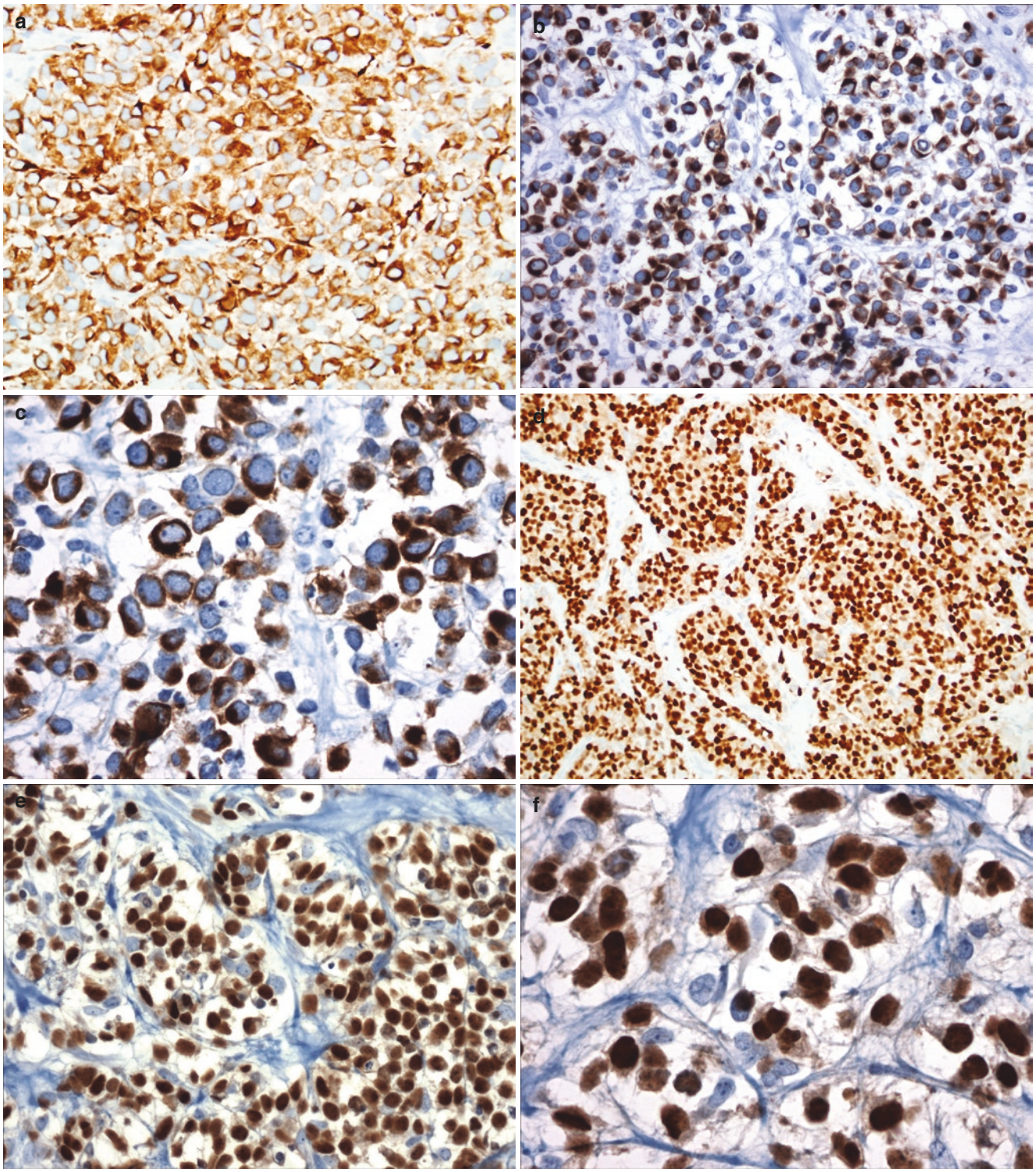

Fig. 11.33 Alveolar RMS. Diffuse desmin (cytoplasmic) (**a**, **b**, **c**) and myogenin (nuclear) positivity in tumor cells (**d**, **e**, **f**)

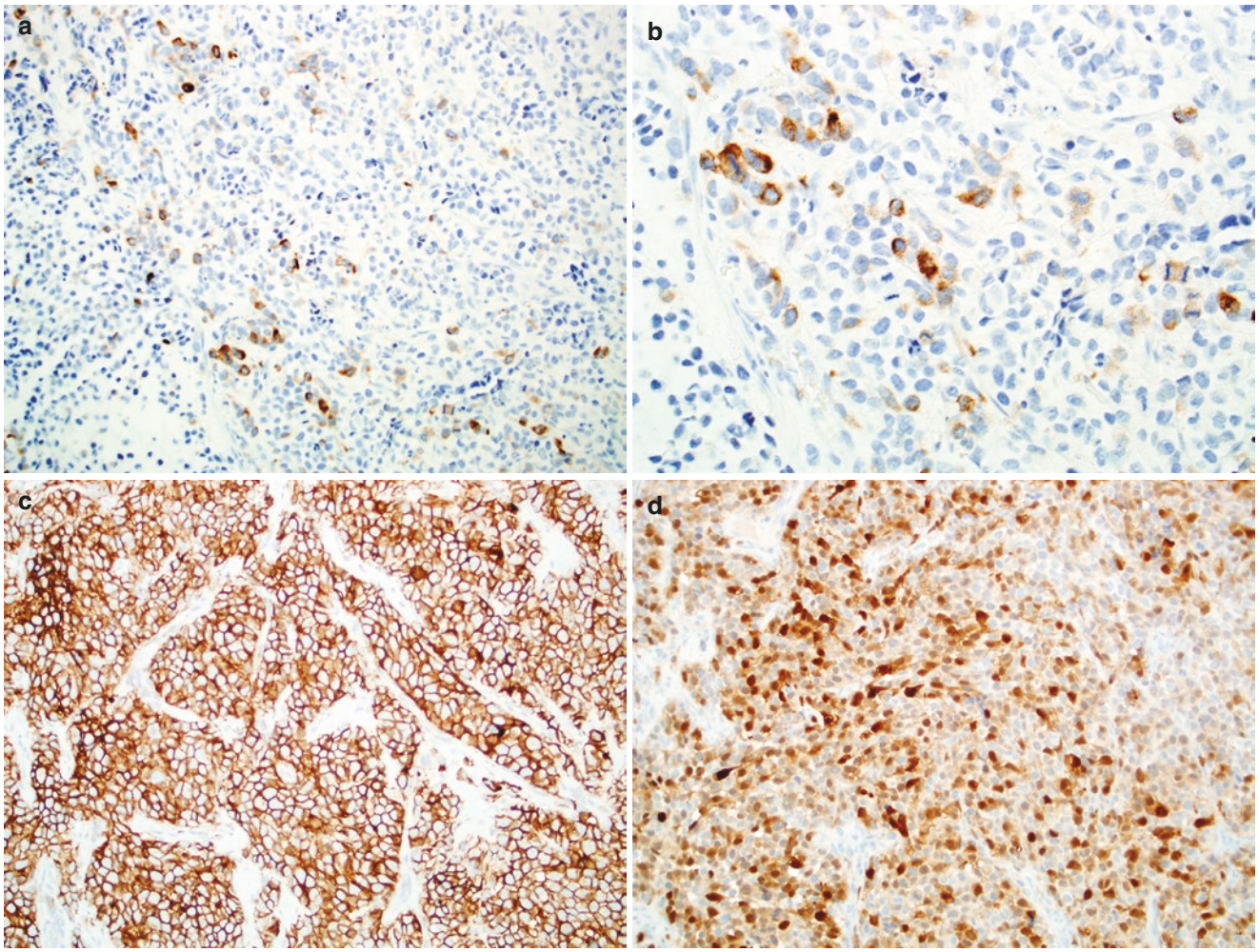

Fig. 11.34 Alveolar RMS. Rare expression of keratin (**a**, **b**), CD56 (**c**), and S-100 protein (**d**)

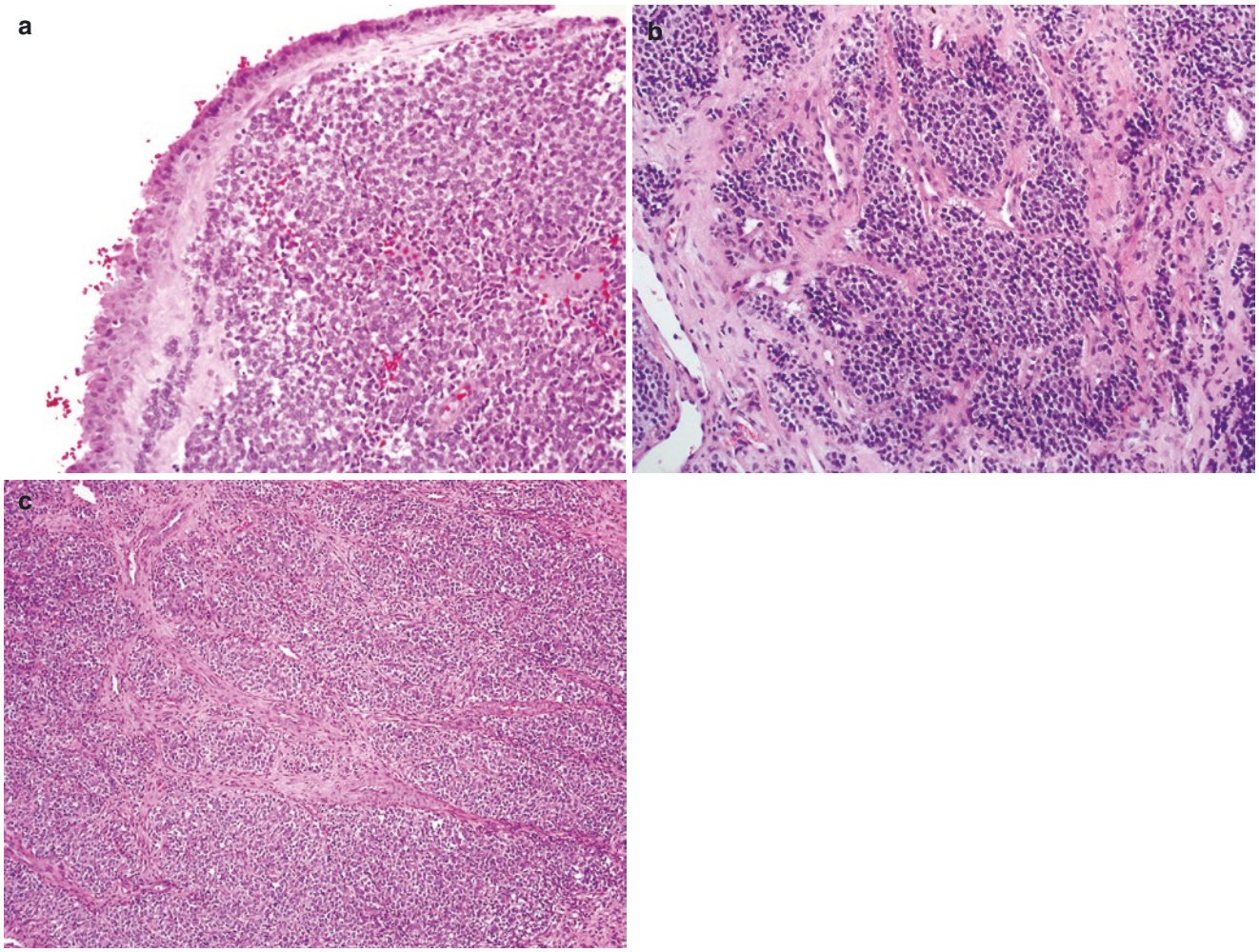

Fig. 11.35 Ewing Sarcoma. A cellular tumor present beneath the respiratory epithelium (**a**) in sinonasal region. Uniform small round cells arranged in nests and clusters in a fibrous stroma (**b**, **c**)

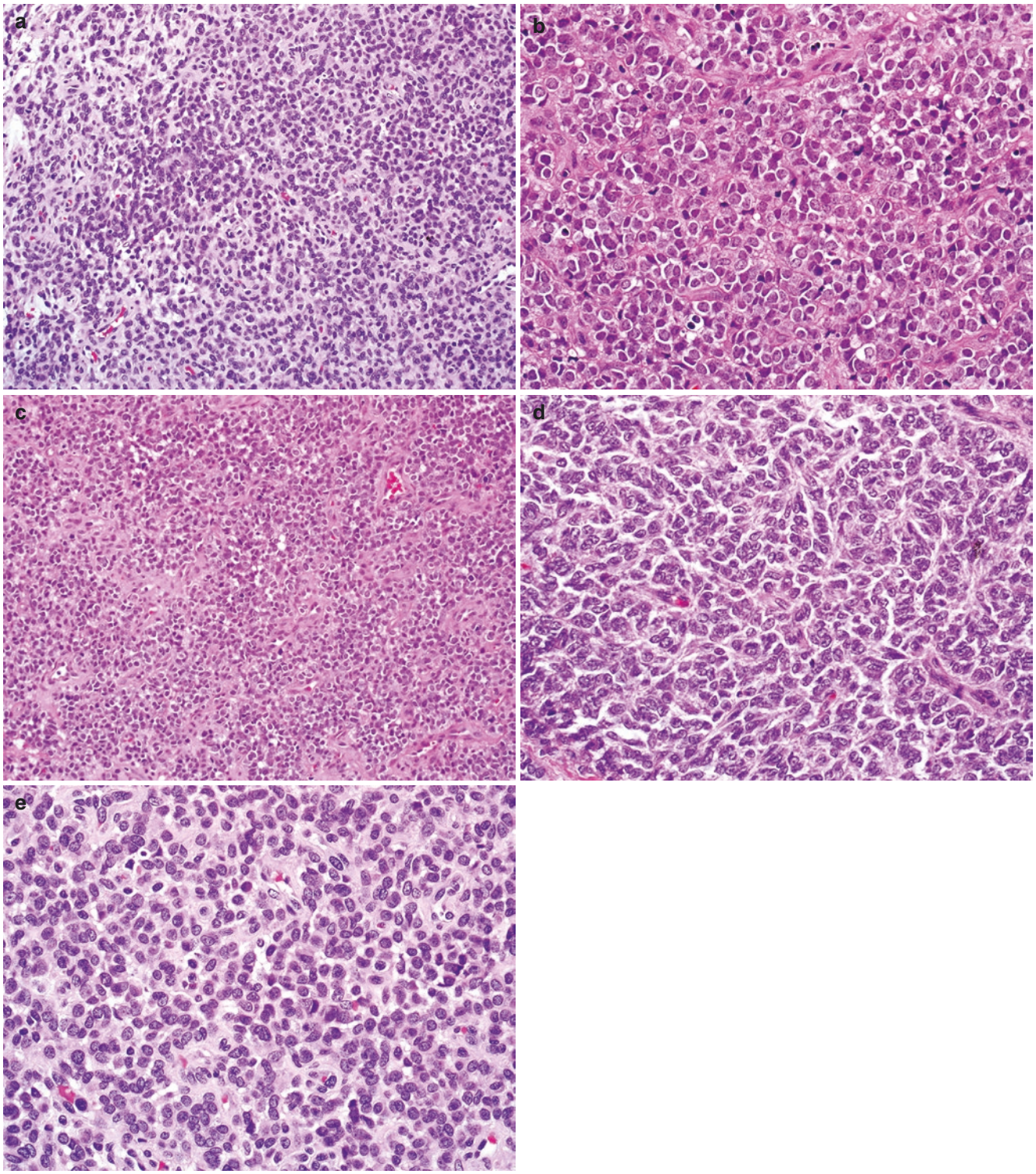

Fig. 11.36 Ewing Sarcoma. Higher magnification shows hyperchromatic nuclei with fine, stippled chromatin and inconspicuous nucleoli (**a**–**e**)

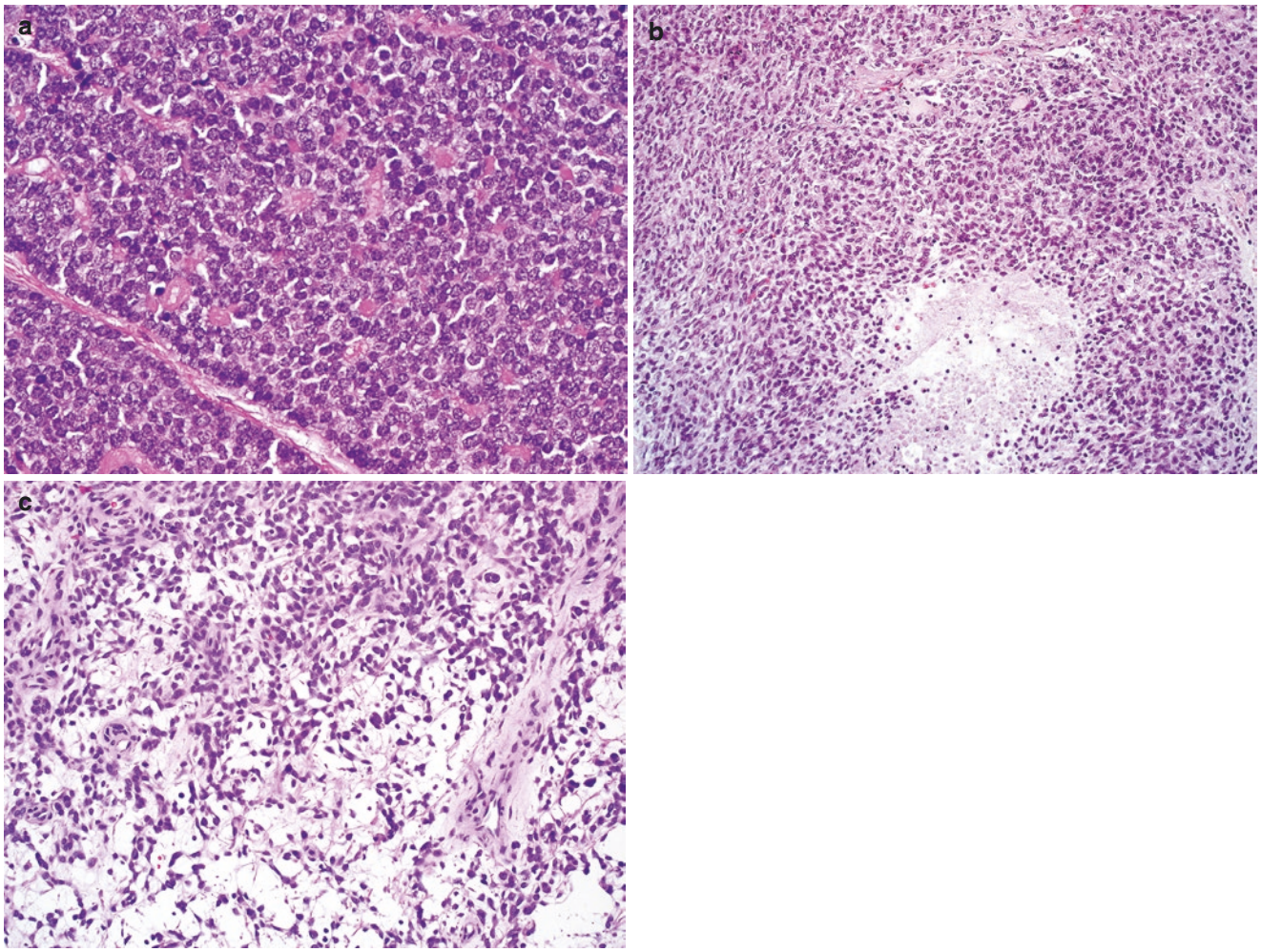

Fig. 11.37 Ewing Sarcoma. Subset of tumors show rosettes (neuroectodermal differentiation) (**a**), spindling of tumor cells (**b**), and myxoid stromal change (**c**)

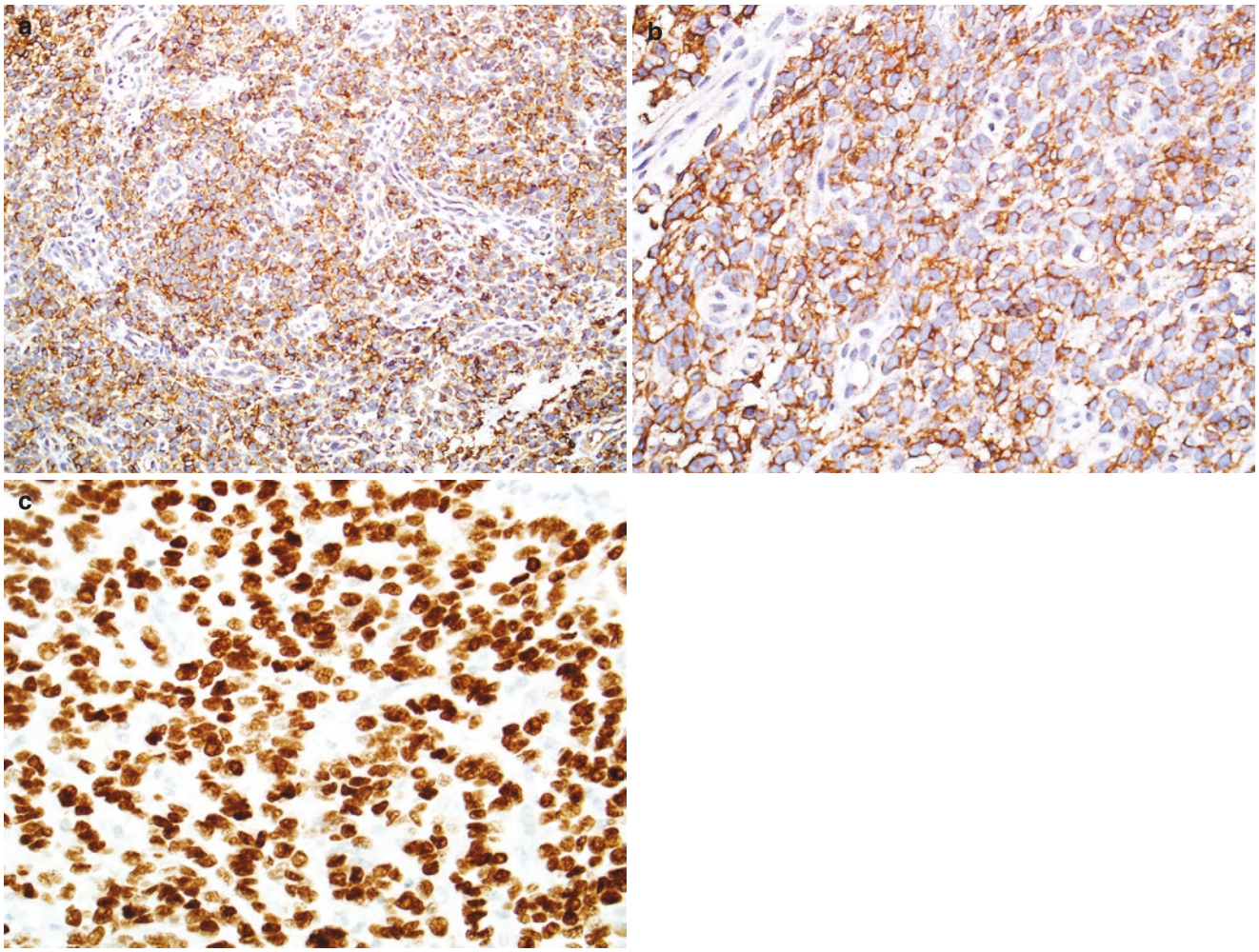

Fig. 11.38 Ewing Sarcoma. CD99 shows diffuse membranous (**a**, **b**) and NKX2.2 shows diffuse nuclear expression (**c**)

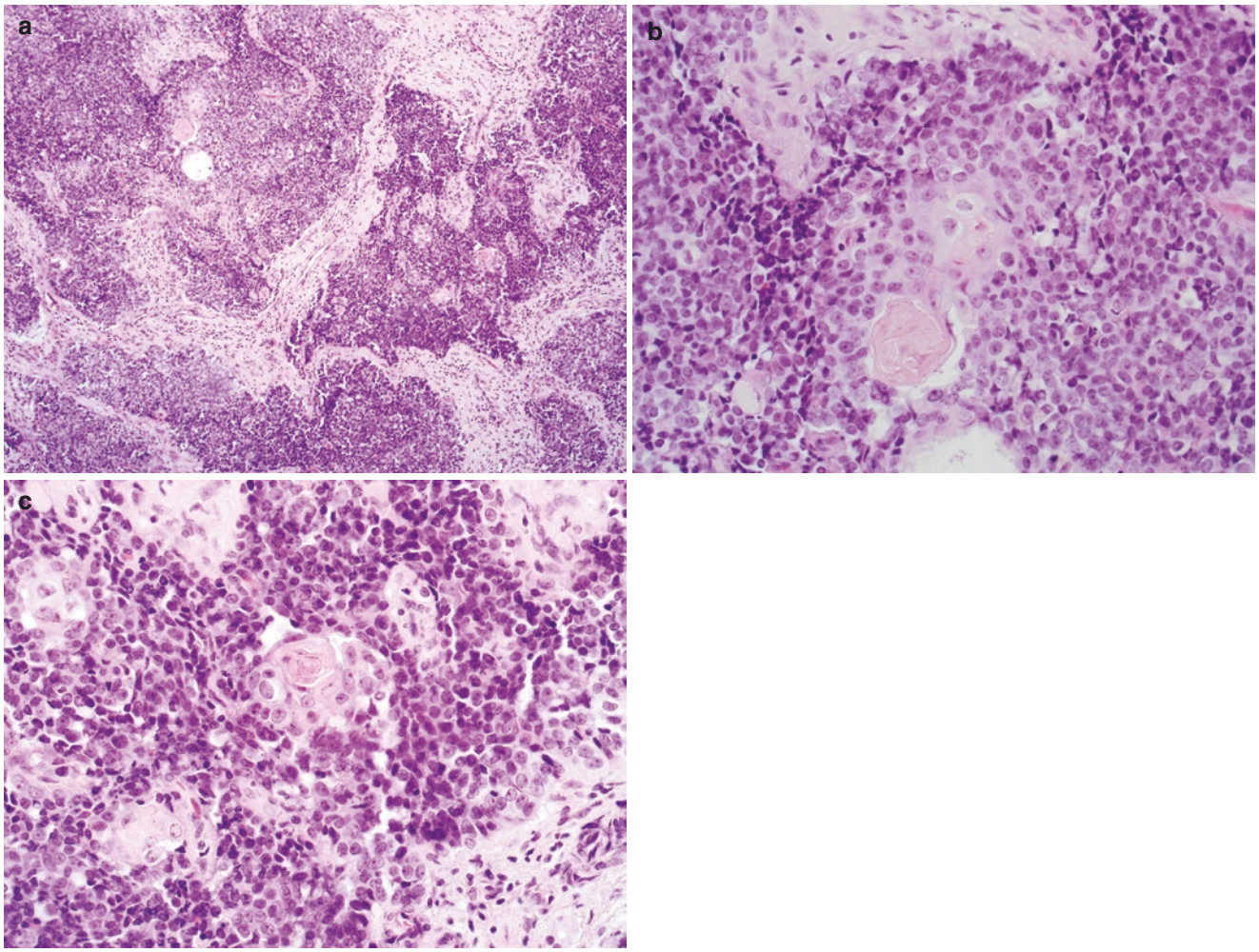

Fig. 11.39 Adamantinoma like Ewing Sarcoma. Islands of undifferentiated tumor cells in fibrous stroma (**a**) which on higher magnification shows squamous islands with keratin pearls (**b**, **c**)

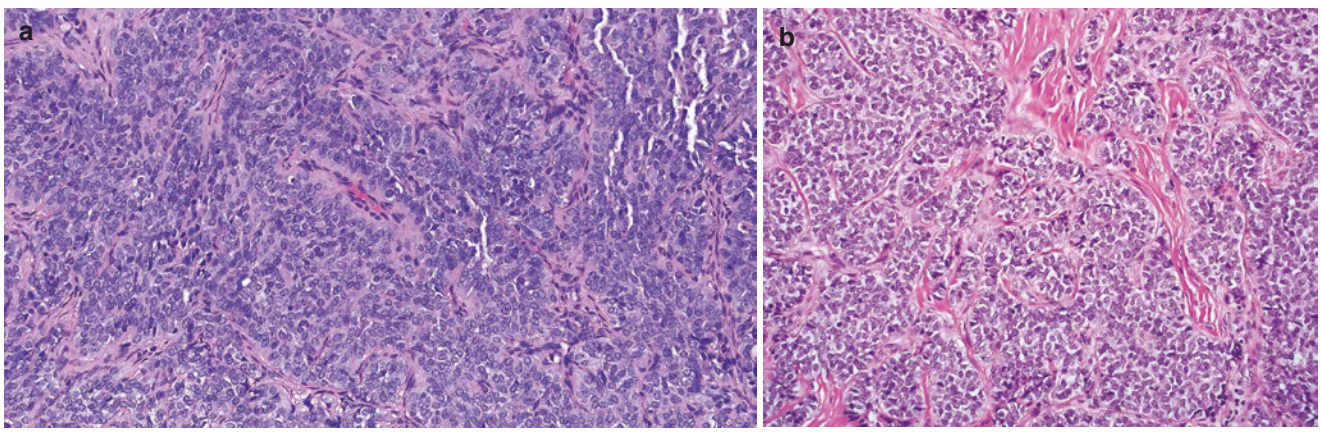

Fig. 11.40 Adamantinoma like Ewing Sarcoma. Peripheral palisading is conspicuous in this example (**a**) with lobules of undifferentiated cells present in hyalinized stroma (**b**)

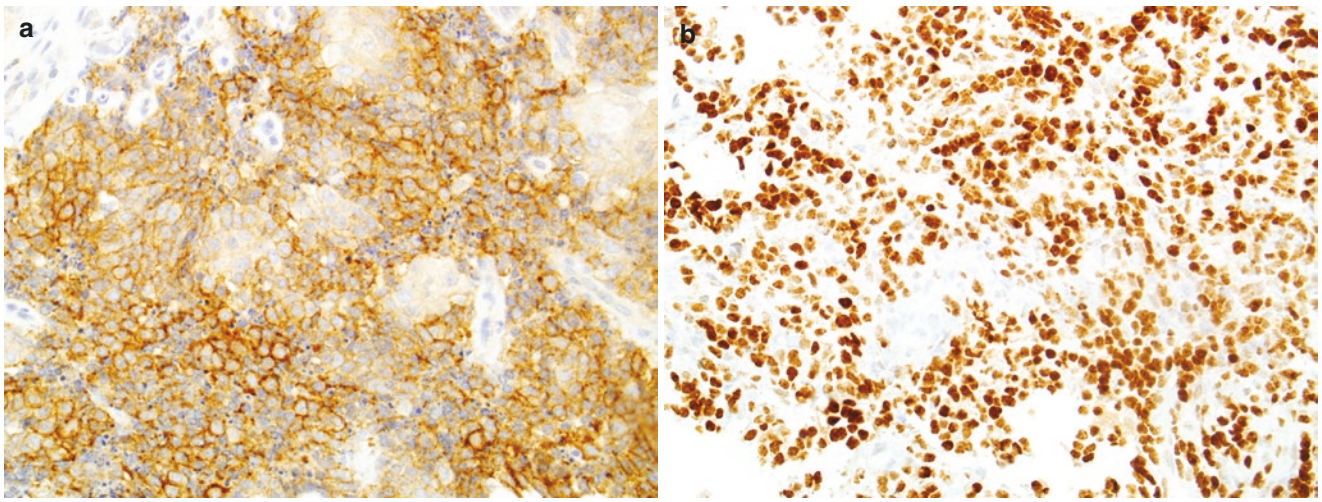

Fig. 11.41 Adamantinoma like Ewing Sarcoma. CD99 (membranous, **a**) and NKX2.2 (nuclear, **b**) are positive

11.5 Conclusion

Malignant mesenchymal tumors of SN tract are rare; however, all of these show a peculiar histomorphology and characteristic immunophenotype and molecular aberrations. A correct clinically oriented approach and high index of suspicion is imperative in establishing a correct diagnosis.

References

1. WHO Classification of Tumours Editorial Board. Head and neck tumours [internet; beta version ahead of print]. Lyon: International Agency for Research on Cancer; 2022 [cited July 6, 2022]. (WHO classification of tumours series, 5th ed.; vol. 9). Available from: https://tumourclassification.iarc.who.int/chapters/52.
2. Carter CS, East EG, McHugh JB. Biphenotypic Sinonasal sarcoma: a review and update. Arch Pathol Lab Med. 2018;142(10):1196–201.
3. Gross J, Fritchie K. Soft tissue special issue: Biphenotypic Sinonasal sarcoma: a review with emphasis on differential diagnosis. Head Neck Pathol. 2020;14(1):33–42.
4. Surrey LF, Davis JL. NTRK-rearranged soft tissue neoplasms: a review of evolving diagnostic entities and algorithmic detection methods. Cancer Genet. 2022;260-261:6–13.
5. Wasserman JK, Gravel D, Purgina B. Chordoma of the head and neck: a review. Head Neck Pathol. 2018;12(2):261–8.
6. Ozair MZ, Shah PP, Mathios D, Lim M, Moss NS. New prospects for molecular targets for Chordomas. Neurosurg Clin N Am. 2020;31(2):289–300.
7. Agaimy A, Michal M, Chiosea S, Petersson F, Hadravsky L, Kristiansen G, Horch RE, Schmolders J, Hartmann A, Haller F, Michal M. Phosphaturic mesenchymal tumors: Clinicopathologic, Immunohistochemical and molecular analysis of 22 cases expanding their morphologic and Immunophenotypic Spectrum. Am J Surg Pathol. 2017;41(10):1371–80.
8. Sun L, Dehner C, Kenney J, McNulty SM, Zhu X, Pfeifer JD, Maluf HM, Chrisinger JSA. Clinicopathologic and molecular features of six cases of phosphaturic mesenchymal tumor. Virchows Arch. 2021;478(4):757–65.
9. Folpe AL. Phosphaturic mesenchymal tumors: a review and update. Semin Diagn Pathol. 2019;36(4):260–8.
10. Zhao Z, Yin Y, Zhang J, Qi J, Zhang D, Ma Y, Wang Y, Li S, Zhou J. Spindle cell/sclerosing rhabdomyosarcoma: case series from a single institution emphasizing morphology, immunohistochemistry and follow-up. Int J Clin Exp Pathol. 2015;8(11):13814–20.
11. Thompson LDR, Jo VY, Agaimy A, Llombart-Bosch A, Morales GN, Machado I, Flucke U, Wakely PE Jr, Miettinen M, Bishop JA. Sinonasal tract alveolar rhabdomyosarcoma in adults: a Clinicopathologic and Immunophenotypic study of fifty-two cases with emphasis on epithelial immunoreactivity. Head Neck Pathol. 2018;12(2):181–92.
12. Thompson LD. Small round blue cell tumors of the sinonasal tract: a differential diagnosis approach. Mod Pathol. 2017;30(s1):S1–S26.

Hematolymphoid Tumors of the Sinonasal Tract

12

Flavia G. Rosado and Mingyi Chen

12.1 Introduction

This section provides an overview of the hematolymphoid neoplasms that involve the sinonasal mucosa, as well as adjacent sites such as the upper airways and Waldeyer tonsillar ring. In the Western world, these tumors are more frequently non-Hodgkin B cell lymphomas, namely, diffuse large B cell lymphoma (DLBCL) and Burkitt lymphoma, and extraosseous plasmacytoma [1–3]. Hematolymphoid malignancies such as extranodal NK/T cell lymphoma nasal type and plasmablastic lymphoma are uncommon, but show predilection for involvement of the upper respiratory tract and oropharynx [2]. History of immunosuppression, either iatrogenic types or secondary to Human Immunodeficiency Virus (HIV) infection and histologic demonstration of Epstein–Barr virus (EBV) association is key to the diagnosis of many of these tumors.

Here we provide an algorithm that summarizes a general approach to the differential diagnosis of sinonasal hematolymphoid tumors (see Fig. 12.1). The algorithm starts with careful evaluation of high quality H&E-stained sections to determine the cell size of the neoplasm and other useful morphologic features. In this initial step, the atypical infiltrate can be categorized based on the degree of atypia as minimal or severe, the predominant cell size as large, medium or small, and the cellular composition of the infiltrate as either monomorphic or polymorphic. Notably, the assessment of cell size is not as useful in the differential of T cell lymphomas compared to B cell lymphomas, since many T cell lymphoma categories are more heterogeneous regarding cell size. A brief review and pictures (see Figs. 12.2, 12.3, 12.4, 12.5, 12.6, 12.7, 12.8, 12.9, 12.10, 12.11, 12.12, 12.13, 12.14, 12.15 and 12.16) of the entities included in each category discussed in the algorithm is provided below. A summary of the key points is also provided (see Table 12.1).

F. G. Rosado (✉)
University of Texas Southwestern Medical Center, Dallas, TX, USA

Pathology, University of Pittsburgh Medical Center, Pittsburgh, USA
e-mail: rosadofg@upmc.edu

M. Chen
University of Texas Southwestern Medical Center, Dallas, TX, USA
e-mail: mingyi.chen@utsouthwestern.edu

D. Jain, J. A. Bishop (eds.), *Atlas of Sinonasal Tract Pathology*, https://doi.org/10.1007/978-981-19-7315-4_12

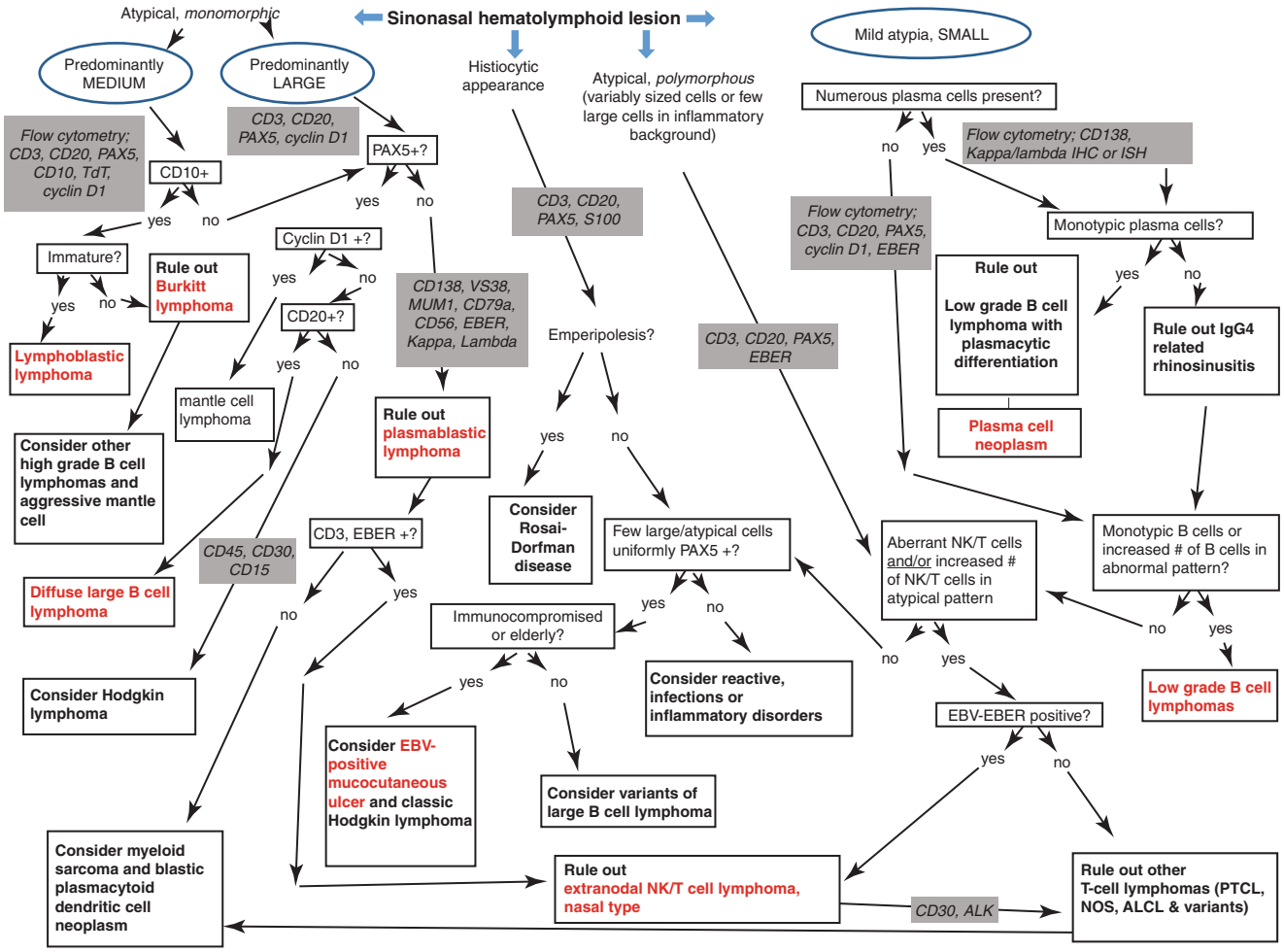

Fig. 12.1 Algorithm for the differential diagnosis of hematolymphoid neoplasms of the sinonasal tract

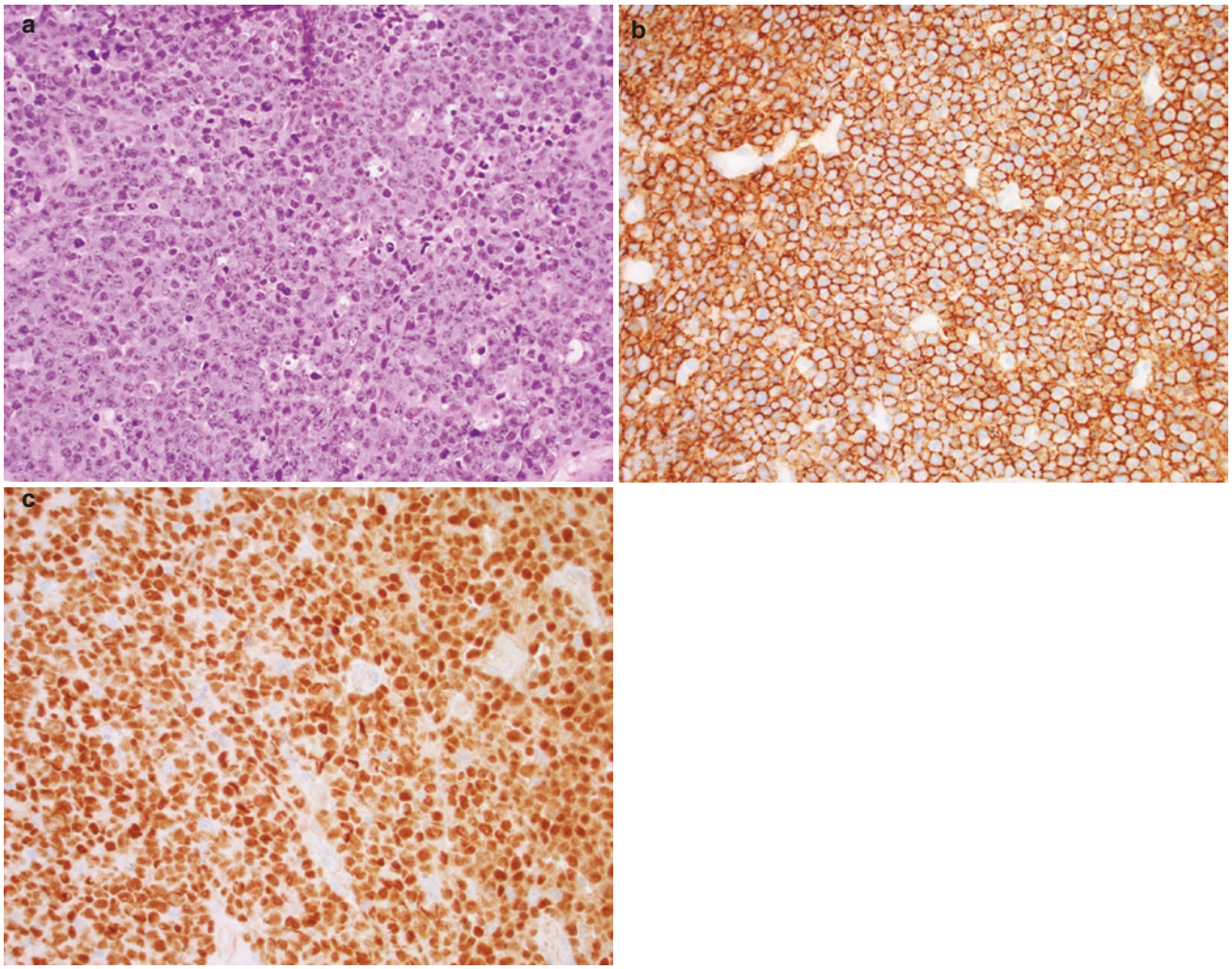

Fig. 12.2 (**a–c**) Diffuse large B cell lymphoma: Diffuse infiltrate of large cells with irregular nuclei and multiple nucleoli (**a**, H&E stain, 40X). The tumor cells show strong and uniform expression of CD20 (**b**, CD20 immunostain, 40X) and PAX5 (**c**, PAX5 immunostain, 40X)

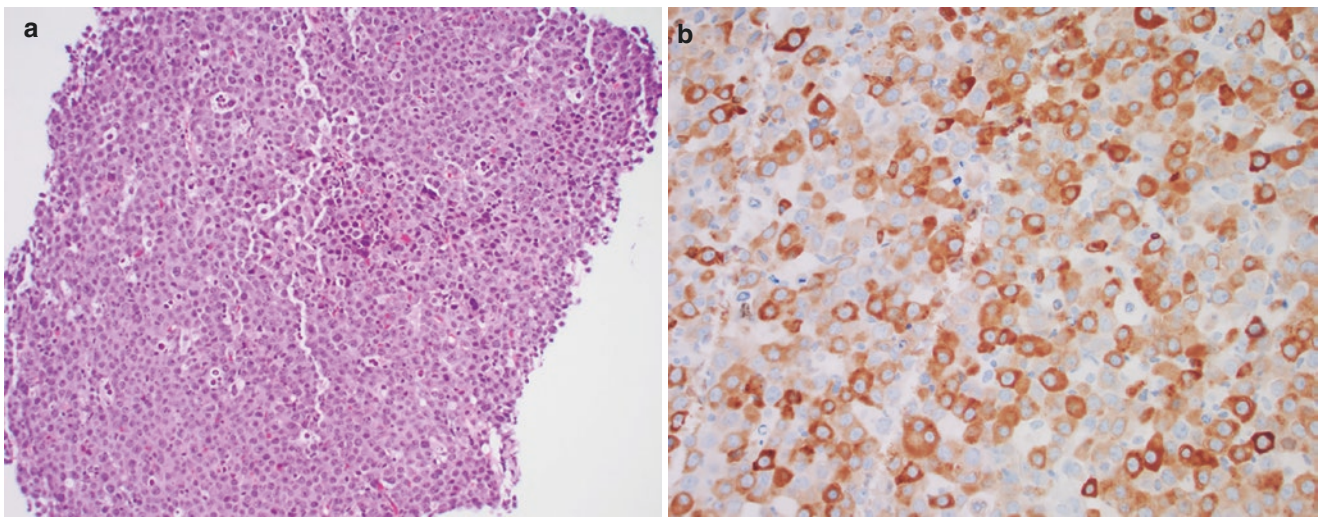

Fig. 12.3 (**a**, **b**) Plasmablastic lymphoma: Diffuse infiltrate of large cells with slightly off center nuclei, moderate amount of slightly basophilic cytoplasm, and single prominent nucleoli (**a**, H&E stain, 20X). The tumor cells are negative for PAX5 and variably express plasma cell markers CD138, VS38, and CD79a (**b**, CD79a immunostain, 40X)

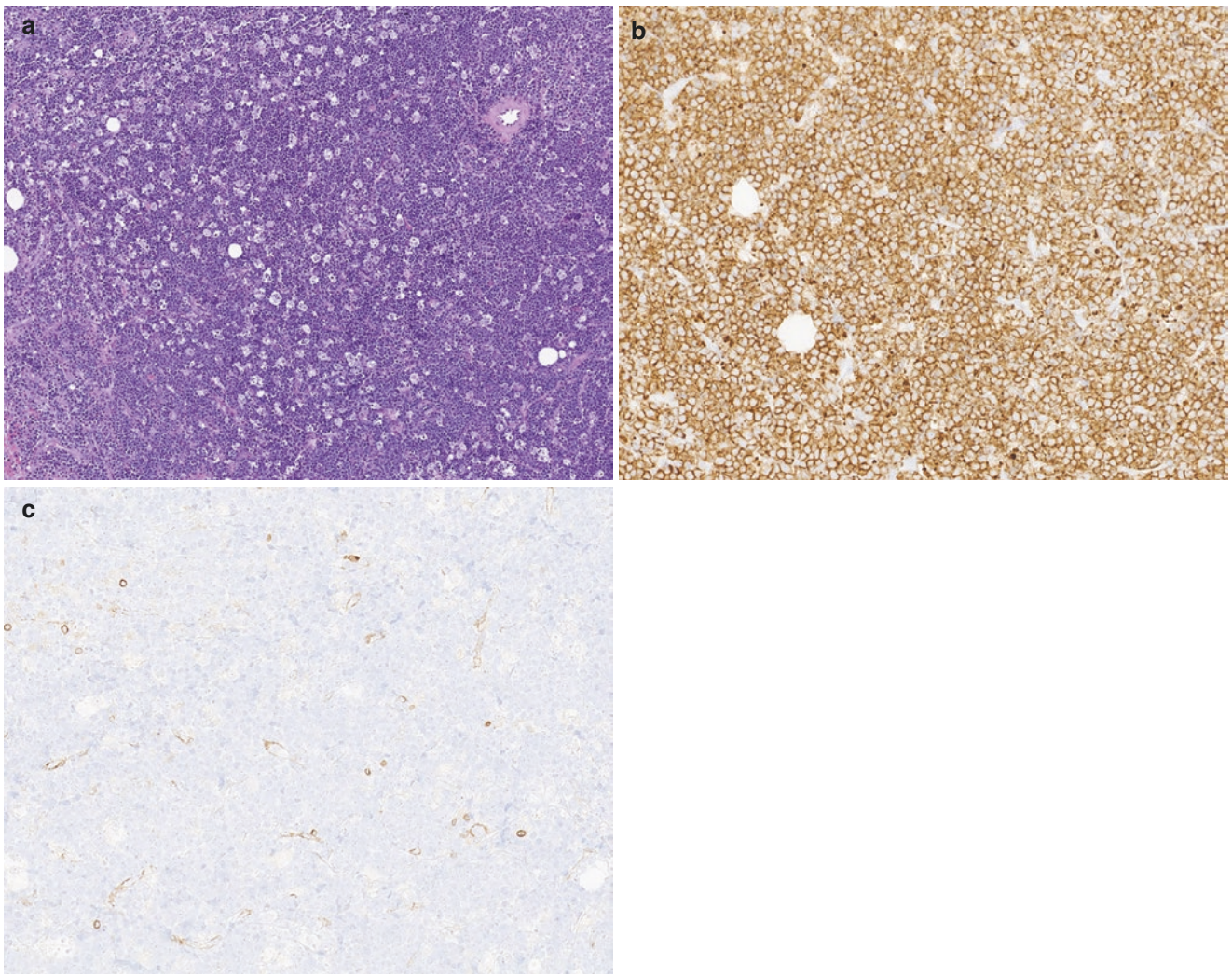

Fig. 12.4 (**a**–**c**) Burkitt lymphoma: Diffuse infiltrate of monomorphic medium-sized cells with squared off cytoplasm and scattered apoptotic bodies imparting the typical "starry-sky" appearance (**a**, H&E stain, 10X). The tumor cells are positive for CD10 (**b**, CD10 immunostain, 20X) and negative for bcl2 (**c**, Bcl2 immunostain, 20X)

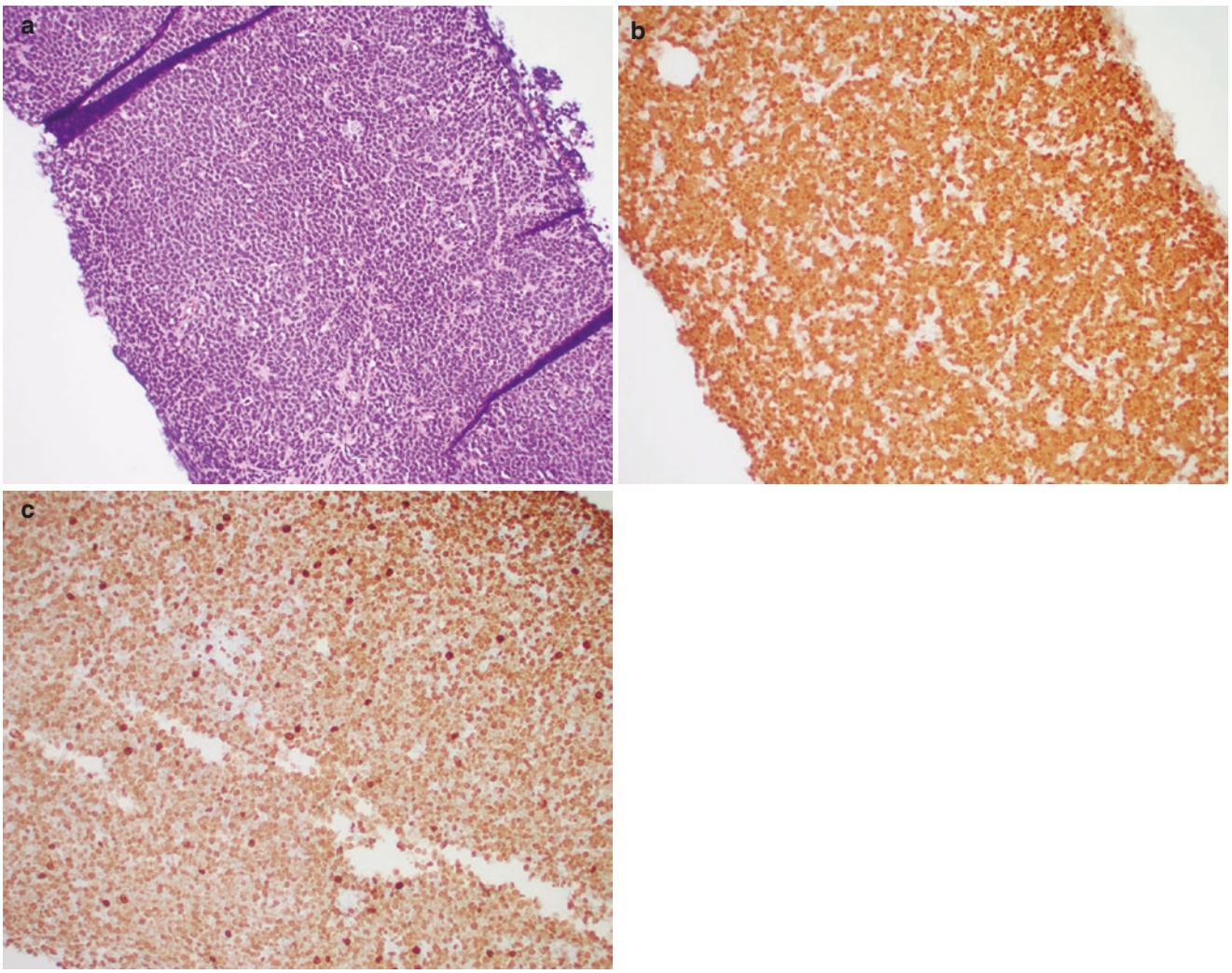

Fig. 12.5 (**a**–**c**) Mantle cell lymphoma, blastoid variant: diffuse monomorphic infiltrate of medium-sized B cells (**a**, H&E stain, 10X). The diffuse and strong nuclear staining with cyclin D1 is diagnostic (**b**, Cyclin D1 immunostain, 10X). Unlike conventional type of mantle cell lymphoma, this aggressive variant shows extremely high Ki-67 proliferation rate (**c**, Ki-67 immunostain, 20X)

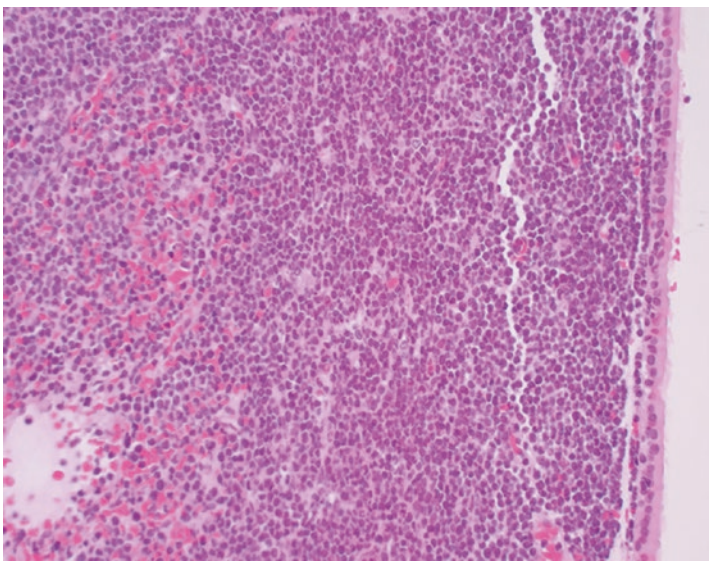

Fig. 12.6 B-lymphoblastic lymphoma: diffuse infiltrate of medium-sized cells with overlying normal respiratory-type epithelium (H&E stain, 20X)

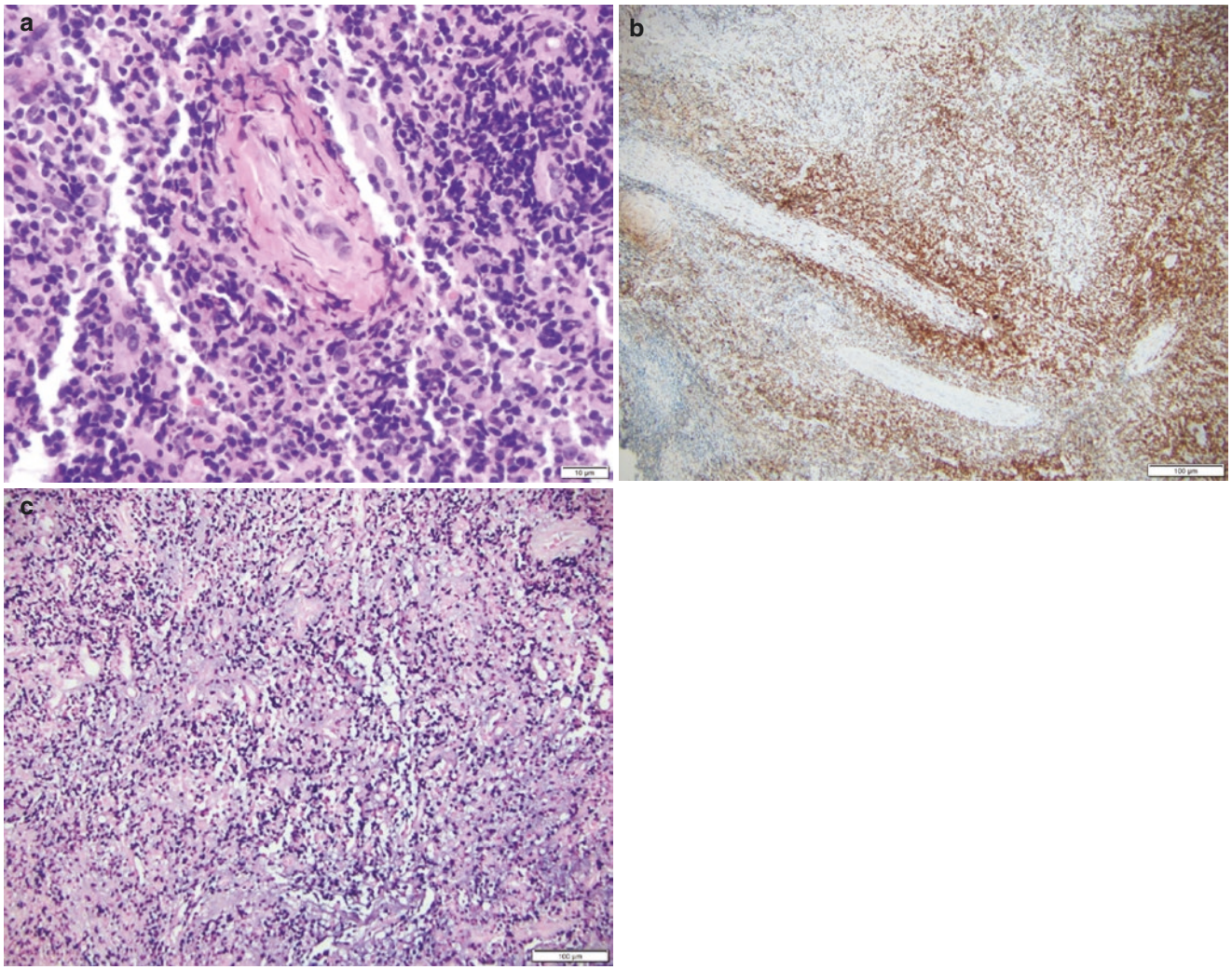

Fig. 12.7 (**a**–**c**) Extranodal NK/T cell lymphoma, nasal type: infiltrate of small- to medium-sized lymphocytes with mild atypia; may be difficult to distinguish from reactive lymphocytes especially in extensively necrotic samples (**a**, H&E stain, 40X); a CD3 immunostain highlights the angiocentric distribution of the neoplastic lymphocytes (**b**, CD3 immunostain, 20X); the neoplastic cells display cytotoxic T cell or NK cell phenotype and are positive for Epstein–Barr virus using *in-situ* hybridization studies (**c**, EBER ISH, 20X)

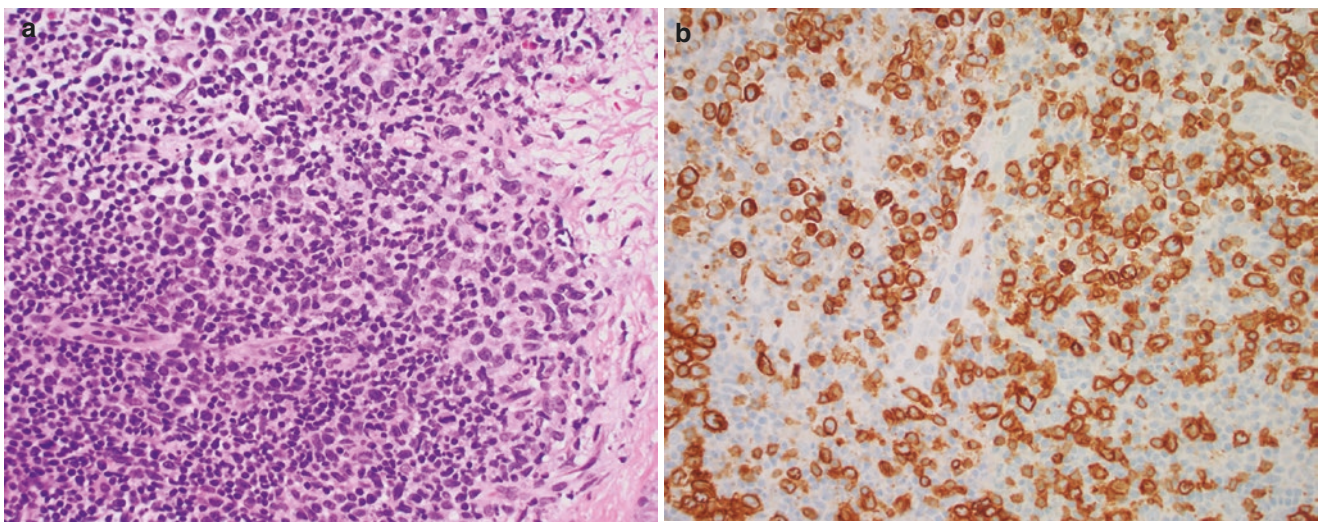

Fig. 12.8 (**a**, **b**) Peripheral T cell lymphoma, not otherwise specified: Atypical medium to large sized T cells with numerous infiltrating reactive lymphocytes (**a**, H&E stain, 40X). A CD3 immunostain highlights nuclear irregularities of the neoplastic cells (**b**, CD3 immunostain, 40X)

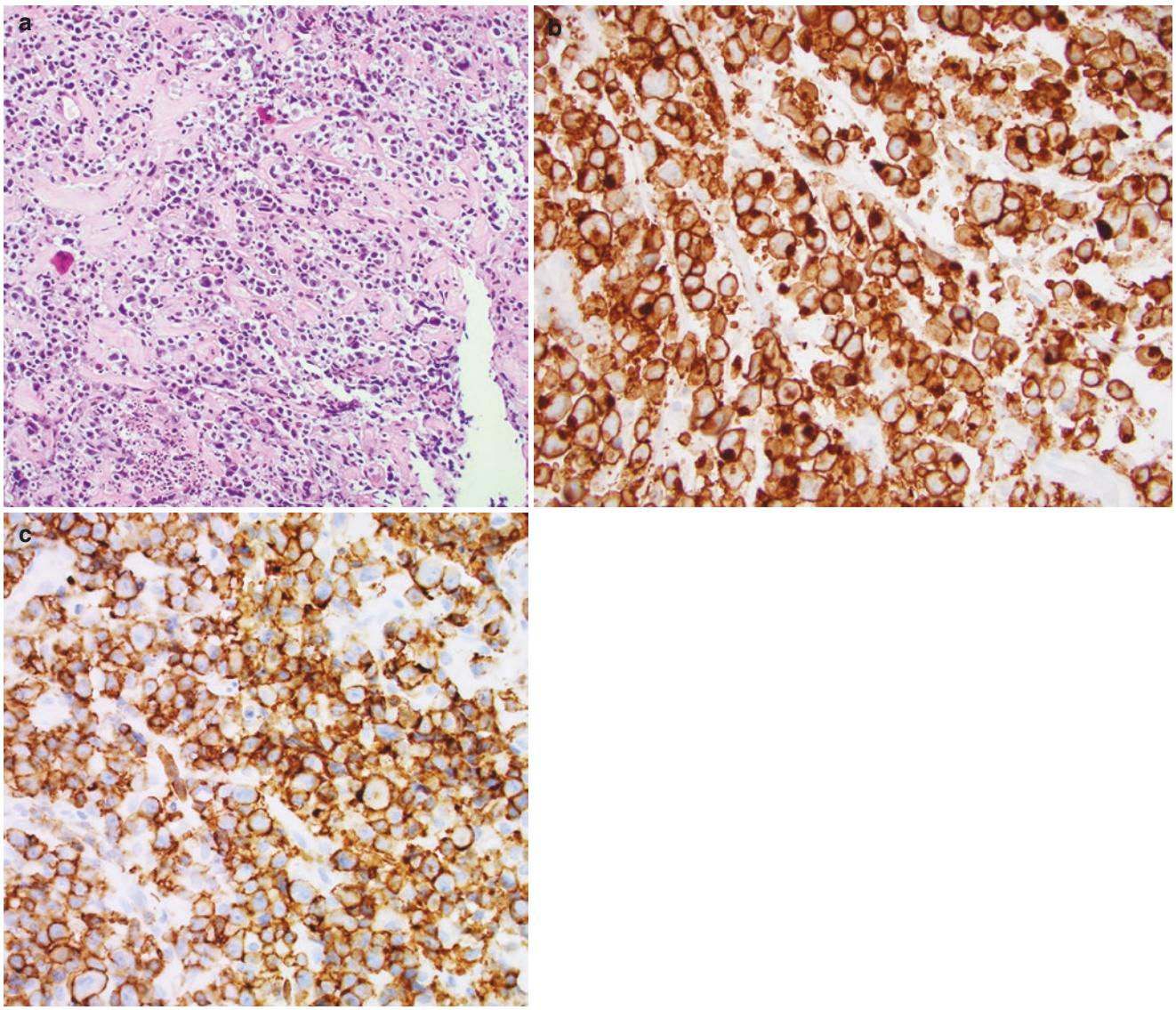

Fig. 12.9 (**a**–**c**) Anaplastic large cell lymphoma: diffuse infiltrate of large pleomorphic cells (**a**, H&E stain, 20X). The atypical cells are neoplastic T cells showing strong and uniform expression of CD30 (**b**, CD30 immunostain, 40X). In cases with loss of CD45 and T cell markers, a CD43 help demonstrate hematolymphoid origin (**c**, CD43 immunostain, 40X)

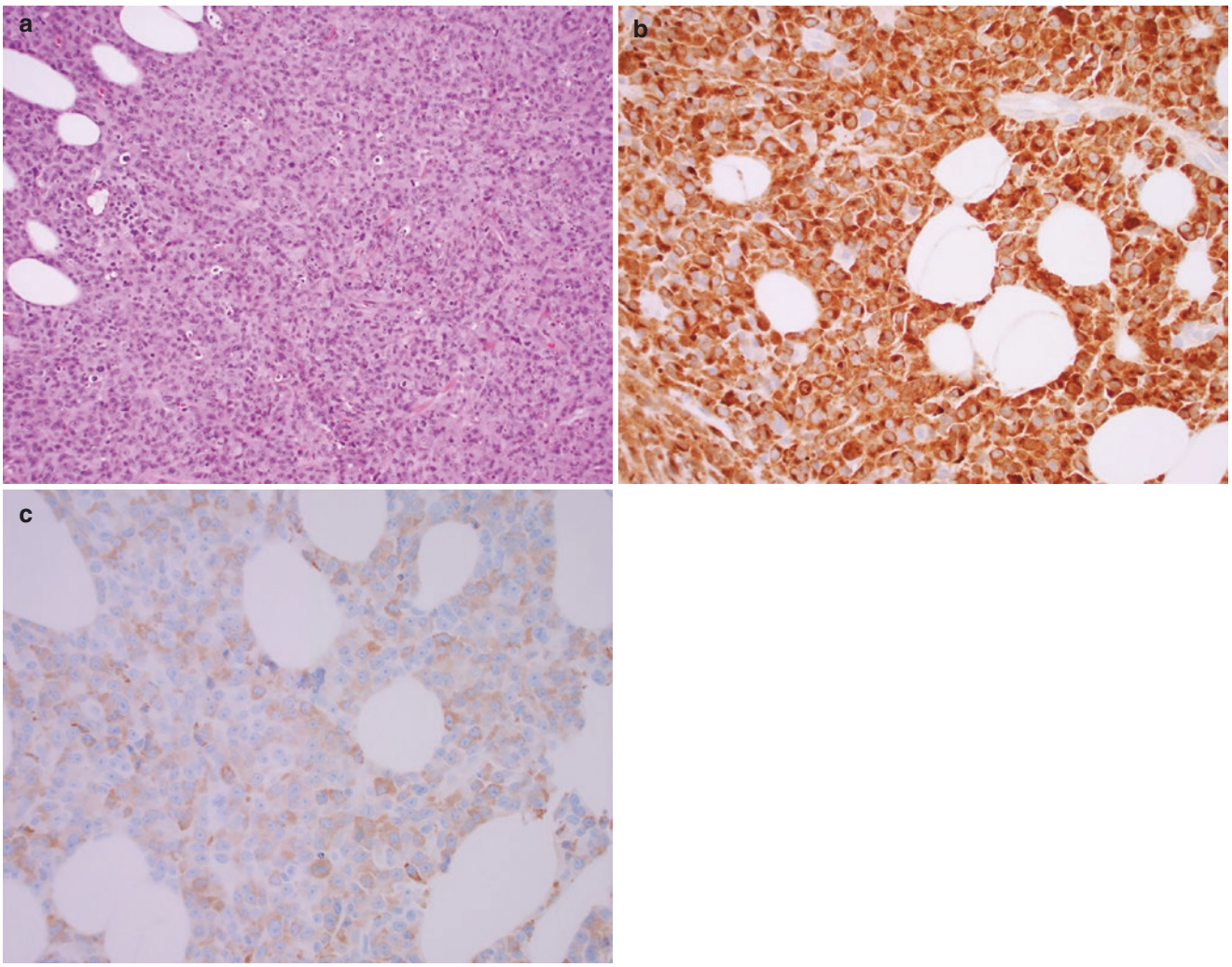

Fig. 12.10 (**a**–**c**) Myeloid sarcoma: sheets of highly atypical cells negative for initial screening markers CD3, CD20 and sometimes CD45 (**a**, H&E stain, 20X). A lysozyme immunostain helps demonstrate myeloid lineage (**b**, lysozyme immunostain, 40X). Staining with myeloperoxidase may be weak and variable (**c**, MPO immunostain, 40X)

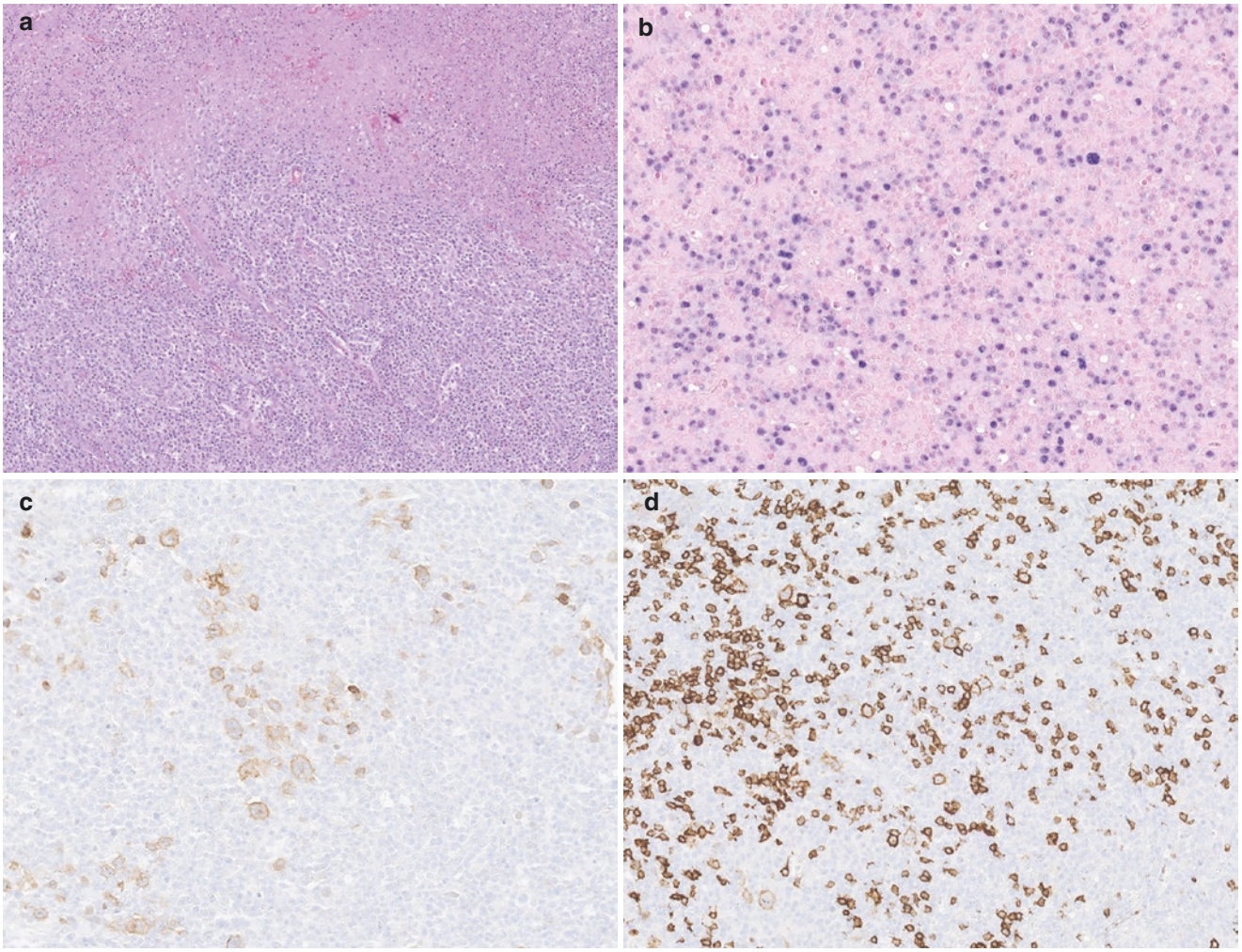

Fig. 12.11 (**a**–**d**) EBV-positive mucocutaneous ulcer: necroinflammatory debris from the superficial ulcer is microscopically delineated by a polymorphic infiltrate composed of few large cells, variably sized activated lymphocytes including immunoblasts, few plasma cells and histiocytes (**a**, H&E stain, 10X). An EBV *in-situ* hybridization study is positive in numerous cells within the infiltrate (**b**, EBER *in-situ* hybridization, 20X). A few of the large transformed cells resemble Hodgkin cells and express CD30 (**c**, CD30 immunostain, 40X). Staining with CD20 may be weak and variable in the Hodgkin-like large cells, a feature that overlaps with that seen in classic Hodgkin lymphoma (**d**, CD20 immunostain, 40X)

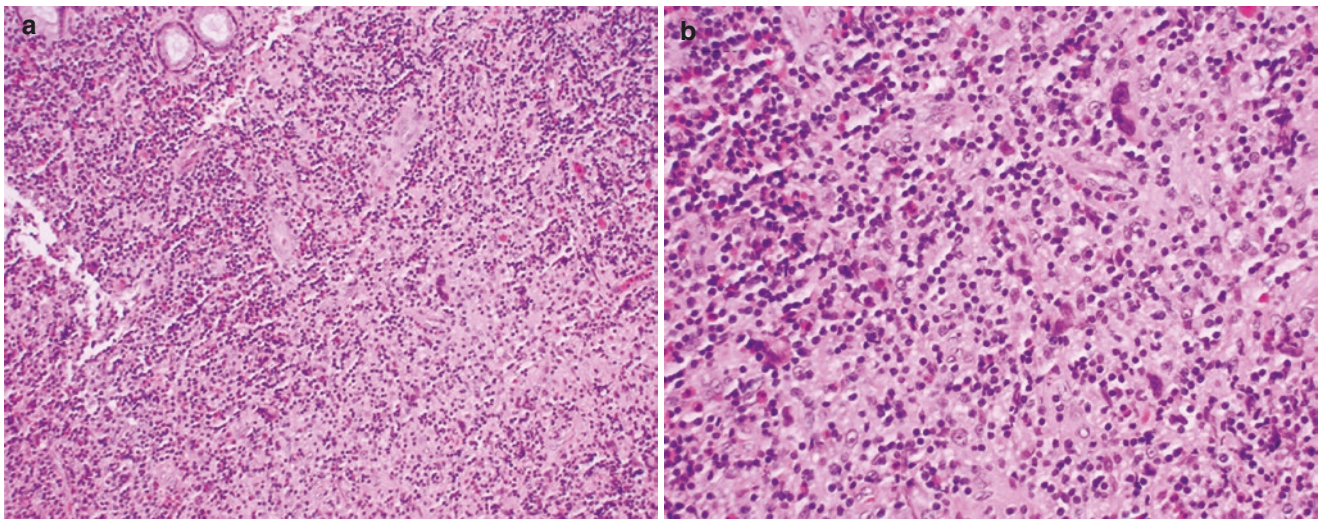

Fig. 12.12 (**a**, **b**) Classic Hodgkin lymphoma, iatrogenic lymphoproliferative disorder: this polymorphic infiltrate with few large cells in a background of numerous small lymphocytes, eosinophils, and histiocytes formed an extranodal mass in a patient with history of iatrogenic immunosuppression (**a**, H&E stain, 20X). High power image shows the mummified large cells which are multilobated, features of Hodgkin cells (**b**, H&E stain, 20X). The diagnosis requires demonstration of the classic Hodgkin phenotype

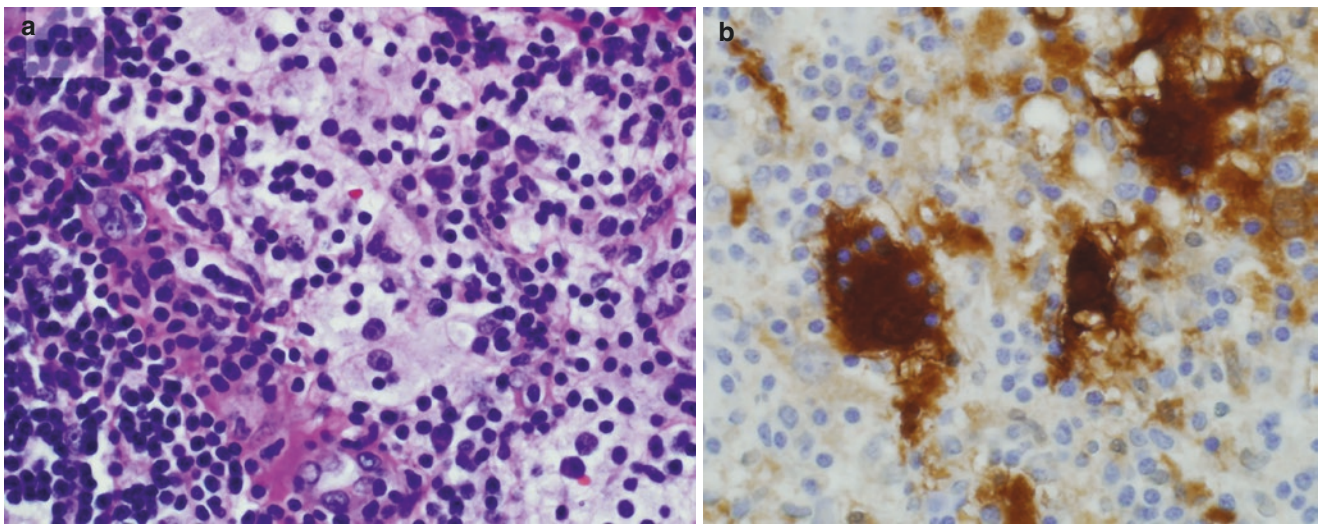

Fig. 12.13 (**a**, **b**) Rosai–Dorfman disease: infiltrate of foamy histiocytes and numerous small lymphocytes, some of which seen within the cytoplasm of the histiocytes, a phenomenon known as emperipolesis (**a**, H&E stain, 100X oil). The histiocytes express S100, which is helpful to highlight the emperipolesis (**b**, S100 immunostain, 100X oil)

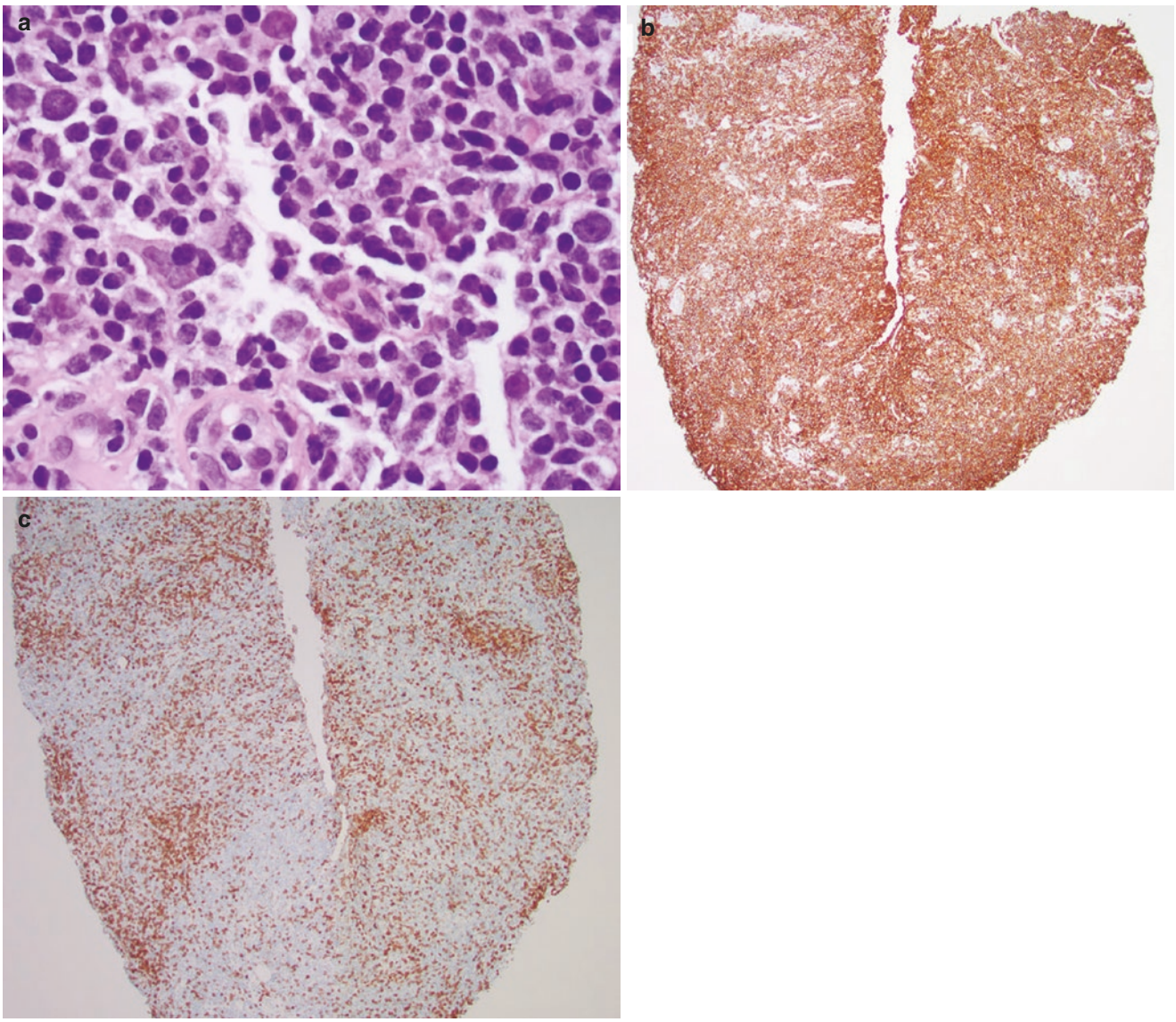

Fig. 12.14 (**a–c**) Low grade B lymphoma, marginal zone: the neoplastic cells are mature, small- to medium-sized lymphocytes with slight nuclear irregularities and abundant cytoplasm (**a**, H&E stain, 100X oil). A CD20 immunostain demonstrates distinctively abnormal pattern, with a predominance of B lymphocytes in a diffuse arrangement (**b**, CD20 immunostain, 4X) and fewer accompanying CD3-positive T lymphocytes (**c**, CD3 immunostain, 4X)

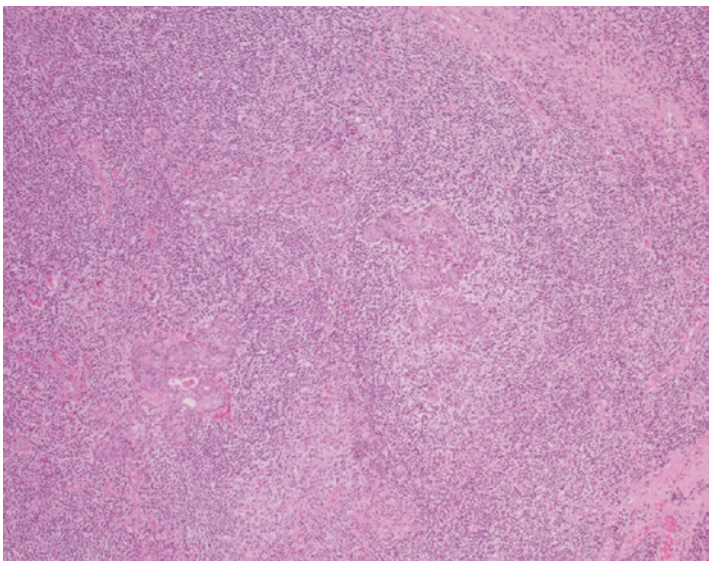

Fig. 12.15 Extranodal marginal zone lymphoma of mucosa associated lymphoid tissue (MALT lymphoma): low power image of the lymphoma shows a mottled appearance due to cells with abundant cytoplasm and infiltration of epithelial cells (15, H&E stain, 10X)

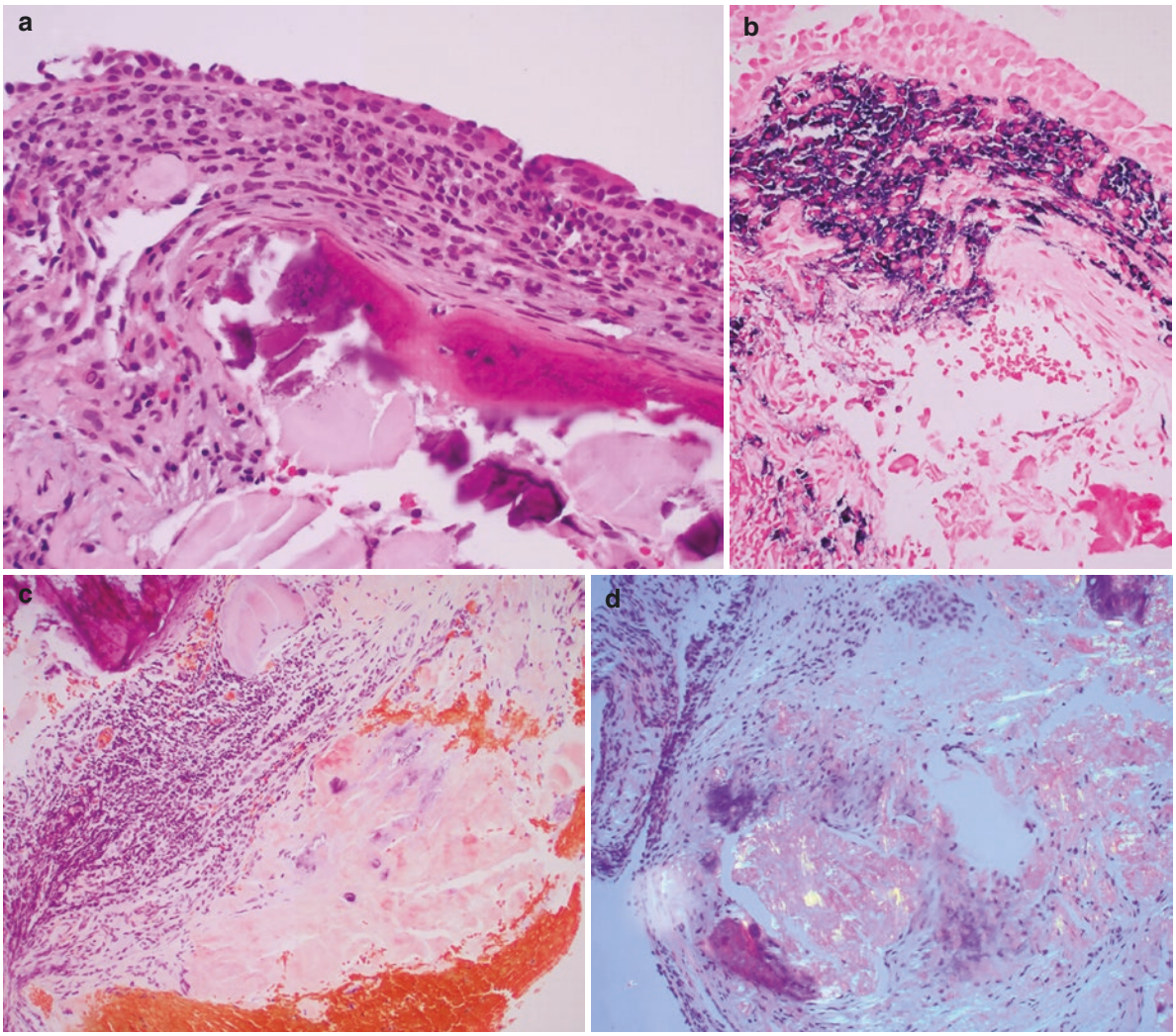

Fig. 12.16 (**a–d**) Primary amyloidosis: atypical plasma cells with intranuclear immunoglobulin inclusions (Dutcher bodies) are seen underneath respiratory epithelium and surrounding deposits of amorphous material with dystrophic calcification (**a**, H&E stain, 40X). The plasma cells are kappa-restricted (**b**, Kappa *in-situ* hybridization, 40X). The deposits are congophilic with Congo red stain (**c**, Congo red stain, 20X) and under polarized light display the apple green birefringence diagnostic of amyloid (**d**, Congo red stain, 20X)

Table 12.1 Differential diagnosis of hematolymphoid tumors of the sinonasal tract

Histologic pattern	Initial ancillary studies	Differential Diagnosis	Additional ancillary studies	Pitfalls and other considerations
Monomorphic, predominantly large cells	IHC CD3, CD56, CD20, PAX5, cyclin D1, CD138, EBER ISH	*B cell phenotype—PAX5(+)* • Diffuse large B cell lymphoma, NOS • EBV-positive DLBCL	In DLBCL, FISH for *MYC*, *BCL2,* BCL6, cell of origin determination with Hans algorithm (MUM1, bcl6, CD10) and double expresser status (c-myc, bcl2)	Consider alternative diagnosis in cases with variable and/or weak expression of CD20
		• Large cell lymphoma with IRF4 rearrangement	IRF4 FISH	Indicated in cases arising in Waldeyer ring, strong expression MUM1, young individuals
		• Aggressive pleomorphic mantle cell lymphoma	Cyclin D1 (+), high Ki-67	Cyclin D1 or SOX11 strongly uniformly positive; weak focal cyclin D1 is non-specific
		Plasma cell phenotype PAX5(−) CD138(+) • Plasmablastic lymphoma	If PAX5(−) CD138(−), add additional plasma cell markers CD79a, VS38, kappa, lambda, MUM1	T cell markers may be expressed
		T/NK cell phenotype (cytoplasmic CD3+, PAX5-, CD20-, CD56 +, EBER+) • Extranodal NK/T cell lymphoma nasal type	If CD56(−), add additional cytotoxic markers	Cell size varies, small cell size may be less aggressive; CD56 (−) cases require positive expression of other cytotoxic markers and EBER; Consider other T cell lymphomas if EBER (−) Surface CD3 is negative by flow cytometry in cases with NK cell phenotype
		Null phenotype (CD3 -/CD20−/ CD138−/ PAX5 -) • Anaplastic large cell lymphoma • Plasmablastic lymphoma • Myeloid sarcoma • Blastic plasmacytoid dendritic cell neoplasm • Non-hematopoietic tumors	CD43, CD30, CD45, T/ cytotoxic markers, CD2, CD4, CD56, TIA1, ALK, Granzyme B, plasma cell markers VS38, myeloid markers lysozyme, myeloperoxidase	Null phenotype ALCL may be only positive for CD43; CD43 is positive in ALCL, myeloid sarcoma, and plasmablastic lymphoma; CD43 is a good screening marker for hematopoietic tumors that are CD45 negative; CD30 positive tumors include classic Hodgkin lymphoma, ALCL, and germ cell tumors; consider blastic plasmacytoid dendritic cell neoplasm in CD4(+) CD56(+) cases

(continued)

Table 12.1 (continued)

Histologic pattern	Initial ancillary studies	Differential Diagnosis	Additional ancillary studies	Pitfalls and other considerations
Medium-sized cells	Flow cytometry; IHC: CD3, CD10, bcl2, CD20, cyclin D1, PAX5, TDT, ki-67	*CD10 (+) B cells* • Burkitt lymphoma • Burkitt-like lymphoma with 11q aberration • High grade B cell lymphoma • Lymphoblastic lymphoma • Aggressive blastoid mantle cell lymphoma • Indolent T lymphoblastic proliferation	SOX11 if cyclin D1(−) CD5(+) MYC/IgH for suspected Burkitt lymphoma; consider 11q aberration if no MYC rearrangement detected; FISH for MYC, BCL2, and BCL6 rearrangements Flow cytometry to demonstrate normal T lymphoblastic maturation pattern	Aggressive variants of mantle cell lymphoma may show unusual phenotype CD10(+) CD5(−); High grade B cell lymphoma, not otherwise specified if morphologically resembling Burkitt but lacking MYC/IgH, non-Burkitt phenotype bcl2 (+) CD10(−); negative 11q aberration; no double hit/triple hit Sensitivity for MYC/IgH depends on design of FISH probes
Variably sized cells, polymorphic	CD3, CD15, CD20, CD30, CD45, PAX5, EBER	• EBV-positive mucocutaneous ulcer • CHL • EBV-positive DLBCL	Additional markers for distinction between Hodgkin and non-Hodgkin lymphoma: CD19, CD79a, OCT2, BOB1	History of immunosuppression increases the incidence of extranodal CHL
Small lymphocytes	Flow cytometry; IHC CD3, CD20, CD21, Ki67, cyclin D1	• Low grade B cell lymphomas • Reactive	CD5, CD10, CD23, CD43 MyD88 mutation analysis in cases suspected of lymphoplasmacytic lymphoma	Rare cases of marginal zone lymphoma positive for MyD88 mutation
Plasma cells	Flow cytometry; IHC CD19, CD138, ISH or IHC kappa, lambda	• Extraosseous plasmacytoma • Primary amyloidosis • Low grade B cell lymphoma with extensive plasmacytic differentiation • Reactive • IgG4-related rhinosinusitis	Congo red special stain MyD88 mutation analysis in cases suspected of lymphoplasmacytic lymphoma IgG4/IgG IHC	Plasma cells in plasma cell neoplasms are more likely CD19(−) CD56(+), in low grade B cell lymphomas with plasmacytic differentiation CD19(+) CD56 (−) Correlation with serum IgG4 levels recommended
Histiocytic	GMS, AFB special stains S100, CD1a, CD3, CD20, PAX5	• Rosai–Dorfman disease • T cell/ histiocyte-rich large B cell lymphoma • Reactive, infectious	EBER if T cell histiocyte rich vs other EBV-positive lymphoproliferative disorders considered	S100 highlights emperipolesis in Rosai–Dorfman disease; CD1a positive cells may indicate abnormal Langerhans cell proliferation EBER (+) most likely to fit under EBV(+) DLBCL than T cell/histiocyte-rich large B cell lymphoma

IHC Immunohistochemistry, *FISH* Fluorescence *in-situ* hybridization, *DLBCL* Diffuse large B cell lymphoma, *ALCL* anaplastic large cell lymphoma, *EBV* Epstein–Barr virus, *CHL* classic Hodgkin lymphoma, *EBER* EBV encoded RNA *in-situ* hybridization, *ISH in-situ* hybridization, *NOS* Not otherwise specified

12.2 Large Cell Size

A monomorphic infiltrate of predominantly large cells is more likely to be diffuse large B cell lymphoma (DLBCL), either not otherwise specified, or specific categories such as EBV-positive diffuse large B cell lymphoma, and the new large B cell lymphoma with IRF4 rearrangement. In this location, the differential diagnosis for DLBCL includes plasmablastic lymphoma, particularly in HIV positive or otherwise immunosuppressed individuals, extranodal NK/T cell lymphomas nasal type, and double hit/triple hit lymphomas. An initial panel of immunohistochemical and *in-situ* hybridization (ISH) studies to include CD3, CD56, CD20, PAX5, cyclin D1, CD138, Epstein–Barr encoded RNA (EBER) ISH is likely to be informative in most cases. An infiltrate of large cells that is negative for CD3, CD20, PAX5, and CD138 and in which plasmablastic lymphoma has been excluded with additional plasma cell markers warrants consideration for alternative less common diagnoses such as anaplastic large cell lymphoma and myeloid sarcoma. While non-hematopoietic tumors may also be considered in this scenario, a lack of CD45 expression in isolation cannot be used to rule out some hematolymphoid origin, as neoplasms such as in anaplastic large cell lymphoma (ALCL), myeloid sarcoma, dendritic cells tumors, plasmablastic lymphoma, and classic Hodgkin lymphoma may be negative for CD45 [4–9].

12.2.1 Large B Cell Lymphomas

Diffuse large B cell lymphoma (DLBCL) is a type of non-Hodgkin B cell lymphoma characterized by diffuse infiltrate of predominantly large B cells, typically, with strong and diffuse expression of CD20 and PAX5 by immunohistochemistry (Fig. 12.2a–c) [1]. DLBCL displays a variety of morphologic appearances, ranging from monotonous to highly pleomorphic cytology, distributed in either cohesive sheets or in a more loosely arrangement of cells in an inflammatory background. The "not otherwise specified" categorization of DLBCL requires exclusion of features that would warrant a more specific WHO classification. Cases rich in histiocytes and reactive small lymphocytes with few scattered large neoplastic cells raise consideration for the specific subtype of DLBCL, **T cell/histiocyte-rich large B cell lymphoma**. Cases of DLBCL positive for EBV by EBER are classified as **EBV-positive DLBCL** [10]. In cases with strong expression of MUM1/IRF arising in the Waldeyer ring of young patients, fluorescence *in-situ* hybridization (FISH) testing for IRF4 rearrangement may be considered to rule out the new provisional category of **large B cell lymphoma with *IRF4* rearrangement** [11]. FISH studies to identify rearrangements of MYC, BCL2, and BCL6 to exclude **high grade B cell lymphoma with rearrangements of *MYC* and *BCL2* and/or *BCL6*** (double hit/triple hit lymphomas) are recommended in all cases of DLBCL [10, 12]. Additional immunohistochemical stains are recommended in DLBCL for prognostication and selection for targeted therapy [12, 13]. Determination of cell of origin using immunohistochemical algorithms, such as the Hans algorithm with CD10, Bcl6, and MUM1, is widely utilized in current practices to distinguish germinal center phenotype (better prognosis) from non-germinal center phenotype (worse prognosis) [12].
Adding cyclin D1 immunostain to an initial panel of immunostain is helpful to rule out the pleomorphic variant of mantle cell lymphoma, an aggressive subtype of mantle cell lymphoma**,** in which strong and diffuse expression of cyclin D1 and SOX11 is typically present [14].

12.2.2 Plasmablastic Lymphoma

Plasmablastic lymphoma (PBL) is a rare type of aggressive lymphoma that characteristically affects patients with acquired immunodeficiency syndrome (AIDS) or other types of immunosuppression. In the setting of AIDS, PBL is frequently positive for EBV and *MYC* gene rearrangements and tends to arise in the oropharynx [2, 6, 15, 16]. In plasmablastic lymphoma, the tumor cells are terminally differentiated B cells, negative for immunohistochemical markers PAX5 and CD45, and positive for CD138 and MUM1 (Fig. 12.3a, b) [2, 9, 15, 16]. In some cases, there is loss of typical plasma cell markers and additional markers are needed to demonstrate the plasma cell phenotype, such as VS38 and cytoplasmic light chain Kappa and Lambda [6, 9]. Variants of plasmablastic lymphoma with a higher number of mature plasma cells and aberrant expression of T cell markers may complicate the distinction from plasma cell neoplasms and T cell lymphomas, respectively [6, 15]. In addition to plasmablastic lymphoma, the differential diagnosis for tumors with plasmablastic features may include plasmablastic myeloma, ALK-positive large B cell lymphoma, extracavitary primary effusion lymphoma, and HHV8-positive diffuse large B cell lymphoma [16].

12.3 Medium-Sized Cells

A diffuse infiltrate of uniformly medium-sized cells is typically associated with aggressive types of mature non-Hodgkin B cell lymphomas, lymphoblastic lymphoma, and aggressive variants of mantle cell lymphoma. Mature T cell lymphomas, including extranodal NK/T cell lymphoma nasal type, may also be uniformly medium sized [10, 17, 18].

The most common medium-sized B cell lymphoma in the sinonasal tract is **Burkitt Lymphoma**. In these tumors, the presence of scattered apoptotic cells (macrophages with

apoptotic debris) imparting a "starry-sky" appearance is characteristic, albeit not specific nor required for the diagnosis (Fig. 12.4a). In a typical case of Burkitt, the cells display squared off cytoplasm and multiple peripheral small nucleoli. As a mature type of B cell lymphoma, the Burkitt cells are strongly and diffusely positive for PAX5, CD20, CD19, are negative for CD34 and TdT, and are typically surface light chain restricted [2, 19, 20]. The extremely high proliferation rate is evident by high expression of CD38 by flow cytometry and high ki-67 > 99% by immunohistochemistry. Unlike other aggressive B cell lymphomas, in Burkitt lymphoma the tumor cells are positive for CD10 and bcl6, negative for bcl2 and cyclin D1, with high c-myc expression (Fig. 12.4b, c). A *MYC/IG* rearrangement is usually demonstrable by appropriate FISH testing [20]. Cases that resemble Burkitt lymphoma morphologically and phenotypically, but lack MYC/Ig rearrangement may fit into the newly described category of **Burkitt-like lymphoma with 11q aberration** [20]. Cases in which there is demonstration of MYC rearrangements associated with either BCL2 and BCL6 rearrangements are classified as **high grade B cell lymphoma with rearrangements of *MYC*, *BCL2,* and *BCL6*** regardless of specific morphology or phenotype. A strong and diffuse expression of cyclin D1 by immunohistochemistry is diagnostic for **"blastoid" variant of mantle cell lymphoma** (Fig. 12.5a–c). This aggressive variant of mantle cell lymphoma may show aberrant phenotypes such as positivity with CD10 and/or lack of CD5 [15, 20]. The presence of CD10-positive mature blastoid cells in a follicular/nodular pattern associated with CD21-positive dendritic meshworks requires consideration for **pediatric-type follicular lymphoma**, particularly in young individuals. Unlike other types of follicular lymphoma, this variant lacks expression of bcl2 [21].

The identification of CD10-positive cells that lack surface immunoglobulin by flow cytometry and are medium sized warrant exclusion of **lymphoblastic lymphoma,** although some cases of mature B cell lymphoma may also lack surface immunoglobulin [2, 20]. The demonstration of an immature phenotype with CD34 and/or uniform TdT expression establishes the diagnosis of lymphoblastic lymphoma. Determination of lineage is based on demonstration of lineage-defining markers cytoplasmic CD3 for T cell lineage or CD19, CD79a, or CD22 for B cell lineage (Fig. 12.6) [2]. **Indolent T lymphoblastic proliferation** may be identified in the sinuses presenting as non-destructive sheets of aggregates of morphologically and phenotypically immature T-lineage cells. By flow cytometry, there is a normal maturation pattern of T cells and no aberrancies. This is indolent and requires no treatment [2].

A rare type of blastoid tumor is **blastoid plasmacytoid dendritic cell neoplasm**, a malignant neoplasm that typically arises in the skin and spreads to blood and bone marrow. Involvement of the nasal cavity has been reported [8, 22]. Cases with "blastoid" or Burkitt-like appearance that do not fulfill diagnostic criteria for any of the above-discussed entities are likely to fit under the classification of **high grade B cell lymphoma, unclassifiable** [20].

12.3.1 Mature T Cell Lymphomas

T cell lymphomas are less frequent than B cell lymphomas, and most cases in the sinonasal tract are small to medium in size [1, 2]. Antigens normally expressed on T cells or NK cells including CD2, CD3, CD5, CD7, and CD56 are variably lost in these neoplasms [2, 17]. The expression of cytoplasmic CD3, TIA1, Granzyme B, T cell receptors by immunohistochemistry or positive T cell receptor gene rearrangements by molecular testing can be used to establish T cell lineage. Although the precise determination of T cell versus NK cell origin may not be possible, by flow cytometry, NK cells are characteristically negative for surface CD3 expression and positive for cytoplasmic CD3 molecules [2, 17].

Of all mature T cell lymphomas, **extranodal NK/T cell lymphoma (ENKTCL), nasal type** is a highly aggressive neoplasm of NK cells or cytotoxic T cells uniformly associated with EBV, more frequently seen in the sinonasal tract than other extranodal sites [1, 2, 17]. Biopsies of these tumors show extensive coagulative necrosis with apoptotic debris, and a high suspicion for this should be in necrotic masses in the sinonasal tract regardless of the cytologic appearance [2, 17]. The infiltrate is frequently medium sized with a characteristic perivascular accentuation (Fig. 12.7a–c), but may also be composed of small cells, large or pleomorphic cells [2, 17]. The neoplastic cells are positive for CD3 by immunohistochemistry, which may help highlight atypical nuclear irregularities. The cells are usually positive for CD2, CD43, and CD56; other T cell markers including CD4, CD8, CD16, and CD57 are often negative [2, 17]. Tumors with cytotoxic T cell phenotype may be positive for CD5, CD8, and T cell receptors, and cytotoxic molecular granzyme B, TIA1, and perforin. Cases negative for CD56 require demonstration of other cytotoxic markers and EBV association for the diagnosis [2, 17]. The differential for ENKTCL is **peripheral T cell lymphoma, not otherwise classified** (PTCL, NOS), should be considered in T cell tumors that are EBV negative or that otherwise phenotypically not compatible with ENKTCL (Fig. 12.8a, b).

12.3.2 Pleomorphic T Cell Lymphomas

Exceedingly rare in the United States, **Adult T cell leukemia/Lymphoma (ATLL)** may be on the differential for lymphomatous proliferations in individuals originated from Southwestern Japan, the Caribbean, parts of Central Africa,

the Middle East, Papua New Guinea, and South America. In these geographic areas, the human T-lymphotropic virus-1 (HTLV-1) that is strongly associated with ATLL is endemic. Correlation with clinical history and demonstration of HTLV1 association is key to establish the diagnosis in non-endemic areas [2, 18, 23]. The typical presentation includes generalized lymphadenopathy, abnormal circulating T lymphocytes, hypercalcemia, and skin rash, with subsequent dissemination to extranodal sites, including the head and neck [2, 23]. The abnormal T cells display a wide range of cytologic appearances, but the presence of the highly pleomorphic "flower cells" is characteristic. The neoplastic cells are characteristically positive for CD4 and CD25, with frequent co-expression of CD2, CD3, and CD5, and aberrant loss of CD7. Cases that are negative for CD4 and positive for CD8, or double negative CD4 and CD8 are recognized [2, 23]. CD30 may be positive, complicating the distinction with other pleomorphic T cell neoplasms such as ALCL [23]. Unlike ALCL, in ATLL the cytotoxic molecules TIA1, Granzyme B, and perforin are negative, and unlike extranodal NK/T cell lymphoma, EBER is negative in ATLL [23]. The lack of ALK expression in ATLL may help in the distinction from ALK-positive ALCL. **Anaplastic large cell lymphoma (ALCL)** is subdivided in ALK-positive, ALK negative and primary cutaneous subtypes and is a diagnostic consideration in all EBV-negative T cell neoplasms expressing CD30 (Fig. 12.9a–c). The null phenotype of ALCL, in which the tumor cells aberrantly lack all T cell/cytotoxic molecules, require exclusion of classic Hodgkin lymphoma and other CD30-positive CD45-negative malignancies including **myeloid sarcoma** (Fig. 12.10a–c) [4]. In such instances, CD43 is a marker to be considered to demonstrate hematolymphoid origin (Fig. 12.9c) [4, 5, 7–9].

12.4 Polymorphic Infiltrates

Polymorphic infiltrates may be seen in association with EBV-positive lymphoproliferative disorders and are characterized by variably sized activated large atypical cells in a mixed inflammatory background that includes eosinophils, plasma cells, and histiocytes. An ulcerated mass arising in the skin or mucosal sites, particularly the oropharynx and gastrointestinal tract, and that shows a polymorphic lymphoid infiltrate microscopically warrants consideration for the diagnosis of **EBV-positive Mucocutaneous ulcer (EBV MCU)** [24]. This is a newly recognized entity that occurs in patients with age-related, HIV-related or iatrogenic immunosuppression. Demonstrable association with EBV is required for the diagnosis. The large cells are transformed B cells with cytologic features of immunoblasts or Hodgkin-like cells, positive for PAX5, OCT2, and CD45, with variable expression of CD20. The expression of CD30 and CD15 (in a subset) may complicate the distinction from classic Hodgkin lymphoma (Fig. 12.11a–d). The numerous T cells are often CD8+ and may make a dense rim between the infiltrate and the uninvolved adjacent soft tissue [24]. In cases with focal and weak CD20 expression, the distinction from EBV-positive DLBCL or **classic Hodgkin lymphoma (CHL)** may be challenging (Fig. 12.11c) [24, 25]. While classic Hodgkin lymphoma is typically nodal disease, it may arise in Waldeyer ring or be seen in extranodal sites in immunosuppressed individuals (Fig. 12.12a, b) [24, 25].

12.5 Histiocytic Lesions

Non-granulomatous histiocytic proliferations may occur associated with a variety of malignant hematolymphoid neoplasms. Along with numerous small lymphocytes, histiocytes make up the characteristic background of **T cell/histiocyte-rich large B cell lymphoma** [26, 27]. B cell markers such as PAX5 and CD20 will highlight the large atypical cells allowing for the diagnosis. This type of lymphoma typically affects nodal sites, liver, spleen, and bone marrow, although reports of tumors arising primarily in the sinonasal and upper respiratory tract exist [26].

Other histiocytic lesions that are uncommon, but that may be identified in nodal and extranodal sites including the sinonasal tract, facial bones, and orbital sites encompass **Rosai–Dorfman disease (RDD)** along with other histiocytosis in this group, Erdheim-Chester and Langerhans cell histiocytosis [1, 2, 28]. Initially thought to be an inflammatory proliferation of histiocytes, the identification of mutations associated with RDD, specifically the mutually exclusive *KRAS* and *MAP2K1* mutations [28], support the consideration for a clonal/neoplastic biology for these tumors. The defining histopathologic feature of RDD is the identification of histiocytes displaying emperipolesis, presence of intact cells in the cytoplasm of the histiocytes. Unlike Erdheim-Chester, RDD usually shows strong staining with S100, which helps highlight the emperipolesis (Fig. 12.13a, b). Unlike Langerhans cell histiocytosis, the proliferating cells are negative for Langerhans cell markers CD1a and Langerin (CD207) [28].

12.6 Small Cells or Normal-Appearing Cells

Aside from ENKTCL, a mass forming proliferation of small lymphocytes in the sinonasal region is likely either a low grade B cell lymphoma or a reactive-non-specific process. Flow cytometry is particularly helpful to demonstrate light chain restriction indicative of a clonal neoplastic B cell proliferation or T cell aberrancies. Immunostains with CD3 and CD20 may be useful to demonstrate an increase in B cells (B

cells more numerous than T cells), diffusely dispersed rather than in the normal follicular/aggregated arrangement, or in prominent crowded nodules, suggesting a low grade B cell lymphoma (Fig. 12.14a–c). The presence of numerous plasma cells, even without cytologic atypia, may require exclusion of clonal plasma cell proliferation with kappa/lambda immunophenotyping. In the appropriate clinical setting, the diagnosis of IgG4-related rhinosinusitis may be considered.

12.6.1 Low Grade B Cell Lymphomas

Low grade B cell lymphomas are less common in the sinonasal mucosa than aggressive types of non-Hodgkin lymphoma and may arise either primarily in the upper respiratory tract lymphoid tissue or represent tissue infiltration from lymphoma arising in other sites [2, 29, 30]. Cases of **extranodal marginal zone lymphoma of mucosa associated lymphoid tissue (MALT lymphoma)** arising primarily in the paranasal sinus are rare, developing rarely in patients with long-standing history of chronic sinusitis [29, 31]. However, cases arising in minor salivary glands or periocular adnexa may extend to the paranasal sinus [30, 31]. The infiltrate is composed of diffuse infiltrate of small- to medium-sized CD20-positive B lymphocytes with only mild irregularities and often abundant amount of cytoplasm (Fig. 12.15). Residual follicles may be demonstrated with CD21 staining, and follicular colonization may occur. The B cells may aberrantly express CD43, which is helpful to demonstrate their neoplastic nature.

Cases with extensive plasmacytic differentiation may be difficult to distinguish from **lymphoplasmacytic lymphoma** [32]. While the presence of *MyD88* mutation may help to confirm cases of lymphoplasmacytic lymphoma, the mutation is known to occur in rare cases of MALT lymphoma [33]. Cases with plasmacytic differentiation show presence of a plasma cell component with the same light chain restriction as the B cells. By flow cytometry, the plasma cells show a CD19-positive CD56-negative phenotype, which is distinct from the plasma cell clones present in plasma cell neoplasms [34]. Prominent follicular colonization expands the follicles and may create difficulty in the distinction with follicular lymphoma. Case series of sinonasal lymphomas report **follicular lymphoma** more frequently than other low grade B cell lymphomas [3, 35]. **Chronic lymphocytic leukemia/small lymphocytic lymphoma** of the sinonasal areas occur more likely from infiltration from other sites of involvement [2].

12.7 Plasma Cell Neoplasms

The presence of numerous mature plasma cells may be seen in the setting of reactive processes, plasma cell neoplasms, or low grade B cell neoplasms with plasmacytic differentiation. Plasma cell neoplasms are among one of the most frequent hematolymphoid malignancies identified in the sinonasal area and include extraosseous plasmacytoma and primary amyloidosis [1, 2, 29]. **Extraosseous plasmacytoma** presents as tissue-based lesions composed of mature-appearing plasma cells often with minimal cytologic atypia [36]. The distinction from reactive proliferations relies on the demonstration of light chain restriction by either flow cytometry or *in-situ* hybridization [1, 2, 29]. Amyloid deposition in **primary amyloidosis** (AL type) appears histologically as a deposit of amorphous lightly eosinophilic material [37]. Associated neoplastic plasma cells, frequently lambda light chain restricted, may be present in the biopsy (Fig. 12.16a, b). Staining with Congo red demonstrates apple green birefringence diagnostic of amyloid protein (Fig. 12.16c, d) under polarized lens or green color by Sulfated Alcian Blue (SAB) stain [37].

12.8 Reactive/Inflammatory

A variety of neoplastic and non-neoplastic lesions of the nasal cavity and sinonasal tract may induce non-specific reactive acute and/or chronic inflammation [38]. Among inflammatory disorders that affect this site, the newly recognized IgG4 related rhinosinusitis may be associated with unilateral mass-forming solid lesions and fall on the differential of other hematolymphoid proliferations and inflammatory disorders such as Rosai–Dorfman disease and granulomatosis with polyangiitis [2, 28, 39]. In most patients, there is an association with chronic sinusitis and bilateral changes on imaging. There is currently no consensus diagnostic criteria for this newly proposed clinical entity in the sinonasal tract. In other sites, the diagnosis of IgG4-related disease requires the presence of mass formation, elevated serum IgG4, a lymphoplasmacytic infiltrate with an increased number of IgG4 positive plasma cells (IgG4+/IgG+ cells >40% and > 10 IgG4+ plasma cells/HPF), background of storiform fibrosis, and obliterating phlebitis [39, 40].

12.9 Conclusion

In conclusion, hematolymphoid lesions in the sinonasal tract are overall infrequent. The most common entities to affect this site are non-Hodgkin B cell lymphomas such as DLBCL and Burkitt lymphoma, followed by extraosseous plasmacytoma [1, 2, 29, 36]. EBV-related hematolymphoid disorders such as extranodal NK T cell lymphoma nasal type, plasmablastic lymphoma, and EBV mucocutaneous ulcer show predilection for nasal and oral cavities among other extranodal sites. Other entities rarely described in the sinonasal tract include lymphoblastic lymphoma, histiocytic proliferations, Hodgkin lymphomas, myeloid sarcoma, low grade B cell lymphomas, and other T cell lymphomas. An algorithmic approach based on morphologic assessment of the cell size (small, medium, or large) and overall pattern of the infiltrate (monomorphic vs polymorphic) with targeted immunophenotyping narrows down the differential diagnosis in most cases.

References

1. Kreise FH. Hematolymphoid lesions of the Sinonasal tract. Head Neck Pathol. 2016;10:109–11.
2. Crane GM, Duffield AS. Hematolymphoid lesions of the sinonasal tract. Semin Diagn Pathol. 2016;33(2):71–80.
3. Azarpira N, Ashraf MJ, Monabati A, Makarempour A, Khademi B, Hakimzadeh A, Abedi E, Valibeigi B. Primary lymphoma of nasal cavity and paranasal sinuses. Lab Medicine. 2012;43(6):294–9.
4. Medeiros LJ, Elenitoba-Johnson KS. Anaplastic large cell lymphoma. Am J Clin Pathol. 2007;127(5):707–22.
5. Kaygusuz G, Kankaya D, Ekinci C, Topçuoğlu P, Kuzu I. Myeloid sarcomas: a clinicopathologic study of 20 cases. Miyeloid Sarkomlar: 20 Olguluk Klinikopatolojik Çalışma. Turk J Haematol. 2015;32(1):35–42.
6. Harmon CM, Smith LB. Plasmablastic lymphoma: a review of Clinicopathologic features and differential diagnosis. Arch Pathol Lab Med. 2016;140(10):1074–8.
7. Wang HY, Zu Y. Diagnostic algorithm of common mature B-cell lymphomas by immunohistochemistry. Arch Pathol Lab Med. 2017;141(9):1236–46.
8. Reichard KK, Burks EJ, Foucar MK, Wilson CS, Viswanatha DS, Hozier JC, Larson RS. CD4(+) CD56(+) lineage-negative malignancies are rare tumors of plasmacytoid dendritic cells. Am J Surg Pathol. 2005;29(10):1274–83.
9. Al Shaarani M, Shackelford RE, Master SR, Mills GM, AlZubaidi Y, Mamilly A, Wei EX. Plasmablastic lymphoma, a rare entity in bone marrow with unusual Immunophenotype and challenging differential diagnosis. Case Rep Hematol. 2019; Sep;2:1586328.
10. King JF, Lam JT. A practical approach to diagnosis of B-cell lymphomas with diffuse large cell morphology. Arch Pathol Lab Med. 2020;144(2):160–7.
11. Pittaluga S, Harris NL, Siebert R, Salaverria I. Large B-cell lymphoma with *IRF4* rearrangement. In: Swerdlow SH, Campo E, Harris NL, et al, eds. WHO classification of tumors of Haematopoietic and lymphoid tissues. Revised 4th Ed. Lyon: IARC; 2017:280–281.
12. Jamil MO, Mehta A. Diffuse large B-cell lymphoma: prognostic markers and their impact on therapy. Expert Rev Hematol. 2016;9(5):471–7.
13. Thapa B, Caimi PF, Ardeshna KM, Solh M, Carlo-Stella C, Kahl BS. Mehdi Hamadani; CD19 antibody-drug conjugate therapy in DLBCL does not preclude subsequent responses to CD19-directed CAR T-cell therapy. Blood Adv. 2020;4(16):3850–2.
14. Swerdlow S.H. Campo E. Seto M. Müller-Hermelink H.K. Mantle cell lymphoma. In: Swerdlow SH, Campo E, Harris NL, et al, eds. WHO classification of tumors of Haematopoietic and lymphoid tissues. Revised 4th Ed. Lyon: IARC; 2017:432.
15. Pan Z, Chen M, Zhang Q, Wang E, Yin L, Xu Y, Huang Q, Yuan Y, Zhang X, Zheng G, Yuan J. CD3-positive plasmablastic B-cell neoplasms: a diagnostic pitfall. Mod Pathol. 2018;31(5):718–31.
16. Ahn JS, Okal R, Vos JA, Smolkin M, Kanate AS, Rosado FG. Plasmablastic lymphoma versus plasmablastic myeloma: an ongoing diagnostic dilemma. J Clin Pathol. 2017 Sep;70(9):775–80.
17. Chan JKC, Quintanilla-Martinez L, Ferry JA. Extranodal NK/T-cell lymphoma, nasal type. In: Swerdlow SH, Campo E, Harris NL, et al, eds. WHO classification of tumors of Haematopoietic and lymphoid tissues. Revised 4th Ed. Lyon: IARC; 2017:368–371.
18. Pileri SA, Weisenburger DD, Sng I, Nakamura S, Müller-Hermelink HK, Chan WC, Jaffe ES. Peripheral T-cell lymphoma, NOS. In: Swerdlow SH, Campo E, Harris NL, et al, eds. WHO classification of tumors of Haematopoietic and lymphoid tissues. Revised 4th Ed. Lyon: IARC; 2017:403–407.
19. Chiu A, Frizzera G, Mathew S, Hyjek EM, Chadburn A, Tam W, Knowles DM, Orazi A. Diffuse blastoid B-cell lymphoma: a histologically aggressive variant of t(14;18)-negative follicular lymphoma. Mod Pathol. 2009;22(11):1507–17.
20. Chen BJ, Fend F, Campo E, Quintanilla-Martinez L. Aggressive B-cell lymphomas—from morphology to molecular pathogenesis. Annals of Lymphoma. 2019;3:1.
21. Jaffe ES, Harris NL, Siebert R. Pediatric-type follicular lymphoma. In: Swerdlow SH, Campo E, Harris NL, et al, eds. WHO classification of tumors of Haematopoietic and lymphoid tissues. Revised 4th Ed. Lyon: IARC; 2017:278–279.
22. Lee SE, Park HY, Kwon D, Jeon YK, Kim WY. Blastic plasmacytoid dendritic cell neoplasm with unusual extracutaneous manifestation: two case reports and literature review. Medicine (Baltimore). 2019;98(6):e14344.
23. Ohshima K, Jaffe ES, Yoshino T, Siebert R. Adult T-cell leukaemia/lymphoma. In: Swerdlow SH, Campo E, Harris NL, et al, eds. WHO classification of tumors of Haematopoietic and lymphoid tissues. Revised 4th Ed. Lyon: IARC; 2017:363–367.
24. Ikeda T, Gion Y, Yoshino T, Sato Y. A review of EBV-positive mucocutaneous ulcers focusing on clinical and pathological aspects. J Clin Exp Hematop. 2019;59(2):64–71.
25. Men Y, Sun X, Wei D, Yu Z. Primary extranodal head and neck classical Hodgkin lymphoma: a rare clinical case report. Exp Ther Med. 2016;12(2):1007–11.
26. Wang J, Sun NC, Weinstein SM, Canalis R. Primary T-cell-rich B-cell lymphoma of the ethmoid sinus. A case report with 5 years of follow-up. Arch Pathol Lab Med. 2000;124(8):1213–6.
27. Ott G, Delabie J, Gascoyne RD, Campo E, Stein H, Jaffe ES. T-cell/histiocyte-rich large B-cell lymphoma. In: Swerdlow SH, Campo E, Harris NL, et al, eds. WHO classification of tumors of Haematopoietic and lymphoid tissues. Revised 4th Ed. Lyon: IARC; 2017:298–299.
28. Goyal G, Ravindran A, Young JR, Shah MV, Bennani NN, Patnaik MM, Nowakowski GS, Thanarajasingam G, Habermann TM, Vassallo R, Sher T, Parikh SA, Rech KL, Go RS, & Mayo Clinic Histiocytosis Working Group. Clinicopathological features, treatment approaches, and outcomes in Rosai-Dorfman disease. Haematologica. 2020;105(2):348–57.
29. Babb MJ, Cruz RM, Puligandla B. Sinonasal mucosa-associated lymphoid tissue lymphoma. Arch Otolaryngol Head Neck Surg. 1999;125(5):585–8.

30. Young W, Scofield-Kaplan SM, Levy RE, Rosado F, Mancini R. Conjunctival lymphoma with nasal spread through the nasolacrimal duct. Ophthal Plast Reconstr Surg. 2021;37(1):e3–5.
31. Tauber S, Nerlich A, Lang S. MALT lymphoma of the paranasal sinuses and the hard palate: report of two cases and review of the literature. Eur Arch Otorhinolaryngol. 2006 Jan;263(1):19–22.
32. Ma S, Jug R, Shen S, Zhang WL, Xu HT, Yang LH. Marginal zone lymphoma of palatine tonsil with prominent plasmacytic differentiation: a CARE-compliant article and review of literature. Medicine (Baltimore). 2018;97(2):e9648.
33. Li ZM, Rinaldi A, Cavalli A, et al. MYD88 somatic mutations in MALT lymphomas. Br J Haematol. 2012;158(5):662–4.
34. Rosado FG, Morice WG, He R, Howard MT, Timm M, McPhail ED. Immunophenotypic features by multiparameter flow cytometry can help distinguish low grade B-cell lymphomas with plasmacytic differentiation from plasma cell proliferative disorders with an unrelated clonal B-cell process. Br J Haematol. 2015;169(3):368–76.
35. Chalastras T, Elefteriadou A, Giotakis J, et al. Non-Hodgkin's lymphoma of nasal cavity and paranasal sinuses. A clinicopathological and immunohistochemical study. Acta Otorhinolaryngol Ital. 2007;27(1):6–9.
36. D'Aguillo C, Soni RS, Gordhan C, Liu JK, Baredes S, Eloy JA. Sinonasal extramedullary plasmacytoma: a systematic review of 175 patients. Int Forum Allergy Rhinol. 2013;00:X–XX.
37. Wahid NW, Abed T, Meghji S, Gilbertson J, Barnes M. Localized Sinonasal Amyloidosis. Allergy Rhinol (Providence). 2019;10:2152656719860821.
38. Momeni AK, Roberts CC, Chew FS. Imaging of chronic and exotic sinonasal disease: review. AJR Am J Roentgenol. 2007;189(6 Suppl):S35–45.
39. Moteki H, Yasuo M, Hamano H, Uehara T, Usami S. IgG4-related chronic rhinosinusitis: a new clinical entity of nasal disease. Acta Otolaryngol. 2011 May;131(5):518–26.
40. Piao Y, Zhang Y, Yue C, Wang C, Zhang L. Immunoglobulin G4-related chronic rhinosinusitis: a pitfall in the differential diagnosis of granulomatosis with polyangiitis, Rosai-Dorfman disease, and fungal rhinosinusitis. Hum Pathol. 2018;73:82–8.

Neuroectodermal and Melanocytic Tumors of the Sinonasal Tract

13

Matthew Gabrielson and Lisa M. Rooper

13.1 Introduction

Historically, classifications of sinonasal tumors have placed several entities thought to arise from derivatives of the embryonic neural crest, including Ewing sarcoma, malignant mucosal melanoma, and olfactory neuroblastoma, in the broad category of neuroectodermal tumors [1–4]. However, conceptualization of these tumors based on cell of origin has increasingly fallen out of favor as better understanding of their specific genetic underpinnings and phenotypic characteristics has revealed few similarities between the various entities in this historical group. Nevertheless, it remains convenient to discuss tumors of presumed neuroectodermal and melanocytic origin together, as these unique and diverse tumors do not neatly fit into other groups of sinonasal malignancies. Furthermore, a rare subset of sinonasal tumors, including teratocarcinosarcoma and the emerging category of olfactory carcinoma, actually show neuroectodermal differentiation and can also be addressed within this category.

13.2 Ewing Sarcoma

Ewing sarcoma is a primitive small round cell sarcoma defined by the presence of fusions between genes in the FET and ETS families, most commonly *EWSR1::FLI1* [5–12]. While the term primitive neuroectodermal tumor was previously used synonymously with Ewing sarcoma, this designation has fallen out of favor with recognition that these tumors are defined by their pathognomonic fusions and are distinct from the neuroectodermal neoplasms that arise in the central nervous system [13]. Ewing sarcomas most commonly arise in adolescents and young adults, with approximately 50% in patients under 18 and 85% in the first four decades [14, 15] Approximately 10% of all Ewing sarcomas occur in the head and neck including a significant subset in the sinonasal tract [14, 16]. In general, those Ewing sarcomas that do arise in the head and neck tend to have a better prognosis than in other anatomic sites, likely because of lower stage and smaller size at presentation [14]. Ewing sarcoma consistently demonstrates diffuse membranous CD99 expression and nuclear NKX2.2 positivity that can differentiate it from a broad range of other sinonasal small round blue cell tumors. Although tumors with neuroendocrine differentiation can also label with NKX2.2 [17–20]. FLI1 expression correlates with fusion status but has limited specificity [21, 22]. The morphologic and immunohistochemical profile of Ewing sarcoma is detailed below (Figs. 13.1, 13.2, 13.3, 13.4, 13.5, 13.6, 13.7, 13.8, 13.9, and 13.10).

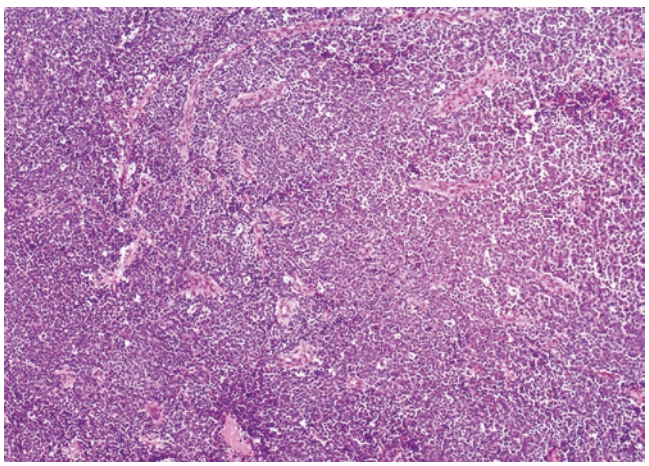

Fig. 13.1 Ewing sarcoma is composed of small round blue cells that show diffuse sheet-like growth (10x)

M. Gabrielson
Department of Pathology, The Johns Hopkins University School of Medicine, Baltimore, MD, USA
e-mail: mgabrie8@jhmi.edu

L. M. Rooper (✉)
Department of Pathology, The Johns Hopkins University School of Medicine, Baltimore, MD, USA

Department of Oncology, The Johns Hopkins University School of Medicine, Baltimore, MD, USA
e-mail: rooper@jhmi.edu

D. Jain, J. A. Bishop (eds.), *Atlas of Sinonasal Tract Pathology*, https://doi.org/10.1007/978-981-19-7315-4_13

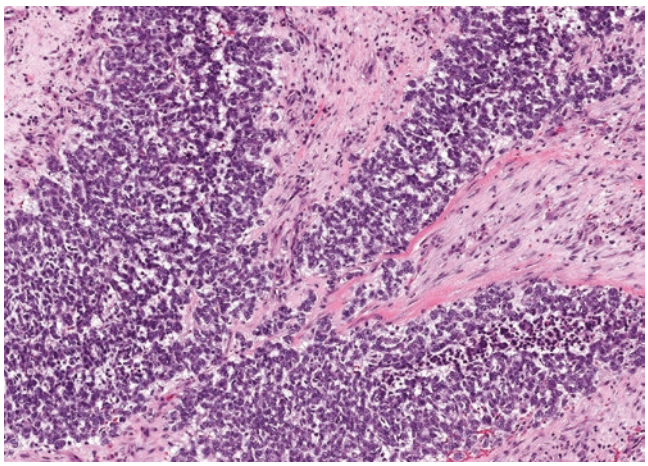

Fig. 13.2 A subset of Ewing sarcoma cases has more lobulated or nested architecture (20x)

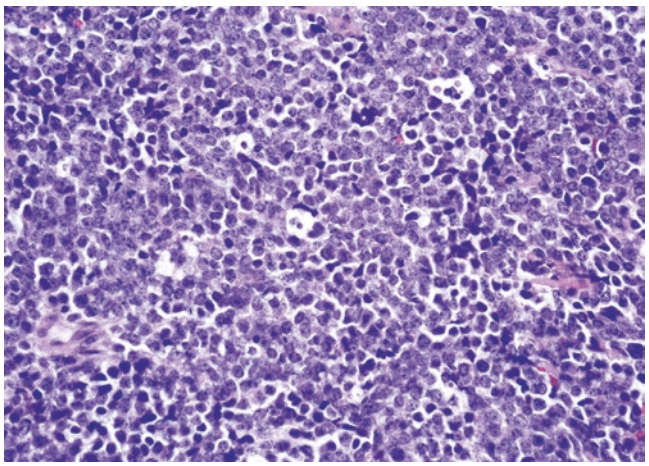

Fig. 13.5 Nuclei in Ewing sarcoma are usually round to oval with fine chromatin and small nucleoli (40x)

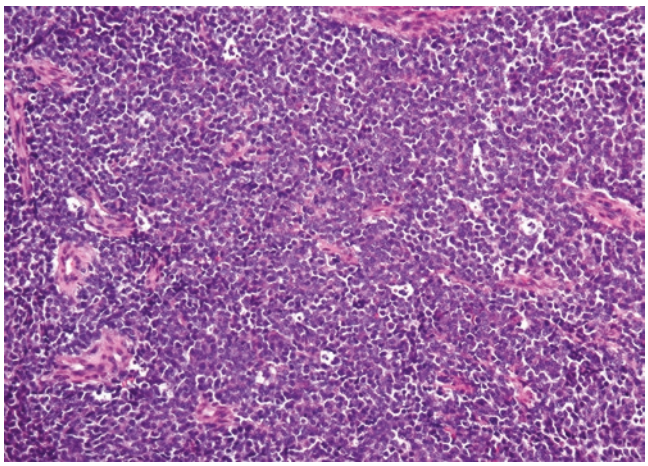

Fig. 13.3 Tumor cells in Ewing sarcoma have a syncytial appearance with indistinct cell borders (20x)

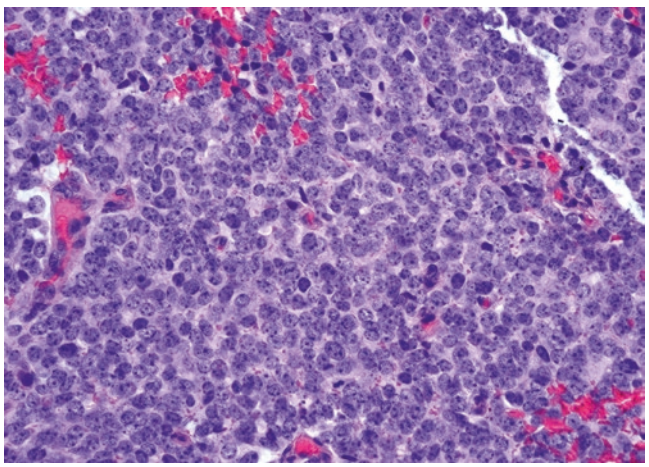

Fig. 13.6 Despite its nuclear monotony, Ewing sarcoma can show an elevated mitotic rate (40x)

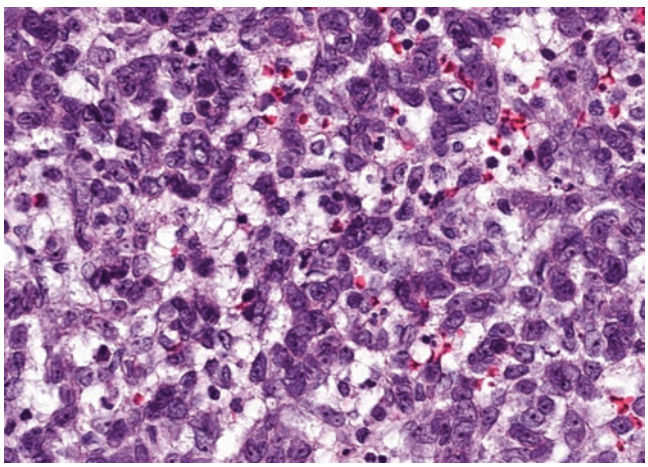

Fig. 13.4 Ewing sarcoma tumor cells demonstrate variable amounts of clear glycogenated cytoplasm (40x)

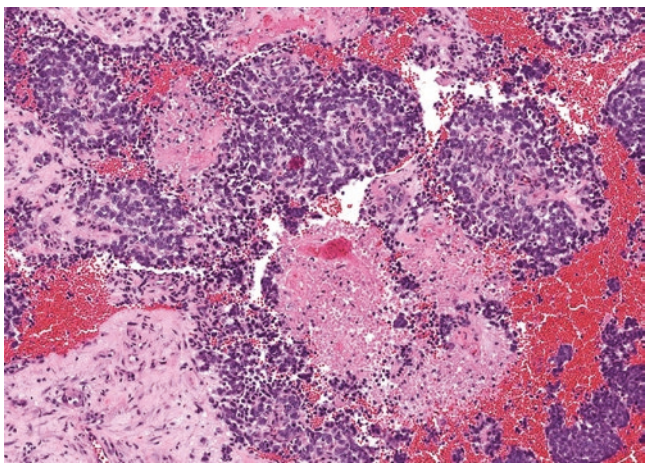

Fig. 13.7 Ewing sarcoma also frequently shows geographic zones of tumor necrosis (10x)

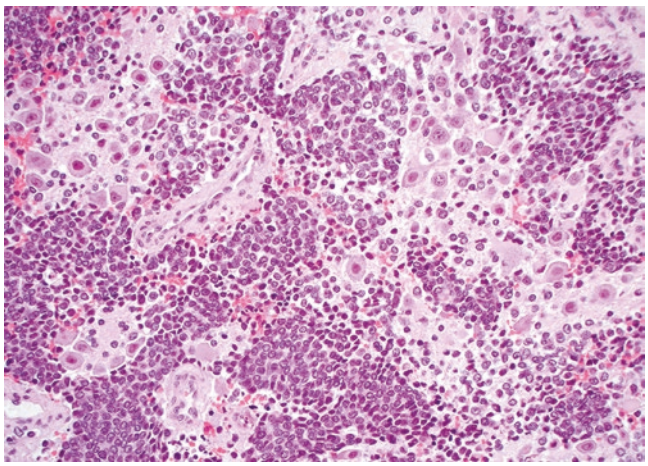

Fig. 13.8 Rare Ewing sarcoma cases demonstrate overt neural differentiation with neuropil and ganglion cell formation, generally after therapy [23–25] (20x)

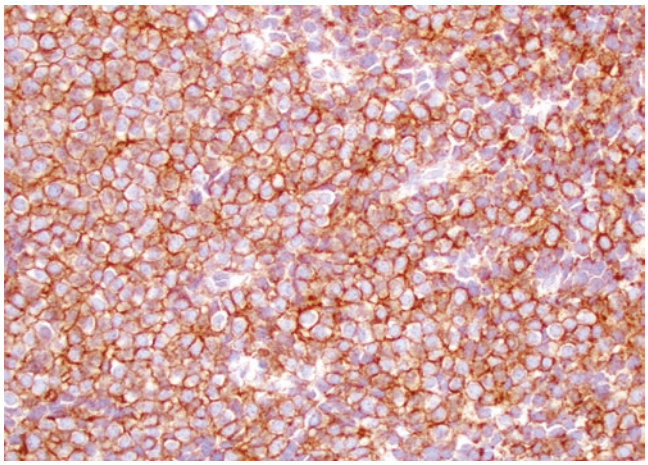

Fig. 13.9 Ewing sarcoma consistently displays membranous positivity for CD99 (40x)

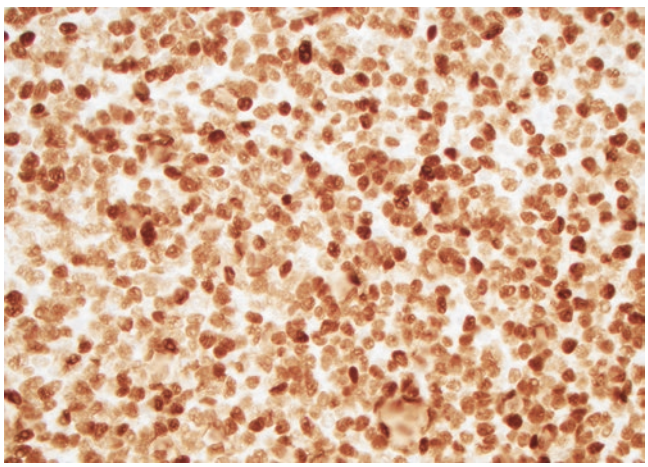

Fig. 13.10 Ewing sarcoma also is positive for transcription factor NKX2.2 (40x)

13.3 Adamantinoma-Like Ewing Sarcoma

Adamantinoma-like Ewing sarcoma (ALES) is a rare variant of Ewing sarcoma that is defined by overt squamous differentiation, including occasional formation of keratin pearls and diffuse immunohistochemical positivity for AE1/AE3 as well as p63 and p40 [26, 27]. Nevertheless, it still harbors the *EWSR1::FLI1* fusion characteristic of Ewing sarcoma and consistently expresses CD99 and NKX2.2 [28]. While there is some controversy as to whether tumors with these features truly are a variant of Ewing sarcoma or instead represent a carcinoma with *EWSR1::FLI1* fusion, they currently are classified under the Ewing sarcoma umbrella and are unquestionably a distinctive entity regardless of terminology [13, 28–30]. ALES was originally reported in the extremities but has since predominantly been recognized in head and neck sites, including the salivary glands, thyroid gland, and sinonasal tract [31–39]. Patients with ALES tend to be slightly older than those with conventional Ewing sarcoma [28]. Although this variant is extremely rare and follow-up data is limited, the majority of cases reported to date have had good outcomes [28]]. The pathologic findings in ALES are depicted below. (Figs. 13.11, 13.12, 13.13, 13.14, 13.15, 13.16, 13.17, and 13.18).

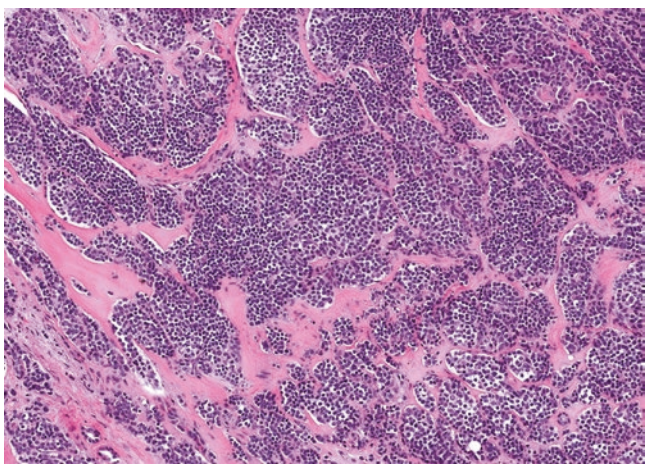

Fig. 13.11 ALES is composed of highly infiltrative nests of basaloid cells (10x)

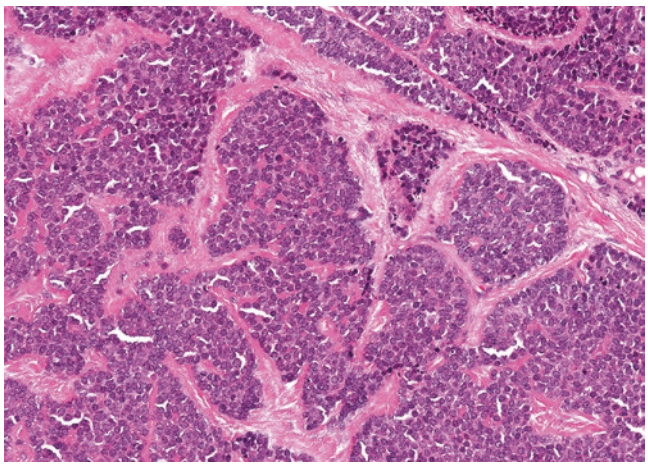

Fig. 13.12 Occasional peripheral palisading and rosette formation can be seen in ALES (20x)

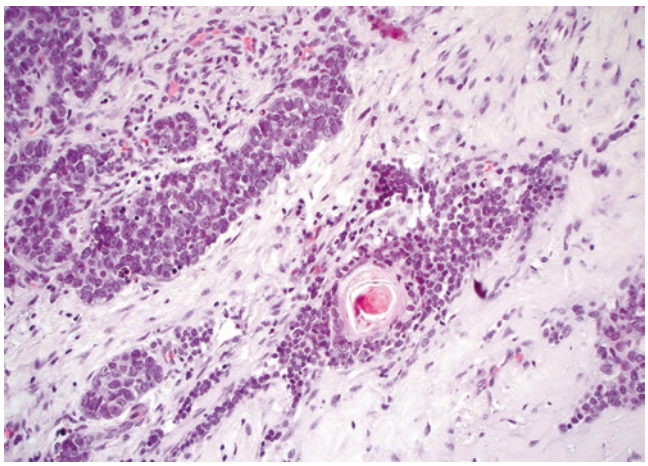

Fig. 13.13 While not seen in every case, a subset of ALES demonstrate compact keratin pearl formation (40x)

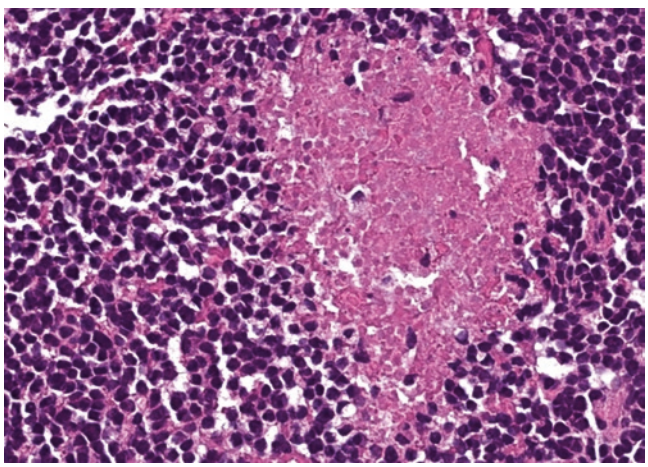

Fig. 13.14 Similar to conventional Ewing sarcoma, the tumor cells in ALES are monotonous despite necrosis or mitotic figures (40x)

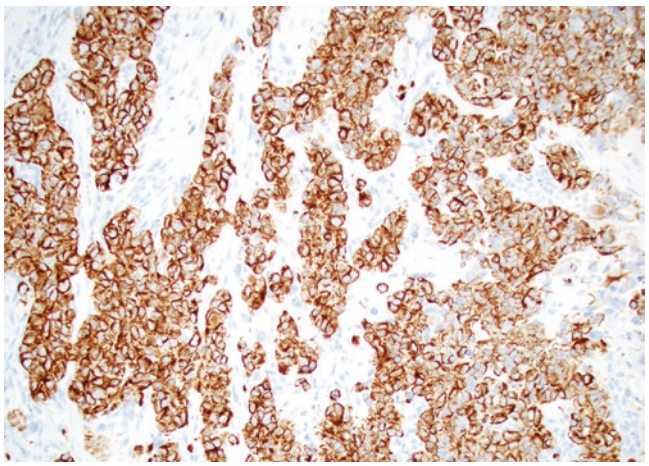

Fig. 13.15 ALES are diffusely positive for AE1/AE3 (20x)

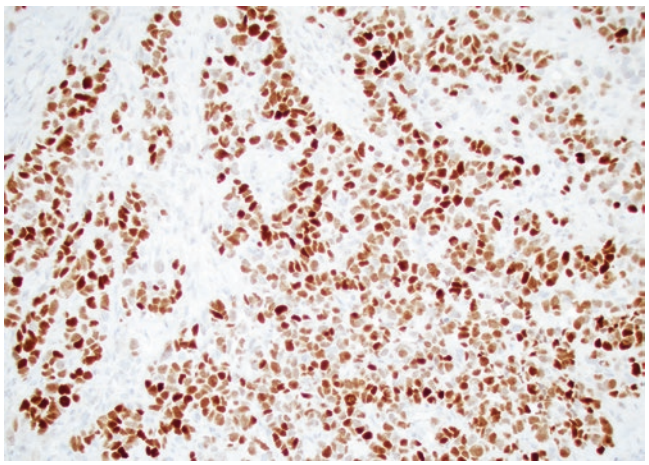

Fig. 13.16 ALES also consistently express squamous markers such as p40 (20x)

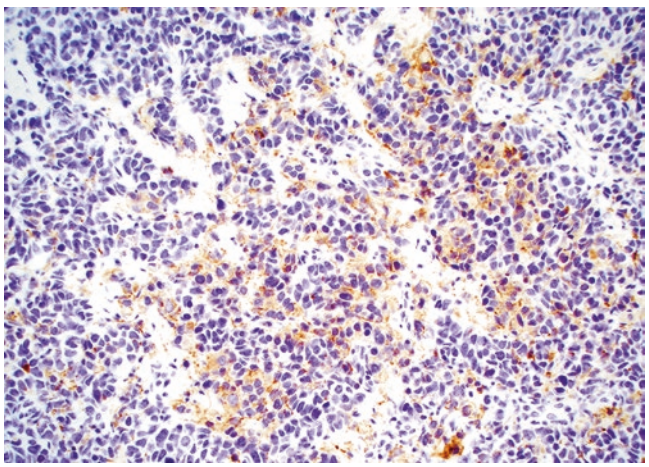

Fig. 13.17 A subset of ALES can also show synaptophysin expression, which should trigger consideration of this diagnosis when seen in combination with p40 (20x)

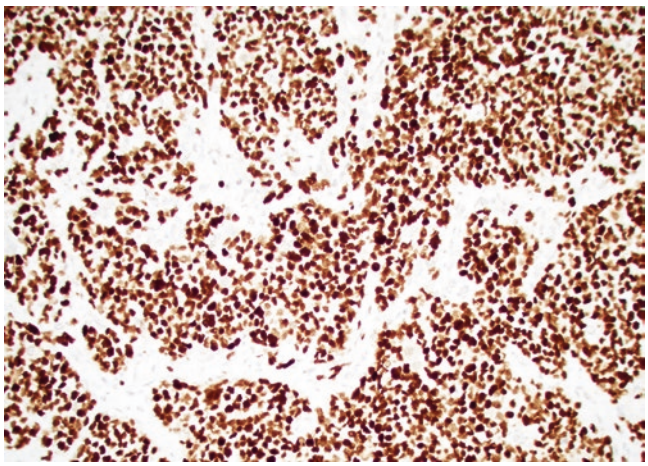

Fig. 13.18 As with other Ewing sarcomas, ALES are positive for NKX2.2 (20x)

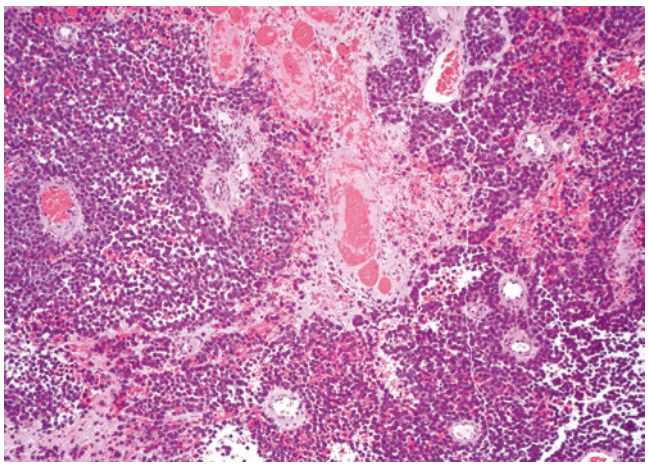

Fig. 13.19 Mucosal melanoma commonly grows in diffuse sheets (10x)

13.4 Mucosal Melanoma

Malignant mucosal melanomas arising in the sinonasal tract are rare, encompassing less than 1% of melanomas overall and just 4% of sinonasal malignancies [40–42]. However, sinonasal melanomas do represent a significant proportion of non-cutaneous melanomas, with approximately 80% of mucosal melanomas occurring in head and neck sites [40]. They most frequently occur in elderly patients in the seventh or eighth decade and are extremely rare before age 30 [41, 43]. Although they are sometimes associated with mucosal melanosis, there are no known environmental or occupational risk factors [44–46]. Similar to its cutaneous counterpart, mucosal melanoma is defined by melanocytic differentiation, with consistent expression of melanocytic markers S100, SOX10, HMB-45, Melan A, and MITF, and occasional endogenous melanin pigment production. Mucosal melanomas are driven by different genetic pathways than cutaneous melanomas, with frequent *KIT* mutations, no ultraviolet-light mutational signatures, and only rare involvement of *BRAF* and *NRAS* [47–50]. They are highly aggressive tumors that carry a poor prognosis, with outcomes dependent on tumor size and stage [43, 44]. Major prognostic indicators such as Breslow thickness used in cutaneous melanoma are not applicable in this site. Due to their protean morphology, mucosal melanomas can overlap with a wide range of sinonasal tumors and should be considered in the differential diagnosis of virtually all sinonasal small round blue cell tumors. The histologic findings in sinonasal mucosal melanomas are described below (Figs. 13.19, 13.20, 13.21, 13.22, 13.23, 13.24, 13.25, 13.26, 13.27, 13.28, 13.29, and 13.30).

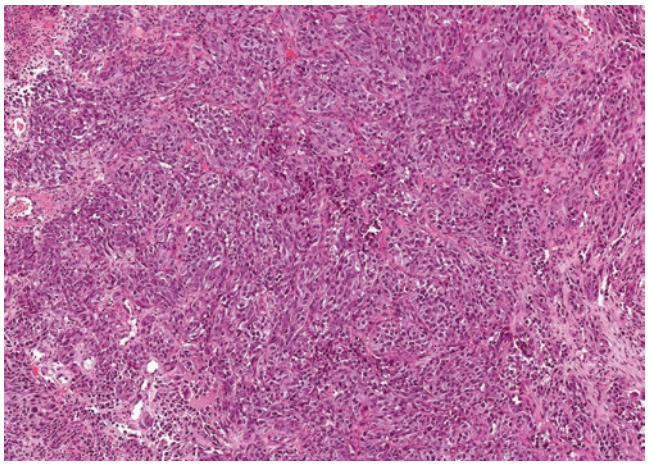

Fig. 13.20 Other cases of mucosal melanoma show a more nested pattern (10x)

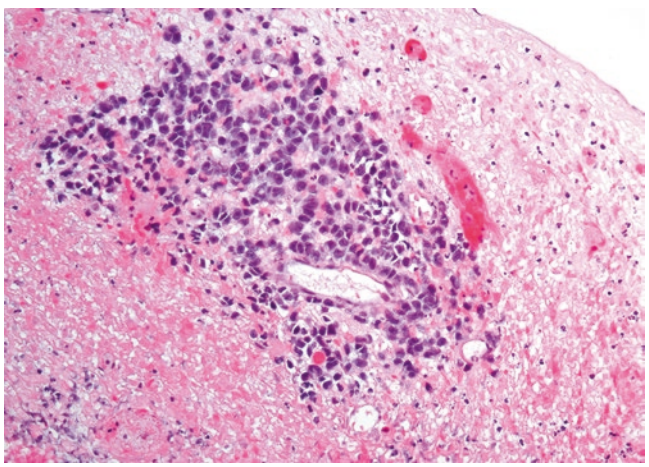

Fig. 13.21 Peritheliomatous growth in a background of extensive necrosis is particularly characteristic of mucosal melanoma (20x)

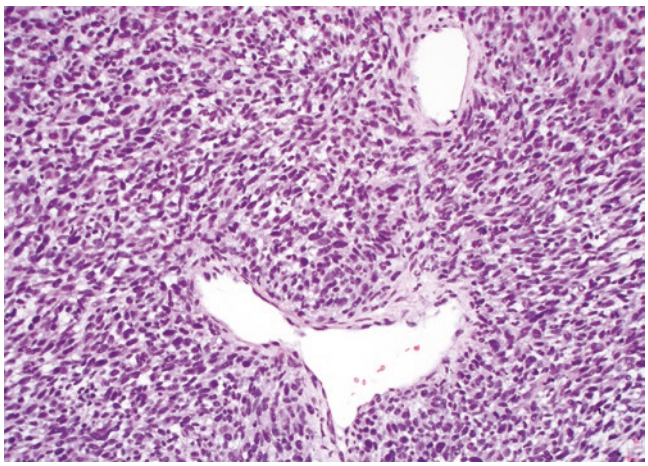

Fig. 13.22 Mucosal melanoma can show a variably epithelioid and spindled histologic appearance (20x)

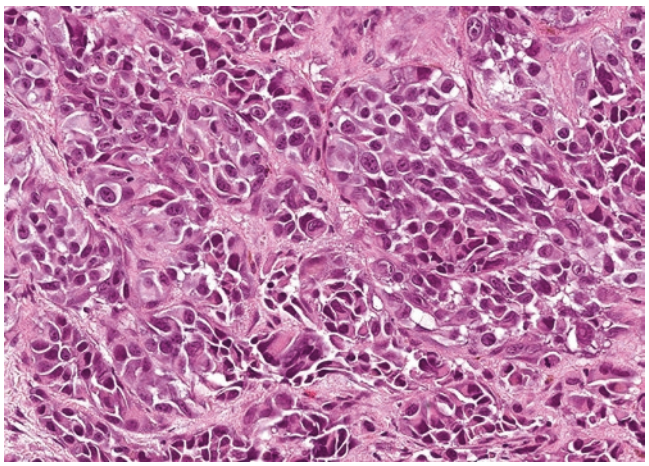

Fig. 13.25 Mucosal melanomas display variable amounts of cytoplasmic pigmentation (40x)

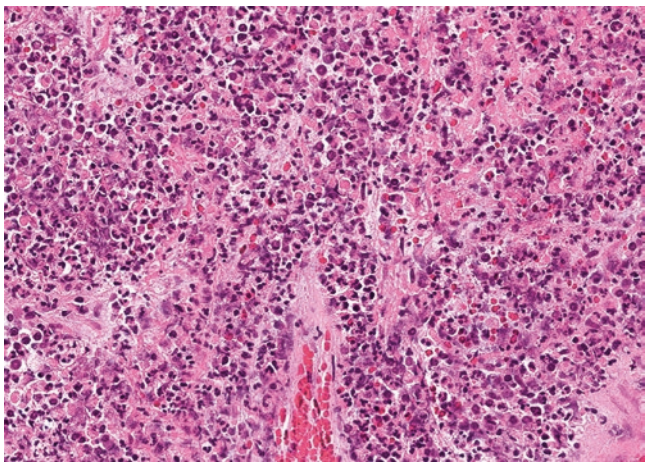

Fig. 13.23 A subset of mucosal melanomas are strikingly plasmacytoid or rhabdoid with eccentric eosinophilic cytoplasm (20x)

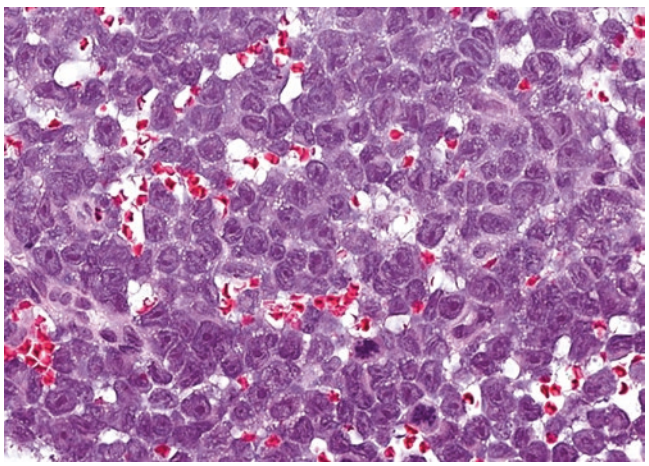

Fig. 13.26 Mucosal melanomas frequently have vesicular chromatin with prominent cherry-red nucleoli (40x)

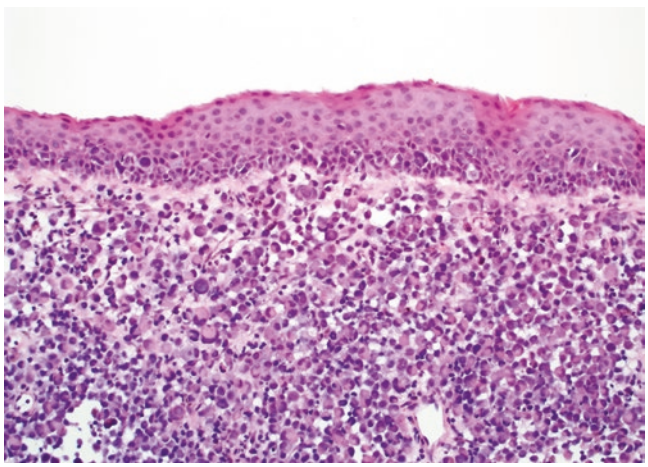

Fig. 13.24 The presence of pagetoid spread in the overlying epithelium can help suggest the diagnosis of mucosal melanoma (20x)

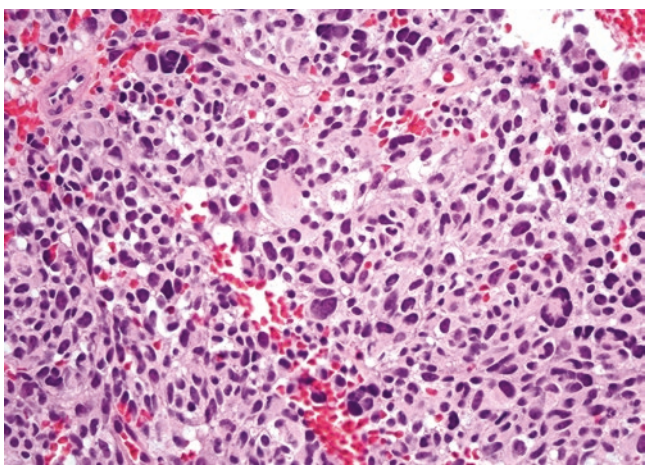

Fig. 13.27 Multinucleation with floret-like cells can occasionally be seen in mucosal melanoma (20x)

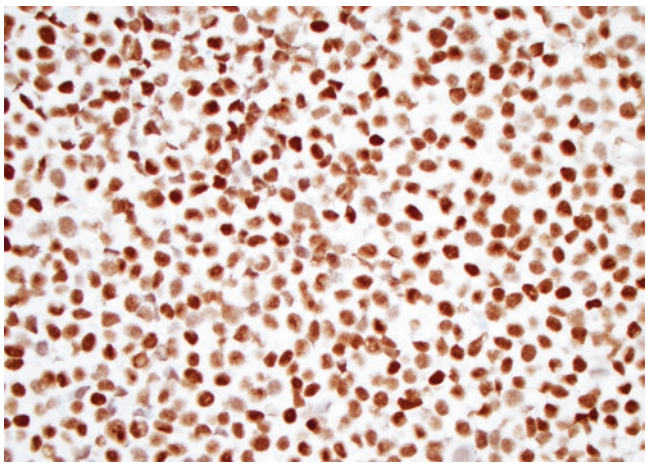

Fig. 13.28 Mucosal melanomas are consistently positive for SOX10 (40x)

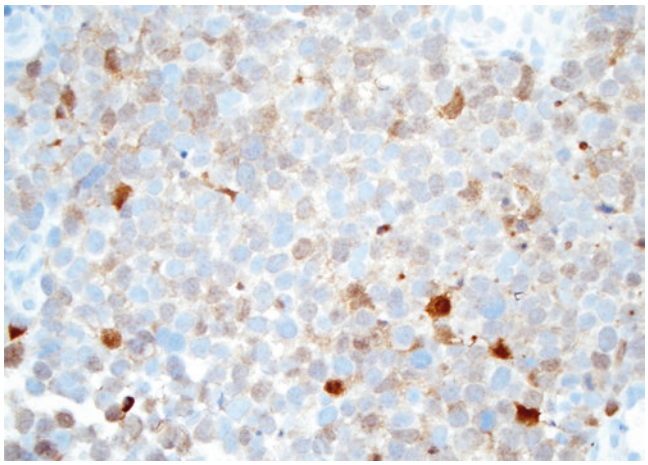

Fig. 13.29 Although S100 is positive in most mucosal melanomas, it can be focal and is less consistently expressed in this site than in cutaneous cases [51] (40x)

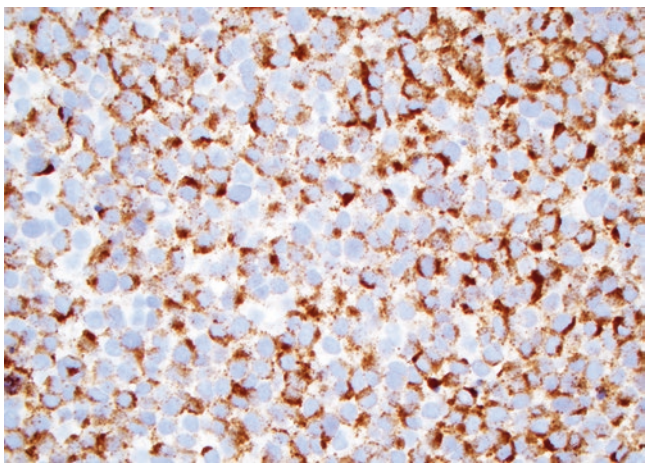

Fig. 13.30 Most mucosal melanomas show cytoplasmic expression of HMB45 (40x)

13.5 Olfactory neuroblastoma

Olfactory neuroblastoma (ONB) is a rare sinonasal tumor that is thought to arise from the specialized olfactory sensory neuroepithelium. It can occur across a wide range of ages, with a peak in the fifth and sixth decade of life [52–54]. ONB virtually always involves the cribriform plate and has characteristic imaging findings of a dumbbell-shaped mass extending intracranially from the superior nasal cavity [55, 56]. ONB displays well-developed immunohistochemical evidence of neuroendocrine differentiation including diffuse strong positivity for specific neuroendocrine markers synaptophysin, chromogranin, and INSM1, with a characteristic network of S100-positive sustentacular cells; only focal cytokeratin expression is allowable [55–57]. Calretinin is also a relatively specific marker of ONB in the sinonasal tract [58]. Although no tumor-defining molecular alterations have been identified to date in ONB, a variety of somatic mutations have been reported in smaller groups of cases [59–62]. Survival is largely dependent on tumor stage at presentation, which is most frequently determined using the Kadish-Morita system [63, 64]. Histologic grade, as assessed using the Hyams system, can also accurately predict prognosis [65–69]. ONB overlaps with a wide range of sinonasal small round blue cell tumors, and comprehensive immunohistochemical workup is recommended for specific classification. The pathologic appearance of ONB is discussed in detail below (Figs. 13.31, 13.32, 13.33, 13.34, 13.35, 13.36, 13.37, 13.38, 13.39, 13.40, 13.41, 13.42, and 13.43).

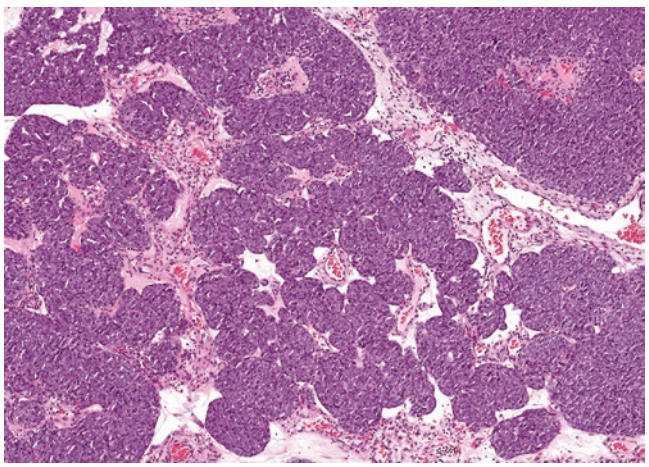

Fig. 13.31 ONB generally demonstrates nested to lobulated architecture with prominent vascular stroma (10x)

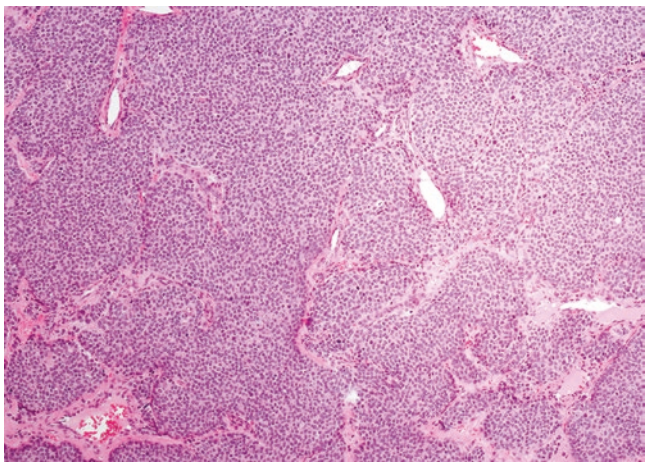

Fig. 13.32 Some cases of ONB display more solid growth (10x)

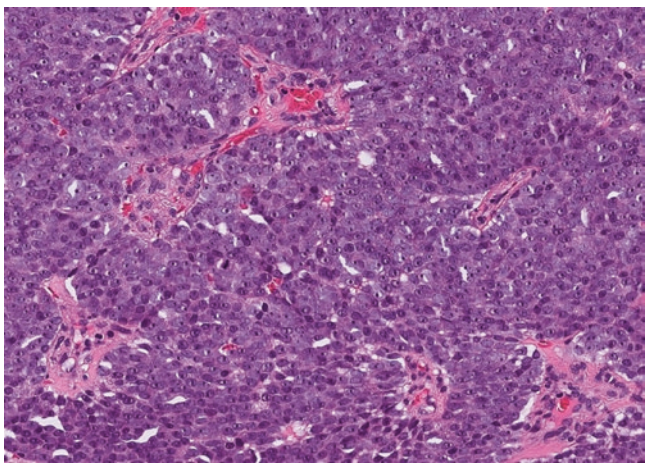

Fig. 13.33 ONB is composed of syncytial small round cells with indistinct cytoplasmic membranes (20x)

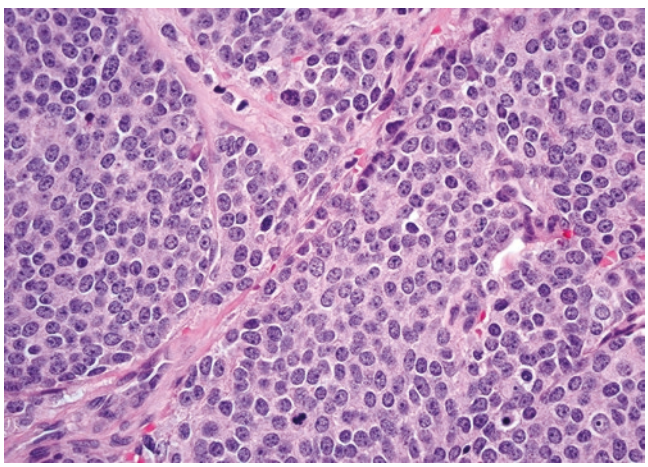

Fig. 13.34 Nuclei are round to oval and display characteristic speckled "salt and pepper" chromatin (40x)

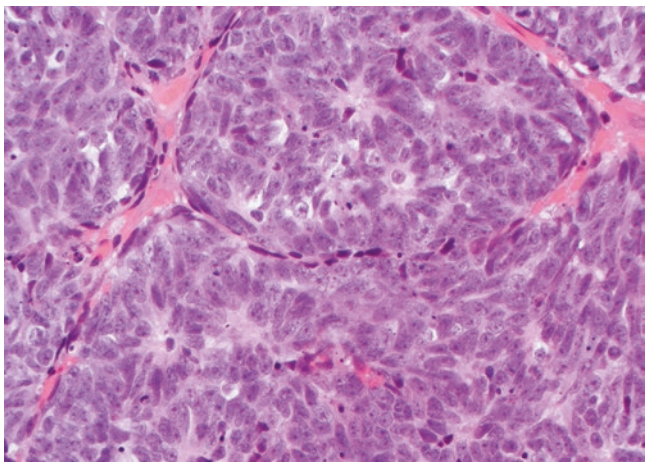

Fig. 13.35 Both Homer Wright pseudorosettes and Flexner–Wintersteiner true rosettes can be seen in ONB (40x)

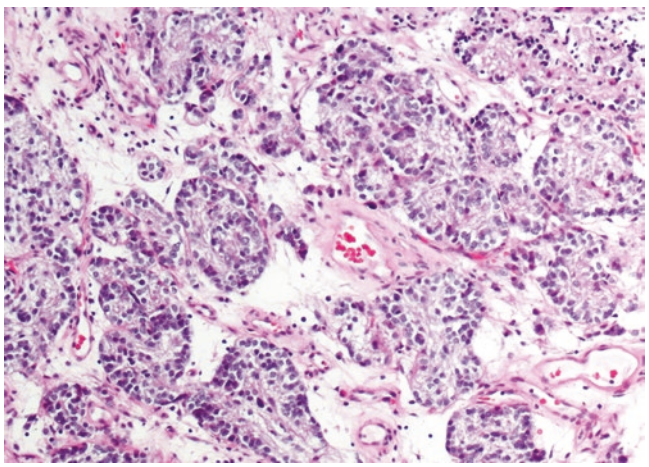

Fig. 13.36 Grade 1 ONB is defined by nested growth, abundant neurofibrillary stroma, and monotonous cytology (20x)

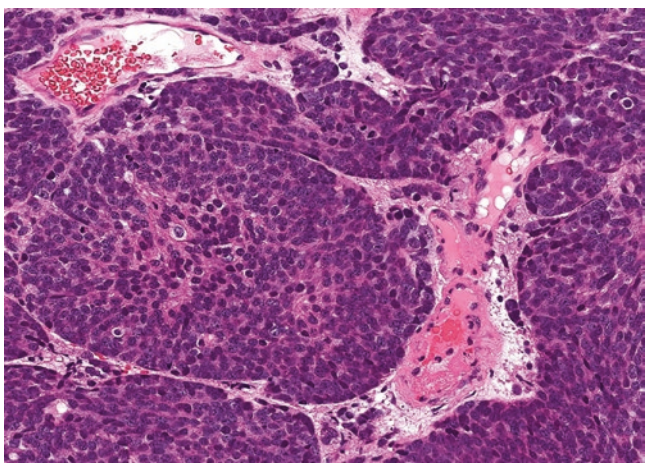

Fig. 13.37 Grade 2 ONB has less neurofibrillary stroma and can show increased cellularity and scattered mitotic figures (20x)

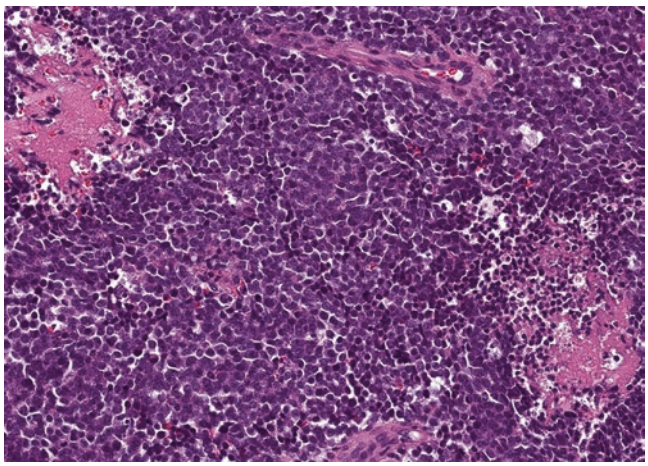

Fig. 13.38 Grade 3 ONB demonstrates an elevated mitotic rate, zones of necrosis, and increased nuclear atypia (20x)

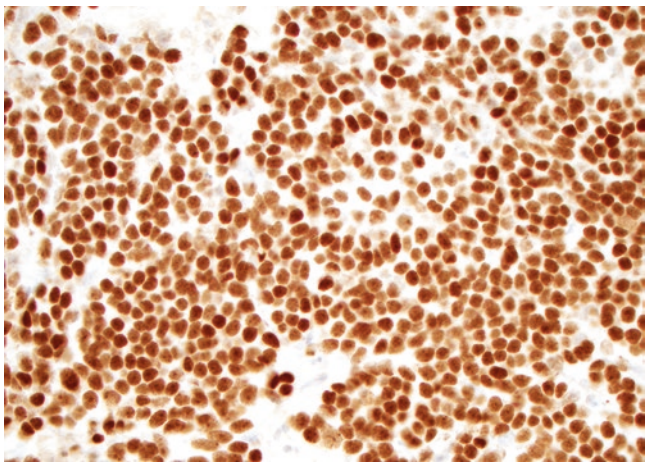

Fig. 13.41 ONB is also consistently positive for the emerging neuroendocrine transcription factor INSM1 [57] (40x)

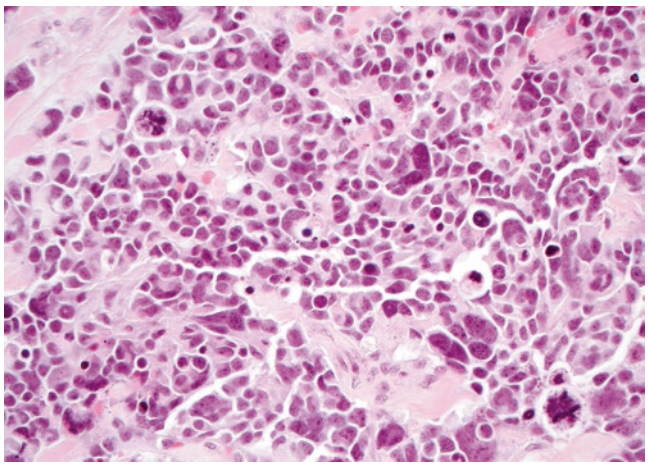

Fig. 13.39 Grade 4 ONB displays overt nuclear pleomorphism and prominent necrosis and mitosis; because of overlap with other sinonasal tumors, high grade ONB should be diagnosed only after comprehensive immunohistochemical evaluation (20x)

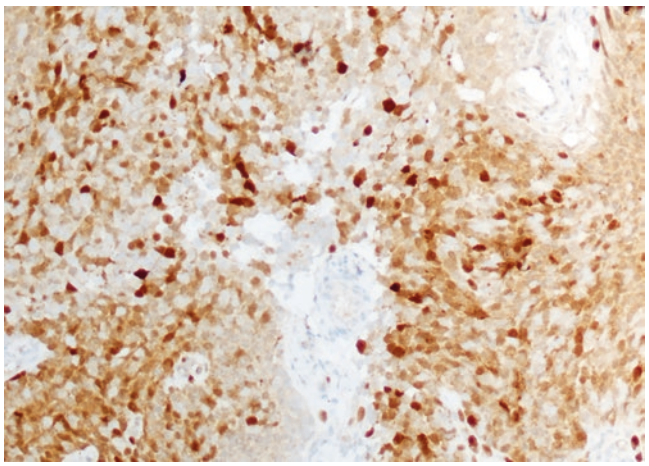

Fig. 13.42 Calretinin is a relatively specific marker of ONB in the sinonasal tract [58] (40x)

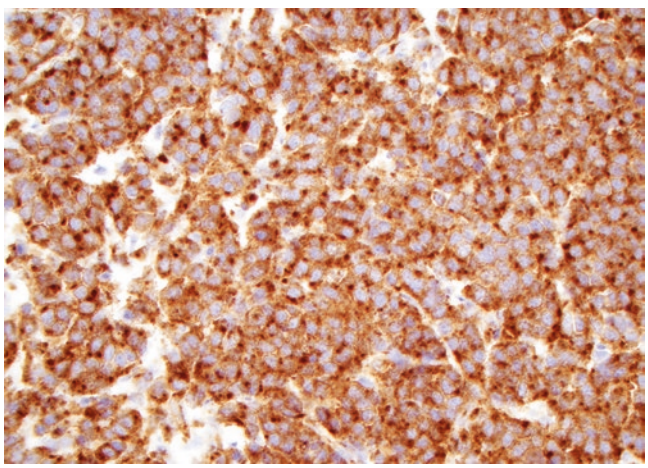

Fig. 13.40 ONB demonstrates diffuse strong positivity with markers of neuroendocrine differentiation including synaptophysin (40x)

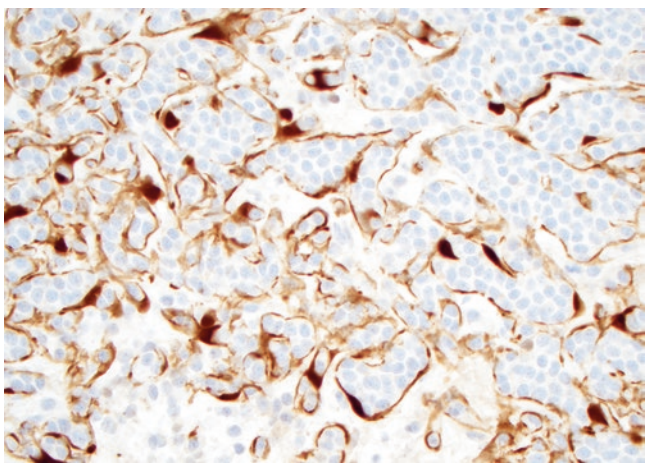

Fig. 13.43 ONB classically shows a sustentacular pattern of staining with S100 (40x)

13.6 Olfactory Carcinoma

Olfactory carcinoma is an emerging sinonasal tumor that shows some histologic and immunohistochemical similarities to ONB but demonstrates well-developed epithelial differentiation including diffuse cytokeratin positivity and gland formation that blurs the line between ONB and sinonasal carcinoma [70–72]. This tumor type has also been reported under several other names including olfactory neuroblastoma with divergent epithelial differentiation, mixed olfactory neuroblastoma and carcinoma, olfactory neuroepithelioma, and mixed lineage olfactory neuroblastoma, but is increasingly thought to be a distinctive entity [70, 72–78]. Histologically, olfactory carcinomas should have a closer histologic resemblance to ONB than neuroendocrine carcinoma with nested growth and neurofibrillary stroma, and frequently also overlap with sinonasal adenocarcinoma with intermixed glands that even show cilia formation [71, 72, 79, 80]. They also show more cytokeratin expression than is allowable in ONB with decreased expression of neuroendocrine markers [71, 72, 79]. Although the clinical features and outcomes have not been well-characterized, in limited experience, these tumors tend to occur at the superior aspect of the nasal cavity and behave in an aggressive fashion [69, 70, 72–79, 81]. The histologic and immunohistochemical profile of olfactory carcinoma is further detailed below (Figs. 13.44, 13.45, 13.46, 13.47, 13.48, 13.49, 13.50 and 13.51).

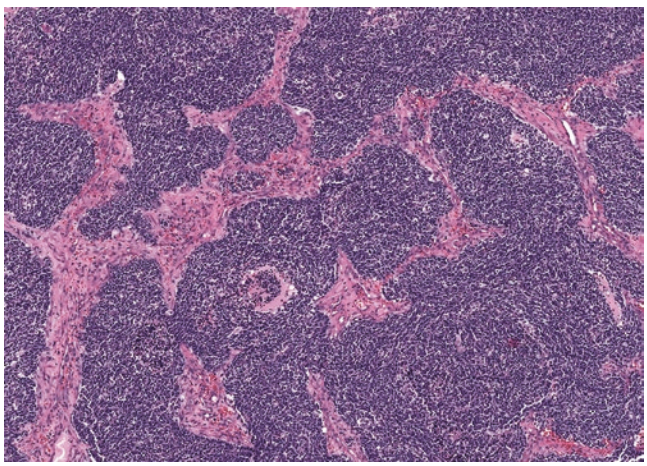

Fig. 13.44 Olfactory carcinoma often demonstrates nested architecture and prominent vascular stroma similar to ONB (10x)

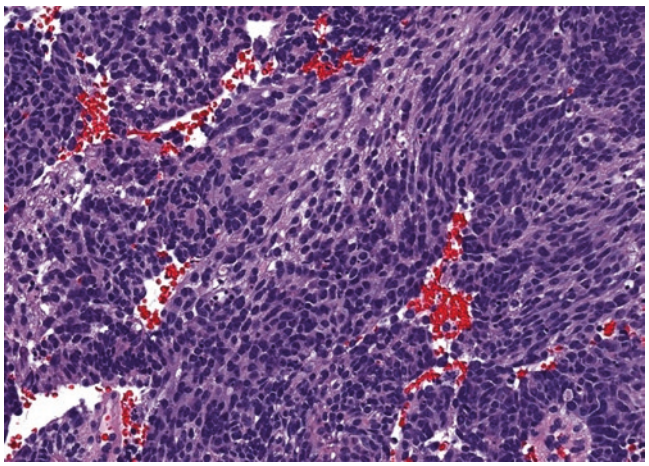

Fig. 13.45 Olfactory carcinoma is predominantly composed of neuroepithelial cells with hyperchromatic nuclei and scant neurofibrillary stroma (20x)

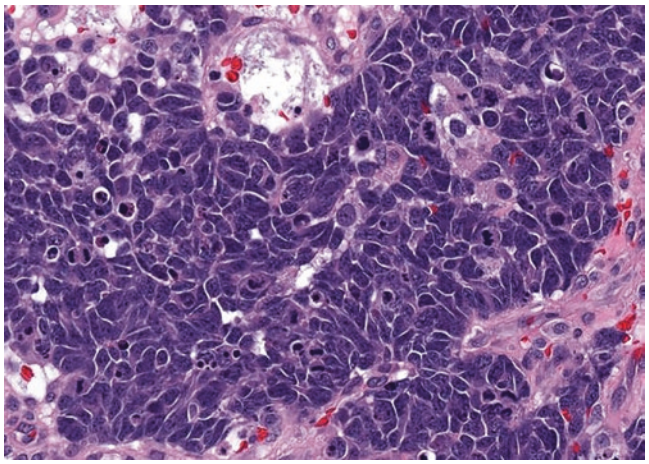

Fig. 13.46 These nuclei demonstrate increased atypia with nuclear wrapping, vesicular chromatin, numerous apoptotic bodies, and numerous mitotic figures and necrosis (40x)

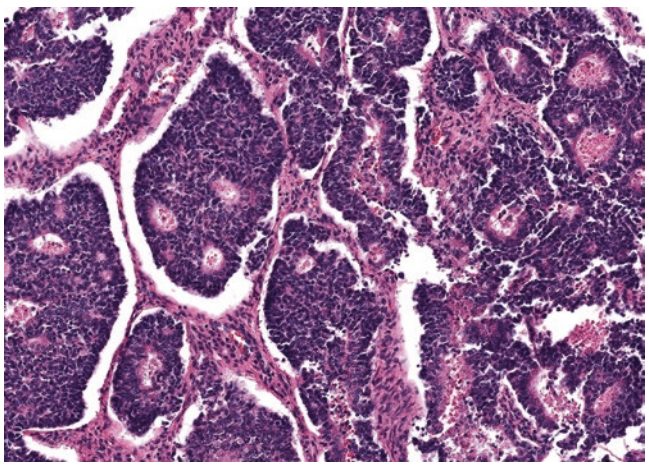

Fig. 13.47 Most olfactory carcinoma demonstrate a prominent glandular component that is intermixed with the neuroepithelial component (10x)

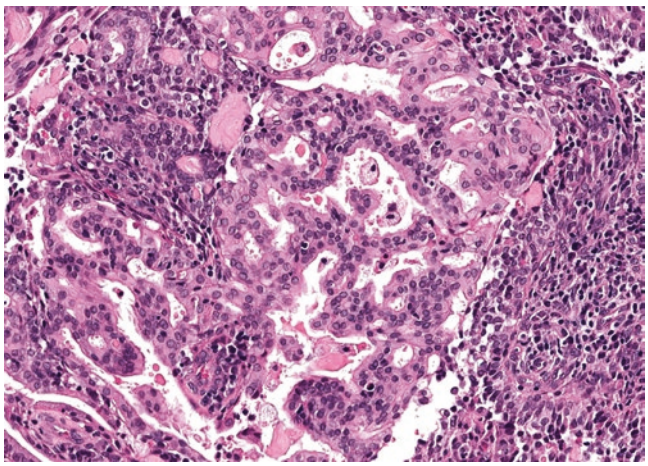

Fig. 13.48 The glandular component is frequently composed of large cells with eosinophilic cytoplasm, occasional mucin production, and more uniform oval nuclei (20x)

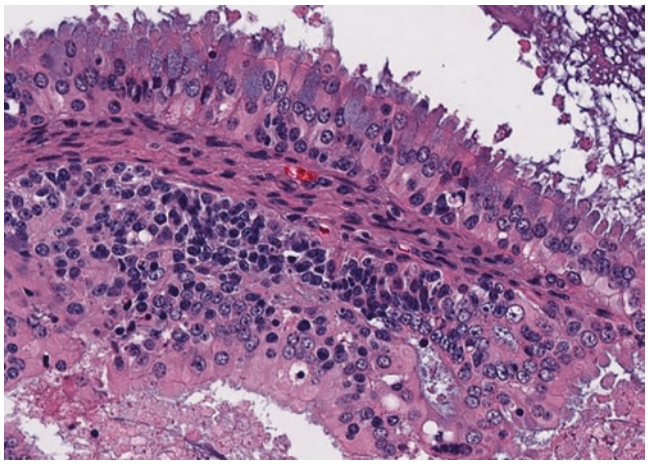

Fig. 13.49 Many olfactory carcinomas demonstrate cilia on the glandular component (40x)

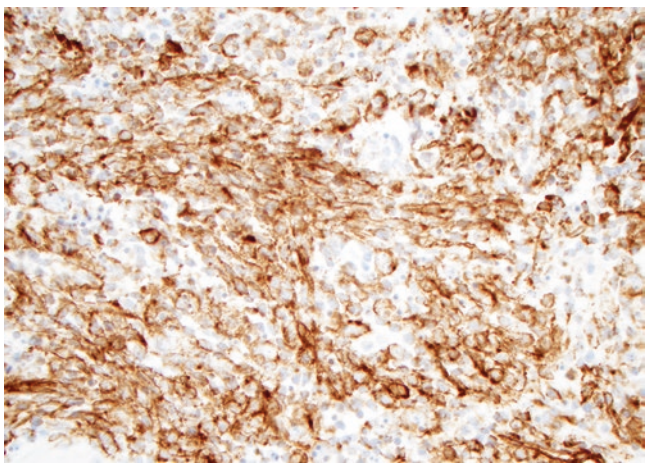

Fig. 13.50 Olfactory carcinoma displays diffuse keratin positivity, which should not be seen in ONB (40x)

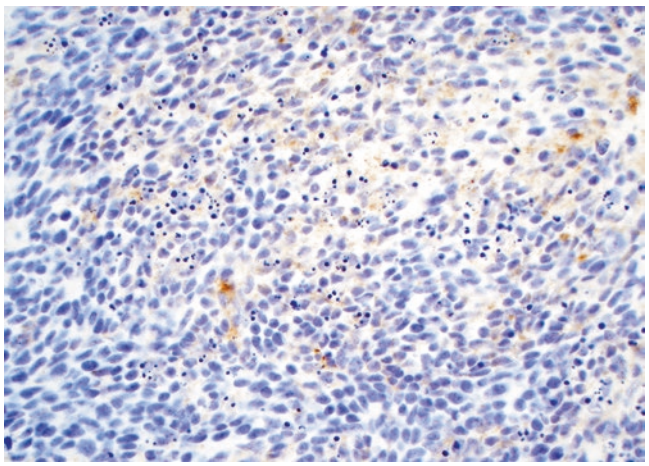

Fig. 13.51 Although olfactory carcinoma is positive for neuroendocrine markers like synaptophysin, the staining is not as strong as in ONB (40x)

13.7 Teratocarcinosarcoma

Sinonasal teratocarcinosarcoma (TCS) is a rare and distinctive sinonasal malignancy defined by intermixed epithelial, mesenchymal, and primitive neuroepithelial elements [82]. These components can vary widely in composition and cytologic atypia, with epithelial components including squamous or glandular elements often with a fetal-like clear cell appearance, mesenchymal components including spindle cell proliferations with occasional heterologous differentiation, and neuroepithelial components including primitive epithelioid cells with neurofibrillary background. Immunohistochemical findings correlate with the differentiation of each component. TCS occur in the superior aspect of the nasal cavity and are most common in adults in their fourth or fifth decade, with 80% of tumors occurring in males [83–85]. Although TCS are aggressive tumors that frequently present at high stage, they have shown improved outcomes in recent years with multimodality therapy [83, 86]. Recently, recurrent *SMARCA4* inactivation and activating *CTNNB1* mutations have been identified in TCS—findings that suggest they may be related to SMARCA4-deficient sinonasal carcinomas or other high grade sinonasal carcinomas with neuroendocrine differentiation [87–91]. Because the various components of TCS overlap with a wide range of sinonasal neoplasms, corresponding loss of SMARCA4/BRG1 expression and nuclear b-catenin accumulation can help suggest the diagnosis in cases where multilineage differentiation is not apparent histologically [90–92]. The morphologic profile of TCS is depicted below (Figs. 13.52, 13.53, 13.54, 13.55, 13.56, 13.57, 13.58, 13.59, 13.60, 13.61, and 13.62).

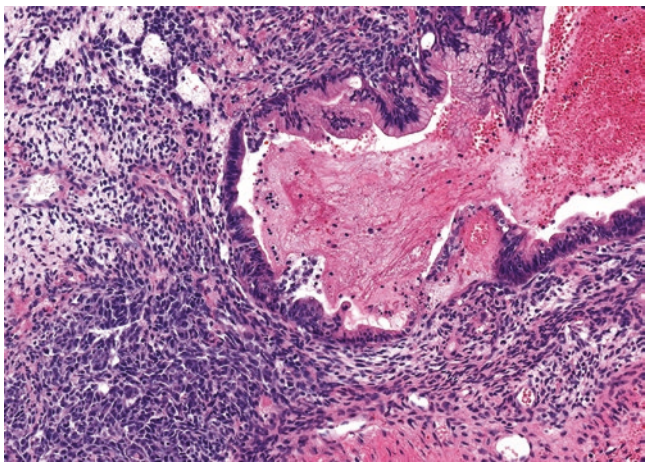

Fig. 13.52 Sinonasal TCS demonstrate a mix of epithelial, mesenchymal, and primitive neuroepithelial elements with varying degrees of cytologic atypia (10x)

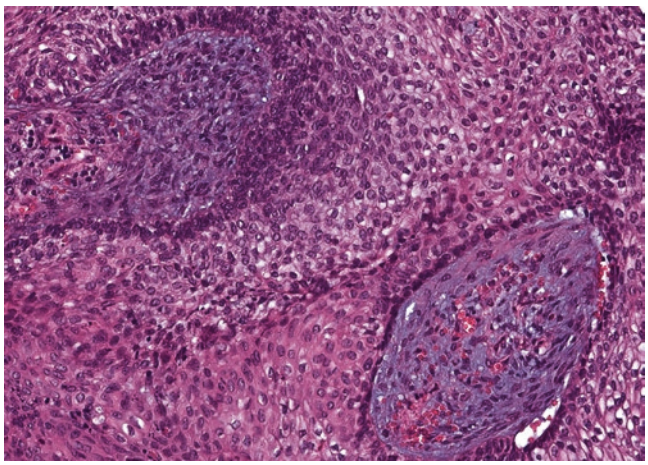

Fig. 13.53 Squamous elements in TCS can be keratinizing or non-keratinizing and frequently have a fetal-like clear cell appearance (20x)

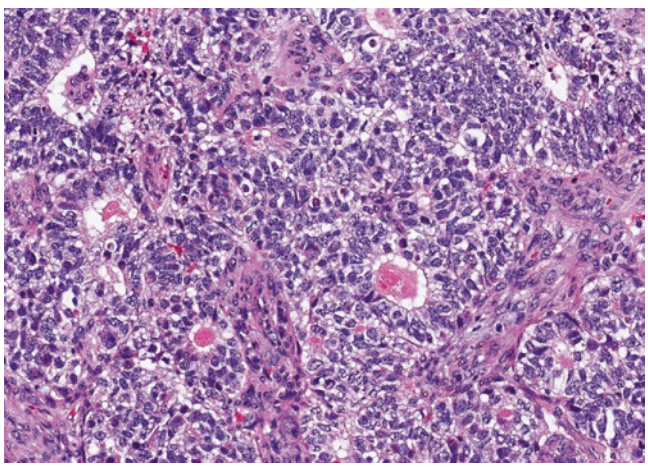

Fig. 13.54 Glandular elements can also demonstrate a prominent fetal-like clear cell appearance (20x)

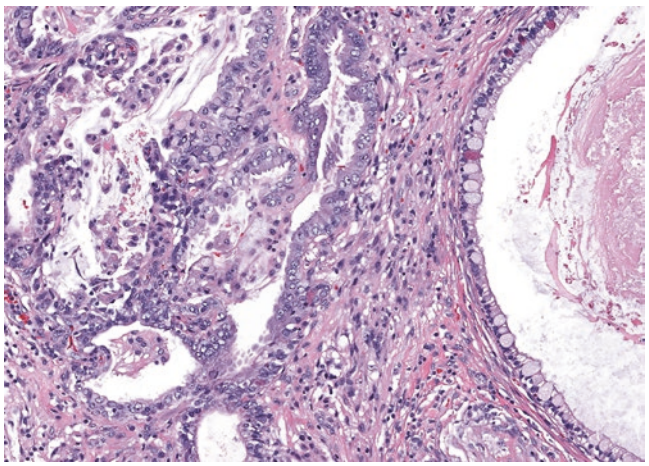

Fig. 13.55 Glandular elements in TCS can demonstrate prominent mucin production (20x)

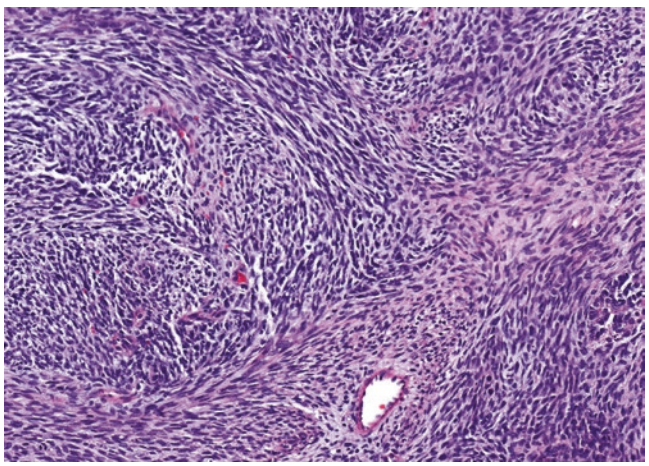

Fig. 13.56 The mesenchymal component of TCS most commonly consists of hypercellular fascicles of nondescript spindled cells (20x)

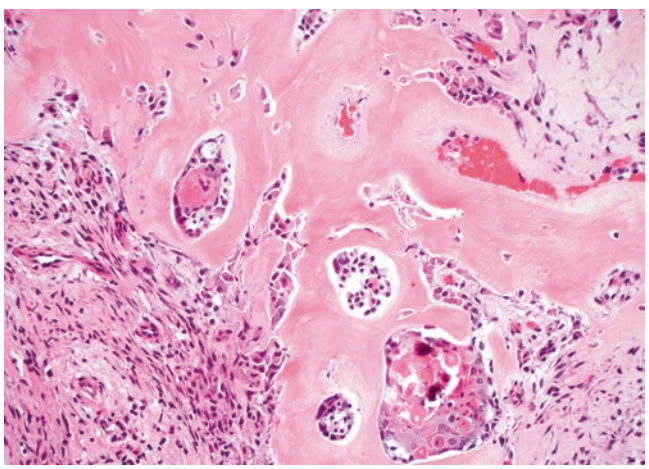

Fig. 13.57 Occasional heterologous differentiation such as osteoid formation can be seen in TCS (20x)

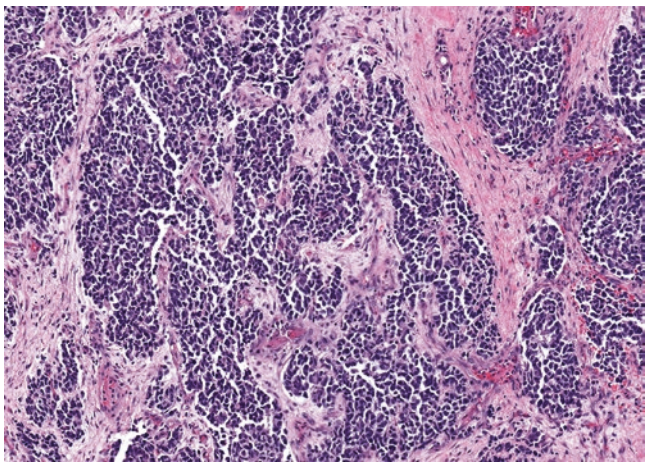

Fig. 13.58 The neuroepithelial component of TCS is usually composed of nests of primitive cells with hyperchromatic nuclei and scant cytoplasm (10x)

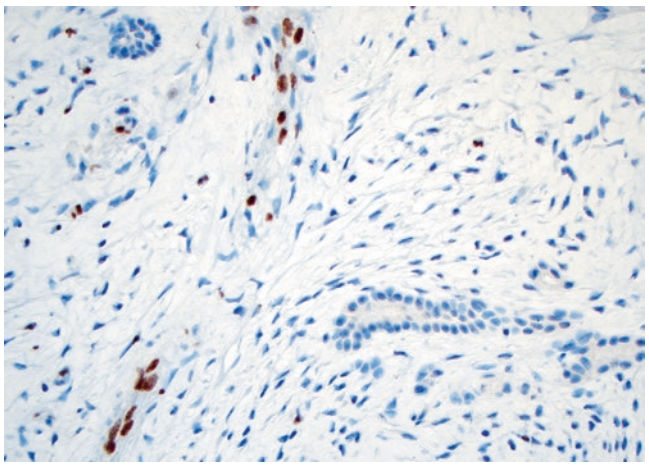

Fig. 13.61 Approximately 70% of TCS show total loss of nuclear SMARCA4 expression with retained expression in normal background blood vessels (40x)

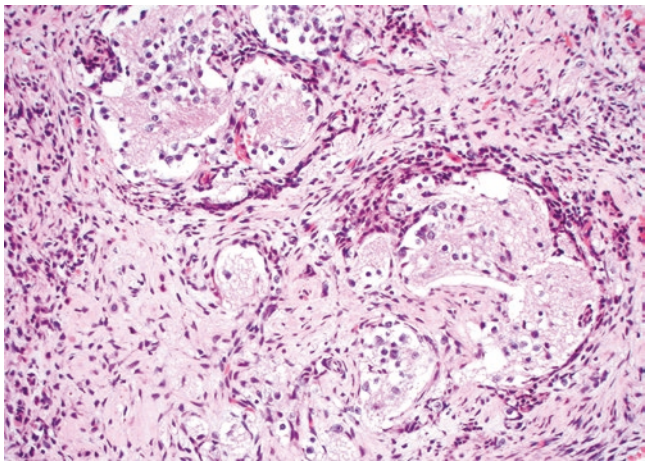

Fig. 13.59 Rare areas with mature ganglion cells and abundant neurofibrillary matrix material also can be seen in TCS (20x)

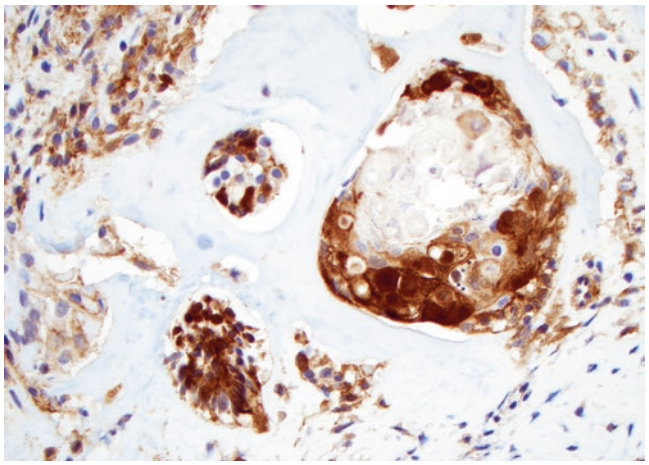

Fig. 13.62 A subset of TCS also demonstrate nuclear b-catenin positivity (40x)

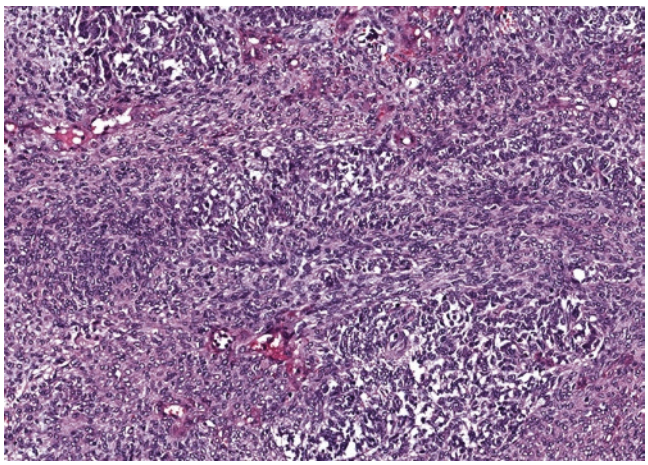

Fig. 13.60 The epithelial, stromal, and neuroepithelial components of TCS can occasionally merge together and be difficult to distinguish (20x)

13.8 Conclusion

Overall, the category of sinonasal tumors with neuroectodermal or melanocytic differentiation includes a diverse group of rare entities, many of which show entirely distinct origins and pathogenesis that belie the heterogeneous nature of this classification. Indeed, the molecular underpinnings and histological and immunohistochemical features of several of these entities have only become clear in recent years and may further shift the classification of these tumors in the future. Nevertheless, because these tumor types can show substantial morphologic and immunophenotypic overlap, careful consideration of all of these entities is necessary for successful diagnosis of high grade sinonasal malignancies.

References

1. Wenig BM, Dulguerov P, Kapadia SB, Prasad ML, Fanburg-Smith JC, Thompson LD. Neuroectodermal tumours. In: Barnes L, Eveson JW, Reichart P, Sidransky D, International Agency for Research on Cancer, editors. Pathology and genetics of head and neck tumours. World Health Organization classification of tumours. Lyon: IARC; 2005. 430 p.
2. Wenig BM, Flucke U, Thompson LDR. Ewing sarcoma/primitive neuroectodermal tumor. In: El-Naggar A, Chan JK, Grandis JR, Takata T, Slootweg PJ, editors. WHO classification of head and neck tumors. Lyon: International Agency for Research on Cancer; 2017. p. 56–7.
3. Bell D, Franchi A, Gillison M, Thompson LDR, Wenig BM. Olfactory neuroblastoma. In: El-Naggar A, Chan JK, Grandis JR, Takata T, Slootweg PJ, editors. WHO classification of head and neck tumors. Lyon: International Agency for Research on Cancer; 2017. p. 57–9.
4. Williams MD, Speight P, Wenig BM. Mucosal Melanoma. In: El-Naggar A, Chan JK, Grandis JR, Takata T, Slootweg PJ, editors. WHO classification of head and neck tumors. Lyon: International Agency for Research on Cancer; 2017. p. 60–1.
5. Delattre O, Zucman J, Melot T, Garau XS, Zucker JM, Lenoir GM, et al. The Ewing family of tumors--a subgroup of small-round-cell tumors defined by specific chimeric transcripts. N Engl J Med. 1994;331(5):294–9.
6. Jeon IS, Davis JN, Braun BS, Sublett JE, Roussel MF, Denny CT, et al. A variant Ewing's sarcoma translocation (7;22) fuses the EWS gene to the ETS gene ETV1. Oncogene. 1995;10(6):1229–34.
7. Kaneko Y, Yoshida K, Handa M, Toyoda Y, Nishihira H, Tanaka Y, et al. Fusion of an ETS-family gene, EIAF, to EWS by t(17;22)(q12;q12) chromosome translocation in an undifferentiated sarcoma of infancy. Genes Chromosomes Cancer. 1996;15(2):115–21.
8. Ng TL, O'Sullivan MJ, Pallen CJ, Hayes M, Clarkson PW, Winstanley M, et al. Ewing sarcoma with novel translocation t(2;16) producing an in-frame fusion of FUS and FEV. J Mol Diagn. 2007;9(4):459–63.
9. Peter M, Couturier J, Pacquement H, Michon J, Thomas G, Magdelenat H, et al. A new member of the ETS family fused to EWS in Ewing tumors. Oncogene. 1997;14(10):1159–64.
10. Shing DC, McMullan DJ, Roberts P, Smith K, Chin SF, Nicholson J, et al. FUS/ERG gene fusions in Ewing's tumors. Cancer Res. 2003;63(15):4568–76.
11. Sorensen PH, Lessnick SL, Lopez-Terrada D, Liu XF, Triche TJ, Denny CT. A second Ewing's sarcoma translocation, t(21;22), fuses the EWS gene to another ETS-family transcription factor, ERG. Nat Genet. 1994;6(2):146–51.
12. Turc-Carel C, Aurias A, Mugneret F, Lizard S, Sidaner I, Volk C, et al. Chromosomes in Ewing's sarcoma. I. An evaluation of 85 cases of remarkable consistency of t(11;22)(q24;q12). Cancer Genet Cytogenet. 1988;32(2):229–38.
13. de Alava E, Lessnick SL, Stamenkovic I. Ewing Sarcoma. In: WHO Classification of Tumours Editorial Board, editor. WHO Classification of Soft Tissue and Bone Tumours. Lyon: International Agency for Research on Cancer; 2020. p. 323–5.
14. Ellis MA, Gerry DR, Neskey DM, Lentsch EJ. Ewing sarcoma of the head and neck. Ann Otol Rhinol Laryngol. 2017;126(3):179–84.
15. Torabi SJ, Izreig S, Kasle DA, Benchetrit L, Salehi PP, Judson BL. Clinical characteristics and treatment-associated survival of head and neck Ewing sarcoma. Laryngoscope. 2020;130(10):2385–92.
16. Whaley JT, Indelicato DJ, Morris CG, Hinerman RW, Amdur RJ, Mendenhall WM, et al. Ewing tumors of the head and neck. Am J Clin Oncol. 2010;33(4):321–6.
17. Ambros IM, Ambros PF, Strehl S, Kovar H, Gadner H, Salzer-Kuntschik M. MIC2 is a specific marker for Ewing's sarcoma and peripheral primitive neuroectodermal tumors. Evidence for a common histogenesis of Ewing's sarcoma and peripheral primitive neuroectodermal tumors from MIC2 expression and specific chromosome aberration. Cancer. 1991;67(7):1886–93.
18. Hung YP, Fletcher CD, Hornick JL. Evaluation of NKX2-2 expression in round cell sarcomas and other tumors with EWSR1 rearrangement: imperfect specificity for Ewing sarcoma. Mod Pathol. 2016;29(4):370–80.
19. Machado I, Yoshida A, Morales MGN, Abrahao-Machado LF, Navarro S, Cruz J, et al. Review with novel markers facilitates precise categorization of 41 cases of diagnostically challenging, "undifferentiated small round cell tumors". A clinicopathologic, immunophenotypic and molecular analysis. Ann Diagn Pathol. 2018;34:1–12.
20. McCuiston A, Bishop JA. Usefulness of NKX2.2 immunohistochemistry for distinguishing Ewing sarcoma from other Sinonasal small round blue cell tumors. Head Neck Pathol. 2018;12(1):89–94.
21. Folpe AL, Hill CE, Parham DM, O'Shea PA, Weiss SW. Immunohistochemical detection of FLI-1 protein expression: a study of 132 round cell tumors with emphasis on CD99-positive mimics of Ewing's sarcoma/primitive neuroectodermal tumor. Am J Surg Pathol. 2000;24(12):1657–62.
22. Llombart-Bosch A, Machado I, Navarro S, Bertoni F, Bacchini P, Alberghini M, et al. Histological heterogeneity of Ewing's sarcoma/PNET: an immunohistochemical analysis of 415 genetically confirmed cases with clinical support. Virchows Arch. 2009;455(5):397–411.
23. Collini P, Mezzelani A, Modena P, Dagrada P, Tamborini E, Luksch R, et al. Evidence of neural differentiation in a case of post-therapy primitive neuroectodermal tumor/Ewing sarcoma of bone. Am J Surg Pathol. 2003;27(8):1161–6.
24. Erdogan KE, Deveci MA, Hakkoymaz ZR, Gonlusen G. Therapy-induced neural differentiation in Ewing's sarcoma: a case report and review of the literature. Turk Patoloji Derg. 2019;35(2):139–43.
25. Weissferdt A, Kalhor N, Moran CA. Ewing sarcoma with extensive neural differentiation: a clinicopathologic, immunohistochemical, and molecular analysis of three cases. Am J Clin Pathol. 2015;143(5):659–64.
26. Bridge JA, Fidler ME, Neff JR, Degenhardt J, Wang M, Walker C, et al. Adamantinoma-like Ewing's sarcoma: genomic confirmation, phenotypic drift. Am J Surg Pathol. 1999;23(2):159–65.
27. Folpe AL, Goldblum JR, Rubin BP, Shehata BM, Liu W, Dei Tos AP, et al. Morphologic and immunophenotypic diversity in Ewing family tumors: a study of 66 genetically confirmed cases. Am J Surg Pathol. 2005;29(8):1025–33.
28. Rooper LM, Bishop JA. Soft tissue special issue: Adamantinoma-like Ewing sarcoma of the head and neck: a practical review of a challenging emerging entity. Head Neck Pathol. 2020;14(1):59–69.
29. Eloy C, Cameselle-Teijeiro J, Vieira J, Teixeira MR, Cruz J, Sobrinho-Simoes M. Carcinoma of the thyroid with Ewing/PNET family tumor elements: a tumor of unknown histogenesis. Int J Surg Pathol. 2014;22(6):579–81.
30. Eloy C, Oliveira M, Vieira J, Teixeira MR, Cruz J, Sobrinho-Simoes M. Carcinoma of the thyroid with Ewing family tumor elements and favorable prognosis: report of a second case. Int J Surg Pathol. 2014;22(3):260–5.
31. Alexiev BA, Tumer Y, Bishop JA. Sinonasal adamantinoma-like Ewing sarcoma: A case report. Pathol Res Pract. 2017;213(4):422–6.
32. Bishop JA, Alaggio R, Zhang L, Seethala RR, Antonescu CR. Adamantinoma-like Ewing family tumors of the head and neck: a pitfall in the differential diagnosis of basaloid and myoepithelial carcinomas. Am J Surg Pathol. 2015;39(9):1267–74.
33. Kikuchi Y, Kishimoto T, Ota S, Kambe M, Yonemori Y, Chazono H, et al. Adamantinoma-like Ewing family tumor of soft tissue associated with the vagus nerve: a case report and review of the literature. Am J Surg Pathol. 2013;37(5):772–9.

34. Lezcano C, Clarke MR, Zhang L, Antonescu CR, Seethala RR. Adamantinoma-like Ewing sarcoma mimicking basal cell adenocarcinoma of the parotid gland: a case report and review of the literature. Head Neck Pathol. 2015;9(2):280–5.
35. Mahadevan P, Ramkumar S, Gangadharan VP. Adamantinoma-like Ewing's family tumor of the Sino nasal region: a case report and a brief review of literature. Case Rep Pathol. 2019;2019:6.
36. Morlote D, Harada S, Lindeman B, Stevens TM. Adamantinoma-like Ewing sarcoma of the thyroid: a case report and review of the literature. Head Neck Pathol. 2019;13:618.
37. Rooper LM, Jo VY, Antonescu CR, Nose V, Westra WH, Seethala RR, et al. Adamantinoma-like Ewing sarcoma of the salivary glands: a newly recognized mimicker of basaloid salivary carcinomas. Am J Surg Pathol. 2019;43(2):187–94.
38. Weinreb I, Goldstein D, Perez-Ordonez B. Primary extraskeletal Ewing family tumor with complex epithelial differentiation: a unique case arising in the lateral neck presenting with Horner syndrome. Am J Surg Pathol. 2008;32(11):1742–8.
39. Alnuaim H, Alzahrani M, Ghandurah S, Dababo M. Adamantinoma-like Ewing sarcoma of the parotid gland: report of two cases and review of literature. Cureus. 2020;12(12):e11870.
40. Lopez F, Rodrigo JP, Cardesa A, Triantafyllou A, Devaney KO, Mendenhall WM, et al. Update on primary head and neck mucosal melanoma. Head Neck. 2016;38(1):147–55.
41. Gal TJ, Silver N, Huang B. Demographics and treatment trends in sinonasal mucosal melanoma. Laryngoscope. 2011;121(9):2026–33.
42. Moreno MA, Roberts DB, Kupferman ME, DeMonte F, El-Naggar AK, Williams M, et al. Mucosal melanoma of the nose and paranasal sinuses, a contemporary experience from the M D. Anderson Cancer Center. Cancer. 2010;116(9):2215–23.
43. Moya-Plana A, Auperin A, Obongo R, Baglin A, Ferrand FR, Baujat B, et al. Oncologic outcomes, prognostic factor analysis and therapeutic algorithm evaluation of head and neck mucosal melanomas in France. Eur J Cancer. 2019;123:1–10.
44. Ascierto PA, Accorona R, Botti G, Farina D, Fossati P, Gatta G, et al. Mucosal melanoma of the head and neck. Crit Rev Oncol Hematol. 2017;112:136–52.
45. Lyu J, Wu Y, Li C, Wang R, Song H, Ren G, et al. Mutation scanning of BRAF, NRAS, KIT, and GNAQ/GNA11 in oral mucosal melanoma: a study of 57 cases. J Oral Pathol Med. 2016;45(4):295–301.
46. Merkel EA, Gerami P. Malignant melanoma of sun-protected sites: a review of clinical, histological, and molecular features. Lab Investig. 2017;97(6):630–5.
47. Hintzsche JD, Gorden NT, Amato CM, Kim J, Wuensch KE, Robinson SE, et al. Whole-exome sequencing identifies recurrent SF3B1 R625 mutation and comutation of NF1 and KIT in mucosal melanoma. Melanoma Res. 2017;27(3):189–99.
48. Nassar KW, Tan AC. The mutational landscape of mucosal melanoma. Semin Cancer Biol. 2020;61:139–48.
49. Newell F, Kong Y, Wilmott JS, Johansson PA, Ferguson PM, Cui C, et al. Whole-genome landscape of mucosal melanoma reveals diverse drivers and therapeutic targets. Nat Commun. 2019;10(1):3163.
50. Zebary A, Jangard M, Omholt K, Ragnarsson-Olding B, Hansson J. KIT, NRAS and BRAF mutations in sinonasal mucosal melanoma: a study of 56 cases. Br J Cancer. 2013;109(3):559–64.
51. Xu X, Palsgrove D, Kurian E, Yan S, Oliai BR, Bishop JA. Variable Expression of S100 Protein in Sinonasal Malignant Mucosal Melanoma: A Potential Diagnostic Pitfall. Head Neck Pathol. 2020;14(4):929–35.
52. Broich G, Pagliari A, Ottaviani F. Esthesioneuroblastoma: a general review of the cases published since the discovery of the tumour in 1924. Anticancer Res. 1997;17(4A):2683–706.
53. Jethanamest D, Morris LG, Sikora AG, Kutler DI. Esthesioneuroblastoma: a population-based analysis of survival and prognostic factors. Arch Otolaryngol Head Neck Surg. 2007;133(3):276–80.
54. Platek ME, Merzianu M, Mashtare TL, Popat SR, Rigual NR, Warren GW, et al. Improved survival following surgery and radiation therapy for olfactory neuroblastoma: analysis of the SEER database. Radiat Oncol. 2011;6:41.
55. Mills SE. Neuroectodermal neoplasms of the head and neck with emphasis on neuroendocrine carcinomas. Mod Pathol. 2002;15(3):264–78.
56. Thompson LD. Olfactory neuroblastoma. Head Neck Pathol. 2009;3(3):252–9.
57. Rooper LM, Bishop JA, Westra WH. INSM1 is a sensitive and specific marker of neuroendocrine differentiation in head and neck tumors. Am J Surg Pathol. 2018;42(5):665–71.
58. Wooff JC, Weinreb I, Perez-Ordonez B, Magee JF, Bullock MJ. Calretinin staining facilitates differentiation of olfactory neuroblastoma from other small round blue cell tumors in the sinonasal tract. Am J Surg Pathol. 2011;35(12):1786–93.
59. Capper D, Engel NW, Stichel D, Lechner M, Gloss S, Schmid S, et al. DNA methylation-based reclassification of olfactory neuroblastoma. Acta Neuropathol. 2018;136(2):255–71.
60. Classe M, Yao H, Mouawad R, Creighton CJ, Burgess A, Allanic F, et al. Integrated multi-omic analysis of Esthesioneuroblastomas identifies two subgroups linked to cell ontogeny. Cell Rep. 2018;25(3):811–21 e5.
61. Gallia GL, Zhang M, Ning Y, Haffner MC, Batista D, Binder ZA, et al. Genomic analysis identifies frequent deletions of dystrophin in olfactory neuroblastoma. Nat Commun. 2018;9(1):5410.
62. Lazo de la Vega L, McHugh JB, Cani AK, Kunder K, Walocko FM, Liu CJ, et al. Comprehensive molecular profiling of Olfactory neuroblastoma identifies potentially targetable FGFR3 amplifications. Mol Cancer Res. 2017;15(11):1551–7.
63. Kadish S, Goodman M, Wang CC, Olfactory neuroblastoma. A clinical analysis of 17 cases. Cancer. 1976;37(3):1571–6.
64. Morita A, Ebersold MJ, Olsen KD, Foote RL, Lewis JE, Quast LM. Esthesioneuroblastoma: prognosis and management. Neurosurgery. 1993;32(5):706–14. discussion 14–5
65. Bell D, Saade R, Roberts D, Ow TJ, Kupferman M, DeMonte F, et al. Prognostic utility of Hyams histological grading and Kadish-Morita staging systems for esthesioneuroblastoma outcomes. Head Neck Pathol. 2015;9(1):51–9.
66. Goshtasbi K, Abiri A, Abouzari M, Sahyouni R, Wang BY, Tajudeen BA, et al. Hyams grading as a predictor of metastasis and overall survival in esthesioneuroblastoma: a meta-analysis. Int Forum Allergy Rhinol. 2019;9(9):1054–62.
67. Kaur G, Kane AJ, Sughrue ME, Madden M, Oh MC, Sun MZ, et al. The prognostic implications of Hyam's subtype for patients with Kadish stage C esthesioneuroblastoma. J Clin Neurosci. 2013;20(2):281–6.
68. Malouf GG, Casiraghi O, Deutsch E, Guigay J, Temam S, Bourhis J. Low- and high-grade esthesioneuroblastomas display a distinct natural history and outcome. Eur J Cancer. 2013;49(6):1324–34.
69. Van Gompel JJ, Giannini C, Olsen KD, Moore E, Piccirilli M, Foote RL, et al. Long-term outcome of esthesioneuroblastoma: hyams grade predicts patient survival. J Neurol Surg B Skull Base. 2012;73(5):331–6.
70. Seethala RR, Wenig BM, Barnes EL, Hunt JL. Olfactory neuroblastoma with divergent differentiation: from Ganglioneuroblastoma to carcinoma. Mod Pathol. 2007;20(2):229A.
71. Wenig BM. Olfactory carcinoma. Atlas of head and neck pathology. Cambridge, MA: Elsevier; 2015. p. 155–6.
72. Rooper LM, Bishop JA, Faquin WC, Foss RD, Gallia GL, Jo VY, Lewis JS, Nishino M, Stelow EB, Thompson LDR, Wenig BM, Westra WH. Sinonasal tumors with neuroepithelial differentiation (olfactory carcinoma). Am J Surg Pathol. 2022;46(8):1025–35. https://doi.org/10.1097/PAS.0000000000001908.
73. Gandhoke CS, Dewan A, Gupta D, Syal SK, Jagetia A, Saran RK, et al. A rare case report of mixed olfactory neuroblas-

toma: carcinoma with review of literature. Surg Neurol Int. 2017;8:83.
74. Lao WP, Thompson JM, Evans L, Kim Y, Denham L, Lee SC. Mixed olfactory neuroblastoma and neuroendocrine carcinoma: an unusual case report and literature review. Surg Neurol Int. 2020;11:97.
75. Meyer C, Hamersley ERS, Manosalva RE, Torske K, McIntyre N, Mitchell A. Olfactory neuroblastoma with divergent differentiation: an unusual histologic finding in a rare tumor. Head Neck Pathol. 2017;11(4):531–6.
76. Miller DC, Goodman ML, Pilch BZ, Shi SR, Dickersin GR, Halpern H, et al. Mixed olfactory neuroblastoma and carcinoma. Cancer. 1984;54(9):2019–28.
77. Miura K, Mineta H, Yokota N, Tsutsui Y. Olfactory neuroblastoma with epithelial and endocrine differentiation transformed into ganglioneuroma after chemoradiotherapy. Pathol Int. 2001;51(12):942–7.
78. Sugita Y, Kusano K, Tokunaga O, Mineta T, Abe M, Harada H, et al. Olfactory neuroepithelioma: an immunohistochemical and ultrastructural study. Neuropathology. 2006;26(5):400–8.
79. Rooper LM, Gallia GL, Thompson LDR, Bishop JA, Westra WH. High grade Neuroepithelial carcinoma of the Sinonasal tract: a distinctive entity at the intersection of Olfactory neuroblastoma, neuroendocrine carcinoma, and Sinonasal adenocarcinoma. Mod Pathol. 2020;33(2)
80. Stelow EB, Mills SE, Jo VY, Carlson DL. Adenocarcinoma of the upper aerodigestive tract. Adv Anat Pathol. 2010;17(4):262–9.
81. Shintaku M, Ohta M, Kataoka K, Okabe H. Olfactory neuroblastoma associated with extensive "in situ" lesion and aberrant glandular and rhabdomyosarcomatous differentiation. Neuropathology. 2021;41(4):273–80.
82. Franchi A, Wenig BM. Teratocarcinosarcoma. In: Lloyd RV, Osamura RY, Kloppel G, Rosai J, editors. WHO classification of Tumours of endocrine organs. Lyon: International Agency for Research on Cancer; 2017. p. 26–7.
83. Chapurin N, Totten DJ, Morse JC, Khurram MS, Louis PC, Sinard RJ, et al. Treatment of Sinonasal Teratocarcinosarcoma: a systematic review and survival analysis. Am J Rhinol Allergy. 2021;35(1):132–41.
84. Heffner DK, Hyams VJ. Teratocarcinosarcoma (malignant teratoma?) of the nasal cavity and paranasal sinuses a clinicopathologic study of 20 cases. Cancer. 1984;53(10):2140–54.
85. Smith SL, Hessel AC, Luna MA, Malpica A, Rosenthal DI, El-Naggar AK. Sinonasal teratocarcinosarcoma of the head and neck: a report of 10 patients treated at a single institution and comparison with reported series. Arch Otolaryngol Head Neck Surg. 2008;134(6):592–5.
86. Budrukkar A, Agarwal JP, Kane S, Siddha M, Laskar SG, Pai P, et al. Management and clinical outcome of sinonasal teratocarcinosarcoma: single institution experience. J Laryngol Otol. 2010;124(7):739–43.
87. Agaimy A, Jain D, Uddin N, Rooper LM, Bishop JA. SMARCA4-deficient Sinonasal carcinoma: a series of 10 cases expanding the genetic Spectrum of SWI/SNF-driven Sinonasal malignancies. Am J Surg Pathol. 2020;44:703.
88. Birkeland AC, Burgin SJ, Yanik M, Scott MV, Bradford CR, McHugh JB, et al. Pathogenetic analysis of Sinonasal Teratocarcinosarcomas reveal actionable beta-catenin overexpression and a beta-catenin mutation. J Neurol Surg B Skull Base. 2017;78(4):346–52.
89. Dogan S, Vasudevaraja V, Xu B, Serrano J, Ptashkin RN, Jung HJ, et al. DNA methylation-based classification of sinonasal undifferentiated carcinoma. Mod Pathol. 2019;32(10):1447–59.
90. Rooper LM, Uddin N, Gagan J, Brosens LAA, Magliocca KR, Edgar MA, et al. Recurrent loss of SMARCA4 in Sinonasal Teratocarcinosarcoma. Am J Surg Pathol. 2020;44(10):1331–9.
91. Rooper LM, Agaimy A, Gagan J, Simpson RHW Thompson LDR, Trzcinska AM, Uddin N, Bishop JA. Comprehensive molecular profiling of sinonasal teratocarcinosarcoma highlights recurrent SMARCA4 inactivation and CTNNB1 mutations. Am J Surg Pathol. Publish Ahead of Print. 2022. https://doi.org/10.1097/PAS.0000000000001976.
92. Compton ML, Lewis JS Jr, Faquin WC, Cipriani NA, Shi Q, Ely KA. SALL-4 and Beta-Catenin Expression in Sinonasal Teratocarcinosarcoma. Head Neck Pathol. 2021;16(1):229–35.

Secondary/Metastatic Tumors of Sinonasal Tract

14

Haider A. Mejbel and Todd M. Stevens

14.1 Introduction

The sinonasal tract (SNT) is a complex anatomic location that rarely serves as the "soil" for metastatic cancers from diverse sites. Among the many subsites of the SNT, the maxillary sinus, followed by, in descending order of frequency, the sphenoid, ethmoid, frontal sinus, and nasal cavity may be sites of metastasis [1]. Radiologic examination typically shows a mass lesion with features indicating malignant behavior such as bone invasion. However, the radiologic findings are often nonspecific and usually cannot distinguish between primary and metastatic lesions in the absence of clinical history of known primary malignancy, and therefore a tissue biopsy for diagnosis is often ultimately performed. Lastly, direct invasion into the SNT from adjacent oral cavity, skin, major salivary gland, and sellar tumors may also occur.

Histologically, metastatic tumors usually show similar morphologic and immunophenotypic profiles as that of their corresponding primary lesions; however, altered differentiation or immunophenotypic switching may occur. Further, metastatic tumors may mimic primary sinonasal tumors, which are already of numerous and overlapping types. Thus, diagnosis of metastatic cancer to the SNT can be challenging.

Due to its rarity, the proportional incidence of primary tumors metastatic to the SNT are variably reported. López et al. [2] found renal cell carcinoma (RCC) to be the most common neoplasm to metastasize to the sinonasal tract, accounting for 56% of the reported cases in their study. Whereas in Huang et al. [3] metastatic tumors to the SNT were found to originate from the gastrointestinal tract in 29% of the cases, followed by liver (17.6%), kidney (17.6%), breast (17.6%), thyroid gland (12%), and lung (6%). Nonetheless, any malignant neoplasm may metastasize to the SNT including, but not limited to, melanoma, pancreatic adenocarcinoma [4], pulmonary neuroendocrine carcinoma [5], and bone and soft tissue sarcomas such as leiomyosarcoma and osteosarcoma [6]. In most cases, the prognosis of metastatic tumor of the sinonasal tract is poor reflecting high-stage disease, and treatment is typically palliative and directed toward controlling symptoms of nasal obstruction and bleeding.

In this chapter, we discuss the most common metastatic/secondary neoplasms of the sinonasal tract, illustrating their salient pathologic features, and briefly explain the most common relevant differential diagnosis of each example (Table 14.1).

H. A. Mejbel
Gastrointestinal and Molecular Genetics Pathology, Emory University School of Medicine, Emory University Hospital, Atlanta, GA, USA
e-mail: Haider.A.Mejbel@emory.edu

T. M. Stevens (✉)
Department of Pathology, Kansas University Medical Center, Kansas City, KS, USA
e-mail: tstevens2@kumc.edu

D. Jain, J. A. Bishop (eds.), *Atlas of Sinonasal Tract Pathology*, https://doi.org/10.1007/978-981-19-7315-4_14

Table 14.1 Common tumors metastasize to the sinonasal tract and their salient pathologic features and differential diagnosis

Metastatic/Secondary neoplasm in SNT	Typical morphologic features	Salient ancillary studies	Main differential diagnosis
Clear cell renal cell carcinoma	• Polygonal cells with clear cytoplasm. • Tumor cells arranged in sheets or nested pattern with delicate vascular network.	• (+) PAX8, CA-IX • (−) CK 7	• Sinonasal renal cell-like adenocarcinoma. • Clear cell carcinoma of salivary gland. • Sebaceous carcinoma.
Lung adenocarcinoma	• Well-formed glands to poorly differentiated carcinoma.	• (+) TTF-1, Napsin A, and CK7 • (−) p40 and p63.	• Sinonasal non-intestinal-type adenocarcinoma (non-ITAC). • Sinonasal undifferentiated carcinoma (SNUC). • Salivary gland adenocarcinomas. • Seromucinous hamartoma. • Papillary sinusitis.
Breast carcinoma	• Variable, depends on subtype, and grade. • Lymphovascular invasion common.	• GATA-3, GCDFP-15, and mammaglobin (+) typically in low-grade tumors. • Variable ER, PR, and HER2/neu.	• Salivary duct carcinoma. • Secretory carcinoma. • HPV-related multiphenotypic sinonasal carcinoma.
Papillary thyroid carcinoma	• Characteristic nuclear features. • Tumor arranged in variable papillary, follicular, solid, or trabecular growth patterns.	• (+) TTF-1 and PAX-8 and variable thyroglobulin expression.	• Low-grade nasopharyngeal papillary adenocarcinoma. • Polymorphous adenocarcinoma/ cribriform adenocarcinoma of salivary glands. • Secretory carcinoma. • Microsecretory carcinoma.
Colorectal adenocarcinoma	• Malignant glands with elongated, "pencillate" nuclei. • "Dirty necrosis" common.	• (+) CK20, SATB2, and CDX-2 • (−) CK7	• Sinonasal intestinal-type adenocarcinoma. • High-grade adenoid cystic carcinoma.
Hepatocellular carcinoma	• Polygonal cells with vesicular nuclei and prominent nucleoli. • Endothelial wrapping of hepatocytes is a diagnostic clue. • Tumor arranged in solid sheets or trabecular growth pattern; bile pigment may be seen.	• (+) Arginase-1 and HepPar1 • Often negative for both CK7 and CK20.	• SMARCB1-deficient sinonasal carcinoma. • Rhabdomyosarcoma.
Seminoma	• Polygonal cells with abundant clear to amphophilic cytoplasm forming nests or sheets of cells. • Distinct cell borders divided by lymphocytic-rich fibrous septa.	• (+) SALL-4, OCT3/4, CD117, and D2–40 • (−)EMA, keratins, α-fetoprotein, HCG, inhibin-α, CD30, and glypican-3.	• Olfactory neuroblastoma. • Neuroendocrine carcinoma. • Sinonasal teratocarcinosarcoma. • Extranodal NK/T-cell lymphoma.
Melanoma	• Broad morphologic spectrum that includes epithelioid, spindled, rhabdoid, and small cell cytomorphology. • Prominent "cherry-red" nucleoli with frequent mitosis and tumor necrosis. • Should lack *in-situ* component.	• (+) S100, SOX10, with variable Melan-A, and HMB-45 antigen • (−) cytokeratins [can be focally or patchy positive in rare cases] • *BRAF* mutation. • Lack of *EWSR1::ATF1*.	• Primary mucosal melanoma. • Metastatic clear cell sarcoma. • Biphenotypic sinonasal sarcoma.
Prostatic adenocarcinoma	• Variable morphology depending on histologic type and Gleason grade. • Acinar type shows well-formed glands with relatively monomorphic cells with abundant cytoplasm and prominent nucleoli.	• (+) NKX3.1, PSA, and prostein • Correlation with serum PSA may be useful.	• Sinonasal non-intestinal-type adenocarcinoma. • Salivary gland adenocarcinomas.

14.2 Renal Cell Carcinoma

Renal cell carcinoma (RCC) is the most common malignant neoplasm to metastasize to SNT accounting for up to 54% of all sinonasal metastatic tumors [2]. Clinically, metastatic RCC in the sinonasal tract presents with local symptoms of pain, nasal obstruction, and bleeding, as the tumor features a rich vascular network [7].

Histology

Clear cell renal cell carcinoma (ccRCC) is most common subtype of RCC and appears to represent most of the reported cases of metastatic RCC to the SNT [8]. Histologically, tumors show polygonal cells with clear cytoplasm arranged in sheets or nested pattern set among a delicate vascular network (Fig. 14.1). The nuclei are irregular and usually show high nucleolar grade. Sarcomatoid or rhabdoid features may also be seen. Immunohistochemically, ccRCC is positive for pancytokeratin, renal cell carcinoma antigen, carbonic anhydrase IX (CA-IX), and PAX-8, and negative for CK7, AMACR, and Cathepsin-K.

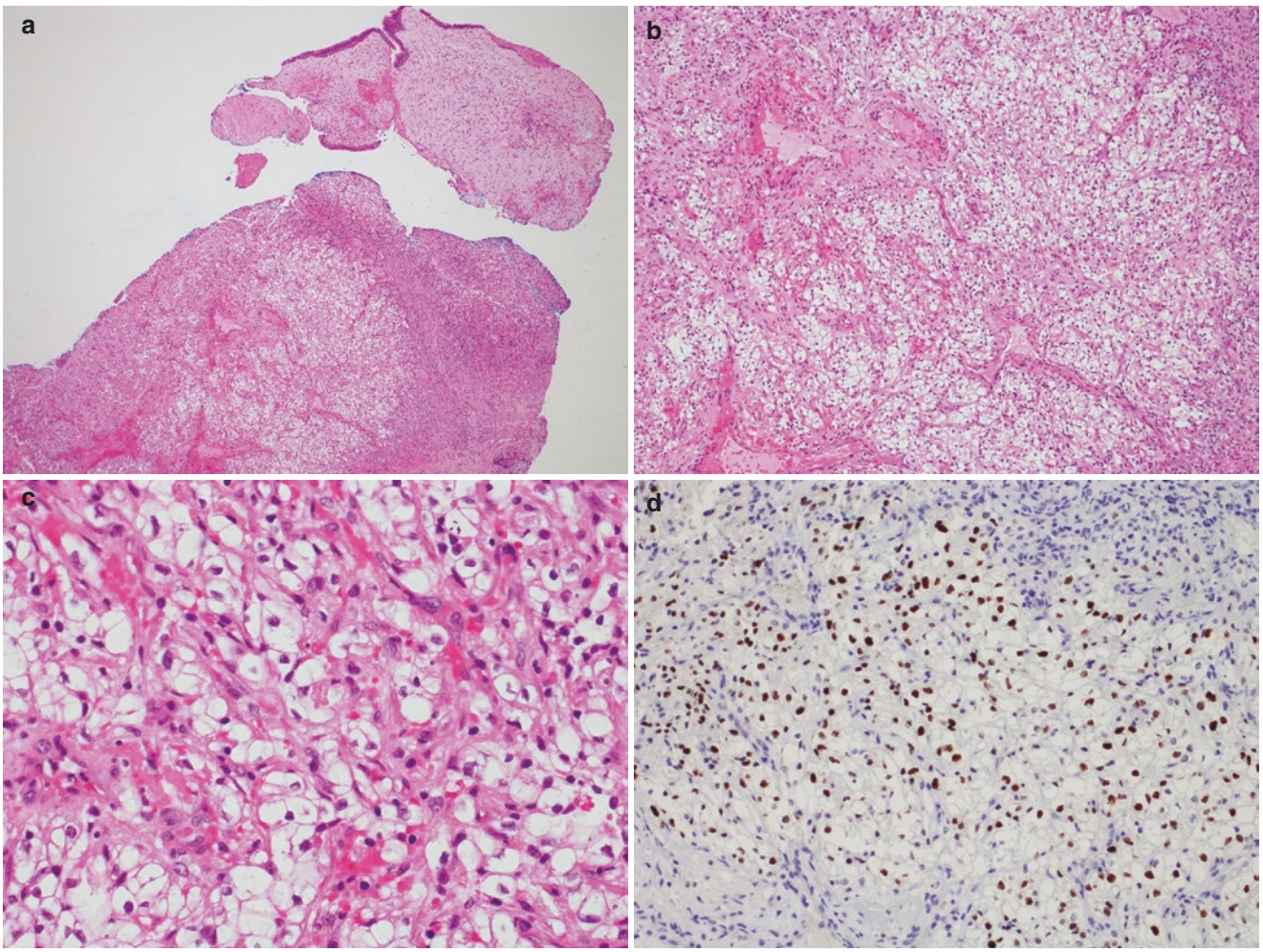

Fig. 14.1 (contributed by Manish Bundele). An example of a clear cell renal cell carcinoma metastatic to the sinonasal tract. (**a** and **b**) A clear cell carcinoma is seen involving sinonasal mucosa (H&E, A-40x, B-100x). (**c**) The delicate vascular network characteristic of clear cell type renal cell carcinoma is noted (H&E, 400x). (**d**) Diffuse expression of PAX8 is typical in renal cell carcinomas (200x)

14.3 Lung Carcinoma

About 40% of patients with non-small cell lung carcinoma (NSCLC) develop distant metastasis to other organs including the brain, liver, bone, and adrenal gland. Metastatic NSCLC to the SNT is extremely rare and accounts for 9% of all metastatic malignant neoplasms of the sinonasal tract. Clinical presentation is variable and includes local pain and nasal obstruction and most patients have wide-spread disease at the time of metastasis to the SNT [9]. The prognosis of metastatic NSCLC is poor and the 5-year survival rates are less than 10%.

Histology

Adenocarcinoma is the most common type of NSCLC to develop distant metastasis. The histologic features depend on the adenocarcinoma subtype and its degree of differentiation that ranges from well-differentiated adenocarcinoma featuring well-formed glands to poorly differentiated carcinoma growing in sheets (Fig. 14.2). Tumor necrosis and lymphovascular invasion are common. Lung adenocarcinoma is usually positive for TTF-1, Napsin A, and CK7, and negative for p40 and p63.

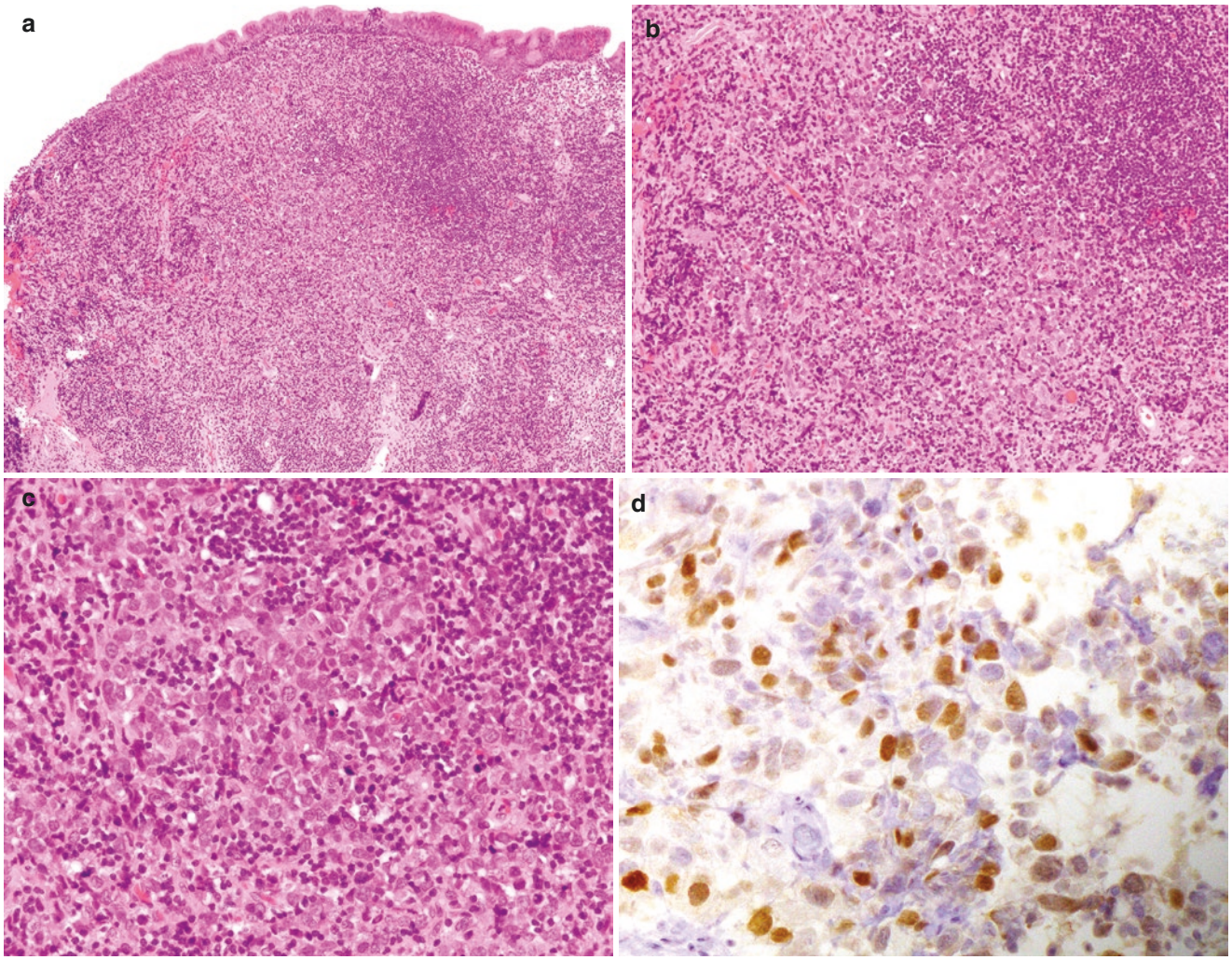

Fig. 14.2 Example of a metastatic poorly differentiated lung carcinoma involving mucosa of the maxillary sinus (**a**, H&E; 40X). Poorly differentiated carcinoma growing in solid pattern with no evident glandular formation (**b**, H&E; 100X). Cytomorphologically, the tumor cells are intermediate to large in size with striking nuclear pleomorphism, associated with lymphoid response in this example (**c**, H&E; 400X). The differential diagnosis of this particular case would be broad and would include SNUC, lymphoepithelial carcinoma, etc.; however, nuclear expression for TTF-1 (**d**, IHC; 400X) and history of lung adenocarcinoma would confirm the diagnosis. This case was CK7 positive and CK20 negative (not shown)

Squamous cell carcinoma of lung, or for that matter a squamous cell carcinoma from any site, could metastasize to the SNT and would be challenging to distinguish from a primary squamous cell carcinoma of the SNT without clinical history. Areas of squamous dysplasia and carcinoma *in-situ* would favor a primary sinonasal tumor. High-risk HPV positivity, present in approximately 20% of squamous cell carcinoma of SNT [10], would favor a sinonasal primary assuming direct extension from an oropharyngeal primary and metastasis from other HPV-positive squamous carcinomas such as uterine cervical and anus are excluded. Lastly, metastatic squamous cell carcinoma to SNT would have to be differentiated from NUT carcinoma. The latter is a high-grade, monomorphic carcinoma and often shows areas of "abrupt" keratinization that can now be easily diagnosed using a commercially available monoclonal NUT antibody [11].

14.4 Breast Carcinoma

Generally, more than 50% of breast cancer patients experience metastatic disease in their lifetimes, yet metastatic breast carcinoma to the head and neck is still uncommon. Breast carcinoma metastasis to the SNT and base of skull may occur through the vertebral venous plexus or transcribrosal spread from meningeal involvement [12]. Clinically, metastatic breast carcinoma to the SNT presents with mass effect with or without symptoms of rhinosinusitis. The prognosis is generally poor; however, early diagnosis and treatment may prolong survival.

Histology

Given its rarity, studies elaborating on the specific subtypes of breast carcinoma to metastasize to the SNT are not available. However, invasive ductal carcinoma (IDC) accounts for more than 75% of primary breast cancers and thus likely accounts for the majority of breast carcinoma cases to metastasize to the SNT. The histologic features of IDC vary according to tumor grade and degree of differentiation from well-formed tubules to solid sheets to single tumor cells (Fig. 14.3). The nuclear grade is usually high, with associated necrosis, and lymphovascular invasion and frequent mitosis are identified.

Metastatic breast carcinomas show expression of cytokeratins and variable expression of the breast markers GATA-3, GCDFP-15, and mammaglobin [13]. However, GATA-3 may be negative especially in high-grade breast carcinoma [14]. Breast biomarkers including Estrogen Receptor (ER), Progesterone Receptor (PR), and HER2/neu (ERBB2) studies are usually performed on all metastatic breast carcinomas to provide prognostic and therapeutic information for targeted therapy. In addition, comparison of ER, PR, and HER2/neu status with the primary breast tumor may provide supportive evidence of breast primary.

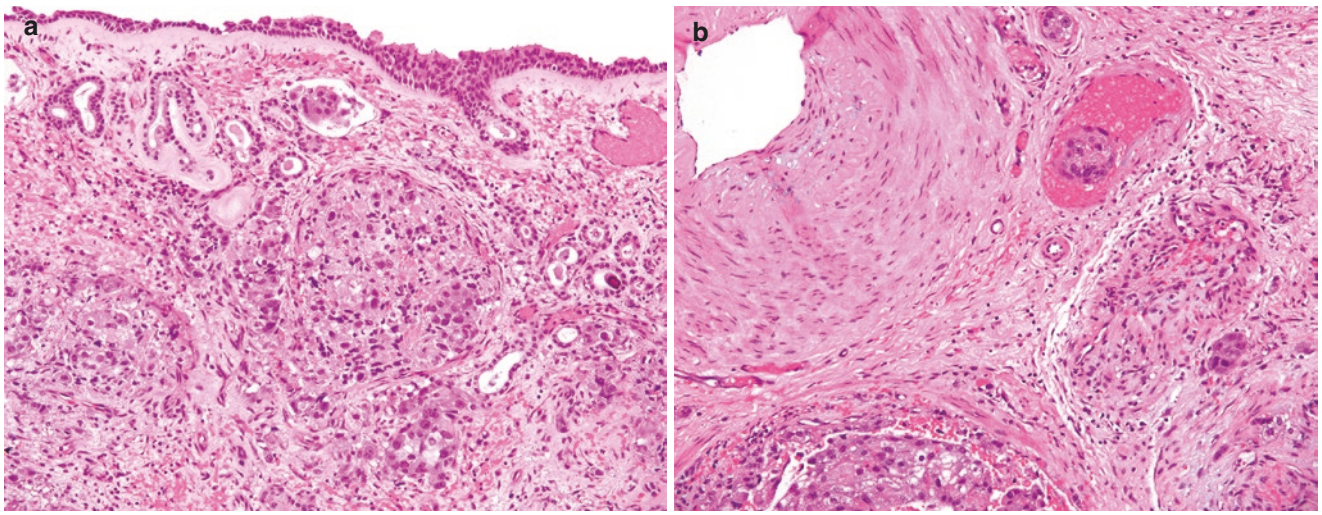

Fig. 14.3 Example of ductal carcinoma of the breast metastatic to the sinonasal tract (**a**, H&E; 400X). Nests of metastatic carcinoma cells involve the sinonasal mucosa with intact surface epithelium. Lymphovascular invasion can be seen in **a** and in **b** (**b**, H&E; 200X). GATA3 (**c**, IHC; 200X) and Estrogen Receptor (**d**, IHC; 400x) are both positive supporting breast primary

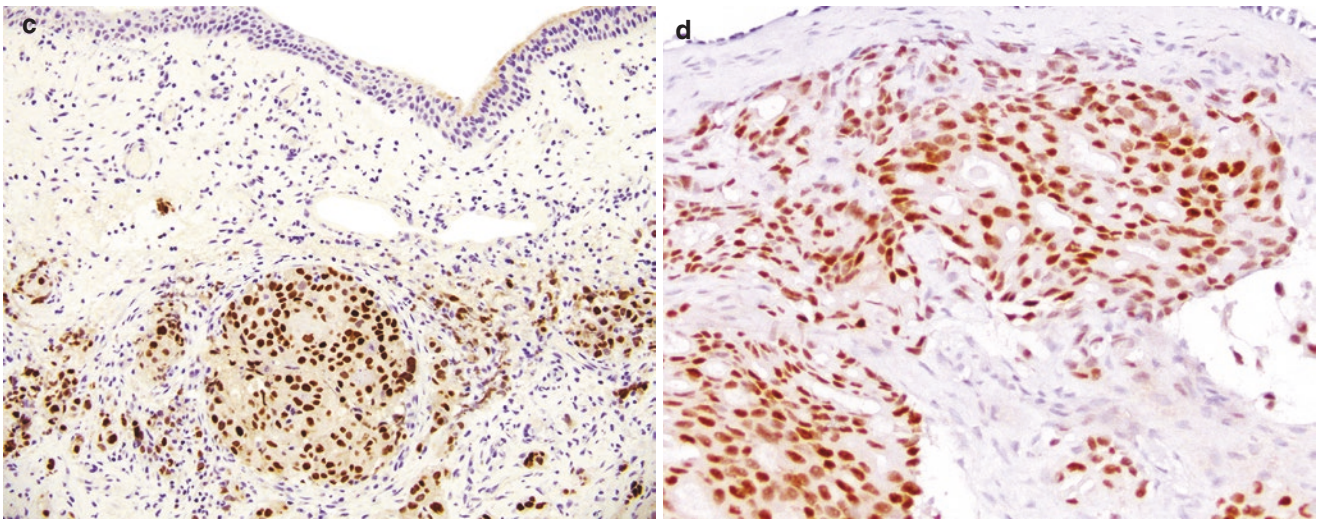

Fig. 14.3 (continued)

14.5 Thyroid Carcinoma

With the current advanced cytologic evaluation of thyroid nodules, most thyroid carcinomas are detected at their early stages. When metastatic, thyroid carcinoma typically involves the lung, liver, and bones [15]. However, the SNT may rarely be involved by metastatic thyroid carcinoma.

Histology

Papillary thyroid carcinoma (PTC) is the most common type of malignant thyroid neoplasm and is the most commonly reported subtype of thyroid carcinoma to metastasize to the SNT (Fig. 14.4). However, metastasis of other histologic types of thyroid carcinoma such as follicular thyroid carcinoma to SNT have been reported [4]. Conventional PTC shows the characteristic nuclear features including nuclear enlargement, irregularity, grooves, small peripheral nucleoli, and nuclear pseudoinclusions, arranged in variable papillary, follicular, solid, or trabecular growth patterns [16]. Additional features such as colloid material and psammoma bodies may also be seen. Co-expression of TTF-1, PAX-8, and variable thyroglobulin will help in confirming the diagnosis.

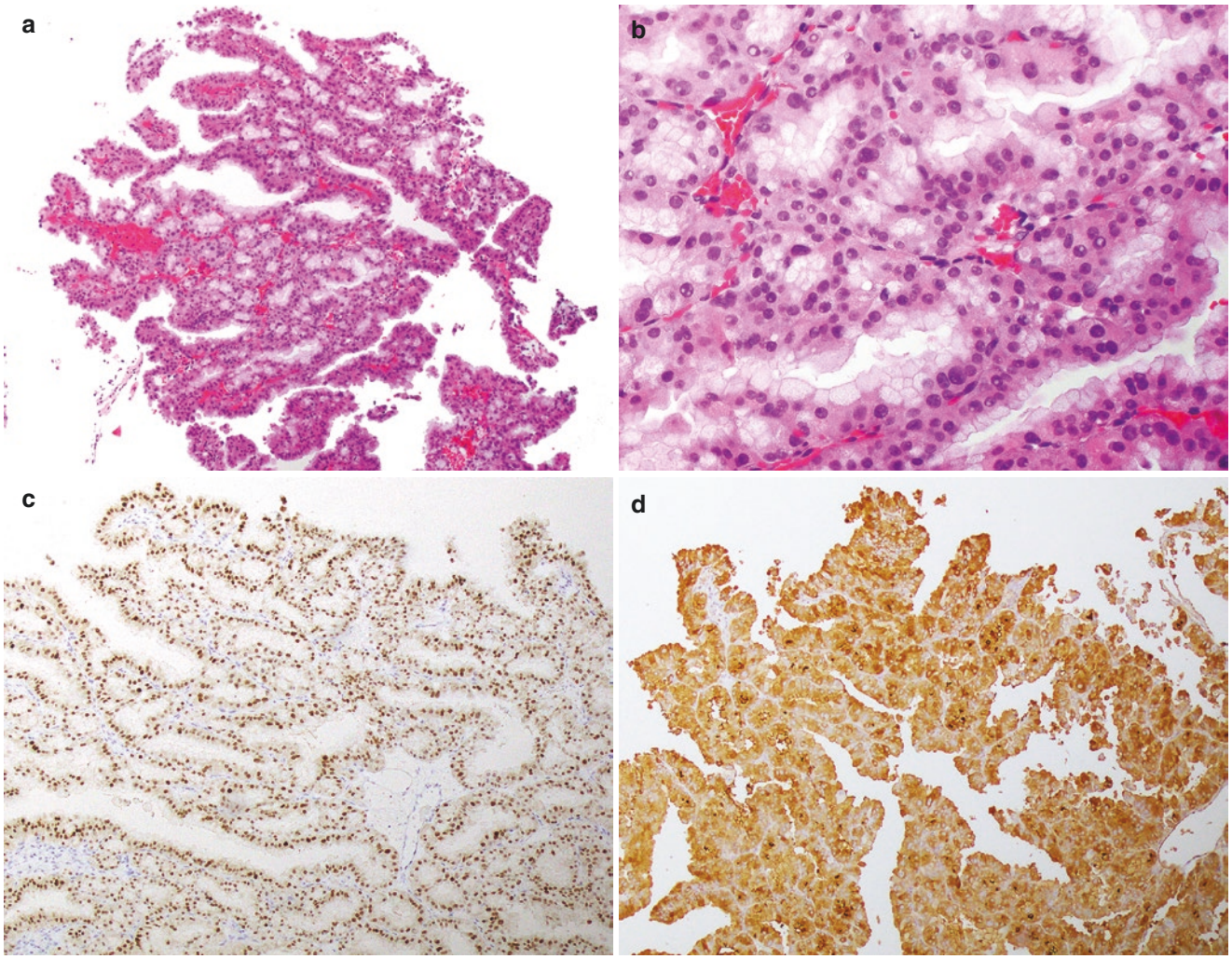

Fig. 14.4 A skull base tumor showing adenocarcinoma with papillary features (**a**, H&E; 100X). The tumor cells show oncocytic and mucinous changes with many nuclear pseudoinclusions (**b**, H&E; 400X). Tumor cells were diffusely positive for TTF-1 (**c**, IHC; 100X) and thyroglobulin (**d**, IHC; 100x), consistent with thyroid primary

14.6 Colorectal Carcinoma

Colorectal adenocarcinoma is considered the most common gastrointestinal neoplasm to metastasize to the sinonasal tract. However, other gastrointestinal neoplasms such as adenocarcinomas of gastric, small bowel, and esophageal primaries are also reported to metastasize to SNT [17, 18]. Treatment is often palliative and prognosis is poor.

Histology

The histologic features of colorectal carcinoma vary depending on its type and its degree of differentiation. Adenocarcinoma is the most common histologic type of colorectal carcinoma and typically shows malignant glands made up of elongated nuclei with visible nucleoli, frequent mitosis, and apoptosis. So-called "dirty necrosis" is common and can serve as a useful clue for colorectal origin. Colorectal adenocarcinoma is positive for CK20, CDX-2, SATB2, and MUC2 and usually negative for CK7.

14.7 Hepatocellular Carcinoma

In addition to regional lymph nodes metastases, hepatocellular carcinoma (HCC) most commonly metastasizes to the lung, adrenal gland, and bone. Metastatic HCC to the sinonasal tract (Fig. 14.5) is uncommon but does occur [19]. Patients typically present with a new mass lesion in the sinonasal tract with known history of HCC. Serum alpha-fetoprotein may be elevated [20]. Radiologic examination shows an enhancing lesion within the sinonasal tract. Histologic examination of metastatic conventional

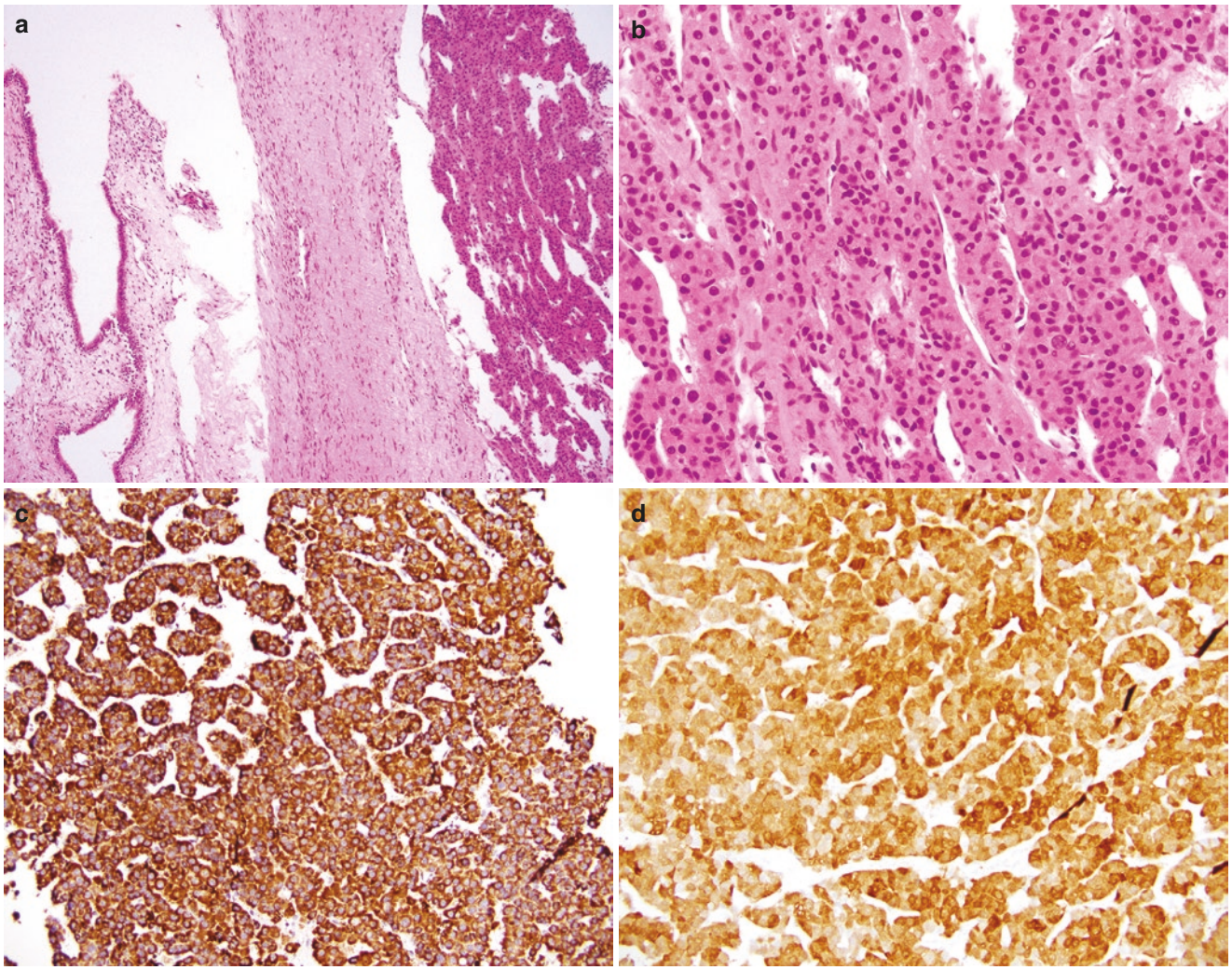

Fig. 14.5 Metastatic hepatocellular carcinoma (HCC) to sinonasal tract (**a**, H&E; 100X). HCC cells with abundant eosinophilic cytoplasm and thick trabecular arrangement with endothelial cell wrapping (**b**, H&E; 400X). HCC shows cytoplasmic expression of Hep-Par1 (**c**, IHC; 200X) and Arginase-1 (**d**, IHC; 200X)

HCC shows tumor with trabecular growth patterns formed of polygonal malignant hepatocytes with vesicular nuclei and prominent nucleoli as well as wrapping of hepatocyte groups by endothelium. Clear cells secondary to accumulation of glycogen and multinucleated giant cells might be seen. Bile pigment may be identified and would help in distinguishing HCC from its mimics [21]. In conjunction with the clinicopathologic presentation, immunohistochemical staining with Arginase-1, HepPar1, and Glypican-3 can help confirm the diagnosis [22]. Treatment options are limited to surgical debulking and chemotherapy.

14.8 Germ Cell Tumors

SNT involvement by a metastatic germ cell tumor may occur [23], and thus, correlation with any history of primary gonadal or mediastinal germ cell tumor should be first attempted before considering a diagnosis of a primary sinonasal germ cell tumor. The latter is an exceedingly rare group of neoplasms that encompasses sinonasal teratoma, choriocarcinoma, and yolk sac tumor [24, 25]. A combination of clinical history, serum tumor markers, histologic examination, and immunohistochemical study can help confirm the diagnosis of metastatic germ cell tumor. Stage IV germ cell

tumors are typically treated with chemotherapy with periodic monitoring of serum tumor marker as indicator of treatment response. Prognosis depends on the type of metastatic germ cell tumor and its response to therapy [26].

Histology

Metastatic seminoma/dysgerminoma typically shows large, round to polygonal cells with abundant clear to amphophilic cytoplasm forming nests or sheets of cells. The tumor cells show distinct cell borders and are divided by fibrous septa that contain prominent lymphocytic infiltration (Fig. 14.6). Cells are relatively uniform with large central nuclei that show one or two prominent nucleoli. Yolk sac tumor may feature microcystic, reticular, solid, papillary, glandular and even hepatoid patterns made up of primitive cells with variable atypia and often clear cytoplasm with hyaline globules. Of note, yolk sac-like areas have been described in INI-1 deficient sinonasal carcinomas and thus this entity should be excluded before diagnosing yolk sac tumor in the SNT.[51] Choriocarcinoma shows a dimorphic morphology of malignant cytotrophoblast and syncytiotrophoblasts and will express GATA-3 and bHCG. A comprehensive immunohistochemical panel is often needed to arrive at an accurate diagnosis [27].

All germ cell tumors will be positive for SALL-4 and variably positive for placental-like alkaline phosphatase (PLAP). Note that SALL-4 can also be expressed in other somatic malignancies and thus is not entirely specific for germ cell tumors [28]. Seminoma is positive for OCT3/4, CD117, and D2–40 and negative for EMA, α-fetoprotein,

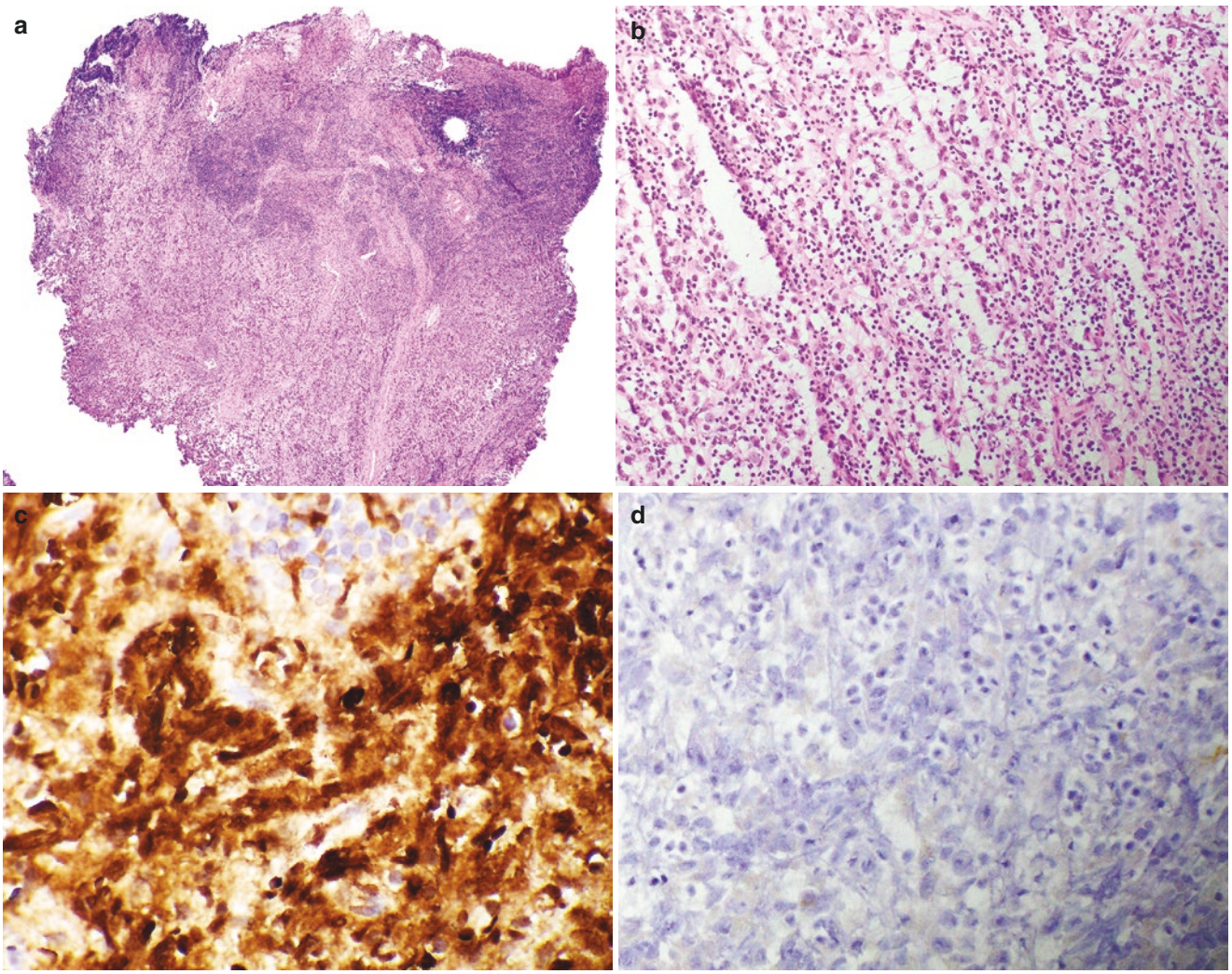

Fig. 14.6 Low-power view of a seminoma metastatic to the sinonasal cavity (**a**, H&E; 40X). The classic architecture of sheets of enlarged, malignant cells with fibrovascular septa with lymphocytic infiltrate were best preserved in the frozen section slides from this case (**b**, H&E, frozen section; 200x). Clinical history of testicular tumor and positive OCT3/4 (**c**, IHC; 600x), albeit with high background staining in this example, and negativity for CD30 (**d**, IHC; 400x) supported the diagnosis

HCG, inhibin-α, CD30, and glypican-3. Cytokeratin expression is usually negative in seminoma. Yolk sac tumors are often positive for pankeratins, AFP and glypican-3, but negative for CK7 [29] and OCT3/4. Choriocarcinoma is positive for hCG and negative for OCT3/4 and AFP with variable expression of glypican-3.

14.9 Metastatic Melanoma

Melanoma of the SNT can be generally categorized into primary mucosal melanoma and secondary melanoma [30]. The latter might be due to direct extension from a nearby cutaneous primary or a metastatic lesion. The lack of melanoma *in-situ* at the mucosal surface should always raise the possibility of metastatic/secondary lesion, as primary sinonasal melanomas often harbor an *in-situ* component. Molecular genetic testing with a next-generation melanoma panel is typically performed on metastatic melanoma to provide helpful prognostic and therapeutic information. Irrespective of melanoma histologic type, the prognosis for stage IV melanoma is very poor with 5-year survival rate of less than 5%.

Histology

Melanoma features a broad morphologic spectrum (Fig. 14.7) that includes epithelioid, spindled, rhabdoid, and small cell cytomorphology. The nuclei often show vesicular chromatin with prominent nucleoli associated with frequent mitosis and tumor necrosis. Melanoma is usually positive for melanocytic markers including S100

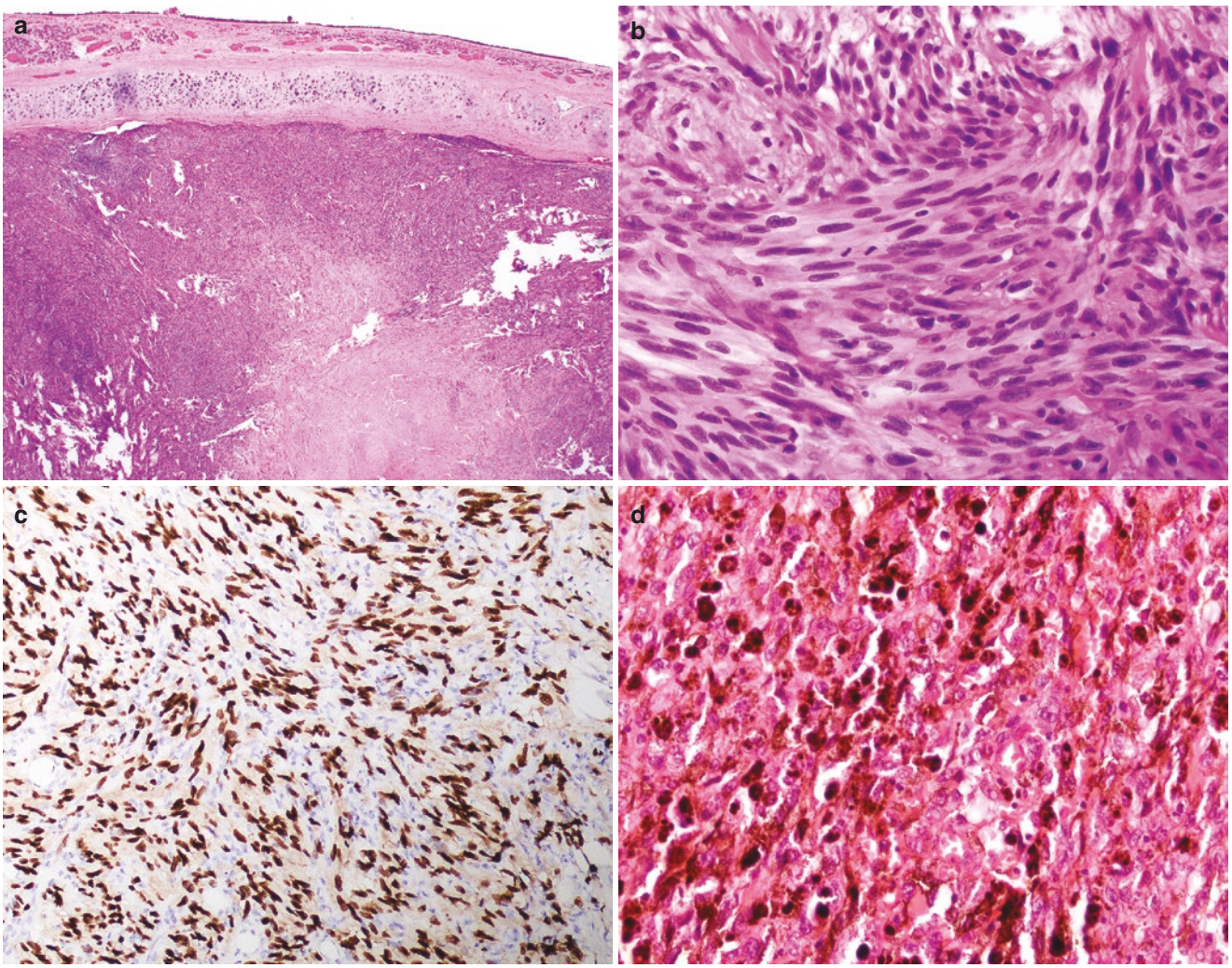

Fig. 14.7 An example of a cutaneous melanoma invading the sinonasal tract by direct extension, seen here undermining the septal cartilage (**a**, H&E; 20x). This particular melanoma grew in spindle cell pattern (**b**, H&E; 400x). The diagnosis was supported by the clinical history and diffuse SOX10 expression (**c**, IHC; 200x). A separate example of melanoma metastatic to sinonasal tract with obvious melanin pigment and epithelioid features with prominent nucleoli (**d**, H&E; 400x)

protein, SOX10, Melan-A, and HMB-45 antigen. However, dedifferentiation and tumor heterogeneity with loss of expression of one or more melanocytic markers are commonly encountered in metastatic melanoma. Furthermore, rare melanoma examples can express cytokeratins [31]. Therefore, multiple melanocytic markers may be needed to arrive at a correct diagnosis.

14.10 Conclusion

Secondary/metastatic neoplasms of the sinonasal tract are far less common than the already rare primary sinonasal neoplasms. Renal cell carcinoma and breast carcinoma are the most common carcinomas to secondarily involve the SNT. Other primary tumors such as thyroid carcinoma, lung adenocarcinoma, hepatocellular carcinoma, germ cell tumors, melanoma, etc. may also metastasize to the SNT. Epistaxis and nasal obstruction are the most common symptoms of the metastatic lesions. Radiologic findings are often nonspecific. Clinical history of another primary neoplasm is very helpful in excluding a primary sinonasal tumor, especially as the latter are often already challenging to accurately diagnose. As expected, patients who suffer from metastatic disease of the sinonasal tract generally experience poor outcomes that often depend on the biology of the primary cancer and other clinicopathologic details.

References

1. Weber AL, Stanton AC. Malignant tumors of the paranasal sinuses: radiologic, clinical, and histopathologic evaluation of 200 cases. Head Neck Surg. 1984;6(3):761–76.
2. López F, Devaney KO, Hanna EY, Rinaldo A, Ferlito A. Metastases to nasal cavity and paranasal sinuses. Head Neck. 2016;38(12):1847–54.
3. Huang HH, Fang TJ, Chang PH, Lee TJ. Sinonasal metastatic tumors in Taiwan. Chang Gung Med J. 2008;31(5):457–62.
4. Duque-Fisher CS, Casiano R, Vélez-Hoyos A, Londoño-Bustamente AF. Metastasis to the sinonasal region. Acta Otorrinolaringol Esp. 2009;60(6):428–31.
5. Haymes A, Mahalingam S, Choudhury N. Small cell lung cancer presenting as unilateral rhinorrhoea. BMJ Case Rep. 2017;2017:bcr-2017.
6. Chang MH, Kuo YJ, Ho CY, Kuan EC, Lan MY. metastatic tumors of the sinonasal cavity: a 15-year review of 17 cases. J Clin Med. 2019;8(4):539.
7. Pereira Arias JG, Ullate Jaime V, Valcárcel Martín F, et al. Epistaxis as initial manifestation of disseminated renal adenocarcinoma. Actas Urol Esp. 2002;26(5):361–5.
8. Petruzzelli GJ, Shook T, Campbell WJ, Gupta S. Paranasal sinus metastases of renal cell carcinoma: a case report and comprehensive literature review. Ann Clin Case Rep. 2019;4:1642.
9. Huang CT, Hong RL. Nasion swelling as the presenting symptom of lung adenocarcinoma. J Thorac Oncol. 2009;4(4):555–8.
10. Stevens TM, Bishop JA. HPV-related carcinomas of the head and neck: morphologic features, variants, and practical considerations for the surgical pathologist. Virchows Arch. 2017;471(2):295–307.
11. Haack H, Johnson LA, Fry CJ, et al. Diagnosis of NUT midline carcinoma using a NUT-specific monoclonal antibody. Am J Surg Pathol. 2009;33(7):984–91.
12. Monserez D, Vlaminck S, Kuhweide R, Casselman J. Symmetrical ethmoidal metastases from ductal carcinoma of the breast, suggesting transcribrosal spread. Acta Otorhinolaryngol Belg. 2001;55(3):251–7.
13. Bhargava R, Dabbs DJ. Use of immunohistochemistry in diagnosis of breast epithelial lesions. Adv Anat Pathol. 2007;14(2):93–107.
14. McCleskey BC, Penedo TL, Zhang K, Hameed O, Siegal GP, Wei S. GATA3 expression in advanced breast cancer: prognostic value and organ-specific relapse. Am J Clin Pathol. 2015;144(5):756–63.
15. Bhansali A, Kataria RN, Subrahmanyam KA, Radotra BD, Mathur SK. Maxillary mass as the presenting manifestation of papillary thyroid carcinoma. Indian J Cancer. 2003;40(2):80–1.
16. Shimmura H, Mori E, Sekine R, Tei M, Otori N. Metastasis of papillary thyroid carcinoma to the maxillary sinus: case report and review of the literature. Case Rep Otolaryngol. 2020;2020:4056901.
17. bin Sabir Husin Athar PP, bte Ahmad Norhan N, bin Saim L, bin Md Rose I, bte Ramli R. Metastasis to the sinonasal tract from sigmoid colon adenocarcinoma. Ann Acad Med Singap. 2008;37(9):788–3.
18. Cama E, Agostino S, Ricci R, Scarano E. A rare case of metastases to the maxillary sinus from sigmoid colon adenocarcinoma. ORL J Otorhinolaryngol Relat Spec. 2002;64(5):364–7.
19. Matsuda H, Tanigaki Y, Yoshida T, Matsuda R, Tsukuda M. A case of metastatic hepatocellular carcinoma in the nasal cavity. Eur Arch Otorhinolaryngol. 2006;263(4):305–7.
20. Zhang J, Chen G, Zhang P, et al. The threshold of alpha-fetoprotein (AFP) for the diagnosis of hepatocellular carcinoma: a systematic review and meta-analysis. PLoS One. 2020;15(2):e0228857.
21. Conrad R, Castelino-Prabhu S, Cobb C, Raza A. Cytopathologic diagnosis of liver mass lesions. J Gastrointest Oncol. 2013;4(1):53–61.
22. Timek DT, Shi J, Liu H, Lin F. Arginase-1, HepPar-1, and Glypican-3 are the most effective panel of markers in distinguishing hepatocellular carcinoma from metastatic tumor on fine-needle aspiration specimens. Am J Clin Pathol. 2012;138(2):203–10.
23. Andaz C, Alsanjari N, Garth RJ, Dearnaley DP. Metastatic seminoma of the sphenoid sinus. J Laryngol Otol. 1991;105(12):1075–8.
24. Bell DM, Porras G, Tortoledo ME, Luna MA. Primary sinonasal choriocarcinoma. Ann Diagn Pathol. 2009;13(2):96–100.
25. Filho BC, McHugh JB, Carrau RL, Kassam AB. Yolk sac tumor in the nasal cavity. Am J Otolaryngol. 2008;29(4):250–4.
26. van Dijk MR, Steyerberg EW, Stenning SP, Dusseldorp E, Habbema JD. Survival of patients with nonseminomatous germ cell cancer: a review of the IGCC classification by cox regression and recursive partitioning. Br J Cancer. 2004;90(6):1176–83.
27. Ulbright TM, Tickoo SK, Berney DM, Srigley JR. Best practices recommendations in the application of immunohistochemistry in testicular tumors: report from the International Society of Urological Pathology consensus conference. Am J Surg Pathol. 2014;38(8):e50–9.
28. Miettinen M, McCue PA, Sarlomo-Rikala M, et al. GATA3: a multispecific but potentially useful marker in surgical pathology: a systematic analysis of 2500 epithelial and nonepithelial tumors. Am J Surg Pathol. 2014;38(1):13–22.
29. Ramalingam P, Malpica A, Silva EG, Gershenson DM, Liu JL, Deavers MT. The use of cytokeratin 7 and EMA in differentiating ovarian yolk sac tumors from endometrioid and clear cell carcinomas. Am J Surg Pathol. 2004;28(11):1499–505.
30. Lund VJ. Sinonasal Malignant Melanoma. Adv Otorhinolaryngol. 2020;84:185–96.
31. Chen N, Gong J, Chen X, et al. Cytokeratin expression in malignant melanoma: potential application of in-situ hybridization analysis of mRNA. Melanoma Res. 2009;19(2):87–93.